Vol 26, No 6, June 2020

EMERGING INFECTIOUS DISEASES®

CDC
CENTERS FOR DISEASE CONTROL AND PREVENTION

Prions

June 2020

Jacopo Carucci Pontormo (1494–1557). *Portrait of Maria Salviati and Giulia de' Medici* (c. 1537). Oil on panel, 34.65 in × 28.07 in/88 cm × 71.3 cm. Digital image courtesy of The Walters Art Museum, Baltimore, Maryland, USA.

EMERGING INFECTIOUS DISEASES

Pages 1061–1352

EMERGING INFECTIOUS DISEASES®

Emerging Infectious Diseases is published monthly by the Centers for Disease Control and Prevention, 1600 Clifton Rd NE, Mailstop H16-2, Atlanta, GA 30329-4027, USA. Telephone 404-639-1960; email, eideditor@cdc.gov.

EMERGING INFECTIOUS DISEASES®

Prions **June 2020**

On the Cover

Jacopo Carucci Pontormo (1494–1557). *Portrait of Maria Salviati and Giulia de' Medici* (c. 1537). Oil on panel, 34.65 in × 28.07 in/88 cm × 71.3 cm. Digital image courtesy of The Walters Art Museum, Baltimore, Maryland, USA.

About the Cover p. 1349

Perspective

Synopses

Medscape EDUCATION ACTIVITY

Research

EMERGING INFECTIOUS DISEASES®
June 2020

Historical Review

Dispatches

Research Letters

EMERGING INFECTIOUS DISEASES®
June 2020

Books and Media

About the Cover

Readers may learn more about this month's cover image, Portrait of Maria Salviati and Giulia de' Medici by reading the historical review article **Syphilis in Maria Salviati (1499–1543), *Wife of Giovanni de' Medici of the Black Bands***, which appears in this issue (https://wwwnc.cdc.gov/eid/article/26/6/18-0786_article). **1350**

Etymologia

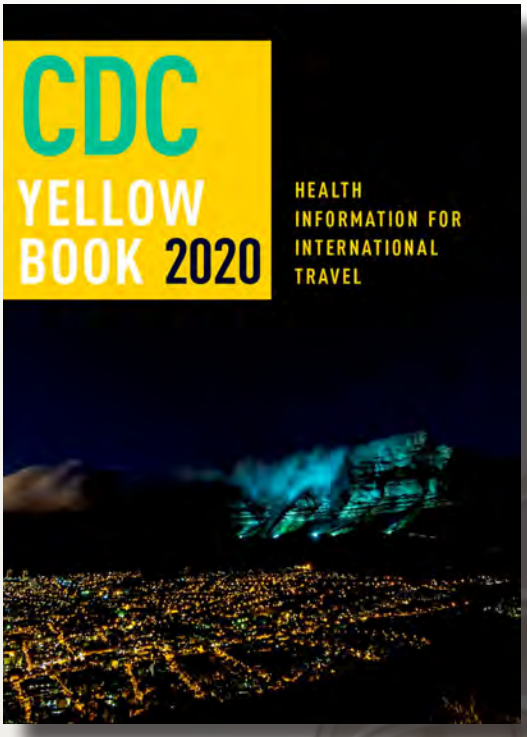

Available Now
Yellow Book 2020

The fully revised and updated CDC Yellow Book 2020: Health Information for International Travel codifies the US government's most current health guidelines and information for clinicians advising international travelers, including pretravel vaccine recommendations, destination-specific health advice, and easy-to-reference maps, tables, and charts.

ISBN: 978-0-19-006597-3 | $115.00 | May 2019 | Hardback | 720 pages

ISBN: 978-0-19-092893-3 | $55.00 | May 2019 | Paperback | 687 pages

Yellow Book 2020 includes important travel medicine updates

- **The latest information on emerging infectious disease threats, such as Zika, Ebola, and henipaviruses**
- **Considerations for treating infectious diseases in the face of increasing antimicrobial resistance**
- **Legal issues facing clinicians who provide travel health care**
- **Special considerations for unique types of travel, such as wilderness expeditions, work-related travel, and study abroad**

OXFORD
UNIVERSITY PRESS

Order your copy at:
www.oup.com/academic

Identifying and Interrupting Superspreading Events—Implications for Control of Severe Acute Respiratory Syndrome Coronavirus 2

Thomas R. Frieden,[1] Christopher T. Lee[1]

It appears inevitable that severe acute respiratory syndrome coronavirus 2 will continue to spread. Although we still have limited information on the epidemiology of this virus, there have been multiple reports of superspreading events (SSEs), which are associated with both explosive growth early in an outbreak and sustained transmission in later stages. Although SSEs appear to be difficult to predict and therefore difficult to prevent, core public health actions can prevent and reduce the number and impact of SSEs. To prevent and control of SSEs, speed is essential. Prevention and mitigation of SSEs depends, first and foremost, on quickly recognizing and understanding these events, particularly within healthcare settings. Better understanding transmission dynamics associated with SSEs, identifying and mitigating high-risk settings, strict adherence to healthcare infection prevention and control measures, and timely implementation of nonpharmaceutical interventions can help prevent and control severe acute respiratory syndrome coronavirus 2, as well as future infectious disease outbreaks.

Severe acute respiratory syndrome (SARS) coronavirus 2 (SARS-CoV-2) continues to spread (*1*). Although we still have limited information on the epidemiology of coronavirus disease (COVID-19), there have been multiple reports of superspreading events (SSEs) (*2*–*4*). During recent severe outbreaks of SARS, Middle East respiratory syndrome (MERS), and Ebola virus disease, SSEs were associated with explosive growth early in an outbreak and sustained transmission in later stages (*5*–*7*). Here, we review the factors that contribute to SSEs and implications for control of SARS-CoV-2.

Author affiliation: Resolve to Save Lives, New York, New York, USA

DOI: https://doi.org/eid2606.200495

SSEs are not limited to emerging infectious diseases. In the early 20th century, Mary Mallon (Typhoid Mary), an asymptomatic typhoid carrier who worked as a cook, infected ≥50 persons (*8*–*10*). An ingenious and elegant but little-known study of tuberculosis demonstrated that many patients, even those with smear-positive, cavitary tuberculosis, were not highly infectious but that 3 of 77 patients accounted for 73% of the infectious burden (*11*). In 1997, Woolhouse et al. observed that 20% of the population contributed to ≥80% of transmission and suggested targeting interventions to the core 20% (*12*). SSEs have also caused explosive outbreaks of measles, including among vaccinated persons (*13*).

During the 2003 SARS epidemic in Beijing, China, 1 hospitalized index patient was the source of 4 generations of transmission to 76 patients, visitors, and healthcare workers (*14*). During the MERS outbreak in South Korea, 166 (89%) of 186 confirmed primary cases did not further transmit the disease, but 5 patients led to 154 secondary cases (*15*). The index patient transmitted MERS to 28 other persons, and 3 of these secondary cases infected 84, 23, and 7 persons. During Ebola, SSEs played a key role sustaining the epidemic: 3% of cases were estimated to be responsible for 61% of infections (*6*).

SSEs highlight a major limitation of the concept of R_0. The basic reproductive number R_0, when presented as a mean or median value, does not capture the heterogeneity of transmission among infected persons (*16*); 2 pathogens with identical R_0 estimates may have markedly different patterns of transmission. Furthermore, the goal of a public health response is to drive the reproductive number to a value

[1]These authors contributed equally to this article.

<1, something that might not be possible in some situations without better prevention, recognition, and response to SSEs. A meta-analysis estimated that the initial median R_0 for COVID-19 is 2.79 (meaning that 1 infected person will on average infect 2.79 others), although current estimates might be biased because of insufficient data (*17*).

Countermeasures can substantially reduce the reproductive number; on the Diamond Princess cruise ship, an initial estimated R_0 of 14.8 (≈4 times higher than the R_0 in the epicenter of the outbreak in Wuhan, China) was reduced to an estimated effective reproductive number of 1.78 after on-board isolation and quarantine measures were implemented (*18*). In Wuhan, aggressive implementation of nonpharmaceutical interventions (NPIs) in the community, including a cordon sanitaire of the city; suspension of public transport, school, and most work; and cancellation of all public events reduced the reproductive number from 3.86 to 0.32 over a 5-week period (C. Wang et al., unpub. data, https://doi.org/10.1101/2020.03.03.20030593). However, these interventions might not be sustainable.

Drivers of SSEs

Although SSEs appear to be difficult to predict and therefore difficult to prevent, understanding the pathogen, host, environmental, and behavioral drivers of SSEs can inform strategies for SSE prevention and control (*19*,*20*) (Table). The potential impact of these factors has been analyzed (*5*). We summarize the evidence for multiple pathogens to facilitate a more generalized approach that can be applied to the current COVID-19 pandemic.

Pathogen-specific factors include binding sites (*29*), environmental persistence, virulence, and infectious dose. Strains of some organisms might be more readily transmissible than other strains of the same species (*21*,*22*). Mutation can potentially lead to increased infectivity (*6*); one preliminary report suggested that SARS-CoV-2 might have 2 distinct genetic subtypes, with the less lethal form becoming more dominant as a result of treating and isolating infected persons (*30*). Monitoring for genetic adaptation, both by whole-genome sequencing and epidemiologic investigation, will determine whether transmissibility of SARS-CoV-2 is evolving and whether variants of the virus are more readily transmitted.

Host factors include duration of infection (prolonged carriage), location and burden of infection (e.g., laryngeal or cavitary tuberculosis), and symptomatology (e.g., transmission of influenza during the prodromal phase) (*23*). All SARS superspreaders were symptomatic. The potential for and extent of transmission of COVID-19 from asymptomatic infected persons has not yet been fully characterized, although probable asymptomatic transmission has been documented in at least 1 family cluster (*31*). Epidemiologic analysis is required to understand the proportion of COVID-19 transmission which occurs before symptom onset, whether children are effective transmitters, and to identify host factors that might be associated with increased infectivity (*32*).

Environmental factors include population density and the availability and use of infection prevention and control measures in healthcare facilities. SARS and MERS had relatively low rates of person-to-person transmission but caused explosive outbreaks in healthcare settings (*28*). Rapid person-to-person transmission of COVID-19 appears likely to have occurred in healthcare settings, on a cruise ship, and in a church (*3*). In a study of 110 case-patients from 11 clusters in Japan, all clusters were associated with closed environments, including fitness centers, shared eating environments, and hospitals; the odds for transmission from a primary case-patient were 18.7 times higher than in open-air environments (H. Nishiura et al., unpub. data, https://doi.org/10.1101/2020.02.28.20029272). SARS-CoV-2 is present in stool (*33*); ensuring cleanliness of toilets and other potentially contaminated surfaces is needed, and measures to prevent aerosolization from plumbing, as might have occurred in the Amoy Garden outbreak of SARS (*24*), might need to be implemented. Evidence of environmental contamination by SARS-CoV-2 through respiratory droplets and fecal shedding highlights the need for effective decontamination efforts and strict adherence to environmental hygiene, which are pertinent to prevention and control of transmission, including SSEs (*34*).

Behavioral factors include cough hygiene, social customs, health-seeking behavior, and adherence to public health guidance. The risk for SSEs varies widely on the basis of cultural and socioeconomic context. In Sierra Leone, 1 traditional funeral was associated with 28 laboratory-confirmed cases of Ebola (*26*,*35*). Perceptions of risk can influence behavior and the likelihood of SSEs. Underestimation of risk in healthcare facilities resulted in transmission that prolonged the Ebola outbreak in Guinea (*27*). During the MERS outbreak in South Korea, doctor shopping (visiting multiple healthcare facilities after symptoms developed) was associated with SSEs (*36*). For control of COVID-19, behavioral recommendations for the general population to wash hands, cover coughs, and minimize exposing others,

Table. Factors that increase the risk for superspreading events and implications for prevention and control of COVID-19*

Factor	Disease	Epidemiologic role	Implications for control of COVID-19
Pathogen	Tuberculosis	Certain strains of *Mycobacterium tuberculosis* are more infectious, and patients ill with these strains should be prioritized for examination of a larger circle of contacts (*21*,*22*)	Continued monitoring for genetic change and for changes in the epidemiology of transmission
Host	Influenza	Viral shedding and risk for transmission among asymptomatic and presymptomatic persons can result in influenza transmission (*23*), particularly in closed settings with minimal ventilation (H. Nishiura et al., unpub. data, https://doi.org/10.1101/2020.02.28.20029272)	Identification of factors associated with increased transmissibility and rapid intervention to prevent transmission from similar patients prospectively; further characterization of risk for asymptomatic transmission
Environment	SARS	Airborne transmission of SARS can result in environmental spread of disease in community (*24*) and healthcare settings (*25*)	Assess changes in plumbing and ventilation that may be needed to reduce risk for spread; increase social distancing; reduce mass gatherings in closed environments; ensure effective triage, isolation, and general infection control in healthcare facilities
Behavior	Ebola	Inaccurate perceptions of Ebola risk can result in behaviors that increase the probability of transmission (*26*,*27*)	Promote handwashing, cough etiquette, and safer care-seeking behavior, including mask-wearing by persons who are ill, and ensure that timely and accurate messaging about risk and behavioral preventive measures are tailored to and reach affected populations
Response	MERS	Timely implementation of control measures can reduce outbreak duration and number of transmission events (*28*)	Rapidly identify and isolate cases to reduce transmission; implement large-scale NPIs in affected areas within 1 week

*COVID-19, coronavirus disease; MERS, Middle East respiratory syndrome; NPIs, nonpharmaceutical interventions; SARS, severe acute respiratory syndrome.

as well as rigorous infection control for healthcare workers, are needed.

Response factors include the timely and effective implementation of prevention and control measures within the community and in healthcare settings. These factors can reduce outbreak duration and decrease the reproductive number, thereby reducing the number of persons infected. Because delay of diagnosis is the most common cause of SSEs (*16*), timeliness is critical to prevent or limit their extent (*20*). Rapid identification and isolation of cases will reduce transmission; where necessary, large-scale NPIs should also be implemented in affected areas within 1 week (*37*). Effective case isolation and contact tracing might be sufficient to control a cluster of COVID-19, but the probability of control will decrease with delays in patient isolation from symptom onset (*38*).

Prevention and Mitigation of SSEs

SSE prevention and mitigation depends, first and foremost, on quickly recognizing and understanding these events. This recognition and understanding enables implementation of control measures specific to the incident and identification of measures, which can reduce the risk for future SSEs. During the SARS epidemic, rapid quarantine and isolation reduced outbreak extent and speed (*19*), and the lack of early detection was the primary cause of a hospital MERS outbreak in South Korea (*39*). An analysis of available data from Hong Kong, Vietnam, Singapore, and Canada found that delaying SARS control measures by just a week could have tripled the size of the epidemic (*7*). A modeling study of control interventions and SSEs in South Korea found that timely interventions (within 1 week), including a government announcement of affected hospitals, reduced the size and duration of MERS transmission (*28*).

Healthcare facilities are critical for prevention and control of SSEs. Targeted control measures include rapid identification and isolation of all potentially infectious patients, including a high index of suspicion for transmissible diseases, and implementation of universal infection control procedures in all areas of all facilities (*20*,*40*). Because individual superspreaders can only be identified retrospectively, universal implementation of triage procedures, rapid diagnosis and isolation, administrative controls (e.g., flow patterns and procedures for patients, visitors, and staff), and engineering controls (e.g., isolation rooms, partitions to protect against respiratory droplets, ventilation systems) are all necessary (*28*). Meticulous infection control is especially needed when performing procedures such as bronchoscopy, intubation, suctioning, sputum induction, and nebulizer therapies, which can enable what would normally be a droplet-transmitted infection to become aerosolized and therefore able to be more widely disseminated. If these types of procedures are needed, they should

be performed by using strict infection control procedures and, when possible, in airborne infection isolation units.

SSEs in healthcare settings can be associated with increased illness and death because many infections occur among patients with underlying conditions, which can delay diagnosis and exacerbate pathologic changes (*41*,*42*). Most tuberculosis is spread by patients who have not yet been given a diagnosis, rather than by failure to effectively isolate these patients (*43*). Risk factors for SSEs of SARS among 86 wards in Guangzhou, China, and 38 wards in Hong Kong were related to inadequate infection prevention and control, including insufficient availability of washing and changing facilities for staff, performing resuscitation on the ward, staff working while experiencing symptoms, and use of oxygen therapy or positive pressure ventilation (*25*). One patient in China who had only abdominal symptoms was not initially suspected of having COVID-19 and was admitted to a surgical ward; >10 healthcare workers and ≥4 patients were presumed to have been infected by this patient (*3*). It is essential that healthcare facilities implement infection control guidelines for COVID-19 rigorously. It is also essential that any nosocomial transmission is analyzed to identify the modes of spread, which will inform best strategies for prevention.

SSEs also occur in settings other than healthcare settings (*44*). The SARS outbreak in Hong Kong was characterized by 2 SSEs responsible for >400 infections (*45*); 1 guest at the Metropole Hotel was the index case for 4 national and international clusters (*46*). Community-wide NPIs, including risk communication to the public on social distancing, hand and respiratory hygiene, and criteria for either self-isolation or safer presentation to the hospital, can limit community transmission. During the SARS outbreak, effective communication appears to have reduced time from symptom onset to hospital admission and decreased the number of persons with whom patients had contact before isolation (*25*). The combination of facility-based and population-based interventions ended SARS transmission (*19*,*47*).

A study modeling the impact of interventions in Wuhan found that, although early identification and isolation reduced the number of infections somewhat, integrated implementation of NPIs decreased the number of cases rapidly and substantially and drove the reproductive number to <1 (C. Wang et al., unpub. data, https://doi.org/10.1101/2020.03.03.20030593). If NPIs had been implemented 2 weeks earlier, an estimated 86% of cases might have been prevented (*48*). For COVID-19, broad infection prevention and control measures include cough and hand hygiene, self-isolation by staying home if sick, and avoiding infection during care-seeking and caregiving.

Conclusions

COVID-19 has already killed more persons than SARS and MERS combined. Both of these coronavirus infections were fueled by SSEs. Understanding transmission dynamics associated with SSEs and their control during other coronavirus outbreaks can help inform current public health approaches to SARS-CoV-2. Anticipated heterogeneity in transmission should be used to plan disease control programs and risk-stratify populations for public health interventions. Countries should develop and implement protocols for implementation of rapid identification, diagnosis, and isolation of patients; effective infection prevention and control practices in healthcare facilities; and timely and relevant risk communication. Such measures can mitigate the impact of SSEs, which have been major drivers of recent epidemics.

Because delay in diagnosis and failure to rapidly implement isolation and response measures have fueled previous SSEs, countries should have plans and operational capacities in place during the containment phase of the response for immediate investigation and implementation of control measures. During the later mitigation phase, when surveillance and laboratory resources are limited, surveillance and focused response efforts should prioritize environments and settings at high risk for SSEs, including closed environments such as healthcare facilities, nursing homes, prisons, homeless shelters, schools, and sites of mass gatherings while community-wide NPIs are implemented more broadly.

Targeted and rapidly implemented public health interventions to prevent and mitigate SSEs are critical for early interruption of transmission during the containment phase and to reduce the effect on the disruption of healthcare services and society during the mitigation phase. Because of the societal and cultural underpinnings of behavioral and environmental factors including the local acceptability of adoption of NPIs, early engagement of communities, including an in-depth understanding of knowledge, attitudes, and practices relevant to the pandemic will be critical to response efforts during all phases.

Acknowledgments

We thank Cyrus Shahpar and Amanda McClelland for providing contributions to the manuscript and Drew Blakeman for providing assistance with manuscript preparation.

About the Authors

Dr. Frieden is a physician, president, and chief executive officer at Resolve to Save Lives, New York, NY, a global initiative and part of the global nonprofit Vital Strategies that works with countries to prevent 100 million deaths from cardiovascular disease and make the world safer from epidemics. He is former director of the US Centers for Disease Control and Prevention and former commissioner of the New York City Health Department. His research interests include epidemiology of infectious diseases and public health.

Dr. Lee is a medical epidemiologist and senior technical advisor at Resolve to Save Lives. He previously served as medical officer with the Measles Elimination Team, Global Immunization Division, Centers for Disease Control and Prevention and as an Epidemic Intelligence Service Officer assigned to the New York City Health Department. He previously worked on migration health and disaster response. His research interests include causes and consequences of forced migration, homelessness, and infectious disease epidemiology.

References

1. World Health Organization. Coronavirus disease 2019 (COVID-19) situation reports, 2020 [cited 2020 Mar 8]. https://www.who.int/emergencies/diseases/novel-coronavirus-2019/situation-reports
2. Why 14 doctors in Wuhan were infected: no eyepieces and masks were worn during surgery Shanghai: Shanghai First Finance Media Limited, January 22, 2020 [cited 2020 Mar 8]. https://www.yicai.com/news/100477916.html
3. Wang D, Hu B, Hu C, Zhu F, Liu X, Zhang J, et al. Clinical characteristics of 138 hospitalized patients with 2019 novel coronavirus-infected pneumonia in Wuhan, China. JAMA. 2020 [Epub ahead of print]. https://doi.org/10.1001/jama.2020.1585
4. South Korean city on high alert as coronavirus cases soar at 'cult' church. New York: The Guardian, February 20, 2020 [cited 2020 Mar 8]. https://www.theguardian.com/world/2020/feb/20/south-korean-city-daegu-lockdown-coronavirus-outbreak-cases-soar-at-church-cult-cluster
5. Wong G, Liu W, Liu Y, Zhou B, Bi Y, Gao GF. MERS, SARS, and Ebola: the role of super-spreaders in infectious disease. Cell Host Microbe. 2015;18:398–401. https://doi.org/10.1016/j.chom.2015.09.013
6. Lau MS, Dalziel BD, Funk S, McClelland A, Tiffany A, Riley S, et al. Spatial and temporal dynamics of superspreading events in the 2014–2015 West Africa Ebola epidemic. Proc Natl Acad Sci U S A. 2017;114:2337–42. https://doi.org/10.1073/pnas.1614595114
7. Wallinga J, Teunis P. Different epidemic curves for severe acute respiratory syndrome reveal similar impacts of control measures. Am J Epidemiol. 2004;160:509–16. https://doi.org/10.1093/aje/kwh255
8. Leavitt J. Typhoid Mary: captive to the public's health. Boston: Beacon Press; 1996.
9. Marineli F, Tsoucalas G, Karamanou M, Androutsos G. Mary Mallon (1869–1938) and the history of typhoid fever. Ann Gastroenterol. 2013;26:132–4.
10. Prouty AM, Schwesinger WH, Gunn JS. Biofilm formation and interaction with the surfaces of gallstones by *Salmonella* spp. Infect Immun. 2002;70:2640–9. https://doi.org/10.1128/IAI.70.5.2640-2649.2002
11. Riley RL, Mills CC, O'Grady F, Sultan LU, Wittstadt F, Shivpuri DN. Infectiousness of air from a tuberculosis ward. Ultraviolet irradiation of infected air: comparative infectiousness of different patients. Am Rev Respir Dis. 1962;85:511–25.
12. Woolhouse ME, Dye C, Etard JF, Smith T, Charlwood JD, Garnett GP, et al. Heterogeneities in the transmission of infectious agents: implications for the design of control programs. Proc Natl Acad Sci U S A. 1997;94:338–42. https://doi.org/10.1073/pnas.94.1.338
13. Shimizu K, Kinoshita R, Yoshii K, Akhmetzhanov AR, Jung S, Lee H, et al. An investigation of a measles outbreak in Japan and China, Taiwan, China, March–May 2018. Western Pac Surveill Response J. 2018;9:25–31. https://doi.org/10.5365/wpsar.2018.9.2.005
14. Shen Z, Ning F, Zhou W, He X, Lin C, Chin DP, et al. Superspreading SARS events, Beijing, 2003. Emerg Infect Dis. 2004;10:256–60. https://doi.org/10.3201/eid1002.030732
15. Chun BC. Understanding and modeling the super-spreading events of the Middle East respiratory syndrome outbreak in Korea. Infect Chemother. 2016;48:147–9. https://doi.org/10.3947/ic.2016.48.2.147
16. Lloyd-Smith JO, Schreiber SJ, Kopp PE, Getz WM. Superspreading and the effect of individual variation on disease emergence. Nature. 2005;438:355–9. https://doi.org/10.1038/nature04153
17. Liu Y, Gayle AA, Wilder-Smith A, Rocklöv J. The reproductive number of COVID-19 is higher compared to SARS coronavirus. J Travel Med. 2020;Feb 13:[Epub ahead of print]. https://doi.org/10.1093/jtm/taaa021
18. Rocklöv J, Sjödin H, Wilder-Smith A. COVID-19 outbreak on the Diamond Princess cruise ship: estimating the epidemic potential and effectiveness of public health countermeasures. J Travel Med. 2020;Feb 28:[Epub ahead of print]. https://doi.org/10.1093/jtm/taaa030
19. Bauch CT, Lloyd-Smith JO, Coffee MP, Galvani AP. Dynamically modeling SARS and other newly emerging respiratory illnesses: past, present, and future. Epidemiology. 2005;16:791–801. https://doi.org/10.1097/01.ede.0000181633.80269.4c
20. Lloyd-Smith JO, Galvani AP, Getz WM. Curtailing transmission of severe acute respiratory syndrome within a community and its hospital. Proc Biol Sci. 2003;270:1979–89. https://doi.org/10.1098/rspb.2003.2481
21. Luo T, Comas I, Luo D, Lu B, Wu J, Wei L, et al. Southern east Asian origin and coexpansion of *Mycobacterium tuberculosis* Beijing family with Han Chinese. Proc Natl Acad Sci U S A. 2015;112:8136–41. https://doi.org/10.1073/pnas.1424063112
22. Holt KE, McAdam P, Thai PV, Thuong NT, Ha DT, Lan NN, et al. Frequent transmission of the *Mycobacterium tuberculosis* Beijing lineage and positive selection for the EsxW Beijing variant in Vietnam. Nat Genet. 2018;50:849–56. https://doi.org/10.1038/s41588-018-0117-9
23. Ip DK, Lau LL, Leung NH, Fang VJ, Chan KH, Chu DK, et al. Viral shedding and transmission potential of asymptomatic and paucisymptomatic influenza virus infections in the community. Clin Infect Dis. 2017;64:736–42.
24. Yu IT, Li Y, Wong TW, Tam W, Chan AT, Lee JH, et al. Evidence of airborne transmission of the severe acute respiratory syndrome virus. N Engl J Med. 2004;350:1731–9. https://doi.org/10.1056/NEJMoa032867

25. Yu IT, Xie ZH, Tsoi KK, Chiu YL, Lok SW, Tang XP, et al. Why did outbreaks of severe acute respiratory syndrome occur in some hospital wards but not in others? Clin Infect Dis. 2007;44:1017–25. https://doi.org/10.1086/512819
26. Nielsen CF, Kidd S, Sillah AR, Davis E, Mermin J, Kilmarx PH; Centers for Disease Control and Prevention. Improving burial practices and cemetery management during an Ebola virus disease epidemic—Sierra Leone, 2014. MMWR Morb Mortal Wkly Rep. 2015;64:20–7.
27. Faye O, Boëlle PY, Heleze E, Faye O, Loucoubar C, Magassouba N, et al. Chains of transmission and control of Ebola virus disease in Conakry, Guinea, in 2014: an observational study. Lancet Infect Dis. 2015;15:320–6. https://doi.org/10.1016/S1473-3099(14)71075-8
28. Lee J, Chowell G, Jung E. A dynamic compartmental model for the Middle East respiratory syndrome outbreak in the Republic of Korea: a retrospective analysis on control interventions and superspreading events. J Theor Biol. 2016;408:118–26. https://doi.org/10.1016/j.jtbi.2016.08.009
29. Richard M, Fouchier RA. Influenza A virus transmission via respiratory aerosols or droplets as it relates to pandemic potential. FEMS Microbiol Rev. 2016;40:68–85. https://doi.org/10.1093/femsre/fuv039
30. Tang X, Wu C, Li X, Song Y, Yao X, Wu X, et al. On the origin and continuing evolution of SARS-CoV-2. National Science Review. 2020;Mar 3:[Epub ahead of print]. https://doi.org/10.1093/nsr/nwaa036
31. Yu P, Zhu J, Zhang Z, Han Y, Huang L. A familial cluster of infection associated with the 2019 novel coronavirus indicating potential person-to-person transmission during the incubation period. J Infect Dis. 2020;Feb 18:[Epub ahead of print]. https://doi.org/10.1093/infdis/jiaa077
32. Kupperscmidt K. Study claiming new coronavirus can be transmitted by people without symptoms was flawed. Washington: American Association for the Advancement of Science, February 3, 2020 [cited 2020 Mar 8]. https://www.sciencemag.org/news/2020/02/paper-non-symptomatic-patient-transmitting-coronavirus-wrong
33. Gu J, Han B, Wang J. COVID-19: Gastrointestinal manifestations and potential fecal-oral transmission. Gastroenterology. 2020;Mar 3:pii: S0016-5085(20)30281-X. Epub ahead of print]. https://doi.org/10.1053/j.gastro.2020.02.054
34. Ong SW, Tan YK, Chia PY, Lee TH, Ng OT, Wong MS, et al. Air, surface environmental, and personal protective equipment contamination by severe acute respiratory syndrome coronavirus 2 (SARS-CoV-2) from a symptomatic patient. JAMA. 2020 Mar 4 [Epub ahead of print]. https://doi.org/10.1001/jama.2020.3227
35. Curran KG, Gibson JJ, Marke D, Caulker V, Bomeh J, Redd JT, et al. Cluster of Ebola virus disease linked to a single funeral—Moyamba District, Sierra Leone, 2014. MMWR Morb Mortal Wkly Rep. 2016;65:202–5. https://doi.org/10.15585/mmwr.mm6508a2
36. Kim SW, Park JW, Jung HD, Yang JS, Park YS, Lee C, et al. Risk factors for transmission of Middle East respiratory syndrome coronavirus infection during the 2015 outbreak in South Korea. Clin Infect Dis. 2017;64:551–7.
37. Zhao S, Lin Q, Ran J, Musa SS, Yang G, Wang W, et al. Preliminary estimation of the basic reproduction number of novel coronavirus (2019-nCoV) in China, from 2019 to 2020: a data-driven analysis in the early phase of the outbreak. Int J Infect Dis. 2020;92:214–7. https://doi.org/10.1016/j.ijid.2020.01.050
38. Hellewell J, Abbott S, Gimma A, Bosse NI, Jarvis CI, Russell TW, et al.; Centre for the Mathematical Modelling of Infectious Diseases COVID-19 Working Group. Feasibility of controlling COVID-19 outbreaks by isolation of cases and contacts. Lancet Glob Health. 2020 Feb 28 [Epub ahead of print]. https://doi.org/10.1016/S2214-109X(20)30074-7
39. Park GE, Ko JH, Peck KR, Lee JY, Lee JY, Cho SY, et al. Control of an outbreak of Middle East respiratory syndrome in a tertiary hospital in Korea. Ann Intern Med. 2016;165:87–93. https://doi.org/10.7326/M15-2495
40. World Health Organization. Clinical management of severe acute respiratory infection when novel coronavirus (2019-nCoV) infection is suspected: interim guidance, January 28, 2020 [cited 2020 Mar 8]. https://www.who.int/publications-detail/clinical-management-of-severe-acute-respiratory-infection-when-novel-coronavirus-(ncov)-infection-is-suspected
41. Amer H, Alqahtani AS, Alzoman H, Aljerian N, Memish ZA. Unusual presentation of Middle East respiratory syndrome coronavirus leading to a large outbreak in Riyadh during 2017. Am J Infect Control. 2018;46:1022–5. https://doi.org/10.1016/j.ajic.2018.02.023
42. Lee CT, Hagan JE, Jantsansengee B, Tumurbaatar OE, Altanchimeg S, Yadamsuren B, et al. Increase in infant measles deaths during a nationwide measles outbreak, Mongolia, 2015–2016. J Infect Dis. 2019;220:1771–9. https://doi.org/10.1093/infdis/jiz140
43. Frieden TR, Sherman LF, Maw KL, Fujiwara PI, Crawford JT, Nivin B, et al. A multi-institutional outbreak of highly drug-resistant tuberculosis: epidemiology and clinical outcomes. JAMA. 1996;276:1229–35. https://doi.org/10.1001/jama.1996.03540150031027
44. Liang W, Zhu Z, Guo J, Liu Z, Zhou W, Chin DP, et al.; Beijing Joint SARS Expert Group. Severe acute respiratory syndrome, Beijing, 2003. Emerg Infect Dis. 2004;10:25–31. https://doi.org/10.3201/eid1001.030553
45. Riley S, Fraser C, Donnelly CA, Ghani AC, Abu-Raddad LJ, Hedley AJ, et al. Transmission dynamics of the etiological agent of SARS in Hong Kong: impact of public health interventions. Science. 2003;300:1961–6. https://doi.org/10.1126/science.1086478
46. Centers for Disease Control and Prevention. Update: outbreak of severe acute respiratory syndrome—worldwide, 2003. MMWR Morb Mortal Wkly Rep. 2003;52:241–6, 248.
47. Anderson RM, Fraser C, Ghani AC, Donnelly CA, Riley S, Ferguson NM, et al. Epidemiology, transmission dynamics and control of SARS: the 2002–2003 epidemic. Philos Trans R Soc Lond B Biol Sci. 2004;359:1091–105. https://doi.org/10.1098/rstb.2004.1490
48. Lai S, Ruktanonchai NW, Zhou L, Prosper O, Luo W, Wesolowski A, et al. Effect of nonpharmaceutical interventions for containing the COVID-19 outbreak: an observational and modelling study. World Population. 2020 Mar 4 [cited 2020 Mar 8]. https://www.worldpop.org/events/COVID_NPI

Address for correspondence: Thomas R. Frieden, Resolve to Save Lives, 100 Broadway, 4th Fl, New York, NY 10005, USA; email: tfrieden@rtsl.org

Risks Related to Chikungunya Infections among European Union Travelers, 2012–2018

Céline M. Gossner, Nelly Fournet, Joana Gomes Dias, Beatriz Fernández Martínez, Martina Del Manso, Johanna J. Young, Hervé Zeller, Denis Coulombier

Autochthonous outbreaks of chikungunya have occurred in the European Union (EU) after virus introduction by infected travelers. We reviewed the surveillance data of travel-related cases reported in the EU during 2012–2018 to document factors associated with increased infection rates among travelers and to assess how surveillance data could support preparedness against secondary transmission and timely control of outbreaks. Thirteen EU countries reported 2,616 travel-related chikungunya cases. We observed 3 successive epidemiologic periods; the highest number of cases (75%) occurred during 2014–2015, when most cases were associated with the Caribbean and South America. The highest infection rates among travelers were observed during the same phase. Although surveillance of travel-related cases is relevant for estimating the infection risk for travelers, we could not identify a relationship between the number of infected travelers and a higher likelihood of secondary transmission in the EU.

Chikungunya is a disease carried by *Aedes* mosquitoes that affects >100 countries, mostly in the tropics and subtropics (*1*). In the European Union (EU), chikungunya is not endemic, even though some outbreaks were reported in France and Italy after introduction of chikungunya virus by travelers into receptive areas (areas in which *Aedes albopictus* mosquitoes were established and active) (*2*–*6*).

To limit secondary transmission, it is crucial to monitor the distribution and activity of the mosquito vectors of the virus, reduce the likelihood of introduction of the virus by travelers, detect infections among returning travelers early, and implement timely control measures for cases in receptive areas. Consequently, surveillance of chikungunya was implemented during 2008 by the EU, whose goal was supporting these objectives (*7*).

We reviewed the surveillance data of travel-associated chikungunya cases reported in the EU during 2012–2018 with 2 aims. The first aim was to document factors associated with increased infection rates among travelers so that travelers, travel clinics, and public health authorities have relevant information to mitigate risks for infection. The second aim was to review how surveillance data could support preparedness against secondary transmission and timely control of outbreaks in susceptible areas.

Methods

Travelers

We obtained traveler data for 2012–2017 from the International Air Transport Association, which records passengers on commercial flights. We did not have access to 2018 data and considered it equal to 2017 data. We analyzed the number of travelers flying from chikungunya-affected countries to EU countries per month. We considered the departure and arrival countries irrespectively of connecting flights and assumed that case-patients were flying from the country in which infection occurred.

Travel-Related Cases

We defined a travel-related case-patient as a person reported by an EU country, later called reporting countries, with a probable or confirmed chikungunya infection acquired outside their country of residence during 2012–2018. Cases were reported to the European Centre for Disease Prevention and Control (ECDC) (*8*). For time-related analysis we used, in

Author affiliations: European Centre for Disease Prevention and Control, Solna, Sweden (C.M. Gossner, J. Gomes Dias, J.J. Young, H. Zeller, D. Coulombier); Santé Publique France, Saint-Maurice, France (N. Fournet); Instituto de Salud Carlos III, Madrid, Spain (B. Fernández Martínez); Istituto Superiore di Sanita, Rome, Italy (M. Del Manso)

DOI: https://doi.org/10.3201/eid2606.190490

order of preference, the date of onset, the date of diagnostics, or the date of notification. When none of these dates were available and if the date used for statistics was earlier than any of the dates mentioned, we used the date used for statistics, which is an unspecified, mandatory date.

We defined a probable case-patient as a person who had fever, returned from an area with ongoing chikungunya transmission within 2 weeks before onset of symptoms, and had virus-specific IgM in 1 serum sample (*9*). We defined a confirmed case-patient as a person satisfying any of the following laboratory criteria: detection of virus nucleic acid or virus isolation from a clinical specimen, virus-specific IgM in 1 serum sample plus confirmation by neutralization, or seroconversion or 4-fold antibody titer increase of specific antibodies in paired serum samples (*9*).

Vector Distribution and Population

For each year, we obtained data on establishment of *Ae. albopictus* mosquitoes at the regional level (third level of the Nomenclature of Territorial Units for Statistics [*10*]) from the VectorNet database (*11*) and the French Ministry of Health website (*12*) and the population in reporting countries from Eurostat (*13*). We calculated the percentage of the population in regions in which the vector was established (population living in regions in which *Ae. albopictus* mosquitoes were established × 100/total population in the country). We grouped countries per geographic regions according to the United Nations Statistics Division definitions (*14*).

Inclusion Criteria

The applied inclusion criteria (Appendix Figure, https://wwwnc.cdc.gov/EID/article/26/6/19-0490-App1.pdf) aimed to account for possible errors in gathering or reporting travel history/exposure of case-patients and lack of specificity of IgM serologic testing (*15,16*). We included probable and confirmed travel-related cases. Cases related to the French overseas territories (e.g., Martinique, French Polynesia) were considered as travel-related cases and those overseas territories as countries of infection. We also included reporting countries that submitted data every year and provided country of infection for ≥50% of their cases (arbitrary cutoff value) over the study period. When multiple countries of infection were reported for 1 case, the country of infection was changed to unknown. Finally, we included cases with a known country of infection; countries of infections that were associated with ≥2 cases, of which ≥1 was a confirmed case, and that were either reported by 2 reporting countries or reported over multiple years; and countries of infection that had travelers data available.

Analysis

To obtain information that could support prevention of cases among travelers, we performed a descriptive analysis of travel patterns, case characteristics, reporting countries, and countries of infection. As a proxy of the risk for infection, we calculated infection rates among travelers (TIR = no. cases/100,000 travelers).

To define the risk for secondary transmission, we conducted a (nonsystematic) literature search on occurrences of secondary transmission in the EU during 2012–2018 and estimated the number of cases that could have led to autochthonous outbreaks. We considered that travel-related cases were distributed evenly within the reporting countries; for each year and reporting country, we multiplied the number of travel-related cases that occurred during June–October (when the vector is more abundant and active) by the percentage of population in regions where *Ae. albopictus* mosquitoes were established. We did not consider secondary transmission by donations of substances of human origin. We performed statistical analyses by using STATA/SE 14.0 software (https://www.stata.com) and Microsoft Excel 2016 (https://www.microsoft.com).

Results

We identified 13 reporting countries and 59 countries of infection (Figure 1). During 2012–2018, a total of 146 million travelers arrived in reporting countries from countries of infection (Appendix Table). Most of these travelers arrived from Southeast Asia (27%), southern Asia (19%), and the Caribbean (15%). More specifically, 12% arrived from India, 12% from Thailand, and 8% from Brazil. The United Kingdom (31%), France (22%), and Germany (16%) received the highest number of travelers.

Travelers from the Caribbean (41%) and Polynesia (74%) arrived primarily in France. Travelers from South (32%) and Central (29%) America arrived mainly in Spain. Travelers from Southeast (32%) and southern (55%) Asia and from eastern Africa (44%) arrived primarily in the United Kingdom.

The overall yearly number of travelers increased during 2012–2018 from 18 million to 24 million. The highest increases in travelers during that period were for Northern Africa (88%), Central America (71%), and the Caribbean (54%). There were also large annual variations in number of travelers returning

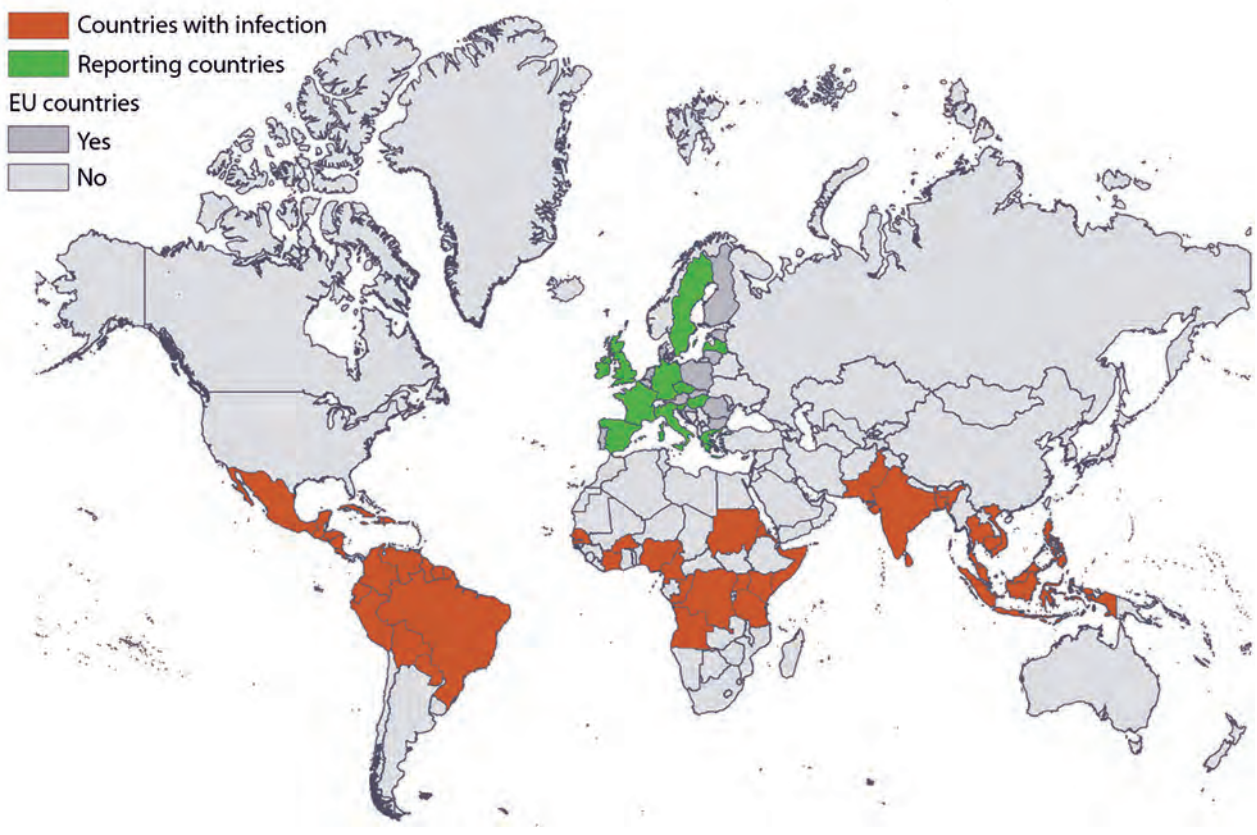

Figure 1. Risks related to chikungunya infections among EU travelers, 2012–2018. Countries with infection and reporting countries are indicated. Map produced on January 8, 2020. Administrative boundaries were obtained from EuroGeographics and the United Nations Food and Agriculture Organization. EU, European Union.

from specific countries of infection. For instance, the number of travelers from Venezuela decreased by 58% during 2013–2015 largely because of domestic insecurity and political crisis.

The number of EU travelers exhibited a seasonal pattern with peaks related to holiday periods (January, March, and August). Peak periods varied among reporting countries: March and August for France; January and March for Germany; July–September for Spain; January for Sweden; and January, April, and August for the United Kingdom.

Risk for Infection among Travelers

During 2012–2018, there were 2,616 travel-related chikungunya cases, among which 1,766 were confirmed cases and 850 were probable cases (Table 1). France (918), the United Kingdom (593), Spain (587), and Germany (359) reported 94% of the cases. Although most reporting countries reported mostly confirmed cases, 60% of the cases reported by France and 31% of the cases reported by the United Kingdom were confirmed. The global TIR was 1.8 cases/100,000 travelers (Appendix Table).

The number of cases and global TIR fluctuated over the study period (Table 1; Figure 2; Appendix Table); both values peaked in 2014. There was a seasonal increase in cases during May–September, with a peak in May–June for Spain, May–August for France, September–November for Germany, and October–November for the United Kingdom. The global TIR was highest in May, June, and July. The median age of travel-related case-patients was 43 years (interquartile range 32–55 years), and the female-to-male ratio was 1.1:4.

We observed 3 successive epidemiologic periods (Figures 2–5). The first phase, 2012–2013, had few cases, most (84%) associated with southern and Southeast Asia; the global TIR was 0.2. In November 2013, one case was associated with the Caribbean, marking the start of epidemics in the Americas (*17*).

The second phase, 2014–2015, corresponded to the globalization of virus circulation; the global TIR was 4.8. Most cases were associated with the Caribbean (68%) and South America (17%). In 2014, the TIR for travelers from the Caribbean reached 45.9; in 2015 it decreased in travelers from the Caribbean (1.6), but

Table 1. Characteristics of 2,616 persons with travel-related chikungunya infections, 2012–2018

Characteristic	No. case-patients (%)
Case classification	
Probable	850 (32)
Confirmed	1,766 (68)
Sex	
F	1,517 (58)
M	1,088 (42)
Unknown	11 (<1)
Age group, y	
<1–4	25 (1)
5–14	79 (4)
15–24	154 (7)
25–44	936 (43)
45–64	775 (35)
≥65	221 (10)
Unknown	426 (16)
Year of infection	
2012	37 (1)
2013	45 (2)
2014	1,431 (55)
2015	448 (17)
2016	365 (14)
2017	171 (7)
2018	119 (6)
Month of infection	
January	133 (5)
February	89 (3)
March	96 (3)
April	150(5)
May	296 (11)
June	392 (15)
July	340 (13)
August	284 (11)
September	240 (9)
October	220 (8)
November	209 (8)
December	167 (6)

it increased for travelers from South America (6.3) and Central America (6.1). In 2014, there was a high TIR for travelers returning from Haiti (266.6) and Dominica (193.6), and during 2015, a high TIR was associated with Honduras (78.1) and Nicaragua (76.5).

During the 2014–2015 phase, a high TIR was associated with Polynesia (36.8), which matched the intense epidemic in the region; in French Polynesia for instance, a few months after introduction of the virus, 25% of the population had been affected (*18*). In Africa, high TIRs were observed in travelers returning from Angola (12.0) during 2014 and Equatorial Guinea (9.2) during 2015. During that phase, travelers arriving in France and Spain had the highest TIRs: 9.5 for France and 9.8 for Spain.

The third phase, 2016–2018, was marked by a decrease in the global TIR. During that phase, a large percentage of case-patients were returning from southern Asia (45%) and South America (24%); regional TIRs were 2.1 for southern Asia and 1.4 for South America. During 2016, there were high TIRs for travelers returning from Bolivia (21.4) and Nicaragua (18.2). In Africa, high TIRs were seen for travelers from Somalia during 2016 (68.3) and Kenya during 2018 (6.6); a large epidemic affected Mombasa County in Kenya during 2018 (*19*). During 2016–2018, travelers arriving in Germany, Spain, Sweden, and the United Kingdom had TIRs ranging from 1.0 to 2.1, and travelers arriving in France had a TIR of 0.5.

Risk for Secondary Transmission within the EU

During 2012–2018, a total of 3 autochthonous chikungunya outbreaks occurred in the EU. Two occurred in France in Hérault Department (September–October 2014) and Var Department (August 2017) (*3*,*4*). For the outbreak in Hérault, the index case-patient returned from Cameroon. For the outbreak in Var, the virus originated in Central Africa. One large outbreak occurred in the Lazio and Calabria regions of Italy (June–November 2017) (*5*). The index case-patient was not identified, but the virus originated in Pakistan or India (*6*,*20*).

During the study period, 10 case-patients returned from Cameroon (1–2/year). France reported the only case-patient during 2014; the TIR for travelers from France that year was 0.9. The highest TIR related to Cameroon was during 2017 for travelers from Spain (TIR = 28.5). During 2012–2018, a total of 38 case-patients were reported from Central Africa, 6 of them during 2017: 2 by France (TIR = 1.0) and 4 by Spain (TIR = 15.3). The highest TIRs related to Central Africa were in 2014 and 2017 among travelers from Spain (TIR = 17.3 during 2014 and 15.3 during 2017). During the study period, we detected 328 case-patients infected in India or Pakistan, 72 of them during 2017. Italy did not report any cases from these countries during 2017. During 2017, the TIR for travelers returning either from India or Pakistan was highest in the United Kingdom. The highest TIRs related to India or Pakistan were during 2016 among travelers from Malta and Slovenia. During 2014, travelers from France who had the highest TIRs (>600) were returning from Dominica, Suriname, and Tonga. During 2017, among travelers from France and Italy, those who had the highest TIRs returned from Bangladesh (TIR = 12.5 for travelers from France and 8.7 for travelers from Italy).

Among the reporting countries, France, Germany, Greece, Italy, Malta, Slovenia, and Spain had receptive areas (Table 2). The percentage of the population in regions in those countries colonized by *Ae. albopictus* mosquitoes increased during 2012–2018, from 28% in 2012 to 45% in 2018. We estimated that 270 travel-related case-patients returned to receptive areas during 2012–2018; 171 (63%) were in 2014. Among

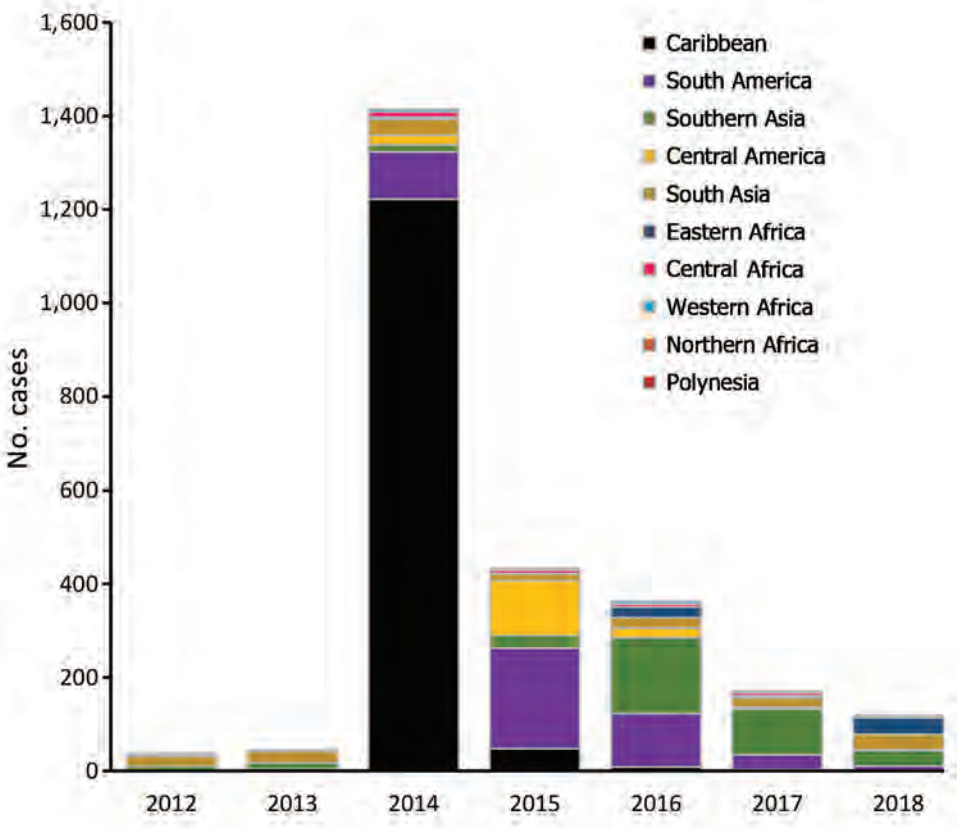

Figure 2. Number of travel-related chikungunya cases during 2012–2018, by region of infection and year.

the estimated case-patients, 163 arrived in France, 79 in Spain, and 25 in Italy.

Discussion

We documented factors associated with increased travel-associated chikungunya cases reported in the EU during 2012–2018. Travel patterns (i.e., volume of travelers, country visited, and period of travel) were specific to each of the reporting countries. These patterns also reflect the geopolitical context, historical and cultural links, and preferences of travelers.

The TIR fluctuated according to the region/country visited, the reporting country, and the period of travel. The difference in TIR and seasonality among reporting countries was likely caused by difference in places visited within the countries of infection, intensity of virus circulation at the time of the visit, and reason for travel (e.g., business versus holidays). Generally, we observed a much higher TIR for travelers visiting a country with historical links to the reporting country (i.e., travelers from Spain visiting countries in Central America or travelers from France visiting French Overseas Countries and Territories). This finding might be explained by a high number of travelers visiting friends or relatives (VFR travelers). These travelers are less likely to receive pretravel advice than other types of travelers (*21*), might stay longer in the visited country, and might use fewer protective measures. Therefore, EU countries should consider issuing their own specific travel advice on the basis of countries most visited and those that have a higher risk for infection for their citizens. Prevention campaigns could be strengthened before and during peaks of cases and TIR, and be tailored to at-risk populations (e.g., VFR travelers). To reach these populations, travel advice could be provided online when flight tickets are purchased or through social media.

A high number of cases or high TIR might also highlight a sensitive surveillance system. This suggestion explains a slightly higher TIR among travelers from Sweden compared with other travelers during the 2012–2013 and 2016–2018 phases. With an overall number of travelers that is relatively low and a sensitive surveillance system, Sweden was able to test most possible case-patients and therefore detect a high proportion of cases among travelers.

As highlighted in other reports (*22*,*23*), travel-related cases are good indicators of the epidemiologic situation of the country visited because outbreaks are reflected by an increase in travel-related cases. Our results accurately highlighted the spread of the virus throughout the Americas, Polynesia, and eastern

Africa. Therefore, travelers can be considered as sentinels, particularly in countries in which disease surveillance is limited (e.g., Somalia).

If there are few travelers, the likelihood of observing cases is limited. Therefore, having no cases associated with a specific country does not necessarily mean that no virus is circulating. It is useful to consider traveler data, and TIR provides a more accurate estimation of the risk for infection for travelers.

The higher proportion of female case-patients could be explained by the fact that women are at higher risk for development of severe symptoms and are therefore are more likely to seek medical attention (*24*). In addition, more female travelers might be exposed. For instance, in Spain, 61% of the travel-related cases were VFR travelers (*25*); those travelers are expected to be persons who emigrated to Spain from disease-endemic countries, mostly from the Americas. A high proportion of persons born in Central America/Caribbean (64.5%) and South America (55.6%) and living in Spain are women (*26*). Therefore, we might consider that more female travelers were going to the Americas as VFR travelers and became infected during that visit.

The number of cases and TIR do not seem to correlate with the likelihood of occurrence of autochthonous outbreaks in reporting countries and the origin of the imported outbreak strain. We found no autochthonous outbreaks associated with epidemics in the Americas during 2014–2015. In contrast, we

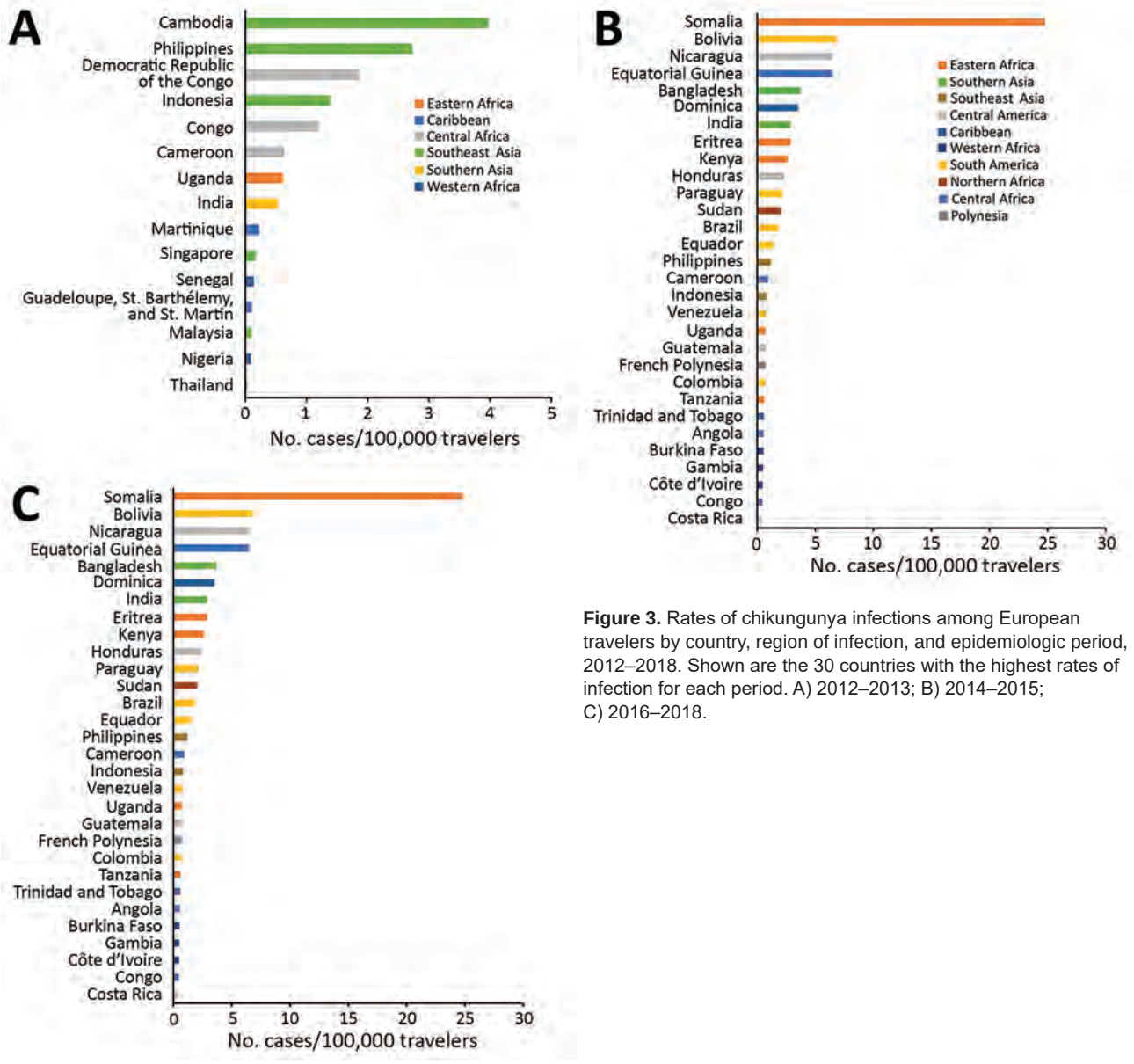

Figure 3. Rates of chikungunya infections among European travelers by country, region of infection, and epidemiologic period, 2012–2018. Shown are the 30 countries with the highest rates of infection for each period. A) 2012–2013; B) 2014–2015; C) 2016–2018.

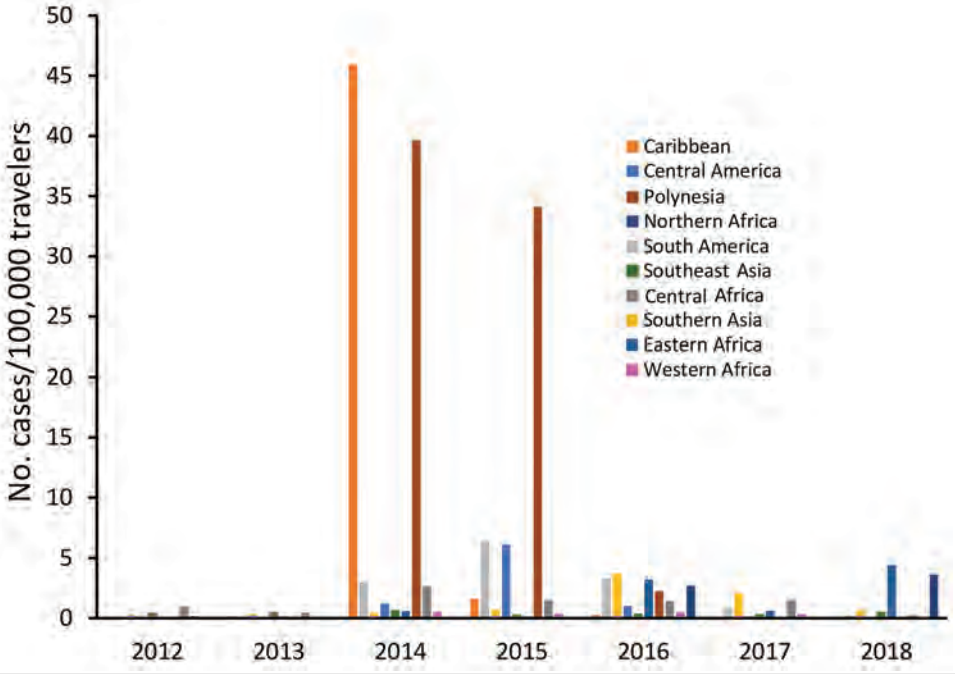

Figure 4. Rates of chikungunya infections among European Union travelers by region of infection and year, 2012–2018.

found 2 autochthonous outbreaks during 2017 despite the relatively lower number of imported cases than in previous years. The autochthonous outbreaks that occurred in the EU were not consistently associated with regions/countries of infections with most cases or high TIRs. In addition, although we estimated that pressure of introduction in receptive areas in Spain was higher than that for those in Italy, no outbreaks were reported in Spain. Also, outbreaks have not occurred in years that had higher pressure of introduction. Many other factors account for allowing an autochthonous outbreak, including activity and abundance of the vector, environmental factors, adaptation of the virus strain to the local vector, surveillance sensitivity, and timeliness of control measures implemented for imported cases (*27*–*29*). Consequently, although monitoring of outbreaks worldwide is relevant for estimating the risk for infection to travelers, this monitoring does not seem to be as relevant for estimation of the risk for secondary transmission.

In the absence of valid data on vector competence of local *Ae. Albopictus* mosquito populations and the particular chikungunya virus strain, each imported case should be considered as a potential index case. Control measures should then be implemented for the case to limit the likelihood of virus and disease spread.

In the context of the global climatic and ecologic changes, it is expected that *Ae. albopictus* mosquitoes will colonize new areas of the EU, thus creating new areas at risk for local transmission (*30*,*31*). Furthermore, the *Ae. aegypti* mosquito, another competent vector, is threatening to establish itself on the continent, increasing even more the risk for local transmission (*32*).

Surveillance systems in EU countries are diverse and have evolved over time (e.g., chikungunya became a mandatory reportable disease in Spain during 2014). Detailed information about national surveillance systems is available in the ECDC annual epidemiologic reports (*33*). Large outbreaks worldwide increased awareness among physicians, potentially enhancing testing of potential cases. Consequently,

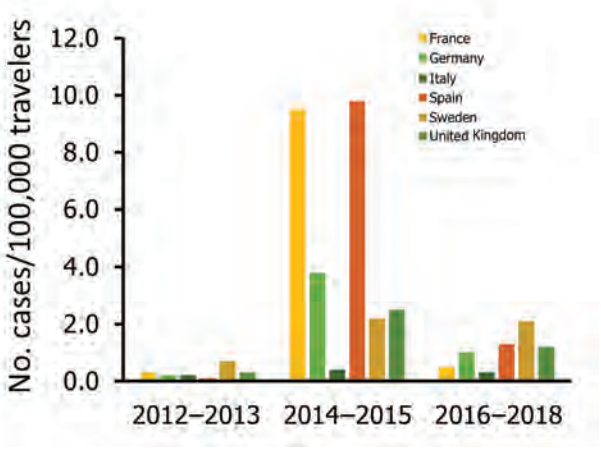

Figure 5. Rates of chikungunya infections among European Union travelers returning from countries of infection, by reporting country and epidemiologic periods, 2012–2018. Only countries reporting the highest number of cases were included.

Table 2. Estimated number of travel-related cases of chikungunya that could have led to secondary transmissions on the basis of cases reported during June–October and proportion of population in countries in which *Aedes albopictus* mosquitoes are established, per year and reporting country, 2012–2018

Characteristic, year	France	Germany	Greece	Italy	Malta	Slovenia	Spain	Total
No. travel-related case during June–October								
2012	7	3	0	2	0	0	0	12
2013	6	0	0	3	0	0	1	10
2014	540	85	1	0	0	0	180	806
2015	35	29	0	9	0	0	87	160
2016	16	28	1	9	0	1	31	86
2017	10	11	0	3	0	0	14	38
2018	5	7	1	2	0	0	2	17
% Population in regions in which *Ae. albopictus* mosquitoes are established								
2012	21	0	6	83	92	11	20	28
2013	23	0	17	84	93	11	20	29
2014	25	0	25	86	93	14	20	31
2015	34	0	27	81	93	31	30	34
2016	36	0	76	99	93	57	33	41
2017	43	0	49	100	93	57	42	43
2018	55	1	83	100	93	57	42	45
Estimated no. cases in regions in which *Ae. albopictus* are established								
2012	1	0	0	2	0	0	0	3
2013	1	0	0	3	0	0	0	4
2014	135*	0	0	0	0	0	36	171
2015	12	0	0	7	0	0	26	45
2016	6	0	1	9	0	1	10	26
2017	4*	0	0	3*	0	0	6	13
2018	3	0	1	2	0	0	1	6
Total no. cases in regions in which *Ae. albopictus* are established								
2012–2018	163	0	2	25	0	1	79	270

*When an outbreak occurred.

comparisons between years and between reporting countries should be made cautiously.

Vector presence and activity in countries of infection vary at the local level, whereas we analyzed country level data. We did not have information about the reason for travel (e.g., tourism, business, VFR) and length of stay, 2 variables that are likely to influence the risk for infection (*34*,*35*). This limitation prevented us from identifying recommendations at the subnational level and targeted to the travelers categories.

The reported travel-related cases only represent a fraction of the actual infections because ≤25% of infected persons remain asymptomatic (*36*). In parallel, 34% of cases were probable cases, diagnosed with 1 IgM test, a highly unspecific test that leads to a high number of false-positive results and, in some instances, indicates a previous infection (*15*,*16*,*37*,*38*). These biases were likely to be constant over time and place and therefore did not affect interpretation of our results.

We considered that all reported case-patients had viremia while in the EU and therefore could have contributed to secondary transmission. However, a study published in 2007 estimated that 63% of infected travelers were viremic upon return to their home country (*39*), which would suggest that we overestimated the number of potential index cases.

Several studies that assessed risk for travelers related to chikungunya and dengue used travelers data from the United Nation World Tourism Organization (*22*,*40*) or national databases *41*,*42*). As highlighted in another report (*43*), there are major differences in the number of travelers between databases. The International Air Transport Association collects the number of flight passengers from 1 departure airport to an arrival airport, whereas other databases also include multicountry journeys and other types of travel mode, such as cruise ships; in addition, some databases might count travelers on the basis of their nationality instead of place of departure. We compared our results with those of 1 study that assessed the risk for chikungunya infection among travelers from Spain during 2008–2014 (*22*). Although results from the 2 studies are not in disagreement, they are not directly comparable. We believe that main difference in methods was that we used travelers data adjusted per year (except for 2018) and that the authors of the other study used mean annual number of travelers from previous years. If one considers major variations in number of travelers per year (e.g., Venezuela), we recommend researchers to used yearly number of travelers to estimate TIR. This recommendation emphasizes that comparison of TIRs between studies should be made with caution.

In conclusion, monitoring the number of travel-related chikungunya cases and the TIR among travelers can support travel advice. However, our results showed no indication that these factors can be useful in estimating the risk for autochthonous outbreaks in EU countries.

Acknowledgments

We thank the members of the emerging and vector-borne disease network of the ECDC for their support of surveillance for chikungunya in the EU by providing chikungunya data and Henriette de Valk for reviewing and providing pertinent comments that helped improve the manuscript.

About the Author

Dr. Gossner is a veterinarian and principal expert in emerging and vector-borne diseases at the European Centre for Disease Prevention and Control, Solna, Sweden. Her primary research interests are emerging and vector-borne diseases.

References

1. Centers for Disease Control and Prevention. Where has chikungunya virus been found. 2018 May 29 [cited 2018 Dec 4]. https://www.cdc.gov/chikungunya/geo/index.html
2. Rezza G, Nicoletti L, Angelini R, Romi R, Finarelli AC, Panning M, et al.; CHIKV study group. Infection with chikungunya virus in Italy: an outbreak in a temperate region. Lancet. 2007;370:1840–6. https://doi.org/10.1016/S0140-6736(07)61779-6
3. Delisle E, Rousseau C, Broche B, Leparc-Goffart I, L'Ambert G, Cochet A, et al. Chikungunya outbreak in Montpellier, France, September to October 2014. Euro Surveill. 2015;20:21108. https://doi.org/10.2807/1560-7917.ES2015.20.17.21108
4. Calba C, Guerbois-Galla M, Franke F, Jeannin C, Auzet-Caillaud M, Grard G, et al. Preliminary report of an autochthonous chikungunya outbreak in France, July to September 2017. Euro Surveill. 2017;22. https://doi.org/10.2807/1560-7917.ES.2017.22.39.17-00647
5. Vairo F, Mammone A, Lanini S, Nicastri E, Castilletti C, Carletti F, et al.; Chikungunya Lazio Outbreak Group. Local transmission of chikungunya in Rome and the Lazio region, Italy. PLoS One. 2018;13:e0208896. https://doi.org/10.1371/journal.pone.0208896
6. Venturi G, Di Luca M, Fortuna C, Remoli ME, Riccardo F, Severini F, et al. Detection of a chikungunya outbreak in Central Italy, August to September 2017. Euro Surveill. 2017;22. https://doi.org/10.2807/1560-7917.ES.2017.22.39.17-00646
7. European Centre for Disease Prevention and Control. ECDC strategic multi-annual programme 2014–2020, 2014 [cited 2020 Mar 1]. https://ecdc.europa.eu/sites/portal/files/media/en/aboutus/Key%20Documents/Strategic-multiannual-programme-2014-2020.pdf
8. European Centre for Disease Prevention and Control. The European Surveillance System (TESSy) [cited 2018 Mar 7]. https://ecdc.europa.eu/en/publications-data/european-surveillance-system-tessy
9. European Commission. Commission implementing decision 2018/945 of 22 June 2018 on the communicable diseases and related special health issues to be covered by epidemiological surveillance as well as relevant case definitions. Luxembourg: Office of the European Union; 6.7.2018:L170/1 [cited 2020 Mar 3]. https://eur-lex.europa.eu/legal-content/EN/TXT/PDF/?uri=CELEX:32018D0945&from=EN#page=13
10. European Commission. Eurostat. Nomenclature of territorial units for statistics [cited 2019 Feb 5]. http://ec.europa.eu/eurostat/web/nuts/overview
11. European Centre for Disease Prevention and Control (ECDC), European Food Safety Authority (EFSA). VectorNet: a European network for sharing data on the geographic distribution of arthropod vectors, transmitting human and animal disease agents. Mosquito maps [cited 2018 Dec4]. https://ecdc.europa.eu/en/disease-vectors/surveillance-and-disease-data/mosquito-maps
12. Ministry of Solidarity and Health. Presence maps of the tiger mosquito (*Aedes albopictus*) in mainland France, Nov 28, 2018 [in French] [cited 2019 Feb 7]. https://solidarites-sante.gouv.fr/sante-et-environnement/risques-microbiologiques-physiques-et-chimiques/especes-nuisibles-et-parasites/article/cartes-de-presence-du-moustique-tigre-aedes-albopictus-en-france-metropolitaine
13. Eurostat, the statistical office of the European Union. Population on 1 January by age group, sex and NUTS 3 region [cited 2019 Mar 9]. https://ec.europa.eu/eurostat/web/products-datasets/product?code=demo_r_pjangrp3
14. United Nations Statistics Division. Standard country or area codes for statistical use [cited 2017 Dec 15]. https://unstats.un.org/unsd/methodology/m49
15. Calba C, Franke F, Brottet E, Terpant G, Fournet N, Ovize A, et al. Specificity of chikungunya serology and epidemiological surveillance. Presented at: 39th Interdisciplinary Meeting of Anti-Infectious Chemotherapy; 2019 Dec 16–17; Paris, France [cited 2020 Mar 1]. https://sdblb.org/wp-content/uploads/2019/09/RICAI_Programme.pdf
16. Prat CM, Flusin O, Panella A, Tenebray B, Lanciotti R, Leparc-Goffart I. Evaluation of commercially available serologic diagnostic tests for chikungunya virus. Emerg Infect Dis. 2014;20:2129–32. https://doi.org/10.3201/eid2012.141269
17. Staples JE, Fischer M. Chikungunya virus in the Americas: what a vectorborne pathogen can do. N Engl J Med. 2014;371:887–9. https://doi.org/10.1056/NEJMp1407698
18. World Health Organization, Regional Office of Western Pacific. Pacific syndromic surveillance report, Week 4 ending 25 Jan 2015 [cited 2019 Jan 30]. http://www.wpro.who.int/southpacific/programmes/communicable_diseases/disease_surveillance_response/PSS-25-January-2014/en
19. World Health Organization. Disease outbreak news: chikungunya—Mombasa, Kenya, Feb 27, 2018 [cited 2018 Dec 6]. https://www.who.int/csr/don/27-february-2018-chikungunya-kenya/en
20. Lindh E, Argentini C, Remoli ME, Fortuna C, Faggioni G, Benedetti E, et al. The Italian 2017 outbreak chikungunya virus belongs to an emerging *Aedes albopictus* – –adapted virus cluster introduced from the Indian subcontinent. Open Forum Infect Dis. 2018;6:ofy321.
21. Warne B, Weld LH, Cramer JP, Field VK, Grobusch MP, Caumes E, et al.; EuroTravNet Network. Travel-related infection in European travelers, EuroTravNet 2011. J Travel Med. 2014;21:248–54. https://doi.org/10.1111/jtm.12120
22. Fernandez-Garcia MD, Bangert M, de Ory F, Potente A, Hernandez L, Lasala F, et al. Chikungunya virus infections among travellers returning to Spain, 2008 to 2014. Euro

Surveill. 2016;21:30336. https://doi.org/10.2807/1560-7917.ES.2016.21.36.30336
23. Nakayama E, Tajima S, Kotaki A, Shibasaki KI, Itokawa K, Kato K, et al. A summary of the imported cases of chikungunya fever in Japan from 2006 to June 2016. J Travel Med. 2018;25. https://doi.org/10.1093/jtm/tax072
24. Delgado-Enciso I, Paz-Michel B, Melnikov V, Guzman-Esquivel J, Espinoza-Gomez F, Soriano-Hernandez AD, et al. Smoking and female sex as key risk factors associated with severe arthralgia in acute and chronic phases of chikungunya virus infection. Exp Ther Med. 2018;15:2634–42.
25. National Center for Epidemiology, CIBER Epidemiology and Public Health (CIBERESP), Carlos III Health Institute. Results for epidemiological surveillance on communicable diseases. Annual report 2016, 2018 [in Spanish] [cited 2020 Mar 1]. www.isciii.es/ISCIII/es/contenidos/fd-servicios-cientifico-tecnicos/fd-vigilancias-alertas/fd-enfermedades/RENAVE_INFORME_ANUAL_2016
26. National Institute of Statistics. Foreign population per country of birth, age (five-year grouping) and gender, Jan 1, 2018 [in Spanish] [cited 2020 Mar 1]. https://www.ine.es/dynt3/inebase/es/index.htm?type=pcaxis&path=/t20/e245/p08/&file=pcaxis&dh=0&capsel=0
27. Manica M, Guzzetta G, Poletti P, Filipponi F, Solimini A, Caputo B, et al. Transmission dynamics of the ongoing chikungunya outbreak in central Italy: from coastal areas to the metropolitan city of Rome, summer 2017. Euro Surveill. 2017;22. https://doi.org/10.2807/1560-7917.ES.2017.22.44.17-00685
28. Tjaden NB, Suk JE, Fischer D, Thomas SM, Beierkuhnlein C, Semenza JC. Modelling the effects of global climate change on chikungunya transmission in the 21st century. Sci Rep. 2017;7:3813. https://doi.org/10.1038/s41598-017-03566-3
29. Solimini AG, Manica M, Rosà R, Della Torre A, Caputo B. Estimating the risk of dengue, chikungunya and Zika outbreaks in a large European city. Sci Rep. 2018;8:16435. https://doi.org/10.1038/s41598-018-34664-5
30. Gossner CM, Ducheyne E, Schaffner F. Increased risk for autochthonous vector-borne infections transmitted by *Aedes albopictus* in continental Europe. Euro Surveill. 2018;23. https://doi.org/10.2807/1560-7917.ES.2018.23.24.1800268
31. Cunze S, Kochmann J, Koch LK, Klimpel S. *Aedes albopictus* and its environmental limits in Europe. PLoS One. 2016;11:e0162116. https://doi.org/10.1371/journal.pone.0162116
32. Kraemer MU, Sinka ME, Duda KA, Mylne AQ, Shearer FM, Barker CM, et al. The global distribution of the arbovirus vectors *Aedes aegypti* and *Ae. albopictus*. eLife. 2015;4:e08347. https://doi.org/10.7554/eLife.08347
33. European Centre for Disease Prevention and Control. Annual epidemiological reports (AERs) [cited 2019 Dev 17]. https://www.ecdc.europa.eu/en/annual-epidemiological-reports
34. Massad E, Rocklov J, Wilder-Smith A. Dengue infections in non-immune travellers to Thailand. Epidemiol Infect. 2013;141:412–7. https://doi.org/10.1017/S0950268812000507
35. Schwartz E, Weld LH, Wilder-Smith A, von Sonnenburg F, Keystone JS, Kain KC, et al.; GeoSentinel Surveillance Network. Seasonality, annual trends, and characteristics of dengue among ill returned travelers, 1997–2006. Emerg Infect Dis. 2008;14:1081–8. https://doi.org/10.3201/eid1407.071412
36. Centers for Disease Control and Prevention. Infectious diseases related to travel: chikungunya. In: CDC Yellow Book, 2018: Health Information for International Travel. New York: Oxford University Press; 2017.
37. Borgherini G, Poubeau P, Jossaume A, Gouix A, Cotte L, Michault A, et al. Persistent arthralgia associated with chikungunya virus: a study of 88 adult patients on reunion island. Clin Infect Dis. 2008;47:469–75. https://doi.org/10.1086/590003
38. Grivard P, Le Roux K, Laurent P, Fianu A, Perrau J, Gigan J, et al. Molecular and serological diagnosis of chikungunya virus infection. Pathol Biol (Paris). 2007;55:490–4. https://doi.org/10.1016/j.patbio.2007.07.002
39. Lambert J, Couturier E, Vaillant V. Chikungunya infection, descriptive study of cases imported into mainland France, 2005–2006; 2007. Saint Maurice: InVS [in French] [cited 2020 Mar 1]. https://www.vie-publique.fr/sites/default/files/rapport/pdf/074000355.pdf
40. Rocklöv J, Lohr W, Hjertqvist M, Wilder-Smith A. Attack rates of dengue fever in Swedish travellers. Scand J Infect Dis. 2014;46:412–7. https://doi.org/10.3109/00365548.2014.887222
41. Fukusumi M, Arashiro T, Arima Y, Matsui T, Shimada T, Kinoshita H, et al. Dengue sentinel traveler surveillance: monthly and yearly notification trends among Japanese travelers, 2006–2014. PLoS Negl Trop Dis. 2016;10:e0004924. https://doi.org/10.1371/journal.pntd.0004924
42. Lau CL, Weinstein P, Slaney D. Dengue surveillance by proxy: travellers as sentinels for outbreaks in the Pacific Islands. Epidemiol Infect. 2013;141:2328–34. https://doi.org/10.1017/S0950268813000058
43. Behrens RH, Carroll B. The challenges of disease risk ascertainment using accessible data sources for numbers of travelers. J Travel Med. 2013;20:296–302. https://doi.org/10.1111/jtm.12062

Address for correspondence: Céline M. Gossner, European Centre for Disease Prevention and Control, Gustav III:s Blvd 40, 168 73 Solna, Sweden; email: celine.gossner@ecdc.europa.eu

Manifestations of Toxic Shock Syndrome in Children, Columbus, Ohio, USA, 2010–2017[1]

Aliza Cook,[2] Sarah Janse, Joshua R. Watson, Guliz Erdem

Medscape EDUCATION ACTIVITY

In support of improving patient care, this activity has been planned and implemented by Medscape, LLC and Emerging Infectious Diseases. Medscape, LLC is jointly accredited by the Accreditation Council for Continuing Medical Education (ACCME), the Accreditation Council for Pharmacy Education (ACPE), and the American Nurses Credentialing Center (ANCC), to provide continuing education for the healthcare team.

Medscape, LLC designates this Journal-based CME activity for a maximum of 1.00 ***AMA PRA Category 1 Credit(s)™***. Physicians should claim only the credit commensurate with the extent of their participation in the activity.

Successful completion of this CME activity, which includes participation in the evaluation component, enables the participant to earn up to 1.0 MOC points in the American Board of Internal Medicine's (ABIM) Maintenance of Certification (MOC) program. Participants will earn MOC points equivalent to the amount of CME credits claimed for the activity. It is the CME activity provider's responsibility to submit participant completion information to ACCME for the purpose of granting ABIM MOC credit.

All other clinicians completing this activity will be issued a certificate of participation. To participate in this journal CME activity: (1) review the learning objectives and author disclosures; (2) study the education content; (3) take the post-test with a 75% minimum passing score and complete the evaluation at http://www.medscape.org/journal/eid; and (4) view/print certificate. For CME questions, see page 1352.

Release date: May 14, 2020; Expiration date: May 14, 2021

Learning Objectives

Upon completion of this activity, participants will be able to:

- Evaluate the clinical characteristics of pediatric toxic shock syndrome (TSS) in a large tertiary care center, based on a retrospective chart review
- Determine diagnostic decisions regarding pediatric TSS in a large tertiary care center, and their implications for published criteria, based on a retrospective chart review
- Assess the treatment and management of pediatric TSS, based on a retrospective chart review from a large tertiary care center

CME Editor

Karen L. Foster, Technical Writer/Editor, Emerging Infectious Diseases. *Disclosure: Karen L. Foster has disclosed no relevant financial relationships.*

CME Author

Laurie Barclay, MD, freelance writer and reviewer, Medscape, LLC. *Disclosure: Laurie Barclay, MD, has disclosed no relevant financial relationships.*

Authors

Disclosures: ***Aliza Cook, MD; Sarah Janse, PhD; Joshua R. Watson, MD;*** *and* ***Guliz Erdem, MD,*** *have disclosed no relevant financial relationships.*

Author affiliations: The Ohio State University, Columbus, Ohio, USA (A. Cook, S. Janse, J.R. Watson, G. Erdem); Nationwide Children's Hospital, Columbus (S. Janse, J.R. Watson, G. Erdem)

DOI: https://doi.org/10.3201/eid2606.190783

[1]Preliminary results from this study were presented at the Pediatric Academic Societies Meeting, May 6–9, 2017, San Diego, California, USA; and at IDWeek 2018, October 3–7, 2018, San Francisco, California, USA.

[2]Current affiliation: Yale New Haven Hospital, New Haven, Connecticut, USA.

Data are limited on the incidence and management of streptococcal toxic shock syndrome (TSS) and nonstreptococcal TSS in children. We aimed to define the clinical patterns of TSS at Nationwide Children's Hospital in Ohio as they relate to published criteria, diagnostic decisions, and treatment options. Through retrospective chart reviews, we identified 58 patients with TSS (27 streptococcal, 31 nonstreptococcal) during January 2010–September 2017. We observed clinical and laboratory findings that are not part of TSS criteria, such as pyuria in streptococcal TSS (50% of patients) and pulmonary involvement (85%) and coagulopathy (92%) in nonstreptococcal TSS patients. Recommended treatment with clindamycin and intravenous immunoglobulin was delayed in streptococcal TSS patients without rash (3.37 days vs. 0.87 days in patients with rash), leading to prolonged hospitalization and complications. Incorporation of additional TSS signs and symptoms would be helpful in TSS diagnosis and management.

Toxic shock syndrome (TSS) is a severe acute illness caused by toxin-producing strains of *Streptococcus pyogenes* (streptococcal TSS [STSS]) and *Staphylococcus aureus* (nonstreptococcal TSS [NSTSS]) (*1*–*5*). Data are limited on the incidence, management, and outcomes for children with TSS (*6*–*8*). Most epidemiologic and clinical studies of TSS have reported predominantly streptococcal cases. The incidence of severe streptococcal infections, including TSS, has been increasing in North America since the 1990s. Studies from the United States and Canada report incidence rates of 3.8–10.24 invasive group A *Streptococcus* (GAS) cases per 100,000 persons per year (*9*,*10*). Reported death rates vary from 4.2% to 56% for STSS (*2*,*3*,*7*,*8*,*11*–*15*) and are up to 22% for NSTSS (*3*,*12*).

The uncontrolled cytokine stimulation by bacterial toxins results in several clinical manifestations of TSS, such as hypotension, fever, rash, and organ dysfunction (*3*,*8*). On the basis of these clinical signs, the Centers for Disease Control and Prevention (CDC) defined criteria for TSS and updated these criteria in 2010 for STSS and in 2011 for NSTSS (*4*,*5*). Despite recognition of illness and CDC disease definitions, TSS diagnosis remains challenging because some clinical findings, such as hypotension, could be transient and some, such as rash, might be absent.

CDC criteria do not differentiate between children and adults. In children, differentiating TSS from septic shock, Kawasaki disease with shock, and drug reaction with eosinophilia and systemic symptoms syndrome poses additional challenges (*3*,*16*). In addition to these diagnostic difficulties, challenges and controversies exist for managing TSS. Our objective was to differentiate the clinical patterns of TSS in children in a large tertiary center as they relate to published criteria, diagnostic decisions, and treatment options.

Methods

The Nationwide Children's Hospital Institutional Review Board approved the study. We queried electronic medical records during January 2010–December 2017 for diagnosis codes from the International Classification of Diseases, 10th Revision, for toxic shock syndrome, severe sepsis with septic shock, GAS bacteremia, and necrotizing fasciitis. The addition of diagnoses other than TSS helped us identify 7 STSS patients who were discharged with diagnoses of sepsis and septic shock. In addition to discharge and admission diagnoses, we considered any diagnosis during the hospitalization period associated with these billing codes. We also reviewed preadmission records related to the admission diagnoses. We included patients in the study if their illness met criteria for definite or probable TSS. Where all CDC criteria for either STSS or NSTSS were fulfilled, we defined cases as definite (*4*,*5*). Where a single criterion was missing because of incomplete data or because GAS was isolated from a nonsterile site, we classified the case as probable (*4*). Data collected were age, sex, height, weight, body mass index, date of presentation, and clinical signs and symptoms (Table 1). We also collected duration of hospitalization; use and type of antimicrobial agents; use and timing of clindamycin, intravenous immunoglobulin (IVIg), or both after initial evaluation; and clinical outcomes, including mechanical intubation, amputation, and death. We reviewed several admission laboratory and radiologic parameters: complete blood count, urinalysis, blood urea nitrogen, creatinine, estimated glomerular filtration rate, alanine transaminase, aspartate transaminase, total bilirubin, creatinine kinase, coagulation studies, and chest radiographs. We also reviewed additional studies and any imaging study done during the hospitalization period that identified possible sites and sources of infection.

Statistical Analysis

We compared the demographic, clinical, laboratory, and treatment data between patients with STSS and NSTSS. We used Student *t* tests to compare normally distributed continuous variables between STSS and NSTSS groups, the Wilcoxon rank-sum test to analyze skewed continuous variables, and a Fisher exact test to analyze categorical variables. Continuous variables are presented as means with SDs for normally

Table 1. Characteristics of patients with STSS and NSTSS, Nationwide Children's Hospital, Columbus, Ohio, USA, 2010–2017*

Characteristic†	STSS, n = 27	NSTSS, n = 31	Total, N = 58	p value
Demographic				
Sex, no. (%)				
F	15 (55.6)	21 (67.7)	36 (62.1)	0.42
M	12 (44.4)	10 (32.3)		
Mean age, y (SD)	9.4 (5.9)	13.2 (4.1)	11.4 (5.3)	<0.05
Mean BMI (SD)	18.9 (4.9)	22.7 (7.9)	20.9 (6.9)	<0.05
Clinical findings				
Vomiting	18 (66.7)	26 (83.9)	44 (75.9)	0.22
Diarrhea	9 (33.3)	14 (45.2)	23 (39.7)	0.43
Myalgia	9 (37.5)	12 (44.4)	21 (41.2)	0.78
Fever at presentation, mean (SD)	39.5 (0.8)	39.6 (0.6)	39.5 (0.7)	0.65
Generalized erythematous rash	14 (51.9)	30 (96.8)	44 (75.9)	<0.05
Desquamation	6 (22.2)	14 (45.2)	20 (34.5)	0.1
Altered mental status	10 (41.7)	11 (36.7)	21 (38.9)	0.83
Fasciitis/tissue necrosis	5 (20.0)	1 (3.3)	6 (10.9)	0.08
Pharyngeal hyperemia	6 (22.2)	23 (74.2)	29 (50.0)	<0.05
Pulmonary Infiltrates	22 (88.0)	19 (61.3)	41 (73.2)	<0.05
PPV and inotropic support	25 (92.6)	29 (93.5)	54 (93.1)	1.0
Capillary leak‡	21 (84.0)	18 (58.1)	39 (69.6)	<0.05
Admission laboratory findings§				
Thrombocyte count, $\times 10^3/\mu L$, mean (SD)	120.1 (81.6)	119.2 (76.9)	119.6 (78.4)	0.97
Abnormal coagulation tests, PT, PTT, INR, s, n = 49	24 (100)	23 (92.0)	47 (95.9)	0.49
Pyuria, n = 24	12 (50.0)	12 (50.0)	24 (50.0)	1.00
BUN, mg/dL, median (IQR), n = 57	14 (8–26)	13 (11–41)	14 (11–27)	0.73
Creatinine, g/day median (IQR)	0.8 (0.5–1.2)	0.9 (0.7–2.0)	0.8 (0.5–1.6)	0.12
eGFR, mL/min/m², mean (SD)	72.8 (34.2)	71.9 (39.8)	72.3 (37.0)	0.93
ALT, U/L, median (IQR)	49 (28–129)	40 (29–95)	47 (29–95)	0.55
AST, U/L, median (IQR)	52 (28–132)	52 (25–84)	52 (28–102)	0.62
Total bilirubin, md/dL, median (IQR), n = 57	0.9 (0.5–1.6)	0.9 (0.4–1.8)	0.9 (0.4–1.6)	0.79
CPK, U/L, median (IQR), n = 17	154 (73–674)	130 (67–304)	137 (69–304)	0.67
Treatment				
IVIg and clindamycin	14 (51.9%)	14 (45.2)	28 (48.3)	<0.05
Clindamycin only	8 (29.6%)	16 (51.6)	24 (41.4)	
IVIg only	0 (0.0%)	1 (3.2)	1 (1.7)	
Neither IVIg nor clindamycin	5 (18.5%)	0	5 (8.6)	

*ALT, alanine aminotransferase; AST, aspartate aminotransferase; BMI, body mass index; BUN, blood urea nitrogen; CPK, creatinine phosphokinase; eGFR, estimated glomerular filtration rate; INR, international normalized ratio; IQR, interquartile range; IVIg, intravenous immunoglobulin; NSTSS, nonstreptococcal TSS; PPV, positive pressure ventilation; PT, prothrombin time; PTT, partial thromboplastin time; STSS, streptococcal TSS; TSS, toxic shock syndrome.
†Continuous variables are presented as means with SDs; categorical variables are presented as counts with percentages. If data were not available for all patients, the number of patients is indicated.
‡Capillary leak indicates hypotension, hypoalbuminemia, and hemoconcentration.
§Reference values: thrombocyte count, 140–440 $\times 10^3/\mu L$; PT, 12.4–14.7 s; PTT, 24–36 s; INR, ≤1.1; BUN, 5–18 mg/dL; creatinine, varies by patient age and sex; eGFR, >60 mL/min/1.73 m²; ALT, <40 U/L); AST, 15–50 U/L); bilirubin, 0.1–1.0 mg/dL; CPK, 37–430 U/L.

distributed variables and as median and interquartile range for skewed variables; categorical variables are presented as counts with percentages.

We conducted all analyses on log-transformed values of the time from admission outcomes to satisfy model assumptions. We used Student *t* tests to compare STSS with NSTSS and a linear mixed model to compare groups of antimicrobial drugs. For ease of interpretation, raw means and SDs are presented for each group, and the mean difference of the log-transformed values are presented as the ratio of geometric means with 95% CI.

Results

During the study period, 456 patients had diagnosis codes of TSS, severe sepsis with septic shock, GAS bacteremia, and necrotizing fasciitis at admission, discharge, or both. Our review of electronic medical records indicated that illnesses of 58 patients met the CDC diagnostic criteria for TSS. None of the patients had a prolonged preadmission course that would affect their treatment start time. Twenty-seven (47%) patients had STSS and 31 (53%) had NSTSS. Of the STSS patients, 16 had confirmed and 11 had probable STSS. Of the NSTSS patients, 11 had confirmed and 20 had probable NSTSS.

Clinical and Laboratory Findings

Fever was not always documented during initial examinations, although most patients had history of fever requiring antipyretic medication or had fever develop during hospitalization (Table 1). Vomiting and rash were present in most patients with TSS. However, of the 27 patients with STSS, 13 (48%) had

no rash. Altered mental status was observed in ≈40% of patients.

Of patients with confirmed STSS, GAS was isolated from blood (3 patients), deep tissue (4 patients from necrotic tongue, subdural empyema, orbital abscess, and sinus aspirations), pleural fluid and deep endotracheal tube suction (4 patients), peritoneal fluid (1 patient), endotracheal tube suction and blood (3 patients), and urine and blood (1 patient). Patients with probable STSS had GAS obtained from rapid streptococcal screening test and throat cultures. Patients with NSTSS had staphylococci isolated from skin lesions and abscesses (10 patients); sterile sites, including bone (3 patients); urine (1 patient); and vaginal and genital area swab samples (7 patients).

Several patients with NSTSS, for which only thrombocytopenia is listed in the hematologic category of the CDC definition, had other coagulation abnormalities. Of 25 patients who had coagulation tests on admission, 17 (68%) had increased prothrombin time, 7 (28%) had increased prothrombin and partial thromboplastin time, and 1 patient had prolonged partial thromboplastin time.

Inflammatory markers were not tested in all patients at admission. For the 20 patients for whom erythrocyte sedimentation rate (ESR) was tested on admission, median ESR was 22 mm/h (IQR 15.0–36.0 mm/h; reference 0–13 mm/h). ESR levels were higher in patients with STSS. Of 15 patients with NSTSS, median ESR was 22 mm/h (IQR 15.0–32.5 mm/h); of 5 patients with STSS, median ESR was 36 mm/h (IQR 14.5–39 mm/h). Of 34 patients for whom C-reactive protein (CRP) was tested on admission, median CRP was 12.75 mg/dL (IQR 6.8–23.8 mg/dL; reference <1.2 mg/dL). Of 18 patients with NSTSS, median CRP was 8.3 mg/dL (IQR 5.8–20.6 mg/dL), and of 16 patients with STSS, median CRP was 20.4 mg/dL (IQR 6.9–26.3mg/dL). CRP levels were significantly higher for patients with STSS than for those with NSTSS ($p = 0.0443$).

Pulmonary infiltrates were present in most (42 patients) patients with TSS at diagnosis and admission. Only 7 (12%) patients had primary admission and discharge diagnoses for pneumonia. Median arterial oxygen partial pressure to fractional inspired oxygen (PaO2:FiO2) ratio was also decreased in these patients. Of the 31 patients with NSTSS, for which pulmonary involvement is not a CDC diagnostic criterion, 19 (61%) had diffuse pulmonary infiltrates.

Of the clinical criteria listed for TSS and NSTSS and evaluated on admission, creatine phosphokinase was not elevated in the 17 patients for whom results were available. Similarly, renal and hepatic involvement criteria for both STSS and NSTSS did not vary significantly from age-based normal values for most of the patients. Twelve (21%) patients had elevated alanine transaminase, 14 (24%) had elevated aspartate transaminase, and 17 (29%) had elevated serum creatinine. However, pyuria (≥10 leukocytes/high-power field), which is not a CDC clinical criterion for STSS, was present in half the patients with STSS who had a urinalysis on admission (median urine leukocyte count 17.5/high-power field). We also reviewed microbiological studies. For 21 (68%) patients with NSTSS, *Staphylococcus aureus* grew from superficial and sterile site cultures.

We found significant differences between patients with STSS and NSTSS. Patients with STSS were significantly younger, had lower body mass index, were less likely to have an erythematous rash, and had more capillary leak and pulmonary infiltrates at presentation. Patients with NSTSS were less likely to have pulmonary infiltrates and capillary leak and to have less tissue necrosis or mental status changes (Table 1).

Management of Patients

Patients with NSTSS received clindamycin and IVIg sooner than patients with STSS. Five patients who did not receive clindamycin or IVIg had STSS. Patients with NSTSS stayed ≈57% fewer inpatient days (Tables 1, 2; Appendix, https://wwwnc.cdc.gov/EID/article/26/6/19-0783-App1.pdf). One patient had necrotizing infection of the tongue that was promptly recognized and operatively debrided. One patient with STSS died. We examined the differences between patients receiving only clindamycin, only IVIg, both, or neither. None of the outcomes differed significantly among groups (Appendix).

Management of STSS patients with rash differed from management of those without rash. We found no difference in the requirement for vasopressor support between patients with or without rash, yet clindamycin was initiated ≈66% sooner for patients

Table 2. Time from hospital admission for patients who had streptococcal toxic shock syndrome with and without rash and treatments received, Nationwide Children's Hospital, Columbus, Ohio, USA, 2010–2017

Time from admission, d	Rash, mean (± SD)	No rash, mean (± SD)	Ratio of geometric means (95% CI)	p value
Start of antimicrobial drugs	0.45 (0.49)	1.08 (1.57)	0.47 (0.16–1.40)	0.17
Start of clindamycin	0.87 (0.61)	3.37 (2.36)	0.24 (0.10–0.59)	<0.05
Start of intravenous immunoglobulin	1.47 (0.60)	1.48 (0.49)	0.97 (0.58–1.60)	0.89

with rash than for patients without rash (Table 2). Patients with STSS and without a rash had longer hospital stays than did those with rash. Clindamycin with or without IVIg infusion was delayed in treatment of STSS patients without rash, and for 5 patients (19% of patients without rash), neither clindamycin nor IVIg was administered.

Discussion

Data are limited on the incidence and management of children with TSS (*3*,*8*). Our large, single-institution retrospective analysis of 58 cases showed similarities and unexpected findings among children with TSS. In comparison with patients with NSTSS, children with STSS were younger, experienced more severe illness with higher rates of capillary leak and pulmonary symptoms, and had longer hospital stays. Similar to our findings, STSS has been associated with more severe disease and worse outcomes than NSTSS in the literature (*2*,*3*,*7*,*8*,*15*,*17*). Unlike our findings, those studies do not indicate whether late recognition and treatment of STSS in patients without rash played any role in the reported disease outcomes and hospitalization duration.

Case definitions for streptococcal and NSTSS are generally designed to optimize specificity rather than sensitivity. Our data suggest that unified criteria for TSS, rather than separate criteria for STSS and NSTSS, might improve sensitivity. We found that certain clinical and laboratory findings were common in both STSS and NSTSS but only included in the case definition of one or the other. First, although pyuria is a criterion for NSTSS but not for STSS (*4*,*5*), half the urinalyses performed in both groups demonstrated pyuria. Second, acute respiratory distress syndrome is a criterion for STSS but not for NSTSS. However, 61% of the patients in our study with NSTSS had diffuse pulmonary infiltrates and decreased PaO2:FiO2 ratio <200. Finally, coagulation abnormalities are included in the case definition of STSS but not NSTSS, yet most patients in both groups had abnormalities. The pulmonary involvement, pyuria, and coagulation abnormalities were common and were observed at admission. Case definitions are generally designed to have high specificity, sometimes at the expense of sensitivity. If the relatively inexpensive evaluation methods, such as urinalysis, chest radiograph, PaO2:FiO2 ratio of <200 and coagulation panels were incorporated into TSS evaluations, our data suggest that they might have aided accurate and timely diagnosis. Consideration of these additional organ dysfunctions, and considering TSS as a unifying diagnosis rather than as STSS and NSTSS, could potentially strengthen the conclusive diagnosis rather than discrediting it.

Data from published literature illustrate the importance of prompt recognition of TSS and early treatment (*7*,*18*–*24*). Complementary treatment with clindamycin improves the survival of patients with STSS by reducing toxin release (*7*,*18*–*24*). Although IVIg is suggested as a possible adjunctive agent, published patient outcomes have varied (*24*–*28*). IVIg functions by inhibiting T-cell activation that would result in decreased cytokine release, downregulation of adhesion molecules, chemokine and chemokine-receptor expression, and neutralization of superantigens (*25*–*28*). In some studies, IVIg did not show significant benefit in treatment of patients with STSS (*20*,*24*,*29*). One report that pooled 5 studies of clindamycin and IVIg treatment for STSS showed the death rates decreased from 33.7% to 15.7% (*30*). We did not identify significant differences in hospitalization rates and duration of mechanical ventilation among patients treated with or without IVIg. Fewer than half the patients in our study received clindamycin and IVIg. Similarly, only 50%–67% of patients with severe GAS infection have received clindamycin (*2*,*18*,*20*,*24*). Our results suggest that the lack of appropriate treatment may be associated with absence of rash at the time of presentation. In our study, in STSS patients without rash, sepsis alone was often diagnosed, and the patients were not treated with clindamycin or IVIg. These patients also experienced delays in diagnosis and had longer hospital stays than those with a rash.

Our study had several limitations. Although Nationwide Children's Hospital serves almost all of central Ohio's children, our data were not population based and were from 1 pediatric center. We might not have identified all patients with NSTSS because we were unable to review individual charts for patients with staphylococcal bacteremia if they did not have additional diagnoses of sepsis or septic shock. Despite our efforts to capture the clinical and laboratory changes at the time of initial evaluation, the duration of illness, as well as rapidly changing signs such as rash, might not have been accurately recorded in the patient charts, which would affect the overall diagnosis and possibly lead to misclassification of patients. In addition, because of the retrospective nature of our study, none of the bacterial isolates were archived for further typing or microbiological analysis.

Our findings indicate organ system involvement in TSS beyond that predicted by existing CDC criteria. Because clinicians appear to rely on archetypal presentations of TSS (e.g., fever, hypotension, and

rash) to diagnose TSS, updated clinical and diagnostic criteria would facilitate early accurate diagnosis and treatment. Physicians should be aware of TSS presentations without rash. Furthermore, the updated criteria may benefit from a unifying definition.

About the Author

Dr. Cook is an internal medicine resident at Yale New Haven Hospital in New Haven, Connecticut. Her primary research interests include primary care innovations, hospital-to-home transitions, quality improvement, and health equity.

References

1. Stevens DL, Tanner MH, Winship J, Swarts R, Ries KM, Schlievert PM, et al. Severe group A streptococcal infections associated with a toxic shock–like syndrome and scarlet fever toxin A. N Engl J Med. 1989;321:1–7. https://doi.org/10.1056/NEJM198907063210101
2. Adalat S, Dawson T, Hackett SJ, Clark JE; in association with the British Paediatric Surveillance Unit. Toxic shock syndrome surveillance in UK children. Arch Dis Child. 2014;99:1078–82. https://doi.org/10.1136/archdischild-2013-304741
3. Javouhey E, Bolze PA, Jamen C, Lina G, Badiou C, Poyart C, et al. Similarities and differences between staphylococcal and streptococcal toxic shock syndromes in children: results from a 30-case cohort. Front Pediatr. 2018;6:360. https://doi.org/10.3389/fped.2018.00360
4. Centers for Disease Control and Prevention. Streptococcal toxic shock syndrome (STSS) (*Streptococcus pyogenes*) 2010 case definition [cited 2019 May 23]. https://wwwn.cdc.gov/nndss/conditions/streptococcal-toxic-shock-syndrome/case-definition/2010
5. Centers for Disease Control and Prevention. Toxic shock syndrome (other than streptococcal) (TSS) 2011 case definition [cited 2019 May 23]. https://wwwn.cdc.gov/nndss/conditions/toxic-shock-syndrome-other-than-streptococcal/case-definition/2011
6. O'Brien KL, Beall B, Barrett NL, Cieslak PR, Reingold A, Farley MM, et al. Epidemiology of invasive group a streptococcus disease in the United States, 1995–1999. Clin Infect Dis. 2002;35:268–76. https://doi.org/10.1086/341409
7. Chen KY, Cheung M, Burgner DP, Curtis N. Toxic shock syndrome in Australian children. Arch Dis Child. 2016;101:736–40. https://doi.org/10.1136/archdischild-2015-310121
8. Chuang YY, Huang YC, Lin TY. Toxic shock syndrome in children: epidemiology, pathogenesis, and management. Paediatr Drugs. 2005;7:11–25. https://doi.org/10.2165/00148581-200507010-00002
9. Nelson GE, Pondo T, Toews KA, Farley MM, Lindegren ML, Lynfield R, et al. Epidemiology of invasive group A streptococcal infections in the United States, 2005–2012. Clin Infect Dis. 2016;63:478–86. https://doi.org/10.1093/cid/ciw248
10. Tyrrell GJ, Fathima S, Kakulphimp J, Bell C. Increasing rates of invasive group A streptococcal disease in Alberta, Canada; 2003–2017. Open Forum Infect Dis. 2018;5:ofy177. https://doi.org/10.1093/ofid/ofy177
11. Davies HD, Matlow A, Scriver SR, Schlievert P, Lovgren M, Talbot JA, et al. Apparent lower rates of streptococcal toxic shock syndrome and lower mortality in children with invasive group A streptococcal infections compared with adults. Pediatr Infect Dis J. 1994;13:49–56. https://doi.org/10.1097/00006454-199401000-00011
12. Descloux E, Perpoint T, Ferry T, Lina G, Bes M, Vandenesch F, et al. One in five mortality in non-menstrual toxic shock syndrome versus no mortality in menstrual cases in a balanced French series of 55 cases. Eur J Clin Microbiol Infect Dis. 2008;27:37–43. https://doi.org/10.1007/s10096-007-0405-2
13. Rodríguez-Nuñez A, Dosil-Gallardo S, Jordan I; ad hoc Streptococcal Toxic Shock Syndrome collaborative group of Spanish Society of Pediatric Intensive Care. Clinical characteristics of children with group A streptococcal toxic shock syndrome admitted to pediatric intensive care units. Eur J Pediatr. 2011;170:639–44. https://doi.org/10.1007/s00431-010-1337-x
14. Shah SS, Hall M, Srivastava R, Subramony A, Levin JE. Intravenous immunoglobulin in children with streptococcal toxic shock syndrome. Clin Infect Dis. 2009;49:1369–76. https://doi.org/10.1086/606048
15. Timmis A, Parkins K, Kustos I, Riordan FA, Efstratiou A, Carrol ED. Invasive group A streptococcal infections in children presenting to a paediatric intensive care unit in the North West of England. J Infect. 2010;60:183–6. https://doi.org/10.1016/j.jinf.2009.12.001
16. Lin YJ, Cheng MC, Lo MH, Chien SJ. Early differentiation of Kawasaki disease shock syndrome and toxic shock syndrome in a pediatric intensive care unit. Pediatr Infect Dis J. 2015;347. https://doi.org/10.1097/INF.0000000000000852
17. Lithgow A, Duke T, Steer A, Smeesters PR. Severe group A streptococcal infections in a paediatric intensive care unit. J Paediatr Child Health. 2014;50:687–92. https://doi.org/10.1111/jpc.12601
18. Linnér A, Darenberg J, Sjölin J, Henriques-Normark B, Norrby-Teglund A. Clinical efficacy of polyspecific intravenous immunoglobulin therapy in patients with streptococcal toxic shock syndrome: a comparative observational study. Clin Infect Dis. 2014;59:851–7. https://doi.org/10.1093/cid/ciu449
19. Andreoni F, Zürcher C, Tarnutzer A, Schilcher K, Neff A, Keller N, et al. Clindamycin affects group A streptococcus virulence factors and improves clinical outcome. J Infect Dis. 2017;215:269–77.
20. Couture-Cossette A, Carignan A, Mercier A, Desruisseaux C, Valiquette L, Pépin J. Secular trends in incidence of invasive beta-hemolytic streptococci and efficacy of adjunctive therapy in Quebec, Canada, 1996–2016. PLoS One. 2018;13:e0206289. https://doi.org/10.1371/journal.pone.0206289
21. Stevens DL, Gibbons AE, Bergstrom R, Winn V. The Eagle effect revisited: efficacy of clindamycin, erythromycin, and penicillin in the treatment of streptococcal myositis. J Infect Dis. 1988;158:23–8. https://doi.org/10.1093/infdis/158.1.23
22. Sriskandan S, McKee A, Hall L, Cohen J. Comparative effects of clindamycin and ampicillin on superantigenic activity of *Streptococcus pyogenes*. J Antimicrob Chemother. 1997;40:275–7. https://doi.org/10.1093/jac/40.2.275
23. Zimbelman J, Palmer A, Todd J. Improved outcome of clindamycin compared with beta-lactam antibiotic treatment for invasive *Streptococcus pyogenes* infection. Pediatr Infect Dis J. 1999;18:1096–100. https://doi.org/10.1097/00006454-199912000-00014
24. Carapetis JR, Jacoby P, Carville K, Ang SJ, Curtis N, Andrews R. Effectiveness of clindamycin and intravenous immunoglobulin, and risk of disease in contacts, in invasive

group a streptococcal infections. Clin Infect Dis. 2014; 59:358–65. https://doi.org/10.1093/cid/ciu304
25. Norrby-Teglund A, Muller MP, Mcgeer A, Gan BS, Guru V, Bohnen J, et al. Successful management of severe group A streptococcal soft tissue infections using an aggressive medical regimen including intravenous polyspecific immunoglobulin together with a conservative surgical approach. Scand J Infect Dis. 2005;37:166–72. https://doi.org/10.1080/00365540410020866
26. Schlievert PM. Use of intravenous immunoglobulin in the treatment of staphylococcal and streptococcal toxic shock syndromes and related illnesses. J Allergy Clin Immunol. 2001;108(Suppl):S107–10. https://doi.org/10.1067/mai.2001.117820
27. Valiquette L, Low DE, McGeer AJ. Assessing the impact of intravenous immunoglobulin in the management of streptococcal toxic shock syndrome: a noble but difficult quest. Clin Infect Dis. 2009;49:1377–9. https://doi.org/10.1086/606049
28. Low DE. Toxic shock syndrome: major advances in pathogenesis, but not treatment. Crit Care Clin. 2013;29:651–75. https://doi.org/10.1016/j.ccc.2013.03.012
29. Kadri SS, Swihart BJ, Bonne SL, Hohmann SF, Hennessy LV, Louras P, et al. Impact of intravenous immunoglobulin on survival in necrotizing fasciitis with vasopressor-dependent shock: a propensity score-matched analysis from 130 US hospitals. Clin Infect Dis. 2017;64:877–85.
30. Parks T, Wilson C, Curtis N, Norrby-Teglund A, Sriskandan S. Polyspecific intravenous immunoglobulin in clindamycin-treated patients with streptococcal toxic shock syndrome: a systematic review and meta-analysis. Clin Infect Dis. 2018;67:1434–6. https://doi.org/10.1093/cid/ciy401

Address for correspondence: Guliz Erdem, Nationwide Children's Hospital, 700 Children's Dr, Columbus, OH 43205, USA; email: guliz.erdem@nationwidechildrens.org

Genomic Epidemiology of 2015–2016 Zika Virus Outbreak in Cape Verde

Oumar Faye,[1] Maria de Lourdes Monteiro,[1] Bram Vrancken,[1] Matthieu Prot,[1] Sebastian Lequime, Maryam Diarra, Oumar Ndiaye, Tomas Valdez, Sandra Tavarez, Jessica Ramos, Silvânia da Veiga Leal, Cecilio Pires, Antonio Moreira, Maria Filomena Tavares, Linete Fernandes, Jorge Noel Barreto, Maria do Céu Teixeira, Maria da Luz de Lima Mendonça, Carolina Cardoso da Silva Leite Gomes, Mariano Salazar Castellon, Laurence Ma, Frédéric Lemoine, Fabiana Gámbaro-Roglia, Déborah Delaune, Gamou Fall, Ibrahima Socé Fall, Mamadou Diop, Anavaj Sakuntabhai, Cheikh Loucoubar, Philippe Lemey, Edward C. Holmes, Ousmane Faye, Amadou Alpha Sall,[2] Etienne Simon-Loriere[2]

During 2015–2016, Cape Verde, an island nation off the coast of West Africa, experienced a Zika virus (ZIKV) outbreak involving 7,580 suspected Zika cases and 18 microcephaly cases. Analysis of the complete genomes of 3 ZIKV isolates from the outbreak indicated the strain was of the Asian (not African) lineage. The Cape Verde ZIKV sequences formed a distinct monophylogenetic group and possessed 1–2 (T659A, I756V) unique amino acid changes in the envelope protein. Phylogeographic and serologic evidence support earlier introduction of this lineage into Cape Verde, possibly from northeast Brazil, between June 2014 and August 2015, suggesting cryptic circulation of the virus before the initial wave of cases were detected in October 2015. These findings underscore the utility of genomic-scale epidemiology for outbreak investigations.

Author affiliations: Institut Pasteur, Dakar, Senegal (Oumar Faye, M. Diarra, O. Ndiaye, G. Fall, M. Diop, C. Loucoubar, Ousmane Faye, A.A. Sall); Ministerio da Saude, Praia, Cape Verde (M. de Lourdes Monteiro, T. Valdez, S. Tavarez, J. Ramos, S. da Veiga Leal, C. Pires, A. Moreira, M.F. Tavares, L. Fernandes, J.N. Barreto, M. do Céu Teixeira, M.L. de Lima Mendonça); Katholieke Universiteit Leuven, Leuven, Belgium (B. Vrancken, S. Lequime, P. Lemey); Institut Pasteur, Paris, France (M. Prot, L. Ma, F. Gámbaro-Roglia, D. Delaune, E. Simon-Loriere); World Health Organization, Praia (C.C. da Silva Leite Gomes, M.S. Castellon, I.S. Fall); CNRS USR 3756, Paris (F. Lemoine); Université de Paris, Sorbonne Paris Cité, Paris (F. Gámbaro-Roglia); Université Paris-Sud/Paris-Saclay, Orsay, France (D. Delaune); Institut de Recherche Biomédicale des Armées, Brétigny-sur-Orge, France (D. Delaune); CNRS UMR 2000, Paris (A. Sakuntabhai); The University of Sydney, Sydney, New South Wales, Australia (E.C. Holmes)

DOI: https://doi.org/10.3201/eid2606.190928

Zika virus (ZIKV), first discovered in Uganda in 1947 and sporadically found in Africa and Asia, was long believed to only cause mild disease in humans (*1*). ZIKV isolates are classified into 1 of 2 lineages, representing the African and Asian genotypes. ZIKVs of the African lineage have been isolated from many regions of Africa (*2*), mostly through entomologic investigations, and serologic evidence suggests that ZIKV infections in humans are frequent (*3*). However, until the 2000s, the virus had seldom been detected in humans. The Asian lineage has spread throughout the Pacific, causing outbreaks in humans in Yap, Federated States of Micronesia, in 2007 and in French Polynesia during 2013–2014, where an association with neurologic afflictions was first detected (*4*). Zika cases were first reported in Brazil in May 2015, and from there, the virus quickly spread to most of the Americas (*5*). The high number of cases led to the discovery of an association between congenital ZIKV infection and neonatal neurologic complications, particularly microcephaly (*6*,*7*).

In October 2015, an epidemic of rash, conjunctivitis, and arthralgia was noted by physicians in Praia, the capital of Cape Verde, an archipelago nation located in the Atlantic Ocean, west of the coast of Senegal. Blood samples sent to the regional reference laboratory of the Institut Pasteur de Dakar (Dakar, Senegal) confirmed the epidemic involved ZIKV infection. By the end of the outbreak in May 2016, a total of 7,580 suspected Zika cases and 18 microcephaly cases were

[1]These first authors contributed equally to this article.

[2]These senior authors contributed equally to this article.

reported in the 4 most densely populated southern islands of the Cape Verde archipelago (Brava, Fogo, Maio, and Santiago; Figure 1) (*8*). Overall, ≈50% of confirmed microcephaly cases were linked to reports of Zika-related symptoms in the mother during the first trimester of gestation (*8*).

Experimental Procedures

Sample Collection

In October 2015, Cape Verde reported a ZIKV outbreak and initiated a surveillance system to investigate the circulation of the virus in the country. All healthcare facilities were alerted to report suspected Zika cases according to the case definition of rash with or without fever and ≥1 of the following symptoms: conjunctivitis, headache, pruritus, arthralgia, myalgia, diarrhea, vomiting, adenopathy, or retro-orbital pain. In total, 1,226 sample sets (including blood and sometimes matching urine) of the original 7,580 sample sets from patients with suspected ZIKV infections (*9*) were sent to the Virology Laboratory at the Achadinha Health Center (Praia, Cape Verde) for ZIKV diagnosis. Only a fraction of the original sample set was sent because ZIKV testing was performed at the discretion of each healthcare facility's medical practitioners. Staff also sent samples from patients not fitting the Zika case definition (i.e., patients with only rash or only fever) for Zika testing.

Ethics

In this study, we used samples collected as part of approved ongoing surveillance conducted by the Institut Pasteur de Dakar (a World Health Organization Collaborating Centre for Arboviruses and Haemorrhagic Fever Reference and Research). All samples from humans were de-identified before we performed virus characterization and analyses; thus, no patient information can be reported.

Molecular Tests

We tested acute serum samples (obtained <5 days after symptom onset; n = 387) and, when available, matched urine samples (n = 82) by quantitative reverse transcription PCR (qRT-PCR). We extracted RNA from serum or urine samples using the QIAamp Viral RNA Mini Kit (QIAGEN, https://www.qiagen.com) according to the manufacturer's recommendations and performed a 1-step real-time PCR assay (*10*) on an ABI7500 instrument (Applied Biosystems, https://www.thermofisher.com) using the QuantiTect Probe RT-PCR Kit (QIAGEN).

Figure 1. Locations of suspected Zika cases (dark gray shading), Cape Verde, 2015–2016. Only 2 cases on Boa Vista were confirmed, and those might have been imported.

Serologic Tests

We tested serum samples (collected <10 days after symptom onset; n = 1,226) by ELISA for ZIKV IgM and IgG. For ZIKV antibody–positive samples, we tested for antibodies against other flaviviruses (yellow fever virus [YFV], dengue virus [DENV], and West Nile virus [WNV]) endemic in the West Africa region to rule out cross-reactions.

For the IgM ELISA, we coated 96-well microtiter plates with a monoclonal IgM capture antibody (goat anti-human IgM; KPL, https://www.seracare.com) in carbonate bicarbonate buffer (pH 9.6) and incubated overnight at 4°C. After washing the plate 3 times with phosphate-buffered saline plus 0.05% tween, we added heat-inactivated (56°C, 30 min) patient serum samples and controls (all diluted 1:100 in phosphate-buffered saline plus 0.05% tween and 1% milk powder) in duplicate into plate wells and incubated at 37°C for 1 h. We washed wells 3 times; added ZIKV, DENV, WNV, or YFV antigens into plate wells; and incubated the plate for 1 h. After 3 washes, we added ZIKV-, DENV-, WNV-, or YFV-specific immune ascites from mice to each well and incubated for 1 h at 37°C. After 3 washes, we added peroxidase-labeled antibody specific to mouse IgG for 1 h at 37°C. Last, we added a tetramethylbenzidine substrate to the IgM conjugate complex and stopped the color reaction using a sulfuric acid solution. For the indirect IgG ELISA, we captured ZIKV antigen on 96-well plates coated with ZIKV-specific mouse hyperimmune ascitic fluid. We added patient serum samples (1:100) and then horseradish peroxidase–conjugated goat anti-human IgG. We considered serum samples positive

if the optical density at 450 nm was >0.20 above the negative serum sample average and the ratio between the sample and the negative control was >2.

We analyzed samples positive for ZIKV IgM or IgG by ELISA for ZIKV-neutralizing antibodies using the plaque reduction neutralization test (PRNT) as described by De Madrid and Porterfield (*11*). In brief, we mixed 2-fold serial dilutions of serum samples (starting at 1:10) with equal volumes of medium containing 800 PFU/mL of the ZIKV reference strain MR766 and incubated for 1 h at 37°C. We then used serum–virus mixtures to infect Vero cell monolayers in 24-well plates. After 1 h at 37°C, we covered cells with DMEM containing 2% FBS and 0.4% carboxymethylcellulose and incubated for 4 days. We determined neutralizing antibody titers using an 80% cutoff value and classified samples as positive if their titers were ≥20 IU/mL.

Untargeted Sequencing

We treated RNA samples first with Turbo DNase (Ambion, https://www.thermofisher.com) and then depleted host rRNA using the NEBNext rRNA Depletion Kit (New England Biolabs, https://www.neb.com). We used rRNA-depleted RNA samples for cDNA synthesis using random primers and Superscript IV (ThermoFisher, https://www.thermofisher.com) and used cDNA for library preparation (Nextera XT DNA Library Prep Kit; Illumina, https://www.illumina.com). We sequenced libraries on an Illumina NextSeq500.

Amplicon-Based Sequencing

We sequenced amplicons from 3 samples following the protocol described by Quick et al. (*12*). We prepared sequencing libraries using the NEBNext Ultra II DNA Library Prep Kit for Illumina and barcoded with NEBNext Multiplex Oligos for Illumina (Dual Index Primers Set 1) (New England Biolabs for both). We sequenced prepared libraries on an Illumina MiSeq using MiSeq Reagent Kit v3 (600 cycles) at the Biomics platform of Institut Pasteur (Paris, France). We used Trimmomatic (http://www.usadellab.org) to remove adaptor and primer sequences (first 24 nt from 5′ end of reads, which is the maximum length of primers used for multiplexed PCRs). Then, we aligned reads to the complete genome sequence of a 2016 ZIKV isolate from the Dominican Republic (GenBank accession no. KU853012) using the CLC Genomics Suite (QIAGEN). We used SAMtools (http://samtools.sourceforge.net) to sort the aligned bam files and generate alignment statistics. We visually inspected ZIKV-aligned reads using Geneious version 9.1 (https://www.geneious.com) before generating consensus sequences and required a minimum of a 5× read-depth coverage to make a base call. We deposited all sequences we obtained in GenBank (accession nos. MK241415–*7*).

Sequence Dataset Compilation

To determine the origin of ZIKV in Cape Verde, we created a comprehensive dataset of all publicly available ZIKV sequences from GenBank. We then removed from this dataset all laboratory, patented, African genotype, and pre-2000 Asian genotype isolates. We concatenated all genome fragments of the same isolate to retain 1 representative sequence per isolate. For sequences with incomplete information on sampling time and location in GenBank records, we attempted to retrieve this information from published studies and other online resources. For cases in which the origin of the imported case of ZIKV infection was known, we set the sampling location as the location of origin. Last, we removed sequences that were not linked to a publication or associated with a known sampling time or location. This data pruning resulted in a final dataset of 459 ZIKV sequences. We created a multiple sequence alignment of these data using MAFFT (*13*) and manually edited the alignment by using AliView (*14*).

Phylogenetic Inference

We performed Bayesian phylogenetic and phylogeographic analyses using BEAST version 1.10.4 (*15*). We employed an uncorrelated relaxed-clock model (with rates drawn from an underlying log-normal distribution) (*16*) and a skygrid coalescent tree prior distribution (*17*) in combination with a codon-partitioned substitution model (SRD06) (*18*). We inferred migration history using a discrete phylogeographic model that incorporates a model-averaging procedure (i.e., the Bayesian stochastic search variable selection procedure) (*19*) to identify the subset of migration flows that adequately explain the diffusion process. We assessed convergence and mixing properties of the Markov chains with Tracer version 1.7 (*20*) and combined samples of several independent chains post burn-in. We generated maximum clade credibility trees summarizing the combined post burn in Markov chain Monte Carlo samples with the use of TreeAnnotator version 1.10.4 (http://beast.community/programs).

Results and Discussion

We report the findings of samples from 1,226 patients with suspected ZIKV infections (Table), as well as patients not fitting the Zika case definition. Samples

were tested over the course of the Cape Verde outbreak. The practice of sending samples from cases not fulfilling the strict Zika case definition for ZIKV testing resulted in a surge of tests being performed during the latter part of the outbreak (Figure 2). The peak of acute infections (as detected by IgM ELISA or qRT-PCR) occurred 3 weeks before the peak of suspected cases. The presence of IgG-positive, IgM-negative, qRT-PCR–negative cases in April 2016 indicates that many infections were not detected during their acute phase and highlights the challenge of capturing the timing and extent of outbreaks when a large proportion of the infected population is asymptomatic. Indeed, 80% of ZIKV infections are asymptomatic (*21*). The early detection of samples positive for ZIKV IgG (confirmed by PRNT) and negative for ZIKV IgM and RNA (including samples with sampling dates before October 2015 that were also received for ZIKV testing though not fitting the Zika case definition) is compatible with the silent circulation of ZIKV before the major wave of reported cases.

Table. Confirmed Zika cases during 2015–2016 outbreak, Cape Verde*

Category	No. confirmed/ no. tested
Confirmed recent ZIKV infections	226/1,226
qRT-PCR+/IgM–	18
qRT-PCR+/IgM+	6
qRT-PCR–/IgM+	202
Confirmed previous ZIKV infections: IgG+/PRNT+/qRT-PCR–/IgM–	311/1,226

*PRNT, plaque reduction neutralization test; qRT-PCR, quantitative reverse transcription PCR; ZIKV, Zika virus; –, negative; +, positive.

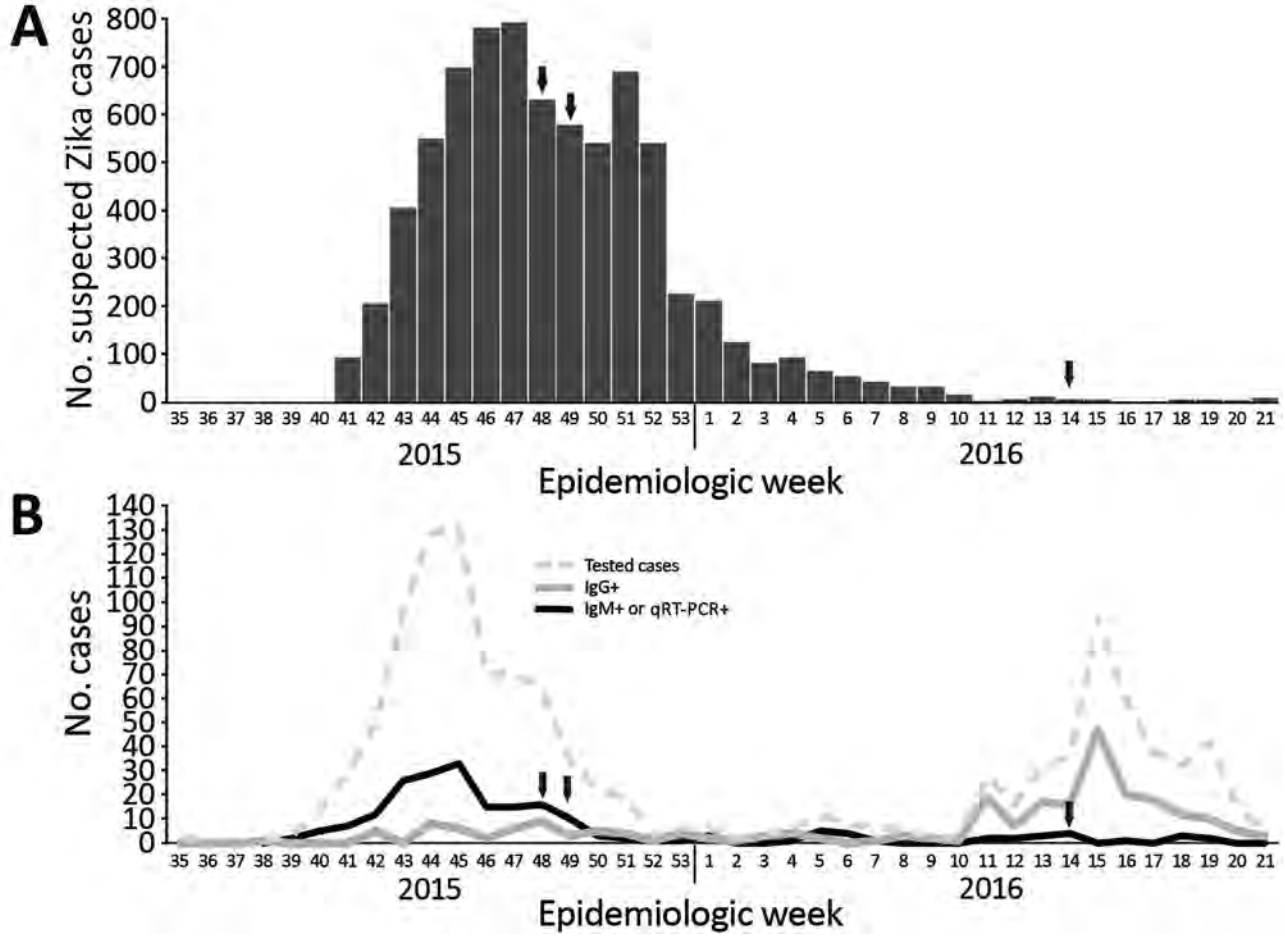

Figure 2. Suspected Zika cases, cases tested for Zika virus (ZIKV) infection, ZIKV antibody–positive cases, and ZIKV RNA–positive cases, Cape Verde, 2015–2016, by epidemiologic week. A) Cases of suspected ZIKV infection (n = 7,580) (*9*). B) Cases tested for ZIKV infection, ZIKV antibody–positive cases, and ZIKV RNA–positive cases. Only 1,226 of 7,580 cases of suspected ZIKV infection are included among those tested for ZIKV infection. In addition, some patients with fever only or rash only who did not fit the Zika case definition were also tested for ZIKV infection and included on this graph. ZIKV IgG–positive cases were negative by qRT-PCR and IgM ELISA and confirmed positive for ZIKV IgG by plaque reduction neutralization test. Arrows indicate the time of patient sampling for the 3 sequenced ZIKV isolates (GenBank accession nos. MK241415–7). qRT-PCR, quantitative reverse transcription PCR; –, negative; +, positive.

Although the high population densities of the southern islands (with >50% of the Cape Verde population living on Santiago Island) may explain why these islands experienced intense outbreaks, determining other factors that might have helped prevent further spread of the virus within the archipelago during the outbreak will be of value for future application.

Before this outbreak on the Cape Verde archipelago, no Zika outbreaks or ZIKV-associated microcephaly cases had been reported in Africa, and

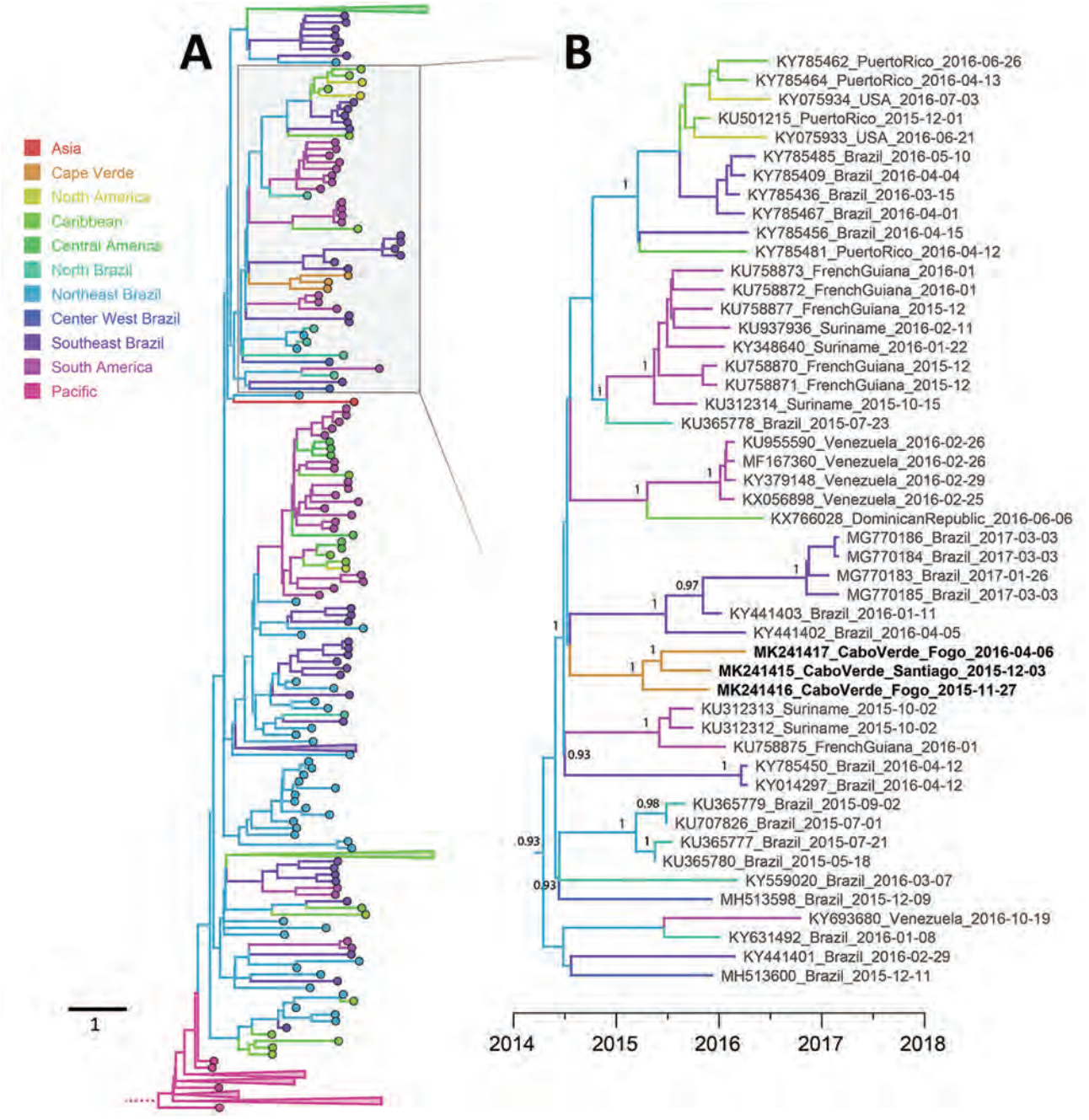

Figure 3. Maximum clade credibility phylogenetic tree demonstrating migration history of Zika virus (ZIKV) Asian lineage, 2014–2018. A) Phylogeny of 459 ZIKV isolates. The tree base was removed for ease of presentation. Tips of tree are colored according to their sampling location and branches according to their most probable geographic location. Note that sequences from the 2016 Angola outbreak (*23*) were published during the later stages of preparation of this manuscript and therefore were not included in this Bayesian analysis. Scale bar indicates years. See Appendix Figure 1 (https://wwwnc.cdc.gov/EID/article/26/6/19-0928-App1.pdf) for fully annotated tree. B) Expansion of tree containing Cape Verde ZIKV sequences (bold). Clade posterior probabilities are shown at well-supported nodes (>0.9). GenBank accession number, country of origin, and sampling date are provided for each ZIKV sequence.

only the Asian lineage of ZIKV had been found to be associated with neurologic and congenital afflictions. Because Cape Verde is situated in an area (near Senegal) where the African lineage of ZIKV has been regularly detected (*22*) and the Cape Verde outbreak involved cases of microcephaly, we needed to determine the origin and genotype of the ZIKV that caused this outbreak. We assessed virus origin and genotype through sequencing and phylogenetic analysis of ZIKVs sampled from patients in Cape Verde. Although our attempts at untargeted sequencing with rRNA-depleted samples were unsuccessful, we were able to Sanger sequence a small fragment of the envelope gene, which revealed that the virus was a part of the Asian lineage. We shared this information with the World Health Organization in May 2016.

We subsequently used a published overlapping PCR amplicon scheme to amplify and sequence the ZIKV genomes of preserved samples (*12*). This procedure enabled us to construct libraries that we could sequence and resulted in us obtaining 3 complete ZIKV genomes. These 3 sequences were obtained from samples acquired in November 2015 (Fogo), December 2015 (Santiago), and April 2016 (Fogo). Bayesian phylogenetic analysis of publicly available ZIKV sequences indicated that all 3 Cape Verde ZIKV genomes were related to the Asian genotype and formed a single, separate, well-supported monophyletic group (posterior probability 1, Figure 3; Appendix Figure 1, https://wwwnc.cdc.gov/EID/article/26/6/19-0928-App1.pdf), confirming our initial inference that was based on a partial envelope gene fragment. Of note, all sequences of Cape Verde ZIKVs contained a unique nonsynonymous substitution in the envelope protein (I756V), and a second amino acid change (T659A) also in the envelope gene was present in 2 of the isolates (those acquired December 2015 and April 2016). Additional work is needed to determine whether these mutations arose by chance or if they facilitate adaptation to local conditions, such as growth in mosquito species of Africa.

Phylogeographic analyses indicated that the Cape Verde ZIKV clade shares a common ancestor with lineages circulating in Brazil (posterior probability 0.798) and is most likely from northeast Brazil (posterior probability 0.574). Both Brazil and Cape Verde are Portuguese-speaking countries, and direct flights between northeast Brazil (Fortaleza) and Cape Verde (Praia) occurred daily during the outbreak. Although our data suggest that the ZIKV responsible for the Cape Verde outbreak originated in northeast Brazil, a lack of genomic sampling from many ZIKV-affected regions in the Americas makes excluding transmission through these other locations impossible. The median estimated date for the most recent common ancestor of the Cape Verde ZIKV clade was June 2015 (95% highest posterior density March 2015–August 2015; Figure 3). The median estimated date of divergence of this clade from the sequences sampled outside Cape Verde was November 2014 (95% highest posterior density July 2014–March 2015). Hence, these results indicate that ZIKV was most likely introduced into Cape Verde between June 2014 and August 2015, clearly before the first wave of documented clinical cases. This estimated virus introduction date is also supported by the finding of persons with ZIKV IgG and neutralizing antibodies early during the outbreak (Figure 2).

This study has 2 main limitations. First, because only a fraction of suspected Zika case samples were tested, bias in the reported distribution of confirmed cases is possible. Second, only 3 ZIKV genome sequences were recovered from this outbreak, perhaps limiting the power of our phylodynamic and phylogeographic analyses.

In conclusion, our analysis indicates that the Asian lineage of ZIKV reached Cape Verde in 2015 and triggered a relatively large epidemic. Of note, the Cape Verde ZIKV clade is distinct from the ZIKV of the 2017 Angola outbreak (Appendix Figure 2), which also involved microcephaly cases (*23*,*24*). The introduction of ZIKV into Cape Verde from Brazil and silent circulation in Cape Verde was likely to have occurred before the wave of cases in October 2015, as revealed by both phylogenetic and serologic data. The time scale we report is consistent with those estimated for the initial movement of ZIKV from Brazil to neighboring countries in South America and islands of the Caribbean (Appendix Figure 1) (*10*,*25*,*26*).

Acknowledgements

We thank 2 anonymous reviewers whose suggestions helped to improve this manuscript.

This work was supported by Institut Pasteur de Dakar. P.L. received funding by the European Research Council under the European Union's Horizon 2020 Research and Innovation Programme (grant agreement no. 725422-ReservoirDOCS) and by the Wellcome Trust through project 206298/Z/17/Z. S.L. and B.V. are supported by the Fonds Wetenschappelijk Onderzoek (Belgium). E.S.-L. received funding from the INCEPTION program (Investissements d'Avenir grant ANR-16-CONV-0005) and Institut Pasteur. F.G.-R. is part of the Pasteur-Paris University International doctoral program, BioSPC doctoral school. E.C.H. is funded by an Australian Research Council Australian Laureate Fellowship (FL170100022).

About the Author

Dr. Oumar Faye is a virologist often working on outbreak responses at Institut Pasteur de Dakar in Dakar, Senegal. His research interests focus on the development of diagnostic tools and the characterization of arboviruses and hemorrhagic fever viruses.

References

1. Baud D, Gubler DJ, Schaub B, Lanteri MC, Musso D. An update on Zika virus infection. Lancet. 2017;390:2099–109. http://dx.doi.org/10.1016/S0140-6736(17)31450-2
2. Faye O, Freire CC, Iamarino A, Faye O, de Oliveira JV, Diallo M, et al. Molecular evolution of Zika virus during its emergence in the 20th century. PLoS Negl Trop Dis. 2014;8:e2636. http://dx.doi.org/10.1371/journal.pntd.0002636
3. Posen HJ, Keystone JS, Gubbay JB, Morris SK. Epidemiology of Zika virus, 1947–2007. BMJ Glob Health. 2016;1:e000087. http://dx.doi.org/10.1136/bmjgh-2016-000087
4. Cao-Lormeau VM, Blake A, Mons S, Lastère S, Roche C, Vanhomwegen J, et al. Guillain-Barré syndrome outbreak associated with Zika virus infection in French Polynesia: a case-control study. Lancet. 2016;387:1531–9. http://dx.doi.org/10.1016/S0140-6736(16)00562-6
5. Pan American Health Organization; World Health Organization. Zika cases and congenital syndrome associated with Zika virus reported by countries and territories in the Americas, 2015–2018, cumulative cases. 2018 Jan 4 [cited 2019 Oct 15]. https://www.paho.org/hq/index.php?option=com_docman&task=doc_download&gid=43296
6. de Araújo TVB, Ximenes RAA, Miranda-Filho DB, Souza WV, Montarroyos UR, de Melo APL, et al.; Investigators from the Microcephaly Epidemic Research Group; Brazilian Ministry of Health; Pan American Health Organization; Instituto de Medicina Integral Professor Fernando Figueira; State Health Department of Pernambuco. Association between microcephaly, Zika virus infection, and other risk factors in Brazil: final report of a case-control study. Lancet Infect Dis. 2018;18:328–36. http://dx.doi.org/10.1016/S1473-3099(17)30727-2
7. Mlakar J, Korva M, Tul N, Popović M, Poljšak-Prijatelj M, Mraz J, et al. Zika virus associated with microcephaly. N Engl J Med. 2016;374:951–8. http://dx.doi.org/10.1056/NEJMoa1600651
8. Lourenço J, de Lourdes Monteiro M, Valdez T, Monteiro Rodrigues J, Pybus O, Rodrigues Faria N. Epidemiology of the Zika virus outbreak in the Cabo Verde Islands, West Africa. PLoS Curr. 2018;10:10.
9. Serviço de Vigilância Integrada e Resposta a Epidemias, Ministério da Saúde e da Segurança Social. Boletim informativo seminal, infeção por vírus Zika (ZIKV), ano 2016, (semanas 1 a 21). 2016 [cited 2019 Jul 1]. http://www.minsaude.gov.cv/index.php/documentosite/zika-1/341-boletim-informativo-semanal-da-infecao-por-virus-zika-semana-21-ano-2016/file
10. Faria NR, Azevedo RDSDS, Kraemer MUG, Souza R, Cunha MS, Hill SC, et al. Zika virus in the Americas: early epidemiological and genetic findings. Science. 2016; 352:345–9. http://dx.doi.org/10.1126/science.aaf5036
11. De Madrid AT, Porterfield JS. A simple micro-culture method for the study of group B arboviruses. Bull World Health Organ. 1969;40:113–21.
12. Quick J, Grubaugh ND, Pullan ST, Claro IM, Smith AD, Gangavarapu K, et al. Multiplex PCR method for MinION and Illumina sequencing of Zika and other virus genomes directly from clinical samples. Nat Protoc. 2017;12:1261–76. http://dx.doi.org/10.1038/nprot.2017.066
13. Katoh K, Standley DM. MAFFT multiple sequence alignment software version 7: improvements in performance and usability. Mol Biol Evol. 2013;30:772–80. http://dx.doi.org/10.1093/molbev/mst010
14. Larsson A. AliView: a fast and lightweight alignment viewer and editor for large datasets. Bioinformatics. 2014;30:3276–8. http://dx.doi.org/10.1093/bioinformatics/btu531
15. Suchard MA, Lemey P, Baele G, Ayres DL, Drummond AJ, Rambaut A. Bayesian phylogenetic and phylodynamic data integration using BEAST 1.10. Virus Evol. 2018;4:vey016. http://dx.doi.org/10.1093/ve/vey016
16. Drummond AJ, Ho SY, Phillips MJ, Rambaut A. Relaxed phylogenetics and dating with confidence. PLoS Biol. 2006;4:e88. http://dx.doi.org/10.1371/journal.pbio.0040088
17. Gill MS, Lemey P, Faria NR, Rambaut A, Shapiro B, Suchard MA. Improving Bayesian population dynamics inference: a coalescent-based model for multiple loci. Mol Biol Evol. 2013;30:713–24. http://dx.doi.org/10.1093/molbev/mss265
18. Shapiro B, Rambaut A, Drummond AJ. Choosing appropriate substitution models for the phylogenetic analysis of protein-coding sequences. Mol Biol Evol. 2006;23:7–9. http://dx.doi.org/10.1093/molbev/msj021
19. Lemey P, Rambaut A, Drummond AJ, Suchard MA. Bayesian phylogeography finds its roots. PLOS Comput Biol. 2009;5:e1000520. http://dx.doi.org/10.1371/journal.pcbi.1000520
20. Rambaut A, Drummond AJ, Xie D, Baele G, Suchard MA. Posterior summarization in Bayesian phylogenetics using Tracer 1.7. Syst Biol. 2018;67:901–4. http://dx.doi.org/10.1093/sysbio/syy032
21. Duffy MR, Chen TH, Hancock WT, Powers AM, Kool JL, Lanciotti RS, et al. Zika virus outbreak on Yap Island, Federated States of Micronesia. N Engl J Med. 2009;360: 2536–43. http://dx.doi.org/10.1056/NEJMoa0805715
22. Sow A, Loucoubar C, Diallo D, Faye O, Ndiaye Y, Senghor CS, et al. Concurrent malaria and arbovirus infections in Kedougou, southeastern Senegal. Malar J. 2016;15:47. http://dx.doi.org/10.1186/s12936-016-1100-5
23. Hill SC, Vasconcelos J, Neto Z, Jandondo D, Zé-Zé L, Aguiar RS, et al. Emergence of the Asian lineage of Zika virus in Angola: an outbreak investigation. Lancet Infect Dis. 2019;19:1138–47. http://dx.doi.org/10.1016/S1473-3099(19)30293-2
24. Sassetti M, Zé-Zé L, Franco J, Cunha JD, Gomes A, Tomé A, et al. First case of confirmed congenital Zika syndrome in continental Africa. Trans R Soc Trop Med Hyg. 2018;112: 458–62. http://dx.doi.org/10.1093/trstmh/try074
25. Faria NR, Quick J, Claro IM, Thézé J, de Jesus JG, Giovanetti M, et al. Establishment and cryptic transmission of Zika virus in Brazil and the Americas. Nature. 2017;546:406–10. http://dx.doi.org/10.1038/nature22401
26. Thézé J, Li T, du Plessis L, Bouquet J, Kraemer MUG, Somasekar S, et al. Genomic epidemiology reconstructs the introduction and spread of Zika virus in Central America and Mexico. Cell Host Microbe. 2018;23:855–864.e7. http://dx.doi.org/10.1016/j.chom.2018.04.017

Address for correspondence: Etienne Simon-Loriere, Institut Pasteur, 28 rue du Docteur Roux, 75724 Paris CEDEX 15, France; email: etienne.simon-loriere@pasteur.fr

Epidemiologic Changes of Scrub Typhus in China, 1952–2016

Zhongjie Li,[1] Hualei Xin,[1] Junling Sun,[1] Shengjie Lai, Lingjia Zeng, Canjun Zheng, Sarah E. Ray, Nicole Davis Weaver, Liping Wang, Jianxing Yu, Zijian Feng,[2] Simon I. Hay, George F. Gao[2]

Scrub typhus, a miteborne rickettsiosis, has emerged in many areas globally. We analyzed the incidence and spatial–temporal distribution of scrub typhus in China during 1952–1989 and 2006–2016 using national disease surveillance data. A total of 133,623 cases and 174 deaths were recorded. The average annual incidence was 0.13 cases/100,000 population during 1952–1989; incidence increased sharply from 0.09/100,000 population in 2006 to 1.60/100,000 population in 2016. The disease, historically endemic to southern China, has expanded to all the provinces across both rural and urban areas. We identified 3 distinct seasonal patterns nationwide; infections peaked in summer in the southwest, summer-autumn in the southeast, and autumn in the middle-east. Persons ≥40 years of age and in nonfarming occupations had a higher risk for death. The changing epidemiology of scrub typhus in China warrants an enhanced disease control and prevention program.

Scrub typhus is a life-threatening disease caused by *Orientia tsutsugamushi*, an obligate intracellular bacterium transmitted by the larvae of trombiculid mites (*1*). Only biting larvae of Asian scrub typhus chiggers (*Leptotrombidium* spp.) can transmit the disease. After the bite of an infective mite, a characteristic necrotic inoculation lesion (an eschar) can develop. The microorganism then spreads through the lymphatic fluid and blood, causing manifestations including fever, headache, rash, lymphadenopathy, and mental changes (*1*). Without appropriate treatment with specific antimicrobial drugs (e.g., tetracycline, chloramphenicol, doxycycline, or azithromycin), >6% of infected patients will die (*2*,*3*). There is no licensed human vaccine to prevent scrub typhus infection.

Globally, scrub typhus is traditionally regarded as a disease endemic to a region called the Asia-Pacific tsutsugamushi triangle, which extends from Pakistan in the west to far eastern Russia in the east to northern Australia in the south. In some countries of Southeast Asia, scrub typhus is a leading cause of treatable nonmalarial febrile illness (*4*–*6*). It is estimated that scrub typhus threatens >1 billion persons, causes at least 1 million clinical cases per year, and is associated with substantial mortality rates globally (*1*,*7*). The 2010s saw a widespread reemergence of scrub typhus in endemic regions such as India, Korea, Laos, and the Maldives (*3*,*6*,*8*). The recent emergence of scrub typhus in the Arabian Peninsula, Chile, and possibly Kenya suggests wider global distribution of this disease in tropical and subtropical regions, far from the tsutsugamushi triangle (*9*–*12*). Although scrub typhus poses the greatest threat to residents of eastern and southern Asia as well as tourists traveling to these regions, it remains a neglected disease globally. The lack of both research and a nationwide surveillance system within many endemic regions have resulted in poorly understood epidemiologic characteristics and disease burden of scrub typhus at global, national, and subnational levels (*7*). The Global Burden of Disease Study publishes estimates for 333 diseases and injuries, but currently bundles scrub typhus with other neglected tropical diseases, rather than providing specific burden estimates (*13*).

In China, scrub typhus cases were recorded in the early 1950s, and a disease surveillance system for scrub typhus was established in 1952 (*14*,*15*). *Leptotrombidium deliense* and *L. scutellare* mites are the 2 principal vectors transmitting the disease in the country (*16*). *L. deliense* mites inhabit southern China and emerge in April, peaking in June–August, and decreasing

Author affiliations: Chinese Center for Disease Control and Prevention, Beijing, China (Z. Li, H. Xin, S. Lai, L. Zeng, C. Zheng, L. Wang, J. Yu, Z. Feng, G.F. Gao); Qingdao City Center for Disease Control and Prevention, Shandong, China (H. Xin); University of Southampton, Southampton, UK (S. Lai); University of Washington, Seattle, Washington, USA (S.E. Ray, N.D. Weaver, S.I. Hay); Chinese Academy of Sciences, Beijing (G.F. Gao)

DOI: https://doi.org/10.3201/eid2606.191168

[1]These first authors contributed equally to this article.

[2]These senior authors contributed equally to this article.

September–December, whereas *L. scutellare* is widespread in China, emerging annually in October–December, and is the main mite species in northern China (*17*). Several studies have revealed that the incidence of scrub typhus is rising nationwide (*18*,*19*); however, the changing epidemiologic characteristics of scrub typhus at the subnational level and among the subgroups are not fully illustrated. After the SARS outbreak in 2003, a nationwide population-based infectious disease surveillance system was developed in China to collect epidemiologic information at the patient level, enabling study of the epidemiologic features of a disease at the smaller scale of a geographic region and specific population (*20*,*21*).

In this study, we systematically collated longitudinal nationwide surveillance data of scrub typhus in China from 1952–1990 and 2006–2016. We explored changes in the disease's epidemiologic characteristics, both spatiotemporally and seasonally, and changes in high-risk population groups at both national and subnational levels.

Materials and Methods

National Surveillance of Scrub Typhus

In China, the national surveillance program on scrub typhus (Appendix Tables 1, 2, https://wwwnc.cdc.gov/EID/article/26/6/19-1168-App1.pdf) varied through 3 time periods. Initially, mail-based reporting of monthly aggregated data occurred in 1952–1989. Beginning in 1952, data on scrub typhus were reported on a voluntary basis in certain areas of China. In 1955, scrub typhus became a statutorily notifiable disease, and reporting all suspected, probable, and laboratory-confirmed scrub typhus cases was required. Reporting was suspended during 1990–2005; in 1990, scrub typhus was removed from the list of notifiable diseases, due to its relatively low threat. Therefore, nationwide data on the disease are not available from 1990–2005. Internet-based reporting of individual cases occurred in 2006–2016; in 2006, scrub typhus was added as a reporting disease in the National Notifiable Infectious Disease Reporting Information System at the Chinese Centers for Disease Control and Prevention (China CDC). The information on individual cases includes patient demographic information (name, sex, occupation, residence), date of illness onset, case classification (confirmed, probable, suspected), date of diagnosis, date of report, reporter institution, and date of death (if applicable).

The National Health Commission of the People's Republic of China determined that the collection of data on human cases of scrub typhus was part of a routine public health investigation and was exempt from institutional review board assessment. All data in this study are anonymous so that individual patients cannot be identified.

Case Definition

Scrub typhus cases have been classified as probable (clinically diagnosed) or confirmed (laboratory confirmed) in accordance with the diagnosis criteria and case classification guidelines issued by the Chinese national health authorities (Appendix Table 2). Probable cases are diagnosed by local experienced physicians according to epidemiologic exposure (travel to a disease-endemic area and contact with chiggers or rodents ≤3 weeks before the onset of illness) and clinical manifestations (such as high fever, lymphadenopathy, skin rash, and eschars or ulcers). Confirmed cases are probable cases with 1 positive result among the following tests: Weil-Felix test, indirect immunofluorescence antibody assay, PCR, or isolation of *Orientia tsutsugamushi* (*22*).

Data Analysis

Our analysis comprised all probable and confirmed human scrub typhus cases in 1952–1989 and 2006–2016 (Appendix Tables 3, 4). We calculated the annual incidence rate by dividing the number of human scrub typhus cases by the corresponding population at the end of a given year. We obtained population data used to calculate incidence rates from the National Bureau of Statistics of China (*23*). We calculated the case-fatality ratio by dividing the number of human scrub typhus deaths by the number of scrub typhus cases. We used Joinpoint regression models to examine the incidence trends from 1952–2016 and calculated annual percentage changes (*24*).

We created a heat map of yearly incidence rates (standardized range 0–1) to visualize the long-term change over the 49-year period by province (Appendix Table 5, Figure 3). To assess the changing spatial and temporal patterns of the affected areas from 2006–2016, we plotted the newly affected and previously affected counties and townships by year in both the rural and urban areas where each case resided. In our study, the rural areas refer to the village or rural town, and urban areas refer to the city community or urban town. We identified epidemiologically related regions of scrub typhus based on hierarchical cluster analysis with Ward's minimum variance method, using the Pearson correlation coefficient matrix of average weekly cases between paired provinces as distance.

To quantify the characteristics of scrub typhus season, we fitted multiple linear regression models

to time series of the weekly number of scrub typhus cases during 2006–2016, including harmonic terms representing annual and semiannual periodic cycles as described previously (*25*–*27*). We defined scrub typhus season as the period of consecutive weeks in which >95% of the total annual cases occurred and as the smallest number of consecutive weeks. We characterized scrub typhus season by plotting the season onset, peak (the week with the highest case number in the fitted seasonal curve), and offset against the calendar week of the year. We used a multivariable logistic regression model to explore the predictors of death for scrub typhus. We used R statistical software version 3.4.1 (https://www.r-project.org) to produce graphs and perform statistical analyses (*28*) and ArcGIS version 10.2.2 (ESRI, https://www.arcgis.com) to plot geographic patterns. We used Joinpoint version 4.5.0.0 (US National Cancer Institute, https://surveillance.cancer.gov/joinpoint) to examine incidence trends.

Results

Overall Incidence

During the 49 years covered in this study (1952–1989 and 2006–2016), a total of 133,623 scrub typhus cases were recorded throughout the country. During 1952–1989, the occurrence of the disease remained at a stable, low level, with a mean annual incidence rate of 0.13 (95% CI 0.11–0.15) per 100,000 population (Figure 1, panel A). Since 2006, the annual incidence rate has increased sharply, changing from 0.09/100,000 population in 2006 to 1.60/100,000 population in 2016 (>16-fold increase) (Table 1), with an annual percent change of 32% (95% CI 30%–34%) (Appendix Figure 1).

Demographic Features

From 2006–2016, the mean age of case-patients was 48 years (range 1 month–98 years). The median age increased from 46 years (interquartile range 27–58 years) in 2006 to 53 years (interquartile range 41–64 years) in 2016. Overall, case-patients ≥45 years of age were the most common (66%); the highest incidence was among those 60–64 years (1.67 cases/100,000 population) and 65–69 years (1.71 cases/100,000 population). However, a subgroup of children <5 years of age had the highest incidence rate in the southwest disease-endemic regions (4.30 cases/100,000 population for Yunnan and Sichuan provinces combined) (Table 1). The sex ratio of male to female changed from 1.09:1 in 2006–2009 to 0.85:1 in 2010–2016. In general, farmers (73%) were the most affected group, with 86% of cases occurring in rural areas.

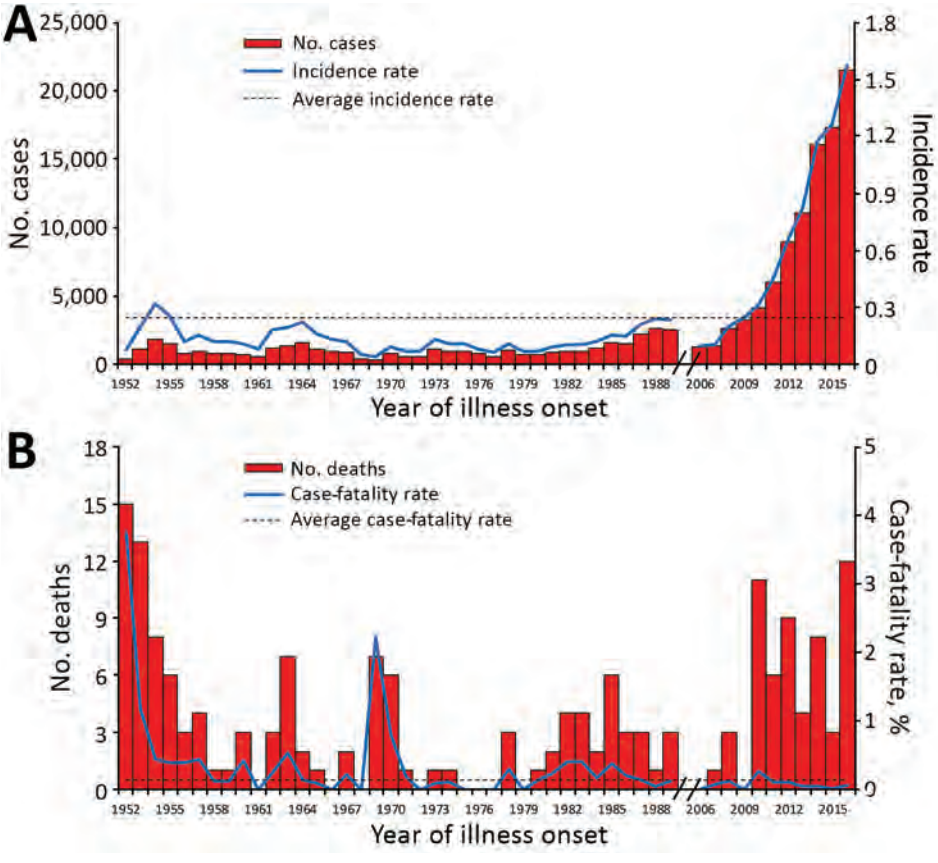

Figure 1. Reported cases and deaths of scrub typhus in China, 1952–2016. A) Aggregated number of cases by year (red bars), annual incidence rate (blue line), and average annual incidence rate (black dashed line) per 100,000 residents. B) Aggregated number of deaths by year (red bars), case-fatality ratio (blue line), and average annual case-fatality ratio (black dashed line). The data from 1990–2005 are missing because surveillance for scrub typhus was suspended during the period.

Table 1. Characteristics of reported scrub typhus cases, China, 2006–2016*

Characteristic	2006	2007	2008	2009	2010	2011	2012	2013	2014	2015	2016
No. cases	1,254	1,340	2,613	3,237	4,088	6,020	8,928	11,111	16,035	17,293	21,562
No. probable cases	1,049	1,187	2,360	2,939	3,811	5,630	8,555	10,536	15,339	16,696	20,997
No. confirmed cases	205	153	253	298	277	390	373	575	696	597	565
Incidence†	0.09	0.10	0.19	0.24	0.30	0.45	0.66	0.82	1.19	1.28	1.60
Sex											
M	642	711	1,385	1,660	2,040	2,884	4,228	4,910	7,222	8,021	9,871
	(51)	(53)	(53)	(51)	(50)	(48)	(47)	(44)	(45)	(46)	(46)
F	612	629	1,228	1,577	2,048	3,136	4,700	6,201	8,813	9,272	11,691
	(49)	(47)	(47)	(49)	(50)	(52)	(53)	(56)	(55)	(54)	(54)
Age, y, median	46	46	48	44	46	50	50	51	52	53	53
(IQR)‡	(27–58)	(27–59)	(30–60)	(25–57)	(28–59)	(33–61)	(36–62)	(38–62)	(39–63)	(42–64)	(41–64)
<5	86 (7)	92 (7)	198 (8)	279 (9)	358 (9)	423 (7)	606 (7)	638 (6)	775 (5)	681 (4)	928 (4)
5–14	143 (11)	139 (10)	173 (7)	341 (11)	344 (8)	401 (7)	539 (6)	629 (6)	811 (5)	716 (4)	899 (4)
15–44	373	402	783	1,012	1,200	1,543	2,147	2,589	3,683	3,738	4,578
	(30)	(30)	(30)	(31)	(29)	(26)	(24)	(23)	(23)	(22)	(21)
45–60	397	415	878	1,001	1,320	2,035	3,169	4,038	5,791	6,339	7,797
	(32)	(31)	(34)	(31)	(32)	(34)	(35)	(36)	(36)	(37)	(36)
≥61	255	292	581	604	866	1,618	2,467	3,217	4,975	5,819	7,360
	(20)	(22)	(22)	(19)	(21)	(27)	(28)	(29)	(31)	(34)	(34)
Residence§											
Rural	892	1,023	2,108	2,758	3,512	5,231	7,725	9,622	13,803	15,058	18,597
	(76)	(79)	(83)	(87)	(88)	(88)	(87)	(87)	(87)	(88)	(89)
Urban	279	264	424	408	477	718	1,170	1,443	2,105	2,051	2,414
	(24)	(21)	(17)	(13)	(12)	(12)	(13)	(13)	(13)	(12)	(11)
Occupation,	733	859	1,700	2,079	2,721	4,250	6,179	7,853	11,842	13,230	16,670
farmer	(58)	(64)	(65)	(64)	(67)	(71)	(69)	(71)	(74)	(77)	(77)
No. in endemic province	16	19	18	22	20	20	23	21	27	26	25
No. in endemic county	222	225	327	372	431	509	582	692	769	809	883
No. in endemic township	616	683	1,183	1,283	1,523	2,088	2,644	3,264	4,125	4,353	5,025
No. deaths	0	1	3	0	11	6	9	4	8	3	12

*Values are no. (%) except as indicated. IQR, interquartile range.
†No. cases/100,000 population.
‡Some columns do not add up to 100% because of rounding.
§Some columns do not add up to equal the total because of missing data.

Spatial-Temporal Distribution

During the 28 years from 1952–1979, nearly all cases (99.9%) occurred in the southern provinces of China; sporadic cases were recorded in several northern provinces. Beginning in 1980, the disease began to expand slowly northward and westward; the number of affected provinces gradually increased from 17 during 1952–1989 to all 31 provinces during 2011–2016 (Figure 2). We saw dramatic expansion in both rural and urban areas. In rural areas, the affected townships increased nearly 10-fold, from 422 in 2006 to 4,083 in 2016, and the affected urban townships expanded from 194 in 2006 to 942 in 2016 (Figure 3). As of 2016, a total of 28% (883/3,101) of all counties and 11% (5,025/44,539) of all townships recorded cases of scrub typhus throughout the country (Appendix Figure 2).

During 2006–2016, nearly all cases (93,187/93,481; 99.7%) occurred in the 15 provinces that had a cumulative case count ≥100. Among these provinces, we identified 3 epidemiologic regions using hierarchical cluster analysis (Figure 4, panels A, B): middle-east (latitude range 31°–41°N, longitude range 105°–125°E); southwest (latitude range 21°–31°N, longitude range 95°–105°E); and southeast China (latitude range 21°–31°N, longitude range 105°–125°E).

Seasonal Pattern

Nationally, the seasonal pattern of scrub typhus incidence begins to increase rapidly in May, reaches a peak in October, and falls in November; 94% of cases occurred from May through November in both periods, 1980–1989 and 2006–2016. Heat maps showed consistent seasonal patterns of scrub typhus within each province and between the 2 periods of 1980–1989 and 2006–2016 (Appendix Figure 3), but we observed geographic diversity of seasonal patterns across China. Multiple linear regression models of time series data confirmed and quantified seasonal characteristics of scrub typhus activity in the 3 epidemiologic regions ($p<0.001$ for all) (Appendix Tables 6, 7). Specifically, the scrub typhus season

in the southeast extended from calendar week 17 (early May) to calendar week 50 (mid-December), lasting for 34 weeks and capturing 95% of the total reported cases from this region. In the southwest, the season extended from calendar week 21 (late May) to calendar week 48 (early December), for 28 weeks of duration, capturing 95% of total reported cases in the region. In the middle-east, scrub typhus season lasted 12 weeks, from calendar week 38 (late September) to calendar week 49 (mid-December), capturing 97% of total reported cases in the region (Figure 5, panels A, B).

Risk for Death

A total of 174 deaths were recorded throughout the country during the 49 years of this study (1952–1989 and 2006–2016). The overall case-fatality ratio was 0.13% (95% CI 0.11%–0.15%); the case fatality ratio from 2006–2016 was significantly lower than that

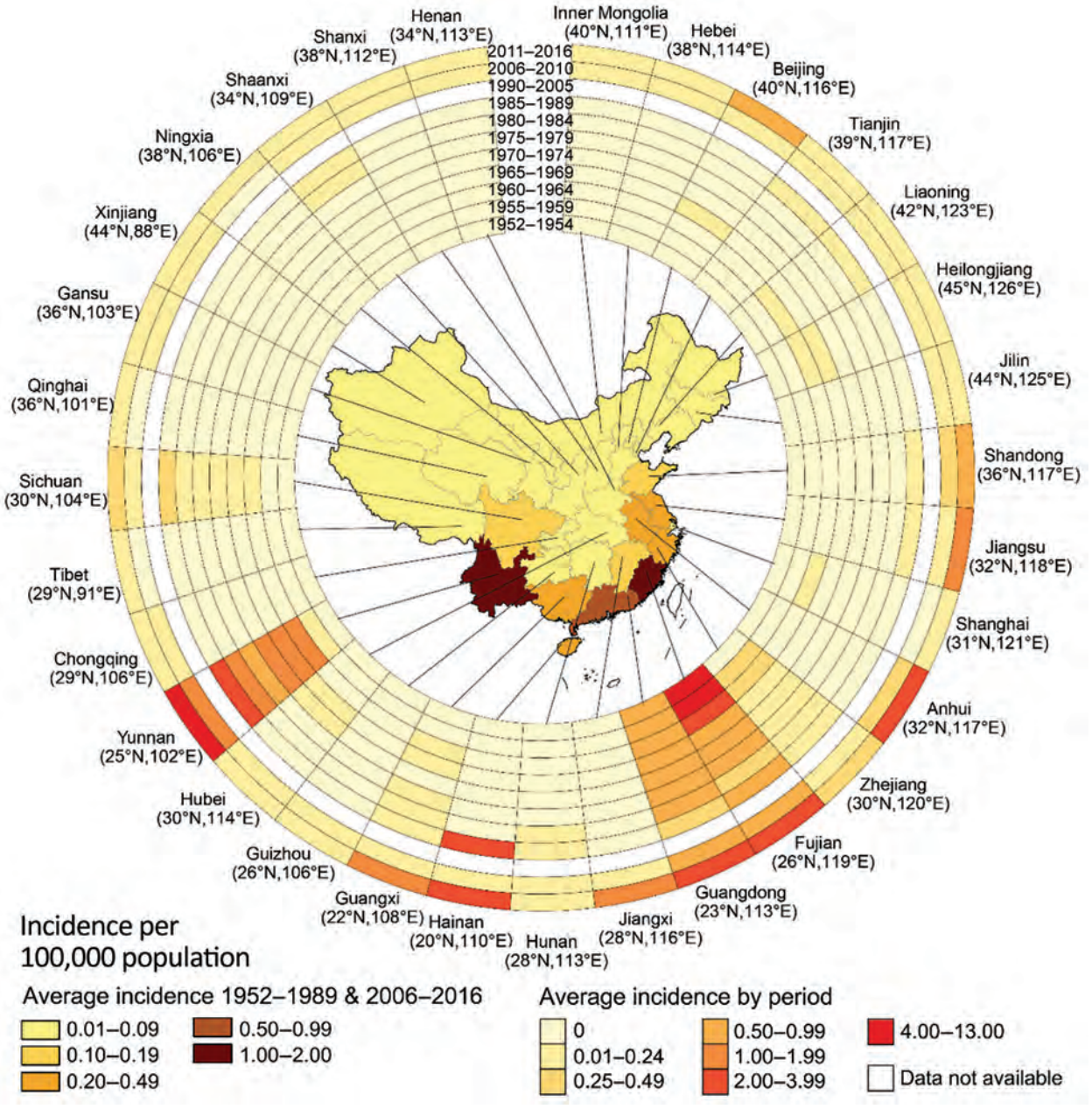

Figure 2. Incidence rate of scrub typhus for each province of China during 1952–1989 and 2006–2016, by time period. Annual average incidence of scrub typhus per 100,000 population in the 31 provinces investigated is shown. The rings contain data for 11 periods studied; the innermost ring shows data for early periods of 1952–1954, and the outermost ring data for 2011–2016. The latitude and longitude of the capital city of each province are shown.

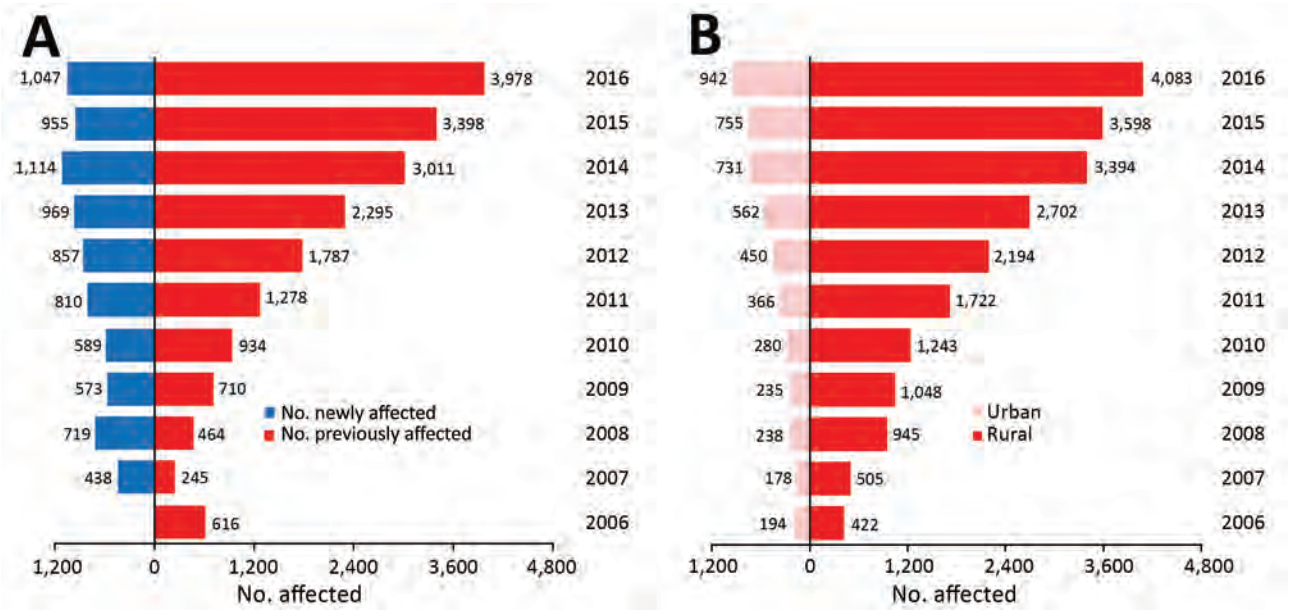

Figure 3. Number of townships with scrub typhus cases reported in China during 2006–2016, by year. A) Number of affected townships for each year, divided by those that were affected in previous years (red bars) and those newly affected townships for each year (blue bars). B) Total number of affected townships for each year in rural (red bars) and urban (light pink bars).

from 1952–1989 (0.06% vs. 0.29%; p<0.001). The following subgroups had a higher risk for death: age ≥40 years (adjusted odds ratio [aOR] 3.43, 95% CI 1.69–7.72), nonfarmer occupation (aOR 3.56, 95% CI 1.97–6.43), and interval of illness onset to diagnosis ≥8 days (aOR 2.36, 95% CI 1.07–5.19) (Table 2).

Discussion

In this study of a longitudinal surveillance dataset spanning 49 years, we found the occurrence of scrub typhus in China has been maintained at a relatively low level from the 1950s–1980s. However, in the 2000s, incidence rates increased in an unprecedented manner, in both the historically endemic areas and in new areas not previously identified as having cases. In addition, profound epidemiologic changes, including geographic expansion, varying age and sex distribution, and diverse seasonal patterns were further discovered during the period 2006–2016.

In China, some novel natural and socioeconomic factors may have contributed to the increased risk for scrub typhus infection. During the past decade, the reduction of industrial land use, recovering forests and wetlands, and the banning of traditional burning of straw within rural areas have provided a favorable setting for the breeding of rodents and mites, increasing the possibility of human exposure, and the forming of new natural foci for scrub typhus in previously unaffected areas (*29*). In some other scrub typhus–endemic countries, evidence suggests that a combination of climate change and the expansion of humans into previously uninhabited areas may play roles in both the reemergence and the apparent rising incidence of scrub typhus (*30*,*31*).

Globally, the application of improved surveillance mechanisms and enhanced awareness of clinicians have contributed to greater recognition of scrub typhus in some countries, such as India (*1*), South Korea (*1*,*6*), Laos (*6*), and Japan (*3*,*32*). In China, the overall incidence of all notifiable infectious diseases was relatively stable during 2006–2013 (*20*). We believe changes in surveillance may have played a minor role in the increase of scrub typhus in China; although the reincorporating of the disease in the National Notifiable Infectious Disease Reporting Information System and the issuing of 2009 national guidelines may have influenced disease awareness among reporters while the increased use of diagnostic tools such as PCR enabled identification of more cases, the change in reporting alone could not fully explain the drastic changes in the geographic and demographic distribution of scrub typhus. More investigations into the pathogen, the vectors, the environment, and the hosts driving the changing epidemiology of scrub typhus in the country should be conducted.

In this study, we determined that most cases of scrub typhus occur in rural areas and in older persons. During 1990–2020, in rural areas of China, a large number of young and middle-aged male persons have traveled to metropolitan areas seeking

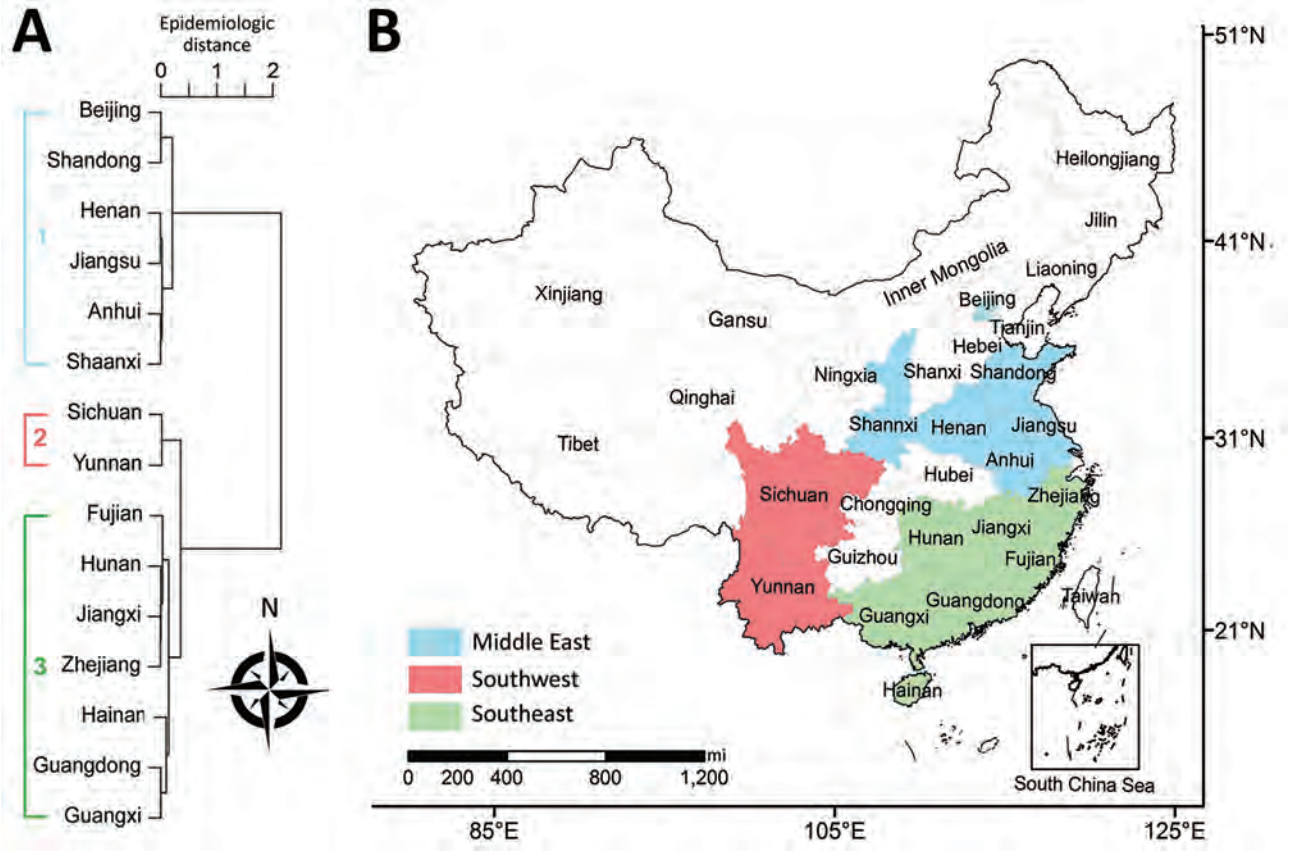

Figure 4. Epidemiologic regions of scrub typhus in China, 2006–2016. A) Epidemiologic regions based on hierarchical clustering, using the Pearson correlation coefficient matrix between average weekly scrub typhus time series of paired provinces that had a cumulative number of cases >100 in 2006–2016 combined. B) Map of identified epidemiologic regions identified by hierarchical clustering), e.g., middle-east (latitude range 31°–41°N and longitude range 105°–125°E), southwest (latitude range 21°–31°N and longitude range 95°–105°E), southeast of China (latitude range 21°–31°N and longitude range 105°–125°E). Other provinces had a combined total of <100 cases in 2006–2016.

better jobs and higher incomes, often leaving their older, younger, or female family members in rural areas. Older family members >60 years of age commonly performed routine farming activities and so are at higher risk for infection. However, the high incidence of scrub typhus cases in patients <5 years of age in 2 specific provinces, Yunnan and Sichuan, should be addressed, and possible risk factors must be further explored.

We discovered that both the number of scrub typhus cases and the number of affected urban areas are rapidly increasing. Because of improved economic and living conditions in China, more persons live in urban areas and travel to rural areas for recreation and entertainment (e.g., fishing, hiking, picnicking, camping, and picking fruit) on the weekends and on holidays. For urban groups susceptible to scrub typhus, frequent outdoor activities in endemic areas increase the risk for infection (*30*,*33*). In 2012, an outbreak of scrub typhus was detected in a city park, implying that the rodent host and mites may inhabit urban settings. In addition, frequent transportation of farmed goods may lead to the migration of rodents carrying infected mites, which may cause the expansion of scrub typhus to more urban and non–typhus-endemic areas (*33*,*34*).

Our study revealed varying seasonal patterns of the scrub typhus epidemic in China, which have also previously been reported in certain nearby countries. In Japan, 2 types of seasonal patterns peaked in weeks 18–25 (April–May) and weeks 43–52 (November–December) and were located north and south of 37°N latitude (*35*); in South Korea, a single seasonal pattern peaking in October–November was reported (*8*). The appearance of larvae determines the seasonality of scrub typhus. The heterogeneous geographic distribution of *L. deliense* and *L. scutellare* mites may well explain the diverse seasonal patterns of scrub typhus in the southeast, southwest, and middle-east parts of China (*17*). Because of the complex interactions among

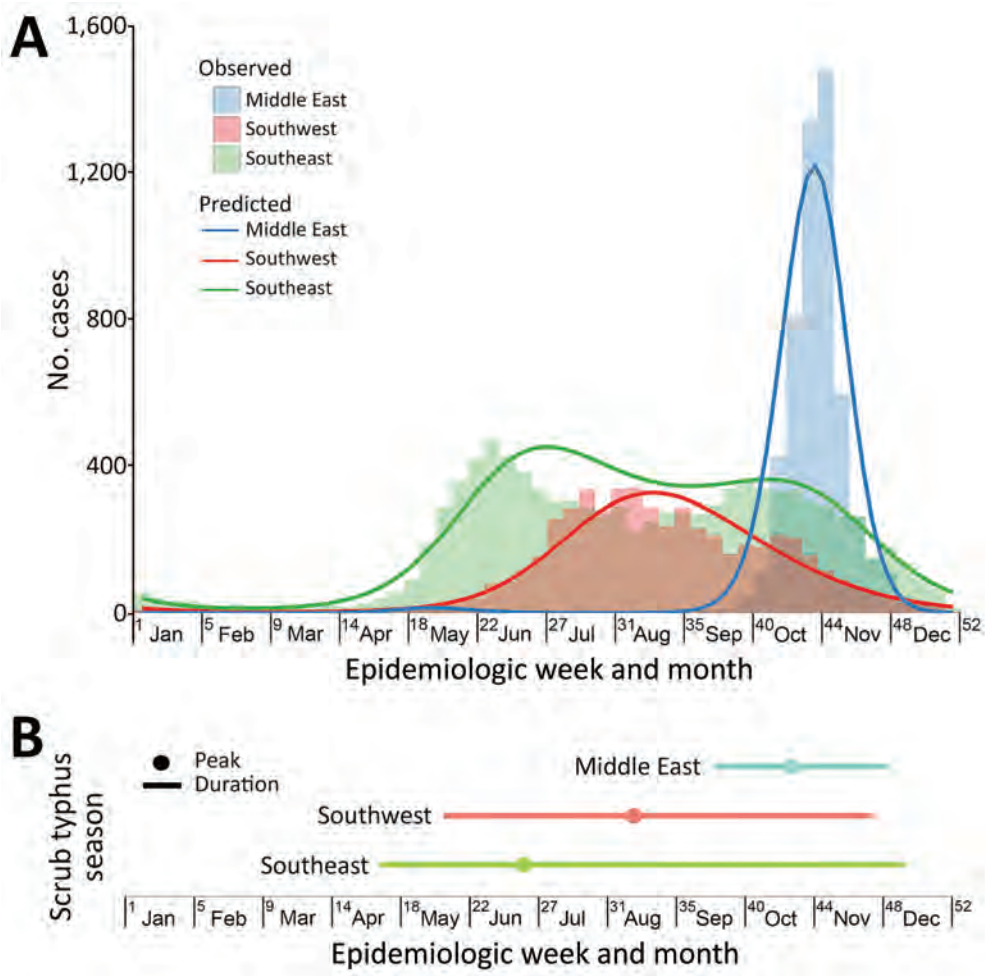

Figure 5. Seasonal characteristics of scrub typhus in China, 2006–2016. A) The weekly number of scrub typhus in year 2016, with a fitted seasonal curve superimposed, by epidemiologic regions identified. B) Duration and peak of scrub typhus seasons in epidemiologic regions. Scrub typhus season was defined as starting with the week in which a fast increase of average weekly case numbers began and ending with the week that the cumulative case numbers captured in the interval between the start and end accounted for >95% of the reported cases in 2006–2016. The colored dot in each region indicates the week with the highest predicted number of scrub typhus cases in the fitted seasonal curve (the peak). The colored bar indicates the number of weeks between season start and end (duration).

vectors, hosts, and humans, as well as climatic factors, the seasonal distribution of scrub typhus outbreaks may also vary locally; a spring outbreak of scrub typhus has occurred on an island in Fujian Province (in the southeastern coastal area) during 2000–2005 (*36*). Knowing the exact timing of scrub typhus activity at both national and subnational levels is important to healthcare providers and health officials who use this data to guide diagnostic testing, conduct disease surveillance, plan vector control measures, respond to outbreaks, and provide antimicrobial treatment to febrile patients. Travel precautions for those entering scrub typhus–endemic regions, and strategies for controlling mites, should be given before the beginning of scrub typhus season.

Because scrub typhus is a disease that is treatable with specific antimicrobial medicine, early and accurate diagnosis is essential to reduce the risk for severe complications and death. The case-fatality rate of scrub typhus in China was reduced from 13%–16% to 0.2%–0.4% after the introduction of antirickettsial drugs (*14*). However, the absence of definitive signs and symptoms make difficult the differentiation of scrub typhus from other common febrile diseases, such as murine typhus, typhoid fever, and leptospirosis. Our study reveals that, compared with diagnosis within 2 days after illness onset, diagnosis later than 8 days after the onset of illness poses a 2.36 times higher risk of death for the patient.

The immunofluorescence assay is the reference diagnostic test for scrub typhus recommended by the World Health Organization (*37*), but the need for standardization has hampered the method's widespread use. PCR assay targeting on the gene encoding the 56-kDa type-specific antigen is highly sensitive and useful (*38*,*39*) but also has limited uses because of the lack of standardized reagents or commercial diagnostic kits. Currently, the Weil-Felix test, despite its lack of sensitivity and specificity (*40*), is widely accessible throughout China, specifically in conjunction with a previous exposure history or specific eschars of scrub typhus (*41*). The finding that delayed diagnosis is associated with death highlights the need for research and development of inexpensive, accurate point-of-

Table 2. Risk factors associated with death from scrub typhus, China, 2006–2016

Factor	No. cases	No. deaths	Case-fatality ratio	Crude odds ratio (95% CI)	Adjusted odds ratio (95% CI)*
Sex					
F	49,907	22	0.04	1.00	1.00
M	43,574	35	0.08	**1.82 (1.07–3.11)**	**1.75 (1.02–3.01)**
Age group, y					
<40	25,261	9	0.04	1.00	1.00
40–59	37,660	19	0.05	1.50 (0.68–3.30)	**2.86 (1.22–6.69)**
≥60	30,560	29	0.09	**2.70 (1.27–5.72)**	**5.88 (2.55–13.55)**
Residence					
Rural	80,329	37	0.05	1.00	1.00
Urban	11,753	20	0.17	**3.31 (1.92–5.70)**	**1.89 (1.05–3.42)**
Region					
Middle-east	25,186	2	0.01	1.00	1.00
Southeast	45,043	44	0.10	**12.31 (2.98–50.79)**	**10.05 (2.41–41.86)**
Southwest	23,202	11	0.05	**5.97 (1.32–26.95)**	**9.48 (2.05–43.94)**
North and west	50	0	0	NA	NA
Occupation					
Farmer	68,116	24	0.04	1.00	1.00
Nonfarmer	25,365	33	0.13	**3.7 (2.18–6.25)**	**3.56 (1.97–6.43)**
Time from illness onset to diagnosis, d					
<2	20,775	8	0.04	1.00	1.00
2–7	42,875	22	0.05	1.33 (0.59–2.99)	1.67 (0.74–3.77)
≥8	29,831	27	0.09	**2.35 (1.07–5.18)**	**2.36 (1·07–5.19)**

*Result from multivariable logistic regression. Boldface type indicates significance (p<0.05). NA, not available.

care diagnostic tests for the acute phase of infection in clinical settings.

Our study has 3 limitations. First, we collected all study data used from a passive surveillance system and, therefore, data quality may be influenced by the availability of diagnostic technology, underreporting, and the completeness and accuracy of the data over the years. Diagnosis and notification of cases may vary across areas, affecting the geographic comparisons of incidence. Second, individual case data with demographic information were not reported from 1952–1989; therefore, we could only analyze population characteristics, case distributions, and death risk factors from the period 2006–2016. Furthermore, because scrub typhus was removed from the notifiable disease list in 1990, the lack of surveillance data during 1990–2005 limits the consecutiveness of epidemic trend analysis. Third, data on *O. tsutsugamushi* strains and on the accurate distribution of *Leptotrombidium* mite species were unavailable in this study, making it impossible for us to present the whole picture of scrub typhus in China involving human cases, pathogens, hosts, and vectors. However, data used in this study were the most comprehensive and reliable data on scrub typhus available at national and subnational levels in China; these nationwide report data demonstrate striking changes in epidemiologic features of scrub typhus in China, highlighting the need to conduct further high-quality investigations to better interpret the findings from passive surveillance data.

Among the dozens of countries with endemic scrub typhus, China is one of the few that has established a nationwide surveillance system. By using these long-term incidence data, we thoroughly described the epidemiologic change of scrub typhus over time; our findings are a starting point for further studies to explore additional information related to the global disease burden of scrub typhus. This study may also benefit other scrub typhus–endemic regions outside of China; our findings suggest the possibility of similar epidemiologic changes in areas with similar social and ecologic environments.

As a whole, after ≈40 years of low-level transmission, scrub typhus has become a markedly greater threat in China than previously understood, warranting a higher degree of scrutiny and study to inform health policy. Furthermore, the epidemiologic changes resulting from geographic expansion, demographic transition, and multiple seasonal patterns highlight the need to adjust and enhance current disease prevention and control strategies at national and subnational levels.

Acknowledgments

We acknowledge staff members of the county-, district-, and province-level Centers for Disease Control and Prevention of China for their assistance in the field investigation and data collection. We also thank Bob Thompson for his help in manuscript improvement.

This study was supported by grants from the Ministry of Science and Technology of China (2018ZX10101002, 2018ZX10713001, 2018ZX10713001, 2018ZX10713001-005, 2018ZX10101002-003-002) and Emergency Response

Mechanism Operation Program from the Chinese Center for Disease Control and Prevention (131031001000015001). S.E.R., N.D.W., and S.I.H. are primarily supported by the Bill & Melinda Gates Foundation (grant no. OPP1132415).

About the Author

Dr. Zhongjie Li is an epidemiologist at the Chinese Center for Disease Control and Prevention. His research interests include the epidemiology of infectious disease, disease surveillance, and early-warning systems on disease outbreak detection.

References

1. Walker DH. Scrub typhus—scientific neglect, ever-widening impact. N Engl J Med. 2016;375:913–5. https://doi.org/10.1056/NEJMp1608499
2. Taylor AJ, Paris DH, Newton PN. A systematic review of mortality from untreated scrub typhus (*Orientia tsutsugamushi*). PLoS Negl Trop Dis. 2015;9:e0003971. https://doi.org/10.1371/journal.pntd.0003971
3. Bonell A, Lubell Y, Newton PN, Crump JA, Paris DH. Estimating the burden of scrub typhus: a systematic review. PLoS Negl Trop Dis. 2017;11:e0005838. https://doi.org/10.1371/journal.pntd.0005838
4. Kasper MR, Blair PJ, Touch S, Sokhal B, Yasuda CY, Williams M, et al. Infectious etiologies of acute febrile illness among patients seeking health care in south-central Cambodia. Am J Trop Med Hyg. 2012;86:246–53. https://doi.org/10.4269/ajtmh.2012.11-0409
5. Blacksell SD, Sharma NP, Phumratanaprapin W, Jenjaroen K, Peacock SJ, White NJ, et al. Serological and blood culture investigations of Nepalese fever patients. Trans R Soc Trop Med Hyg. 2007;101:686–90. https://doi.org/10.1016/j.trstmh.2007.02.015
6. Mayxay M, Castonguay-Vanier J, Chansamouth V, Dubot-Pérès A, Paris DH, Phetsouvanh R, et al. Causes of non-malarial fever in Laos: a prospective study. Lancet Glob Health. 2013;1:e46–54. https://doi.org/10.1016/S2214-109X(13)70008-1
7. Paris DH, Shelite TR, Day NP, Walker DH. Unresolved problems related to scrub typhus: a seriously neglected life-threatening disease. Am J Trop Med Hyg. 2013;89:301–7. https://doi.org/10.4269/ajtmh.13-0064
8. Lee HW, Cho PY, Moon SU, Na BK, Kang YJ, Sohn Y, et al. Current situation of scrub typhus in South Korea from 2001–2013. Parasit Vectors. 2015;8:238. https://doi.org/10.1186/s13071-015-0858-6
9. Horton KC, Jiang J, Maina A, Dueger E, Zayed A, Ahmed AA, et al. Evidence of *Rickettsia* and *Orientia* infections among abattoir workers in Djibouti. Am J Trop Med Hyg. 2016;95:462–5. https://doi.org/10.4269/ajtmh.15-0775
10. Maina AN, Farris CM, Odhiambo A, Jiang J, Laktabai J, Armstrong J, et al. Q fever, scrub typhus, and rickettsial diseases in children, Kenya, 2011–2012. Emerg Infect Dis. 2016;22:883–6. https://doi.org/10.3201/eid2205.150953
11. Izzard L, Fuller A, Blacksell SD, Paris DH, Richards AL, Aukkanit N, et al. Isolation of a novel *Orientia* species (*O. chuto* sp. nov.) from a patient infected in Dubai. J Clin Microbiol. 2010;48:4404–9. https://doi.org/10.1128/JCM.01526-10
12. Weitzel T, Dittrich S, López J, Phuklia W, Martinez-Valdebenito C, Velásquez K, et al. Endemic scrub typhus in South America. N Engl J Med. 2016;375:954–61. https://doi.org/10.1056/NEJMoa1603657
13. Hay SI, Abajobir AA, Abate KH, Abbafati C, Abbas KM, Abd-Allah F, et al.; GBD 2016 DALYs and HALE Collaborators. Global, regional, and national disability-adjusted life-years (DALYs) for 333 diseases and injuries and healthy life expectancy (HALE) for 195 countries and territories, 1990–2016: a systematic analysis for the Global Burden of Disease Study 2016. Lancet. 2017;390:1260–344. https://doi.org/10.1016/S0140-6736(17)32130-X
14. Fan MY, Walker DH, Yu SR, Liu QH. Epidemiology and ecology of rickettsial diseases in the People's Republic of China. Rev Infect Dis. 1987;9:823–40. https://doi.org/10.1093/clinids/9.4.823
15. Zheng C, Jiang D, Ding F, Fu J, Hao M. Spatiotemporal patterns and risk factors for scrub typhus from 2007 to 2017 in southern China. Clin Infect Dis. 2019;69:1205–11. https://doi.org/10.1093/cid/ciy1050
16. Luo Y, Yin J. Progress in research of *Orientia tsutsugamushi* and its host and vector [in Chinese]. Disease Surveillance. 2019;(10):920–3.
17. Wang G-h, Wang C-j, Li B-j, Jiang Z-k, Ding L-yD, Wang L. General situation on studies of animal hosts of tsutsugamushi disease in China [in Chinese]. Chinese Journal of Hygienic Insecticides & Equipments. 2013;19:370–3.
18. Wu YC, Qian Q, Soares Magalhaes RJ, Han ZH, Hu WB, Haque U, et al. Spatiotemporal dynamics of scrub typhus transmission in mainland China, 2006–2014. PLoS Negl Trop Dis. 2016;10:e0004875. https://doi.org/10.1371/journal.pntd.0004875
19. Sun Y, Wei YH, Yang Y, Ma Y, de Vlas SJ, Yao HW, et al. Rapid increase of scrub typhus incidence in Guangzhou, southern China, 2006–2014. BMC Infect Dis. 2017;17:13. https://doi.org/10.1186/s12879-016-2153-3
20. Li Z, Gao GF. Infectious disease trends in China since the SARS outbreak. Lancet Infect Dis. 2017;17:1113–5. https://doi.org/10.1016/S1473-3099(17)30579-0
21. Wang L, Wang Y, Jin S, Wu Z, Chin DP, Koplan JP, et al. Emergence and control of infectious diseases in China. Lancet. 2008;372:1598–605. https://doi.org/10.1016/S0140-6736(08)61365-3
22. Chinese Center for Disease Control and Prevention. National guideline of scrub typhus control and prevention [in Chinese]. 2009 [cited 2017 Mar 16]. http://www.chinacdc.cn/tzgg/200901/t20090105_40316.html
23. National Bureau of Statistics of China. National data [in Chinese]. 2018 [cited 2020 Mar 27]. http://data.stats.gov.cn/english/index.htm
24. Kim HJ, Fay MP, Feuer EJ, Midthune DN. Permutation tests for Joinpoint regression with applications to cancer rates. Stat Med. 2000;19:335–51. https://doi.org/10.1002/(SICI)1097-0258(20000215)19:3<335::AID-SIM336>3.0.CO;2-Z
25. Yu H, Alonso WJ, Feng L, Tan Y, Shu Y, Yang W, et al. Characterization of regional influenza seasonality patterns in China and implications for vaccination strategies: spatio-temporal modeling of surveillance data. PLoS Med. 2013;10:e1001552. https://doi.org/10.1371/journal.pmed.1001552
26. Naumova EN, Jagai JS, Matyas B, DeMaria A Jr, MacNeill IB, Griffiths JK. Seasonality in six enterically transmitted diseases and ambient temperature. Epidemiol Infect. 2007;135:281–92. https://doi.org/10.1017/S0950268806006698
27. Xing W, Liao Q, Viboud C, Zhang J, Sun J, Wu JT, et al. Hand, foot, and mouth disease in China, 2008–12: an

epidemiological study. Lancet Infect Dis. 2014;14:308–18. https://doi.org/10.1016/S1473-3099(13)70342-6
28. R Core Team. R: A language and environment for statistical computing. Vienna (Austria): R Foundation for Statistical Computing; 2013.
29. Liu J, Li S, Ouyang Z, Tam C, Chen X. Ecological and socioeconomic effects of China's policies for ecosystem services. Proc Natl Acad Sci U S A. 2008;105:9477–82. https://doi.org/10.1073/pnas.0706436105
30. Tsai PJ, Yeh HC. Scrub typhus islands in the Taiwan area and the association between scrub typhus disease and forest land use and farmer population density: geographically weighted regression. BMC Infect Dis. 2013;13:191. https://doi.org/10.1186/1471-2334-13-191
31. Li T, Yang Z, Dong Z, Wang M. Meteorological factors and risk of scrub typhus in Guangzhou, southern China, 2006–2012. BMC Infect Dis. 2014;14:139. https://doi.org/10.1186/1471-2334-14-139
32. Matsui T, Kramer MH, Mendlein JM, Osaka K, Ohyama T, Takahashi H, et al. Evaluation of national tsutsugamushi disease surveillance—Japan, 2000. Jpn J Infect Dis. 2002; 55:197–203.
33. Park SW, Ha NY, Ryu B, Bang JH, Song H, Kim Y, et al. Urbanization of scrub typhus disease in South Korea. PLoS Negl Trop Dis. 2015;9:e0003814. https://doi.org/10.1371/journal.pntd.0003814
34. Yang LP, Liu J, Wang XJ, Ma W, Jia CX, Jiang BF. Effects of meteorological factors on scrub typhus in a temperate region of China. Epidemiol Infect. 2014;142:2217–26. https://doi.org/10.1017/S0950268813003208
35. Yoshikura H. Geographical distribution of Japanese spotted fever and tsutsugamushi disease in Japan—possible effect of environmental temperature. Jpn J Infect Dis. 2017;70:349–51. https://doi.org/10.7883/yoken.JJID.2016.274
36. Cao M, Guo H, Tang T, Wang C, Li X, Pan X, et al. Spring scrub typhus, People's Republic of China. Emerg Infect Dis. 2006;12:1463–5. https://doi.org/10.3201/eid1209.060257
37. Janardhanan J, Trowbridge P, Varghese GM. Diagnosis of scrub typhus. Expert Rev Anti Infect Ther. 2014;12:1533–40. https://doi.org/10.1586/14787210.2014.974559
38. Fournier PE, Siritantikorn S, Rolain JM, Suputtamongkol Y, Hoontrakul S, Charoenwat S, et al. Detection of new genotypes of *Orientia tsutsugamushi* infecting humans in Thailand. Clin Microbiol Infect. 2008;14:168–73. https://doi.org/10.1111/j.1469-0691.2007.01889.x
39. Bechah Y, Socolovschi C, Raoult D. Identification of rickettsial infections by using cutaneous swab specimens and PCR. Emerg Infect Dis. 2011;17:83–6. https://doi.org/10.3201/eid1701.100854
40. Kovácová E, Kazár J. Rickettsial diseases and their serological diagnosis. Clin Lab. 2000;46:239–45.
41. Zheng MH, Shi KQ, Chen YP. Skin lesion in a critically ill man. BMJ. 2015;351:h4570. https://doi.org/10.1136/bmj.h4570

Address for correspondence: Jianxing Yu, State Key Laboratory of Infectious Disease Prevention and Control, National Institute for Communicable Disease Control and Prevention, Chinese Center for Disease Control and Prevention, Changbai Rd 155#, Changping District, Beijing, 102206, China; email: yujianxing@icdc.cn

Pharmacologic Treatments and Supportive Care for Middle East Respiratory Syndrome

Taylor Kain, Patrick J. Lindsay, Neill K.J. Adhikari, Yaseen M. Arabi, Maria D. Van Kerkhove, Robert A. Fowler

Available animal and cell line models have suggested that specific therapeutics might be effective in treating Middle East respiratory syndrome (MERS). We conducted a systematic review of evidence for treatment with pharmacologic and supportive therapies. We developed a protocol and searched 5 databases for studies describing treatment of MERS and deaths in MERS patients. Risk of bias (RoB) was assessed by using ROBINS-I tool. We retrieved 3,660 unique citations; 20 observational studies met eligibility, and we studied 13 therapies. Most studies were at serious or critical RoB; no studies were at low RoB. One study, at moderate RoB, showed reduced mortality rates in severe MERS patients with extracorporeal membrane oxygenation; no other studies showed a significant lifesaving benefit to any treatment. The existing literature on treatments for MERS is observational and at moderate to critical RoB. Clinical trials are needed to guide treatment decisions.

Middle East respiratory syndrome (MERS), which is now known to be caused by MERS coronavirus (MERS-CoV), was first reported in September 2012 in Saudi Arabia (*1*). Since then, it has spread to 26 other countries (*2*). As of November 30, 2019, a total of 2,494 confirmed cases and 858 deaths had been reported to the World Health Organization (WHO); the case-fatality rate was 34.4% (*3*). To date, all cases have been linked to travel or residence in the Arabian Peninsula. MERS-CoV is a human betacoronavirus that is found in humans and dromedary camels and is similar to other human coronaviruses (e.g., severe acute respiratory syndrome coronavirus [SARS-CoV] and SARS-CoV-2, the cause of coronavirus disease [COVID-19]) (*4*). Infected patients generally have fever, cough, dyspnea, and abnormal chest imaging (*5*). Many patients have onset of respiratory failure and require noninvasive ventilation (NIV) or invasive mechanical ventilation; advanced supportive care techniques, such as extracorporeal membrane oxygenation (ECMO), have been used. Most of these patients are cared for in an intensive care unit (ICU).

No vaccination against MERS-CoV infection exists, and WHO and the US Centers for Disease Control and Prevention (CDC) recommend general infection prevention measures when caring for patients (*1*,*6*). As with other coronaviruses, no evidence-based recommended pharmacologic therapy for the treatment of MERS-CoV infection exists; however, limited data from available animal and cell line models have led to multiple different combinations of antiviral drugs and other adjunctive therapies to be proposed and used in humans (*7*,*8*). We conducted a systematic review to summarize the current evidence base for treatment of MERS, including specific treatments against MERS, adjunctive pharmacologic therapies, and supportive care.

Methods

Literature Search and Selection Criteria

We developed a protocol that considered the Preferred Reporting Items for Systematic Reviews and Meta-Analyses checklist (*9*), which was registered with the International Prospective Register of Systematic Reviews (reference no. CRD42018114622). We searched for relevant studies in 5 databases (MEDLINE, PubMed, Embase, Cochrane, and Cumulative Index to Nursing and Allied Health Literature) in August 2018 and updated the results in October 2019

Author affiliations: University of Toronto, Toronto, Ontario, Canada (T. Kain, P.J. Lindsay, N.K.J. Adhikari, R.A. Fowler); Harvard University, Boston, Massachusetts, USA (P.J. Lindsay); Sunnybrook Health Sciences Center, Toronto (N.K.J. Adhikari, R.A. Fowler); King Saud Bin Abdulaziz University for Health Center, Riyadh, Saudi Arabia (Y.M. Arabi); King Abdullah International Medical Research Center, Riyadh (Y.M. Arabi); World Health Organization, Geneva, Switzerland (M.D. Van Kerkhove)

DOI: https://doi.org/10.3201/eid2606.200037

(Appendix Figure, https://wwwnc.cdc.gov/EID/article/26/6/20-0037-App1.pdf). We imposed no language restrictions. We also searched reference lists of studies included in the review, as well as ClinicalTrials.gov for any ongoing or completed trials.

We imported all abstracts into Covidence (Veritas Health Innovation, https://www.covidence.org) for review. After we removed duplicates, 2 authors (T.K. and P.L.) independently and in duplicate screened titles and abstracts of references generated from the literature search. The population studied was patients of any age admitted to a hospital with laboratory-confirmed MERS. We included studies with ≥5 cases in patients who received a therapy targeting MERS or that examined supportive care for MERS. Specific and supportive care therapies included, but were not limited to, antiviral drugs, immunomodulatory medications (e.g., corticosteroids), antibody-based pharmaceuticals, and alternative oxygen-delivery therapies (e.g., ECMO and NIV). We included studies that reported our primary outcome of interest, death at any point of illness. We also recorded information regarding secondary outcomes where available, including hospital length of stay, ICU length of stay, mechanical ventilation days, and adverse events. Eligible studies included randomized controlled trials (RCTs), nonrandomized single-arm intervention studies (with or without a control group), prospective and retrospective cohort studies, and case series. We used the term "cohort studies" to describe those in which an association between an exposure and outcome was reported for an eligibility criteria–defined complete group of consecutive patients, and only if the exposure was relevant to this review. If exposure was not relevant, then we reclassified the study as a case series. We intended to only include studies with a comparator or control group, but because of the varying quality of papers retrieved, we deviated from our original methodologic plan and included any study describing patients given a treatment of interest, even if no specific control group was available. We excluded all preclinical studies (i.e., those performed on animals or human cell lines).

Two review authors (T.K. and P.L.) compared screening results and discussed differences. Any disagreement on eligibility was resolved through consensus with 2 other authors (R.A.F., N.K.J.A.). We constructed a PRISMA diagram of the included studies (Figure).

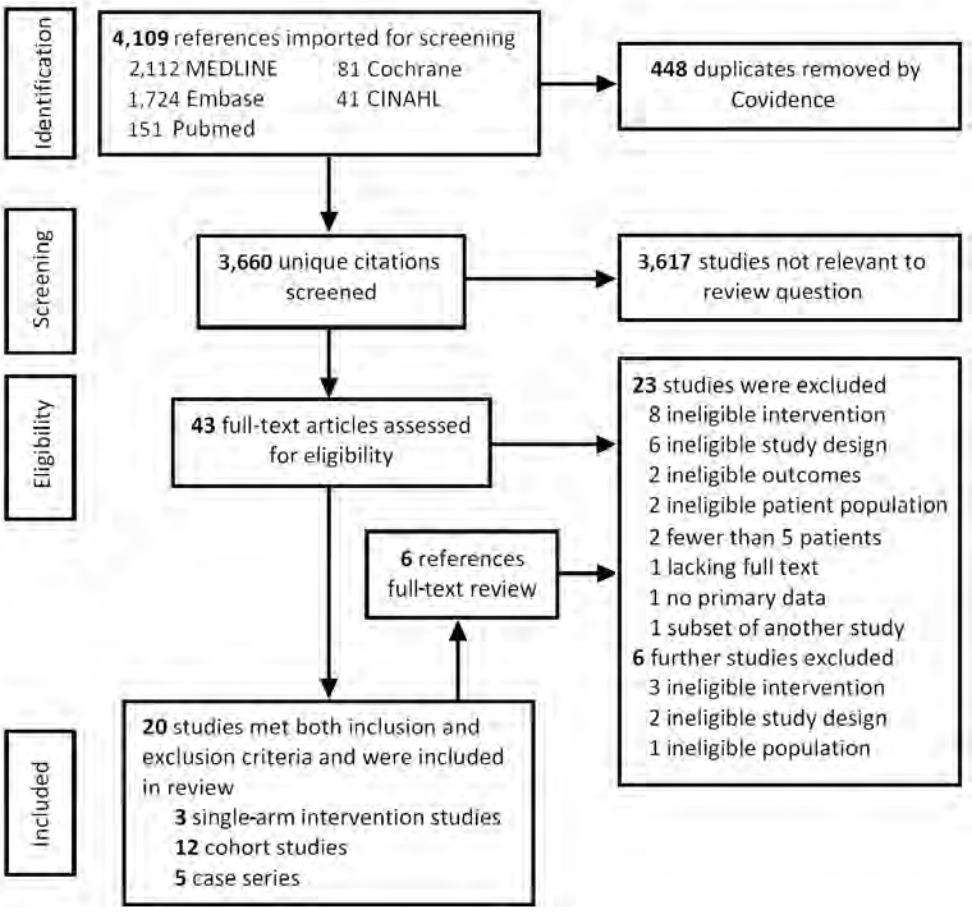

Figure. Preferred Reporting Items for Systematic Reviews and Meta-Analyses diagram of literature search results, screening performed, and reasons for exclusion of full text reviews from a systematic review of evidence for MERS treatment with pharmacologic and supportive therapies. CINAHL, Cumulative Index to Nursing and Allied Health Literature.

Data Extraction

For each included study, 2 authors (T.K. and P.L.) independently and in duplicate extracted data, including publication year, location of study, patient location (e.g., ICU or ward), dates of subject enrollment, study design, baseline characteristics (e.g., age and underlying conditions), study interventions and co-interventions, and clinical outcomes of interest (including death). Given the small pool of patients, we observed a substantial overlap in patients reported among the studies; therefore, we estimated the number of unique patients among all studies, attempting to contact primary authors for clarification when needed.

Quality Assessment and Statistical Analysis

Two authors (T.K. and P.L.) assessed the risk of bias (RoB) by using the ROBINS-I tool for nonrandomized intervention and cohort studies (*10*). Other authors (R.A.F. and N.K.J.A.) verified selected methodologic details of these studies. We did not assess the methodologic quality of case series in the absence of a validated tool. We assessed the overall certainty of evidence by using the GRADE framework (*11*), considering RoB, inconsistency, imprecision, and publication bias of trials.

Results

Search Results

We retrieved 4,108 citations, of which 448 were duplicates, leaving 3,660 unique citations; we determined that 3,167 were not relevant. After full-text screening the remaining 43 studies, we found 20 that met eligibility criteria (Figure): 3 nonrandomized single-arm intervention studies (*12*–*14*), 12 prospective and retrospective cohort studies (*15*–*26*), and 5 case series with ≥5 patients (*27*–*31*). We then reviewed the references of these papers; an additional 6 papers underwent full review, but none met eligibility. No RCTs had been completed at the time of review.

The included studies enrolled patients during September 2012–March 2018. We estimated the number of unique patients among studies to be 678–865, representing 31%–40% of the 2,189 patients with MERS during that period (*32*). The diversity of different specific therapies studied and the substantial overlap in patients among studies precluded formal meta-analyses.

Patient and Study Characteristics

Of the 20 included studies, 19 were conducted in Saudi Arabia; 1 was conducted in South Korea during the 2015 outbreak (Table 1). During the trials, the median or mean age of patients was 45–66 years (Table 2). Many had >1 underlying condition; diabetes and chronic kidney disease were the most common. Mortality rates in studies were high, ranging from 20% to 100%. An overall mortality rate could not be accurately calculated because of the substantial overlap in patients included in multiple studies.

Specific Treatments

These 20 studies collectively examined 11 different pharmaceutical treatments for MERS: 6 antiviral drugs, 2 antibody-mediated therapies, 2 immunomodulatory medications, and 1 antibiotic with possible immunomodulatory effects (*33*) (Appendix Table 1). The studies also examined 2 specific methods of supportive care: NIV and ECMO (Appendix Table 2). Narrative description of studies based on intervention and effect on primary outcome is shown in Table 3. No studies included data on secondary outcomes by treatment provided, and so only mortality rate is described in this report. RoB is shown for all studies in Table 4. Unless otherwise specified, all comparisons described are between patients who received a treatment versus patients who did not (controls).

Specific Antiviral Drugs

Four types of antiviral drugs were used for treatment of MERS in the 20 included studies: lopinavir/ritonavir, oseltamivir, ribavirin, and interferons (α2a, α2b, and β1a). Lopinavir/ritonavir was only used in a single study (*15*), and all patients were treated with the combination, so the effect on the mortality rate could not be elucidated. Oseltamivir was used in most the studies, probably as empiric treatment for influenza. Outcome data were only reported from a single study (*18*) in which authors reported no difference in the crude 90-day mortality rate for patients treated with oseltamivir (112/177 [63%] vs. 105/213 [49%]; p = 0.31).

Ribavirin

Outcome data for ribavirin were available in 7 studies (*14*,*18*–*22*,*26*); 3 smaller studies (*18*,*19*,*21*) overlapped with other patient datasets, so we abstracted outcomes from a subsequent larger study (*26*). The effect of ribavirin combined with interferon (IFN) on the mortality rate, as studied by Arabi et al. (*26*) and Omrani et al. (*14*), is described separately. In a retrospective cohort study, Al Ghamdi et al. (*22*) found no association of ribavirin treatment with the crude mortality rate (6/19 [32%] vs. 13/32 [41%]; p = 0.56). Multivariate logistic regression indicated no

Table 1. Demographic information and main intervention (where applicable) for studies included in a systematic review of evidence for MERS treatment with pharmacologic and supportive therapies, by type of study*

Reference	Location (no. centers)	Study period	No. patients	Intervention group	Comparator group	Primary outcome
Nonrandomized, single-arm intervention study with historical comparisons						
(*12*)	Jeddah, Saudi Arabia (1)	April–June 2014	32	IFN-β1a (May–Jun); 11 patients	IFN-α2a (Apr); 13 patients	Mortality rate (unspecified)
(*13*)	Saudi Arabia (5)	Sept 2012–Dec 2015	35	ECMO; 17 patients	No ECMO 18 patients	90-d mortality rate
(*14*)	Riyadh, Saudi Arabia (1)	Oct 2012–May 2014	70 (44 included)	RBV/IFN-α2a; 20 patients	Supportive care 24 patients	14-d and 28-d mortality rate
Prospective cohort study						
(*15*)	Seoul, South Korea (3)	May–July 2015	30	NA	NA	NA
(*16*)	Jedda, Saudi Arabia (1)	Mar–Jun 2014	8	NA	NA	NA
Retrospective cohort study						
(*17*)	Saudi Arabia (14)	Sept 2012–Oct 2015	309	Steroids; 151 patients	No steroids 157 patients	90-d all-cause mortality rate
(*18*)	Saudi Arabia (14)	Sept 2012–Oct 2015	330 MERS	MERS	Non-MERS SARI	90-d mortality rate
(*19*)	Riyadh, Saudi Arabia (1)	Oct 2012–May 2014	70 (31 included)	NA	NA	NA
(*20*)	Al-Madinah City, Saudi Arabia (2)	Mar–May 2014	29	NA	NA	NA
(*21*)	Jeddah, Saudi Arabia (1)	April–May 2014	14	NA	NA	Survival at 1 y
(*22*)	Jedda, Saudi Arabia (1)	Jan–Dec 2014	51	NA	NA	NA
(*23*)	Riyadh, Saudi Arabia (1)	April 2014–Mar 2018	314	NA	NA	Mortality rate (unspecified)
(*24*)	Saudi Arabia (14)	Sept 2012–Jan 2018	349	Macrolides	No macrolides	90-d mortality rate
(*25*)	Saudi Arabia (14)	Sept 2012–Oct 2015	302	NIV	Invasive ventilation	90-d mortality rate
(*26*)	Saudi Arabia (14)	Sept 2012–Jan 2018	349	RBVIFN	No RBV/IFN	90-d mortality rate
Case series without evaluation of treatments						
(*27*)	Al-Hasa, Saudi Arabia (1)	April–May 2013	5	NA	NA	NA
(*28*)	Riyadh, Saudi Arabia (1)	Dec 2012–Aug 2013	11	NA	NA	NA
(*29*)	Al-Hasa, Saudi Arabia (1)	April 2012–Nov 2016	107	NA	NA	NA
(*30*)	Riyadh, Saudi Arabia (1)	Before Oct 2014	6	NA	NA	NA
(*31*)	Riyadh, Saudi Arabia (1)	July–Oct 2015	63 (8 included)	NA	NA	NA

*ECMO, extracorporeal membrane oxygenation; IFN, interferon; MERS, Middle East respiratory syndrome; NA, not applicable; NIV, noninvasive ventilation; NS, nonsurvivors; RBV, ribavirin; SARI, severe acute respiratory infection.

association of ribavirin treatment with the mortality rate (adjusted odds ratio [aOR] 0.66, 95% CI 0.04–12.36; p = 0.78). This study was at serious RoB because of residual confounding and small sample size.

Sherbini et al. (*20*) found no difference in the mortality rate for patients treated with ribavirin (3/10 [30%] vs. 7/19 [37%]; p = 1.0). This study was at critical RoB because of unmeasured and uncontrolled confounding. Another study (*15*) used ribavirin in all patients, precluding determination of a treatment effect, whereas a final study (*23*) found that ribavirin was not associated with the mortality rate in the patient cohort studied, but no additional data were provided.

IFN

Outcomes data for treatment with IFN were available for 8 studies (*12*,*14*,*18*–*22*,*26*); 3 smaller studies (*18*,*19*,*21*) overlapped with other datasets, so we abstracted outcomes from a subsequent larger study (*26*). In a retrospective cohort study, Arabi et al. (*26*) studied the effect of ribavirin and IFN on the 90-day mortality rate in patients with MERS; 144/349 patients (41%) were treated with ribavirin/IFN (58% IFN-α2a, 17% IFN-α2b, and 27% IFN-β1a). No information was available on the mortality rate for each type of IFN. The crude mortality rate was higher in patients treated with ribavirin/IFN (106/144 [74%] vs. 126/205 [62%]; p = 0.02). However, after adjustment for time-varying confounders, ribavirin/IFN treatment was not associated with the 90-day mortality rate (aOR 1.03, 95% CI 0.73–1.44; p = 0.87) or clearance of MERS-CoV RNA (adjusted hazard ratio [aHR] 0.65, 95% CI 0.3–1.44; p = 0.29). This study was at moderate overall RoB.

In a nonrandomized single-arm intervention study, Shalhoub et al. (*12*) compared IFN-α2a with IFN-β1a, where all patients were co-treated with ribavirin. No difference was observed in the unadjusted mortality rate (11/13 [85%] vs. 7/11 [64%]; p = 0.24),

Table 2. Underlying conditions, age of study populations, overall mortality rates, and mortality rates by intervention (where applicable) for studies included in a systematic review of evidence for MERS treatment with pharmacologic and supportive therapies, by type of study*

		Underlying conditions				Mortality rate		
Reference	Age, y	≥1	Diabetes mellitus	CKD	Intervention	Intervention	Comparison	Total
Nonrandomized, single-arm intervention study with historical comparisons								
(*12*)	66 (median)	NR	15 (47%)	16 (50%) 6 (19%) on dialysis	IFN-β1a vs IFN-α2a	64% IFN-β1a	85% IFN-α2a	69%
(*13*)	46 (median ECMO); 50 (median no ECMO)	NR	18 (51%)	5 (14%)	ECMO	65%	100%	83%
(*14*)	66 y (mean)	NR	30 (68%)	11 (26%)	RBV + IFN-α2a	14d: 30%; 28d: 70%	14d: 71%,28d: 83%	52% at 14 d; 77% at 28 d
Prospective cohort study								
(*15*)	49 (mean)	11 (47%)	4 (13%) NS 1 (25%)	1 (3%) NS 0 (0%)	NA	NA	NA	20%
(*16*)	57 (median)	NR	5 (63%)	NR	NA	NA	NA	75%
Retrospective cohort study								
(*17*)	58 (mean steroids); 55 (mean no steroids)	132 (87%) steroids 115 (73%) no steroids	87 (58%) steroids 69 (44%) no steroids	43 (29%) steroids 47 (30%) no steroids	Steroids	90-d 74% Hospital 78%	58% 90-d Hospital 58%	66%
(*18*)	58 (median)	265 (80%) NS 199 (75%)	162 (49%) NS 124 (77%)	100 (30%) NS 80 (80%)	MERS vs non-MERS SARI	66%	31%	NA
(*19*)	59 (median)	NR	17 (55%) NS 13 (77%)	6 (19%) NS 4 (75%)	NA	NA	NA	70%
(*20*)	45 (median)	NR	9 (31%) NS 7 (78%)	8 (28%) NS 8 (100%)	NA	NA	NA	35%
(*21*)	54 (median)	12 (86%)	6 (43%)	6 (42%) 3 (21%) on dialysis	NA	NA	NA	64% 90 d, 43% 28 d
(*22*)	54 (median)	36 (71%)	17 (33%) NS 8 (47%)	14 (28%) had ESRD NS 8 (57%)	NA	NA	NA	37%
(*23*)	48 (mean)	NR	NR	NR	NA	NA	NA	25%
(*24*)	56 (median macrolides); 58 (median no macrolides)	106 (78%) vs. 175 (82%)	72 (53%) vs. 98 (46%)	41 (30%) vs. 68 (32%)	Macrolides	60%	70%	66%
(*25*)	60 (median NIV); 58 (median IMV)	88 (84%) vs. 164 (83%)	62 (59%) vs. 95 (48%)	31 (30%) vs. 68 (35%)	NIV	69%	76%	73%
(*26*)	58 (median RBV/IFN); 58 (no RBV/IFN)	121 (84%) vs. 160 (78%)	84 (58%) vs. 86 (42%)	53 (37%) vs. 56 (27%)	RBVIFN	74%	62%	66%
Case series without evaluation of treatment								
(*27*)	58 (mean)	5 (100%)	4 (80%)	5 (100%)	NA	NA	NA	100%
(*28*)	59 (median)	NR	8 (67%)	5 (42%)	NA	NA	NA	58% at 90 d, 42% at 28 d
(*29*)	57 vs 52 (median)	NR	52 (49%)	21 (20%)	NA	39%	54%	51%
(*30*)	59 (mean)	3 (50%)	0 (0%)	0 (0%)	NA	NA	NA	60%
(*31*)	58 (mean)	NR	NR	NR	NA	NA	NA	63% (0% in included patients)

*CKD, chronic kidney disease; ESRD, end-stage renal disease; HCW, health-care workers; IFN, interferon; IMV, invasive mechanical ventilation; MERS, Middle East respiratory syndrome; NIV, noninvasive ventilation; NR, not reported; NS, nonsurvivors; NA, not applicable; RBV, ribavirin; SARI, severe acute respiratory infection.

or adjusted mortality rate using multivariable models (aOR [IFN-α] 0.16, 95% CI 0.02–1.38; p = 0.09; aOR [IFN-β] 0.28, 95% CI 0.03–2.33, p = 0.24). This study is at serious RoB because of uncontrolled confounding and selection bias, as well as exclusion of patients crossing over from 1 treatment to another.

In a nonrandomized single-arm intervention study, Omrani et al. (*14*) compared ribavirin/IFN-α2a with supportive care, finding a significantly lower crude 14-day mortality rate for ribavirin/IFN-α2a (6/20 [30%] vs. 17/24 [71%]; p = 0.04) but not a significantly lower crude 28-day mortality rate (14/20 [70%] vs. 20/24 [83%]; p = 0.054). The study was at serious RoB because of selection of patients and unmeasured confounding.

Al Ghamdi et al. (*22*) performed a retrospective cohort study in which 8 patients were treated with IFN-α and 23 patients with IFN-β. They found no association between IFN-α and the crude mortality rate (2/8 [25%] vs. 17/43 [40%]; p = 0.69), but they observed an increase in the crude mortality rate in patients treated with IFN-β (5/23 [22%] vs. 14/28 [50%]; p = 0.05). However, multivariable logistic regression adjusting for severity of illness found no association between IFN-α or IFN-β and the mortality rate (aOR [IFN-α] 0.47, 95% CI 0.02–10.4; p = 0.63; aOR [IFNβ] 0.68, 95% CI 0.04–10.3; p = 0.78). This study had a serious RoB because of the high likelihood of residual confounding and small sample size.

In a retrospective cohort study, Sherbini et al. (*20*) found no difference in the mortality rate among patients treated with IFN (6/19 [32%] vs. 4/10 [40%]; p = 0.7). This study was at critical risk for bias because of unmeasured and uncontrolled confounding. Another study (*15*) used IFN-α2a in all patients in the cohort, whereas a final study (*23*) stated that IFN was not associated with the mortality rate, but no additional data were provided.

Immunomodulatory Medications

Corticosteroids

Eight studies reported outcomes for patients treated with corticosteroids of varying amounts and types (*15*,*17*–*23*); 3 studies (*18*,*19*,*21*) were subsets of another larger study (*17*). In a retrospective cohort study, Arabi et al. (*17*) found that patients who received corticosteroids had a higher crude 90-day mortality rate (112/151 [74%] vs. 91/158 [58%]; p = 0.002). However, by using marginal structural modeling to account for time-varying confounders, they found that corticosteroid therapy was not associated with the 90-day mortality rate (aOR 0.75, 95% CI 0.52–1.07; p = 0.12) and was associated with longer time to MERS-CoV RNA clearance (aHR 0.35, 95% CI 0.17–0.72; p = 0.005). This study was at moderate RoB because it used modeling techniques to control for known confounders.

In a retrospective cohort study, Al Ghamdi et al. (*22*) reported no association between the mortality rate and treatment with hydrocortisone (2/5 [40%] vs. 17/46 [37%]; p = 0.35). They also found no association when adjusting for severity of illness (aOR 2.92, 95% CI 0.1–63.6; p = 0.5). This study was at serious RoB because of a high likelihood of residual confounding. In a prospective cohort study, Hong et al. (*15*) reported on 30 patients with MERS in South Korea. Only 1 patient was treated with corticosteroids, and no association with the mortality rate was observed (1/1 [100%] vs. 5/29 [17%]; p = 0.2). This study was at critical RoB because of unmeasured confounders and bias in participant selection.

In a retrospective cohort study, Alfaraj et al. (*23*) reported that corticosteroids were associated with an increased mortality rate (aOR 3.84, 95% CI 1.95–7.57; p<0.0001), but no further details were provided. Lack of information prevented scoring for all domains of bias, but the paper was judged to be at critical RoB overall because of its uncontrolled design and unmeasured confounding. In a study by Sherbini et al. (*20*), no outcome data could be assessed because all patients were treated with corticosteroids.

Macrolides

Mortality rates for patients treated with macrolide therapy were described in 2 studies (*20*,*24*), but 1 study (*20*) was a subset of the other (*24*). In a retrospective cohort study, Arabi et al. (*24*) examined the association of macrolide therapy with the 90-day mortality rate by using multivariable logistic regression and on MERS-CoV RNA plasma clearance by using a Cox proportional hazards model. Macrolide therapy was not independently associated with the mortality rate (aOR 0.84, 95% CI 0.47–1.51; p = 0.56) or RNA clearance (aHR 0.88, 95% CI 0.47–1.64; p = 0.68). This study was at moderate overall RoB given the use of regression models to attempt to account for confounding.

Mycophenolate Mofetil

Mycophenolate mofetil was only used in a single study by Al Ghamdi et al. (*22*) and was associated with a decrease in the crude mortality rate (0/8 [0%] vs. 19/43 [44%]; p = 0.02). Mycophenolate mofetil could not be evaluated in a multivariable model because all patients survived. This study was at serious RoB because of the high likelihood of residual confounding.

Table 3. Narrative summary of treatments for MERS in humans, based on a systematic review of evidence for MERS treatment with pharmacologic and supportive therapies*

Reference	Patients treated, no.	Study type	Specifics of intervention or analysis	RoB	Outcome†	Certainty of evidence
Ribavirin						
(*22*)	19	Retrospective cohort study	Multivariate logistic regression	Serious	aOR 0.66, 95% CI 0.04–12.36, p = 0.78	Very low evidence; no benefit
(*20*)	10	Retrospective cohort study	Unadjusted	Critical	3/10 (30%) vs. 7/19 (37%), p = 1.0	
Interferons: IFN-α2a, IFN-α2b, INF-β1a						
(*12*)	13 (IFN-α2a); 11 (IFN-β1a)	Nonrandomized single-arm intervention	IFN-α2a vs IFN-β1a; all co-treated with RBV; unadjusted	Serious	aOR (IFN-α) 0.16, 95% CI 0.02–1.38, p = 0.09; aOR (IFN-β) 0.28, 95% CI 0.03–2.33, p = 0.24	Very low evidence; no benefit of IFN-α2a or IFN-β1a
(*22*)	8 (IFN-α); 23 (IFN-β)	Retrospective cohort	Multivariate logistic regression	Serious	aOR 0.47, 95% CI 0.02–10.4, p = 0.63 (IFN-α); aOR 0.68, 95% CI 0.04–10.3, p = 0.78 (IFN-β)	
(*20*)	19	Retrospective cohort	Unadjusted	Critical	6/19 (32%) vs. 4/10 (40%), p = 0.70	
Ribavirin and IFN						
(*26*)	144	Retrospective cohort	Cox-proportional hazards model Marginal structural model	Moderate	aHR 1.52, 95% CI 1.13–2.06, p = 0.006; aOR 1.03, 95% CI 0.73–1.44, p = 0.87	Low evidence no benefit; very low evidence harm
(*14*)	20	Nonrandomized single-arm intervention	Unadjusted	Serious	14d: 6/20 (30%) vs. 17/24 (71%), p = 0.04; 28d: 14/20 (70%) vs. 20/24 (83%), p = 0.05	
Corticosteroids						
(*17*)	151	Retrospective cohort	Marginal structural model	Moderate	aOR (mortality rate) 0.75; 95% CI 0.52–1.07, p = 0.12; aHR (RNA clearance) 0.35; 95% CI 0.17–0.72, p = 0.005	Low evidence no benefit; very low evidence harm
(*22*)	5	Retrospective cohort	Multivariate logistic regression	Serious	aOR 2.92, 95% CI 0.1–63.6, p = 0.5	
(*15*)	1	Prospective cohort	Unadjusted	Critical	0/24 (0%) vs. 1/6 (17%), p = 0.2	
(*23*)	NI	Retrospective cohort	Multivariate logistic regression Paper lacking data	Critical	aOR 3.84, 95% CI 1.95–7.57, p<0.0001	
Macrolide therapy						
(*24*)	136	Retrospective cohort	Multivariate logistic regression Cox-proportional hazards model	Moderate	aOR (mortality rate) 0.84, 95% CI 0.47–1.51, p = 0.56; aHR (RNA clearance) 0.88, 95% CI 0.47–1.64, p = 0.68	Low evidence no benefit
Mycophenolate mofetil						
(*22*)	8	Retrospective cohort	Unadjusted	Serious	8/8 (100%) vs. 0/19 (0%), p = 0.02	Very low evidence of benefit
IVIG						
(*18*)	23	Retrospective cohort	Unadjusted	Moderate	7/113 (6%) vs. 16/217 (7%), p = 0.7	Very low evidence of harm
(*15*)	3	Prospective cohort	Unadjusted	Critical	3/6 (50%) vs. 0/2 (0%), p = 0.005	
Convalescent plasma						
(*16*)	2	Retrospective cohort	Unadjusted	Critical	1/24 (4%) vs. 1/6 (17%), p = 0.37	Very low evidence no benefit
Extracorporeal membrane oxygenation						
(*13*)	17	Nonrandomized single-arm intervention	Unadjusted	Moderate	11/17 (65%) vs. 18/18 (100%), p = 0.02	Low evidence of benefit
(*15*)	2	Retrospective cohort	Unadjusted	Critical	1/24 (4%) vs. 1/6 (17%), p = 0.4	
Noninvasive ventilation						
(*25*)	105	Retrospective cohort	Multivariate logistic regression	Moderate	aOR 0.61, 95% CI 0.23–1.6, p = 0.27	Low evidence no benefit

*Narrative description was decided through consensus among authors based on RoB, type of study, and numbers of patients treated. aHR, adjusted hazard ratio; aOR; adjusted odds ratio; IFN, interferon; IVIg, intravenous immunoglobulin; NI, no information; RoB, risk of bias.
†Percentages in parentheses indicate mortality rates.

Antibody-Mediated Pharmaceuticals

Intravenous Immunoglobulin and Convalescent Plasma

Mortality rates for patients treated with intravenous immunoglobulin (IVIg) were reported in 2 studies (*15*,*18*). One retrospective cohort study (*18*) at moderate RoB reported no association between IVIg and the mortality rate (16/23 [70%] vs. 201/307 [65%]; p = 0.69). Another study (*15*) at critical RoB reported a significant increase in the mortality rate in patients treated with IVIg (3/3 [100%] vs. 3/27 [11%]; p = 0.005). A single study (*15*) at critical RoB reported no association between treatment with convalescent plasma and the mortality rate (1/2 patients [50%] vs. 5/28 [18%]; p = 0.37).

Supportive Care

ECMO

Six studies reported outcome data for treatment of MERS with ECMO (*13*,*15*,*16*,*18*,*19*,*22*). One study (*13*) looking specifically at ECMO provided more detailed information and captured all ECMO-treated patients included in 4 other studies (*16*,*18*,*19*,*22*). In a nonrandomized, single-arm intervention study, Alshahrani et al. (*13*) reported a lower mortality rate among patients treated with ECMO versus supportive care (11/17 [65%] vs. 18/18 [100%]; p = 0.02). The study attempted to control for bias by identifying patients in the pre-ECMO period who would have been eligible for ECMO if available. The study was still at moderate overall RoB because of unmeasured and unknown confounding. Hong et al. (*15*) found no association between ECMO and the mortality rate at any time point (1/2 [50%] vs. 5/28 [4%]; p = 0.4); however, this study was at critical RoB.

NIV

Three studies reported mortality rates for MERS patients treated with NIV (*18*,*19*,*25*), but 2 studies (*18*,*19*) were subsets of another study (*25*). In a retrospective cohort study, Alraddadi et al. (*25*) reviewed the cases of patients who were initially managed with NIV (105/302 [35%]) compared with those managed with invasive ventilation alone. Most (92%) of the NIV group required invasive mechanical ventilation. NIV was not independently associated with the 90-day mortality rate (aOR 0.61, 95% CI 0.23–1.6; p = 0.27). This study was at moderate overall RoB because it used propensity scores to adjust for known confounders.

Case Series

No meaningful outcome data based on specific treatments or supportive care could be derived from any of the case series. This lack of data was attributable to inadequate reported information or

Table 4. Summary of RoB for all single-arm intervention and cohort studies calculated using the ROBBINS-I tool in a systematic review of evidence for MERS treatment with pharmacologic and supportive therapies*

	Reason for RoB determination							
Reference	Confounding	Selection of participants	Classification of interventions	Deviations from intended interventions	Missing outcome data	Outcome measurements	Selection of results reported	Overall RoB
Nonrandomized, single-arm intervention study with historical comparisons								
(*12*)	Serious	Low	Low	Low	Moderate	Low	Moderate	Serious
(*13*)	Moderate	Moderate	Moderate	Moderate	Low	Low	Moderate	Moderate
(*14*)	Serious	Low	Low	Moderate	Low	Low	Moderate	Serious
Prospective cohort study								
(*15*)	Critical	Moderate	Low	Moderate	Low	Low	Moderate	Critical
(*16*)	Serious	Low	Moderate	Moderate	Low	Low	Moderate	Serious
Retrospective cohort study								
(*17*)	Moderate	Low	Low	Moderate	Low	Low	Moderate	Moderate
(*18*)	Moderate	Low	Low	Moderate	Low	Low	Moderate	Moderate
(*19*)	Critical	Serious	Moderate	Moderate	Low	Low	Moderate	Critical
(*20*)	Critical	Moderate	Moderate	Moderate	Low	Low	Moderate	Critical
(*21*)	Critical	Moderate	Moderate	Moderate	Low	Low	Moderate	Critical
(*22*)	Serious	Moderate	Moderate	Moderate	Low	Low	Moderate	Serious
(*23*)	Critical	Serious	Serious	NI	NI	Low	Serious	Critical
(*24*)	Moderate	Low	Low	Low	Low	Low	Moderate	Moderate
(*25*)	Moderate	Moderate	Low	Moderate	Low	Low	Moderate	Moderate
(*26*)	Moderate	Low	Low	Moderate	Low	Low	Moderate	Moderate
Case series without evaluation of treatments								
(*27*)	NA	NA	NA	NA	NA	NA	NA	NA
(*28*)	NA	NA	NA	NA	NA	NA	NA	NA
(*29*)	NA	NA	NA	NA	NA	NA	NA	NA
(*30*)	NA	NA	NA	NA	NA	NA	NA	NA
(*31*)	NA	NA	NA	NA	NA	NA	NA	NA

*NA, not applicable; NI, no information; RoB, risk of bias.

because all patients in the case series were treated with identical therapies.

Overall Certainty of Evidence

In terms of assessing MERS patient mortality rates, the certainty of evidence is low or very low because all 20 studies had at least moderate RoB and because of the imprecision of estimates of treatment effect. We did not downgrade for inconsistency because meta-analyses were not possible and statistical heterogeneity could not be assessed. Studies generally had appropriate inclusion criteria for MERS patients and therefore provided direct evidence. We found no evidence that might suggest publication bias.

Discussion

In this systematic review we identified 3 nonrandomized single-arm intervention studies, 12 cohort studies, and 5 case series evaluating specific treatments and supportive care for MERS patients. Most studies were at serious or critical RoB because of confounding and selection bias.

Low-quality evidence suggests no benefit from corticosteroids or combination of ribavirin with any type of IFN but also very low evidence of harm. Low-quality evidence from a single study suggests no benefit from macrolide therapy. Low-quality evidence indicated a benefit from ECMO for severe MERS cases from a single study. Low-quality evidence suggests no benefit from NIV. All other treatments assessed had very low-quality of evidence. On the basis of this review, no specific pharmacologic therapies have sufficient evidence of effectiveness to warrant a treatment recommendation, although ECMO might be considered for severe MERS.

Our study has several strengths, including a broad review of the published literature, assessment of RoB according to the Cochrane framework, and duplicate independent data extraction. Although ours is not the first systematic review of treatment for MERS, we report on a large number of patients (*34*,*35*). We estimate the number of unique cases to be ≈678–865. Our study also specifically evaluated both pharmacologic treatments and supportive care for MERS.

Our study has limitations. We are limited in any inferences we can draw from these reviewed studies because of substantial RoB and low-quality of evidence in most publications. Few studies evaluating a single intervention, the substantial heterogeneity in study populations and design, and overlap in patient populations precluded meta-analyses. Assessing the effect of pharmaceutical interventions is challenging because of the substantial heterogeneity in timing and dose of treatments administered. Also, many studies had no contemporaneous similar comparator group, and most were retrospective in nature. Overall, the quality of evidence bearing on any individual treatment we reviewed was very low to low, owing to RoB and the imprecision of included studies. Ongoing research might provide additional rigorous data on specific treatments (e.g., the MIRACLE trial, an RCT of lopinavir/ritonavir and IFN-β1b [https://clinicaltrials.gov/ct2/show/NCT02845843]).

Several treatment options in earlier phases of clinical study were not within the scope of this systematic review and did not meet inclusion criteria for our study but are worth highlighting as potential future directions of research. Many of these studies have been included in prior systematic reviews of preclinical studies (*35*). One example is SAB-301, a polyclonal antibody directed at the MERS-CoV spike protein that is derived from transchromosomic cows. A phase 1 trial published in 2018 demonstrated the safety and tolerability of this treatment (*36*). Another example is a phase 1 trial from 2019 that demonstrated the safety and tolerability of the GLS-5300 MERS coronavirus vaccine in humans (*37*). Other potential treatment options still in early phases of development have been summarized elsewhere (*38*,*39*). The high mortality rate, lack of proven effective treatments, ongoing potential for human-to-human transmission, and the emergence of novel coronaviruses (*40*) underscore the importance of developing research capacity in regions prone to MERS outbreaks as well as the capacity to perform collaborative clinical trials to improve the treatment evidence base.

In this systematic review of potential therapies for MERS, we found existing studies to be at moderate to critical RoB. Low-quality evidence (based on a single study) indicates a benefit from ECMO in severe MERS cases. Low-quality evidence also exists showing no benefit of corticosteroids, NIV, macrolides, or combination of ribavirin with any type of IFN. Collaborative clinical trials evaluating potential therapies are urgently needed to guide treatment decisions (*41*,*42*).

Acknowledgments

The authors would like to thank Rebecca Grant for her early work in drafting preliminary tables of available MERS therapeutics.

About the Author

Dr. Kain is a critical care medicine trainee at the University of Toronto in 2018. He will start a training program in infectious diseases at New York University in 2020.

References

1. ProMED-mail. Novel coronavirus—Saudi Arabia: human isolate. 2012 [cited 2018 Oct 29]. http://www.promedmail.org/direct.php?id=20120920.1302733
2. World Health Organization. Middle East respiratory syndrome coronavirus (MERS-CoV). 2018 [cited 2019 Oct 10]. http://www.who.int/news-room/fact-sheets/detail/middle-east-respiratory-syndrome-coronavirus-(mers-cov)
3. World Health Organization. Epidemic and pandemic prone diseases—MERS situation update. 2018 [cited 2019 Oct 10]. http://www.emro.who.int/pandemic-epidemic-diseases/mers-cov/mers-situation-update-september-2018.html
4. Zaki AM, van Boheemen S, Bestebroer TM, Osterhaus AD, Fouchier RA. Isolation of a novel coronavirus from a man with pneumonia in Saudi Arabia. N Engl J Med. 2012;367:1814–20. https://doi.org/10.1056/NEJMoa1211721
5. Assiri A, Al-Tawfiq JA, Al-Rabeeah AA, Al-Rabiah FA, Al-Hajjar S, Al-Barrak A, et al. Epidemiological, demographic, and clinical characteristics of 47 cases of Middle East respiratory syndrome coronavirus disease from Saudi Arabia: a descriptive study. Lancet Infect Dis. 2013;13:752–61. https://doi.org/10.1016/S1473-3099(13)70204-4
6. Centers for Disease Control and Prevention. Fact sheet about Middle East respiratory syndrome (MERS). 2018 [cited 2018 Aug 1]. https://www.cdc.gov/coronavirus/mers/downloads/factsheet-mers_en.pdf
7. Falzarano D, de Wit E, Martellaro C, Callison J, Munster VJ, Feldmann H. Inhibition of novel β coronavirus replication by a combination of interferon-α2b and ribavirin. Sci Rep. 2013;3:1686. https://doi.org/10.1038/srep01686
8. Falzarano D, de Wit E, Rasmussen AL, Feldmann F, Okumura A, Scott DP, et al. Treatment with interferon-α2b and ribavirin improves outcome in MERS-CoV–infected rhesus macaques. Nat Med. 2013;19:1313–7. https://doi.org/10.1038/nm.3362
9. Moher D, Liberati A, Tetzlaff J, Altman DG; PRISMA Group. Preferred reporting items for systematic reviews and meta-analyses: the PRISMA statement. Int J Surg. 2010;8:336–41. https://doi.org/10.1016/j.ijsu.2010.02.007
10. Sterne JA, Hernán MA, Reeves BC, Savović J, Berkman ND, Viswanathan M, et al. ROBINS-I: a tool for assessing risk of bias in non-randomised studies of interventions. BMJ. 2016;355:i4919. https://doi.org/10.1136/bmj.i4919
11. Guyatt GH, Oxman AD, Vist GE, Kunz R, Falck-Ytter Y, Alonso-Coello P, et al.; GRADE Working Group. GRADE: an emerging consensus on rating quality of evidence and strength of recommendations. BMJ. 2008;336:924–6. https://doi.org/10.1136/bmj.39489.470347.AD
12. Shalhoub S, Farahat F, Al-Jiffri A, Simhairi R, Shamma O, Siddiqi N, et al. IFN-α2a or IFN-β1a in combination with ribavirin to treat Middle East respiratory syndrome coronavirus pneumonia: a retrospective study. J Antimicrob Chemother. 2015;70:2129–32. https://doi.org/10.1093/jac/dkv085
13. Alshahrani MS, Sindi A, Alshamsi F, Al-Omari A, El Tahan M, Alahmadi B, et al. Extracorporeal membrane oxygenation for severe Middle East respiratory syndrome coronavirus. Ann Intensive Care. 2018;8:3. https://doi.org/10.1186/s13613-017-0350-x
14. Omrani AS, Saad MM, Baig K, Bahloul A, Abdul-Matin M, Alaidaroos AY, et al. Ribavirin and interferon alfa-2a for severe Middle East respiratory syndrome coronavirus infection: a retrospective cohort study. Lancet Infect Dis. 2014;14:1090–5. https://doi.org/10.1016/S1473-3099(14)70920-X
15. Hong KH, Choi JP, Hong SH, Lee J, Kwon JS, Kim SM, et al. Predictors of mortality in Middle East respiratory syndrome (MERS). Thorax. 2018;73:286–9. https://doi.org/10.1136/thoraxjnl-2016-209313
16. Al-Hameed F, Wahla AS, Siddiqui S, Ghabashi A, Al-Shomrani M, Al-Thaqafi A, et al. Characteristics and outcomes of Middle East respiratory syndrome coronavirus patients admitted to an intensive care unit in Jeddah, Saudi Arabia. J Intensive Care Med. 2016;31:344–8. https://doi.org/10.1177/0885066615579858
17. Arabi YM, Mandourah Y, Al-Hameed F, Sindi AA, Almekhlafi GA, Hussein MA, et al.; Saudi Critical Care Trial Group. Corticosteroid therapy for critically ill patients with Middle East respiratory syndrome. Am J Respir Crit Care Med. 2018;197:757–67. https://doi.org/10.1164/rccm.201706-1172OC
18. Arabi YM, Al-Omari A, Mandourah Y, Al-Hameed F, Sindi AA, Alraddadi B, et al.; Saudi Critical Care Trial Group. Critically ill patients with the Middle East respiratory syndrome: a multicenter retrospective cohort study. Crit Care Med. 2017;45:1683–95. https://doi.org/10.1097/CCM.0000000000002621
19. Almekhlafi GA, Albarrak MM, Mandourah Y, Hassan S, Alwan A, Abudayah A, et al. Presentation and outcome of Middle East respiratory syndrome in Saudi intensive care unit patients. Crit Care. 2016;20:123. https://doi.org/10.1186/s13054-016-1303-8
20. Sherbini N, Iskandrani A, Kharaba A, Khalid G, Abduljawad M, Al-Jahdali H. Middle East respiratory syndrome coronavirus in Al-Madinah City, Saudi Arabia: demographic, clinical and survival data. J Epidemiol Glob Health. 2017;7:29–36. https://doi.org/10.1016/j.jegh.2016.05.002
21. Khalid I, Alraddadi BM, Dairi Y, Khalid TJ, Kadri M, Alshukairi AN, et al. Acute management and long-term survival among subjects with Middle East respiratory syndrome coronavirus pneumonia and ARDS. Respir Care. 2016;61:340–8. https://doi.org/10.4187/respcare.04325
22. Al Ghamdi M, Alghamdi KM, Ghandoora Y, Alzahrani A, Salah F, Alsulami A, et al. Treatment outcomes for patients with Middle Eastern respiratory syndrome coronavirus (MERS CoV) infection at a coronavirus referral center in the Kingdom of Saudi Arabia. BMC Infect Dis. 2016;16:174. https://doi.org/10.1186/s12879-016-1492-4
23. Alfaraj SH, Al-Tawfiq JA, Assiri AY, Alzahrani NA, Alanazi AA, Memish ZA. Clinical predictors of mortality of Middle East respiratory syndrome coronavirus (MERS-CoV) infection: a cohort study. Travel Med Infect Dis. 2019;29:48–50. https://doi.org/10.1016/j.tmaid.2019.03.004
24. Arabi YM, Deeb AM, Al-Hameed F, Mandourah Y, Almekhlafi GA, Sindi AA, et al.; Saudi Critical Care Trials Group. Macrolides in critically ill patients with Middle East respiratory syndrome. Int J Infect Dis. 2019;81:184–90. https://doi.org/10.1016/j.ijid.2019.01.041
25. Alraddadi BM, Qushmaq I, Al-Hameed FM, Mandourah Y, Almekhlafi GA, Jose J, et al.; Saudi Critical Care Trials Group. Noninvasive ventilation in critically ill patients with the Middle East respiratory syndrome. Influenza Other Respir Viruses. 2019;13:382–90. https://doi.org/10.1111/irv.12635
26. Arabi YM, Shalhoub S, Mandourah Y, Al-Hameed F, Al-Omari A, Al Qasim E, et al. Ribavirin and interferon therapy for critically ill patients with Middle East respiratory syndrome: a multicenter observational study. Clin Infect Dis. 2019;Jun 25:ciz544. https://doi.org/10.1093/cid/ciz544

27. Al-Tawfiq JA, Momattin H, Dib J, Memish ZA. Ribavirin and interferon therapy in patients infected with the Middle East respiratory syndrome coronavirus: an observational study. Int J Infect Dis. 2014;20:42–6. https://doi.org/10.1016/j.ijid.2013.12.003
28. Arabi YM, Arifi AA, Balkhy HH, Najm H, Aldawood AS, Ghabashi A, et al. Clinical course and outcomes of critically ill patients with Middle East respiratory syndrome coronavirus infection. Ann Intern Med. 2014;160:389–97. https://doi.org/10.7326/M13-2486
29. Alhumaid S, Tobaiqy M, Albagshi M, Alrubaya A, Algharib F, Aldera A, et al. MERS-CoV transmitted from animal-to-human vs MERS-CoV transmitted from human-to-human: comparison of virulence and therapeutic outcomes in a Saudi hospital. Trop J Pharm Res. 2018;17:1155–64. https://doi.org/10.4314/tjpr.v17i6.23
30. Khalid M, Khan B, Al Rabiah F, Alismaili R, Saleemi S, Rehan-Khaliq AM, et al. Middle Eastern respiratory syndrome corona virus (MERS CoV): case reports from a tertiary care hospital in Saudi Arabia. Ann Saudi Med. 2014;34:396–400. https://doi.org/10.5144/0256-4947.2014.396
31. Al-Dorzi HM, Aldawood AS, Khan R, Baharoon S, Alchin JD, Matroud AA, et al. The critical care response to a hospital outbreak of Middle East respiratory syndrome coronavirus (MERS-CoV) infection: an observational study. Ann Intensive Care. 2016;6:101–12. https://doi.org/10.1186/s13613-016-0203-z
32. World Health Organization. Middle East respiratory syndrome coronavirus (MERS-CoV) maps and epicurves Oct 2015. 2015 [cited 2019 Jul 25]. https://www.who.int/csr/disease/coronavirus_infections/maps-epicurves-19-october-2015
33. Amsden GW. Anti-inflammatory effects of macrolides—an underappreciated benefit in the treatment of community-acquired respiratory tract infections and chronic inflammatory pulmonary conditions? J Antimicrob Chemother. 2005;55:10–21. https://doi.org/10.1093/jac/dkh519
34. Morra ME, Van Thanh L, Kamel MG, Ghazy AA, Altibi AMA, Dat LM, et al. Clinical outcomes of current medical approaches for Middle East respiratory syndrome: a systematic review and meta-analysis. Rev Med Virol. 2018;28:e1977. https://doi.org/10.1002/rmv.1977
35. Momattin H, Al-Ali AY, Al-Tawfiq JA. A systematic review of therapeutic agents for the treatment of Middle East respiratory syndrome coronavirus (MERS-CoV). Travel Med Infect Dis. 2019;30:9–18. https://doi.org/10.1016/j.tmaid.2019.06.012
36. Beigel JH, Voell J, Kumar P, Raviprakash K, Wu H, Jiao JA, et al. A randomized placebo-controlled phase 1 safety and tolerability study of a novel human anti-MERS coronavirus polyclonal intravenous immunoglobulin produced from transchromosomic cattle. Lancet Infect Dis. 2018;18:410–8. https://doi.org/10.1016/S1473-3099(18)30002-1
37. Modjarrad K, Roberts CC, Mills KT, Castellano AR, Paolino K, Muthumani K, et al. Safety and immunogenicity of an anti-Middle East respiratory syndrome coronavirus DNA vaccine: a phase 1, open-label, single-arm, dose-escalation trial. Lancet Infect Dis. 2019;19:1013–22. https://doi.org/10.1016/S1473-3099(19)30266-X
38. Xu J, Jia W, Wang P, Zhang S, Shi X, Wang X, et al. Antibodies and vaccines against Middle East respiratory syndrome coronavirus. Emerg Microbes Infect. 2019;8:841–56. https://doi.org/10.1080/22221751.2019.1624482
39. Han HJ, Liu JW, Yu H, Yu XJ. Neutralizing monoclonal antibodies as promising therapeutics against Middle East respiratory syndrome coronavirus infection. Viruses. 2018;10:680–90. https://doi.org/10.3390/v10120680
40. Wuhan Municipal Health Commission. Report of clustering pneumonia of unknown etiology in Wuhan City. 2019 [cited 2020 Feb 15]. http://wjw.wuhan.gov.cn/front/web/showDetail/2019123108989
41. Aguanno R, Elldrissi A, Elkholy AA, Embarek PB, Gardner E, Grant R, et al.; FAO-OIE-WHO MERS Technical Working Group. MERS: progress on the global response, remaining challenges and the way forward. Antiviral Res. 2018;159:35–44. https://doi.org/10.1016/j.antiviral.2018.09.002
42. World Health Organization. WHO consultation on MERS-CoV therapeutics and vaccine evaluation. 2018 [cited 2020 Mar 14]. https://www.who.int/blueprint/what/norms-standards/meeting-report-30-november-2018.pdf

Address for correspondence: Robert Fowler, Sunnybrook Hospital, Rm D1.08, 2075 Bayview Ave, Toronto, ON M4N 3M5, Canada; email: rob.fowler@sunnybrook.ca

Distribution of Streptococcal Pharyngitis and Acute Rheumatic Fever, Auckland, New Zealand, 2010–2016

Jane Oliver, Arlo Upton, Susan J. Jack, Nevil Pierse, Deborah A. Williamson, Michael G. Baker

Group A *Streptococcus* (GAS) pharyngitis is a key initiator of acute rheumatic fever (ARF). In New Zealand, ARF cases occur more frequently among persons of certain ethnic and socioeconomic groups. We compared GAS pharyngitis estimates (1,257,058 throat swab samples) with ARF incidence (792 hospitalizations) in Auckland during 2010–2016. Among children 5–14 years of age in primary healthcare clinics, GAS pharyngitis was detected in similar proportions across ethnic groups (≈19%). Relative risk for GAS pharyngitis was moderately elevated among children of Pacific Islander and Māori ethnicities compared with those of European/other ethnicities, but risk for ARF was highly elevated for children of Pacific Islander and Māori ethnicity compared with those of European/other ethnicity. That ethnic disparities are much higher among children with ARF than among those with GAS pharyngitis implies that ARF is driven by factors other than rate of GAS pharyngitis alone.

Acute rheumatic fever (ARF) can cause rheumatic heart disease, which in turn may produce permanent heart damage (*1*). ARF is an autoimmune disease triggered in response to group A *Streptococcus* (GAS) infection. GAS pharyngitis is generally considered the major initiator of ARF, but GAS skin infection may also play a role. Substantial knowledge gaps with regard to ARF risk factors and pathogenesis impair disease prevention and control (*2*,*3*). If GAS pharyngitis is the sole initiator of ARF, then we would expect this infection to be most common in groups in which incidence of ARF is highest. ARF rates peak among children 5–14 years of age (*4*).

ARF and rheumatic heart disease exert a major burden on developing countries. Disease rates are also particularly high among persons of Māori and Pacific Islander ethnicity in New Zealand (*4*–*6*). During 2000–2009, among children 5–14 years of age, ARF incidence among Māori children was 40.2 cases/100,000 children, and among Pacific Islander children, it was 81.2/100,000. By contrast, the incidence for non-Māori, non–Pacific Islander children in New Zealand was 2.1/100,000. Associations between ARF and socioeconomic deprivation have inconsistently been observed (*6*–*10*). During 2010–2013, persons living in the most deprived New Zealand neighborhoods were 33 (95% CI 19–58) times more likely to be hospitalized with ARF for the first time compared with persons living in the least deprived neighborhoods (*6*).

In 2011, the New Zealand government announced a major national Rheumatic Fever Prevention Programme (RFPP), aiming to reduce the national incidence of ARF by two thirds (to 1.4 cases/100,000 persons) by mid-2017 (*11*,*12*). The RFPP strongly emphasized primary prevention of ARF through sore throat management; that is, prompt detection and antimicrobial treatment of GAS pharyngitis before development of ARF (*11*,*12*). In areas with high rates of ARF, the sore throat management aspect of the RFPP had 2 components: school-based throat swabbing clinics and rapid-response primary healthcare clinics (PHCs). School-based clinics operated only when schools were in session. Children with a self-reported sore throat could have their throat swabbed free of charge, either at school or at a rapid-response PHC when certain conditions were met. If the swab sample culture produced GAS, a 10-day course of oral amoxicillin was recommended (*13*). The RFPP was reportedly the largest sore throat management program for ARF prevention

Author affiliations: Murdoch Children's Research Institute, Melbourne, Victoria, Australia (J. Oliver); University of Otago Wellington, Wellington, New Zealand (J. Oliver, N. Pierse, M.G. Baker); University of Melbourne, Melbourne (J. Oliver, D.A. Williamson); Labtests Ltd, Auckland, New Zealand (A. Upton); University of Otago, Dunedin, New Zealand (S.J. Jack)

DOI: https://doi.org/10.3201/eid2606.181462

ever conducted (*14*). As of 2014, school clinics included ≈50,000 children (*12*). By December 2013, a total of 83% of school clinics had been implemented and additional rapid-response clinics were being set up in PHCs. Public health messages about the value of seeking throat swabbing for those experiencing sore throat symptoms were promoted to populations considered at high risk for ARF (*15*).

The RFPP resulted in a large collection of high-quality diagnostic throat swab sample data, which provided a unique opportunity to describe the distribution of GAS pharyngitis across an entire population and correlate the data with ARF rates. Most RFPP throat swab samples were collected in Auckland, where ≈50% of ARF patients in New Zealand reside (*15*). Our aim was to describe the distribution of GAS pharyngitis in the Auckland population and compare it with the distribution of ARF.

Methods

Setting

In 2013, the population of New Zealand was ≈4.5 million persons. The largest city is Auckland, where around one third of the population resides. In the 2013 census, 10% of persons in Auckland identified their ethnicity as Māori, 12% Pacific Islander, 21% Asian, and 57% European/other (*16*). Auckland comprises 3 district health boards (DHBs): Waitemata, Auckland, and Counties Manukau. Many Auckland schools (n = 75) participated in the RFPP school program. Rapid-response clinics were widely implemented (*15*).

The National Health Index (NHI) is a unique patient identifier widely used in New Zealand health data; it can be encrypted to protect patient privacy. Demographic information encoded by the NHI includes New Zealand resident status, prioritized ethnicity, sex, birth date, DHB, and New Zealand Deprivation Index (NZDep) score. The prioritized ethnicity classification system allocates persons to a single ethnic group based on a prioritized order of Māori, Pacific Islander, Asian, and European/other. The European/other group refers to non-Māori, non–Pacific Islander, and non-Asian persons (*17*). The NZDep score is an ecologic measure of socioeconomic deprivation corresponding to a neighborhood (*18*). Deciles 1–2 (quintile 1) represent the least deprived neighborhoods, and deciles 9–10 (quintile 5) represent the most deprived.

Persons eligible to have their throat swabbed and receive antimicrobial treatment through the RFPP were Māori and Pacific Islander children 4–19 years of age, all children in that age group living in quintile 5 neighborhoods, and eligible children's household contacts 3–35 years of age if they visited a school or rapid-response clinic with a self-reported sore throat. Other persons contributed throat swab samples in PHCs when clinicians decided to collect a sample separately from the RFPP (*15*).

Throat Swab Sample Data Collection

Since mid-2009, the sole community pathology laboratory service provider for the entire Auckland region has been Labtests (*19*). We obtained data on all throat swab samples cultured at Labtests during 2010–2016: patient encrypted NHI, age, date of swab sample collection, sample source (i.e., school clinic or PHC), and culture result (e.g., GAS). Although swab samples collected in school clinics could be distinguished from those collected in PHCs, we could not distinguish between samples collected in rapid-response clinics and those in regular PHCs.

ARF Data Collection

We obtained data on ARF diagnoses during 1988–2016 from the Ministry of Health (International Classification of Diseases, 10th Revision [ICD-10], codes I00-I02 and ICD International Classification of Diseases, 9th Revision [ICD-9], codes 390–392). We also obtained rheumatic heart disease diagnoses for the same period (ICD-10 codes I05-I09 and ICD-9 codes 393–398). The encrypted NHI was provided for each entry along with the demographic information it encoded. We identified the first ARF entry for each child and removed all later entries. Because ARF precedes rheumatic heart disease in the causal pathway, when identifying initial ARF hospitalizations, we excluded all persons who had been hospitalized for rheumatic heart disease before their first hospitalization for ARF. We excluded from study all admissions for non–New Zealand citizens. We also excluded hospital transfers; thus, only the first record was included for each ARF admission. In so doing, we attempted to limit the dataset to initial presentations of ARF, in accordance with the method adopted by the Ministry of Health in 2013 (*18*). We created a dataset of initial ARF hospitalizations in Auckland during 2010–2016, the initial ARF dataset, and performed basic demographic analyses.

Statistical Analyses

We performed descriptive epidemiologic analyses according to key outcome measures, stratified according to selected demographic characteristics and whether GAS pharyngitis was detected. We considered a throat swab sample that produced GAS on culture to indicate a case of GAS pharyngitis. Key outcome measures were incidence of throat swab samples (no.

samples collected/total no. children sampled), incidence of GAS pharyngitis, and the proportion of total throat swab samples that indicated GAS pharyngitis.

For all analyses, we used R version 3.3.1 (*20*). Because the RFPP was still being implemented in 2013, our later analyses focused on 2014–2016. After 2013, the annual number of swab samples collected peaked, remaining relatively stable with high population coverage. Most analyses concentrated on children 5–14 years of age (*4*). The focus is largely on samples from PHCs because the school programs intensely targeted high-risk populations on the basis of ARF incidence. When calculating seasonal rates, we multiplied numerator (swab) data by 4 to produce annualized rates.

Rate Calculations

If a person contributed >1 swab sample, that person would be counted >1 time in the numerator. We calculated intercensus population estimates and projections by interpolation and extrapolation, using denominator data from 2006 and 2013 population censuses (*21*). When calculating mean rates, we used the population estimate for the middle of the period. We calculated relative risks (RRs) and 95% CIs for initial ARF and GAS pharyngitis from the number of cases detected in the population.

Results

Settings and Time Trends in Throat Swab Sample Collection and GAS Pharyngitis

During 2010–2016, a total of 1,257,058 throat swabs were collected in Auckland. The total number of throat swab samples collected each year increased dramatically; 8 times more samples were collected in 2016 than in 2010. During 2011–2016, swabbing increased in school clinics but also increased 4-fold in PHCs. The throat swabbing incidence for the Auckland population plateaued in 2014–16; swabbing in school clinics peaked in 2014 (130.8 samples/1,000 person-years) and in PHCs peaked in 2015 (114.5 samples/1,000 person-years; Figure 1; Appendix Table 1, https://wwwnc.cdc.gov/EID/article/26/6/18-1462-App1.pdf).

Of the swab samples, 163,534 were positive for GAS (13.0% total samples); 64,036 were positive for streptococci of group C, group G, or both (5.1% total). The annual proportion of samples positive for GAS decreased from 15.3% in 2010 to 10.7% in 2011 before increasing to 15.1% in 2016 (Figure 1). However, the annual incidence of GAS pharyngitis increased nearly 8-fold from 2010 to 2016. The proportion of positive GAS swab samples was higher among those collected in PHCs (15.0%) than in school clinics (12.6%) (Figure 1; Appendix Table 1).

Sociodemographic Characteristics of Populations Contributing Throat Swab Samples

We determined the sociodemographic characteristics of populations who contributed throat swab samples in detail for 2014–2016. Sample collection in PHCs was highest among children 5–9 years of age (100,406 total swab samples, 356.6 swab samples/1,000 children), followed by children 10–14 years (72,980 swab samples, 266.5/1,000 children), and then children <5 years of age (68,548 swab samples, 229.1 samples/1,000 children).

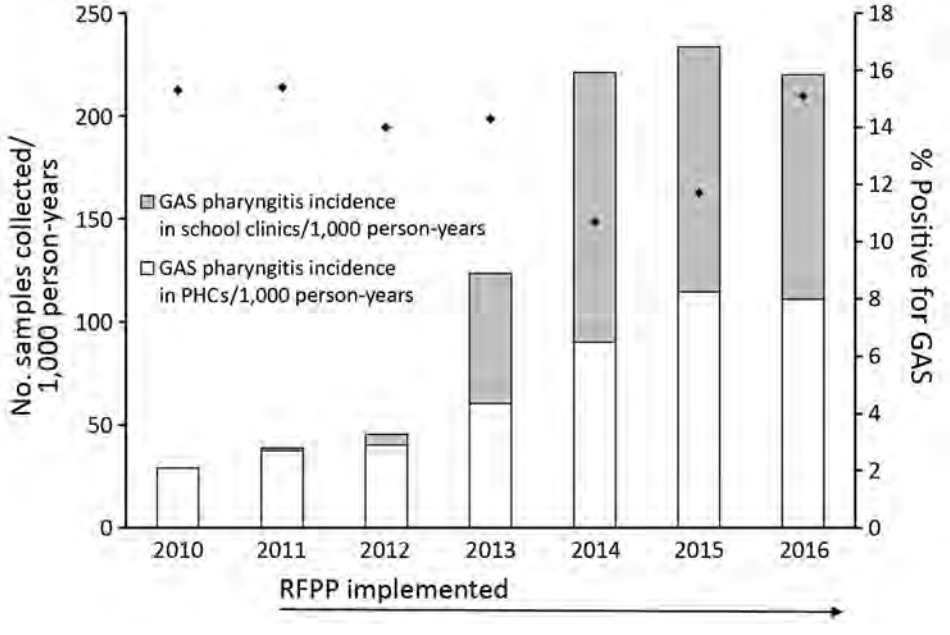

Figure 1. Number of throat swab samples collected and GAS-positive swab samples, by year, Auckland, New Zealand, 2010–2016. Diamonds indicate percentages of swab sample cultures positive for GAS. GAS, group A *Streptococcus*; PHC, private healthcare clinic.

The incidence of GAS pharyngitis was highest among children 5–9 years of age (82.9 cases/1,000 person-years), followed by children 10–14 years of age (44.3 cases/1,000 person-years). GAS was uncommon in throat swab samples from persons ≥50 years of age, although ≈15,000 swabs were collected from persons in this age group each year. A much smaller secondary peak in incidence of GAS pharyngitis was seen among adults 30–39 years of age, and 66.2% of those affected were female (Figure 2; Appendix Table 2).

In school clinics, the incidence of swab collection was highest among children 5–9 years of age (1151.3 swabs/1,000 person-years), as was the incidence of GAS pharyngitis (121.8 swabs/1,000 person-years). Of the total school clinic swab samples collected, 96.2% were from children 5–14 years of age, the target age group.

During the study period, 792 persons were hospitalized for initial ARF; 398 (50.3%) were children 5–14 years of age. Because incidence of GAS pharyngitis and ARF were both highest among children 5–14 years of age, we further restricted our analysis to this group.

Seasonal Distribution of Swab Sample Collection and GAS Pharyngitis

The incidence (and RR) of throat swab collection was highest in winter, both in PHCs (480.3/1,000 children 5–14 years of age) and overall; incidence of GAS pharyngitis was also highest in winter (Table; Figure 3, panel A; Appendix Table 3). In winter, the incidence of GAS detected by swab samples collected in PHCs (87.9 samples/1,000 person-years) was more than twice the rate detected by samples collected in the summer. By contrast, the proportion of GAS-positive samples was lower in winter and spring than in summer and autumn. The seasonal pattern of ARF incidence rates was roughly similar to that of GAS pharyngitis; ARF rates were highest in autumn and winter (Figure 3, panel B).

Throat Swab Sample Collection and Incidence of GAS Pharyngitis by Ethnicity

Nearly one quarter of all Pacific Islander children and one fifth of all Māori children contributed ≥1 swab in PHCs, compared with approximately one sixth of European/other children. The proportion of samples positive for GAS was similar between these groups (20.1%–22.3%), but incidence of GAS pharyngitis was significantly higher among Pacific Islander (99.6 cases/1,000 person-years) and Māori (79.0 cases/1,000 person-years) children compared with those of European/other ethnicity (58.3 cases/1,000 person-years). Incidence of GAS pharyngitis was lowest among Asian children (Figure 4; Appendix Table 3).

Distribution of Throat Swab Sample Collection and Incidence of GAS Pharyngitis

Most throat swab samples were collected from children living in the most deprived neighborhoods; ≥1 throat swab sample was contributed by approximately one quarter of all children from quintile 5, compared with one eighth of all children from quintiles 1 and 2. The proportion of GAS-positive swab samples from children across quintiles was similar (19.5%–21.8%), but incidence of GAS pharyngitis increased with area deprivation. For children in quintile 1,

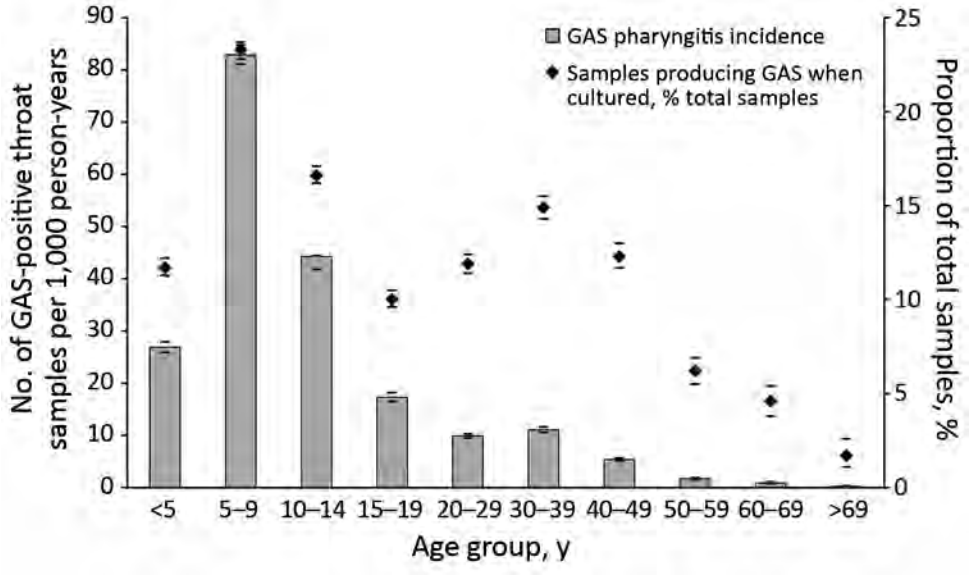

Figure 2. Mean annual distribution of GAS pharyngitis in PHCs, by age group, Auckland, New Zealand, 2014–2016. Diamonds indicate percentages of swab sample cultures positive for GAS; bars above and below indicate 95% CIs. GAS, group A *Streptococcus*; PHC private healthcare clinic.

Table. Comparison of GAS pharyngitis and ARF rates in the Auckland region, New Zealand, 2014–2016*

Characteristic	GAS pharyngitis in PHCs		GAS pharyngitis in PHCs and schools		Initial ARF hospitalizations	
	Mean annual incidence†	RR (95% CI)	Mean annual incidence†	RR (95% CI)	Mean annual incidence†	RR (95% CI)
Total	15.7	Referent NA	28.1	Referent NA	0.1	Referent NA
Age group, y						
0–4	26.9	2.7 (2.6–2.9)	28.7	2.8 (2.6–2.9)	0.7	0.1 (0.0–0.4)
5–9	82.9	8.2 (7.8–8.6)	204.8	18.1 (17.4–18.9)	17.8	2.5 (1.7–3.8)
10–14	44.3	4.5 (4.2–4.7)	99.7	9.3 (8.9–9.7)	32.5	4.7 (3.3–6.7)
15–19	17.3	1.8 (1.6–1.9)	20.4	2.0 (1.9–2.1)	9.2	1.3 (0.8–2.1)
20–29	9.9	Referent	10.3	Referent	7.1	Referent
30–39	11.1	1.1 (1.1–1.2)	11.5	1.1 (1.0–1.2)	1.7	0.2 (0.1–0.5)
≥40	2.5	0.3 (0.2–0.3)	2.6	0.2 (0.2–0.3)	0.0	0.0 (0.0–0.1)
Children age 5–14 y						
Total	62.8	Referent NA	150.6	Referent NA	25.0	Referent NA
M	63.3	Referent	153.4	Referent	25.6	Referent
F	62.5	1.0 (1.0–1.0)	147.6	1.0 (0.9–1.0)	23.7	0.9 (0.7–1.3)
Prioritized ethnicity						
Māori	79.0	1.3 (1.3–1.4)	248.7	3.4 (3.3–3.5)	35.5	86.9 (11.9–635.0)
Pacific Islander	99.6	1.7 (1.6–1.8)	383.4	4.8 (4.7–5.0)	98.3	240.4 (33.5–1,722.6)
Asian	29.2	0.5 (0.5–0.5)	41.0	0.6 (0.6–0.7)	0.0	0.7 (0.0–18.0)
European/Other	58.3	Referent	66.9	Referent	0.4	Referent
2013 New Zealand Deprivation Index quintile						
1	43.5	Referent	45.4	Referent	3.0	Referent
2	39.2	0.9 (0.8–1.0)	45.6	1.0 (0.9–1.1)	2.6	0.9 (0.2–3.8)
3	50.0	1.1 (1.1–1.2)	61.6	1.4 (1.3–1.4)	6.5	2.1 (0.6–7.6)
4	82.4	1.9 (1.7–2.0)	125.7	2.7 (2.5–2.8)	24.7	8.1 (2.8–23.7)
5	103.1	2.3 (2.2–2.5)	427.6	7.7 (7.4–8.1)	76.9	25.2 (9.3–68.5)
Season						
Summer	39.3	Referent	77.0	Referent	25.5	Referent
Autumn	62.3	1.6 (1.5–1.6)	185.3	2.3 (2.3–2.4)	32.6	1.3 (0.8–1.9)
Winter	87.9	2.2 (2.2–2.3)	201.7	2.5 (2.5–2.6)	31.9	1.3 (0.9–1.8)
Spring	62.1	1.6 (1.5–1.6)	138.5	1.8 (1.7–1.8)	8.5	0.3 (0.2–0.6)
District health board						
Waitemata	54.4	1.0 (0.9–1.0)	67.3	0.8 (0.8–0.9)	13.4	0.6 (0.3–0.9)
Auckland	54.9	Referent	80.1	Referent	24.1	Referent
Countries Manukau	72.1	1.3 (1.2–1.4)	270.9	3.0 (2.9–3.1)	36.8	1.5 (1.0–2.3)

*ARF, acute rheumatic fever; GAS, group A *Streptococcus;* PHC, primary healthcare clinic; referent NA, referent not available; RR, relative risk.
†Per 1,000 person-years.

incidence was 43.5 cases/1,000 person-years, but in quintile 5, incidence was 103.1 cases/1,000 person-years (Figure 5; Appendix Table 3).

Comparison of GAS Pharyngitis and ARF Incidence

We compared mean annual incidence of GAS pharyngitis during 2014–2016, by selected demographic characteristics and swab sample source (i.e., PHC and total), with the mean annual incidence of ARF (Table). The RR for initial ARF was highest among children 10–14 years of age; however, the RR for GAS pharyngitis was highest among children 5–9 years of age. Although ARF was rare among children <5 years of age, GAS pharyngitis was relatively common. The RR for initial ARF was 240.4 (95% CI 33.5–1,722.6) for children of Pacific Islander ethnicity compared with those of European/other ethnicity and was also extremely elevated for Māori children (RR 86.9, 95% CI 11.9–635.0). Of children who contributed throat swab samples in a PHC, the RR for GAS pharyngitis was highest among Pacific Islanders (RR 1.7, 95% CI 1.6–1.8), followed by Māori children, yet this discrepancy was not nearly as extreme as the RR for ARF. Higher RRs for GAS pharyngitis were also estimated for Māori and Pacific Islander children regardless of the sample collection setting. A similar pattern was noted for differences between NZDep quintiles. Seasonality was more pronounced for GAS pharyngitis incidence than for ARF incidence; at PHCs, GAS pharyngitis was least likely in summer and most likely in winter (RR 2.2, 95% CI 2.2–2.3).

Discussion

The RFPP provided a unique opportunity to assess the distribution of GAS pharyngitis across a well-defined region over a sustained period and compare it with the distribution of ARF. To our knowledge, the RFPP produced the largest ever compilation of throat swab sample data; 1.3 million swab samples were collected in Auckland from 2010 (before RFPP) through 2016. These comprehensive throat swab sample data showed the following: the proportion of GAS-positive swab samples was fairly consistent across the

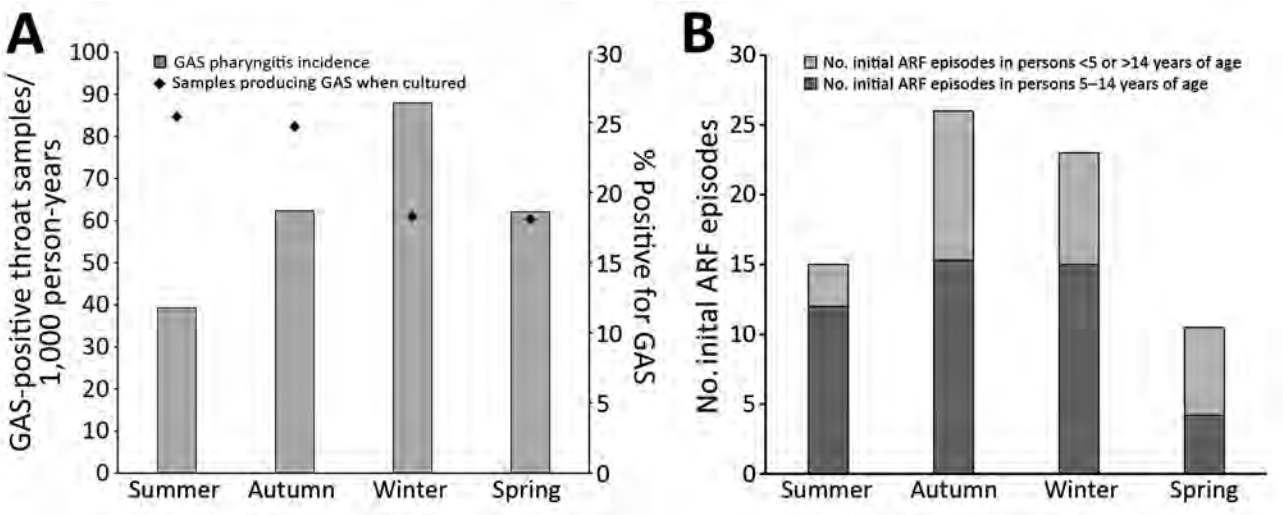

Figure 3. Mean annual distribution of GAS pharyngitis and ARF cases, by season, Auckland, New Zealand, 2014–2016. A) GAS-positive throat swab samples collected from children 5–14 years of age in PHCs. Diamonds indicate percentages of swab sample cultures positive for GAS. B) Mean annual number of first ARF episodes. ARF, acute rheumatic fever; GAS, group A *Streptococcus*; PHC, private healthcare clinic.

population of children 5–14 years of age but varied between PHC and school clinic settings, suggesting that sample collection thresholds differed by setting; GAS pharyngitis is seasonal and shares some similarities with ARF; unlike ARF, GAS pharyngitis occurs across a wide range of age groups (*4*); and ethnic and socioeconomic differences in GAS pharyngitis are insufficient to explain the marked inequities in ARF incidence.

A striking feature of GAS pharyngitis is the consistent difference in the proportion of GAS-positive samples collected in PHCs and school clinics. The proportion of GAS-positive samples collected from Māori and Pacific Islander children 5–14 years of age in PHCs (20%–21%) was nearly twice that observed for those collected by school programs (11%). At PHCs, the proportion of GAS-positive samples was similar between ethnic groups and NZDep quintiles (except somewhat lower for Asian children). One possible explanation could be that as children approach the level where their caregiver feels they are sufficiently unwell to warrant visiting a PHC, the likelihood of them having GAS pharyngitis is much the same across ethnic groups and deprivation quintiles. Consequently, the proportion of GAS-positive samples by health service may reveal information about the threshold at which persons seek treatment there. Furthermore, the literature describes GAS pharyngitis as a severely painful sore throat (*22*). It is debatable whether many affected children would therefore attend school; many may have visited a rapid response PHC instead. Consequently, GAS-positive samples from school clinics may have largely detected GAS carriage. To support this view, the proportion of GAS-positive samples from school clinics was slightly lower than the estimated prevalence of asymptomatic pharyngeal GAS carriage reported (12%) (*23*). This threshold effect has several implications. First, we should concentrate on findings from PHCs, where the threshold for attendance seems to be higher and a moderate proportion of cases are likely to represent true GAS pharyngitis (not viral pharyngitis with coincidental GAS detection on swab culture) (*24*). Second, GAS pharyngitis incidence rates are likely to provide a better indication of the distribution of this condition compared with the proportion of GAS-positive samples overall. The

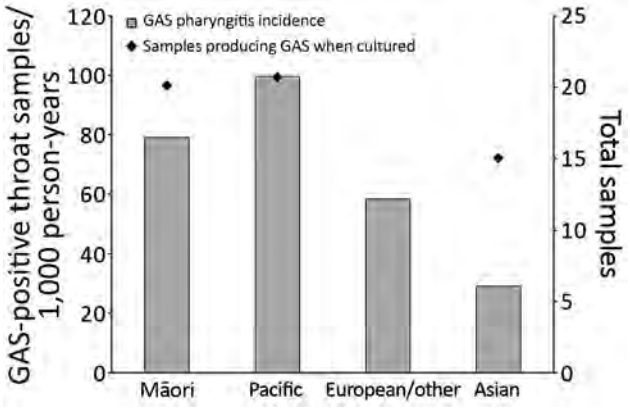

Figure 4. Mean annual distribution of GAS pharyngitis in PHCs among children 5–14 years of age, by ethnic group, Auckland, New Zealand, 2014–2016. Diamonds indicate percentages of swab sample cultures positive for GAS. GAS, group A *Streptococcus*; PHC, private healthcare clinic.

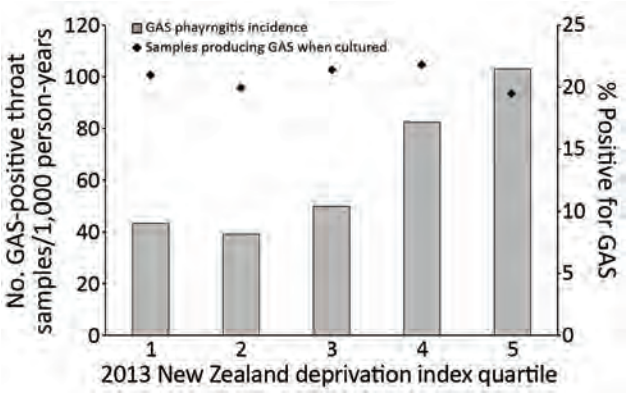

Figure 5. Mean annual distribution of GAS pharyngitis in PHCs among children 5–14 years of age, by NZDep quintile, Auckland, New Zealand, 2014–2016. Diamonds indicate percentages of swab sample cultures positive for GAS. GAS, group A *Streptococcus*; NZDep, New Zealand Deprivation Index; PHC, private healthcare clinic.

consistently lower proportion of GAS-positive samples from the school program, at a level equivalent to asymptomatic detection, raises questions about the effectiveness of basing the RFPP in this setting at all. There are potential ways to improve the accuracy of GAS pharyngitis diagnosis, such as through clinical decision rules, although the validity and practicality of such methods are debated (*25*–*28*).

The value of observing the incidence of GAS pharyngitis in PHC settings is illustrated by seasonal distribution patterns. GAS pharyngitis was more common in winter, when incidence was more than twice that in summer. Paradoxically, the proportion of GAS-positive swab samples showed the opposite pattern, being highest in summer. This effect was caused by the large increase in sample collection during winter. Most pharyngitis has a viral cause (*27*); thus, more GAS-negative children reporting a sore throat visited a PHC in winter, reducing the proportion of swab samples that produced GAS in culture. The increase in sample collection during winter was somewhat appropriate given the increased rate of ARF.

Differences in the proportion of GAS swabs across ethnic and socioeconomic groups were insufficient for explaining the marked inequities in ARF incidence rates. Māori and Pacific Islander children, among whom risk of acquiring ARF is highest, were well targeted by the RFPP. Very low rates of ARF in non-Māori, non–Pacific Islander populations in New Zealand have been reported (*29*,*30*), along with ≈200 throat swabs collected/1,000 persons (Appendix Table 3). This observation raises the question of whether intensive swabbing of non-Māori, non–Pacific Islander populations is appropriate. The evidence for reducing swab sample collection from young children is less certain. Although the incidence of GAS pharyngitis was elevated in groups at highest risk for ARF, the age distribution was much broader. If, as hypothesized, ARF is caused by repeated untreated GAS pharyngitis, which eventually triggers autoimmune reactions (priming) (*1*), then concentrating sore throat management strategies on young children is probably justifiable. The extreme disparities in ARF rates between ethnic and socioeconomic groups were not seen for GAS pharyngitis rates. These observations do not support the hypothesis that differences in observed GAS pharyngitis are a key pathway propelling the observed ARF inequities. Consequently, other factors that may drive ARF need to be considered, including the role of GAS skin infections (*31*). Ethnic and socioeconomic differences in exposures to environmental cofactors or host factors also need to be considered as key drivers of ARF inequities (*31*–*37*).

Strengths of our study include complete dataset coverage of a large, well-defined population. Well-characterized numerators and denominators permitted analysis by key demographic attributes. Microbiological analyses were performed by a single provider (Labtests) using standardized protocols. A limitation is that swab sample data reflect healthcare service use rather than representative population sampling, particularly because accurate RFPP coverage data were never collected. In addition, the RFPP deliberately targeted persons in groups at high risk for ARF, for whom GAS pharyngitis risk is potentially higher. These data cannot therefore directly measure the distribution of GAS pharyngitis. A second limitation with this study, and with the RFPP in general, is that it is impossible to know which GAS-positive children have true GAS pharyngitis and which have pharyngitis from other causes and coincidental GAS carriage. No information about clinical manifestations was collected, and serologic confirmation of infection was not sought in the RFPP (and was neither recommended nor practical) (*38*). It is likely that many persons for whom antimicrobial drugs were prescribed had viral infections and may not have benefited from treatment. Last, because the RFPP was not set up to be evaluated, it is impossible to know which swab samples were collected in rapid-response clinics and which as part of routine healthcare. Regardless, the increase in PHC swabbing correlates strongly with, and is most likely attributable to, RFPP implementation (*15*).

A priority for future research is to establish the pathogenic significance of GAS detection in pharyngeal swab sample cultures across different settings. Future analyses could assess the frequency of throat sample

collection and GAS pharyngitis for an entire birth cohort of children in Auckland. Population incidence (cohort) studies could be useful for establishing accurate risk measures, particularly of the type conducted in Melbourne, Victoria, Australia, where GAS pharyngitis surveillance data were collected to investigate prevalence, transmission, and serology (*24*). It would be useful to establish an ongoing surveillance and monitoring program for ARF prevention that could assess specific intervention components, such as rapid-response clinics. A case–control study would be well suited to investigate factors contributing to the greatly elevated ARF risk for Māori and Pacific Islander children, beyond exposure to GAS pharyngitis alone (*39*,*40*). Specimens collected in such a study could be used for immune profiling to investigate the hypothesis that cumulative exposure to GAS is indeed a risk factor for ARF (*41*).

In conclusion, we found that the RFPP dramatically increased rates of throat swab sample collection among children at high risk for ARF. Throat swab sample collection is appropriate, given the goal of reducing ARF. However, because GAS pharyngitis is common in human populations, the RFPP resulted in many persons who were not at high risk for ARF undergoing throat swabbing and, for many, antimicrobial drug treatment. The population incidence of GAS pharyngitis shows some correlation with ARF risk. However, disparities in ARF incidence are vastly higher across ethnic and socioeconomic groups than are disparities in GAS pharyngitis, as measured by swab sample cultures from persons with self-reported pharyngitis. This inconsistency implies that factors other than exposure to a single episode of GAS pharyngitis alone must drive ARF development. Identifying and mitigating any modifiable risk factors may hold the key to effective ARF prevention.

Acknowledgments

We acknowledge Greg Morris, who extracted the data and provided guidance on data cleaning.

J.O. was supported by a full-time PhD scholarship from Lotteries Health Research.

About the Author

Dr. Oliver is a postdoctoral public health researcher. This study formed part of her doctoral thesis, which concerns ARF, its risk factors, and determinants. She currently works in infectious disease research at the University of Melbourne and at Murdoch Children's Research Institute. Her major focus is on streptococcal diseases and Buruli ulcer.

References

1. Carapetis JR, Currie BJ, Good MF. Towards understanding the pathogenesis of rheumatic fever. Scand J Rheumatol. 1996;25:127–31, 32–3.
2. Parks T, Smeesters PR, Steer AC. Streptococcal skin infection and rheumatic heart disease. Curr Opin Infect Dis. 2012;25:145–53. https://doi.org/10.1097/QCO.0b013e3283511d27
3. Carapetis JR, Beaton A, Cunningham MW, Guilherme L, Karthikeyan G, Mayosi BM, et al. Acute rheumatic fever and rheumatic heart disease. Nat Rev Dis Primers. 2016;2:15084. https://doi.org/10.1038/nrdp.2015.84
4. Carapetis JR, Steer AC, Mulholland EK, Weber M. The global burden of group A streptococcal diseases. Lancet Infect Dis. 2005;5:685–94. https://doi.org/10.1016/S1473-3099(05)70267-X
5. Jaine R, Baker M, Venugopal K. Acute rheumatic fever associated with household crowding in a developed country. Pediatr Infect Dis J. 2011;30:315–9. https://doi.org/10.1097/INF.0b013e3181fbd85b
6. Gurney JK, Stanley J, Baker MG, Wilson NJ, Sarfati D. Estimating the risk of acute rheumatic fever in New Zealand by age, ethnicity and deprivation. Epidemiol Infect. 2016;144:3058–67. https://doi.org/10.1017/S0950268816001291
7. Riaz BK, Selim S, Karim MN, Chowdhury KN, Chowdhury SH, Rahman MR. Risk factors of rheumatic heart disease in Bangladesh: a case-control study. J Health Popul Nutr. 2013;31:70–7. https://doi.org/10.3329/jhpn.v31i1.14751
8. Adanja B, Vlajinac H, Jarebinski M. Socioeconomic factors in the etiology of rheumatic fever. J Hyg Epidemiol Microbiol Immunol. 1988;32:329–35.
9. Zaman MM, Yoshiike N, Chowdhury AH, Jalil MQ, Mahmud RS, Faruque GM, et al. Socio-economic deprivation associated with acute rheumatic fever. A hospital-based case-control study in Bangladesh. Paediatr Perinat Epidemiol. 1997;11:322–32. https://doi.org/10.1111/j.1365-3016.1997.tb00011.x
10. Ba-Saddik IA, Munibari AA, Al-Naqeeb MS, Parry CM, Hart CA, Cuevas LE, et al. Prevalence of rheumatic heart disease among school-children in Aden, Yemen. Ann Trop Paediatr. 2011;31:37–46. https://doi.org/10.1179/1465328110Y.0000000007
11. New Zealand Ministry of Health. Rheumatic fever [cited 2017 Dec 8]. http://www.health.govt.nz/our-work/diseases-and-conditions/rheumatic-fever
12. New Zealand Ministry of Health. Progress on the Better Public Services rheumatic fever target [cited 2018 Feb 10]. http://www.health.govt.nz/about-ministry/what-we-do/strategic-direction/better-public-services/progress-better-public-services-rheumatic-fever-target
13. Lennon D, Kerdemelidis M, Arroll B, Sharpe N. Once-daily amoxicillin for group A streptococcal (GAS) sore throat as the other first-line option: a clarification of the NZ sore throat guidelines. N Z Med J. 2011;124:116–9.
14. Lennon D, Kerdemelidis M, Arroll B. Meta-analysis of trials of streptococcal throat treatment programs to prevent rheumatic fever. Pediatr Infect Dis J. 2009;28:e259–64. https://doi.org/10.1097/INF.0b013e3181a8e12a
15. Jack SJ, Williamson DA, Galloway Y, Pierse N, Zhang J, Oliver J, et al. Primary prevention of rheumatic fever in the 21st century: evaluation of a national programme. Int J Epidemiol. 2018;47:1585–93. https://doi.org/10.1093/ije/dyy150
16. Statistics New Zealand. 2013 Census QuickStats about a place: Auckland Region [cited 2018 Feb 13] http://www.stats.govt.nz/Census/2013-census/profile-and-summary-reports/quickstats-about-a-place.aspx

17. Ministry of Health. HISO 10001:2017 ethnicity data protocols [cited 2018 Feb 13]. https://www.health.govt.nz/publication/hiso-100012017-ethnicity-data-protocols
18. Salmond CE, Crampton P. Development of New Zealand's deprivation index (NZDep) and its uptake as a national policy tool. Can J Public Health. 2012;103(Suppl 2):S7–11.
19. Labtests. About Labtests [cited 2018 Feb 13]. http://www.labtests.co.nz/about-us/about-labtests
20. R Core Team. R: A language and environment for statistical computing. Vienna (Austria): R Foundation for Statistical Computing; 2014.
21. Statistics New Zealand. Estimates and projections [cited 2018 Feb 15]. http://www.stats.govt.nz/browse_for_stats/population/estimates_and_projections.aspx
22. Wannamaker LW. Perplexity and precision in the diagnosis of streptococcal pharyngitis. Am J Dis Child. 1972;124:352–8.
23. Shaikh N, Leonard E, Martin JM. Prevalence of streptococcal pharyngitis and streptococcal carriage in children: a meta-analysis. Pediatrics. 2010;126:e557–64. https://doi.org/10.1542/peds.2009-2648
24. Danchin MH, Rogers S, Kelpie L, Selvaraj G, Curtis N, Carlin JB, et al. Burden of acute sore throat and group A streptococcal pharyngitis in school-aged children and their families in Australia. Pediatrics. 2007;120:950–7. https://doi.org/10.1542/peds.2006-3368
25. Centor RM. When should patients seek care for sore throat? Ann Intern Med. 2013;159:636–7. https://doi.org/10.7326/0003-4819-159-9-201311050-00012
26. Aalbers J, O'Brien KK, Chan WS, Falk GA, Teljeur C, Dimitrov BD, et al. Predicting streptococcal pharyngitis in adults in primary care: a systematic review of the diagnostic accuracy of symptoms and signs and validation of the Centor score. BMC Med. 2011;9:67. https://doi.org/10.1186/1741-7015-9-67
27. Mistik S, Gokahmetoglu S, Balci E, Onuk FA. Sore throat in primary care project: a clinical score to diagnose viral sore throat. Fam Pract. 2015;32:263–8. https://doi.org/10.1093/fampra/cmv015
28. McIsaac WJ, Kellner JD, Aufricht P, Vanjaka A, Low DE. Empirical validation of guidelines for the management of pharyngitis in children and adults. [Erratum s in: JAMA. 2005;294:2700]. JAMA. 2004;291:1587–95. https://doi.org/10.1001/jama.291.13.1587
29. Gurney J. The incidence of acute rheumatic fever in New Zealand, 2010–2013. N Z Med J. 2015;128:65–7.
30. Jaine R, Baker M, Venugopal K. Epidemiology of acute rheumatic fever in New Zealand 1996–2005. J Paediatr Child Health. 2008;44:564–71. https://doi.org/10.1111/j.1440-1754.2008.01384.x
31. Baker MG, Barnard LT, Kvalsvig A, Verrall A, Zhang J, Keall M, et al. Increasing incidence of serious infectious diseases and inequalities in New Zealand: a national epidemiological study. Lancet. 2012;379:1112–9. https://doi.org/10.1016/S0140-6736(11)61780-7
32. Free S, Howden-Chapman P, Pierse N, Viggers H; Housing, Heating and Health Study Research Team. More effective home heating reduces school absences for children with asthma. J Epidemiol Community Health. 2010;64:379–86. https://doi.org/10.1136/jech.2008.086520
33. Pierse N, Arnold R, Keall M, Howden-Chapman P, Crane J, Cunningham M; Heating Housing and Health Study Group. Modelling the effects of low indoor temperatures on the lung function of children with asthma. J Epidemiol Community Health. 2013;67:918–25. https://doi.org/10.1136/jech-2013-202632
34. Anderson P, Craig E, Jackson G, Jackson C. Developing a tool to monitor potentially avoidable and ambulatory care sensitive hospitalisations in New Zealand children. N Z Med J. 2012;125:25–37.
35. Baker MG, McDonald A, Zhang J, Howden-Chapman P. Infectious diseases attributable to household crowding in New Zealand: a systematic review and burden of disease estimate [cited 2020 Mar 20]. https://www.health.govt.nz/publication/infectious-diseases-attributable-household-crowding-new-zealand-systematic-review-and-burden-disease
36. Grimes A, Tim Denne T, Howden-Chapman P, Arnold R, Telfar-Barnard L, Preval N, et al. Cost benefit analysis of the Warm Up New Zealand: Heat Smart Programme [cited 2017 Apr 4]. https://motu.nz/our-work/urban-and-regional/housing/cost-benefit-analysis-of-the-warm-up-new-zealand-heat-smart-programme
37. Woodward A, Crampton P, Howden-Chapman P, Salmond C. Poverty—still a health hazard. N Z Med J. 2000;113:67–8.
38. Heart Foundation of New Zealand. Group A streptococcal sore throat management guideline. 2014 Update [cited 2017 Apr 4]. https://www.heartfoundation.org.nz/resources/group-a-streptococcal-sore-throat-management
39. Oliver JR, Pierse N, Stefanogiannis N, Jackson C, Baker MG. Acute rheumatic fever and exposure to poor housing conditions in New Zealand: a descriptive study. J Paediatr Child Health. 2017;53:358–64. https://doi.org/10.1111/jpc.13421
40. Baker MG, Gurney J, Oliver J, Moreland NJ, Williamson DA, Pierse N, et al. Risk factors for acute rheumatic fever: literature review and protocol for a case-control study in New Zealand. Int J Environ Res Public Health. 2019;16:4515. https://doi.org/10.3390/ijerph16224515
41. Raynes JM, Frost HR, Williamson DA, Young PG, Baker EN, Steemson JD, et al. Serological evidence of immune priming by group A streptococci in patients with acute rheumatic fever. Front Microbiol. 2016;7:1119. https://doi.org/10.3389/fmicb.2016.01119

Address for correspondence: Jane Oliver, 792 Elizabeth St, Melbourne 3000, Victoria, Australia; email: jane.oliver@unimelb.edu.au

Temporary Fertility Decline after Large Rubella Outbreak, Japan

Kenji Mizumoto, Gerardo Chowell

Japan experienced 2 large rubella epidemics in 2004 and 2012–2014. Because of suboptimal immunization levels, the country has been experiencing a third major outbreak during 2018–2020. We conducted time series analyses to evaluate the effect of the 2012–2014 nationwide rubella epidemic on prefecture-level natality in Japan. We identified a statistically significant decline in fertility rates associated with rubella epidemic activity and increased Google searches for the term "rubella." We noted that the timing of fertility declines in 2014 occurred 9–13 months after peak rubella incidence months in 2013 in 4 prefectures with the highest rubella incidence. Public health interventions should focus on enhancing vaccination campaigns against rubella, not only to protect pregnant women from infection but also to mitigate declines in population size and birth rates.

Japan has recently experienced 2 large rubella epidemics. A 2004 epidemic had 4,248 reported cases, and another outbreak during 2012–2014 had 12,614 reported rubella cases and 45 reported cases of severe birth defects in newborns (*1*–*4*). Because of suboptimal immunization levels, Japan is now experiencing a third major rubella outbreak that began in 2018 (*5*–*7*). This epidemic has resulted in 5,296 reported cases as of April 12, 2020, and has affected all 47 prefectures by the 13th week of 2020 (*8*).

Rubella infections during early pregnancy can lead to serious health consequences, including miscarriages, stillbirths, and severe birth defects in newborns, known as congenital rubella syndrome (CRS) (*9*). The continued rubella epidemic in Japan led the US Centers for Disease Control and Prevention to issue a travel alert on October 22, 2018, that urged increased precautions and recommended pregnant women not protected against rubella avoid traveling to Japan (*9*).

Author affiliations: Kyoto University, Kyoto, Japan, and Hokkaido University, Hokkaido, Japan (K. Mizumoto); Georgia State University, Atlanta, GA, USA (K. Mizumoto, G. Chowell) Fogarty International Center, National Institutes of Health, Bethesda, Maryland, USA (G. Chowell)

DOI: https://doi.org/10.3201/eid2606.181718

Past studies have suggested that the 1918–1920 influenza pandemic had a profound effect on those planning to conceive children, which led to declines in birth rates after adjusting for maternal death (*10*,*11*). We examined the effects of Japan's large rubella outbreak during 2012–2014 on behavioral changes among women of childbearing age by quantifying the temporal changes in fertility rates and rubella cases in 4 prefectures of Japan that experienced the brunt of the 2013 rubella epidemic.

Methods

Data Sources

We extracted data on births/month and estimated female population/year stratified by age and prefecture from January 1, 2013–December 31, 2017, for Japan and 4 prefectures with the highest cumulative number of rubella cases in 2013 from the Ministry of Internal Affairs and Communications in Japan (*12*). Then, we calculated monthly estimates of the female population 15–49 years of age during 2013–2018 by using a smoothing cubic spline interpolation-fitting method with a knot at each data point. Because the number of births/age group was not available, we considered the fertility rate to be the proportion of births divided by the number of female persons 15–49 years of age/1,000 population/year.

We collected notifications of rubella and CRS cases from weekly reports published by the National Institute of Infectious Diseases in Japan and converted these to monthly case counts (*8*). Surveillance relies on mandatory notifications and medical institutions must report all diagnosed rubella and CRS cases. Clinical diagnosis of rubella includes symptoms of generalized rash, swollen lymph nodes, and fever.

We also extracted relevant monthly data on Google search terms from Google Trends (https://trends.google.com) to quantify the public attention to the rubella epidemic. We suspect anxiety was driven by a perceived risk rather than actual risk. For example, during a 2014–15 outbreak of Ebola virus,

the public conducted internet searches to collect information related to the epidemic, even in areas with extremely low risk for infection (*13*). Google Trends uses searches for keywords and search terms to provide data on search volume in a geographic region over time and generates an output scale of 0–100 (*14*).

We conducted a search of Google Trends by using the search topic strategy for January 1, 2012–December 31, 2017, and included the Tokyo, Kanagawa, Osaka, and Hyogo prefectures by using the Japanese word for rubella, "fushin." We used data from years after 2013 to exclude demographic changes and perinatal outcomes associated with the Great East Japan Earthquake that occurred on March 11, 2011 (*15*).

Statistical Analysis

Time series data can be decomposed into three components: seasonality, long-term trends, and random (*16*,*17*). For our study, the seasonal and trend components contain effects of long-term changes. Temporal variation in the fertility rate over time can be effected by systematic seasonal changes, such as the number of marriages, and long-term trends, such as population demography. By filtering out these components, we were able to concentrate on a single event. We applied moving averages to extract monthly seasonal- and trend-adjusted elevated fertility rates and their residuals. To detect temporal associations between these time series data, we examined cross-coefficients of fertility rates, rubella cases, and Google searches for "rubella" at different lag intervals (lags or leads ≤12 months) for each combination of 2/3 variables. A more detailed description of this procedure is published elsewhere (*10*,*18*,*19*). Then, we used an augmented Dickey-Fuller test for stationarity analysis. We used the Mann-Kendall test for trend analysis and null hypotheses of 0 cross-correlation for each of the estimated correlation coefficients.

We used a bootstrap method with 1,000 replications to calculate mean monthly and annual fertility rates in 2014 and corresponding confidence intervals. We performed statistical analyses in R version 3.2.3 (R Foundation for Statistical Computing, https://www.r-project.org).

Results

We assessed geospatial variation in cumulative rubella cases across Japan in 2013 (Figure 1, panel A). The highest rubella incidence occurred in Tokyo (2,547 cases), Osaka (2,241 cases), Kanagawa (1,230 cases), and Hyogo (941 cases). The distribution of cumulative rubella cases across all prefectures was highly skewed to the right with a median of 44.0 (interquartile range 20.5–106.5). We assessed the number of rubella and CRS cases by month during 2013–2019. During the 2012–2014 outbreak, the highest incidence of rubella was 2,513 cases in May 2013 and the highest incidence of CRS was 7 cases in October 2013 (Figure 1, panel B).

We assessed the seasonal variation of fertility rates for the 4 prefectures with the highest rubella burden (Figure 2). We observed fertility rate declines for 2014 during 5 months in Tokyo, 2 months in Kanagawa, 3 months in Osaka, and 4 months in Hyogo, after which rates increased during 6 months in Tokyo, 5 months in Kanagawa, 2 months in Osaka, and 4 months in Hyogo. Of note, fertility rate declines in 2014 occurred in the first half of the year, which corresponds to 9–13 months after rubella incidence peaked in Tokyo, 11–12 months after peak incidence in Kanagawa, 9–11 months after peak incidence in Osaka, and 8–12 months after peak incidence in Hyogo (Table). We believe behavioral changes occurred around the peak rubella incidences and calculated times after the peak incidence of rubella cases.

We plotted the time series of rubella cases, Google searches for "rubella," and seasonality- and trend-adjusted fertility rates for the 4 prefectures with the highest rubella incidence (Figure 3). We found that peaks in rubella cases and Google searches for "rubella" were synchronized across the 4 prefectures with the most rubella cases. However, troughs in elevated fertility rates occurred 9–11 months after the peak in rubella cases and Google searches for "rubella" (Table). To statistically assess the timescale of the association between rubella cases, Google searches for "rubella," and elevated fertility rates, we calculated cross-correlations between these 3 signals in the time series. In Tokyo, we found a negative association between rubella incidence and fertility rates at a time lag of 9 months (r = –0.280), 10 months (r = –0.390), 11 months (r = –0.408), and 12 months (r = –0.284) and between Google searches for "rubella" and fertility rates at time lags of 9 months (r = –0.382), 10 months (r = –0.468), and 11 months (r = –0.397) (Figure 4; Appendix Table 1, http://wwwnc.cdc.gov/EID/article/26/6/18-1718-App1.pdf). We also identified negative associations between rubella incidence and fertility rates in Kanagawa at time lags of 9 months (r = –0.320), 10 months (r = –0.428), and 11 months (r = –0.446) and between Google searches for "rubella" and fertility rates at time lags of 9 months (r = –0.385), 10 months (r = –0.461), and 11 months (r = –0.432) (Appendix Table 2, Figure 1). In Osaka, we found positive and negative associations between rubella cases and fertility rates at a time lag of 5 months (r = 0.296), 9 months (r = –0.365), 10 months (r = –0.424), and 11 months (r = –0.319) and

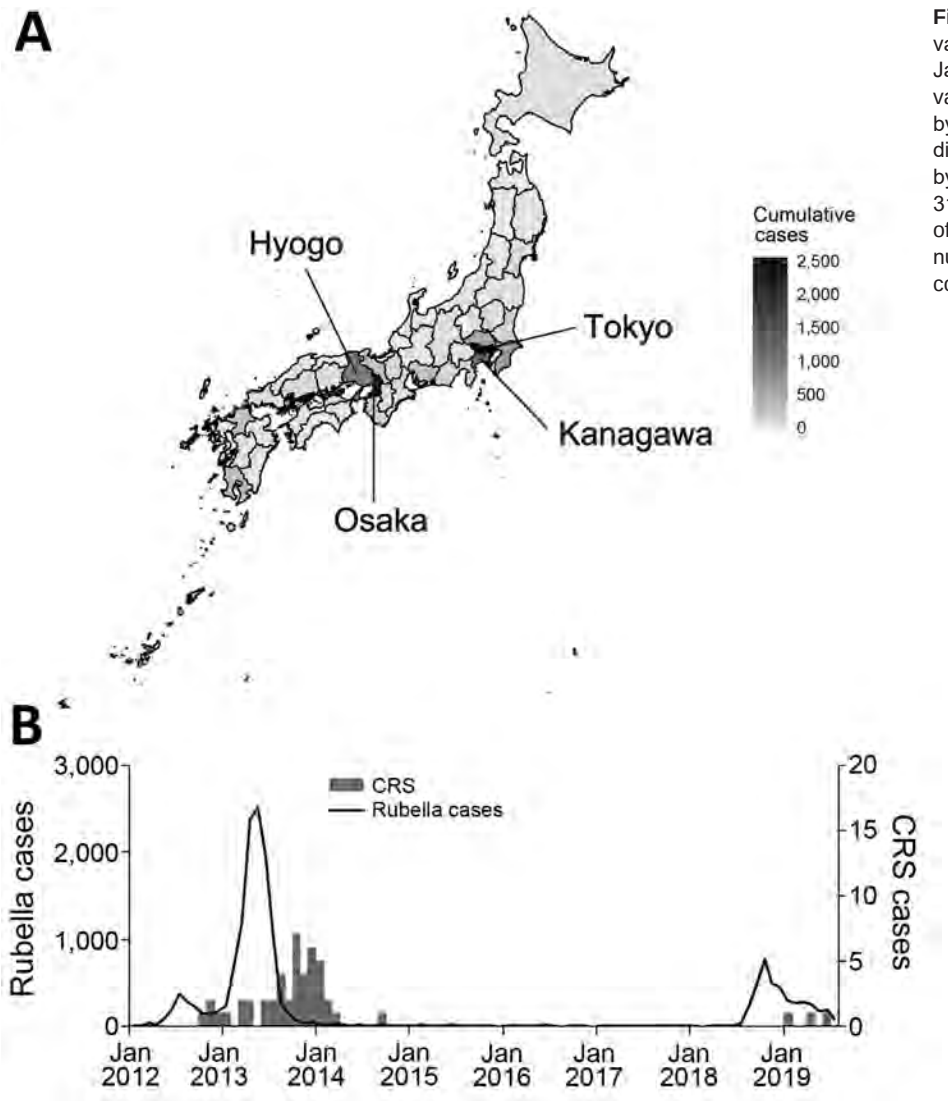

Figure 1. Spatial and temporal variations of rubella and CRS in Japan, 2013–2019. A) Geospatial variation in cumulative rubella cases by prefecture, 2013. B) Temporal distribution of rubella and CRS cases by month during January 1, 2012–July 31, 2019. Black line indicates number of cases of rubella. Gray bars indicate number of cases of CRS. CRS, congenital rubella syndrome.

between Google searches for "rubella" and fertility rates at 4 months (r = 0.286), 5 months (r = 0.316), 9 months (r = –0.356), 10 months (r = –0.437), and 11 months (r = –0.361) (Appendix Table 3, Figure 2). In Hyogo, we identified positive and negative associations between rubella cases and fertility rates at a time lag of 5 months (r = 0.347), 9 months (r = –0.309), 10 months (r = –0.410), and 11 months (r = –0.402) and between Google searches for "rubella" and fertility rates at 0 months (r = –0.298), 5 months (r = 0.346), 9 months (r = –0.310), 10 months (r = –0.398), and 11 months (r = –0.393) (Appendix Table 4, Figure 3). We observed several positive associations between rubella incidence and Google searches for "rubella" in all 4 prefectures.

We decomposed time series data of fertility rates for Tokyo, Kanagawa, Osaka, and Hyogo (Appendix Figure 4). We observed downward trends in fertility rates but a small peak during 2015 and an upward trend before 2015 in Tokyo. Seasonally, fertility rates tend to decrease in the first half of the year and increase in the second half of the year.

We did not find statistically significant differences in fertility rates between 2014 and the control years. Fertility rate differences between 2014 and control years were 34.87 (95% CI 34.01–35.20)/1,000 women of childbearing age in Tokyo, 36.52 (95% CI 35.06–36.92)/1,000 women of childbearing age in Kanagawa, 35.95 (95% CI 35.25–36.6)/1,000 women of childbearing age in Osaka, and 37.97 (95% CI 37.15–38.53)/1,000 women of childbearing age in Hyogo.

Discussion

We assessed the effect of the 2012–2014 rubella epidemic on prefecture-level natality in Japan. We identified a statistically significant decline in fertility rates associated with rubella epidemic activity and

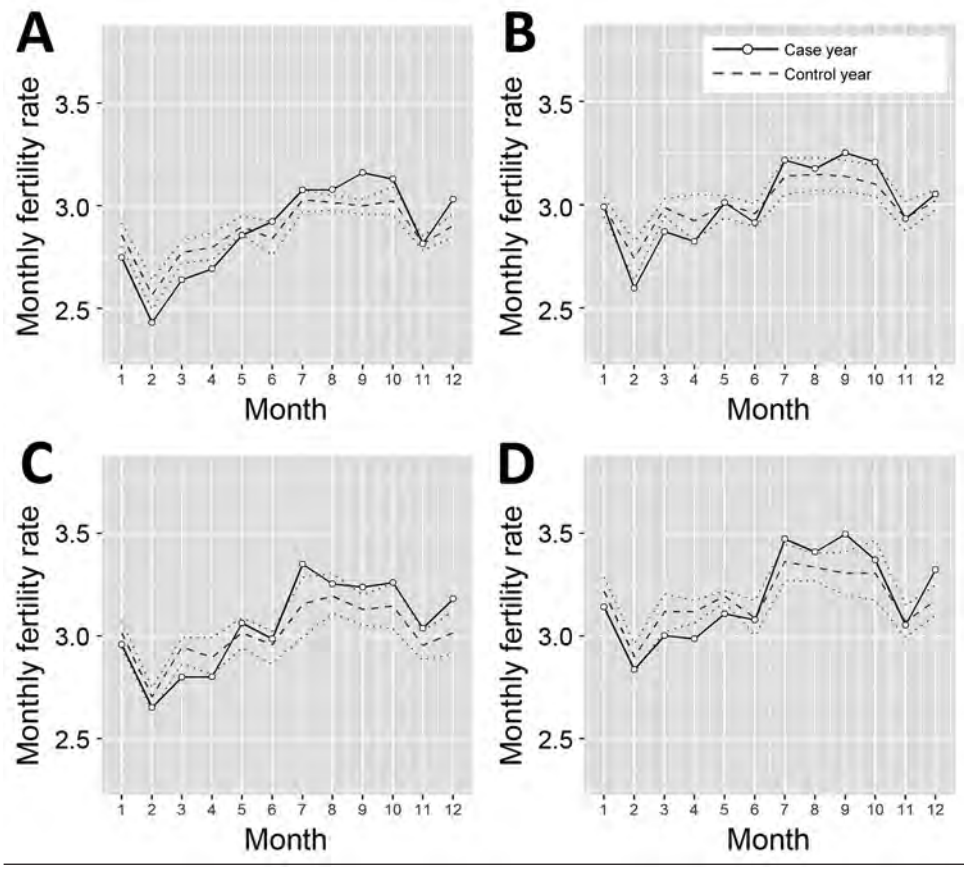

Figure 2. Temporal variation of fertility rates by prefecture in Japan, 2013–2017. A) Tokyo; B) Kanagawa; C) Osaka; and D) Hyogo. Solid line indicates average fertility rate during the case year, 2014. Dashed line indicates the average fertility rate during the combined control years, 2013, 2015, 2016, and 2017. Dotted lines indicate upper and lower limits of 95% CI for control years.

Google searches for "rubella." We noted declines in fertility rates in 2014 that occurred after each peak month of rubella case incidence in 2013, which was 9–13 months after peaks in Tokyo, 11–12 months in Kanagawa, 9–11 months in Osaka, and 8–12 months in Hyogo. Considering the relatively small number of rubella cases during 2012–2014, we do not think the reduction in fertility was caused by miscarriages or stillbirths but by voluntary pregnancy delays because of perceived risk for CRS, which is reflected in increases in Google searches for "rubella."

Birth rate declines associated with infectious disease epidemics could exacerbate the effects of demographic changes in Japan, which are characterized by decreased population, declines in birth rates, and a delayed childbearing trend. According to the 2010 census, the population of Japan is ≈127.09 million, a decrease of 962,607 from the previous census (*20*). In addition, the fertility rate was 1.44/1,000 female persons 15–49 years of age in 2016, much lower than the replacement-level fertility of 2.1/1,000, the minimum level needed to sustain population size (*21*). Similarly, the average age of women at first childbirth rose from 25.6 years of age in 1970 to 30.7 years of age in 2016. Older maternal age is associated with increased risks for adverse pregnancy and birth outcomes (*22*–*26*).

We found no statistically significant differences in birth rates between 2014 and the control years (2013, 2015, 2016, and 2017). However, pregnancy delays related to fear of infection and the increased proportion of late-age childbearing exacerbate the declining birth trend for the ongoing and future rubella epidemics.

Table. Summary results on the timing of peak rubella cases and deficit fertility rates for 4 prefectures in Japan, 2013*

	Rubella case peaks, 2013			Decreased fertility, 2014		Lag time troughs, mo.	
Prefecture	Month	No. cases	Peak month for Google searches, 2013	Month of lowest birth rates	Deficit rate at lowest month†	Peak rubella incidence–fertility rate decline	Peak Google search–fertility rate decline
Tokyo	Apr	571	Apr	Mar	–0.090	11	11
Kanagawa	Apr	305	Apr	Mar	–0.130	11	11
Osaka	May	730	May	Feb	–0.120	9	9
Hyogo	May	260	May	Apr	–0.111	11	11

*Data on Google searches collected from Google Trends (https://trends.google.com).
†Irregular only.

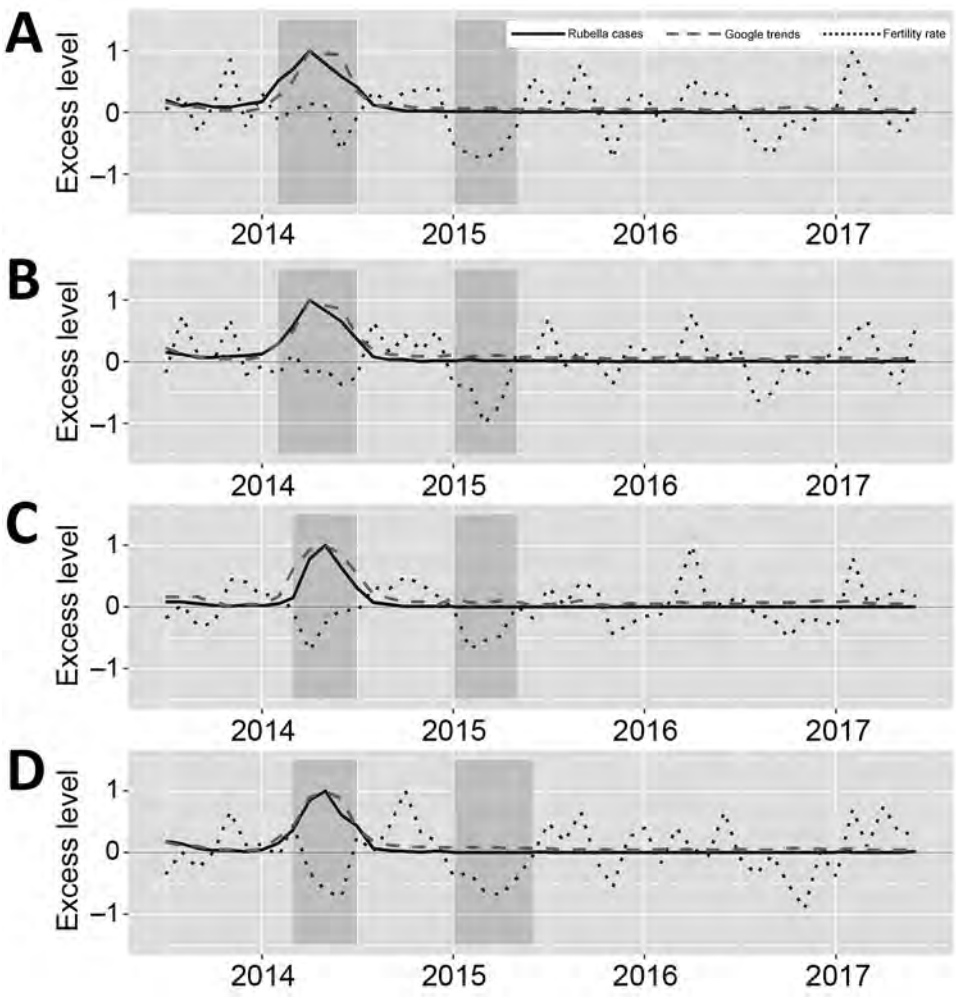

Figure 3. Cross-correlation between rubella cases, Google searches for "rubella," and elevated fertility rates, Tokyo, Japan, 2012–2016. Cross-correlation coefficients were calculated in each lag, –12 months, lead period, +12 months, and at 0. Bars indicate cross-correlation coefficients between A) fertility rate and rubella case time-series; B) fertility rate and Google searches for "rubella" time-series; and C) rubella cases and Google searches for "rubella" time series. Horizontal dashed lines are the confidence limits (upper limit, 0.28; lower limit, –0.28) for the null hypothesis of 0 true cross-correlation coefficients between the 2 time-series. Google search data collected from Google Trends (https://trends.google.com).

Therefore, Japan's government should implement public health interventions to rapidly curtail rubella transmission, protect childbearing mothers, and sustain birth rates.

Our study has several limitations. First, we did not establish a causal relationship between an increase of rubella cases and a decrease of fertility rate, but studies have suggested a person's behavior will change not only because of actual risk but also because of perceived risk (*13*). Indeed, some segments of the population with low vaccination coverage in Japan, such as women 24–34 years of age who are part of a relatively small group of persons born during 1989–1993 in which only 78.3% are seropositive, presumably worry about infection and CRS (*1*,*6*). In addition, soon after the rubella outbreak occurred, the Ministry of Health, Labour and Welfare issued its first notice to alert the public on May 25, 2012, and subsequently issued an additional 7 notices during the outbreak (*27*). On January 29, 2013, Japan's National Institute of Infectious Diseases published specific guidelines for prevention and control of rubella and CRS (*28*). These approaches likely increased the population's awareness about the risk for rubella infection and its potential consequences. Furthermore, a substantial number of pregnancies likely were delayed until the end of the outbreaks because of concerns about rubella infection, and public awareness, which is partially supported by the internet search activities recorded by Google Trends. In addition, the relationship between the 1918 influenza pandemic and fertility, in which a direct causal relationship was estimated (*10*,*18*,*19*), indicates a remarkable decline in births occurring 9–11 months after the surge in pandemic mortality rates. A similar phenomenon was observed for the Zika virus (ZIKV) epidemic. After the identification of the probable association between ZIKV infection during pregnancy and microcephaly in 2016 (*29*–*31*), public concern over ZIKV quickly increased in Brazil, where a substantial number of microcephaly cases initially were reported.

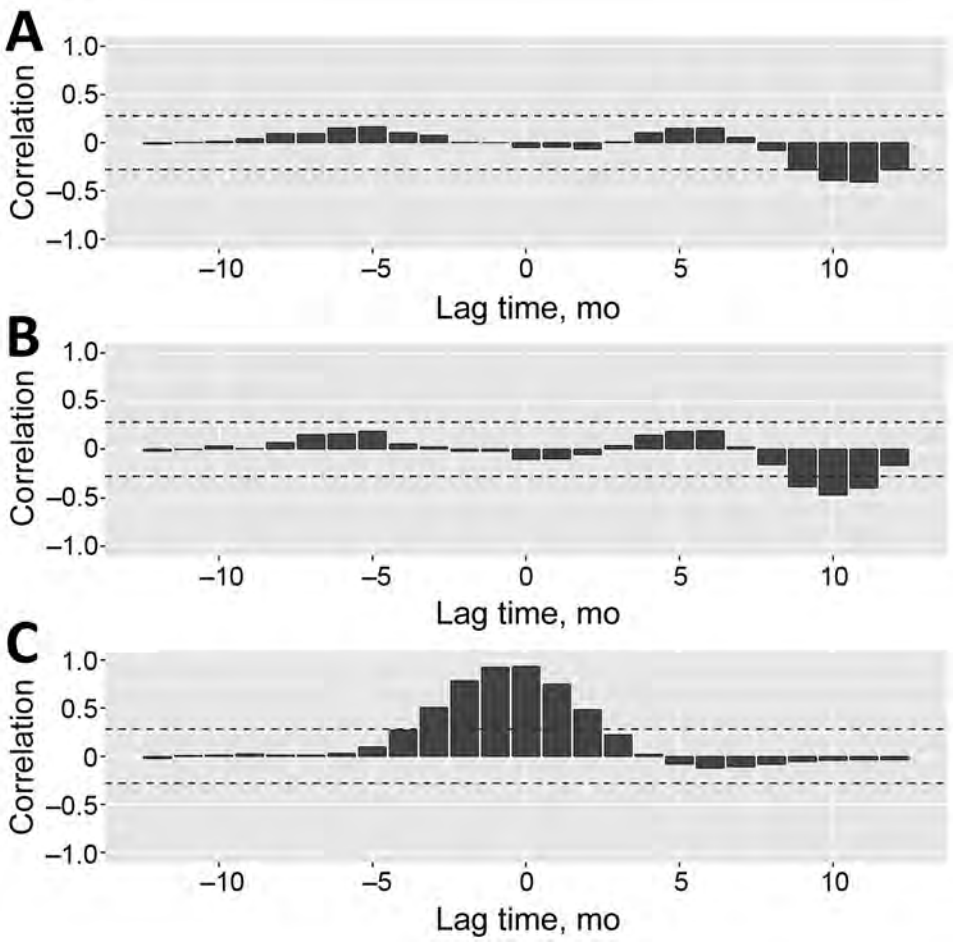

Figure 4. Temporal distribution of rubella cases, Google searches for the term "rubella," and elevated fertility rates by prefecture, 2013–2017, Japan. A) Tokyo; B) Kanagawa; C) Osaka; D) Hyogo Time-series of rubella cases, Google searches for the term "rubella," and seasonally- and trend-adjusted elevated fertility rates. The data are scaled between –1 and 1. Dark gray areas show the peak timing of rubella cases and the corresponding drop timing of fertility rates. Google search data collected from Google Trends (https://trends.google.com).

As a result, birth rates in Brazil's largest cities during the second half of 2016 exhibited substantial reductions ≈9 months after the start of media coverage for the ZIKV epidemic (*32*,*33*). We found a similar fertility decline 9–11 months after the peaks in rubella case incidence and peak Google searches for "rubella" across all 4 prefectures. To reinforce the statistical association, we conducted additional analyses. We used influenza, which does not affect people's fertility decisions, as a control and did not find a decline in fertility associated with influenza case counts or the Google searches for "influenza" (Appendix Tables 5–8, Figures 5–8). We explored wavelet cross-correlation to measure similarity between 2 signals at different scales (*34*,*35*). We identified relatively high coefficients at a lag time of 9–11 months in levels 2 and 3 between rubella incidence and fertility, and between rubella incidence and Google searches for "rubella," consistent with our results (Appendix Tables 9–11, Figures 9–20).

Second, we did not identify the causal relationship for the substantial fertility rate increases ahead of substantial fertility rate declines. Although we examined the association between fertility rates and other factors, including economic index, such as prefectural-level unemployment rates and the Nikkei Index, and the number of marriages (data not shown), we did not identify statistically significant associations. Several interrelated factors likely played a role. In addition, we only observed the lagged increases in Osaka and Hyogo, and the number of the months and the correlation coefficients are relatively small compared with the lagged decrease.

Third, an increase in Google searches for "rubella" might have preceded an outbreak of rubella cases at the prefectural level because media reporting about the outbreaks raised public awareness, potentially leading to large-scale behavior changes in the country. However, the temporal variations of rubella cases and Google searches for "rubella" in all 4 prefectures are highly correlated at a time lag of 0 (Figure 4; Appendix Tables 1–4, Figures 1–3) and rubella case incidence and Google searches for "rubella" mostly were synchronized.

In conclusion, our analyses indicate a substantial temporal decline in the fertility rate in Japan after a

major rubella outbreak in 2012–2014. Public health interventions should focus on enhancing vaccination campaigns against rubella, not only to protect pregnant women from infection but also to mitigate declines in population size and birth rates.

K.M. received support from the Japan Society for the Promotion of Science KAKENHI (grant no. 15K20936), from the Program for Advancing Strategic International Networks to Accelerate the Circulation of Talented Researchers (grant no. G2801), and from the Leading Initiative for Excellent Young Researchers from the Ministry of Education, Culture, Sport, Science & Technology of Japan. G.C. received support from the National Science Foundation (grant no. 1414374) as part of the joint National Science Foundation, National Institutes of Health, and US Department of Agriculture Ecology and Evolution of Infectious Diseases program and a grant from the UK Biotechnology and Biological Sciences Research Council (no. BB/M008894/1).

About the Authors

Dr. Mizumoto works as an assistant professor at the Graduate School of Advanced Integrated Studies in Human Survivability, Kyoto University in Japan. His research interests include mathematical and statistical epidemiology and modeling of infectious diseases. Dr. Chowell is a professor of epidemiology and biostatistics and chair of the Department of Population Health Sciences at the Georgia State University School of Public Health. He is also a senior research fellow at the Fogarty International Center, National Institutes of Health, USA. His research interests include mathematical modeling of infectious disease dynamics and control.

References

1. Ujiie M, Nabae K, Shobayashi T. Rubella outbreak in Japan. Lancet. 2014;383:1460–1. https://doi.org/10.1016/S0140-6736(14)60712-1
2. Minakami H, Kubo T, Unno N. Causes of a nationwide rubella outbreak in Japan, 2012-2013. J Infect. 2014;68:99–101. https://doi.org/10.1016/j.jinf.2013.09.002
3. US Centers for Disease Control and Prevention (CDC). Nationwide rubella epidemic—Japan, 2013. MMWR Morb Mortal Wkly Rep. 2013;62:457–62.
4. Sugishita Y, Shimatani N, Katow S, Takahashi T, Hori N. Epidemiological characteristics of rubella and congenital rubella syndrome in the 2012–2013 epidemics in Tokyo, Japan. Jpn J Infect Dis. 2015;68:159–65. https://doi.org/10.7883/yoken.JJID.2014.195
5. Saito MM, Ejima K, Kinoshita R, Nishiura H. Assessing the effectiveness and cost-benefit of test-and-vaccinate policy for supplementary vaccination against rubella with limited doses. Int J Environ Res Public Health. 2018;15:E572. https://doi.org/10.3390/ijerph15040572
6. Kinoshita R, Nishiura H. Assessing herd immunity against rubella in Japan: a retrospective seroepidemiological analysis of age-dependent transmission dynamics. BMJ Open. 2016;6:e009928. https://doi.org/10.1136/bmjopen-2015-009928
7. Nishiura H, Kinoshita R, Miyamatsu Y, Mizumoto K. Investigating the immunizing effect of the rubella epidemic in Japan, 2012–14. Int J Infect Dis. 2015;38:16–8. https://doi.org/10.1016/j.ijid.2015.07.006
8. Infectious Disease Surveillance Center, National Institute of Infectious Diseases, Japan. Infectious Diseases Weekly Report [in Japanese] [cited 2020 April 12]. https://www.niid.go.jp/niid/ja/idwr.html
9. US Centers for Disease Control and Prevention. Rubella in Japan [cited 2018 Oct 24] https://wwwnc.cdc.gov/travel/notices/alert/rubella-japan
10. Chandra S, Christensen J, Mamelund SE, Paneth N. Short-term birth sequelae of the 1918–20 influenza pandemic in the United States: state-level analysis. Am J Epidemiol. 2018;187:2585–95. https://doi.org/1093/aje/kwy153
11. Bureau of the Census. Birth statistics for the registration area of the United States 1921. Washington, DC: Government Printing Office; 1923 [cited 2018 Nov 2]. https://babel.hathitrust.org/cgi/pt?id=hvd.li4xns;view=1up;seq=3
12. Ministry of Internal Affairs and Communications. Statistics Japan [in Japanese] [cited 2018 Oct 24]. http://www.e-stat.go.jp/SG1/estat/eStatTopPortal.do
13. Fung IC-H, Tse ZT, Cheung CN, Miu AS, Fu KW. Ebola and the social media. Lancet. 2014;384:2207. https://doi.org/10.1016/S0140-6736(14)62418-1
14. Gianfredi V, Bragazzi NL, Mahamid M, Bisharat B, Mahroum N, Amital H, et al. Monitoring public interest toward pertussis outbreaks: an extensive Google Trends–based analysis. Public Health. 2018;165:9–15. https://doi.org/10.1016/j.puhe.2018.09.001
15. Suzuki K, Yamagata Z, Kawado M, Hashimoto S. Effects of the great East Japan Earthquake on secondary sex ratio and perinatal outcomes. J Epidemiol. 2016;26:76–83. https://doi.org/10.2188/jea.JE20150055
16. Brockwell PJ, Davis RA. Introduction to time series and forecasting, second edition. New York: Springer Verlag; 2002.
17. Kendall M, Stuart A, Ord JK. The advanced theory of statistics, vol. 3, 4th ed. High Wycombe (England): Charles Griffin; 1983.
18. Dahal S, Mizumoto K, Bolin B, Viboud C, Chowell G. Natality decline and spatial variation in excess death rates during the 1918–1920 influenza pandemic in Arizona, United States. Am J Epidemiol. 2018;187:2577–84. https://doi.org/10.1093/aje/kwy146
19. Chandra S, Yu Y-L. Fertility decline and the 1918 influenza pandemic in Taiwan. Biodemogr Soc Biol. 2015;61:266–72. https://doi.org/10.1080/19485565.2015.1062718
20. Statistics Bureau, Ministry of Internal Affairs and Communications Japan. Statistical handbook of Japan 2017 [cited 2018 Oct 24]. http://www.stat.go.jp/english/data/handbook/pdf/2017all.pdf
21. World Health Organization South-East Asia. Total fertility rate, health situation and trend assessment [cited 2020 April 12]. http://origin.searo.who.int/entity/health_situation_trends/data/chi/TFR/
22. Kato T, Yorifuji T, Yamakawa M, Inoue S, Doi H, Eboshida A, et al. Association of maternal age with child health: a Japanese longitudinal study. PLoS One. 2017;12:e0172544. https://doi.org/10.1371/journal.pone.0172544

23. Heffner LJ. Advanced maternal age—how old is too old? N Engl J Med. 2004;351:1927–9. https://doi.org/10.1056/NEJMp048087
24. Schmidt L, Sobotka T, Bentzen JG, Nyboe Andersen A; ESHRE Reproduction and Society Task Force. Demographic and medical consequences of the postponement of parenthood. Hum Reprod Update. 2012;18:29–43. https://doi.org/10.1093/humupd/dmr040
25. Carolan M, Frankowska D. Advanced maternal age and adverse perinatal outcome: a review of the evidence. Midwifery. 2011;27:793–801. https://doi.org/10.1016/j.midw.2010.07.006
26. Hsieh TT, Liou JD, Hsu JJ, Lo LM, Chen SF, Hung TH. Advanced maternal age and adverse perinatal outcomes in an Asian population. Eur J Obstet Gynecol Reprod Biol. 2010;148:21–6. https://doi.org/10.1016/j.ejogrb.2009.08.022
27. National Institute of Infectious Diseases. Risk assessment for rubella outbreak and congenital rubella syndrome [in Japanese]. 2013 Sep 30 [cited 2018 Oct 24]. https://www.niid.go.jp/niid/ja/rubella-m-111/2145-rubella-related/3980-rubella-ra-2.html
28. National Institute of Infectious Diseases. Guidance on strengthening measures for prevention and control of rubella and congenital rubella syndrome [in Japanese]. Infectious Agents Surveillance Report. 2013:34;90 [cited 2018 Oct 24] https://www.niid.go.jp/niid/en/iasr-sp/2250-related-articles/related-articles-398/3427-de3981.html
29. Schuler-Faccini L, Ribeiro EM, Feitosa IM, Horovitz DD, Cavalcanti DP, Pessoa A, et al.; Brazilian Medical Genetics Society–Zika Embryopathy Task Force. Possible association between Zika virus infection and microcephaly—Brazil, 2015. MMWR Morb Mortal Wkly Rep. 2016;65:59–62. https://doi.org/10.15585/mmwr.mm6503e2
30. Johansson MA, Mier-y-Teran-Romero L, Reefhuis J, Gilboa SM, Hills SL. Zika and the risk of microcephaly. N Engl J Med. 2016;375:1–4. https://doi.org/10.1056/NEJMp1605367
31. Nishiura H, Mizumoto K, Rock KS, Yasuda Y, Kinoshita R, Miyamatsu Y. A theoretical estimate of the risk of microcephaly during pregnancy with Zika virus infection. Epidemics. 2016;15:66–70. https://doi.org/10.1016/j.epidem.2016.03.001
32. Diaz-Quijano FA, Chiavegatto Filho ADP. Reduction of the birth rate in São Paulo: a probable effect of the panic caused by the Zika-associated microcephaly epidemic. Ann Epidemiol. 2017;27:616–7. https://doi.org/10.1016/j.annepidem.2017.08.009
33. Diaz-Quijano FA, Pelissari DM, Chiavegatto Filho ADP. Zika-associated microcephaly epidemic and birth rate reduction in Brazilian cities. Am J Public Health. 2018;108:514–6. https://doi.org/10.2105/AJPH.2017.304260
34. Cazelles B, Chavez M, Berteaux D, Ménard F, Vik JO, Jenouvrier S, et al. Wavelet analysis of ecological time series. Oecologia. 2008;156:287–304. https://doi.org/ 10.1007/s00442-008-0993-2
35. Metcalf CJE, Walter KS, Wesolowski A, Buckee CO, Shevliakova E, Tatem AJ, et al. Identifying climate drivers of infectious disease dynamics: recent advances and challenges ahead. Proc Biol Sci. 2017;284:20170901. https://doi.org/10.1098/rspb.2017.0901

Address for correspondence: Kenji Mizumoto, Graduate School of Advanced Integrated Studies in Human Survivability, Kyoto University, Yoshida-Nakaadachi-cho, Sakyo-ku, Kyoto 606-8306, Japan; email: mizumoto.kenji.5a@kyoto-u.ac.jp

Radical Change in Zoonotic Abilities of Atypical BSE Prion Strains as Evidenced by Crossing of Sheep Species Barrier in Transgenic Mice

Alba Marín-Moreno,[1] Alvina Huor,[1] Juan Carlos Espinosa, Jean Yves Douet, Patricia Aguilar-Calvo,[2] Naima Aron, Juan Píquer, Sévérine Lugan, Patricia Lorenzo, Cecile Tillier, Hervé Cassard, Olivier Andreoletti, Juan María Torres

Classical bovine spongiform encephalopathy (BSE) is the only zoonotic prion disease described to date. Although the zoonotic potential of atypical BSE prions have been partially studied, an extensive analysis is still needed. We conducted a systematic study by inoculating atypical BSE isolates from different countries in Europe into transgenic mice overexpressing human prion protein (PrP): $TgMet_{129}$, $TgMet/Val_{129}$, and $TgVal_{129}$. L-type BSE showed a higher zoonotic potential in $TgMet_{129}$ mice than classical BSE, whereas Val_{129}-PrP variant was a strong molecular protector against L-type BSE prions, even in heterozygosis. H-type BSE could not be transmitted to any of the mice. We also adapted 1 H- and 1 L-type BSE isolate to sheep-PrP transgenic mice and inoculated them into human-PrP transgenic mice. Atypical BSE prions showed a modification in their zoonotic ability after adaptation to sheep-PrP producing agents able to infect $TgMet_{129}$ and $TgVal_{129}$, bearing features that make them indistinguishable of sporadic Creutzfeldt-Jakob disease prions.

Prion diseases, or transmissible spongiform encephalopathies (TSEs), are a group of rare and lethal neurodegenerative diseases that affect a great number of mammal species, including humans and animals belonging to the human food chain. The conversion of a host encoded cellular protein of unknown function (PrP^C) into a disease-associated isoform (PrP^{Sc}) is the molecular event underlying the development of TSEs. Such conformational change is driven by PrP^{Sc} itself because it recruits and transforms PrP^C molecules, acting as a template (*1*). The conformational change, associated with an increase of β-sheet content, also results in a change in the protein biochemical features (*2*). Although PrP^C is monomeric, protease-sensitive, and soluble in nonionic detergents, PrP^{Sc} has a high tendency to aggregate, is partially resistant to protease digestion, and is insoluble in nonionic detergents (*1*,*3*).

Classical bovine spongiform encephalopathy (C-BSE) caused a major food safety crisis when consumption of contaminated meat was discovered in the late 1990s as the cause of a new prion disease affecting humans, which was called variant Creutzfeldt-Jakob disease (vCJD) (*4*). The first description of C-BSE was made in 1987 in affected cattle in the United Kingdom (*5*). In the years following, ≈200,000 cattle succumbed to the disease (*6*). To date, C-BSE is the only recognized zoonotic prion (*6*) and is responsible for ≥231 human deaths (*7*).

After the implementation of active surveillance in the European Union in 2001, several atypical BSE cases were identified in aged asymptomatic cattle during slaughterhouse testing. Two major phenotypes with pathology and epidemiology distinct from C-BSE were observed, bovine amyloidotic spongiform encephalopathy (or L-BSE) (*8*) and H-BSE (*9*). The biochemical properties of PrP^{Sc} isolated from these cases also differed from C-BSE in terms of the protease-resistant fragment size and ratio of glycoforms on Western blot (WB). It is unclear whether atypical BSE resulted from exposure to an acquired

Author affiliations: Centro de Investigación en Sanidad Animal, Madrid, Spain (A. Marín-Moreno, J.C. Espinosa, P. Aguilar-Calvo, J. Píquer, P. Lorenzo, J.M. Torres); Interactions Hôte Agent Pathogène–École Nationale Vétérinaire de Toulouse, Toulouse, France (A. Huor, J.Y. Douet, N. Aron, S. Lugan, C. Tiller, H. Cassard, O. Andreoletti)

DOI: https://doi.org/10.3201/eid2606.181790

[1]These first authors contributed equally to this article.

[2]Current affiliation: University of California–San Diego, La Jolla, California, USA.

TSE or emerged spontaneously, a theory supported by the occurrence of atypical BSE being maintained at a similar rate in various countries independent of their C-BSE status.

The zoonotic potentials of atypical and C-BSE seemed to differ. One study performed in transgenic mice overexpressing the human Met_{129}–normal brain prion protein (PrP) variant (Tg650) showed that L-BSE has a higher zoonotic potential than C-BSE because a 100% attack rate was observed in the intracranial challenge, whereas H-BSE was unsuccessfully transmitted (*10*). Other intermediate species belonging to the human food chain might play a role in a possible atypical BSE zoonosis. For example, C-BSE can naturally affect goats (*11*). Furthermore, C-BSE virulence in human-PrP transgenic mouse models is increased after passaging in ovine-PrP transgenic mice (*12*). The possible zoonotic potential of atypical BSE after its adaptation to the sheep sequence is not known. At least L-type BSE is efficiently transmitted in sheep (*13*). L-BSE transmission in ovine-PrP transgenic mouse models produced a prion similar to C-BSE in terms of incubation times, histopathologic features, and electrophoretic mobility, although the glycoprofile maintained a more equilibrated proportion between the 3 bands than C-BSE (*14*). Therefore, a deep assessment of the zoonotic potential of atypical BSE prions should include the evaluation of zoonotic potential after adaptation to the sheep-PrP sequence.

Polymorphisms and mutations in the human prion protein gene affect survival and disease development in vCJD and other human TSEs (*15*). The most important genetic variant for disease outcome in humans is the polymorphic codon 129, which can codify methionine (Met_{129}) or valine (Val_{129}) and has been detected as Met_{129} homozygous in all vCJD-diagnosed cases, with the exception of 1 Met/Val_{129} heterozygous vCJD case (*16*,*17*).

The main aim of our study was to assess the zoonotic potential of the atypical BSE prions in transgenic mice that overexpress human-PrP covering the 3 possible 129 codon genotypes. We used a high number of isolates from different sites in Europe and a collection of human-PrP transgenic mouse lines. In addition, we adapted 1 H-BSE and 1 L-BSE isolate to the sheep-PrP sequence and sequentially inoculated them into human-PrP $TgMet_{129}$ and $TgVal_{129}$ mice to assess whether intermediate passage in sheep can modify prion strain features, including prion virulence in humans. We decided to use 2 different ovine-PrP transgenic mouse models to study the effect of the polymorphism Ala/Val_{136} of the sheep-PrP sequence.

Materials and Methods

Ethics Statement

We conducted animal experiments in accordance with the Code for Methods and Welfare Considerations in Behavioral Research with Animals (Directive 2010/63/EU) and made every effort to minimize suffering. Experiments developed in Centro de Investigación en Sanidad Animal–Instituto Nacional de Investigación y Tecnología Agraria y Alimentaria (Madrid, Spain) were evaluated by the Committee on the Ethics of Animal Experiments of the Instituto Nacional de Investigación y Tecnología Agraria y Alimentaria and approved by the General Directorate of the Madrid Community Government (permit nos. PROEX 263/15, PROEX 181/16, and PROEX 228/16). Experiments developed in Institut National de la Recherche Agronomique–École Nationale Vétérinaire de Toulouse (Toulouse, France) were approved by the Institut National de la Recherche Agronomique/École Nationale Vétérinaire de Toulouse Ethics Committee under the auspices of the Ministry of Education and Research of France (permit no. APAFIS-2017044210492380 v2).

Prion Isolates

We used a collection of atypical BSE field isolates from different countries in Europe to ensure the consistency of the results (Appendix Table, https://wwwnc.cdc.gov/EID/article/26/6/18-1790-App1.pdf). We characterized all isolates to differentiate them from C-BSE (data not shown). For comparison, we included C-BSE isolates and other prion isolates in the study. For inoculation, we prepared all isolates from brain tissues as 10% (wt/vol) homogenates in 5% glucose. Second passages were performed by inoculating mice with 10% (wt/vol) homogenates in 5% glucose of brains selected from first passage.

Mouse Transmission Studies

The atypical BSE isolates were inoculated in 3 different mouse models for human-PrP: HuPrP-Tg340-Met_{129} ($TgMet_{129}$) line expressing human Met_{129}-PrP variant (*12*), HuPrP-Tg361-Val_{129} ($TgVal_{129}$) line expressing human Val_{129}-PrP variant (*18*), and HuPrP-Tg351-Met/Val_{129} (TgMet/Val_{129}) line obtained by mating $TgMet_{129}$ and $TgVal_{129}$ mice (*18*). All of these transgenic lines show similar brain PrP^C levels of expression (≈4-fold the level of expression in human brain) on a mouse-PrP null background. For the adaptation to the sheep-PrP sequence, we used 2 different overexpressing sheep-PrP mouse models to include the 2 variants of the Ala/Val_{136} Arg_{154} Gln_{171}

haplotype. The OvPrP-Tg338 (TgVRQ) harbors the VRQ allele and expresses 8–10-fold the level of PrP^C expression in sheep brain (*19*). The OvPrP-TgShXI (TgARQ) harbors the ARQ allele and expresses 3–4-fold the level of PrP^C expression in sheep brain (*20*). We performed subsequent bioassays for the detection of low-level propagation of atypical BSE prions in BoPrP-Tg110 mice (TgBo) (*21*).

We individually anesthetized 6–7-week-old mice with isoflurane and inoculated them with 2 mg equivalent of brain homogenate in the right parietal lobe by using a 25-gauge disposable hypodermic needle. We observed mice daily and assessed their neurologic status twice a week. When progression of a TSE disease was evident or at the established experimental endpoint (700 days postinoculation), we euthanized the animals for ethical reasons, then performed necropsy and removed the brain. We fixed part of the brain by using immersion in neutral-buffered 10% formalin (4% 2-formaldehyde) and used it for histopathology; we froze the rest of the tissue at -20°C and used it for determining the presence of proteinase K–resistant PrP^{Sc} (PrP^{res}) by WB. We calculated survival times as mean ± SD days postinoculation for all the mice that scored positive for PrP^{res}. We defined the attack rate as the proportion of mice that scored positive for PrP^{res} divided by the number of inoculated mice. We used brain homogenates from PrP^{res}-positive mice for further passaging. When all mice were scored negative for PrP^{res} on primary passage, we pooled all PrP^{res}-negative brains and used them for second passage.

Histologic Examination and Paraffin-Embedded Tissue Blotting

We performed all procedures comprising the histopathologic analysis of mouse brains as previously described (*22*). We fixed mouse brain samples in neutral-buffered 10% formalin (4% 2-formaldehyde) and embedded them in paraffin. After deparaffinization, we stained 4-μm-thick tissue slices with hematoxylin and eosin. We established brain lesion profiles according to published methods (*23*). We conducted paraffin-embedded tissue (PET) blots as previously described (*24*) by using the Sha31 monoclonal antibody (mAb) (*25*).

Western Blotting

We homogenized frozen brain tissues (175 + 20 mg) in 5% glucose in distilled water in grinding tubes (Bio-Rad, https://www.bio-rad.com) adjusted to 10% (wt/vol) by using a TeSeE Precess 48TM homogenizer (Bio-Rad). We determined the presence of PrP^{res} in transgenic mouse brains by using WB, using the reagents of the ELISA commercial test TeSeE (Bio-Rad). We prepared brain homogenates (10–100 μL of a 10% [wt/vol]) as previously described (*18*) and loaded samples into 12% Bis-Tris Gel (Criterion XT; Bio-Rad). We transferred proteins electrophoretically onto polyvinylidene fluoride membranes (Millipore, https://www.sigmaaldrich.com) and blocked overnight with 2% bovine serum albumin blocking buffer. We incubated membranes with Sha31 (*25*) mAb at a concentration of 1 μg/mL. Sha31 recognizes the 145-WEDRYYRE-152 epitope of the human-PrP^C sequence, which is conserved in sheep and bovine sequences. We detected immunocomplexes by incubating the membranes for 1 h with horseradish peroxidase conjugated antimouse IgG (GE Healthcare Amersham Biosciences, https://www.gelifesciences.com). We developed immunoblots with enhanced chemiluminescence in ECL Select (GE Healthcare Amersham Biosciences) and captured images by using the ChemiDoc WRS+ System and processed them by using Image Lab 5.2.1 software (both Bio-Rad).

Results

Atypical BSE Transmission to Human-PrP Transgenic Mouse Models

We transmitted a panel of atypical L-type and H-type BSE (2 serial passages) into 3 transgenic mouse lines. These mouse lines were homozygous for Met ($TgMet_{129}$) or Val ($TgVal_{129}$) at codon 129 of human-PrP or were their F1 cross resulting in heterozygous mice ($TgMet/Val_{129}$). The PrP^C level in the brain of all 3 transgenic mice lines has been shown to be approximately 4-fold higher than in human brain tissue (*26*). In parallel, we inoculated C-BSE control isolates (Table 1).

As we reported on a previous study (*18*), only $TgMet_{129}$ mice get infected with C-BSE isolates. However, $TgMet/Val_{129}$ and $TgVal_{129}$ showed no transmission or accumulation of PrP^{res} (Table 1).

L-BSE was efficiently transmitted to $TgMet_{129}$ (Table 1; Figure 1, panel A). The attack rate was 100% for first passage, and incubation time was not reduced on subsequent passaging. In $TgMet_{129}$, the L-BSE PrP^{res} pattern in WB differed from the C-BSE PrP^{res} pattern both in terms of apparent molecular weight and glycoprofile distribution, marked by an evident lower proportion of the diglycosylated band (Figure 1, panel B; Appendix Figure 1). We examined the regional distribution and intensity of PrP^{res} deposition in the brain by using PET blotting. Brains of $TgMet_{129}$ inoculated with L-BSE showed finer

Table 1. Transmission of H- and L-type BSE isolates to TgMet129, TgMet/Val129, and TgVal129 mice in a study of atypical BSE transmission using isolates from different countries in Europe and transgenic mouse models overexpressing human normal brain prion protein*

	Mean survival period, dpi ± SD (n/n_0) (reference)†					
	$TgMet_{129}$		$TgMet/Val_{129}$		$TgVal_{129}$	
Isolate	P1	P2	P1	P2	P1	P2
C-BSE_0	739 (1/6) (*12*,*18*)	633 ± 32 (6/6) (*18*)	>700 (0/6) (*18*)	>700 (0/6) (*18*)	>700 (0/6) (*18*)	>700 (0/6) (*18*)
C-BSE_2	491–707 (0/9) (*12*,*18*)	572 ± 37 (3/4) (*12*,*18*)	>700 (0/5) (*18*)	ND	>700 (0/6) (*18*)	>700 (0/6) (*18*)
C-BSE_3	758–801 (2/6)	615 ± 95 (6/6)	ND	ND	>700 (0/6)	>700 (0/6)
BSE L_1	607 ± 13 (7/7)	487 ± 116 (4/4)	>700 (0/12)	ND	>700 (0/14)	>700 (0/4)
BSE $L_1 \rightarrow TgMet_{129}$	487 ± 116 (4/4)	ND	ND	ND	>700 (0/4)	ND
BSE L_2	629 ± 35 (7/7)	508 ± 97 (5/5)	>700 (0/6)	ND	>700 (0/6)	>700 (0/6)
BSE $L_2 \rightarrow TgMet_{129}$	508 ± 97 (5/5)	ND	>700 (0/7)	ND	>700 (0/6)	>700 (0/6)
BSE L_3	541 ± 70 (7/7)	ND	>700 (0/11)	ND	>700 (0/11)	ND
BSE H_1	>700 (0/19)	>700 (0/6)	>700 (0/14)	ND	>700 (0/13)	>700 (0/6)
BSE H_2	>700 (0/12)	>700 (0/6)	>700 (0/12)	ND	>700 (0/12)	ND
BSE H_3	>700 (0/14)	>700 (0/12)	>700 (0/12)	ND	>700 (0/12)	ND

*BSE, bovine spongiform encephalopathy; C-BSE, classical bovine spongiform encephalopathy; dpi, days postinoculation; ND, not detected; n/n_0, diseased proteinase K–resistant prion protein–positive/inoculated animals; P1, first passage; P2, second passage.
†Survival time is indicated as mean dpi ± SD for all mice that scored positive for proteinase K–resistant prion protein.

staining than the granular PrP deposits typical of C-BSE (Figure 1; Appendix Figure 1). Deposits were mostly restricted to the habenular, geniculate, and dorsal nuclei of the thalamus. Lesion profiles also reflect differences between both strains (Figure 1, panel C). We detected no clinical signs, PrP^{res} accumulation by WB (Table 1), or PrP^{Sc} deposition by PET blotting (data not shown) in the brains of $TgVal_{129}$ or $TgMet/Val_{129}$ L-BSE inoculated mice. These brains were collected and inoculated in TgBo animals; no transmission was observed (data not shown). This finding suggests the absence of subclinical infection in $TgVal_{129}$ and $TgMet/Val_{129}$ mice. We inoculated L-BSE passaged in $TgMet_{129}$ into $TgVal_{129}$ and $TgMet/Val_{129}$ mice and detected no PrP^{res} accumulation (Table 1). After H-BSE inoculation, we detected no clinical signs, PrP^{res} accumulation by WB (Table 1), or PrP^{Sc} deposits by PET blotting (data not shown) in any of the 3 human transgenic mouse models.

Atypical BSE Transmission into Ovine-PrP Transgenic Mouse Models

We transmitted 1 L-BSE isolate and 1 H-BSE isolate (2 iterative passages) to VRQ and ARQ ovine-PrP transgenic mice. L-BSE transmitted in both TgVRQ and TgARQ caused 100% attack rates and short incubation times in the second passage (Table 2).

L-BSE propagation in all TgVRQ and TgARQ infected mice showed a WB PrP^{res} profile with similarities to the one observed after passage of C-BSE in the same model in terms of low molecular mass migration but also a glycoform ratio where the diglycosylated and monoglycosylated bands contain a more equal signal proportion than C-BSE were detected with mAb Sha31, which is more similar to L-BSE or classical scrapie (Figure 2, panel A). These features have previously been reported in ARQ/ARQ and VRQ/VRQ sheep inoculated with L-BSE (*13*). We inoculated brains collected from the second passage in TgBo, causing a clinical disease with similar incubation periods as original L-BSE (Table 3). Both WB and PET blotting patterns (Appendix Figure 2), as well as WB patterns once transmitted back into TgBo (Figure 3), support the view that passage in ovine sequences did not irreversibly alter L-BSE strain properties.

TgARQ mice inoculated with H-BSE isolate did not show any clinical sign or accumulation of PrP^{res} (Table 2). In TgVRQ, first passage produced disease in only 1 out of 6 animals, with long incubation times. On second passage, 100% attack rates were achieved, and incubation times were reduced (Table 2). This finding suggests a substantial transmission barrier for the H-BSE prion agent in this animal model. The WB PrP^{res} profile was characterized by 21 kDa profile (Figure 2, panel B). The prion that propagated in TgVRQ mice inoculated with H-BSE could not be transmitted (2 serial passages) in TgBo mice. These results suggest that, upon adaptation to the VRQ ovine-PrP sequence, the H-BSE strain properties were irreversibly altered (Table 3).

We thus analyzed the neuropathologic phenotypes of the atypical BSE agents transmitted into ovine-PrP transgenic mice by PrP^{res} PET blotting (Appendix Figure 2). Regarding L-BSE, the results support those obtained by WB because TgVRQ ovine passaged L-BSE displays a similar PrP deposition as ovine passaged C-BSE. PrP^{res} deposition predominantly involved several nuclei of the thalamus and regions like the septum and external cortex of the inferior colliculus; we obtained similar results for TgARQ

passaged L-BSE (Appendix Figure 2), as previously described (*14*). Concerning TgVRQ adapted H-BSE prions, the deposition pattern is also strikingly different to that displayed by C-BSE or L-BSE (Appendix Figure 2).

Atypical BSE Transmission into Human-PrP Transgenic Mouse Models after Adaptation to the Sheep-PrP Sequence

We inoculated prions obtained after 2 passages of L-BSE and H-BSE isolates in ovine PrP expressing mice into $TgMet_{129}$ and $TgVal_{129}$. $TgMet_{129}$ mice inoculated with L-BSE passaged into TgVRQ showed neither clinical signs nor PrP^{res} accumulation in their brain (Figure 1, panels A, B). By contrast, $TgVal_{129}$ inoculated with the same isolates had disease characterized by 100% attack rates and short incubation times in the second passage (Figure 1, panel A). The obtained PrP^{res} resembles a sporadic Creutzfeldt-Jakob disease (sCJD) Val/Val_{129} type 2 (sCJD VV2) profile (Figure 1, panel B). PET blotting showed a deposition pattern similar to that of sCJD VV2 in the same mice (Figure 1, panel A). Lesion profiles of both strains also were coincident (Figure 1, panel

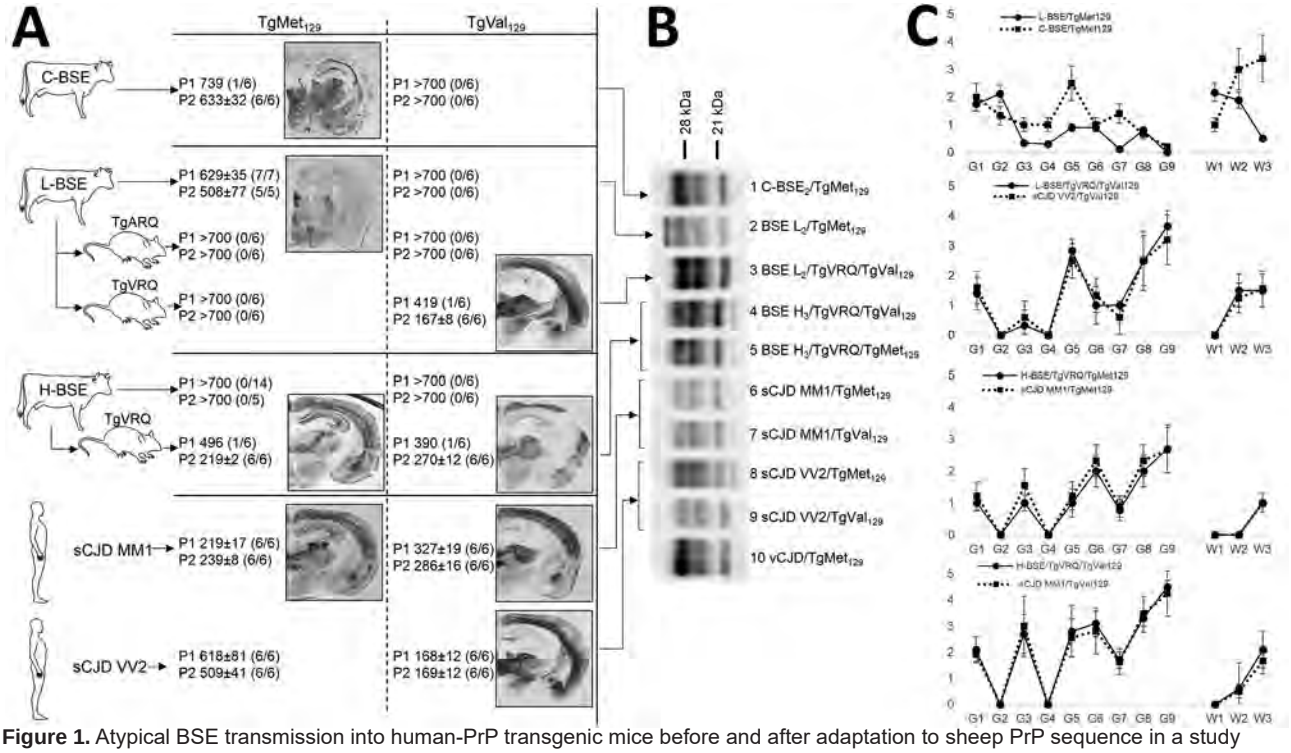

Figure 1. Atypical BSE transmission into human-PrP transgenic mice before and after adaptation to sheep PrP sequence in a study of atypical BSE transmission using isolates from different countries in Europe and transgenic mouse models overexpressing human normal brain prion protein. A) Transmission data including mean survival time ± SD as well as attack rates (diseased PrP^{res} positive/inoculated animals) and PET blot images for all atypical BSE transmission into the human-PrP transgenic mouse models. L-BSE/$TgMet_{129}$ showed fine staining, and deposits were restricted to the several thalamus nuclei. C-BSE/TgMet129 showed granular deposits. L-BSE/TgVRQ/$TgVal_{129}$ and $TgVal_{129}$ PET blotting showed strong deposition in a particular area of the isocortex, thalamus, and midbrain, and mild deposition in the fiber tracts. H-BSE/TgVRQ and sCJD MM1 PET blotting images showed strong deposition in the isocortex area, hippocampus, thalamus, and midbrain in $TgMet_{129}$ and strong deposition in the isocortex area, thalamus, and midbrain in $TgVal_{129}$. B) Brain PrP^{res} profile in $TgMet_{129}$ and $TgVal_{129}$ mice inoculated with atypical BSE prions before or after adaptation to the sheep-PrP sequence immunoblotted with the Sha31 mAb. Human vCJD and different sCJD prion strains inoculated in the same $TgMet_{129}$ and $TgVal_{129}$ mouse models are also included for comparison purposes. L-BSE/TgVRQ/$TgVal_{129}$ (lane 3) is very similar to sCJD VV2/$TgVal_{129}$ (lane 9). By contrast, H-BSE/TgVRQ/$TgMet_{129}$ (lane 5) and sCJD MM1/$TgMet_{129}$ (lane 6) are undistinguishable, as also observed with H-BSE/TgVRQ/$TgVal_{129}$ (lane 4) and sCJD MM1/$TgVal_{129}$ (lane 7). All PrP^{res} profiles are different from those of vCJD/$TgMet_{129}$ (lanes 1 and 10) and L-BSE/$TgMet_{129}$ (lane 2). All inoculated animals were analyzed, and individual variations in the PrP^{res} profile among them were not found. C) Vacuolar lesion profile in brains from human-PrP transgenic mice inoculated with C-BSE or the atypical BSE isolates before and after adaptation to the sheep-PrP sequence. Lesion scoring was conducted for 9 areas of gray matter (G) and 3 areas of white matter (W) in mouse brains: G1, dorsal medulla; G2, cerebellar cortex; G3, superior colliculus; G4, hypothalamus; G5, medial thalamus; G6, hippocampus; G7, septum; G8, medial cerebral cortex at the level of the thalamus; G9, medial cerebral cortex at the level of the septum (G9); W1, cerebellum; W2, mesencephalic tegmentum; W3, pyramidal tract. BSE, bovine spongiform encephalopathy; C-BSE, classical bovine spongiform encephalopathy; mAb, monoclonal antibody; PET, paraffin embedded tissue; PrP, prion protein; PrPres, proteinase K–resistant prion protein; sCJD, sporadic Creutzfeldt-Jakob disease; vCJD, variant Creutzfeldt-Jakob disease.

Table 2. Intracerebral inoculation of TgBo, TgVRQ, and TgARQ mice with atypical BSE isolates to promote adaptation to the sheep-PrP sequence in a study of atypical BSE transmission using isolates from different countries in Europe and transgenic mouse models overexpressing human normal brain prion protein*

	Mean survival time, d ± SD (n/n_0)†					
	TgBo		TgVRQ		TgARQ	
Isolate	P1	P2	P1	P2	P1	P2
BSE L_2	263 ± 31 (6/6)	208 ± 21 (6/6)	438 ± 20 (6/6)	168 ± 22 (6/6)	386‡, 404 (2/6)	155 ± 8 (6/6)
BSE H_3	382 ± 74 (6/6)	262 ± 3 (6/6)	801 (1/6)	408 ± 44 (6/6)	>700 (0/6)	>700 (0/6)

*BSE, bovine spongiform encephalopathy; dpi, days post-inoculation; n/n_0, diseased proteinase K–resistant prion protein–positive/inoculated animals; P1, first passage; P2, second passage.
†Survival time is indicated as mean dpi ± SD for all mice that scored positive for proteinase K–resistant prion protein.
‡Found dead animals without clinical signs and positive for proteinase K–resistant disease-associated isoform.

C). Furthermore, the prion generated in the $TgVal_{129}$ transgenic mouse line is not able to infect back in TgBo (Table 3). By contrast, ARQ-adapted L-BSE loses its ability to infect human-PrP $TgMet_{129}$ transgenic mouse lines (Figure 1, panel A).

VRQ-adapted H-BSE can now infect both human-PrP $TgMet_{129}$ and $TgVal_{129}$ mouse lines, showing 100% attack rates and short incubation times in the second passage (Figure 1, panel A). The obtained PrP^{res} in both cases is similar to that of sCJD Met/Met_{129} type 1 (sCJD MM1) (Figure 1, panel B). PET blotting showed similarities with the deposition patterns typical of sCJD MM1 in $TgMet_{129}$ and $TgVal_{129}$ (Figure 1, panel A). Lesion profiles of both strains also were coincident (Figure 1, panel C). Both generated prions can infect back in TgBo (Table 3; Figure 3).

VRQ-adapted L-BSE reduces its zoonotic potential toward human-PrP $TgMet_{129}$ mice, as shown by a total abolishment of prion replication in $TgMet_{129}$ (Figure 1, panel A). Strikingly, intermediate passage of L-BSE into TgVRQ increased its zoonotic potential toward $TgVal_{129}$ mice (Figure 1, panel A).

Discussion

The zoonotic potential of atypical BSE prions has been partially studied by using both PrP-overexpressing animals and gene-targeted mice (*10*,*27*–*29*). All evidence converges to indicate a higher capacity of L-BSE than of C-BSE to transmit in human-PrP–expressing hosts and a high transmission barrier for H-BSE. Absence of a transmission barrier for L-BSE in $TgMet_{129}$ has already been reported (*10*). Our study (using other transgenic mice with a different PrP^C expression level) expands the investigation to other genotypes. Lack of prion propagation in $TgMet/Val_{129}$ and $TgVal_{129}$ indicates that Val_{129} variant is a strong molecular protector against L-BSE zoonotic transmission even in heterozygosis, as previously reported for C-BSE and related C-BSE prions (*18*). Finally, H-BSE clearly has a robust transmission barrier with respect to the human-PrP sequence, independent of the codon 129 polymorphism.

Once adapted to $TgMet_{129}$, L-BSE did not propagate in $TgMet/Val_{129}$ and $TgVal_{129}$, which precludes secondary infections between persons. In contrast,

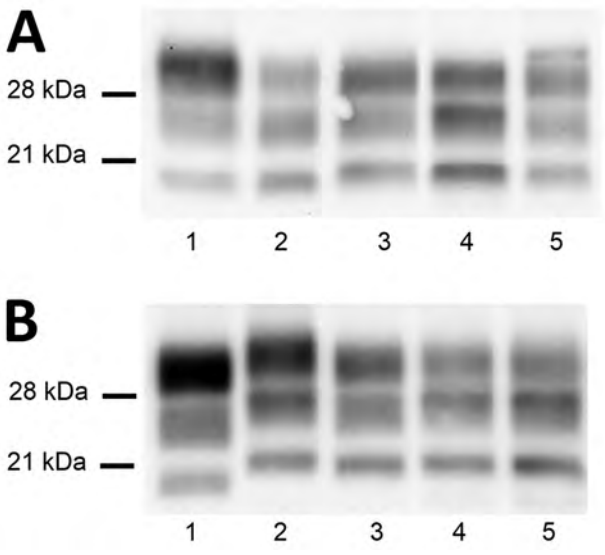

Figure 2. Atypical BSE transmission into sheep PrP transgenic mice in a study of atypical BSE transmission using isolates from different countries in Europe and transgenic mouse models overexpressing human normal brain prion protein. A) Brain PrP^{res} profile of L-BSE prions (lane 2) changed once passaged into TgVRQ (lane 3) and TgARQ (lane 5). L-BSE propagation into TgVRQ and TgARQ produced a PrP^{res} profile with a molecular weight slightly higher than C-BSE (lane 1). L-BSE/TgVRQ transmission into $TgVal_{129}$ mice rendered a PrP^{res} similar to type 2 sCJD profile when transmitted in the same animal model (lane 4). All inoculated animals were analyzed and individual variations in the PrP^{res} profile among them were not found. Lane 1, $C\text{-}BSE_2$; lane 2, BSE L_2; lane 3, BSE L_2/TgVRQ; lane 4, BSE L_2/TgVRQ/TgVal129; lane 5, BSE L_2/TgARQ. B) Brain PrP^{res} profile of H-BSE prions (lane 2) changed once passaged into TgVRQ (lane 3) and produced a 21 kDa PrP^{res} profile very different from that of C-BSE (lane 1). H-BSE/TgVRQ transmission into $TgMet_{129}$ (lane 4) and $TgVal_{129}$ (lane 5) mice rendered a PrP^{res} similar to type 1 sCJD profile when transmitted in the same animal models. All inoculated animals were analyzed and individual variations in the PrP^{res} profile among them were not found. Lane 1, $C\text{-}BSE_2$; lane 2, BSE H_3; lane 3, BSE H_3/TgVRQ; lane 4, BSE H_3/TgVRQ/TgMet129; lane 5, BSE H_3/TgVRQ/TgVal129. BSE, bovine spongiform encephalopathy; C-BSE, classical bovine spongiform encephatlopathy; PrP, prion protein; PrPres, proteinase K–resistant prion protein; sCJD, sporadic Creutzfeldt-Jakob disease.

Table 3. Intracerebral inoculation of TgBo with sCJD, L-BSE, and H-BSE isolates after their adaptation (P2) in various hosts in a study of atypical BSE transmission using isolates from different countries in Europe and transgenic mouse models overexpressing human normal brain prion protein*

Isolate	Mean survival time, days ± SD (n/n_0)†	
	P1	P2
BSE L_2	263 ± 31 (6/6)	204 ± 4 (6/6)
BSE L_2→TgVRQ (P2)	221 ± 3 (6/6)	212 ± 3 (6/6)
BSE L_2→TgARQ (P2)	240 ± 18 (6/6)	215 ± 5 (6/6)
BSE L_2→TgVRQ (P2)→$TgVal_{129}$ (P2)	>650 (0/6)	ND
BSE H_3	382 ± 74 (6/6)	262 ± 3 (6/6)
BSE H_3→TgVRQ (P2)	>650 (0/6)	>650 (0/6)
BSE H_3→TgVRQ (P2)→$TgMet_{129}$ (P2)	671, 699,‡ 759‡ (3/6)	631 ± 34 (5/6)
BSE H_3→TgVRQ (P2)→$TgVal_{129}$ (P2)	627,‡ 689‡ (2/6)	703‡ (1/6)
sCJD MM1→$TgMet_{129}$ (P2)	750 ± 18 (3/6)	ND
sCJD MM1→$TgVal_{129}$ (P2)	737, 763,‡ 833‡ (3/4)	ND
sCJD VV2→$TgVal_{129}$ (P2)	833‡ (1/6)	ND
vCJD→$TgMet_{129}$ (P2)	249 ± 2 (6/6)	236 ± 5 (6/6)

*BSE, bovine spongiform encephalopathy; dpi, days post-inoculation; n/n0, diseased proteinase K–resistant prion protein–positive/inoculated animals; P1, first passage; P2, second passage, sCJD, sporadic Creutzfeldt-Jakob disease; vCJD, variant Creutzfeldt-Jakob disease.
†Survival time is indicated as mean dpi ± SD for all mice that scored positive for proteinase K–resistant prion protein.
‡Found dead animals without clinical signs and positive for proteinase K–resistant disease-associated isoform.

C-BSE propagated in Val_{129} genotypes once adapted to the Met_{129} human-PrP sequence, even when Val_{129} also protected against primary infection (*18*). However, Met/Val_{129} genotypes might be naturally affected by vCJD because a definite vCJD case of a subject heterozygous for codon 129 has already been reported (*16*). Moreover, evidence of potential prion propagation in Val_{129}-homozygous persons has been indicated in examinations of tonsils and appendices (*30*–*32*). These observations are in contrast with our finding of a lack of transmission of C-BSE in Val_{129} genotypes. However, only 1 vCJD case has been reported in a Met/Val-heterozygous person, which might mean that the event is very rare. Moreover, whether the PrP^{res} positivity detected in lymphoid tissues (tonsils and appendix) of Val_{129}-homozygous persons would eventually extend to their central nervous system is still unknown. As a consequence, the risk for L-BSE secondary transmission once adapted to human-PrP sequence should be assessed carefully.

A complete assessment of the zoonotic potential of atypical BSE prions should include the evaluation of zoonotic potential after adaptation to the sheep-PrP sequence given that C-BSE virulence toward human-PrP transgenic mouse models increased after passage in ovine-PrP transgenic mice. Thus, we propagated 1 H-BSE and 1 L-BSE isolate into ovine-PrP transgenic mice. L-BSE has already been transmitted into sheep (*13*), whereas no H-BSE propagation into this host has been reported. Thus, we decided to perform the adaptation to the sheep sequence by using sheep-PrP transgenic mice, although overexpression of PrP^C reportedly could render changes on prion strains features (*33*). The absence of divergent PrP^{res} profiles among the animals and the uniformity of the incubation times after 2 passages into sheep-PrP transgenic mice argue against the occurrence of mutation events attributable to PrP^C overexpression in our study. In

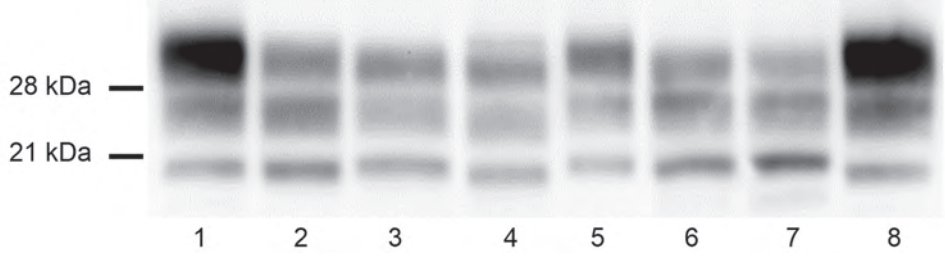

Figure 3. Bovine-PrP transgenic mice challenged with atypical BSEs transmitted into human-PrP transgenic mice before and after adaptation to sheep-PrP sequence in a study of atypical BSE transmission using isolates from different countries in Europe and transgenic mouse models overexpressing human normal brain prion protein. Brain PrPres in TgBo mice inoculated with different atypical BSE either before or after passage into the different transgenic lines. L-BSE biochemical profile (lane 2) changed once passaged into TgVRQ (lane 3) and TgARQ (lane 4). L-BSE/TgVRQ produced a PrPres profile resembling the one of C-BSE (lanes 1 and 8). L-BSE propagation into TgARQ produced a 21kDa PrPres profile. H-BSE (lane 5) can still infect back TgBo line once passaged into TgVRQ and adapted to the human PrP sequence (lanes 6 and 7) and produced a 21 kDa PrPres profile. All inoculated animals were analyzed and individual variations in the PrPres profile among them were not found. Lane 1, C-BSE2; lane 2, BSE L2; lane 3, BSE L2/TgVRQ/TgBo; lane 4, BSE L2/TgARQ/TgBo; lane 5, BSE H3; lane 6, BSE H3/TgVRQ/TgMet129/TgBo; lane 7, BSE H3/TgVRQ/TgVal129/TgBo; lane 8, C-BSE2. BSE, bovine spongiform encephalopathy; C-BSE, classical bovine spongiform encephatlopathy; PrP, prion protein; PrPres, proteinase K–resistant prion protein.

addition, previously reported strain features of L-BSE propagated in sheep (*13*) were similar to those reported in this study using sheep-PrP transgenic mice, which also validates use of these animal models. Our results suggest a moderate but surmountable transmission barrier for L-BSE in the 2 analyzed sheep genotypes, whereas for H-BSE a high transmission barrier exists when transmitted into an ARQ sheep sequence. The polymorphism Ala/Val_{136} present in the sheep-PrP sequence seems to be responsible for the different behavior of the obtained prion agents. Once proved that these isolates could be propagated on sheep-PrP sequence, determining whether they can be differentiated from classical scrapie and C-BSE will be important.

Our results and those provided by other studies indicate that L-BSE adapted to a VRQ sheep sequence resemble C-BSE in its molecular features (*14*). Moreover, L-BSE adapted to ARQ sheep sequence and H-BSE adapted to VRQ sheep sequence generate prions similar to classical scrapie, at least in terms of PrP^{res} glycoprofile. Therefore, in the supposed case of atypical BSE transmission to sheep, early differentiation of both atypical BSE agents from other sheep prions like classical scrapie would be difficult. Nevertheless, the combination of the low incidence of atypical BSE (because of its supposed sporadic nature) and the continued prohibition of meat and bone meal recycling ameliorates the risk for transmission to sheep.

The transmission of atypical BSEs into sheep resulted in the emergence of prions similar to types 1 and 2 sCJD in terms of mean survival times, attack rates, PrP^{res} profile, and PrP^{res} deposition pattern in the brain of human-PrP transgenic mice. The similarities between the sheep-adapted atypical BSE prions propagated into our human-PrP transgenic mouse lines and sCJD prions could suggest a link between them. The well-established dogma that sCJD is a spontaneous disorder unrelated to animal prion disease has been questioned in a previous study given the resemblance of scrapie prions transmitted into human transgenic mouse models to sCJD strains (*26*); however, the data from that study do not unequivocally establish a causative link between exposure to sheep scrapie and the subsequent appearance of sCJD in humans, and the same could apply to our findings. An alternative explanation that cannot be ruled out is that, although being different strains, only a limited number of phenotypes could be generated for the human-PrP, indicating phenotypic convergence. Updates to old epidemiologic research is needed to reconsider all these results involving a possible infectious origin of sCJD. In any case, continuing the characterization of this newly emerged prion strain would be useful to finally discarding or refuting a link with sCJD prions.

Extrapolation of results from prion transmission studies based on transgenic mice should be done with caution, especially when human susceptibility to prions is analyzed. However, our results clearly indicate that atypical BSE adaptation to an ovine-PrP sequence could modify the prion agent to potentially infect humans, showing strain features indistinguishable from those of classic sCJD prions, even though they might or might not be different agents. The supposed sporadic nature of atypical BSE makes its transmission to sheep and later to humans unlikely. However, the expanding range of TSE agents displaying the capacity to transmit in human-PrP–expressing hosts warrants the continuation of the ban on meat and bone meal recycling and underscores the ongoing need for active surveillance.

Acknowledgments

We thank the staff of the Biosafety Level 3 animal facility and the Biosafety Office at Centro de Investigación en Sanidad Animal–Instituto Nacional de Investigación y Tecnología Agraria y Alimentaria (Valdeolmos-Madrid) for their excellent animal care and work, and C. Lacroux for her assistance in organizing the mouse bioassays. In addition, we thank the suppliers of the isolates used in this study.

This work was funded by the Food Standards Agency (grant no. FS231051 to O.A. and J.M.T.), Spanish Ministerio de Economía Industria y Competitividad (grant no. RTA2012-00004 to J.M.T, grant no. AGL2016-78054-R [AEI/FEDER, UE] to J.M.T. and J.C.E., and fellowship BES-2010- 040922 to P.A.C.), Fundació La Marató de TV3 (grant no. 201821-31 to J.C.E.), Instituto Nacional de Investigación y Tecnología Agraria y Agroalimentaria (fellowship INIA-FPI-SGIT-2015-02 to A.M.M.), Alliance BioSecure Research Foundation (grant no. FABS FRM-2014 to J.M.T.), and the FEDER programs POCTEFA (EFA148/16 to O.A.). The funders had no role in study design, data collection and analysis, decision to publish, or preparation of the manuscript.

Conception and design of the study, as well as analysis and interpretation of data and acquisition of funding, were done by J.M.T, J.C.E., and O.A. All authors contributed to data acquisition. A.M.M, J.M.T, J.C.E., and O.A. were involved in drafting the manuscript and revising it critically for important intellectual content. All authors gave final approval of the version to be published.

About the Author

Ms. Marín-Moreno is a PhD student in the Prion Group at Centro de Investigación en Sanidad Animal–Instituto Nacional de Investigación y Tecnología Agraria y Alimentaria, Madrid, Spain. Her primary research interests are the characterization of prion strains and the pathogenesis of prion diseases and their effects on animal and human health.

References

1. Prusiner SB. Prions. Proc Natl Acad Sci U S A. 1998;95:13363–83. https://doi.org/10.1073/pnas.95.23.13363
2. Vázquez-Fernández E, Vos MR, Afanasyev P, Cebey L, Sevillano AM, Vidal E, et al. The structural architecture of an infectious mammalian prion using electron cryomicroscopy. PLoS Pathog. 2016;12:e1005835. https://doi.org/10.1371/journal.ppat.1005835
3. Gielbert A, Davis LA, Sayers AR, Hope J, Gill AC, Sauer MJ. High-resolution differentiation of transmissible spongiform encephalopathy strains by quantitative N-terminal amino acid profiling (N-TAAP) of PK-digested abnormal prion protein. J Mass Spectrom. 2009;44:384–96. https://doi.org/10.1002/jms.1516
4. Will RG, Ironside JW, Zeidler M, Cousens SN, Estibeiro K, Alperovitch A, et al. A new variant of Creutzfeldt-Jakob disease in the UK. Lancet. 1996;347:921–5. https://doi.org/10.1016/S0140-6736(96)91412-9
5. Wells GA, Scott AC, Johnson CT, Gunning RF, Hancock RD, Jeffrey M, et al. A novel progressive spongiform encephalopathy in cattle. Vet Rec. 1987;121:419–20. https://doi.org/10.1136/vr.121.18.419
6. Fernández-Borges N, Marín-Moreno A, Konold T, Espinosa JC, Torres JM. Bovine spongiform encephalopathy (BSE). In: Reference module in neuroscience and biobehavioral psychology. London: Elsevier; 2017. p.1–10.
7. Houston F, Andréoletti O. Animal prion diseases: the risks to human health. Brain Pathol. 2019;29:248–62. https://doi.org/10.1111/bpa.12696
8. Casalone C, Zanusso G, Acutis P, Ferrari S, Capucci L, Tagliavini F, et al. Identification of a second bovine amyloidotic spongiform encephalopathy: molecular similarities with sporadic Creutzfeldt-Jakob disease. Proc Natl Acad Sci U S A. 2004;101:3065–70. https://doi.org/10.1073/pnas.0305777101
9. Biacabe AG, Laplanche JL, Ryder S, Baron T. Distinct molecular phenotypes in bovine prion diseases. EMBO Rep. 2004;5:110–5. https://doi.org/10.1038/sj.embor.7400054
10. Béringue V, Herzog L, Reine F, Le Dur A, Casalone C, Vilotte JL, et al. Transmission of atypical bovine prions to mice transgenic for human prion protein. Emerg Infect Dis. 2008;14:1898–901. https://doi.org/10.3201/eid1412.080941
11. Eloit M, Adjou K, Coulpier M, Fontaine JJ, Hamel R, Lilin T, et al. BSE agent signatures in a goat. Vet Rec. 2005;156:523–4. https://doi.org/10.1136/vr.156.16.523-b
12. Padilla D, Béringue V, Espinosa JC, Andreoletti O, Jaumain E, Reine F, et al. Sheep and goat BSE propagate more efficiently than cattle BSE in human PrP transgenic mice. PLoS Pathog. 2011;7:e1001319. https://doi.org/10.1371/journal.ppat.1001319
13. Simmons MM, Chaplin MJ, Konold T, Casalone C, Beck KE, Thorne L, et al. L-BSE experimentally transmitted to sheep presents as a unique disease phenotype. Vet Res 2016;47:112.
14. Béringue V, Andréoletti O, Le Dur A, Essalmani R, Vilotte JL, Lacroux C, et al. A bovine prion acquires an epidemic bovine spongiform encephalopathy strain-like phenotype on interspecies transmission. J Neurosci. 2007;27:6965–71. https://doi.org/10.1523/JNEUROSCI.0693-07.2007
15. Lloyd SE, Mead S, Collinge J. Genetics of prion diseases. Curr Opin Genet Dev. 2013;23:345–51. https://doi.org/10.1016/j.gde.2013.02.012
16. Mok T, Jaunmuktane Z, Joiner S, Campbell T, Morgan C, Wakerley B, et al. Variant Creutzfeldt-Jakob disease in a patient with heterozygosity at PRNP codon 129. N Engl J Med. 2017;376:292–4. https://doi.org/10.1056/NEJMc1610003
17. Will RG, Zeidler M, Stewart GE, Macleod MA, Ironside JW, Cousens SN, et al. Diagnosis of new variant Creutzfeldt-Jakob disease. Ann Neurol. 2000;47:575–82. https://doi.org/10.1002/1531-8249(200005)47:5<575::AID-ANA4>3.0.CO;2-W
18. Fernández-Borges N, Espinosa JC, Marín-Moreno A, Aguilar-Calvo P, Asante EA, Kitamoto T, et al. Val129-PrP variant is a strong molecular protector against BSE zoonotic transmission but fails to prevent human-to-human vCJD transmission. Emerg Infect Dis. 2017;23:1522–30.
19. Le Dur A, Béringue V, Andréoletti O, Reine F, Laï TL, Baron T, et al. A newly identified type of scrapie agent can naturally infect sheep with resistant PrP genotypes. Proc Natl Acad Sci U S A. 2005;102:16031–6. https://doi.org/10.1073/pnas.0502296102
20. Kupfer L, Eiden M, Buschmann A, Groschup MH. Amino acid sequence and prion strain specific effects on the in vitro and in vivo convertibility of ovine/murine and bovine/murine prion protein chimeras. Biochim Biophys Acta. 2007;1772:704–13. https://doi.org/10.1016/j.bbadis.2006.10.009
21. Castilla J, Gutiérrez Adán A, Brun A, Pintado B, Ramírez MA, Parra B, et al. Early detection of PrPres in BSE-infected bovine PrP transgenic mice. Arch Virol. 2003;148:677–91. https://doi.org/10.1007/s00705-002-0958-4
22. Andréoletti O, Berthon P, Levavasseur E, Marc D, Lantier F, Monks E, et al. Phenotyping of protein-prion (PrPsc)-accumulating cells in lymphoid and neural tissues of naturally scrapie-affected sheep by double-labeling immunohistochemistry. J Histochem Cytochem. 2002;50:1357–70. https://doi.org/10.1177/002215540205001009
23. Fraser H, Dickinson AG. The sequential development of the brain lesion of scrapie in three strains of mice. J Comp Pathol. 1968;78:301–11. https://doi.org/10.1016/0021-9975(68)90006-6
24. Andréoletti O, Simon S, Lacroux C, Morel N, Tabouret G, Chabert A, et al. PrPSc accumulation in myocytes from sheep incubating natural scrapie. Nat Med. 2004;10:591–3. https://doi.org/10.1038/nm1055
25. Féraudet C, Morel N, Simon S, Volland H, Frobert Y, Créminon C, et al. Screening of 145 anti-PrP monoclonal antibodies for their capacity to inhibit PrPSc replication in infected cells. J Biol Chem. 2005;280:11247–58. https://doi.org/10.1074/jbc.M407006200
26. Cassard H, Torres JM, Lacroux C, Douet JY, Benestad SL, Lantier F, et al. Evidence for zoonotic potential of ovine scrapie prions. Nat Commun. 2014;5:5821. https://doi.org/10.1038/ncomms6821
27. Kong Q, Zheng M, Casalone C, Qing L, Huang S, Chakraborty B, et al. Evaluation of the human transmission risk of an atypical bovine spongiform encephalopathy prion strain. J Virol. 2008;82:3697–701. https://doi.org/10.1128/JVI.02561-07

28. Wilson R, Dobie K, Hunter N, Casalone C, Baron T, Barron RM. Presence of subclinical infection in gene-targeted human prion protein transgenic mice exposed to atypical bovine spongiform encephalopathy. J Gen Virol. 2013; 94:2819–27. https://doi.org/10.1099/vir.0.052738-0
29. Wilson R, Plinston C, Hunter N, Casalone C, Corona C, Tagliavini F, et al. Chronic wasting disease and atypical forms of bovine spongiform encephalopathy and scrapie are not transmissible to mice expressing wild-type levels of human prion protein. J Gen Virol. 2012;93:1624–9. https://doi.org/10.1099/vir.0.042507-0
30. Gill ON, Spencer Y, Richard-Loendt A, Kelly C, Dabaghian R, Boyes L, et al. Prevalent abnormal prion protein in human appendixes after bovine spongiform encephalopathy epizootic: large scale survey. BMJ. 2013;347:f5675.
31. Hilton DA, Ghani AC, Conyers L, Edwards P, McCardle L, Ritchie D, et al. Prevalence of lymphoreticular prion protein accumulation in UK tissue samples. J Pathol. 2004;203:733–9. https://doi.org/10.1002/path.1580
32. Ironside JW, Bishop MT, Connolly K, Hegazy D, Lowrie S, Le Grice M, et al. Variant Creutzfeldt-Jakob disease: prion protein genotype analysis of positive appendix tissue samples from a retrospective prevalence study. BMJ. 2006;332:1186–8. https://doi.org/10.1136/bmj.38804.511644.55
33. Le Dur A, Laï TL, Stinnakre MG, Laisné A, Chenais N, Rakotobe S, et al. Divergent prion strain evolution driven by PrP^{C} expression level in transgenic mice. Nat Commun. 2017;8:14170. https://doi.org/10.1038/ncomms14170

Address for correspondence: Juan María Torres, Centro de Investigación en Sanidad Animal–Instituto Nacional de Investigación y Tecnología Agraria y Alimentaria (CISA-INIA), Carretera Algete-El Casar s/n, Valdeolmos, CP 28130, Madrid, Spain; email: jmtorres@inia.es

etymologia

Scrapie [skra'pe]

Ronnie Henry, Lawrence B. Schonburger

Scrapie is a fatal neurodegenerative disease of sheep and goats that was the first of a group of spongiform encephalopathies to be reported (1732 in England) and the first whose transmissibility was demonstrated by Cuille and Chelle in 1936. The name resulted because most affected sheep develop pruritis and compulsively scratch their hides against fixed objects. Like other transmissible spongiform encephalopathies (TSEs), scrapie is associated with an alteration in conformation of a normal neural cell glycoprotein, the prion protein (PrPC). The scrapie agent was first described as a prion (and the term coined) by Stanley Prusiner in 1982, work for which he received the Nobel Prize in 1997.

The altered, misfolded form, designated PrP scrapie (PrPSc), aggregates and is thought to be an essential component of the infectious particle that causes TSEs. PrPSc is often used to designate the infectious particle responsible for all TSEs, including those in humans, such as Creutzfeldt-Jakob disease, even though scrapie does not appear to affect humans.

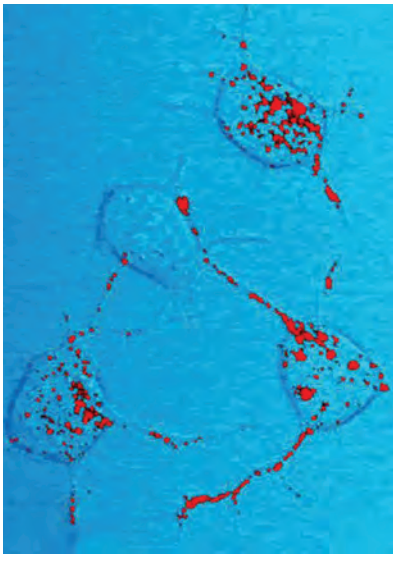

This photomicrograph of a neural tissue specimen, harvested from a scrapie affected mouse, revealed the presence of prion protein stained in red, which was in the process of being trafficked between neurons, by way of their interneuronal connections, known as neurites. Prion proteins can become infectious, causing neurodegenerative diseases such as transmissible spongiform encephalopathies (TSEs), which includes bovine spongiform encephalopathy (BSE), more commonly referred to a mad cow disease. Scrapie is a TSE that is related to BSE, but affects sheep and goats. Iimage credit: National Institute of Allergy and Infectious Diseases (NIAID), 2011.

Sources

1. Brown P, Bradley R. 1755 and all that: a historical primer of transmissible spongiform encephalopathy. BMJ. 1998;317: 1688–92. https://doi.org/10.1136/bmj.317.7174.1688
2. Cuillé J, Chelle PL. The so-called "trembling" disease of sheep: is it inoculable [in French]? Comptes Rendus de l'Académie Sciences. 1936;203:1552.
3. Laplanche J-L, Hunter N, Shinagawa M, Williams E. Scrapie, chronic wasting disease, and transmissible mink encephalopathy. In: Prusiner SB, editor. Prion biology and diseases. Cold Spring Harbor (NY): Cold Spring Harbor Laboratory Press; 1999. p. 393–429.
4. Prusiner SB. Novel proteinaceous infectious particles cause scrapie. Science. 1982;216:136–44. https://doi.org/10.1126/science.6801762

Address for correspondence: Ronnie Henry, Centers for Disease Control and Prevention, 1600 Clifton Rd NE, Mailstop V18-2, Atlanta, GA 30329-4027, USA; email: boq3@cdc.gov

DOI: https://doi.org/10.3201/eid2606.ET2606

Characterization of Sporadic Creutzfeldt-Jakob Disease and History of Neurosurgery to Identify Potential Iatrogenic Cases

Tsuyoshi Hamaguchi, Kenji Sakai, Atsushi Kobayashi, Tetsuyuki Kitamoto, Ryusuke Ae, Yosikazu Nakamura, Nobuo Sanjo, Kimihito Arai, Mizuho Koide, Fumiaki Katada, Masafumi Harada, Hiroyuki Murai, Shigeo Murayama, Tadashi Tsukamoto, Hidehiro Mizusawa, Masahito Yamada

We previously reported a phenotype of Creutzfeldt-Jakob disease (CJD), CJD-MMiK, that could help identify iatrogenic CJD. To find cases mimicking CJD-MMiK, we investigated clinical features and pathology of 1,155 patients with diagnosed sporadic CJD or unclassified CJD with and without history of neurosurgery. Patients with history of neurosurgery more frequently had an absence of periodic sharp-wave complexes on electroencephalogram than patients without a history of neurosurgery. Among 27 patients with history of neurosurgery, 5 had no periodic sharp-wave complexes on electroencephalogram. We confirmed 1 case of CJD-MMiK and suspected another. Both had methionine homozygosity at codon 129 of the prion protein gene and hyperintensity lesions in the thalamus on magnetic resonance images of the brain, which might be a clinical marker of CJD-MMiK. A subgroup with a history of neurosurgery and clinical features mimicking dura mater graft-associated CJD might have been infected during neurosurgery and had symptoms develop after many years.

Author affiliations: Kanazawa University Graduate School of Medical Sciences, Kanazawa, Japan (T. Hamaguchi, K. Sakai, M. Yamada); Hokkaido University, Sapporo, Japan (A. Kobayashi); Tohoku University Graduate School of Medicine, Sendai, Japan (T. Kitamoto); Jichi Medical University, Shimotsuke, Japan (R. Ae, Y. Nakamura); Tokyo Medical and Dental University, Tokyo, Japan (N. Sanjo); National Hospital Organization Chiba-East Hospital, Chiba, Japan (K. Arai, M. Koide); Kameda Medical Center, Chiba (F. Katada); The University of Tokushima, Tokushima, Japan (M. Harada); International University of Health and Welfare, Narita, Japan (H. Murai); Tokyo Metropolitan Institute of Gerontology, Tokyo (S. Murayama); National Center of Neurology and Psychiatry, Kodaira, Japan (T. Tsukamoto, H. Mizusawa)

DOI: https://doi.org/10.3201/eid2606.181969

Prion diseases are fatal, transmissible neurodegenerative disorders characterized by deposition of abnormal prion protein (PrP^{Sc}) in the brain (*1*). Human prion diseases, which include Creutzfeldt-Jakob disease (CJD), are classified into sporadic, genetic, and acquired forms. Acquired forms can be transmitted from humans to humans, as in cases of iatrogenic CJD or kuru, or from animals or humans to humans, as in cases of variant CJD (vCJD). Thus far, >400 cases of iatrogenic CJD have been reported (*2*). Two major medical procedures, intramuscular injection of cadaveric human growth hormone and cadaveric human dura mater grafting, have caused iatrogenic transmission of PrP^{Sc}, and 154 patients, >60% of cases worldwide of dura mater graft–associated CJD (dCJD), have been identified in Japan (*2*,*3*). We previously showed that dCJD could be classified into 2 types, nonplaque and plaque, according to the pathology findings (*4*,*5*). Nonplaque-type dCJD shows clinical features identical to those of typical sporadic CJD (sCJD), but plaque-type dCJD is characterized by atypical pathology and clinical features, including slow disease progression, lack of or late occurrence of periodic sharp-wave complexes (PSWCs) on patients' electroencephalograms (EEGs), and plaque formation in the brain (*4*,*5*).

Molecular features of plaque type dCJD include methionine (M) homozygosity at codon 129 (129MM) of the prion protein gene (*PRNP*) and a distinctive type of PrP^{Sc} with intermediate electrophoretic mobility (-20 kDa) between type 1 and type 2, which has been designated as intermediate type (type i PrP^{Sc}) (*6*,*7*). Clinicopathology studies of patients with dCJD and experimental transmission studies strongly suggest that the combination of 129MM, type i PrP^{Sc}, and kuru plaques (CJD-MMiK) is a distinctive hallmark of

acquired CJD caused by an infection with the V2 sCJD strain to persons with 129MM (*6*,*8*–*10*). We proposed neuropathology and biochemical criteria to identify CJD-MMiK (*8*,*9*). Surprisingly, we discovered 2 cases of diagnosed sCJD that showed clinical, pathologic, and molecular features identical to CJD-MMiK, which might have been iatrogenically transmitted because 1 of the patients had a history of neurosurgery and the other patient was a neurosurgeon (*8*). These results suggested that CJD-MMiK could be a clue to identify acquired CJD cases among patients with sCJD diagnoses. To identify iatrogenic cases, we investigated clinical features and pathology of patients with diagnosed sCJD and a history of neurosurgery to find features similar to CJD-MMiK.

Methods

The Patients

We analyzed patients with suspected prion diseases who were registered by the Creutzfeldt-Jakob Disease Surveillance Committee in Japan during April 1999–February 2016. The surveillance system started in April 1999 and prospectively investigated each patient with a surveillance protocol as previously reported (*5*,*11*,*12*). After obtaining written consent from patients or their families, members of the surveillance committee directly examined the patient and collected data from clinical and pathology records. The surveillance committee reviewed each patient's case files and assessed EEGs, diffusion-weighted magnetic resonance imaging (DW-MRI), ELISA of cerebrospinal fluid (CSF), and history of neurosurgery and then discussed each case to determine which patients had prion disease. The study protocol was approved by the medical ethics committees of Kanazawa University, Tokyo Medical and Dental University, and National Center of Neurology and Psychiatry in Japan.

For patients with a history of neurosurgery, we collected information about the underlying disease, including the date and hospital in which neurosurgery was performed. We determined which patients had undergone a dura mater graft by reviewing surgical records, querying the neurosurgeon, or examining autopsy findings.

Members of the committee assessed EEGs and determined whether PSWCs were typical of prion disease or suggested prion disease. Typical cases were deemed positive for prion disease, and the full committee reviewed and discussed suggested cases to decide whether PSWCs were positive or negative for prion disease.

We examined the cerebral cortices, basal ganglia, and thalamus for hyperintensity lesions on DW-MRI. Committee members defined hyperintensities or submitted scans to the committee's neuroradiology expert for assessment. For ELISA, we examined the value of 14-3-3 protein in CSF, as previously reported (*13*,*14*). We analyzed *PRNP* for M or valine (V) polymorphism in at codon 129 by using the open reading frame after extracting DNA from patient blood, as described earlier (*15*).

We included definite and probable cases of prion disease in this study and classified them into 4 categories: sporadic, acquired, genetic, and unclassified. We used World Health Organization criteria to diagnose sCJD and iatrogenic CJD (*16*). We diagnosed dCJD when we confirmed dura mater grafting, and considered cases as unclassified CJD when insufficient information on dura mater grafting were available. When we confirmed that dura mater graft was not performed during neurosurgery, we diagnosed sCJD even if the patient had history of neurosurgery not related to dura mater. We classified the patients with pathologically confirmed diagnoses of sCJD and unclassified CJD into 9 categories according to *PRNP* polymorphisms, the type of PrP^{Sc}, and pathology seen at autopsy. The 9 subtypes were MM1, MM2-cortical, MM2-thalamic, MM2+1 (pathological features of MM2 and MM1 types of sCJD), MV1, MV2, VV1, VV2, and MMiK. We included patients with definite sCJD and those with probable sCJD and genetic results for *PRNP*, which can distinguish genetic from sporadic prion diseases.

Clinical and Pathology Findings

We investigated 1,161 cases of sCJD in which no dura mater grafting or other iatrogenic causes were proven. We also investigated 3 patients with unclassified CJD and compared them to patients with and without history of neurosurgery. Among the 1,164 patients, 36 had a history of neurosurgery, but we excluded 9 because they underwent neurosurgeries ≤1 year before or after the onset of CJD. Our study included 27 patients with history of neurosurgery and 1,128 without history of neurosurgery.

Statistical Analyses

We used the Student *t* test to compare patients with and without history of neurosurgery, age at onset of CJD, and duration between the onset of CJD and the appearance of akinetic mutism or death. We used the Fisher exact test to analyze sex distribution, negative rate of PSWCs on EEG, and positive rates of 14-3-3 protein and total tau protein (cutoff 1,200 pg/mL) in CSF. We used the χ^2 test to analyze distribution of M and V polymorphisms. We considered $p<0.05$ statistically

Table 1. Comparison of the clinical features of patients with Creutzfeldt-Jakob disease with and without history of neurosurgery*

Patient characteristics	Neurosurgery	No neurosurgery	p value
Total no. patients	27	1,128	
Sex, no. (%)			
F	17 (63.0)	647 (57.4)	0.353
M	10 (37)	481 (42.6)	
Age at onset, y ± SD (range)	71.0 ± 8.8 (49–88)	68.7 ± 9.6 (30–91)	0.217
Disease duration, mo ± SD (range)†	6.1 ± 7.8 (1–28)	6.7 ± 12.0 (0–171)	0.823
Duration from neurosurgery to onset of CJD, y ± SD (range)	15.0 ± 9.1 (1–35)		
Polymorphism at codon 129 of prion protein gene, no. (%)			
MM	25 (92.6)	1,101 (97.6)	0.138
MV	2 (7.4)	22 (1.9)	
VV	0	5 (0.4)	
Negative rate of PSWCs on EEG, no. (%)	5 (18.5)	64/1,121 (5.7)	0.019
14-3-3 protein in CSF, no. tested/no. positive (%)	20/22 (90.9)	675/803 (84.1)	0.300
Tau protein in CSF, cutoff 1,200 pg/mL, no. tested/no. positive (%)	13/14 (92.9)	503/567 (88.7)	0.523

*CJD, Creutzfeldt-Jakob disease; CSF, cerebrospinal fluid; EEG, electroencephalogram; PSWCs, periodic sharp-wave complexes
†Disease duration of CJD: duration between the onset of CJD and the appearance of the akinetic mutism or death in the patients who died without akinetic mutism

significant. We performed statistical analyses by using SPSS Statistics 22 (IBM, https://www.ibm.com).

Results

We evaluated clinical features of the patients with and without history of neurosurgery (Table 1). Among the 27 patients with a history of neurosurgery, 5 (18.5%) had no PSWCs on EEG, but only 64/1,121 (5.7%) patients without history of neurosurgery demonstrated absence of PSWCs on EEG. However, we did not identify statistically significant differences for age at onset of CJD, sex, distribution of polymorphisms, disease duration, or positive rate of 14-3-3 protein or total tau protein in CSF.

Among the 27 sCJD patients with history of neurosurgery, 5 (18.5%) had atypical CJD features, including no PSWCs on EEG during their illnesses (Table 2). Among the 5 patients with atypical sCJD, the median age (± SD) at CJD onset was 65.4 (± 9.6) years (range 49–75 years); 4 were women and 1 was a man. Neurosurgery occurred during 1977–1993. The average time between neurosurgery and onset of CJD was 18.0 (± 8.8) years (9–30 years), and the average time between onset of CJD and the appearance of the akinetic mutism or death was 17.0 (± 7.7) months (6–28 months). Among the 5 patients with atypical sCJD, 2 patients were unclassified because we had no or insufficient information on dura mater graft during neurosurgery. The other 3 patients were determined to have sCJD without a history of dura mater–related neurosurgery. None of the 5 patients with atypical CJD had *PRNP* mutation, but all had 129MM.

DW-MRI was performed in 4/5 atypical patients and we noted hyperintensity lesions in various brain regions (Table 2). In patient 3 (Appendix Figure 1, panel A, https://wwwnc.cdc.gov/EID/article/26/6/18-1969-App1.pdf) and patient 4 (Appendix Figure 1, panel B), images showed hyperintensity lesions in bilateral thalamus and bilateral basal ganglia.

Autopsies were performed on 3/5 patients with atypical CJD (patients 2, 3, and 5); all cases are

Table 2. Patients with history of neurosurgery who had no periodic sharp-wave complexes on electroencephalogram during course of CJD*

Patient no.	Age at CJD onset, y/sex	Year of neurosurgery; reason	Time from neurosurgery to onset of CJD, y	Initial symptoms	Disease duration, mo†	Codon 129 of *PRNP*	Lesions on DW-MRI	Pathology findings
1	75/M	1977; head trauma	30	Dementia	11	MM	CC, BG	ND
2	49/F	1985; subarachnoid hemorrhage	9	Insomnia	28	MM	ND	MM2-T
3	75/F	1985; tumor	14	Drowsiness, gait disturbance	6	MM	BG, Th	CJD-MMiK
4	63/F	1985; tumor	27	Gait disturbance	19	MM	BG, Th	ND
5	64/F	1993; subdural hematoma	10	Visual impairment	21	MM	CC	MM2-C

*Among the patients with history of neurosurgery, average time (± SD) from neurosurgery to onset of CJD was 18.0 (± 9.8) years and average age at neurosurgery was 47.2 (± 10.2) years. However, among 22 patients with PSWCs on EEG, average time (± SD) from neurosurgery to onset of CJD was 14.3 (± 9.1) years and average age at neurosurgery was 58.0 (± 12.2) years. We noted no statistically significant differences between patients with and without PSWCs on EEG in relation to time between neurosurgery and onset of CJD or in age at neurosurgery. BG, basal ganglia; CC, cerebral cortex; CJD, Creutzfeldt-Jakob disease; DW-MRI, diffusion weighted images on magnetic resonance imaging; MM, methionine homozygous; MM2-C, MM2-cortical type sporadic CJD; MM2-T, MM2-thalamic type sporadic CJD; ND, not done; *PRNP*, prion protein gene; Th, thalamus.
†Disease duration is the time between onset of CJD and the appearance of akinetic mutism or death.

Table 3. Patients without history of neurosurgery who had no periodic sharp-wave complexes during duration of CJD and hyperintensity lesions in thalamus diffusion-weighted magnetic resonance imaging of the brain*

Patient no.	Age at CJD onset, y/sex	Codon 129 of *PRNP*	Hyperintensity lesions on DW-MRI	Pathology findings
1	58/F	MM	CC, BG, Th	MM2+1
2	65/M	MM	CC, Th	MM2+1
3	61/F	MM	CC, BG, Th	ND
4	58/M	MV	BG, Th	MV2
5	73/F	MV	CC, Th	MV2
6	65/F	MV	CC, BG, Th	ND
7	65/F	MV	CC, Th	ND
8	75/F	VV	BG, Th	VV2
9	69/M	VV	BG, Th	VV2
10	52/M	VV	CC, BG, Th	ND

*BG, basal ganglia; CC, cerebral cortex; CJD, Creutzfeldt-Jakob disease; DW-MRI, diffusion-weighted magnetic resonance imaging; MM, methionine homozygous; MM2+1, pathological features of MM2 and MM1 types of sporadic CJD; MV, methionine-valine; Th, thalamus; VV, valine homozygous.

reported in detail elsewhere (*8*,*17*–*19*). We assessed the subtypes of CJD with pathology and biochemical analysis of the brain and noted MM2-thalamic type in patient 2, CJD-MMiK in patient 3, and MM2-cortical type sCJD in patient 5 (Table 2). Patient 3 did not receive a dura mater graft according to neurosurgery records, and none was observed at autopsy.

Among patients who had not undergone neurosurgery, 64/1,121 showed no PSWCs on EEG, including 51 (79.7%) with 129MM, 4 (6.3%) with 129VV, and 9 (14.1%) with 129MV. Western blot of brain tissue performed on 25 patients revealed 5 with MM1 type CJD, 9 with MM2 type, 5 with MM2+1 type, 4 with MV2 type, and 2 with VV2 type. DW-MRI was available for 55/64 patients without PSWCs on EEG, 44 patients with 129MM, 8 with 129MV, and 3 with 129VV. On DW-MRI, 10/55 patients had hyperintensity lesions in the thalamus (Table 3), 3 of whom had 129MM, including 2 patients with MM2+1 type. Slight thalamic signal increase was observed in mediodorsal nuclei in all 3 patients with 129MM (Appendix Figure 2).

Discussion

We identified 27/1,155 (2.3%) patients with diagnosed sCJD or unclassified CJD who had neurosurgery ≥1 year before the onset of CJD. We also noted that more patients with history of neurosurgery had an absence of PSWCs on EEG than patients who had not had neurosurgery. Furthermore, 5/27 patients with history of neurosurgery had atypical clinical features, including no PSWCs on EEG for the duration of CJD. Of note, among 5 patients with 129MM, 2 had hyperintensity lesions in the thalamus on DW-MRI, 1 of whom was confirmed to have CJD-MMiK by autopsy.

In our previous study, patients with acquired CJD-MMiK showed no PSWCs ≤1 year after onset of CJD (*4*,*5*). Among 3 autopsies for cases without PSWCs on EEG and a history of neurosurgery, 2 patients were determined to have definite MM2 type sCJD with atypical clinical features (Table 2), as previously reported (*19*–*22*). One had MM2-cortical form and the other had MM2-thalamic form. Our study proved 1 patient had CJD-MMiK (Table 2), which we reported previously (*8*,*17*). Among the patients with history of neurosurgery, no PSWCs on EEG might suggest possibility of acquired CJD-MMiK.

The patient determined to have CJD-MMiK showed hyperintensity lesions in bilateral thalamus in addition to bilateral basal ganglia (Appendix Figure 1, panel A). Several patients with plaque type dCJD showed hyperintensity lesions in thalamus on DW-MRI or proton density-weighted MRI (*5*,*23*–*25*; K. Sakai et al., unpublished data). A previous study on MRI of sCJD showed that the absence of thalamic signal increase differentiated MM1 from other types of sCJD, but thalamic involvement was occasionally observed in MM2-cortical type sCJD (*26*). In our study, thalamic signal increase was observed in 3/44 patients with diagnosed sCJD, and 129MM patients without history of neurosurgery showed only slight signal increases in mediodorsal nuclei. These results suggest that hyperintensity lesions in the thalamus on DW-MRI in patients with 129MM might be a clinical marker of CJD-MMiK, but we cannot exclude the possibility of MM2-cortical type sCJD. Further MRI studies of plaque type dCJD cases with CJD-MMiK is ongoing.

According to a previous study on MRI of sCJD, the most characteristic MRI lesion patterns in the patients with MV2 and VV2 type sCJD, who were infected with V2 sCJD strain, shows predominant involvement of thalamus and basal ganglia (*26*). Because transmission of V2 sCJD strain to persons with 129MM causes CJD-MMiK (*7*–*10*), thalamic involvement frequently was observed, as we noted in the case we identified in this study.

One of the 2 atypical patients with history of neurosurgery, patient 4 (Table 2), did not have an

autopsy but had signs and symptoms of CJD-MMiK. Patient 4 had bilateral hyperintensity lesions in thalamus on DW-MRI (Appendix Figure 1, panel B), no PSWCs on EEG, methionine homozygosity at codon 129 of *PRNP*, gait disturbance as an initial symptom, and long disease duration (19 months), similar to the features of the patients with plaque-type dCJD, suggesting that this patient had CJD-MMiK. However, no information about dura mater grafting at the neurosurgery is available for this patient.

We identified 1 patient with definite CJD-MMiK and another patient with suspected CJD-MMiK among 1,155 patients with diagnosed sCJD or unclassified CJD, suggesting that these 2 patients could have iatrogenic CJD. Several epidemiologic studies have shown no association between surgery and the onset of sCJD, but others show notable association when special conditions are met, such as lag periods >20 years between surgery and CJD onset and when patients are <30 years of age at the time of surgery (*27*,*28*). For the 2 patients with confirmed and suspected CJD-MMiK in our study, patient 3 underwent neurosurgery at 61 years of age, 14 years before CJD onset. Patient 4 underwent neurosurgery at 36 years of age, 27 years before CJD onset. Both of these patients' illness onset fall into the range noted between surgical procedure to illness onset (1–30 years) among 154 patients with dCJD in Japan (*29*). Compared with other surgical procedures, neurosurgery followed by protracted survival is remarkably infrequent and therefore is difficult to study. Our results showed that few patients mimic the findings of MMiK type CJD, which might provide clues supporting the presence of a subgroup of CJD transmitted by neurosurgery after a long time lag without evidence of reuse of contaminated instruments on a CJD patient. An experimental research study provides strong support for an eventual transmission of CJD by general surgery in addition to neurosurgery (*30*), and high-quality epidemiologic research on neurosurgical risk for CJD is needed. Furthermore, we cannot find iatrogenic CJD patients who transmit M1 sCJD strain to persons with 129MM because the transmission would result in MM1 type neuropathology. A new method to detect transmission of M1 sCJD strain to persons with 129MM is needed.

Thus far, a patient with cadaveric pituitary-derived human growth hormone (hGH)–associated CJD in the United Kingdom was reported to have 129MM, type i PrP^{Sc}, and kuru plaques (*31*), suggesting that patients without history of neurosurgery could develop CJD-MMiK. In that case, the patient received hGH through intramuscular injection. Another 2 patients with hGH-associated CJD were reported to have 129MM and type i PrP^{Sc} (*32*,*33*). Unfortunately, detailed clinical information, including brain MRI, is not available for these patients, and we cannot compare the clinical manifestations with those for plaque type dCJD in Japan. Further studies for CJD-MMiK in patients with hGH-associated CJD are needed.

In conclusion, among 1,155 patients with diagnosed sCJD or unclassified type CJD, 2 patients with a history of neurosurgery had atypical clinical and neuropathologic features similar to acquired CJD-MMiK. A subgroup of sCJD mimicking features described in dCJD might have been transmitted by neurosurgery after long time lag. Hyperintensity lesions in the thalamus on DW-MRI in patients with 129MM might be a clinical marker of acquired CJD-MMiK. For epidemiologic surveillance studies, we propose clinical diagnostic criteria of sCJD potentially transmitted by neurosurgical procedures, which includes the criteria of possible, probable, or definite sCJD; methionine homozygosity at codon 129 of *PRNP*; no PSWCs on EEG; and hyperintensity lesions in the thalamus on DW-MRI.

Acknowledgments

The authors thank members of the Creutzfeldt-Jakob Disease Surveillance Committee, Creutzfeldt-Jakob disease specialists, participating physicians in prefectures in Japan, and the patients with Creutzfeldt-Jakob disease and their families for providing important clinical information.

This work was supported by a grant-in-aid from the Research Committee of Prion Disease and Slow Virus Infection, the Ministry of Health, Labour and Welfare of Japan to T.H., R.A., H.M., and M.Y.; a grant-in-aid from the Research Committee of Surveillance and Infection Control of Prion Disease, the Ministry of Health, Labour, and Welfare of Japan to T.K., Y.N., N.S., T.T., H.M., and M.Y.; and a grant-in-aid from the Research Committee of Molecular Pathogenesis and Therapies for Prion Disease and Slow Virus Infection, Agency for Medical Research and Development to T.H., A.K., H.M., and M.Y.

About the Author

Dr. Hamaguchi is an associate professor in the Department of Neurology and Neurobiology of Aging, Kanazawa University Graduate School of Medical Sciences, Kanazawa, Japan. His research interests include transmission of pathogenic protein, such as prion protein and amyloid β protein, among humans.

References

1. Prusiner SB. Prions. Proc Natl Acad Sci USA. 1998;95: 13363–83. https://doi.org/10.1073/pnas.95.23.13363
2. Brown P, Brandel JP, Sato T, Nakamura Y, MacKenzie J, Will RG, et al. Iatrogenic Creutzfeldt-Jakob disease, final assessment. Emerg Infect Dis. 2012;18:901–7. https://doi.org/10.3201/eid1806.120116
3. Brown P, Brandel JP, Preece M, Sato T. Iatrogenic Creutzfeldt-Jakob disease: the waning of an era. Neurology. 2006;67:389–93. https://doi.org/10.1212/01.wnl.0000231528.65069.3f
4. Noguchi-Shinohara M, Hamaguchi T, Kitamoto T, Sato T, Nakamura Y, Mizusawa H, et al. Clinical features and diagnosis of dura mater graft associated Creutzfeldt Jakob disease. Neurology. 2007;69:360–7. https://doi.org/10.1212/01.wnl.0000266624.63387.4a
5. Yamada M, Noguchi-Shinohara M, Hamaguchi T, Nozaki I, Kitamoto T, Sato T, et al. Dura mater graft-associated Creutzfeldt-Jakob disease in Japan: clinicopathological and molecular characterization of the two distinct subtypes. Neuropathology. 2009;29:609–18. https://doi.org/10.1111/j.1440-1789.2008.00987.x
6. Kobayashi A, Asano M, Mohri S, Kitamoto T. Cross-sequence transmission of sporadic Creutzfeldt-Jakob disease creates a new prion strain. J Biol Chem. 2007;282:30022–8. https://doi.org/10.1074/jbc.M704597200
7. Kobayashi A, Sakuma N, Matsuura Y, Mohri S, Aguzzi A, Kitamoto T. Experimental verification of a traceback phenomenon in prion infection. J Virol. 2010;84:3230–8. https://doi.org/10.1128/JVI.02387-09
8. Kobayashi A, Parchi P, Yamada M, Brown P, Saverioni D, Matsuura Y, et al. Transmission properties of atypical Creutzfeldt-Jakob disease: a clue to disease etiology? J Virol. 2015;89:3939–46. https://doi.org/10.1128/JVI.03183-14
9. Kobayashi A, Parchi P, Yamada M, Mohri S, Kitamoto T. Neuropathological and biochemical criteria to identify acquired Creutzfeldt-Jakob disease among presumed sporadic cases. Neuropathology. 2016;36:305–10. https://doi.org/10.1111/neup.12270
10. Kobayashi A, Asano M, Mohri S, Kitamoto T. A traceback phenomenon can reveal the origin of prion infection. Neuropathology. 2009;29:619–24. https://doi.org/10.1111/j.1440-1789.2008.00973.x
11. Nozaki I, Hamaguchi T, Sanjo N, Noguchi-Shinohara M, Sakai K, Nakamura Y, et al. Prospective 10-year surveillance of human prion diseases in Japan. Brain. 2010;133:3043–57. https://doi.org/10.1093/brain/awq216
12. Hamaguchi T, Sakai K, Noguchi-Shinohara M, Nozaki I, Takumi I, Sanjo N, et al. Insight into the frequent occurrence of dura mater graft-associated Creutzfeldt-Jakob disease in Japan. J Neurol Neurosurg Psychiatry. 2013;84:1171–5. https://doi.org/10.1136/jnnp-2012-304850
13. Satoh K, Tobiume M, Matsui Y, Mutsukura K, Nishida N, Shiga Y, et al. Establishment of a standard 14-3-3 protein assay of cerebrospinal fluid as a diagnostic tool for Creutzfeldt-Jakob disease. Lab Invest. 2010;90:1637–44. https://doi.org/10.1038/labinvest.2009.68
14. Schmitz M, Ebert E, Stoeck K, Karch A, Collins S, Calero M, et al. Validation of 14-3-3 protein as a marker in sporadic Creutzfeldt-Jakob disease diagnostic. Mol Neurobiol. 2016;53:2189–99. https://doi.org/10.1007/s12035-015-9167-5
15. Kitamoto T, Ohta M, Doh-ura K, Hitoshi S, Terao Y, Tateishi J. Novel missense variants of prion protein in Creutzfeldt-Jakob disease or Gerstmann-Sträussler syndrome. Biochem Biophys Res Commun. 1993;191:709–14. https://doi.org/10.1006/bbrc.1993.1275
16. World Health Organization. Global surveillance, diagnosis, and therapy of human transmissible spongiform encephalopathies: Report of a WHO consultation, February 9–11, 1998. Geneva: the Organization; 1998.
17. Ishida C, Kakishima A, Okino S, Furukawa Y, Kano M, Oda Y, et al. Sporadic Creutzfeldt-Jakob disease with MM1-type prion protein and plaques. Neurology. 2003; 60:514–7. https://doi.org/10.1212/01.WNL.0000044403.41041.A4
18. Nozaki I, Hamaguchi T, Noguchi-Shinohara M, Ono K, Shirasaki H, Komai K, et al. The MM2-cortical form of sporadic Creutzfeldt-Jakob disease presenting with visual disturbance. Neurology. 2006;67:531–3. https://doi.org/10.1212/01.wnl.0000228224.35678.60
19. Hamaguchi T, Kitamoto T, Sato T, Mizusawa H, Nakamura Y, Noguchi M, et al. Clinical diagnosis of MM2-type sporadic Creutzfeldt-Jakob disease. Neurology. 2005;64:643–8. https://doi.org/10.1212/01.WNL.0000151847.57956.FA
20. Parchi P, Capellari S, Chin S, Schwarz HB, Schecter NP, Butts JD, et al. A subtype of sporadic prion disease mimicking fatal familial insomnia. Neurology. 1999;52: 1757–63. https://doi.org/10.1212/WNL.52.9.1757
21. Parchi P, Giese A, Capellari S, Brown P, Schulz-Schaeffer W, Windl O, et al. Classification of sporadic Creutzfeldt-Jakob disease based on molecular and phenotypic analysis of 300 subjects. Ann Neurol. 1999;46:224–33. https://doi.org/ 10.1002/1531-8249(199908)46:2<224::AID-ANA12>3.0.CO;2-W
22. Krasnianski A, Meissner B, Schulz-Schaeffer W, Kallenberg K, Bartl M, Heinemann U, et al. Clinical features and diagnosis of the MM2 cortical subtype of sporadic Creutzfeldt-Jakob disease. Arch Neurol. 2006;63:876–80. https://doi.org/10.1001/archneur.63.6.876
23. Kretzschmar HA, Sethi S, Földvári Z, Windl O, Querner V, Zerr I, et al. Latrogenic Creutzfeldt-Jakob disease with florid plaques. Brain Pathol. 2003;13:245–9. https://doi.org/10.1111/j.1750-3639.2003.tb00025.x
24. Meissner B, Kallenberg K, Sanchez-Juan P, Ramljak S, Krasnianski A, Heinemann U, et al. MRI and clinical syndrome in dura mater-related Creutzfeldt-Jakob disease. J Neurol. 2009;256:355–63. https://doi.org/10.1007/s00415-009-0026-z
25. Wakisaka Y, Santa N, Doh-ura K, Kitamoto T, Ibayashi S, Iida M, et al. Increased asymmetric pulvinar magnetic resonance imaging signals in Creutzfeldt-Jakob disease with florid plaques following a cadaveric dura mater graft. Neuropathology. 2006;26:82–8. https://doi.org/10.1111/j.1440-1789.2006.00638.x
26. Meissner B, Kallenberg K, Sanchez-Juan P, Collie D, Summers DM, Almonti S, et al. MRI lesion profiles in sporadic Creutzfeldt-Jakob disease. Neurology. 2009; 72:1994–2001. https://doi.org/10.1212/WNL.0b013e3181a96e5d
27. de Pedro-Cuesta J, Mahillo-Fernandez I, Calero M, Rábano A, Cruz M, Siden Å, et al.; EUROSURGYCJD Research Group. Towards an age-dependent transmission model of acquired and sporadic Creutzfeldt-Jakob disease. PLoS One. 2014;9:e109412. https://doi.org/10.1371/journal.pone.0109412
28. López FJG, Ruiz-Tovar M, Almazán-Isla J, Alcalde-Cabero E, Calero M, de Pedro-Cuesta J. Risk of transmission of sporadic Creutzfeldt-Jakob disease by surgical procedures: systematic reviews and quality of evidence. Euro Surveill. 2017;22. https://doi.org/10.2807/1560-7917.ES.2017.22.43.16-00806

29. Ae R, Hamaguchi T, Nakamura Y, Yamada M, Tsukamoto T, Mizusawa H, et al. Update: dura mater graft-associated Creutzfeldt-Jakob disease–Japan, 1975–2017. MMWR Morb Mortal Wkly Rep. 2018;67:274–8. https://doi.org/10.15585/mmwr.mm6709a3
30. Brown P, Gibbs CJ Jr, Rodgers-Johnson P, Asher DM, Sulima MP, Bacote A, et al. Human spongiform encephalopathy: the National Institutes of Health series of 300 cases of experimentally transmitted disease. Ann Neurol. 1994;35:513–29. https://doi.org/10.1002/ana.410350504
31. Ritchie DL, Barria MA, Peden AH, Yull HM, Kirkpatrick J, Adlard P, et al. UK Iatrogenic Creutzfeldt-Jakob disease: investigating human prion transmission across genotypic barriers using human tissue-based and molecular approaches. Acta Neuropathol. 2017;133:579–95. https://doi.org/10.1007/s00401-016-1638-x
32. Cali I, Cohen ML, Haik S, Parchi P, Giaccone G, Collins SJ, et al. Iatrogenic Creutzfeldt-Jakob disease with amyloid-β pathology: an international study. Acta Neuropathol Commun. 2018;6:5. https://doi.org/10.1186/s40478-017-0503-z
33. Duyckaerts C, Sazdovitch V, Ando K, Seilhean D, Privat N, Yilmaz Z, et al. Neuropathology of iatrogenic Creutzfeldt-Jakob disease and immunoassay of French cadaver-sourced growth hormone batches suggest possible transmission of tauopathy and long incubation periods for the transmission of Abeta pathology. Acta Neuropathol. 2018;135:201–12. https://doi.org/10.1007/s00401-017-1791-x

Address for correspondence: Masahito Yamada, Department of Neurology and Neurobiology of Aging, Kanazawa University Graduate School of Medical Science, 13-1 Takara-machi, Kanazawa 920-8640, Japan; email: m-yamada@med.kanazawa-u.ac.jp

Failures of 13-Valent Conjugated Pneumococcal Vaccine in Age-Appropriately Vaccinated Children 2–59 Months of Age, Spain

Sergi Hernández, Fernando Moraga-Llop, Alvaro Díaz, Mariona F. de Sevilla, Pilar Ciruela, Carmen Muñoz-Almagro, Gemma Codina, Magda Campins, Juan José García-García, Cristina Esteva, Conchita Izquierdo, Sebastià González-Peris, Johanna Martínez-Osorio, Sonia Uriona, Luis Salleras, Ángela Domínguez

Vaccination with the 13-valent conjugated pneumococcal disease (PCV13) has reduced invasive pneumococcal disease (IPD), but there have been reports of vaccine failures. We performed a prospective study in children aged 2–59 months who received diagnoses of IPD during January 2012–June 2016 in 3 pediatric hospitals in Catalonia, Spain, a region with a PCV13 vaccination coverage of 63%. We analyzed patients who had been age-appropriately vaccinated but who developed IPD caused by PCV13 serotypes. We detected 24 vaccine failure cases. The serotypes involved were 3 (16 cases); 19A (5 cases); and 1, 6B, and 14 (1 case each). Cases were associated with children without underlying conditions, with complicated pneumonia (OR 6.65, 95% CI 1.91–23.21), and with diagnosis by PCR (OR 5.18, 95% CI 1.84–14.59). Vaccination coverage should be increased to reduce the circulation of vaccine serotypes. Continuous surveillance of cases of IPD using both culture and PCR to characterize vaccine failures is necessary.

Author affiliations: Agència de Salut Pública de Catalunya, Generalitat de Catalunya, Barcelona, Spain (S. Hernández, P. Ciruela, C. Izquierdo); Hospital Universitari Vall d'Hebron, Barcelona (F. Moraga-Llop, M. Campins, S. González-Peris); Hospital de Nens, Barcelona (A. Díaz); Hospital Sant Joan de Déu Barcelona, Barcelona (M.F. de Sevilla, C. Muñoz-Almagro, J.J. García-García, C. Esteva, J. Martínez-Osorio); Institut de Recerca Sant Joan de Déu, Esplugues de Llobregat, Spain (M.F. de Sevilla, C. Muñoz-Almagro, J.J. García-García); CIBER de Epidemiología y Salud Pública, Madrid, Spain (P. Ciruela, J.J. García-García, C. Esteva, L. Salleras, Á. Domínguez); Universitat Internacional de Catalunya, Barcelona (C. Muñoz-Almagro); Vall d'Hebron Institut de Recerca, Barcelona (M. Campins, S. Uriona); Universitat de Barcelona, Barcelona (L. Salleras, Á. Domínguez)

DOI: https://doi.org/10.3201/eid2606.190951

Conjugated pneumococcal vaccines have been shown to be effective in preventing invasive pneumococcal disease (IPD) in children. In February 2001, the European Medicines Agency (EMA) authorized the use of the 7-valent pneumococcal conjugate vaccine (PCV7), which included antigens of serotypes 4, 6B, 9V, 14, 18C, 19F, and 23F (*1*) in children <2 years of age. The introduction of PCV7 led to a reduction in cases of IPD and in hospitalizations caused by vaccine serotypes (*2*,*3*). Cases of IPD with PCV7 vaccine failure represented ≈2% of all reported IPD cases and resulted mainly from bacteremia caused by serotypes 4, 6B, and 19F. Half the patients with vaccine failure had underlying diseases (*4*). In subsequent years, there was an increase in the number of IPD cases caused by non-PCV7 serotypes, mainly serotypes 1, 3, and 19A; pneumonia complicated by empyema, pleural effusion, or both was the most frequent presentation (*5*,*6*).

In April 2009 (*7*), and subsequently in December 2009 (*8*), the European Medicines Agency authorized the marketing of the 10-valent pneumococcal conjugate vaccine (PCV10), which included PCV7 serotypes plus serotypes 1, 5, and 7F. It also authorized the 13-valent conjugated pneumococcal vaccine (PCV13), which included PCV10 serotypes plus serotypes 3, 6A, and 19A. In 2010, the Vaccines Advisory Committee of the Spanish Association of Pediatrics recommended that children should receive PCV13, although the vaccine was not included in the recommended schedule of the National Health System and, therefore, parents had to pay for it. In Catalonia, Spain, PCV13 was included in the vaccination calendar financed by the public health system in July 2016. During 2012–2016, when this study was conducted, the estimated PCV13 coverage in children 7–59 months of age in Catalonia was 63% (*9*).

The introduction of PCV13 in children <5 years of age was associated with a decrease in IPD incidence caused by all vaccine serotypes, except for serotype 3, for which the decrease was not significant (*10*). Previous studies have shown that the immune response against serotype 3 after PCV13 vaccination is lower than that generated against other serotypes (*11*,*12*). Some case-control and cohort studies (*9*,*13*,*14*) have reported no effectiveness, whereas other studies have found the vaccine to be effective (*15*,*16*). Kaplan et al. (*17*) found that most cases of IPD caused by PCV13 serotypes in children receiving ≥1 dose of PCV13 were associated with serotype 19A and generally occurred in children <6 months of age or those with underlying conditions. However, studies have shown several cases of pneumonia complicated with empyema, pleural effusion, or both produced by serotype 3 in children vaccinated with PCV13 (*18*,*19*). We conducted a study to analyze the epidemiologic, clinical, and microbiological characteristics of cases of IPD arising from vaccine failure in children 2–59 months of age who were treated at 3 pediatric hospitals in Catalonia.

Methods

Study Design

We conducted a prospective study in children 2–59 months of age who received diagnoses of IPD during January 1, 2012–June 30, 2016 and were treated in 3 pediatric hospitals in Catalonia: Hospital Sant Joan de Déu, Hospital Maternoinfantil Vall d'Hebron, and Hospital de Nens de Barcelona. We estimated a reference population of 116,279 children <5 years of age (30.4% of the total population of this age in Catalonia) for the 3 hospitals (*9*).

We defined IPD as clinical findings of infection together with the isolation or detection of DNA from *Streptococcus pneumoniae* by real-time PCR in a normally sterile sample. We established the presence of *S. pneumoniae* DNA by amplification of the autolysin (*lytA*) gene and the *wzg* (*cpsA*) gene according to published assays (*20*–*22*). We included in the study only samples that were positive for the *lytA* and *wzg* genes in real-time PCR.

Vaccination Status

We obtained the vaccination status of each case-patient from the vaccination card and the medical record of the primary care center or private center where the child was usually seen. We collected information on the number of PCV13 doses administered and the date of administration. We considered a dose valid if administered after 6 weeks of age, with a minimum interval between doses appropriate to the summary of product characteristics (SmPC) (*8*) and ≥15 days before the onset of IPD.

Patients were considered age-appropriately vaccinated when they had received all doses of PCV13 corresponding to their age (even when the vaccination schedule was incomplete), according to SmPC (*8*) and the Spanish Association of Pediatrics recommendations (*23*). We considered patients age-incorrectly vaccinated when they had received ≥1 doses of PCV13 but did not comply with any vaccination schedule included in the SmPC or had received fewer doses than they should have at disease onset.

Identification, Serotyping, and Classification of *S. pneumoniae*

Strains of *S. pneumoniae* isolated by culture were serotyped, using the Quellung reaction or dot blot, by the National Center for Microbiology, Majadahonda, Madrid (*24*). We performed capsular typing of all culture-negative and PCR-positive samples using 2 methods, depending on the amount of *S. pneumoniae* DNA available. If the amount was low (detection of *LytA* gene DNA and *wzg* [*cpsA*] gene of *S. pneumoniae* by real-time PCR with the cycle threshold [Ct] >30 cycles), we used a previously described real-time multiplex PCR technique that detects all pneumococcal capsular types and differentiates serotypes 1, 3, 4, 5, 6A/C, 6B/D, 7F/A, 8, 9V/A/N/L, 14, 15B/C, 18C/B, 19A, 19F/B/C, 23A and 23F (*20*). If the amount of *S. pneumoniae* DNA was high (PCR-positive samples with Ct ≤30 cycles), we used sequential multiplex PCR combined with fragment analysis and automated fluorescent capillary electrophoresis to differentiate serotypes: 1, 2, 3, 4, 5, 6A/6B, 6C, 6,7C/(7B/40), 7F/7A, 9N/9L, 9V/9A, 10A, 10F/(10C/33C), 11A/11D, 12F/(12A/44/46), 13, 16F, 17F, 18/(18A/18B/18C/18F), 19A, 19F, 20(20A/20B), 21, 22F/22A), 23A, 23B, 24/(24A/24B/24F), 31, 34, 35A/(35C/42), 35B, 35F/47F, 38/25F, 39 (*25*). Because this procedure does not differentiate between serotypes 6A and 6C, and serotypes 7F and 7A, in 2 of the cases recorded, these serotypes were considered as nonvaccine serotypes and classified as 6A/6C and 7F/7A.

Definition of Vaccine Failure and Demographic, Clinical, and Epidemiologic Variables

We used the definition of PCV13 vaccine failure as described by Heininger et al. (*26*). This definition is the occurrence of IPD caused by a specific vaccine-preventable serotype in a person appropriately and fully vaccinated, taking into account the incubation period and the normal delay for protection to be acquired as a result of immunization.

The following demographic, clinical, and epidemiologic variables were recorded for each case-patient: age, sex, date of birth, date of symptom onset, hospitalization date, clinical form of IPD (meningitis, septic shock, uncomplicated pneumonia, complicated pneumonia, occult bacteremia and others), complications during admission, admission to the intensive care unit (ICU), and length of stay. We also recorded medical risk conditions (sickle cell anemia, congenital or acquired asplenia, human immunodeficiency virus infection, cochlear implant, congenital immunodeficiency, chronic heart disease, chronic lung diseases including asthma if treated with a risk dose of oral corticosteroids, cerebrospinal fluid fistula, chronic renal failure including nephrotic syndrome, immunosuppressive treatment or radiotherapy, solid organ or hematopoietic progenitor transplantation, and diabetes mellitus), and date and clinical outcome at discharge (discharge without sequelae, sequelae after 6 months, death).

Statistical Analysis

We compared categorical variables using a Pearson χ^2 test or Fisher exact test and continuous variables using a Student *t* test. In cases of vaccine failure, we calculated the association of serotypes with age group and vaccination status for each specific serotype compared with the remaining serotypes. Values of $p<0.05$ were considered statistically significant. We assumed a bilateral distribution for all p values. We then calculated the odds ratios (ORs) and 95% CIs. We conducted the analyses using SPSS Statistics 19.0 (IBM, https://www.ibm.com).

Data Confidentiality and Ethics Aspects

No diagnostic tests were made or samples taken from any participant in addition to those required by routine care. This study complies with the principles of the Declaration of Helsinki and the legal structure according to international human rights and biomedicine and personal data protection legislation. The Ethics Committee of Hospital Sant Joan de Déu approved the study. Informed consent signed by parents or legal guardians was given for all participants. All data were treated as confidential, and records were accessed anonymously.

Results

During the study period, we recruited 188 patients 2–59 months of age who were admitted to the 3 participating centers with IPD. We identified the *S. pneumoniae* serotype causing IPD in 180 cases (95.7%), of which 104 (57.8%) were caused by PCV13 serotypes. Serotype 3 was the most frequent serotype (42 cases, 23.3%), followed by serotype 1 (19 cases, 10.6%), 19A (17 cases, 9.4%), and 14 (13 cases, 7.2%). Of the 180 case-patients, 102 (56.7%) were not vaccinated, 66 (36.6%) were age-appropriately vaccinated, and 12 (6.7%) were age-incorrectly vaccinated.

Characteristics of Cases of Vaccine Failure

We detected 24 cases of vaccine failure according to the study definition, representing 13.3% of all cases. The serotypes identified were serotype 3 (16 cases, 66.7%); serotype 19A (5 cases, 20.8%); and serotypes 1, 14, and 6B (1 case each). The overall mean age of the 24 case-patients was 31.3 months (range 9–58 months, SD 14.7). Of the 24 case-patients, 66.7% (16) were male, and 62.6% (15) were 24–59 months of age (Table 1). The main age group was 24–59 months in cases caused by serotype 3 (81.3% vs. 25.0%; p = 0.013) and <24 months in cases caused by serotype 19A (80.0% vs. 26.3%; p = 0.047). Of the 24 case-patients, 17 (70.8%) had completed the vaccination schedule, 11 (45.8%) had a 3 + 1 dose schedule, 4 (16.7%) a 2-dose schedule, and 2 (8.3%) a 1-dose schedule. Of the 7 (29.2%) age-appropriately vaccinated patients with an incomplete vaccination schedule, 4 (16.7%) had a 3 + 0 schedule, 2 (8.3%) 1 dose, and 1 (4.2%) 2 doses. Serotype 3 was loosely associated with vaccine failure in age-appropriately vaccinated patients who had completed their vaccination schedule (OR 45.0, 95% CI 3.41–594.12). Serotype 19A was loosely associated with vaccine failure in age-appropriately vaccinated patients with an incomplete vaccination schedule (OR 21.33, 95% CI 1.75–263.67). The most frequent clinical presentation was complicated pneumonia (21/24 cases, 87.5%) and the most frequent complication of these 21 cases was empyema (15/21 cases, 71.4%). Of the 24 cases, 79.2% (19 cases) were diagnosed by PCR alone, 12.5% (3 cases) by culture alone, and 8.3% (2 cases) by PCR and culture. No patient with vaccine failure had underlying conditions.

Distribution of PCV13 Serotypes

Of the 104 cases of IPD caused by PCV13 serotypes, 23.1% (24 cases) were in age-appropriately vaccinated patients. The percentage of vaccine failure varied greatly according to the serotype: 38.1% (16/42) in serotype 3 cases, 29.4% (5/17) in serotype 19A cases, 7.7% (1/13) in serotype 14 cases, and 5.3% (1/19) in serotype 1 cases. Of the PCV13 serotypes, the proportion of serotype 3 in age-appropriately vaccinated patients was higher than in unvaccinated patients (66.7% vs. 27.8%; p = 0.001) (Table 2).

Table 1. Characteristics of age-appropriately vaccinated patients 2–59 months of age with invasive pneumococcal disease caused by PCV13 serotypes, Catalonia, Spain, 2012–2016*

Pt no.	Age, mo/sex	Year	Age at vaccination	Schedule	Clinical manifestation	Complications	Outcome	DT	Ser	Vaccine schedule
1	19/F	2012	12 mo	1	Complicated pneumonia	Pleural effusion	Cured	PCR	19A	UC
2	15/M	2012	3 ,5 mo†	2 + 0	Complicated pneumonia	Empyema, pneumothorax	Cured	Culture, PCR	19A	UC
3	15/F	2012	2, 5, 8 mo	3 + 0	Complicated pneumonia	Empyema, necrotizing pneumonia, bronchoalveolar fistula, pneumothorax	Bronchopleural fistula	PCR	3	UC
4	23/M	2012	17 mo	1	Uncomplicated pneumonia		Cured	Culture	1	UC
5	24/M	2012	2, 4, 6, 18 mo	3 + 1	Complicated pneumonia	Empyema	Cured	PCR	19A	C
6	24/M	2012	12, 21 mo	2	Complicated pneumonia	Empyema	Cured	PCR	3	C
7	21/M	2012	3, 5, 7, 15 mo	3 + 1	Complicated pneumonia	Empyema	Cured	PCR	3	C
8	38/M	2012	30 mo	1	Bacteraemic mastoiditis	Epidural abscess, sigmoid sinus thrombosis	Hydrocephalus	PCR	3	C
9	9/F	2013	2, 3, 4 mo	3 + 0	Complicated pneumonia	Necrotizing pneumonia	Cured	PCR	19A	UC
10	12/M	2013	2, 4, 6 mo	3 + 0	Complicated pneumonia	Empyema, necrotizing pneumonia	Cured	PCR	6B	UC
11	50/F	2013	25 mo	1	Complicated pneumonia	Empyema	Cured	PCR	3	C
12	34/M	2013	3, 6, 9, 15 mo	3 + 1	Complicated pneumonia	Empyema, pneumothorax, bronchopleural fistula	Cured	Culture, PCR	3	C
13	15/M	2014	2, 4, 7 mo	3 + 0	Osteoarticular infection		Cured	Culture	19A	UC
14	43/M	2014	12, 15 mo	2	Complicated pneumonia	Empyema, necrotizing pneumonia, bronchopleural fistula	Cured	PCR	3	C
15	44/F	2014	3, 5, 7, 20 mo	3 + 1	Complicated pneumonia	Empyema	Cured	PCR	3	C
16	25/F	2015	2, 4, 6, 14 mo	3 + 1	Complicated pneumonia	Pleural effusion	Cured	Culture	14	C
17	29/M	2015	3, 5, 7, 18 mo	3 + 1	Complicated pneumonia	Necrotizing pneumonia	Cured	PCR	3	C
18	51/M	2015	2, 4, 6, 16 mo	3 + 1	Complicated pneumonia	Empyema	Cured	PCR	3	C
19	49/F	2015	12,14 mo	2	Complicated pneumonia	Empyema	Cured	PCR	3	C
20	54/F	2015	3, 5, 7,17 mo	3 + 1	Complicated pneumonia	Empyema	Cured	PCR	3	C
21	58/M	2016	14, 16 mo	2	Complicated pneumonia	Empyema, necrotizing pneumonia	Pneumatocele	PCR	3	C
22	35/M	2016	2, 5, 9, 18 mo	3 + 1	Complicated pneumonia	Empyema, necrotizing pneumonia	Cured	PCR	3	C
23	41/M	2016	3, 4, 7, 16 mo	3 + 1	Complicated pneumonia	Necrotizing pneumonia	Cured	PCR	3	C
24	23/M	2016	3, 5, 6, 15 mo	3 + 1	Complicated pneumonia	Pleural effusion	Cured	PCR	3	C

*C, completed; DT, diagnostic technique; Pt, patient; Ser, serotype; UC, uncompleted.
†Patient resident in Andorra (routine immunization schedule 2+1) and transferred to a participating hospital.

Characteristics of IPD According to Vaccine Failure

We found no differences in sex or age group between cases of IPD with and without vaccine failure (Table 3). Cases with vaccine failure were associated with complicated pneumonia (OR 6.65, 95% CI 1.91–23.21). Pneumonia with empyema was the most common form of complicated pneumonia, both in cases of vaccine failure (71.4%) and in the remaining cases (77.5%). Cases of IPD with vaccine failure were associated with the diagnosis only by real-time PCR (OR 5.18, 95% CI 1.84–14.59). We observed no differences between the epidemiologic variables studied.

Table 2. Distribution of PCV13 serotypes causing invasive pneumococcal disease in patients 2–59 months of age in cases of vaccine failure and in unvaccinated patients, Catalonia, Spain, 2012–2016

PCV13 serotype	Vaccine failure, no. (%), n = 24	Unvaccinated patients, no. (%) n = 72	OR (95% CI)	p value
1	1 (4.2)	16 (22.2)	0.15 (0.02–1.21)	0.062
3	16 (66.7)	20 (27.8)	5.20 (1.93–14.04)	0.001
6A	0	1 (1.4)	0	0
6B	1 (4.2)	1 (1.4)	3.09 (0.19–51.35)	0.439
7F	0	3 (4.2)	0	0
9V	0	3 (4.2)	0	0
14	1 (4.2)	12 (16.7)	0.22 (0.03–1.77)	0.174
18C	0	1 (1.4)	0	0
19A	5 (20.8)	12 (16.7)	1.32 (0.41–4.21)	0.634
19F	0	2 (2.8)	0	0
23F	0	1 (1.4)	0	0

Characteristics of IPD Caused by Serotype 3 in Unvaccinated Cases and Cases with Vaccine Failure

Of the 42 case-patients with IPD caused by serotype 3, a total of 20 (47.6%) had received no dose of PCV13, 16 (38.1%) were age-appropriately vaccinated, and 6 (14.3%) were age-incorrectly vaccinated according to the SmPC. We found no significant differences between IPD caused by serotype 3 in unvaccinated patients and age-appropriately vaccinated patients with respect to the distribution by sex, age group, clinical form, and complications (Table 4). None of the severity factors compared (days of hospital admission, stay and days of admission to the ICU, complications, and sequelae at discharge) was associated with either group.

Discussion

Since the introduction of PCV13, several authors have reported cases of IPD caused by vaccine serotypes, both in patients who had received ≥1 dose of PCV13 and in age-appropriately vaccinated patients. In our study, cases with vaccine failure were associated mainly with serotype 3, the clinical presentation of complicated pneumonia, and patients without underlying conditions or other risk factors. This type of vaccine failure coincides with that found by Antachopoulos et al. in Greece (*19*) and confirms the results of Moraga-Llop et al. in Catalonia (*18*).

Kaplan et al. (*17*), in a study carried out in 8 US pediatric hospitals, found that vaccine failures were associated mainly with serotype 19A, age <6 months, and patients with underlying conditions. A retrospective study by Basaranoglu et al. (*27*) of IPD cases in children treated at a tertiary pediatric hospital in Ankara, Turkey, in 2015 reported 2 cases of vaccine failure associated with serotype 19F in patients with underlying neurologic disease. These studies differ from ours in 2 respects. First, they were carried out in a population for which pediatric PCV13 vaccination had been financed since 2010; thus, Basaranoglu et al. (*27*) found that the vaccination coverage in children was 96%. Our study was conducted in a population with an estimated vaccination coverage of 63% (*9*). In addition, although several studies indicate that there has been no decrease in the incidence of serotype 3 after the introduction of PCV13 (*9*,*28*,*29*), only the study in adults by Fukusumi et al. (*29*) included cases diagnosed by real-time PCR; therefore, it cannot be ruled out that, in a population with higher vaccination rates, there were fewer vaccine failures because of herd immunity.

The second aspect is methodological. The studies by Kaplan et al. (*17*) and Basaranoglu et al. (*27*) included only cases diagnosed by culture. In our study, cases diagnosed by PCR were also included; in fact, cases of vaccine failure were associated with a diagnosis by PCR. Selva et al. (*30*) showed the importance of PCR in the diagnosis of IPD caused by serotype 3 in children <5 years of age with negative cultures. Almeida et al. (*31*), in a retrospective study conducted in patients <18 years of age admitted with pneumonia to a tertiary hospital in Portugal during 2012–2014 and diagnosed by PCR, found 4 cases of vaccine failure in patients who had received 4 doses of PCV13, which were all associated with serotype 3. Silva-Costa et al. (*32*) analyzed 152 pleural fluid samples from pediatric patients in Portugal during 2010–2015 to identify and serotype *S. pneumoniae*; 68% of cases were diagnosed only by PCR and, as in our study, the serotypes most frequently identified were 3, 1, and 19A. That study detected 19 cases of PCV13 vaccine failure, of which 17 were related to serotype 3. Serotype 3 was the most frequently identified serotype in children vaccinated with PCV13 in both studies and, although Silva-Costa et al. analyzed only cases of complicated pneumonia, a pathology associated with this serotype, our results, analyzing all clinical presentations of IPD, were identical. We also found a higher frequency of serotype 3 cases in patients with vaccine failure compared with unvaccinated patients, which

is an indicator of the importance of this serotype in the post-PCV13 era. When the 2 studies were carried out, the vaccination coverage in Portugal (61%) was similar to that of Catalonia (63%).

As in the study by Kaplan et al. (*17*), we found that serotype 19A was associated with cases of PCV13 vaccine failure in children <2 years of age, the most frequently isolated serotype in this age group in our setting (*10*). Dominguez et al. (*9*) found that PCV13 effectiveness in the prevention of IPD caused by serotype 19A was 86% for ≥1 dose. The similar results observed by Kaplan et al. (*17*) for this serotype in a population with routine PCV13 vaccination may be explained by the fact that in half of the cases (5/10) reported by Kaplan et al., patients also had some type of underlying condition, whereas in our study, no patient had an underlying condition.

Heininger et al. (*26*) classified vaccine failures according to their cause or origin. Our study found no failures related to usage issues because, in all cases, the dates of vaccine administration and the number of doses administered according to the technical specifications were verified. The data in our study included cases during January 2012–June 2016, so the vaccines administered did not belong to the same batch. Although it is not known whether the preservation or storage of each vaccine was correct, given that vaccine failures occurred mostly in serotype 3 and in cases with complicated pneumonia, it seems unlikely that vaccine failures can be related to any of these factors, because in that case the case-mix of vaccine failures would be much more heterogeneous. Host-related vaccine failures also seem unlikely because no patient had a history of any underlying condition, including immunodeficiency. This finding is reinforced by the absence of differences between cases of IPD caused by serotype 3 in unvaccinated patients and in those with vaccine failure. It may be assumed that, if cases with vaccine failure had some type of immunodeficiency that would have induced a poor immunological response to the PCV13 vaccine, this effect would have manifested as a greater severity of IPD in cases with vaccine failure. The lack of significant differences in the epidemiologic variables between cases with and without vaccine failure makes it unlikely that vaccine failures were related to interference by other infectious agents. The fact that serotype 3 was associated with cases with vaccine failure, and specifically with age-appropriately vaccinated patients who had

Table 3. Characteristics of cases of invasive pneumococcal disease in patients 2–59 months of age with and without vaccine failure, Catalonia, Spain, 2012–2016

Variable	Vaccine failure, no. (%), n = 24	No vaccine failure, no. (%), n = 156	OR (95% CI)	p value
Sex				
F	8 (33.3)	58 (37.2)	Referent	
M	16 (66.7)	98 (62.8)	1.18 (0.48–2.94)	0.716
Age group				
2–23 mo	9 (37.5)	73 (46.8)	Referent	
24–59 mo	15 (62.5)	83 (53.2)	1.46 (0.60–3.55)	0.395
Clinical form				
Meningitis	0	16 (10.3)	0	0
Septic shock	0	4 (2.6)	0	0
Uncomplicated pneumonia	1 (4.2)	26 (16.7)	0.22 (0.03–1.68)	0.134
Complicated pneumonia	21 (87.5)	80 (51.3)	6.65 (1.91 –23.21)	0,001
Occult bacteremia	0	20 (12.8)	0	0
Other	2 (8.3)*	10 (6.4)†	1.33 (0.27–6.46)	0.664
Pneumonia complication				
Empyema	15 (71.4)	62 (77.5)	0.73 (0.25–2.14)	0.561
Pleural effusion	3 (14.3)	23 (28.8)	0.41 (0.11–1.54)	0.263
Necrotizing pneumonia	8 (38.1)	18 (22.5)	2.12 (0.76–5.91)	0.146
Intensive care unit admission	2 (8.3)	35 (22.4)	0.31 (0.07–1.40)	0.173
Sequelae at discharge	3 (12.5)	20 (11.9)	0.96 (0.26–3.53)	1.000
Underlying disease	0	9 (5.8)	0	0
Diagnostic technique				
PCR only	19 (79.2)	66 (42.3)	6.62 (1.47–29.82)	0.014
Culture only	3 (12.5)	44 (28.2)	1.57 (0.25–9.84)	0.631
PCR + culture	2 (8.3)	46 (29.5)	Referent	
Breastfeeding	22 (91.7)	125 (81.2)	2.55 (0.57–11.47)	0.260
School or daycare attendance	20 (83.3)	102 (66.2)	2.55 (0.83–7.85)	0.104
Respiratory infection previous month	17 (70.8)	88 (57.1)	1.82 (0.71–4.65)	0.205
Recurrent otitis media	5 (20.8)	19 (12.3)	1.87 (0.62–5.59)	0.257

*Osteoarticular infection (1); mastoiditis (1).
†Osteoarticular infection (5); mastoiditis (4); orbital cellulitis (1).

Table 4. Characteristics of cases of invasive pneumococcal disease caused by serotype 3 in patients 2–59 months of age with vaccine failure or unvaccinated, Catalonia, Spain, 2012–2016*

Variable	Vaccine failure, no. (%), n = 16	Unvaccinated, no. (%), n = 20	OR (95% CI)	p value
Sex				
F	5 (31.3)	6 (30.0)	Referent	
M	11 (68.8)	14 (70.0)	0.94 (0.23–3.92)	0.936
Days of admission, mean (SD)	14.69 (9.81)	12.25 (6.07)	1.04 (0.95–1.13)	0.367
ICU days, mean (SD)	1.00	3.00 (1.14)	Not calculable	0.540
Age group				
0–23 mo	3 (18.8)	7 (35.0)	Referent	
24–59 mo	13 (81.3)	13 (65.0)	2.33 (0.49–11.06)	0.456
Clinical form				
Septic shock	0	1 (5.0)	0	0
Uncomplicated pneumonia	0	2 (10.0)	0	0
Complicated pneumonia	15 (93.8)	17 (85.0)	2.65 (0.25–28.24)	0.613
Mastoiditis	1 (6.3)	0	0	0
Empyema				
No	3 (20.0)	3 (17.6)	Referent	
Yes	12 (80.0)	14 (82.4)	0.86 (0.15–5.06)	1.000
Pleural effusion				
No	14 (93.3)	13 (76.5)	Referent	
Yes	1 (6.7)	4 (23.5)	0.23 (0.02–2.36)	0.338
Necrotizing pneumonia				
No	9 (60.0)	13 (76.5)	Referent	
Yes	6 (40.0)	4 (23.5)	2.17 (0.47–9.95)	0.450
ICU				
No	15 (93.8)	18 (90.0)	Referent	
Yes	1 (6.3)	2 (10.0)	0.60 (0.05–7.28)	1.000
Sequelae at discharge				
No	13 (81.3)	17 (85.0)	Referent	
Yes	3 (18.8)	3 (15.0)	1.31 (0.23–7.57)	1.000
Underlying disease				
No	16 (100.0)	19 (95.0)		
Yes	0	1 (5.0)		
PCR diagnosis only				
No	1 (6.3)	2 (10.0)	Referent	
Yes	15 (93.8)	18 (90.0)	1.67 (0.14–20.23)	1.000

*ICU, intensive care unit.

completed their vaccination schedule, indicates that vaccine failures could be vaccine related because of low PCV13 effectiveness with respect to serotype 3. This conclusion is in line with the results published by other authors (*9*,*13*,*33*) who studied PCV13 effectiveness in case-control studies and with the results reported on PCV13 effectiveness by Andrews et al. (*14*,*34*) in indirect cohort studies. All those authors observed that the effectiveness for all PCV13 serotypes was high, except for serotype 3, where it was very limited. Vanderkooi et al. (*11*) observed that the level of opsonophagocytic antibodies against serotype 3 was lower than that for the other PCV13 serotypes and Martinón-Torres et al. (*12*) observed that serotype 3 had the lowest levels of immunogenicity after PCV13 vaccination. Van der Linden et al. (*15*), looking at cases diagnosed only by culture, reported a PCV13 effectiveness against serotype 3 in children <24 months of age of 74% (95% CI 2%–93%) for those who had received ≥1 dose of vaccine but a nonsignificant effectiveness of 63% (95% CI -393% to 97%) for those who had received a postbooster dose.

A limitation of the study is that it was not possible to perform a serologic study to determine serotype-specific IgG concentrations. No specific studies were made to rule out immunodeficiency in cases with vaccine failure. However, the absence of a history of disease, the control of patients after discharge (which lasted 6 months in the case of discharge with sequelae), and the fact that IPD in cases with vaccine failure did not present greater severity than unvaccinated cases, support the validity of our results. Another limitation is that serotypes 25F and 38 were negative for the *wzg* (*cpsA*) gene. However, neither of these serotypes are PCV13 serotypes, and of the 89 strains serotyped using the Quellung reaction only 2 were serotype 38 and 1 serotype 25F.

In conclusion, after the introduction of the PCV13 vaccine in Spain, a significant number of IPD cases in Catalonia were recorded in the form of complicated pneumonia produced by PCV13 serotypes in age-appropriately vaccinated children without concurrent

conditions. Serotype 3 represented 66.7% of cases with vaccine failure and was associated with age-appropriately vaccinated patients who had completed their vaccination schedule and with the 24–59 months age group. Serotype 19A represented 20.8% of cases of vaccine failure and was associated with age-appropriately vaccinated patients with an incomplete vaccination schedule and children <2 years of age. In 93.8% of vaccine failures associated with serotype 3, the diagnosis was made only by PCR, which suggests the importance of this diagnostic technique in avoiding underdetection of this serotype. Our findings indicate that vaccine coverage should be increased to reduce the circulation of vaccine serotypes. However, there are doubts as to whether PCV13 vaccination will reduce serotype 3 cases to the same extent as other vaccine serotypes. Continuous surveillance of cases of IPD using not only culture but also PCR to characterize vaccine failures is necessary.

This work was supported by the Plan Nacional I+D+I, ISCIII-Subdirección General de Evaluación y Fomento de la Investigación Sanitaria (project nos. PI11/02081 and PI 11/2345) and cofunded by Fondo Europeo de Desarrollo Regional (FEDER) and the Catalan Agency for the Management of Grants for University Research AGAUR (grant nos. 2017 SGR 1342 and 2017 SGR 0742).

About the Author

Mr. Hernández is a doctoral candidate in public health at the University of Barcelona, Barcelona, Spain. His primary research interest is the epidemiological and public health aspects of invasive pneumococcal disease in children.

References

1. European Medicines Agency. Summary of Prevenar 7 product characteristics. European Medicines Agency, London, United Kingdom. 2011 [cited 2019 May 09]. http://www.ema.europa.eu/docs/en_GB/document_library/EPAR_-_Summary_for_the_public/human/000323/WC500041558.pdf
2. Ben-Shimol S, Greenberg D, Givon-Lavi N, Schlesinger Y, Somekh E, Aviner S, et al. Early impact of sequential introduction of 7-valent and 13-valent pneumococcal conjugate vaccine on IPD in Israeli children <5 years: an active prospective nationwide surveillance. Vaccine. 2014; 32:3452–9. https://doi.org/10.1016/j.vaccine.2014.03.065
3. Lepoutre A, Varon E, Georges S, Dorléans F, Janoir C, Gutmann L, et al.; Microbiologists of Epibac; ORP Networks. Impact of the pneumococcal conjugate vaccines on invasive pneumococcal disease in France, 2001–2012. Vaccine. 2015;33:359–66. https://doi.org/10.1016/j.vaccine.2014.11.011
4. Oligbu G, Hsia Y, Folgori L, Collins S, Ladhani S. Pneumococcal conjugate vaccine failure in children: a systematic review of the literature. Vaccine. 2016;34:6126–32. https://doi.org/10.1016/j.vaccine.2016.10.050
5. Muñoz-Almagro C, Jordan I, Gene A, Latorre C, Garcia-Garcia JJ, Pallares R. Emergence of invasive pneumococcal disease caused by nonvaccine serotypes in the era of 7-valent conjugate vaccine. Clin Infect Dis. 2008;46:174–82. https://doi.org/10.1086/524660
6. Feikin DR, Kagucia EW, Loo JD, Link-Gelles R, Puhan MA, Cherian T, et al.; Serotype Replacement Study Group. Serotype-specific changes in invasive pneumococcal disease after pneumococcal conjugate vaccine introduction: a pooled analysis of multiple surveillance sites. PLoS Med. 2013;10:e1001517. https://doi.org/10.1371/journal.pmed.1001517
7. European Medicines Agency. Summary of Synflorix product characteristics. European Medicines Agency, London, United Kingdom. 2009 [cited 2019 May 09]. http://www.ema.europa.eu/docs/en_GB/document_library/EPAR_-_Pro-duct_Information/human/000973/WC500054346.pdf
8. European Medicines Agency. Summary of Prevenar 13 product characteristics. European Medicines Agency, London, United Kingdom. 2014 [cited 2019 May 09]. https://www.ema.europa.eu/en/documents/overview/prevenar-epar-summary-public_en.pdf
9. Domínguez Á, Ciruela P, Hernández S, García-García JJ, Soldevila N, Izquierdo C, et al. Effectiveness of the 13-valent pneumococcal conjugate vaccine in preventing invasive pneumococcal disease in children aged 7–59 months. A matched case-control study. PLoS One. 2017;12:e0183191. https://doi.org/10.1371/journal.pone.0183191
10. Ciruela P, Izquierdo C, Broner S, Muñoz-Almagro C, Hernández S, Ardanuy C, et al.; Catalan Working Group on Invasive Pneumococcal Disease. The changing epidemiology of invasive pneumococcal disease after PCV13 vaccination in a country with intermediate vaccination coverage. Vaccine. 2018;36:7744–52. https://doi.org/10.1016/j.vaccine.2018.05.026
11. Vanderkooi OG, Scheifele DW, Girgenti D, Halperin SA, Patterson SD, Gruber WC, et al.; Canadian PCV13 Study Group. Safety and immunogenicity of a 13-valent pneumococcal conjugate vaccine in healthy infants and toddlers given with routine pediatric vaccinations in Canada. Pediatr Infect Dis J. 2012;31:72–7. https://doi.org/10.1097/INF.0b013e318233049d
12. Martinón-Torres F, Wysocki J, Center KJ, Czajka H, Majda-Stanislawska E, Omeñaca F, et al. Circulating antibody 1 and 2 years after vaccination with the 13-valent pneumococcal conjugated vaccine in preterm compared with term infants. Pediatr Infect Dis J. 2017;36:326–32. https://doi.org/10.1097/INF.0000000000001428
13. Miller E, Andrews NJ, Waight PA, Slack MP, George RC. Effectiveness of the new serotypes in the 13-valent pneumococcal conjugate vaccine. Vaccine. 2011;29:9127–31. https://doi.org/10.1016/j.vaccine.2011.09.112
14. Andrews N, Kent A, Amin-Chowdhury Z, Sheppard C, Fry N, Ramsay M, et al. Effectiveness of the seven-valent and thirteen-valent pneumococcal conjugate vaccines in England: the indirect cohort design, 2006–2018. Vaccine. 2019;37:4491–8. https://doi.org/10.1016/j.vaccine.2019.06.071
15. van der Linden M, Falkenhorst G, Perniciaro S, Fitzner C, Imöhl M. Effectiveness of pneumococcal conjugate vaccines (PCV7 and PCV13) against invasive pneumococcal disease among children under two years of age in Germany. PLoS One. 2016;11:e0161257. https://doi.org/10.1371/journal.pone.0161257
16. Sings HL, De Wals P, Gessner BD, Isturiz R, Laferriere C, McLaughlin JM, et al. Effectiveness of 13-valent pneumococcal conjugate vaccine against invasive disease

caused by serotype 3 in children: a systematic review and meta-analysis of observational studies. Clin Infect Dis. 2019;68:2135–43. https://doi.org/10.1093/cid/ciy920
17. Kaplan SL, Barson WJ, Lin PL, Romero JR, Bradley JS, Tan TQ, et al. Early trends for invasive pneumococcal infections in children after the introduction of the 13-valent pneumococcal conjugate vaccine. Pediatr Infect Dis J. 2013;32:203–7. https://doi.org/10.1097/INF.0b013e318275614b
18. Moraga-Llop F, Garcia-Garcia JJ, Díaz-Conradi A, Ciruela P, Martínez-Osorio J, González-Peris S, et al. Vaccine failures in patients properly vaccinated with 13-valent pneumococcal conjugate vaccine in Catalonia, a region with low vaccination coverage. Pediatr Infect Dis J. 2016;35:460–3. https://doi.org/10.1097/INF.0000000000001041
19. Antachopoulos C, Tsolia MN, Tzanakaki G, Xirogianni A, Dedousi O, Markou G, et al. Parapneumonic pleural effusions caused by *Streptococcus pneumoniae* serotype 3 in children immunized with 13-valent conjugated pneumococcal vaccine. Pediatr Infect Dis J. 2014;33:81–3. https://doi.org/10.1097/INF.0000000000000041
20. Tarragó D, Fenoll A, Sánchez-Tatay D, Arroyo LA, Muñoz-Almagro C, Esteva C, et al. Identification of pneumococcal serotypes from culture-negative clinical specimens by novel real-time PCR. Clin Microbiol Infect. 2008; 14:828–34. https://doi.org/10.1111/j.1469-0691.2008.02028.x
21. Centers for Disease Control and Prevention (CDC). PCR for detection and characterization of bacterial meningitis pathogens: *Neisseria meningitidis*, *Haemophilus influenzae*, and *Streptococcus pneumoniae*. 2011 [cited 2020 Feb 09]. http://www.cdc.gov/meningitis/lab-manual/chpt10-pcr.html
22. del Amo E, Selva L, de Sevilla MF, Ciruela P, Brotons P, Triviño M, et al. Estimation of the invasive disease potential of *Streptococcus pneumoniae* in children by the use of direct capsular typing in clinical specimens. Eur J Clin Microbiol Infect Dis. 2015;34:705–11. https://doi.org/10.1007/s10096-014-2280-y
23. Moreno-Pérez D, Alvarez García FJ, Aristegui Fernández J, Barrio Corrales F, Cilleruelo Ortega MJ, Corretger Rauet JM, et al.; Advisory Committee on Vaccines of the Spanish Association of Pediatrics. Immunization schedule of the Spanish Association of Pediatrics: 2012 recommendations. An Pediatr (Barc). 2012;76:43.e1–23. https://doi.org/10.1016/j.anpedi.2011.10.008
24. Fenoll A, Jado I, Vicioso D, Casal J. Dot blot assay for the serotyping of pneumococci. J Clin Microbiol. 1997;35:764–6. https://doi.org/10.1128/JCM.35.3.764-766.1997
25. Selva L, Berger C, Garcia-Garcia JJ, de Paz H, Nadal D, Muñoz-Almagro C. Direct identification of *Streptococcus pneumoniae* capsular types in pleural fluids by using multiplex PCR combined with automated fluorescence-based capillary electrophoresis. J Clin Microbiol. 2014;52:2736–7. https://doi.org/10.1128/JCM.00906-14
26. Heininger U, Bachtiar NS, Bahri P, Dana A, Dodoo A, Gidudu J, et al. The concept of vaccination failure. Vaccine. 2012;30:1265–8. https://doi.org/10.1016/j.vaccine.2011.12.048
27. Tanır Basaranoglu S, Karadag Oncel E, Aykac K, Ozsurekci Y, Cengiz AB, Kara A, et al. Invasive pneumococcal disease: from a tertiary care hospital in the post-vaccine era. Hum Vaccin Immunother. 2017;13:962–4. https://doi.org/10.1080/21645515.2016.1256519
28. Slotved HC, Dalby T, Harboe ZB, Valentiner-Branth P, Casadevante VF, Espenhain L, et al. The incidence of invasive pneumococcal serotype 3 disease in the Danish population is not reduced by PCV-13 vaccination. Heliyon. 2016;2:e00198. https://doi.org/10.1016/j.heliyon.2016.e00198
29. Fukusumi M, Chang B, Tanabe Y, Oshima K, Maruyama T, Watanabe H, et al.; Adult IPD Study Group. Invasive pneumococcal disease among adults in Japan, April 2013 to March 2015: disease characteristics and serotype distribution. BMC Infect Dis. 2017;17:2. https://doi.org/10.1186/s12879-016-2113-y
30. Selva L, Ciruela P, Esteva C, de Sevilla MF, Codina G, Hernández S, et al. Serotype 3 is a common serotype causing invasive pneumococcal disease in children less than 5 years old, as identified by real-time PCR. Eur J Clin Microbiol Infect Dis. 2012;31:1487–95. https://doi.org/10.1007/s10096-011-1468-7
31. Almeida AF, Sobrinho-Simões J, Ferraz C, Nunes T, Vaz L. Pneumococcal pneumonia vaccine breakthroughs and failures after 13-valent pneumococcal conjugated vaccine. Eur J Public Health. 2016;26:887–9. https://doi.org/10.1093/eurpub/ckw089
32. Silva-Costa C, Brito MJ, Pinho MD, Friães A, Aguiar SI, Ramirez M, et al.; Portuguese Group for the Study of Streptococcal Infections; Portuguese Study Group of Invasive Pneumococcal Disease of the Pediatric Infectious Disease Society. Pediatric complicated pneumonia caused by *Streptococcus pneumoniae* serotype 3 in 13-valent pneumococcal conjugate vaccinees, Portugal, 2010–2015. Emerg Infect Dis. 2018;24:1307–14. https://doi.org/10.3201/eid2407.180029
33. van der Linden M, Falkenhorst G, Perniciaro S, Fitzner C, Imöhl M. Effectiveness of pneumococcal conjugate vaccines (PCV7 and PCV13) against invasive pneumococcal disease among children under two years of age in Germany. PLoS One. 2016;11:e0161257. https://doi.org/10.1371/journal.pone.0161257
34. Andrews NJ, Waigth PA, Burbidge P, Pearce E, Roalfe L, Zancolli M, et al. Serotype-specific effectiveness and correlates of protection for the 13-valent pneumococcal conjugate vaccine: a postlicensure indirect cohort study. Lancet Infect Dis. 2014;14:839–46. http://doi.org/10.1016/S1473-3099(14)70822-9<jrn>

Address for correspondence: Sergi Hernández, Cardenal Casañas nº10 1°-1ª 08002, Barcelona, Spain; email: 8888hernandez.sergi@gmail.com

Increased Risk for Carbapenem-Resistant *Enterobacteriaceae* Colonization in Intensive Care Units after Hospitalization in Emergency Department

Matias Chiarastelli Salomão, Maristela Pinheiro Freire, Icaro Boszczowski, Sueli F. Raymundo, Ana Rubia Guedes, Anna S. Levin

Carbapenem-resistant *Enterobacteriaceae* (CRE) colonization is common in hospital patients admitted to intensive care units (ICU) from the emergency department. We evaluated the effect of previous hospitalization in the emergency department on CRE colonization at ICU admission. Our case–control study included 103 cases and 201 controls; cases were patients colonized by CRE at admission to ICU and controls were patients admitted to ICU and not colonized. Risk factors were emergency department stay, use of carbapenem, Simplified Acute Physiology Score, upper digestive endoscopy, and transfer from another hospital. We found that ED stay before ICU admission was associated with CRE colonization at admission to the ICU. Our findings indicate that addressing infection control problems in EDs will help to control carbapenem resistance in ICUs.

Klebsiella pneumoniae carbapenemase (KPC), described in 1996, is an enzyme capable of hydrolyzing all β-lactam antimicrobial drugs known at the time (*1*). Since then, other carbapenemases have been described in *Enterobacteriaceae* all over the world, leading to a substantial increase in resistance to antimicrobial drugs (*2*,*3*).

Surveillance data from central line–associated bloodstream infections (CLABSI) in intensive care units (ICUs) in the state of São Paulo, Brazil, demonstrated an increase of carbapenem-resistant *K. pneumoniae*, from 14% in 2011 to 55% in 2017 (*4*). In 2017, *K. pneumoniae* was the most frequent species causing CLABSI (20%) in São Paulo.

Author affiliation: Faculdade de Medicina da Universidade de São Paulo, São Paulo, Brazil

DOI: https://doi.org/10.3201/eid2606.190965

Hospital das Clínicas of the University of São Paulo has routinely performed CRE screening for patients admitted to ICU since January 2014. Early identification and isolation of colonized patients was implemented to decrease secondary colonization. Concomitant training sessions for hand hygiene and contact precautions took place during this period. Despite all efforts, ICUs had a high colonization pressure (17% –29%, mean 21%) due to admission of colonized patients, mainly from EDs (I. Boszczowski, unpub. data).

In 2016, we found that 7% of patients admitted to the ED were positive for CRE. However, among those who were negative at admission, 18% became colonized during their stay in the ED. These findings led us to hypothesize that hospitalization in the ED may be a risk factor for CRE colonization in other units of the hospital (*5*); ≈60% of the patients admitted to ICUs come from hospitalizations in the ED. We evaluated the effect of hospitalization in the ED on CRE colonization at the time of admission to an ICU.

Methods

Setting

Hospital das Clinicas is a 2,200-bed public tertiary-care hospital in São Paulo and is the largest hospital complex in Latin America. The main building has ≈1,000 beds and is the location of the ED and most of the hospital's ICU beds (10 ICUs and 109 intensive care beds).

The ED is a very busy unit. In 2018, 69,000 emergency consultations were performed. The average hospitalization rate in the ED is 150 patients/week, and median length of stay is 6 days. The ED has 50

beds for hospitalization, but occupancy often exceeds 90 beds, with patients on stretchers and often in corridors (Figure 1).

Approximately 60% of ICU patients are admitted from the ED. To monitor and control CRE colonization, CRE surveillance cultures are performed on all patients admitted to ICUs at the time of admission and placed under contact precautions until the return of results. Colonized patients with CRE remain under contact precautions for their entire stay in the unit.

Microbiology

Surveillance cultures are performed at the clinical microbiology laboratory in accordance with the institution's standard methodology. Rectal swab specimens from patients are incubated overnight in thioglycolate broth. Positive growth samples are plated on MacConkey agar with ertapenem, imipenem, and meropenem discs. If there are colonies suggestive of *Enterobacteriaceae* growth within the carbapenems' disk halo, these colonies are isolated and identified by matrix-assisted laser desorption/ionization time-of-flight mass spectrometry, as recommended by Clinical and Laboratory Standards Institute (*6*).

Study Design

We conducted a retrospective case–control study with patients hospitalized in ICUs at HC during September 2015–July 2017. This study used 2 controls for each case. We obtained cases from the infection control department database, which compiles all cases of positive surveillance cultures. Patients who were hospitalized >1 time in ICUs were considered only once, during their first hospitalization.

We defined a case as a patient admitted to one of the ICUs during 2015–2017 who had a positive CRE surveillance culture collected within 2 days of admission. We defined a control as a patient admitted to the ICU whose surveillance cultures collected within the first 2 days of admission were negative. Colonization or prior infection with CRE reported at admission were excluding criteria. We paired controls by ICU and hospitalization period, with a maximum interval of 1 week from the admission of the cases. When >2 patients were eligible as controls for a case, we randomly chose 2 from all the potential controls. The proportion of controls admitted in the ICUs from the ED was similar to the proportion of patients coming from the ED found in our historical series. CRE screening methodologies were the same for all patients in the study period, whether they were cases or controls.

We collected data from medical records for demographic variables, hospitalization records before ICU admission, clinical characteristics at time of ICU admission, severity scores and organ failures, indwelling devices, clinical procedures before ICU admission, concurrent conditions, use of antimicrobial drugs (for ≥48 hours before ICU admission) and

Figure 1. A corridor in the emergency department of Hospital das Clínicas, São Paulo, Brazil, showing patients on stretchers, December 2016.

infection before ICU admission, previous colonization, infection by CRE, length of hospital stay, and death. We defined CLABSI according to the 2018 US Centers for Disease Control and Prevention definition (*7*).

We used REDCap (Research Electronic Data Capture) program (*8*) to create a data collection tool and database. The Ethics and Research Committee of Hospital das Clinicas da Faculdade de Medicina da Universidade de São Paulo approved this study (number CAAE: 91604518.9.0000.0068).

Statistical Analysis

We calculated sample size and determined a minimum requirement of 99 cases and 198 controls for 80% power. We assumed that 35% of the cases had an ED stay >2 days. We performed statistical analysis using Stata version 16 (StataCorp, https://www.stata.com) and SPSS Statistics 11.5 (http://www.ibm.com). We compared cases with controls using the Wilcoxon or McNemar test when appropriate. All tests were 2-tailed, with 95% CIs; we considered p<0.05

Table 1. Characteristics of patients, bivariate analysis, and conditional logistic regression of variables potentially associated with colonization by carbapenem-resistant *Enterobacteriaceae* at ICU admission, Hospital das Clínicas, São Paulo, Brazil, September 2015–July 2017*

	Bivariate analysis				Conditional logistic regression	
Covariate	Cases	Controls	OR (95% CI)	p value	OR (95% CI)	p value
Female sex	34/103 (33)	91/201 (45)	0.58 (0.35–0.95)	0.03		
Mean age, y (range)	50.55 (14–84)	49.78 (4–89)	1.00 (0.99–1.01)	0.62		
Previous hospitalization at ICU admission						
Previous stay in another unit during hospitalization	75/101 (74)	163/201 (81)	0.84 (0.44–1.60)	0.60		
Previous stay in the ED during hospitalization	62/103 (60)	125/201 (62)	1.07 (0.65–0.77)	0.78		
Length of ED stay, d	2 (0–55)	1 (0–37)	1.08 (1.01–1.15)	0.02	1.10 (1.02–1.19)	0.01
ED stay >2 d	34/103 (33)	35/201 (17)	2.45 (1.40–4.32)	0.002		
Days of hospitalization before surveillance culture, median (range)	3 (1–95)	2 (1–37)	0.99 (0.99–0.99)	<0.001		
Transfer from another hospital	43/101 (43)	51/193 (26)	2.79 (1.26–3.68)	0.005	2.52 (1.07–5.89)	0.03
Previous hospitalization	52/85 (61)	63/163 (38)	2.91 (1.53–5.52)	0.001		
Clinical characteristics at ICU admission						
Infection	63/101 (63)	82/194 (42)	2.62 (1.52–4.54)	0.001	1.76 (0.56–5.50)	0.33
Sepsis	46/62 (74)	54/81 (66)	1.41 (0.52–3.85)	0.50		
Surgery before ICU admission	53/102 (52)	106/194 (55)	0.92 (0.53–1.62)	0.78		
Trauma	8/100 (8)	25/194 (13)	0.62 (0.28–1.40)	0.25		
Stroke	5/100 (5)	17/194 (9)	0.61 (0.17–2.18)	0.45		
Severity scores						
SAPS 3, % median (range)	22 (4–92)	16 (0–98)	1.01 (1.002–1.02)	0.01	1.01 (1.002–1.03)	0.02
SOFA, median (range)	5 (0–19)	5 (0–19)	1.09 (0.95–1.07)	0.77		
Invasive procedures and devices						
Dialysis	14/100 (14)	11/194 (6)	2.50 (0.97–6.42)	0.06		
Tracheostomy	2/99 (2)	1/194 (0)	4.92 (0.36–44.67)	0.26		
Colostomy	2/99 (2)	2/194 (1)	2.00 (0.28–14.34)	0.49		
Upper digestive endoscopy	10/101 (10)	5/194 (3)	3.70 (1.11–12.32)	0.003	18.9 (1.83–195.98)	0.01
Colonoscopy	2/101 (2)	0/194 (0)				
Parenteral nutrition	2/101 (2)	1/ 194 (1)	3.77 (0.19–74.94)	0.38		
Underlying conditions						
CCI score, mean (range)	3.10 (0–9)	2.98 (0–11)	0.99 (0.96–1.02)	0.48		
Smoking	25/62 (40)	46/137 (34)	1.17 (0.49–2.78)	0.72		
Diabetes mellitus	20/102 (20)	44/198 (22)	0.86 (0.46–1.62)	0.65		
Malignant neoplasm	9/102 (9)	23/198 (12)	0.77 (0.35–1.70)	0.52		
Rheumatologic or autoimmune disease	11/102 (11)	16/198 (8)	1.44 (0.66–3.15)	0.36		
Cirrhosis	15/102 (15)	11/198 (5)	2.25 (0.85–5.91)	0.10		
Chronic kidney disease	12/102 (12)	14/198 (7)	1.51 (0.56–3.99)	0.40		
Solid organ transplant	8/102 (8)	16/198 (8)	0.62 (0.23–1.64)	0.33		
HIV infection	3/100 (3)	7/198 (4)	1.13 (0.27–4.76)	0.86		
Hematological malignancy	2/102 (2)	6/198 (3)	0.59 (0.13–2.87)	0.52		
Hematopoietic stem cell transplant	1/102 (1)	1/198 (0)	2.00 (0.12–32.42)	0.63		
Antimicrobial drug use						
Any drug at ICU admission†	81/99 (81)	142/193 (71)	1.56 (0.83–2.91)	0.161		
Carbapenem at ICU admission†	25/80 (31)	12/141 (9)	3.92 (1.51–10.21)	0.005	4.62 (1.30–16.40)	0.02
Any drug use in previous 3 mo	50/72 (69)	48/145 (33)	5.38 (2.31–12.53)	<0.001		

*Values are no. (%) except as indicated. CCI, Charlson Comorbidity Index; ED, emergency department; GCS, Glasgow Coma Scale; ICU, intensive care unit; OR, odds ratio; SAPS 3, Simplified Acute Physiology 3, presented as prediction of mortality risk in percentage; SOFA, Sequential Organ Failure Assessment.

Table 2. Multivariate analysis for potential factors associated with colonization by carbapenem-resistant *Enterobacteriaceae* at ICU admission, Hospital das Clínicas, São Paulo, Brazil, September 2015–July 2017*

Covariate	OR (95% CI)	p value
ED stay >2 d	5.85 (1.94–17.65)	0.002
Transfer from another hospital	2.10 (0.95–4.78)	0.076
SAPS 3 score	1.02 (1.003–1.03)	0.02
Carbapenem use on ICU admission, initiated >48 h before ICU admission	4.78 (1.31–17.47)	0.02
Infection at ICU admission	2.86 (1.08–7.55)	0.03
Upper digestive endoscopy	16.40 (2.16–124.50)	0.01

*Model using length of ED stay as dichotomous variable. OR, odds ratio; ED, emergency department; ICU, intensive care unit; SAPS 3, Simplified Acute Physiology Score III.

statistically significant. For variables with p<0.05 in the bivariate analysis, we conducted multivariate analysis with other confounding variables in a conditional logistic regression model. Length of ED stay was a continuous variable and was transformed into a dichotomic variable using SPSS decision tree tool, and for the final model we chose the one with a better fit. We used stepwise backward modeling for the conditional logistic regression and kept the most significant variables in the final model. We used 2 models, one using length of ED stay as a continuous variable and the other as a dichotomous variable. Smoking and sepsis variables comprised more than 40% of missing data (Tables 1 and 2) and were dropped out.

Results

We included 304 patients in the study, 103 cases and 201 controls, and collected surveillance cultures for all patients. Of the 103 case-patients, 99 were colonized by *K. pneumoniae*, 2 by *Enterobacter cloacae,* and 2 by *Escherichia coli*. Of the 304 total patients, 188 patients (62%) were admitted to medical ICUs and 116 (38%) to surgical ICUs. Sixty-five patients were admitted directly to the ICU: 38 transferred from another hospital, 17 came from the operating room, and for 10 patients, this information was not available. Eighty-six patients were transferred from another ward and 152 from the ED; information was not available for 1 patient. Sixty percent of cases and controls stayed in the ED for some time during their hospitalization.

We performed bivariate analysis and demonstrated that 11 characteristics were associated with CRE colonization at ICU admission: sex, ED length of stay, ED stay >2 days, number of hospitalization days before the surveillance culture, transfer from another hospital, previous hospitalization, having an infection on ICU admission, clinical severity (SAPS 3 score), use of antimicrobial drugs in the previous 3 months, carbapenem use on ICU admission (initiated >48 hours before ICU admission), and upper digestive endoscopy (Table 1). The most common infections at ICU admission were pneumonia (37%), skin and soft tissue infection (14%), and CLABSI (10%). The median length of stay in the ED was longer for cases (2 days, range 0–55) than for controls (1 day, range 0–37; p = 0.02) (Figure 2). We analyzed the length of stay in the ED with the decision tree tool; we selected a stay >2 days as cutoff for this variable (χ^2 = 12.799; p = 0.017). We found that 38/62 (61%) of the patients with CRE colonization at ICU admission were already colonized after 3 days of hospitalization in the ED (Figure 3).

We performed multivariate analysis with 2 models, using ED length of stay as a continuous or a dichotomous variable (>2 days). ED stay was a risk factor for colonization by CRE in both analyses: continuous (per day, odds ratio [OR] 1.10, 95% CI 1.02–1.19; p = 0.01) (Table 1) and >2 days of hospitalization (OR 5.85, 95% CI 1.94–17.65; p = 0.002) (Table 2). Use of carbapenem at ICU admission (initiated >48 hours before ICU admission), Simplified Acute Physiology Score III (SAPS 3), transfer from another hospital, and upper digestive endoscopy were risk factors for CRE colonization at ICU admission (Table 1).

Patients colonized by CRE at ICU admission had higher rates of infection by CRE (18 [18%]) than did patients not colonized by CRE when they sought care (11 [6%]; p = 0.001). Colonized patients also had higher in-hospital mortality rates (38 [38%] for patients colonized by CRE and 48 [24%] for those not colonized; p = 0.016).

Discussion

Our results confirm our hypothesis that ED stay is a risk factor for CRE colonization in patients at the time of admission to the ICU. Other risk factors are use of carbapenem at time of ICU admission (carbapenem use initiated >48 hours before ICU admission), SAPS 3, upper digestive endoscopy, and transfer from another hospital (Table 1).

Including ED stay as a risk factor is a notable new finding. A stay in the ED is usually not considered to be a risk factor for CRE colonization (*9*). In a previous study, our group demonstrated that patients admitted to the ED had 6.8% prevalence of CRE colonization at admission to the ED and 18% acquisition rate for patients hos-

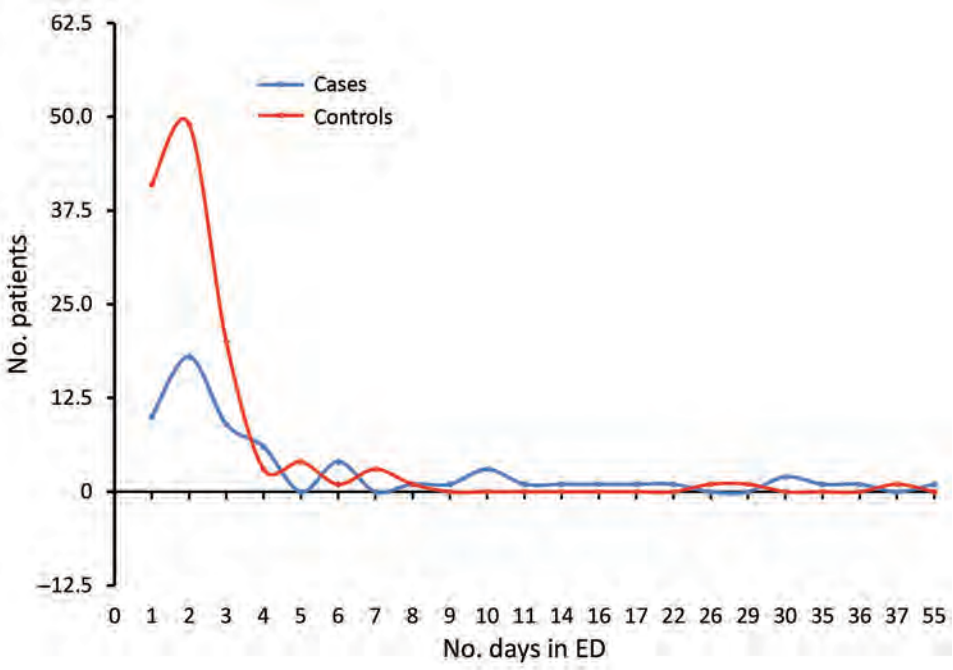

Figure 2. Distribution of days of stay in the emergency department (ED) comparing patients subsequently admitted to an intensive care unit who had a positive carbapenem-resistant *Enterobacteriaceae* culture within 2 days of admission (cases) and patients whose culture was negative (controls), Hospital das Clínicas, São Paulo, Brazil, September 2015–July 2017.

pitalized in the ED for longer than 1 week. Six patients who were not treated in a healthcare facility were colonized by CRE at ED admission, implying circulation of this resistance mechanism in the community (*5*). Our findings show that ED hospitalization is indeed a risk factor for CRE colonization on ICU admission, whereas a previous stay in another hospital unit was not.

Although it is not common, CRE can be found outside the hospital. CRE has been described in community sources of water in Italy (*10*), Brazil (*11*), and Sweden (*12*); in chicken meat in Egypt (*13*); in vegetables imported from Asia (*14*), and in hospital sewage in Brazil, China, and Spain (*15*). Community-acquired CRE infection is difficult to determine; however, up to 30% of patients with CRE infection on hospital admission have had no previous exposure to the healthcare system.

The acquisition or transmission of CRE in the ED may be a result of the work overload. Ours is a tertiary-care public hospital in Brazil with an overcrowded ED. It is not unusual to have patients with high-complexity illness hospitalized on stretchers for longer than a week because of a shortage of ICU or ward beds to which to transfer patients or to have a low ratio of healthcare workers per patient. Prolonged ED stays probably facilitate cross-transmission of multidrug-resistant organisms such as CRE. Although on first thought the problem may be considered a local one, specific to our hospital and setting, this problem extends to other Brazil hospitals. Two other hospitals reported long stays in the ED, with 1 hospital reporting a median length of stay of 3 days (*16*) and another reporting that 21% of patients stayed in the ED for >5 days (*17*). Mortality rates in the EDs of these hospitals are high as well: 7.4% at the first and 3.9% at the second. Furthermore, we expect long ED stay is a problem in other countries, although seldom reported (*18*–*20*). Lack of access to healthcare in developing countries leads to other problems: healthcare-associated infection rates are much higher in developing countries than in high-income countries (*21*), as are drug resistance rates (*22*). In a disadvantaged healthcare system, patients with known risk factors (*23*–*25*) are often hospitalized for prolonged periods in the ED and are a potential source of multidrug-resistant bacteria for other patients in the ED and ICUs.

The need to establish strategies to control CRE transmission in EDs and hospitals is urgent; resistance is not an isolated problem in a specific hospital unit or even in a specific hospital. High workload, understaffing, and turnover of healthcare workers make it difficult to improve adherence to hand hygiene in the ED; additional strategies are needed (26,*27*), and interventions must be multimodal. These interventions must include a change in the workflow of the ED and hospital as well as the entire health system to reduce overcrowding (*26*–*28*). The lack of infrastructure in the ED puts patients in stretchers too near to each other, probably facilitating cross-transmission. In this scenario, good hand hygiene may not be achievable. Dividing patients into cohorts and assigning dedicated

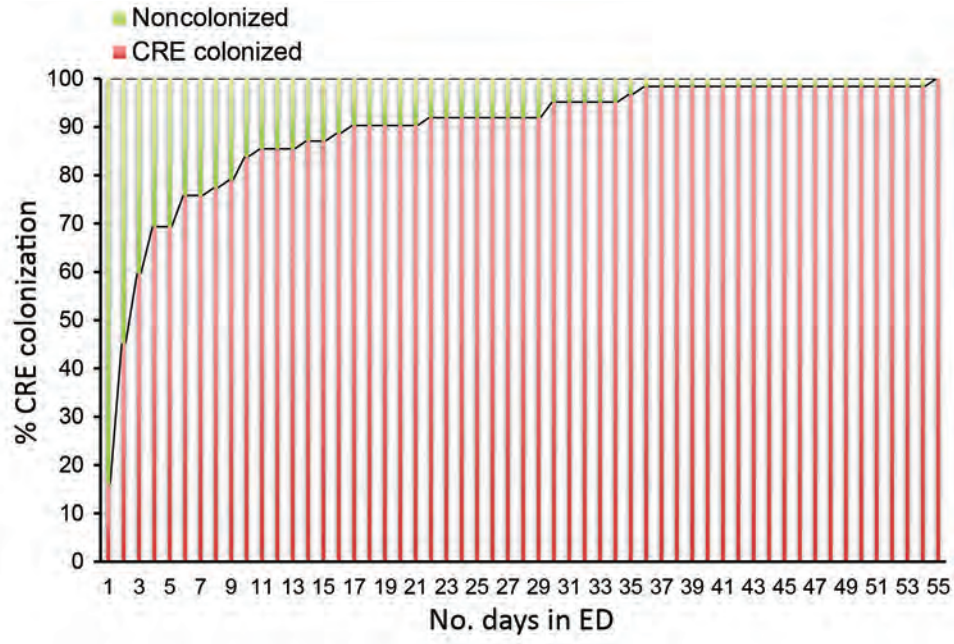

Figure 3. Distribution of colonization of CRE in patients admitted to an intensive care unit after a stay in the ED, Hospital das Clínicas, São Paulo, Brazil, September 2015–July 2017. CRE, carbapenem-resistant *Enterobacteriaceae*; ED, emergency department.

staff may reduce transmission of CRE (*29*). Hospital staff should discuss screening strategies for CRE and early isolation and contact precautions in the ED (*30*). Rising antimicrobial resistance is a substantial threat to global health (*31*), and prolonged ED hospitalization may play a major role in hospital-acquired resistance in low- and middle-income countries.

We found other risk factors that have already been associated with CRE colonization, including transfer from another hospital (*24*,*25*), use of carbapenem (*23*–*25*), SAPS 3, and upper digestive endoscopy (*32*). All of them are associated with previous exposure to healthcare or severity of patients (*33*). The previous use of carbapenems is well described as a risk factor for CRE colonization (*23*–*25*,*33*). In our study, the patients were using carbapenem for ≥48 hours by the time of surveillance culture. Although this timeframe is short, it may have been sufficient for selection of carbapenem-resistant bacteria. We must emphasize that, even though carbapenem use was an independent risk factor in multivariate analysis, the attending physicians may have prescribed it because after a certain length of time in the ED, the patient is at risk for infection by antimicrobial-resistant bacteria.

Of interest, although cirrhosis was not associated with CRE colonization, upper digestive endoscopy was, which suggests that the risk for colonization after endoscopy is probably due to the procedure itself and not to the patient's underlying conditions. We found no clusters of endoscopy-related CRE colonization in the study period, suggesting that it was not an outbreak. Colonization may be a result of improper cleaning procedures. Because this was a retrospective study, we could not test the endoscopes for CRE colonization at the time that colonization occurred. Prospective surveillance for endoscopy-related CRE is underway.

It is difficult to assess the influence of local factors in the hospital ED on colonization by CRE. Factors such as low adherence to hand hygiene and contact precautions, proximity of beds, and others work together to facilitate the transmission of microorganisms. A limitation of this study is that it was not possible to evaluate the effect of each of these variables individually. Other limitations of our study were the retrospective nature of a case–control study; missing data for some variables; potential bias of retrospectively obtaining data from medical records; and the fact that the study was done in only 1 hospital, requiring confirmation in other centers or a multicenter study.

In conclusion, this study demonstrates that prolonged ED stay is a risk factor for CRE colonization at the time of admission to the ICU. Other risk factors were the use of carbapenems at ICU admission (initiated <48 hours before ICU admission), SAPS 3, upper digestive endoscopy, and transfer from another hospital. Clinicians should be aware of the implications of these findings and implement interventions in the ED to control CRE in other hospital units.

Acknowledgments

We thank the medical archive personnel for providing the medical records, Luizegne Donato for organizing the records and files, and Laina Bubach, Lauro Perdigão,

and Maria Luisa Moura for helping to review the medical records.

About the Author

Dr. Salomão is an infectious diseases specialist at the Hospital das Clínicas da Faculdade de Medicina da Universidade de São Paulo. His research focuses on hospital infection control and bacterial resistance.

References

1. Yigit H, Queenan AM, Anderson GJ, Domenech-Sanchez A, Biddle JW, Steward CD, et al. Novel carbapenem-hydrolyzing β-lactamase, KPC-1, from a carbapenem-resistant strain of *Klebsiella pneumoniae*. Antimicrob Agents Chemother. 2001;45:1151–61. https://doi.org/10.1128/AAC.45.4.1151-1161.2001
2. Kumarasamy KK, Toleman MA, Walsh TR, Bagaria J, Butt F, Balakrishnan R, et al. Emergence of a new antibiotic resistance mechanism in India, Pakistan, and the UK: a molecular, biological, and epidemiological study. Lancet Infect Dis. 2010;10:597–602. https://doi.org/10.1016/S1473-3099(10)70143-2
3. Logan LK, Weinstein RA. The epidemiology of carbapenem-resistant *Enterobacteriaceae*: the impact and evolution of a global menace. J Infect Dis. 2017;215(suppl_1):S28–36. https://doi.org/10.1093/infdis/jiw282
4. Center for Epidemiological Surveillance. Data analysis of the epidemiological surveillance system of hospital infections of the state of São Paulo 2017 [in Portuguese]. 2018 [cited 2020 Mar 18]. http://www.saude.sp.gov.br/resources/cve-centro-de-vigilancia-epidemiologica/areas-de-vigilancia/infeccao-hospitalar/aulas/ih18_apresentacao_dados2017.pdf
5. Salomão MC, Guimarães T, Duailibi DF, Perondi MBM, Letaif LSH, Montal AC, et al. Carbapenem-resistant *Enterobacteriaceae* in patients admitted to the emergency department: new risk factors and occurrence in patients coming directly from the community. J Hosp Infect. 2017;97:241–6. https://doi.org/10.1016/j.jhin.2017.08.012
6. Clinical and Laboratory Standards Institute. Performance standards for antimicrobial susceptibility testing. 26th edition supplement (M100S). Wayne (PA): The Institute; 2006.
7. Centers for Disease Control and Prevention. Bloodstream infection event—central line-associated bloodstream infection and non-central line associated bloodstream infection. Device-associated module. 2020 [cited 2020 Mar 27]. /https://www.cdc.gov/nhsn/pdfs/pscmanual/4psc_clabscurrent.pdf
8. Harris PA, Taylor R, Thielke R, Payne J, Gonzalez N, Conde JG. Research electronic data capture (REDCap)—a metadata-driven methodology and workflow process for providing translational research informatics support. J Biomed Inform. 2009;42:377–81. https://doi.org/10.1016/j.jbi.2008.08.010
9. Richter SS, Marchaim D. Screening for carbapenem-resistant *Enterobacteriaceae*: who, when, and how? Virulence. 2017;8:417–26. https://doi.org/10.1080/21505594.2016.1255381
10. Caltagirone M, Nucleo E, Spalla M, Zara F, Novazzi F, Marchetti VM, et al. Occurrence of extended spectrum β-lactamases, KPC-type, and MCR-1.2-producing *Enterobacteriaceae* from wells, river water, and wastewater treatment plants in Oltrepò Pavese area, Northern Italy. Front Microbiol. 2017;8:2232. https://doi.org/10.3389/fmicb.2017.02232
11. Bartley PS, Domitrovic TN, Moretto VT, Santos CS, Ponce-Terashima R, Reis MG, et al. Antibiotic resistance in *Enterobacteriaceae* from surface waters in urban Brazil highlights the risks of poor sanitation. Am J Trop Med Hyg. 2019;100:1369–77.
12. Khan FA, Hellmark B, Ehricht R, Söderquist B, Jass J. Related carbapenemase-producing *Klebsiella* isolates detected in both a hospital and associated aquatic environment in Sweden. Eur J Clin Microbiol Infect Dis. 2018;37:2241–51. https://doi.org/10.1007/s10096-018-3365-9
13. Abdallah HM, Alnaiemi N, Reuland EA, Wintermans BB, Koek A, Abdelwahab AM, et al. Fecal carriage of extended-spectrum β-lactamase- and carbapenemase-producing *Enterobacteriaceae* in Egyptian patients with community-onset gastrointestinal complaints: a hospital-based cross-sectional study. Antimicrob Resist Infect Control. 2017;6:62. https://doi.org/10.1186/s13756-017-0219-7
14. Zurfluh K, Poirel L, Nordmann P, Klumpp J, Stephan R. First detection of *Klebsiella variicola* producing OXA-181 carbapenemase in fresh vegetable imported from Asia to Switzerland. Antimicrob Resist Infect Control. 2015;4:38. https://doi.org/10.1186/s13756-015-0080-5
15. Kelly AM, Mathema B, Larson EL. Carbapenem-resistant *Enterobacteriaceae* in the community: a scoping review. Int J Antimicrob Agents. 2017;50:127–34. https://doi.org/10.1016/j.ijantimicag.2017.03.012
16. Peres RR, Lima SBS, de Souza Magnago TSB, Shardong AC, da Silva Ceron MD, Prochnow A, et al. Clinical-epidemiological profile of patients admitted to the emergency department of a university hospital [in Portuguese]. Rev Saúde (Santa Maria). 2013;39:77–86.
17. Ribeiro RCHM, Rodrigues CC, Canova JCM, Rodrigues CDS, Cesarino CB, Júnior OLS. Stay and outcome of the clinical and surgical patient in the emergency service. Rev Enferm (Lisboa). 2013;7:5426–32. https://periodicos.ufpe.br/revistas/revistaenfermagem/article/download/13670/16557
18. Phua J, Ngerng WJ, Lim TK. The impact of a delay in intensive care unit admission for community-acquired pneumonia. Eur Respir J. 2010;36:826–33. https://doi.org/10.1183/09031936.00154209
19. Cardoso LT, Grion CM, Matsuo T, Anami EH, Kauss IA, Seko L, et al. Impact of delayed admission to intensive care units on mortality of critically ill patients: a cohort study. Crit Care. 2011;15:R28. https://doi.org/10.1186/cc9975
20. Obermeyer Z, Abujaber S, Makar M, Stoll S, Kayden SR, Wallis LA, et al.; Acute Care Development Consortium. Emergency care in 59 low- and middle-income countries: a systematic review. Bull World Health Organ. 2015;93:577–586G. https://doi.org/10.2471/BLT.14.148338
21. Rosenthal VD, Maki DG, Mehta Y, Leblebicioglu H, Memish ZA, Al-Mousa HH, et al.; International Nosocomial Infection Control Consortium. International Nosocomial Infection Control Consortium (INICC) report, data summary of 43 countries for 2007–2012. Device-associated module. Am J Infect Control. 2014;42:942–56. https://doi.org/10.1016/j.ajic.2014.05.029
22. World Health Organization. Antimicrobial resistance global report on surveillance. Geneva: The Organization; 2014 [cited 2020 Mar 18]. http://apps.who.int/iris/bitstream/10665/112642/1/9789241564 748_eng.pdf
23. Papadimitriou-Olivgeris M, Marangos M, Fligou F, Christofidou M, Bartzavali C, Anastassiou ED, et al. Risk factors for KPC-producing *Klebsiella pneumoniae* enteric

colonization upon ICU admission. J Antimicrob Chemother. 2012;67:2976–81.
24. Marchaim D, Chopra T, Bhargava A, Bogan C, Dhar S, Hayakawa K, et al. Recent exposure to antimicrobials and carbapenem-resistant *Enterobacteriaceae*: the role of antimicrobial stewardship. Infect Control Hosp Epidemiol. 2012;33:817–30. https://doi.org/10.1086/666642
25. Schwaber MJ, Klarfeld-Lidji S, Navon-Venezia S, Schwartz D, Leavitt A, Carmeli Y. Predictors of carbapenem-resistant *Klebsiella pneumoniae* acquisition among hospitalized adults and effect of acquisition on mortality. Antimicrob Agents Chemother. 2008;52:1028–33. https://doi.org/10.1128/AAC.01020-07
26. Carter EJ, Wyer P, Giglio J, Jia H, Nelson G, Kauari VE, et al. Environmental factors and their association with emergency department hand hygiene compliance: an observational study. BMJ Qual Saf. 2016;25:372–8. https://doi.org/10.1136/bmjqs-2015-004081
27. Muller MP, Carter E, Siddiqui N, Larson E. Hand hygiene compliance in an emergency department: the effect of crowding. Acad Emerg Med. 2015;22:1218–21. https://doi.org/10.1111/acem.12754
28. Yarmohammadian MH, Rezaei F, Haghshenas A, Tavakoli N. Overcrowding in emergency departments: a review of strategies to decrease future challenges. J Res Med Sci. 2017;22:23.
29. Legeay C, Thépot-Seegers V, Pailhoriès H, Hilliquin D, Zahar JR. Is cohorting the only solution to control carbapenemase-producing *Enterobacteriaceae* outbreaks? A single-centre experience. J Hosp Infect. 2018;99:390–5. https://doi.org/10.1016/j.jhin.2018.02.003
30. Munoz-Price LS, Quinn JP. Deconstructing the infection control bundles for the containment of carbapenem-resistant *Enterobacteriaceae*. Curr Opin Infect Dis. 2013;26:378–87. https://doi.org/10.1097/01.qco.0000431853.71500.77
31. Centers for Disease Control and Prevention. Antibiotic resistance threats in the United States, 2013 [cited 2020 Mar 27]. https://www.cdc.gov/drugresistance/pdf/ar-threats-2013-508.pdf
32. Muscarella LF. Risk of transmission of carbapenem-resistant *Enterobacteriaceae* and related "superbugs" during gastrointestinal endoscopy. World J Gastrointest Endosc. 2014;6:457–74. https://doi.org/10.4253/wjge.v6.i10.457
33. van Loon K, Voor In 't Holt AF, Vos MC. A systematic review and meta-analyses of the clinical epidemiology of carbapenem-resistant *Enterobacteriaceae.* Antimicrob Agents Chemother. 2017;62:e01730-17. https://doi.org/10.1128/AAC.01730-17

Address for correspondence: Matias Chiarastelli Salomão, Av Dr Eneas de Carvalho Aguiar, 255, Instituto Central Hospital das Clínicas da Faculdade de Medicina da Universidade de São Paulo, 5o andar, Subcomissão de Controle de Infecção Hospitalar, São Paulo/SP, CEP 05403-000, Brazil; email: matias.salomao@hc.fm.usp.br

Antimicrobial Resistance in *Salmonella enterica* Serovar Paratyphi B Variant Java in Poultry from Europe and Latin America

L. Ricardo Castellanos,[1] Linda van der Graaf-van Bloois, Pilar Donado-Godoy, Kees Veldman, Francisco Duarte, María T. Acuña, Claudia Jarquín, François-Xavier Weill, Dik J. Mevius, Jaap A. Wagenaar, Joost Hordijk,[2] Aldert L. Zomer[2]

Salmonella enterica serovar Paratyphi B variant Java sequence type 28 is prevalent in poultry and poultry meat. We investigated the evolutionary relatedness between sequence type 28 strains from Europe and Latin America using time-resolved phylogeny and principal component analysis. We sequenced isolates from Colombia, Guatemala, Costa Rica, and the Netherlands and complemented them with publicly available genomes from Europe, Africa, and the Middle East. Phylogenetic time trees and effective population sizes (N_e) showed separate clustering of strains from Latin America and Europe. The separation is estimated to have occurred during the 1980s. N_e of strains increased sharply in Europe around 1995 and in Latin America around 2005. Principal component analysis on noncore genes showed a clear distinction between strains from Europe and Latin America, whereas the plasmid gene content was similar. Regardless of the evolutionary separation, similar features of resistance to β-lactams and quinolones/fluoroquinolones indicated parallel evolution of antimicrobial resistance in both regions.

The d-Tartrate fermenting, nonparatyphoidal variant of *Salmonella enterica* serovar Paratyphi B, contemporarily known as variant Java, was first reported in 1935 by De Moor (*1*). From then until recently, *Salmonella* Paratyphi B var. Java caused sporadic self-limiting gastrointestinal infections in humans (*2*–*4*). Since 1990, reports of human infections increased in Europe (*5*–*10*), North America (*11*–*15*), and Australia (*16*,*17*). Human infections with this serovar were mainly related to exposure to fish or reptiles (*16*–*18*). A dramatic increase in prevalence in poultry and poultry meat in Europe was reported (*19*,*20*), accompanied by an increase in antimicrobial resistance of the strains (*5*,*19*).

Using a multilocus sequence typing (MLST) scheme for *S. enterica* (*21*), strains of *Salmonella* Paratyphi B var. Java were classified into different sequence types (STs). In a previous study, the use of both traditional serotyping and MLST was instrumental in identifying reptiles as the main source of *Salmonella* Paratyphi B var. Java infections in humans in Germany. Isolates originating from poultry were strongly associated with ST28, those from reptiles with ST88, and those from humans mainly with ST43 and ST149 (*18*). Connor et al. confirmed association of *Salmonella* Paratyphi B var. Java ST28 with samples originating from poultry with whole-genome sequence (WGS) data (*22*). Isolates of *Salmonella* Paratyphi B var. Java from poultry and food products have been identified as carriers of *mcr* gene variants conferring resistance to colistin (*23*,*24*) and class 1 integrons in conjugative plasmids (*5*). Furthermore, near-identical plasmids carrying genes conferring resistance to third-generation cephalosporins were identified in *Escherichia coli*, *Salmonella* Paratyphi B var. Java ST28, and other *Salmonella* serovars known to cause infections in humans, such as Heidelberg and Enteritidis (*25*). In these regards, poultry-associated ST28 is of public health concern because it can be a reservoir of antimicrobial

Author affiliations: Utrecht University, Utrecht, the Netherlands (L.R. Castellanos, L. van der Graaf-van Bloois, D.J. Mevius, J.A. Wagenaar, J. Hordijk, A.L. Zomer); Corporación Colombiana de Investigación Agropecuaria–AGROSAVIA, Cundinamarca, Colombia (P. Donado-Godoy); Wageningen Bioveterinary Research, Lelystad, the Netherlands (K. Veldman, D.J. Mevius, J.A. Wagenaar); Instituto Costarricense de Investigación y Enseñanza en Nutrición y Salud, Tres Ríos, Costa Rica (F. Duarte, M.T. Acuña); Universidad del Valle de Guatemala, Guatemala City, Guatemala (C. Jarquín); Institut Pasteur, Paris, France (F.-X. Weill)

DOI: https://doi.org/10.3201/eid2606.191121

[1]Current affiliate: Quadram Institute Bioscience, Norwich, UK.

[2]These authors contributed equally to this article.

resistance to other *Salmonella* serovars of relevance to humans and species of *Enterobacteriaceae* in poultry and food products.

Previous reports from Latin America countries have identified *Salmonella* Paratyphi B var. Java as highly prevalent in poultry and poultry meat (*26*–*30*). Comparisons between strains of *Salmonella* Paratyphi B var. Java ST28 from Colombia and Europe showed a phylogenetic separation between isolates from Colombia and Europe (*31*). We then hypothesized that the separate lineage of Colombia strains could be part of a larger lineage of *Salmonella* Paratyphi B var. Java ST28 circulating in Latin America (*31*). Further investigation of this hypothesis could help identify potential events in poultry management (e.g., farming and trade) leading to the emergence and successful spread of *Salmonella* Paratyphi B var. Java ST28 in both regions. Our objective was to compare the evolutionary and antimicrobial resistance relatedness of poultry-associated *Salmonella* Paratyphi B var. Java ST28 from Europe and Latin America using WGS-based phylogenetic and temporal analysis.

Methods

Strain and Genome Collection

Our study comprised isolates from countries in Latin America and Europe that were previously serotyped as *Salmonella* Paratyphi B var. Java. We selected strains from different countries as follows.

Colombia

We used 259 epidemiologically independent isolates from broilers and broiler meat. We obtained isolates from baseline studies in poultry conducted in Colombia during 2008–2013 that originated from 25 samples from farms, 49 samples from slaughterhouses, and 185 samples from retail meat (*32*). As a rule of thumb, 20% of these isolates were randomly sampled using the select cases option in SPSS Statistics 24 (IBM, https://www.ibm.com). As a result, we selected 52 isolates, 5 originating from samples from farms, 5 from samples from slaughterhouses, and 42 from samples from retail.

Costa Rica

We selected all available strains from a previous study to determine the prevalence of *Salmonella* spp. in chickens at slaughter in the country in 2009 (*33*). The Costa Rican Institute for Research and Training in Nutrition and Health (Tres Ríos, Costa Rica) made 15 isolates available and provided 3 nonbroiler strains of human, reptile, and swine origin.

Guatemala

Available strains from a previous study to determine the prevalence of *Salmonella* in retail raw chicken carcasses in the country were included (*29*). The Center for Health Studies from the Universidad del Valle de Guatemala (Guatemala City, Guatemala) made 5 isolates available.

The Netherlands

Isolates were collected in the Netherlands as part of the Monitoring of Antimicrobial Resistance and Antibiotic Usages in Animals program (*34*). Our study comprised 1,279 isolates obtained during 2000–2016. The isolates originated from broilers, broiler meat, and chicken products (1,100 isolates), human enteric infections (159 isolates), and other animals and food items (20 isolates). A stratified random sampling was performed with the Transform, Rank and Select Cases options in SPSS Statistics 24 for every year within the samples from broilers and broiler meat. In addition, we included 2 randomly selected isolates from the entire pool of human isolates and 2 from other animals and food items as nonbroiler references. As a result, 21 isolates originating from 16 broilers and 1 broiler meat sample, 2 human enteric infections, and 2 from other animals and food products were selected.

Historical *Salmonella* Paratyphi B Var. Java ST28 Strains

Two strains of human origin from Saudi Arabia isolated in 1987 (IP_6155/87) and 1992 (IP_7734/92) and 1 strain from a turkey of Israel origin isolated in Austria in 1988 (IP_6395/88) were identified from their MLST profiles. These strains were the earliest *Salmonella* Paratyphi B var. Java ST28 strains from the EnteroBase database (https://enterobase.warwick.ac.uk) (*35*).

Publicly Available WGS Sequences

We queried EnteroBase for assembled genomes using the "experimental data" search option for strains belonging to "ST28" in the "Achtman 7-gene MLST" scheme (accessed February 22, 2018). We selected 65 strains with metadata available for year and country of isolation for phylogenetic and temporal analysis (Appendix 1, https://wwwnc.cdc.gov/EID/article/26/6/19-1121-App1.xlsx).

WGS and In Silico Screening of Antimicrobial Resistance Genes and Plasmid Content

We isolated genomic DNA from selected strains from the Netherlands, Colombia, Costa Rica, and Guatemala using the UltraClean Microbial DNA Isolation Kit (QIAGEN, https://www.qiagen.com). We performed

WGS on the MiSeq platform using 2 × 250-bp reads and the NextSeq platform using two 2 × 150-bp reads (Illumina, https://www.illumina.com). WGS of historical strains was performed at the Plateforme de microbiologie mutualisée from the Pasteur International Bioresources network (PIBnet, Institut Pasteur, https://www.pasteur.fr) as previously described (*36*). We assembled the genomes of historical and newly sequenced strains with SPAdes version 3.10.1 (*37*) and screened for antimicrobial resistance genes and chromosomal mutations using ResFinder 3.1 (*38*). We subtyped plasmids using PlasmidFinder 2.0 and plasmid MLST (pMLST) 2.0 (*39*). For newly sequenced genomes, we performed 7-gene MLST at the strain level with MLST 1.8 (*40*).

Phylogenetic Time Trees and Effective Population Size Estimates

For phylogenetic single-nucleotide polymorphism (SNP) analysis of the core genome, we aligned WGS of all *Salmonella* Paratyphi B. var. Java ST28 isolates using Parsnp version 1.2 (*41*), excluding non-ST28 strains. We used Gubbins (*42*) to detect and visualize recombination regions in the core genome alignment and performed time-resolved phylogeny on recombination-filtered SNPs of the *Salmonella* Paratyphi B. var. Java ST28 isolates that were extracted from the Gubbins results and used for divergence dating in BEAST (*43*). We included only newly obtained genomes with coverage >30. We used isolation dates as tip dates in the phylogenetic tree, as outlined in the BEAST manual, with the following modifications: 10,000,000× sampling and a general time-reversible model plus γ correction as the distance model. We tested a strict clock, relaxed logarithmic clock, and relaxed exponential clock as the clock model. We used a Bayesian skyline plot with 3 groups as demographic models to adjust for expected population changes and the effective sample size (ESS) method to select the strict clock model because it had the highest ESS values. All ESS values obtained with the strict clock model were >1,000. To generate Bayesian skyline plots for the European and Latin American populations, we repeated time-resolved phylogeny analysis using BEAST on 2 subsets containing the historical isolates and the isolates from Europe and Latin America.

Orthology Prediction and Plasmid/Chromosome Contig Scoring

We annotated genomes using Prokka version 1.13 (*44*), followed by orthology predictions using Roary (*45*). We differentiated chromosome and plasmid contigs with an in-house built tool. In brief, we scored contigs for the presence of known plasmid genes (https://github.com/aldertzomer/RFPlasmid), single-copy chromosomal marker genes (*46*), and kmer profiles and inferred their likely origin (plasmid or chromosomal) using a Random Forest model trained on known plasmid and chromosome assemblies (A.L. Zomer, unpub. data).

Comparison of Accessory Genome

We conducted principal component analysis (PCA) for all isolates on the gene presence/absence tables from the output of orthology predictions. We made comparisons using the accessory (noncore) genome of chromosome contigs, complete plasmid composition with all plasmid contigs, and plasmid composition with only plasmid contigs ≥50 kb. We made additional characterizations of prophage sequences using the PHAge Search Tool Enhanced Release (*47*) and BLAST (https://blast.ncbi.nlm.nih.gov/Blast.cgi).

Data Availability

We deposited sequences of the historical and newly sequenced strains in the short-read archive of the European Nucleotide Archive (ENA) under project no. PRJEB31547. Accession numbers of all collected genomes are provided (Appendix 1 Table 1).

Results

Phylogenetic Time Tree and Effective Population Size of *Salmonella* Paratyphi B var. Java ST28

Most of the strains from poultry that we sequenced from Colombia (48/52), Costa Rica (15/15), Guatemala (4/5), and the Netherlands (17/17) belonged to ST28 (Table). Similarly, nonbroiler strains from a fish product and a turkey in the Netherlands and 1 from a pig carcass in Costa Rica belonged to ST28. Isolates from 3 human and 1 reptile samples from Costa Rica or the Netherlands belonged to STs different from ST28 (Appendix 1 Table 1).

In the phylogenetic trees, the strains collected from the Latin America countries formed a separate cluster. In contrast, the strains collected from the Netherlands clustered with strains originating from other countries in Europe (Figure 1). An additional cluster was formed by the historical strains, which were neither from Europe nor Latin America. The molecular clock was estimated at 3.5×10^{-7} substitutions/site/year (1.7 SNPs/genome/year, 95% CI 1.44–2.0 SNPs/genome/year). The output of BEAST indicated separation between strains from Europe and Latin America occurred in 1987

Table. Newly obtained and publicly available genomes of 155 *Salmonella enterica* serovar Paratyphi B variant Java sequence type 28

Source	Total	No. per source*	Years isolated
Historical			
Saudi Arabia†	2	2 human	1987–1992
Austria†	1	1 poultry‡	1988
Europe			
Belgium§	5	5 unknown	2014
Denmark§	9	8 poultry, 1 unknown	2009–2015
Germany§	5	3 poultry, 1 human, 1 unknown	2001–2013
Ireland§	2	2 human	2015–2016
Nigeria§¶	1	1 poultry	2009
The Netherlands†	19	18 poultry, 1 fish	2000–2016
United Kingdom§	24	18 unknown, 5 human, 1 bovine	2006–2017
Latin America			
Colombia†#	67	67 poultry	2008–2013
Costa Rica†	16	15 poultry, 1 swine	2009–2014
Guatemala†	4	4 poultry	2012

*Source-metadata of publicly available genomes was obtained from EnteroBase (https://enterobase.warwick.ac.uk).
†Newly obtained.
‡Sample from a turkey imported from Israel.
§Publicly available.
¶Phylogenetically related to the European clade.
#19 genomes from previous reports in Colombia were publicly available in EnteroBase (*31*).

(95% CI 1978–1988) (Figure 1; Appendix 2 Figure 1, https://wwwnc.cdc.gov/EID/article/26/6/19-1121-App1.pdf). From the Bayesian Skyline plot, we inferred that the effective population size (N_e) of strains from Europe increased sharply in 1995 (95% CI 1992–1998) and in Latin America in 2005 (95% CI 2001–2007) (Figure 2), 10 years later than in Europe.

In Silico Characterization of Frequent Antimicrobial Resistance Genes and Plasmid Subtypes

We found a chromosomal class 2 integron (with *dfrA1-sat1-aadA1* [GenBank accession no. AB188271.1]) in historical strain IP_6155/87, collected in 1987 in Saudi Arabia. However, this integron was not in the other 2 historical strains from Austria (originating from Israel [IP_6395/88]) and Saudi Arabia [IP_7734/92]). In strain IP_6155/87, the alignment of the class 2 integron was divided into multiple contigs. We also found the integron in all strains from Europe and Latin America in contigs of ≈50 kb carrying the complete integron or divided into multiple contigs. Alignments of ≈50 kb contigs carrying the complete integron, revealed 100% identity within and between strains from European and Latin American clades.

Resistance to β-lactams in strains from Europe was mainly mediated by $bla_{\text{TEM-1B}}$ or $bla_{\text{TEM-1B}}$-like genes. These genes were found in 64% of isolates in the European clade. In strains from the Latin American clade, $bla_{\text{CMY-2}}$ was most prevalent and was carried in 50% of strains (Figure 1). $bla_{\text{TEM-1B}}$ gene is known to confer resistance to aminopenicillins and $bla_{\text{CMY-2}}$ gene to extended-spectrum cephalosporins. In the European clade, $bla_{\text{TEM-1B/1B}}$-like was mainly found on IncI1 plasmids (17/42) and, to a lesser extent, on IncX4 (7/42) and IncHI2 (3/42) plasmids. In strains from the Latin American clade, $bla_{\text{CMY-2}}$ was mainly found on IncI1/ST12 plasmids (25/33) (Figure 1). The *sul2* gene, conferring resistance to sulphonamides, was frequently encountered in strains from Europe (48%) and Latin America (14%). In the European clade, *sul2* was mainly found to co-localize with $bla_{\text{TEM-1B/1B}}$-like on IncI1 plasmids (17/30), whereas in the Latin American clade, *sul2* was found on ColRNAI-like plasmids (9/9). β-lactam and sulphonamide resistance genes in the Latin American clade were observed only in strains from Colombia (Figure 1). In addition, >50% of strains from the European clade exhibited known DNA gyrase mutations conferring resistance to fluoroquinolones. The observed mutations were *gyrA* D87G (16/33), D87Y (10/33), and S83F (7/33) (Figure 1). Although no strains from the Latin American clade carried the chromosomal *gyrA* mutations, they did carry *qnrB19*-harboring plasmids in 96% of the cases. *qnrB19* is known to confer reduced susceptibility to quinolones. This gene was co-localized with ColRNAI-like plasmids in strains from Latin America and in 1 strain from Europe from recent years (2015) (Figure 1).

PCA of Accessory Genomes

We observed a marked distinction for the accessory genes located on chromosome contigs between the European and Latin American clades (Figure 3). The separation in the PCA was associated with the presence of a prophage highly similar to the *Salmonella* phage SEN34 (National Center for Biotechnology Information reference sequence NC_028699.1) in strains from Latin America. This phage was also found in the genome of a *Salmonella* serovar Saintpaul strain submitted in Canada (GenBank accession no.

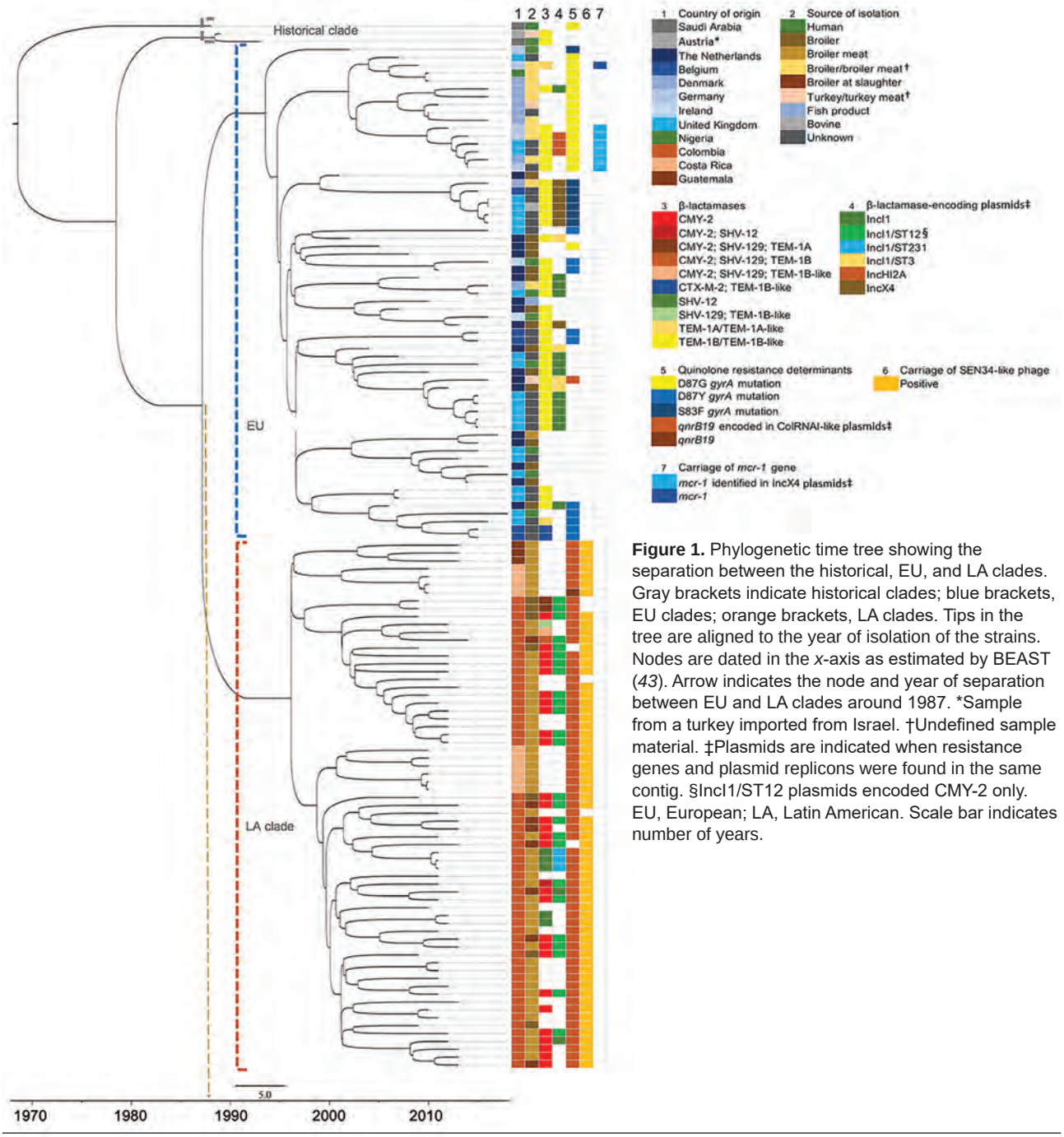

Figure 1. Phylogenetic time tree showing the separation between the historical, EU, and LA clades. Gray brackets indicate historical clades; blue brackets, EU clades; orange brackets, LA clades. Tips in the tree are aligned to the year of isolation of the strains. Nodes are dated in the *x*-axis as estimated by BEAST (*43*). Arrow indicates the node and year of separation between EU and LA clades around 1987. *Sample from a turkey imported from Israel. †Undefined sample material. ‡Plasmids are indicated when resistance genes and plasmid replicons were found in the same contig. §IncI1/ST12 plasmids encoded CMY-2 only. EU, European; LA, Latin American. Scale bar indicates number of years.

CP022491.1). A few strains from Colombia closer to the cluster of strains from Europe in the PCA (UGBOG142, UGVIL373, and SSIII_4_C2) lacked the sequence of this phage. Plasmid composition was similar in strains from Europe and Latin America (Figure 4). The profiles of plasmid composition were characterized by the presence of IncI1 plasmids (cluster I), IncHI2 (cluster II), ColRNAI-like (cluster III), and combinations of IncI1 and IncHI2 plasmids (cluster IV). Although the IncI1 plasmids had different pMLST sequence types, their content appears to be remarkably similar as they are in proximity in the PCA plot (cluster I). When exploring this further using only plasmid contigs ≥50 kb in strains from both European and Latin American clades, we observed that the IncI1 plasmid contigs clearly have near identical content (cluster I in Appendix 2 Figure 2). In strains with multiple plasmid contigs, in addition to the cluster of

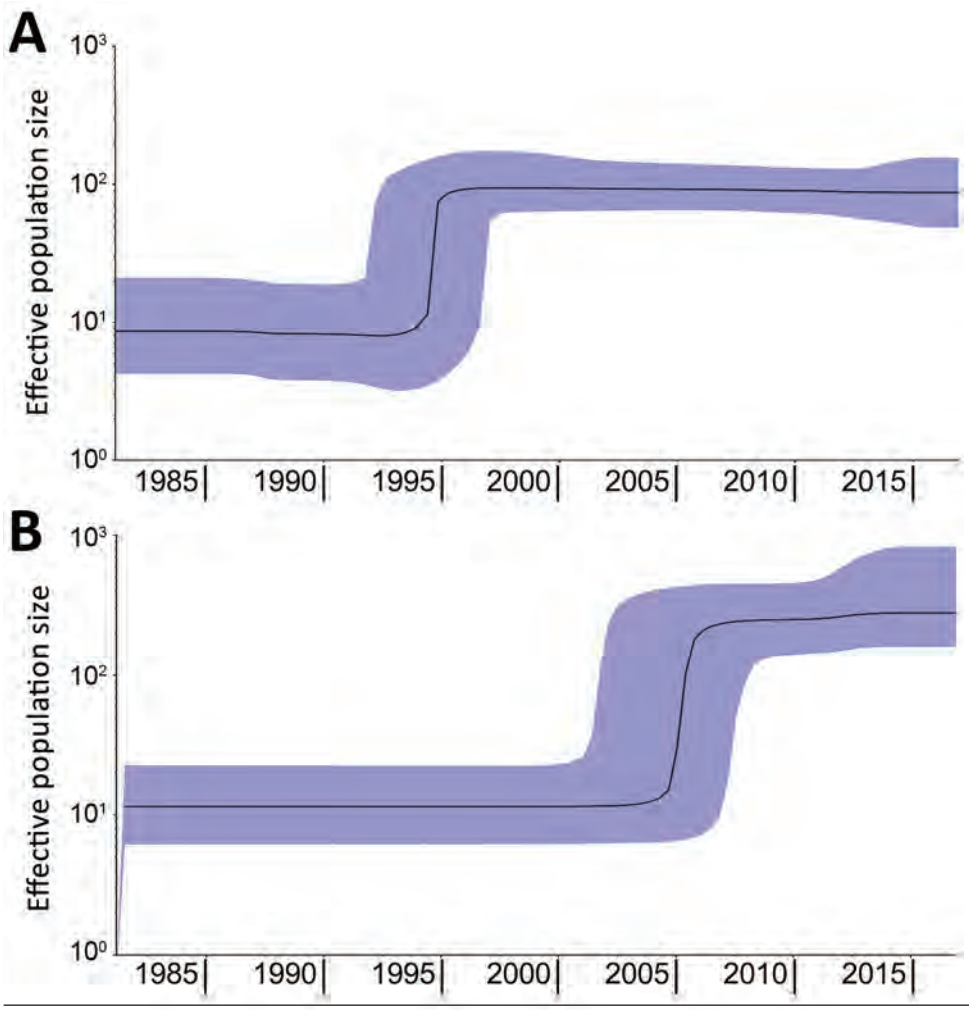

Figure 2. Bayesian skyline plots showing increase in effective population size of *Salmonella enterica* serovar Paratyphi B variant Java sequence type 28. Plots were made separately with strains originating from Europe (A) or Latin America (B). Emergence in Europe occurred in ≈1995 and in Latin America in ≈2005. Black lines indicate estimates of the median population over time; purple shading indicates 95% CIs.

IncI1-like plasmids, IncHI2-like plasmid contigs were differentiated in cluster II (Appendix 2 Figure 2).

Discussion

We selected public genomes using EnteroBase and based on metadata availability and in silico serovar and MLST characterization. In a comparison between EnteroBase, ENA, and GenBank (Appendix 1 Table 2), we found 3,524 genomes associated to BioSamples (i.e., unique identifiers linking metadata and sequencing data) after querying EnteroBase for predicted serovar "Paratyphi B Var. Java." After querying "*Salmonella* AND Java," we found 1,245 in ENA and 1,299 in GenBank. This difference is mainly due to the large number of genomes submitted without serovar information (1,935/3,524) rather than those labeled differently from Paratyphi B or variant Java (71 genomes). In this regard, in silico characterization in EnteroBase helped surpass absent, incorrect, or multiple serovar denominations accompanying genomes submitted to the ENA and GenBank databases.

On the basis of MLST, we found that poultry-associated variant Java ST28 (380 isolates), human-associated ST43 (767 isolates), and reptile-associated ST88 (319 isolates) were among the most abundant STs in EnteroBase. Most (143 isolates) ST28 genomes originated from poultry, and some (24 isolates) originated from humans, which could indicate transfer between these 2 sources. Because metadata were lacking on their year of isolation in EnteroBase (Appendix 1 Table 2), some ST28 genomes were excluded from the phylogenetic time trees in this study. Nevertheless, phylogenetic analysis based on core genome MLST in EnteroBase (*35*) strongly supported the separate clustering of historical strains and those from Europe and Latin America (Appendix 2 Figure 3).

From the time-resolved phylogeny, we observed that strain IP_6155/87 collected in 1987 was ancestral to all the other strains analyzed. IP_6155/87 can be hypothesized to be the strain most closely related to the common ancestor of all analyzed strains, which according to the output from the time-resolved

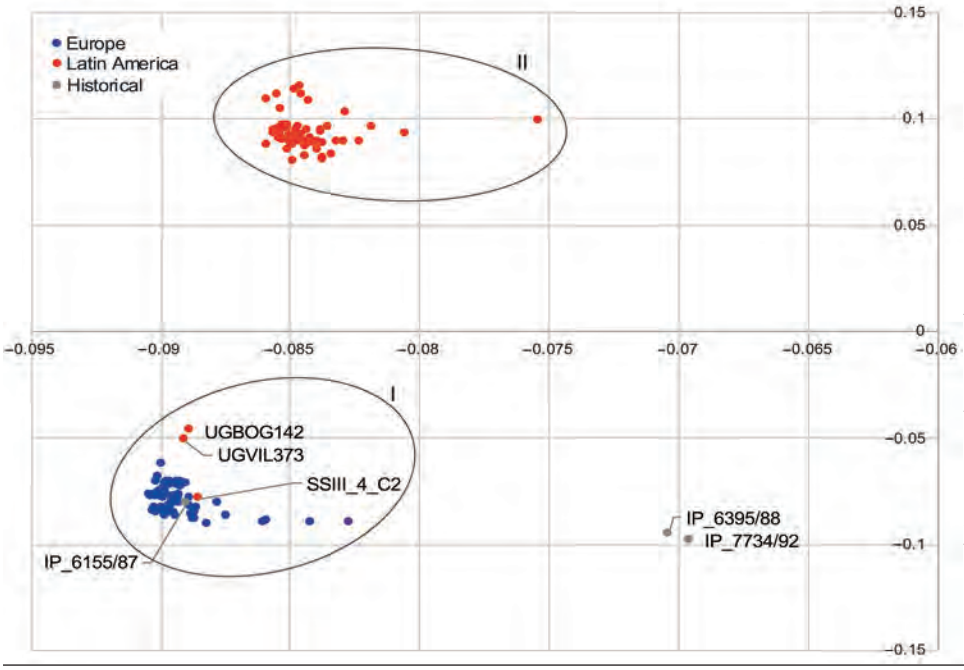

Figure 3. Principal component analysis plot comparing accessory (noncore) genome of chromosome contigs of strains of *Salmonella enterica* serovar Paratyphi B variant Java sequence type 28. Oval rings indicate clusters I and II. Cluster I grouped together historical strain IP_6155/87 with all strains from Europe and some from Latin American. Cluster II grouped Latin America strains only. Cluster II was associated with a prophage sequence highly similar to the *Salmonella* phage SEN34 (National Center for Biotechnology Information reference sequence no. NC_028699.1). The prophage sequence was absent in strains from cluster I.

phylogeny circulated around 1970 (95% CI 1962–1974). This hypothesis is supported by the high level of similarity between the contigs carrying the class 2 integron (with *dfrA1-sat1-aadA1* [GenBank accession no. AB188271.1]) between historical strain IP_6155/87 and strains from Europe and Latin America. Common ancestry of IP_6155/87 was also reflected in the PCAs used to compare the accessory genome. At both chromosome and plasmid levels, the accessory genome of this strain was closely related to strains from Europe, Latin America, or both (Figures 3, 4; Appendix 2 Figure 2).

In comparison with previous estimations of mutation rates for *Salmonella* Typhimurium DT104 (3.4×10^{-7} substitutions/site/year) (*48*), the molecular clock calibrated for *Salmonella* Paratyphi B var. Java ST28 in our study was estimated at 3.5×10^{-7} substitutions/site/year, corresponding to 1.7 SNP/genome/year (95% CI 1.44–2.0 SNP/genome/year). Our results indicate similar mutation rates for these 2 *S. enterica* serovars with distinct ecologic niches.

Previously, genomic characterization of *Salmonella* Paratyphi B var. Java ST28 from Colombia suggested a different clade from the one observed

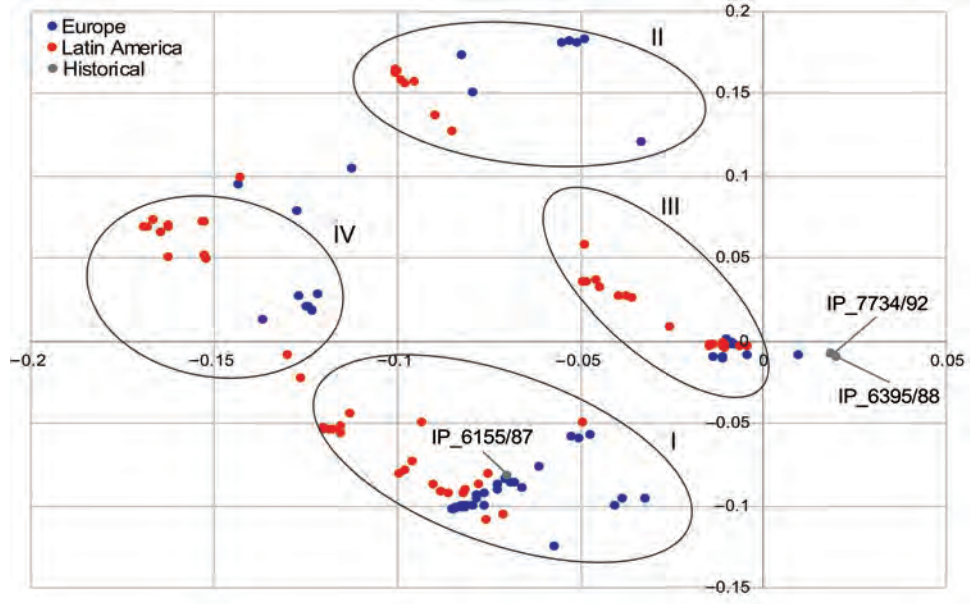

Figure 4. Principal component analysis plot comparing plasmid composition (all plasmid contigs) of strains of *Salmonella enterica* serovar Paratyphi B variant Java sequence type 28. Oval rings indicate clusters I–IV. All clusters grouped strains from Europe and Latin America and were associated with IncI1 plasmids (cluster I), IncHI2 (cluster II), COLRNAI (cluster III), and combinations of IncI1 and IncHI2 plasmids (cluster IV).

in Europe could be circulating in Latin America (*31*). We found a distinct clade of *Salmonella* Paratyphi B var. Java ST28 circulating in poultry from Costa Rica, Guatemala, and Colombia. In Colombia, introduction of foreign technologies for poultry breeding, housing, and processing occurred around 1960 (*49*). Importation of this particular *S. enterica* serovar was anticipated to have occurred around this time. Nevertheless, separation between the European and Latin American clades in our study was estimated with BEAST in the 1980s (Figure 1; Appendix 2 Figure 1). Furthermore, an increase in effective population size in Latin America was observed only in 2005 (95% CI 2001–2007), 10 years after the known increase in Europe, reported in the literature (*19*) and observed with Bayesian skyline in our study (Figure 2). Driving factors that led to the separation of clusters could not be determined based on the availability of data for this study.

The separation between the Latin American and European clades comprised differences at both the core and noncore genome level. Differences in antimicrobial resistance gene content, plasmid replicons, and pMLSTs reflected the evolutionary separation of the 2 clades. Among these differences, DNA gyrase mutations conferring resistance to fluoroquinolones and $bla_{\text{TEM-1B}}$–carrying IncI1 plasmids were characteristic in the European clade. In contrast, *qnrB19*-carrying ColRNAI-like plasmids conferring reduced susceptibility to quinolones and $bla_{\text{CMY-2}}$–carrying IncI1/ST12 plasmids were found in Latin America. In both clades, resistance to β-lactams was mainly carried on IncI1 plasmids, with near-identical gene content (cluster I in Figure 4) but from different pMLST lineages. $bla_{\text{TEM-1B}}$ in Europe was associated with IncI/ST3 in some strains and $bla_{\text{CMY-2}}$ with IncI1/ST12 in Latin America. It is remarkable that the genomic features confer resistance to β-lactam drugs and quinolones/fluoroquinolones in both European and Latin American clades and thus indicate parallel evolution of *Salmonella* Paratyphi B var. Java ST28 in both geographic regions. Acquisition of such antimicrobial resistance traits can be hypothesized to have occurred as a consequence of selection pressure posed by the use of β-lactams and fluoroquinolones in poultry production. As an example, and as previously suggested, the use of aminopenicillins in broiler production potentially could have selected for $bla_{\text{CMY-2}}$–carrying *E. coli* strains in the absence of the use of cephalosporins (*50*). Furthermore, the emergence of *Salmonella* Paratyphi B var. Java in Europe was associated with increased antimicrobial resistance and the use of fluoroquinolones, such as flumequine (*19*) or enrofloxacin, which could also explain the sharp increase in effective population size around 1995. For Latin America, such information is not available because data on the use of antimicrobial drugs in animals is not systematically collected in most countries in the region.

In conclusion, *Salmonella* Paratyphi B var. Java ST28 from poultry in Europe and Latin America form 2 different clades. The separation is estimated to have occurred during the 1980s (95% CI 1978–1988). The years with sharp increase in effective population size were estimated as 1995 for Europe and 2005 for Latin America. Previous reports about the emergence of *Salmonella* Paratyphi B var. Java in poultry in Europe supports these findings for Europe (*6*,*19*); no historical data are available for Latin America. In spite of their evolutionary divergence, the European and Latin American clades have independently acquired different antimicrobial resistance genes on similar plasmids. These genetic determinants confer resistance to β-lactam drugs and quinolones and thus indicate parallel evolution of *Salmonella* Paratyphi B var. Java ST28 in both regions.

Acknowledgments

We thank Birgitta Duim, Arjen Timmerman, Alice Wegener, and Sylvie Issenhuth-Jeanjean for assistance in obtaining the WGS of strains. We also thank Johan F. Bernal, Maribel León, Alejandra Arevalo, María F. Valencia, and Viviana Clavijo for their assistance during the collection and characterization of *Salmonella* strains from Colombia. We thank Walid Alali and Enrique Perez-Gutierrez for their contribution to the projects where the prevalence of *S. enterica* in poultry from Colombia and Guatemala was determined. We thank Jaap Obdam for providing historical information on *Salmonella* serovars in poultry production in the Netherlands. We thank Alison E. Mather for her constructive revision of the manuscript. We acknowledge the World Health Organization Advisory Group on Integrated Surveillance of Antimicrobial Resistance for facilitating the exchange of researchers and knowledge between research groups.

This study was financed by internal funding of Utrecht University, the Netherlands.

About the Author

Dr. Castellanos is a postdoctoral research scientist at the Quadram Institute Bioscience in Norwich, UK. His primary research interests are the evolution of bacteria and plasmids and the reduction of antimicrobial resistance in humans, animals, and food.

References

1. De Moor CE. *Salmonella* infection in Batavia (Java), with particular reference to the diagnosis of the type of infection [in German]. Mededeelingen van den Dienst der Volksgzondheid in Nederlandsch-Indië. 1935;24:98–118.
2. Kristensen M, Kauffmann F. Bakteriologische und klinische Erfahrungen über Infektionen mit d-weinsäurevergärenden Paratyphus B-Bacillen. Z Hyg Infektionskr. 1937;120:149–54. https://doi.org/10.1007/BF02178014
3. Kauffmann F. Differential diagnosis and pathogenicity of *Salmonella* Java and *Salmonella* Paratyphi B [in German]. Z Hyg Infektionskr. 1955;141:546–50. https://doi.org/10.1007/BF02156850
4. Barker RM, Kearney GM, Nicholson P, Blair AL, Porter RC, Crichton PB. Types of *Salmonella* Paratyphi B and their phylogenetic significance. J Med Microbiol. 1988;26:285–93. https://doi.org/10.1099/00222615-26-4-285
5. Miko A, Guerra B, Schroeter A, Dorn C, Helmuth R. Molecular characterization of multiresistant *d*-tartrate–positive *Salmonella enterica* serovar Paratyphi B isolates. J Clin Microbiol. 2002;40:3184–91. https://doi.org/10.1128/JCM.40.9.3184-3191.2002
6. Brown DJ, Mather H, Browning LM, Coia JE. Investigation of human infections with *Salmonella enterica* serovar Java in Scotland and possible association with imported poultry. Euro Surveill. 2003;8:35–40. https://doi.org/10.2807/esm.08.02.00399-en
7. Weill FX, Fabre L, Grandry B, Grimont PAD, Casin I. Multiple-antibiotic resistance in *Salmonella enterica* serotype Paratyphi B isolates collected in France between 2000 and 2003 is due mainly to strains harboring *Salmonella* genomic islands 1, 1-B, and 1-C. Antimicrob Agents Chemother. 2005;49:2793–801. https://doi.org/10.1128/AAC.49.7.2793-2801.2005
8. Threlfall J, Levent B, Hopkins KL, de Pinna E, Ward LR, Brown DJ. Multidrug-resistant *Salmonella* Java. Emerg Infect Dis. 2005;11:170–1. https://doi.org/10.3201/eid1101.031092
9. Denny J, Threlfall J, Takkinen J, Lofdahl S, Westrell T, Varela C, et al. Multinational *Salmonella* Paratyphi B variant Java (*Salmonella* Java) outbreak, August–December 2007. Euro Surveill. 2007;12:E071220.2.
10. Doublet B, Praud K, Nguyen-Ho-Bao T, Argudín MA, Bertrand S, Butaye P, et al. Extended-spectrum β-lactamase- and AmpC β-lactamase–producing D-tartrate–positive *Salmonella enterica* serovar Paratyphi B from broilers and human patients in Belgium, 2008–10. J Antimicrob Chemother. 2014;69:1257–64. https://doi.org/10.1093/jac/dkt504
11. Meunier D, Boyd D, Mulvey MR, Baucheron S, Mammina C, Nastasi A, et al. *Salmonella enterica* serotype Typhimurium DT 104 antibiotic resistance genomic island I in serotype Paratyphi B. Emerg Infect Dis. 2002;8:430–3. https://doi.org/10.3201/eid0804.010213
12. Mulvey MR, Boyd D, Cloeckaert A, Ahmed R, Ng LK; Provincial Public Health Laboratories. Emergence of multidrug-resistant *Salmonella* Paratyphi B dT+, Canada. Emerg Infect Dis. 2004;10:1307–10. https://doi.org/10.3201/eid1007.030862
13. Gaulin C, Vincent C, Ismaïl J. Sporadic infections of *Salmonella* Paratyphi B, var. Java associated with fish tanks. Can J Public Health. 2005;96:471–4. https://doi.org/10.1007/BF03405194
14. Hassan R, Tecle S, Adcock B, Kellis M, Weiss J, Saupe A, et al. Multistate outbreak of *Salmonella* Paratyphi B variant L(+) tartrate(+) and *Salmonella* Weltevreden infections linked to imported frozen raw tuna: USA, March–July 2015. Epidemiol Infect. 2018;146:1461–7. https://doi.org/10.1017/S0950268818001462
15. Heiman Marshall KE, Booth H, Harrang J, Lamba K, Folley A, Ching-Lee M, et al. New product, old problem(s): multistate outbreak of *Salmonella* Paratyphi B variant L(+) tartrate(+) infections linked to raw sprouted nut butters, October 2015. Epidemiol Infect. 2019;8:1–6.
16. Levings RS, Lightfoot D, Hall RM, Djordjevic SP. Aquariums as reservoirs for multidrug-resistant *Salmonella* Paratyphi B. Emerg Infect Dis. 2006;12:507–10. https://doi.org/10.3201/eid1203.051085
17. Djordjevic SP, Cain AK, Evershed NJ, Falconer L, Levings RS, Lightfoot D, et al. Emergence and evolution of multiply antibiotic-resistant *Salmonella enterica* serovar Paratyphi B D-tartrate–utilizing strains containing SGI1. Antimicrob Agents Chemother. 2009;53:2319–26. https://doi.org/10.1128/AAC.01532-08
18. Toboldt A, Tietze E, Helmuth R, Fruth A, Junker E, Malorny B. Human infections attributable to the D-tartrate–fermenting variant of *Salmonella enterica* serovar Paratyphi B in Germany originate in reptiles and, on rare occasions, poultry. Appl Environ Microbiol. 2012;78:7347–57. https://doi.org/10.1128/AEM.01732-12
19. van Pelt W, van der Zee H, Wannet WJ, van de Giessen AW, Mevius DJ, Bolder NM. Explosive increase of *Salmonella* Java in poultry in the Netherlands: consequences for public health. Euro Surveill. 2003;8:31–5. https://doi.org/10.2807/esm.08.02.00398-en
20. Centrum voor Onderzoek in Diergeneeskunde en Agrochemie. Centre d'Etude et des Recherches Vétérinaires et Agrochimiques (CODA-CERVA). *Salmonella* serotypes analysed at the CODA-CERVA in 2013. Technical Report. Federal Public Service Health, Food Chain Security and Environment:Brussels: 2014.
21. Achtman M, Wain J, Weill FX, Nair S, Zhou Z, Sangal V, et al.; S. Enterica MLST Study Group. Multilocus sequence typing as a replacement for serotyping in *Salmonella enterica*. PLoS Pathog. 2012;8:e1002776. https://doi.org/10.1371/journal.ppat.1002776
22. Connor TR, Owen SV, Langridge G, Connell S, Nair S, Reuter S, et al. What's in a name? Species-wide whole-genome sequencing resolves invasive and noninvasive lineages of *Salmonella enterica* serotype Paratyphi B. MBio. 2016;7:1–9. https://doi.org/10.1128/mBio.00527-16
23. Doumith M, Godbole G, Ashton P, Larkin L, Dallman T, Day M, et al. Detection of the plasmid-mediated *mcr-1* gene conferring colistin resistance in human and food isolates of *Salmonella enterica* and *Escherichia coli* in England and Wales. J Antimicrob Chemother. 2016;71:2300–5. https://doi.org/10.1093/jac/dkw093
24. Borowiak M, Fischer J, Hammerl JA, Hendriksen RS, Szabo I, Malorny B. Identification of a novel transposon-associated phosphoethanolamine transferase gene, *mcr-5*, conferring colistin resistance in *d*-tartrate fermenting *Salmonella enterica* subsp. *enterica* serovar Paratyphi B. J Antimicrob Chemother. 2017;72:3317–24. https://doi.org/10.1093/jac/dkx327
25. Castellanos LR, van der Graaf-van Bloois L, Donado-Godoy P, Mevius DJ, Wagenaar JA, Hordijk J, et al. Phylogenomic investigation of IncI1-Iγ plasmids harboring bla_{CMY-2} and bla_{SHV-12} in *Salmonella enterica* and *Escherichia coli* in multiple countries. Antimicrob Agents Chemother. 2019;63:e02546–18. https://doi.org/10.1128/AAC.02546-18
26. Donado-Godoy P, Gardner I, Byrne BA, Leon M, Perez-Gutierrez E, Ovalle MV, et al. Prevalence, risk factors, and antimicrobial resistance profiles of *Salmonella* from commercial broiler farms in two important poultry-producing regions of Colombia. J Food Prot. 2012;75:874–83. https://doi.org/10.4315/0362-028X.JFP-11-458

27. Donado-Godoy P, Clavijo V, León M, Arevalo A, Castellanos R, Bernal J, et al. Counts, serovars, and antimicrobial resistance phenotypes of *Salmonella* on raw chicken meat at retail in Colombia. J Food Prot. 2014;77:227–35. https://doi.org/10.4315/0362-028X.JFP-13-276
28. Donado-Godoy P, Byrne BA, León M, Castellanos R, Vanegas C, Coral A, et al. Prevalence, resistance patterns, and risk factors for antimicrobial resistance in bacteria from retail chicken meat in Colombia. J Food Prot. 2015;78:751–9. https://doi.org/10.4315/0362-028X.JFP-14-349
29. Jarquin C, Alvarez D, Morales O, Morales AJ, López B, Donado P, et al. *Salmonella* on raw poultry in retail markets in Guatemala: levels, antibiotic susceptibility, and serovar distribution. J Food Prot. 2015;78:1642–50. https://doi.org/10.4315/0362-028X.JFP-15-117
30. Boscán-Duque LA, Arzálluz-Fisher AM, Ugarte C, Sánchez D, Wittum TE, Hoet AE. Reduced susceptibility to quinolones among *Salmonella* serotypes isolated from poultry at slaughter in Venezuela. J Food Prot. 2007;70:2030–5. https://doi.org/10.4315/0362-028X-70.9.2030
31. Castellanos LR, van der Graaf-van Bloois L, Donado-Godoy P, León M, Clavijo V, Arévalo A, et al. Genomic characterization of extended-spectrum cephalosporin-resistant *Salmonella enterica* in the Colombian poultry chain. Front Microbiol. 2018;9:2431. https://doi.org/10.3389/fmicb.2018.02431
32. Donado-Godoy P, Castellanos R, León M, Arevalo A, Clavijo V, Bernal J, et al. The establishment of the Colombian Integrated Program for Antimicrobial Resistance Surveillance (COIPARS): a pilot project on poultry farms, slaughterhouses and retail market. Zoonoses Public Health. 2015;62(Suppl 1):58–69. https://doi.org/10.1111/zph.12192
33. Ministerio de Agricultura y Ganadería, Instituto Costarricense de Investigación y Enseñanza en Nutrición y Salud, Ministerio de Salud. Prevalence of *Salmonella* spp. in meat and chicken products. Costa Rica, September–November 2009 [in Spanish]. Technical Report. Ministry of Agriculture and Livestock, Costa Rican Institute for Research and Training in Nutrition and Health and Ministry of Health. San Jose (Costa Rica); 2011.
34. Veldman K, Mevius DJ, Wit B, van Pelt W, Heederik D. MARAN. Monitoring of antimicrobial resistance and antibiotic usage in animals in the Netherlands in 2016. 2017 [cited 2019 Mar 7]. https://www.wur.nl/upload_mm/9/b/4/fe79278b-9361-4912-8cba-03ce17fc086b_Maran%20report%202017.pdf
35. Alikhan NF, Zhou Z, Sergeant MJ, Achtman M. A genomic overview of the population structure of *Salmonella*. PLoS Genet. 2018;14:e1007261. https://doi.org/10.1371/journal.pgen.1007261
36. Kuijpers LMF, Phe T, Veng CH, Lim K, Ieng S, Kham C, et al. The clinical and microbiological characteristics of enteric fever in Cambodia, 2008–2015. PLoS Negl Trop Dis. 2017;11:e0005964. https://doi.org/10.1371/journal.pntd.0005964
37 Bankevich A, Nurk S, Antipov D, Gurevich AA, Dvorkin M, Kulikov AS, et al. SPAdes: a new genome assembly algorithm and its applications to single-cell sequencing. J Comput Biol. 2012;19:455–77. https://doi.org/10.1089/cmb.2012.0021
38. Zankari E, Hasman H, Cosentino S, Vestergaard M, Rasmussen S, Lund O, et al. Identification of acquired antimicrobial resistance genes. J Antimicrob Chemother. 2012;67:2640–4. https://doi.org/10.1093/jac/dks261
39. Carattoli A, Zankari E, García-Fernández A, Voldby Larsen M, Lund O, Villa L, et al. In silico detection and typing of plasmids using PlasmidFinder and plasmid multilocus sequence typing. Antimicrob Agents Chemother. 2014;58:3895–903. https://doi.org/10.1128/AAC.02412-14
40. Larsen MV, Cosentino S, Rasmussen S, Friis C, Hasman H, Marvig RL, et al. Multilocus sequence typing of total-genome-sequenced bacteria. J Clin Microbiol. 2012;50:1355–61. https://doi.org/10.1128/JCM.06094-11
41. Treangen TJ, Ondov BD, Koren S, Phillippy AM. The Harvest suite for rapid core-genome alignment and visualization of thousands of intraspecific microbial genomes. Genome Biol. 2014;15:524. https://doi.org/10.1186/s13059-014-0524-x
42. Croucher NJ, Page AJ, Connor TR, Delaney AJ, Keane JA, Bentley SD, et al. Rapid phylogenetic analysis of large samples of recombinant bacterial whole genome sequences using Gubbins. Nucleic Acids Res. 2015;43:e15. https://doi.org/10.1093/nar/gku1196
43. Drummond AJ, Rambaut A. BEAST: Bayesian evolutionary analysis by sampling trees. BMC Evol Biol. 2007;7:214. https://doi.org/10.1186/1471-2148-7-214
44. Seemann T. Prokka: rapid prokaryotic genome annotation. Bioinformatics. 2014;30:2068–9. https://doi.org/10.1093/bioinformatics/btu153
45. Page AJ, Cummins CA, Hunt M, Wong VK, Reuter S, Holden MTG, et al. Roary: rapid large-scale prokaryote pan genome analysis. Bioinformatics. 2015;31:3691–3. https://doi.org/10.1093/bioinformatics/btv421
46. Parks DH, Imelfort M, Skennerton CT, Hugenholtz P, Tyson GW. CheckM: assessing the quality of microbial genomes recovered from isolates, single cells, and metagenomes. Genome Res. 2015;25:1043–55. https://doi.org/10.1101/gr.186072.114
47. Arndt D, Grant JR, Marcu A, Sajed T, Pon A, Liang Y, et al. PHASTER: a better, faster version of the PHAST phage search tool. Nucleic Acids Res. 2016;44(W1):W16-21. https://doi.org/10.1093/nar/gkw387
48. Mather AE, Reid SWJ, Maskell DJ, Parkhill J, Fookes MC, Harris SR, et al. Distinguishable epidemics of multidrug-resistant *Salmonella* Typhimurium DT104 in different hosts. Science. 2013;341:1514–7. https://doi.org/10.1126/science.1240578
49. Molina LF. Poultry farming in Colombia [in Spanish]. Federación Nacional de Avicultores de Colombia (Fenavi)-Fondo Nacional Avícola (Fonav): Bogotá (Colombia); 2002.
50. Agersø Y, Jensen JD, Hasman H, Pedersen K. Spread of extended spectrum cephalosporinase-producing *Escherichia coli* clones and plasmids from parent animals to broilers and to broiler meat in a production without use of cephalosporins. Foodborne Pathog Dis. 2014;11:740–6. https://doi.org/10.1089/fpd.2014.1742

Address for correspondence: Aldert L. Zomer, Department of Infectious Diseases and Immunology, Faculty of Veterinary Medicine, Utrecht University, Yalelaan 1, 3584CL, Utrecht, the Netherlands; email: a.l.zomer@uu.nl

Invasive Group B *Streptococcus* Infections in Adults, England, 2015–2016

Simon M. Collin, Nandini Shetty, Theresa Lamagni

During 2015–2016, a total of 3,156 episodes of invasive group B *Streptococcus* (iGBS) infection in adults (≥15 years of age) were recorded in England, corresponding to an annual incidence of 4.09/100,000 population. iGBS incidence was highest in older patients and women of childbearing age. The 493 pregnancy-related iGBS episodes correspond to a rate of 1.34/10,000 live births. In adults up to 60–69 years of age and in pregnant women, iGBS incidence increased with higher levels of socioeconomic deprivation. Hospital admissions associated with iGBS were predominantly emergency admissions (73% [2,260/3,099]); only 7% of nonpregnancy iGBS diagnoses were made ≥48 hours after admission. Underlying conditions were highly prevalent in nonpregnant adult case-patients, including cardiovascular (57%), lung (43%), and kidney (45%) disease and diabetes (40%). Post-iGBS episode 30-day and 12-month all-cause mortality rates in nonpregnant adults were 12% and 24%, respectively. No pregnancy-related iGBS deaths were identified.

Streptococcus agalactiae (group B *Streptococcus*; GBS) is implicated in a range of clinical manifestations in adults, including surgical site, skin and soft tissue, and urinary tract infections (*1*–*3*). Invasive GBS (iGBS) disease in adults is of growing clinical and public health concern (*4*–*6*), with incidence in England and Wales during 1996–2010 increasing almost 3-fold (*7*). The increasing prevalence of known risk factors for iGBS disease, including old age and underlying conditions such as diabetes (*8*–*11*), means that considerable healthcare, economic, and social costs will be associated with iGBS disease in adults. The advent of vaccines to prevent neonatal GBS disease raises the possibility of preventing iGBS disease in other patient groups (*12*). However, although neonatal iGBS has been the subject of epidemiologic research for several decades (*13*), adult iGBS disease is less well characterized.

Author affiliation: National Infection Service, Public Health England, London, UK

DOI: https://doi.org/10.3201/eid2606.191141

The aim of this study was to characterize iGBS disease in adults by creating a national retrospective cohort of cases in England identified through laboratory surveillance linked to hospital admissions data. Our objectives were to describe characteristics of adults who received diagnoses of iGBS; time to infection, medical specialty, and healthcare resource use in patients admitted to a hospital within 7 days of diagnosis; concurrent conditions and surgery in current and prior admissions up to 1 year before diagnosis; and all-cause mortality within 30 days and within 1 year of an iGBS episode.

Methods

Case Definition

We defined iGBS infection through the isolation of *S. agalactiae* recorded in specimens from a normally sterile site, such as blood, cerebrospinal fluid, joint fluid, bone, pleural fluid, bronchoalveolar lavage, ascitic fluid, lymph node biopsy/aspirate, pericardial fluid, heart valve, brain abscess, or other organs. We considered laboratory test result records within 14 days to be part of the same episode and merged them accordingly.

PHE Second Generation Surveillance System

We extracted laboratory-confirmed cases of iGBS infection diagnosed from specimens taken during January 1, 2015–December 31, 2016 from the Public Health England (PHE) Second Generation Surveillance System (SGSS), the national communicable disease surveillance database, for analysis. SGSS collates microbiological diagnoses from laboratories across England (including all National Health Service [NHS] laboratories), primarily through automated upload (*14*–*16*). In addition to information about the laboratory, specimen, test method, and type of infection, SGSS records include patient identifiers and demographic data (name, sex, date of birth, and the patient's NHS number).

Hospital Episode Statistics

We identified corresponding hospital admissions for episodes of iGBS infection through record linkage to Hospital Episode Statistics (HES; https://digital.nhs.uk). HES includes all NHS secondary care activity (98% of all hospital activity in the country [*17*]) that requires a hospital bed, including emergency and planned (elective) admissions, day cases, and births. HES admitted patient care data are collated by NHS Digital to reimburse NHS hospitals for the costs of care (using Healthcare Resource Group codes to group diagnoses and interventions). These data provide clinical, demographic and organizational information, including data on diagnoses and procedures, concurrent conditions (by code from the International Classification of Diseases, 10th Revision [ICD-10]), dates of admission, admission method (emergency or elective), care provider, and geographic variables mapped from a patient's postcode.

Data Linkage and Statistical Analysis

Our analysis of hospital admissions associated with iGBS episodes used a dataset created by linking SGSS laboratory records corresponding to iGBS cases with HES hospital admission records (using NHS numbers). Before performing this linkage, we sent patient identifiable data from SGSS records to NHS Digital's Demographic Batch Service to validate recorded NHS numbers, trace missing patient NHS numbers, and obtain dates of death (*18*). We extracted corresponding HES records for a period 1 calendar year before and after the SGSS surveillance period, January 1, 2014–December 31, 2017. To analyze treatment specialties and Healthcare Resource Group when an iGBS episode had >1 associated admission, we selected the admission that was closest to the specimen request date; each admission could be represented by >1 treatment specialty. For each iGBS episode recorded in SGSS, we defined an associated hospital admission as an admission occurring within 7 days of the iGBS specimen request date (proxy for date of diagnosis). Pregnancy-related iGBS episodes were identified by an ICD-10 O or Z370 code for diagnosis at admission. We built multivariable models for risk factors associated with all-cause 30-day and 12-month mortality after iGBS unrelated to pregnancy, including age, sex, socioeconomic deprivation, underlying conditions, and type of hospital admission as a priori risk factors. We performed all analyses in Stata (https://www.stata.com).

Results

During 2015–2016, a total of 3,156 iGBS episodes in adults (≥15 years of age) were recorded in England, corresponding to an incidence rate of 3.48 per 100,000 population per year (Table 1). In 87% (2,753) of recorded episodes, GBS was isolated from a blood culture; the 3 next most common specimen types were from joint (5.6%), bone (2.7%), and bronchoalveolar lavage (2.4%). Of the 3,156 iGBS episodes, 2,999 (95.0%), representing 2,919 patients, could be linked to a hospital admission record within 1 year of iGBS diagnosis and 2,704 (representing 2,647 patients) to an admission within 7 days of iGBS diagnosis (associated hospital admission); of these 2,704 episodes, 479 (17.7%) were pregnancy related (Figure 1). Subtracting this proportion of cases from the 3,156 episodes for England during 2015–2016 gives an estimated incidence rate for iGBS in nonpregnant adults of 2.9/100,000 population/year.

Characteristics of Adults' iGBS Infection

Analysis of sex and age identified that iGBS was most likely to occur in older patients and women of childbearing age (Figure 2). Most (97.6%;

Table 1. Numbers of patients and episodes of iGBS infection among adults in England, 2015–2016*

Age, y	No. iGBS episodes	No. patients	Male sex, no. (%)	No. (%) patients with ≥2 iGBS episodes†	No. (%) iGBS episodes per patient			Annual iGBS incidence‡
					1	2	≥3	
15–19	21	21	7 (33.3)	0 (0.0)	21 (100.0)	0	0	0.33
20–29	241	230	27 (11.7)	3 (1.3)	227 (98.7)	2 (0.9)	1 (0.4)	1.63
30–39	388	376	58 (15.4)	2 (0.5)	374 (99.5)	2 (0.5)	0	2.66
40–49	277	261	128 (49.0)	3 (1.1)	258 (98.9)	2 (0.8)	1 (0.4)	1.87
50–59	363	334	205 (61.4)	13 (3.9)	321 (96.1)	9 (2.7)	4 (1.2)	2.50
60–69	493	466	278 (59.7)	11 (2.4)	455 (97.6)	8 (1.7)	3 (0.6)	4.13
70–79	565	533	304 (57.0)	18 (3.4)	515 (96.6)	17 (3.2)	1 (0.2)	6.76
≥80	808	772	357 (46.2)	22 (2.8)	750 (97.2)	18 (2.3)	4 (0.5)	15.1
Total	3,156	2,993	1,364 (45.6)	72 (2.4)	2,921 (97.6)	58 (1.9)	14 (0.5)	3.48

*iGBS, invasive group B *Streptococcus*.
†Recurrent iGBS episodes detected during Jan 1, 2015–Dec 31, 2016 based on iGBS episodes for which patient's NHS number was recorded in PHE laboratory surveillance system (3084/3156 episodes)
‡Per 100,000 population. Numerator = iGBS episodes/2; denominator = Office for National Statistics mid-2016 population estimates for England (http://www.ons.gov.uk/peoplepopulationandcommunity/populationandmigration/populationestimates/datasets/populationestimatesforukenglandandwalesscotlandandnorthernireland)

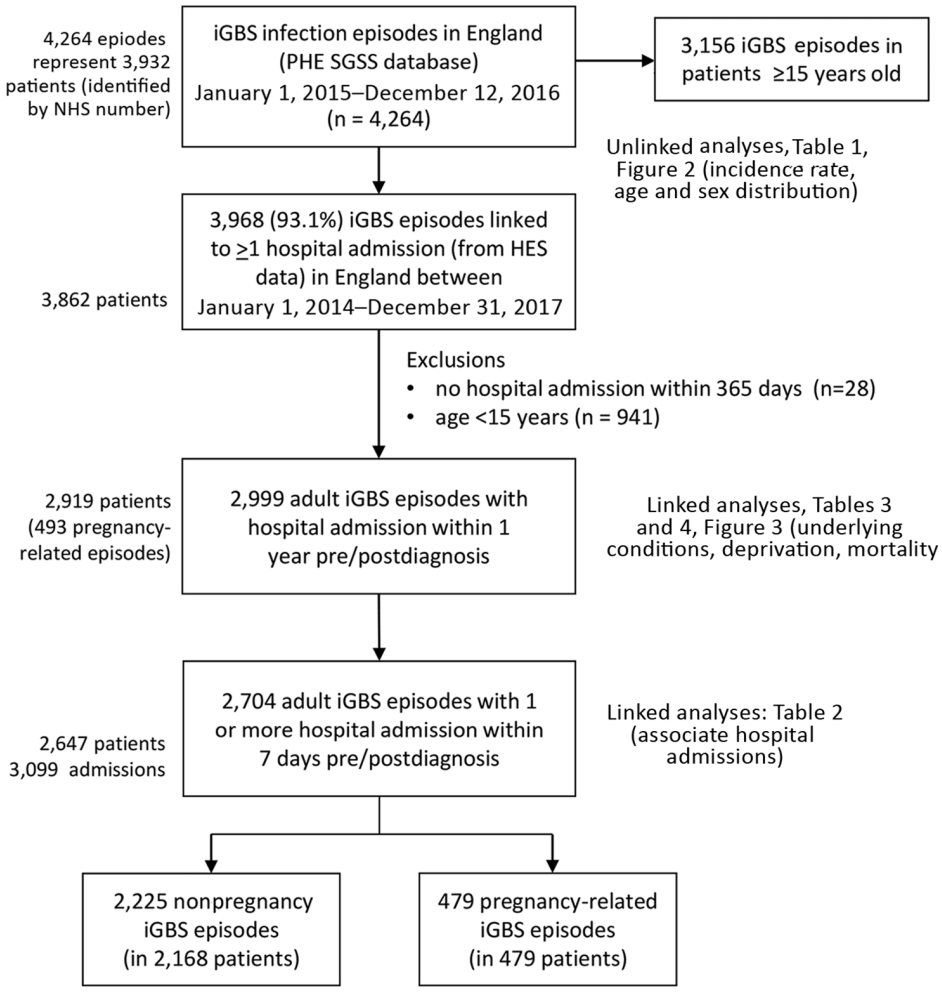

Figure 1. Data flowchart of iGBS infection in England, 2015 and 2016. iGBS, invasive group B *Streptococcus*.

2,921/2,993) patients had a single episode; 1.9% (58) had 2 and 0.5% (14) had ≥3 episodes (Table 1). There were 493 pregnancy-related iGBS episodes (4.09/10,000 live births). Assessment of incidence (excluding maternity cases) by socioeconomic deprivation identified higher rates in more deprived socioeconomic groups in all but the oldest (≥70 years) age groups (Figure 3; Appendix Table 1, https://wwwnc.cdc.gov/EID/article/26/6/19-1141-App1.xlsx). This social gradient was reversed in elderly patients, with adults >80 years of age in the least deprived quintile having a 2.5-fold higher iGBS rate than in the most deprived quintile (23.8 vs. 9.4/100,000 population), an effect that was more pronounced in male than in female patients (Appendix Table 2). Race and ethnicity was broadly representative of the population of England (Appendix Table 3). The proportion who were black (4.0%) was slightly higher than the national figure (3.3%), and the proportion who were mixed race was lower (0.8% vs. 2.2%).

Hospital Admission, Time to Diagnosis, Medical Specialty, and Healthcare Resource Group

Associated admissions (within 7 days of diagnosis) were predominantly through the emergency department (2,260/3,099; 72.9%), except in women 20–39 years of age, for whom most admissions were classified as maternity-related (493/587; 84.0%) (Table 2). In nonpregnancy episodes, most iGBS diagnoses (2,064/2,225; 92.8%) were from specimens taken within 48 hours of admission, suggesting that the infection was community rather than healthcare associated. In pregnancy-related episodes, 37.4% (179/479) of diagnoses were made ≥2 days after admission (Appendix Table 4). Patients were under the care of 57 different medical specialties (Appendix Table 5); general medicine was the most common specialty (1,435/4,011; 35.8%), followed by geriatric medicine (10.9%) and obstetrics (10.9%). Of specialties with >50 associated admissions, the second highest proportion of iGBS diagnosed ≥2 days after admission, after obstetrics and gynecology (37.4%), was in urology (25.7%). The

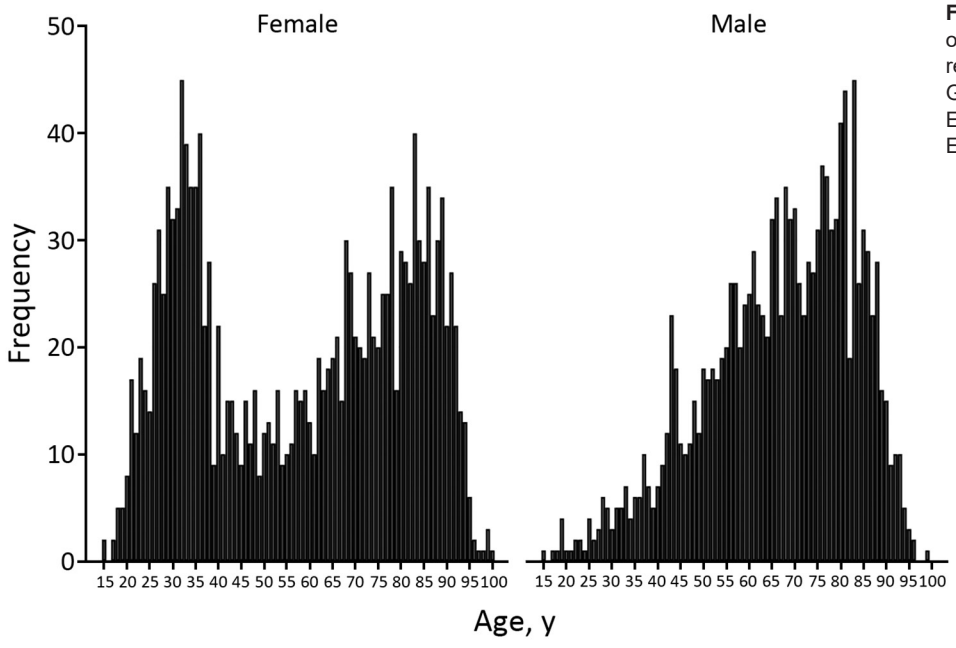

Figure 2. Age and sex distribution of patients ≥15 years of age who received diagnoses of invasive GBS infection, Public Health England laboratory surveillance, England, 2015 and 2016.

top 4 Healthcare Resource Group subchapters were obstetric medicine (451/2,704; 16.7%), infectious diseases and immune system disorders (431/2,704; 15.9%), respiratory system procedures and disorders (366/2,704; 13.5%), and skin disorders (319/2,704; 11.8%) (Appendix Table 6).

Underlying Conditions and Surgery ≤1 Year before iGBS Diagnosis

Analysis of ICD-10 codes recorded in the current and previous (≤1 year pre-iGBS) hospital admissions identified underlying conditions as common in nonpregnant adults with iGBS disease (Table 3). Cardiovascular disease was recorded for 57.5% (1,440/2,506) of all nonpregnancy iGBS episodes, lung disease for 42.9% (1,076/2,506), kidney disease for 44.5% (1,115/2,506), and diabetes for 39.9% (1,000/2,506). Prevalences of underlying conditions were much lower in pregnancy-related cases; most (349/493; 70.8%) had no recorded underlying condition (Appendix Table 7). After diagnostic imaging, testing, and rehabilitation (1,674/2,999; 55.8%), the 4 most commonly recorded current or prior medical procedures by anatomic chapter were arteries and veins (550/2,999; 18.3%); pregnancy, childbirth, and the puerperium (470/2,999; 15.7%); bones and joints (439/2,999; 14.6%); and urinary (433/2,999; 14.4%) (Appendix Table 8).

All-Cause Mortality after iGBS

Overall all-cause mortality in nonpregnant adults in the 30 days after an iGBS episode was 12.5% (313/2,506) (Table 4; Appendix Table 9). With extension to the 12 months after diagnosis, all-cause mortality increased to 29.2% (731/2,506). There were no deaths related to the 493 maternal iGBS episodes. For iGBS unrelated to pregnancy, 30-day mortality after an emergency admission was 13.3% (306/2,299), compared with 3.4% (7/206) for elective admissions ($p<0.001$). In a multivariable model, the strongest predictors of 30-day all-cause mortality for iGBS unrelated to pregnancy were older age (odds ratio [OR] 3.7 [95% CI 1.5–9.3] for age ≥80 years compared with 20–29 years), concurrent conditions (OR 5.3 [95% CI 1.7–16.9] for any of the conditions shown in Table 3 versus none), and emergency admission (OR 3.4 [95% CI 1.6–7.5] versus nonemergency admission) (Appendix Table 10). Estimates suggested an increased risk of death with higher levels of social deprivation, but these apparent effects were not supported by statistical evidence. In relation to concurrent conditions recorded in the current or prior hospital admission(s), we observed the highest 30-day mortality for iGBS unrelated to pregnancy in patients with kidney disease (221/1,115; 19.8%), followed by cancer (81/437; 18.5%), lung disease (186/1,076; 17.3%), and neurologic disorders (138/800; 17.3%) (Appendix Table 11). We observed similar effects for 12-month mortality (Appendix Tables 12, 13).

Discussion

We characterized cases of iGBS disease occurring in England over a 2-year period. The annual incidence rate of 3.48/100,000 population during 2015–2016

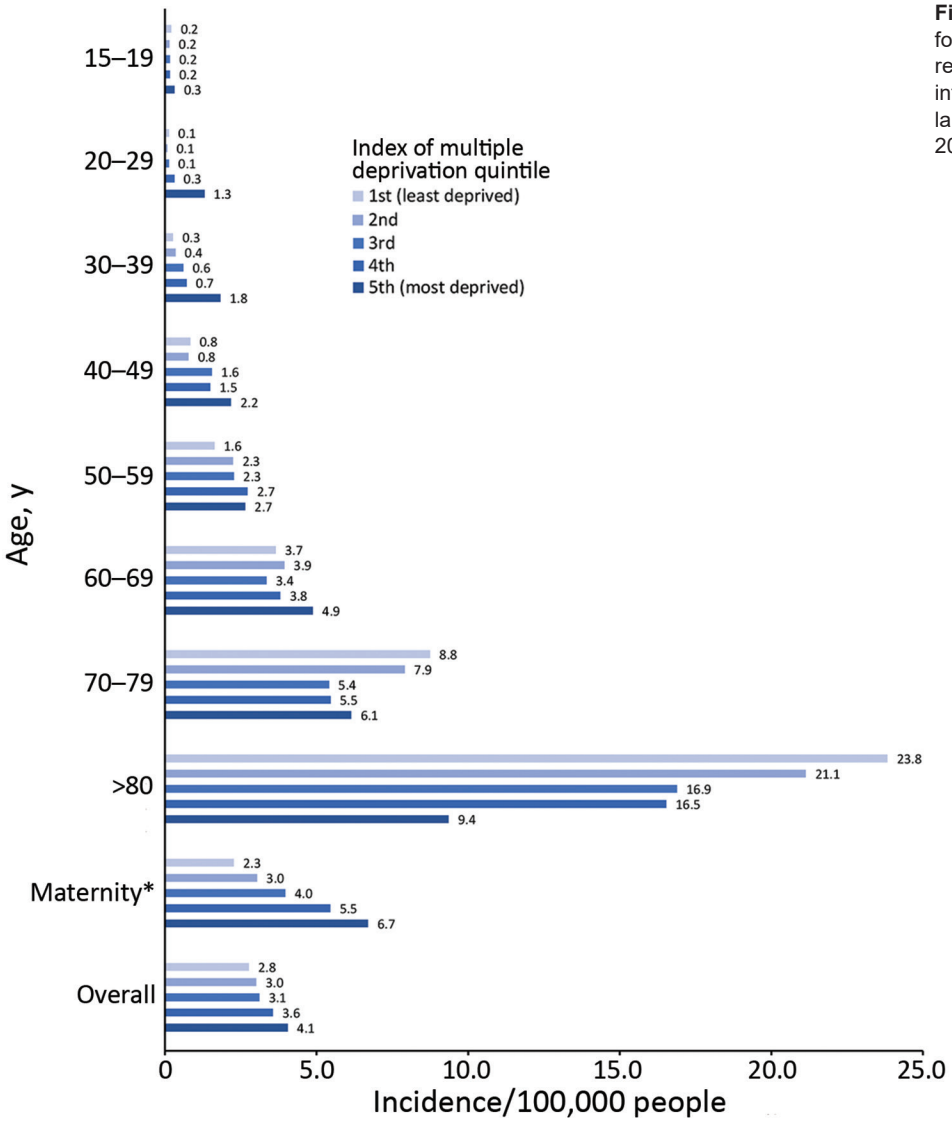

Figure 3. Social deprivation quintiles for patients ≥15 years of age who received diagnoses of invasive GBS infection, Public Health England laboratory surveillance, England, 2015 and 2016.

suggests a continuation of the trend in adults during 1991–2010, when incidence increased from 0.92 to 2.39/100,000 population (*7*). This trend is largely attributable to cases in adults, particularly the elderly. A prominent feature of the iGBS age distribution in England is the relatively higher incidence among women of childbearing age, as also seen in some other countries (*8*). Overall incidence in England for 2015–2016 (≈3/100,000 population, excluding maternity cases) was one third the rate in nonpregnant adults in the United States for the same period (*6*). This finding is the opposite of the reported rates for pregnancy-related iGBS, which are lower in the United States (0.1/1,000 live births) compared with England (0.3/1,000 live births) (*19*), possibly because antenatal GBS screening in the United States leads to widespread use of intrapartum antimicrobial prophylaxis.

Prevalence of underlying conditions appeared to be much higher in iGBS cases than in the adult population in England (*20*). For example, 40% of persons with iGBS had diabetes (compared with 7% in the general population), 17% cancer (2%), 58% cardiovascular disease (1%), 45% kidney disease (4%), and 30% arthritis (1%). These findings are consistent with other studies of iGBS in adults (*5*,*6*,*8*–*11*,*21*,*22*); the increasing prevalence of predisposing medical conditions in the adult population may account for rising rates of iGBS disease (*4*–*8*). Vaccination to prevent iGBS in adults could be a key component of future preventive measures if appropriately targeted. The cost-effectiveness of GBS vaccination has been evaluated (favorably) in relation to neonatal disease (*23*,*24*), but health economic studies encompassing nonpregnancy-associated adult disease are lacking (*25*). Health

Table 2. Hospital admissions among adult patients with iGBS infection in England, 2015–2016*

	Male patients, no. (%)			Female patients, no. (%)			
Age, y	No. admissions	Elective	Emergency	No. admissions	Elective	Emergency	Maternity
15–19	4	2 (50.0)	2 (50.0)	14	0	6 (42.9)	8 (57.1)
20–29	29	2 (6.9)	27 (93.1)	237	5 (2.1)	27 (11.4)	205 (86.5)
30–39	54	2 (3.7)	50 (92.6)	350	10 (2.9)	51 (14.6)	288 (82.3)
40–49	121	9 (7.4)	109 (90.1)	140	12 (8.6)	81 (57.9)	46 (32.9)
50–59	204	30 (14.7)	170 (83.3)	140	34 (24.3)	105 (75.0)	1 (0.7)
60–69	292	35 (12.0)	250 (85.6)	197	25 (12.7)	171 (86.8)	0
70–79	307	23 (7.5)	283 (92.2)	230	16 (7.0)	210 (91.3)	0
≥80	366	26 (7.1)	331 (90.4)	414	19 (4.6)	387 (93.5)	0
Total	1,377	129 (9.4)	1,222 (88.7)	1,722	121 (7.0)	1,038 (60.3)	548 (31.8)

*N = 3,099 associated hospital admissions (within 7 d of specimen date) represent 2,704 invasive GBS episodes in 2,647 patients. iGBS, invasive group B *Streptococcus*.

economic studies of GBS vaccination to prevent GBS disease in adults would need to take into account all manifestations of GBS disease, including noninvasive infections (*26*) and the possible prevention of antimicrobial resistance (*6*,*27*,*28*).

Further prevention measures could be identified through improved understanding of the role of healthcare interventions and the wider hospital environment in enabling disease occurrence (*29*). Although most of the cases in this study were diagnosed at admission, suggesting community acquisition, the high prevalence of underlying conditions and the numbers of patients having medical procedures in the preceding year suggest that prior healthcare exposure was likely for a sizable proportion of patients.

In our study, 30-day mortality (12%) was higher than the case-fatality rate reported recently from a population-based study in the United States (6%) (*6*), but we included all-cause deaths within 30 days of iGBS rather than deaths occurring during hospitalization for iGBS. The high 12-month mortality rate that we observed in the youngest (15–19 years) age group (5/12 cases) reflected deaths in young adults with other medical conditions (2 with cancer, 1 with cardiovascular disease, 1 with multiple concurrent conditions).

The steep gradients observed over quintiles of social deprivation, with more deprived quintiles having higher iGBS incidence up to age 60–69 years but lower incidence thereafter, could be attributed partly to concurrent conditions, although overall prevalence of such conditions did not differ substantially across the quintiles. Social gradients have been reported for different infectious diseases in England (*30*), including incidence increasing with deprivation for invasive group A *Streptococcus*, meningococcal, and pneumococcal infection. Incidence of community-acquired pneumonia in older (≥65 years of age) adults in the United Kingdom showed a steep increase with level of deprivation (*31*), the opposite of the trend that we observed for iGBS in adults ≥70 years of age.

The trend that we observed of increasing maternity-related iGBS incidence with higher levels of social deprivation is entirely consistent with the trend reported for risk of severe maternal sepsis in the United Kingdom (*32*). The potential for iGBS prevention in this group is supported by a study showing that ≥70% of women across all social grades would be likely to accept antenatal GBS vaccination (*33*).

Although PHE's microbiology surveillance database has national coverage (*34*), reporting of GBS infection is not mandatory, and the completeness of reporting is unknown. A comparison of MRSA and

Table 3. Underlying conditions among adult patients with invasive GBS (iGBS) infection unrelated to pregnancy in England, 2015–2016*

	Age, y								
Conditions	15–19	20–29	30–39	40–49	50–59	60–69	70–79	≥80	Total
No. iGBS episodes	12	49	98	204	339	474	545	785	2,506
Diabetes	1 (8.3)	5 (10.2)	17 (17.4)	62 (30.4)	162 (47.8)	212 (44.7)	267 (49.0)	274 (34.9)	1,000 (39.7)
Peripheral vascular disease	1 (8.3)	5 (10.2)	31 (31.6)	46 (22.6)	113 (33.3)	154 (32.5)	203 (37.3)	289 (36.8)	842 (33.6)
Cancer	2 (16.7)	2 (4.1)	1 (1.0)	28 (13.7)	57 (16.8)	77 (16.2)	107 (19.6)	163 (20.8)	437 (17.4)
Cardiovascular disease	3 (25.0)	12 (24.5)	32 (32.7)	58 (28.4)	125 (36.9)	249 (52.5)	355 (65.1)	606 (77.2)	1,440 (57.5)
Lung disease	5 (41.7)	20 (40.8)	39 (39.8)	72 (35.3)	148 (43.7)	193 (40.7)	242 (44.4)	357 (45.5)	1,076 (42.9)
Kidney disease	2 (16.7)	9 (18.4)	19 (19.4)	69 (33.8)	117 (34.5)	197 (41.6)	268 (49.2)	434 (55.3)	1,115 (44.5)
Neurologic disorders	2 (16.7)	11 (22.5)	21 (21.4)	53 (26.0)	111 (32.7)	124 (26.2)	167 (30.6)	311 (39.6)	800 (31.9)
Arthritis	0	5 (10.2)	12 (12.2)	42 (20.6)	74 (21.8)	125 (26.4)	189 (34.7)	294 (37.5)	741 (29.6)
None of these	3 (25.0)	12 (24.5)	23 (23.5)	28 (13.7)	27 (8.0)	39 (8.2)	17 (3.1)	15 (1.9)	164 (6.5)

*Values are no. (%) patients. Predefined conditions (Appendix Table 7, https://wwwnc.cdc.gov/EID/article/26/6/19-1141-App1.pdf) identified in current and prior admissions (up to 1 y prediagnosis). iGBS, invasive group B *Streptococcus*.

Table 4. All-cause 30-day and 12-month mortality among adult patients with iGBS infection in England, 2015–2016*

	Male patients				Female patients, excluding pregnancy-related episodes			
Age, y	No. iGBS episodes	All-cause deaths within 30 d, no. (%)	All-cause deaths within 1 y, no. (%)	Median (IQR) time to death, d	No. iGBS episodes	All-cause deaths within 30 d, no. (%)	All-cause deaths within 1 y, no. (%)	Median (IQR) time to death, d
15–19	6	0	3 (50.0)	39 (33–170)	6	2 (33.3)	2 (33.3)	4 (2–6)
20–29	27	1 (3.7)	2 (7.4)	144 (2–285)	22	0 (0.0)	2 (9.1)	179 (33–325)
30–39	59	4 (6.8)	7 (11.9)	3 (1–159)	39	1 (2.6)	2 (5.1)	58 (2–113)
40–49	120	14 (11.7)	27 (22.5)	26 (2–68)	84	3 (3.6)	8 (9.5)	37 (15–124)
50–59	212	21 (9.9)	44 (20.8)	39 (12–135)	127	3 (2.4)	15 (11.8)	80 (40–177)
60–69	281	21 (7.5)	51 (18.1)	45 (11–168)	193	21 (10.9)	46 (23.8)	72 (3–177)
70–79	310	38 (12.3)	93 (30.0)	57 (13–145)	235	34 (14.5)	66 (28.1)	30 (8–119)
≥80	359	77 (21.4)	177 (49.3)	41 (10–188)	426	73 (17.1)	186 (43.7)	54 (8–136)
Total	1,374	176 (12.8)	404 (29.4)	44 (10–167)	1,132	137 (12.1)	327 (28.9)	53 (8–138)

*iGBS, invasive group B *Streptococcus*; IQR, interquartile range.

E. coli data reported to a separate mandatory surveillance system showed that voluntary reporting represented >80% of records for bacteremia caused by these 2 species (*35*,*36*). A further limitation of our analysis is that, even with linkage to hospital episode data, we lacked sufficiently detailed clinical information on the manifestations and severity of the iGBS cases and outcomes resulting from GBS. This inability to ascertain clinical case characteristics constrained us to analyzing iGBS patients as a homogeneous group, which they will not be in practice (*2*,*5*,*6*,*9*,*37*). Although bronchoalveolar lavage is not universally considered a sterile site sample, we included these specimens in our iGBS case definition to capture lower respiratory tract infections. Although we cannot completely discount the possibility that some of the respiratory isolates were contaminants, national standards for microbiology laboratories provide guidelines to differentiate these from clinically significant infections (*38*).

In conclusion, incidence of iGBS disease in adults continues to increase in England, and high risk groups include the elderly, pregnant women, and adults with underlying conditions. Most nonpregnant adults have emergency cases, and all-cause mortality is high (one quarter of cases). Reasons for the strong social gradients at different ages merit further investigation, as does the potential for prevention of iGBS through vaccination.

Acknowledgments

We thank Nick Hinton at Public Health England for retrieval and linkage of Hospital Episode Statistics (HES) data.

This study was funded by Pfizer Inc.

About the Author

Dr. Collin is a senior scientist in the Healthcare-Associated Infection and Antimicrobial Resistance Division of Public Health England, where his primary research interest is in the epidemiology of group B *Streptococcus* infection.

References

1. Kernéis S, Plainvert C, Barnier JP, Tazi A, Dmytruk N, Gislain B, et al. Clinical and microbiological features associated with group B *Streptococcus* bone and joint infections, France 2004–2014. Eur J Clin Microbiol Infect Dis. 2017;36:1679–84. https://doi.org/10.1007/s10096-017-2983-y
2. Chaiwarith R, Jullaket W, Bunchoo M, Nuntachit N, Sirisanthana T, Supparatpinyo K. *Streptococcus agalactiae* in adults at Chiang Mai University Hospital: a retrospective study. BMC Infect Dis. 2011;11:149. https://doi.org/10.1186/1471-2334-11-149
3. Falagas ME, Rosmarakis ES, Avramopoulos I, Vakalis N. *Streptococcus agalactiae* infections in non-pregnant adults: single center experience of a growing clinical problem. Med Sci Monit. 2006;12:CR447–51.
4. Bjornsdottir ES, Martins ER, Erlendsdottir H, Haraldsson G, Melo-Cristino J, Kristinsson KG, et al. Changing epidemiology of group B streptococcal infections among adults in Iceland: 1975–2014. Clin Microbiol Infect. 2016;22:379.e9–16. https://doi.org/10.1016/j.cmi.2015.11.020
5. Skoff TH, Farley MM, Petit S, Craig AS, Schaffner W, Gershman K, et al. Increasing burden of invasive group B streptococcal disease in nonpregnant adults, 1990–2007. Clin Infect Dis. 2009;49:85–92. https://doi.org/10.1086/599369
6. Francois Watkins LK, McGee L, Schrag SJ, Beall B, Jain JH, Pondo T, et al. Epidemiology of invasive group B streptococcal infections among nonpregnant adults in the United States, 2008–2016. JAMA Intern Med. 2019;179:479–88. https://doi.org/10.1001/jamainternmed.2018.7269
7. Lamagni TL, Keshishian C, Efstratiou A, Guy R, Henderson KL, Broughton K, et al. Emerging trends in the epidemiology of invasive group B streptococcal disease in England and Wales, 1991-2010. Clin Infect Dis. 2013;57:682–8. https://doi.org/10.1093/cid/cit337
8. Ballard MS, Schønheyder HC, Knudsen JD, Lyytikäinen O, Dryden M, Kennedy KJ, et al.; International Bacteremia Surveillance Collaborative. The changing epidemiology of group B streptococcus bloodstream infection: a multi-national population-based assessment. Infect Dis (Lond). 2016;48:386–91. https://doi.org/10.3109/23744235.2015.1131330
9. Camuset G, Picot S, Jaubert J, Borgherini G, Ferdynus C, Foucher A, et al. Invasive group B streptococcal disease in non-pregnant adults, Réunion Island, 2011. Int J Infect Dis. 2015;35:46–50. https://doi.org/10.1016/j.ijid.2015.04.006
10. Lefebvre N, Forestier E, Mohseni-Zadeh M, Remy V, Lesens O, Kuhnert C, et al. Invasive *Streptococcus agalactiae* infections in non-pregnant adults [in French]. Med Mal Infect. 2007;37:796–801. https://doi.org/10.1016/j.medmal.2007.04.003

11. Huang PY, Lee MH, Yang CC, Leu HS. Group B streptococcal bacteremia in non-pregnant adults. J Microbiol Immunol Infect. 2006;39:237–41.
12. Vekemans J, Moorthy V, Friede M, Alderson MR, Sobanjo-Ter Meulen A, Baker CJ, et al. Maternal immunization against Group B streptococcus: World Health Organization research and development technological roadmap and preferred product characteristics. Vaccine. 2019;37:7391–3. https://doi.org/10.1016/j.vaccine.2017.09.087
13. Le Doare K, Heath PT. An overview of global GBS epidemiology. Vaccine. 2013;31(Suppl 4):D7–12. https://doi.org/10.1016/j.vaccine.2013.01.009
14. Freeman R, Charlett A, Hopkins S, O'Connell AM, Andrews N, Freed J, et al. Evaluation of a national microbiological surveillance system to inform automated outbreak detection. J Infect. 2013;67:378–84. https://doi.org/10.1016/j.jinf.2013.07.021
15. PHE Second Generation Surveillance System (SGSS). Laboratory reporting to Public Health England: a guide for diagnostic laboratories. London: Public Health England; 2016.
16. Public Health England. Laboratory surveillance of pyogenic and non-pyogenic streptococcal bacteraemia in England, Wales and Northern Ireland: 2016. London: Public Health England; 2017.
17. Herbert A, Wijlaars L, Zylbersztejn A, Cromwell D, Hardelid P. Data resource profile: Hospital Episode Statistics Admitted Patient Care (HES APC). Int J Epidemiol. 2017;46:1093–1093i. https://doi.org/10.1093/ije/dyx015
18. NHS Digital. Demographics Batch Service Bureau (DBSB): NHS number batch tracing. London: Health and Social Care Information Centre; 2017.
19. Hall J, Adams NH, Bartlett L, Seale AC, Lamagni T, Bianchi-Jassir F, et al. Maternal disease with group B *Streptococcus* and serotype distribution worldwide: systematic review and meta-analyses. Clin Infect Dis. 2017;65(suppl_2):S112–24. https://doi.org/10.1093/cid/cix660
20. NHS Digital. Quality and Outcomes Framework (QOF) 2015–16. 2016 [cited January 2019]. http://digital.nhs.uk/data-and-information/publications/statistical/quality-and-outcomes-framework-achievement-prevalence-and-exceptions-data/quality-and-outcomes-framework-qof-2015–16
21. Schwartz B, Schuchat A, Oxtoby MJ, Cochi SL, Hightower A, Broome CV. Invasive group B streptococcal disease in adults. A population-based study in metropolitan Atlanta. JAMA. 1991;266:1112–4. https://doi.org/10.1001/jama.1991.03470080082034
22. Farley MM, Harvey RC, Stull T, Smith JD, Schuchat A, Wenger JD, et al. A population-based assessment of invasive disease due to group B *Streptococcus* in nonpregnant adults. N Engl J Med. 1993;328:1807–11. https://doi.org/10.1056/NEJM199306243282503
23. Giorgakoudi K, O'Sullivan C, Heath PT, Ladhani S, Lamagni T, Ramsay M, et al. Cost-effectiveness analysis of maternal immunisation against group B *Streptococcus* (GBS) disease: a modelling study. Vaccine. 2018;36:7033–42. https://doi.org/10.1016/j.vaccine.2018.09.058
24. Kim SY, Nguyen C, Russell LB, Tomczyk S, Abdul-Hakeem F, Schrag SJ, et al. Cost-effectiveness of a potential group B streptococcal vaccine for pregnant women in the United States. Vaccine. 2017;35:6238–47. https://doi.org/10.1016/j.vaccine.2017.08.085
25. Cannon JW, Jack S, Wu Y, Zhang J, Baker MG, Geelhoed E, et al. An economic case for a vaccine to prevent group A *Streptococcus* skin infections. Vaccine. 2018;36:6968–78. https://doi.org/10.1016/j.vaccine.2018.10.001
26. Collin SM, Shetty N, Guy R, Nyaga VN, Bull A, Richards MJ, et al. Group B *Streptococcus* in surgical site and non-invasive bacterial infections worldwide: a systematic review and meta-analysis. Int J Infect Dis. 2019;83:116–29. https://doi.org/10.1016/j.ijid.2019.04.017
27. Sevilla JP, Bloom DE, Cadarette D, Jit M, Lipsitch M. Toward economic evaluation of the value of vaccines and other health technologies in addressing AMR. Proc Natl Acad Sci U S A. 2018;115:12911–9. https://doi.org/10.1073/pnas.1717161115
28. Kitamura M, Kimura K, Ido A, Seki T, Banno H, Jin W, et al. Relatively high rates of cefotaxime- and ceftriaxone-non-susceptible isolates among group B streptococci with reduced penicillin susceptibility (PRGBS) in Japan. J Antimicrob Chemother. 2019;74:931–4. https://doi.org/10.1093/jac/dky542
29. Collin SM, Lamb P, Jauneikaite E, Le Doare K, Creti R, Berardi A, et al. Hospital clusters of invasive group B streptococcal disease: a systematic review. J Infect. 2019;79:521–7. https://doi.org/10.1016/j.jinf.2019.11.008
30. Hughes GJ, Gorton R. Inequalities in the incidence of infectious disease in the north east of England: a population-based study. Epidemiol Infect. 2015;143:189–201. https://doi.org/10.1017/S0950268814000533
31. Millett ER, Quint JK, Smeeth L, Daniel RM, Thomas SL. Incidence of community-acquired lower respiratory tract infections and pneumonia among older adults in the United Kingdom: a population-based study. PLoS One. 2013;8:e75131. https://doi.org/10.1371/journal.pone.0075131
32. Acosta CD, Harrison DA, Rowan K, Lucas DN, Kurinczuk JJ, Knight M. Maternal morbidity and mortality from severe sepsis: a national cohort study. BMJ Open. 2016;6:e012323. https://doi.org/10.1136/bmjopen-2016-012323
33. McQuaid F, Jones C, Stevens Z, Plumb J, Hughes R, Bedford H, et al. Factors influencing women's attitudes towards antenatal vaccines, group B *Streptococcus* and clinical trial participation in pregnancy: an online survey. BMJ Open. 2016;6:e010790. https://doi.org/10.1136/bmjopen-2015-010790
34. Public Health England. English Surveillance Programme for Antimicrobial Utilisation and Resistance (ESPAUR). London: Public Health England; 2018.
35. Public Health England. Laboratory surveillance of *Staphylococcus aureus* bacteraemia in England, Wales and Northern Ireland: 2017. London: Public Health England; 2018.
36. Public Health England. Laboratory surveillance of *Escherichia coli* bacteraemia in England, Wales and Northern Ireland: 2017. London: Public Health England; 2018.
37. High KP, Edwards MS, Baker CJ. Group B streptococcal infections in elderly adults. Clin Infect Dis. 2005;41:839–47. https://doi.org/10.1086/432804
38. UK Standards for Microbiology Investigations. Investigation of bronchoalveolar lavage, sputum and associated specimens. London: Public Health England; 2019.

Address for correspondence: Simon M. Collin, Healthcare-Associated Infection and Antimicrobial Resistance Division, National Infection Service, Public Health England, 61 Colindale Ave, London NW9 5EQ, UK; email: simon.collin@phe.gov.uk

Zoonotic Alphaviruses in Fatal and Neurologic Infections in Wildlife and Nonequine Domestic Animals, South Africa

Jumari Steyn, Isabel Fourie, Johan Steyl, June Williams, Voula Stivaktas, Elizabeth Botha, Stefanie van Niekerk, Bjorn Reininghaus, Marietjie Venter

Alphaviruses from Africa, such as Middelburg virus (MIDV), and Sindbis virus (SINV), were detected in horses with neurologic disease in South Africa, but their host ranges remain unknown. We investigated the contribution of alphaviruses to neurologic infections and death in wildlife and domestic animals in this country. During 2010–2018, a total of 608 clinical samples from wildlife and nonequine domestic animals that had febrile, neurologic signs or unexplained deaths were tested for alphaviruses. We identified 32 (5.5%) of 608 alphavirus infections (9 SINV and 23 MIDV), mostly in neurotissue of wildlife, domestic animals, and birds. Phylogenetic analysis of the RNA-dependent RNA polymerase gene confirmed either SINV or MIDV. This study implicates MIDV and SINV as potential causes of neurologic disease in wildlife and nonequine domestic species in Africa and suggests a wide host range and pathogenic potential.

Alphaviruses (family *Togaviridae*) have been recognized as major emerging viruses. New World alphaviruses, such as Western equine encephalitis virus, Eastern equine encephalitis virus, and Venezuelan equine encephalitis virus, are traditionally associated with severe disease, such as encephalitis and a high mortality rate in humans and horses in the Americas and Australia (*1*,*2*). Old World alphaviruses, such as o'nyong nyong virus, chikungunya virus, and Sindbis virus (SINV), are associated mostly with arthralgia, although rare infections with neurologic disease have been reported in humans and equids (*3*). Chikungunya virus was responsible for millions of human infections in new territories, and although the case-fatality rate was low, outbreaks resulted in major illness and long-term sequelae in affected persons (*4*,*5*). Old and New World alphaviruses cluster in separate phylogenetic groups (*6*), but limited information is available about pathogenesis and host range of alphaviruses from Africa and pathogenesis in animals.

SINV is a human pathogen that is distributed across Africa, Europe, Australia, and Asia (*7*). Large outbreaks of infection have been recorded in humans in South Africa since 1974 (*8*). Limited studies on the disease potential of SINV in animals have been conducted. The reservoir hosts are primarily migratory birds (*9*,*10*); various *Culex* mosquitoes are the main vectors. Recent reports suggest that SINV might cause febrile and neurologic disease in horses in South Africa (*11*,*12*).

Middelburg virus (MIDV) was discovered in the late 1950s in *Aedes* species mosquitoes (*13*), although it was only linked to disease in 1990 (*14*) after MIDV was isolated from a horse with signs of infection with African horse sickness virus in Zimbabwe (*14*). Since that time, MIDV has been implicated as the etiologic agent of neurologic and febrile disease in horses in South Africa (*11*). Seroprevalence studies in South Africa during 1959–1960 identified MIDV antibodies in humans, cattle, sheep, and goats (*15*,*16*). The vector status of MIDV is largely unknown; only *Ae. caballus* and *Mansonia africana* mosquitoes have been implicated (*17*). Little is known about the epidemiology of MIDV, including confirmed reservoir hosts, susceptible species, and zoonotic potential. MIDV, recombinant virus originating from Semliki Forest virus and Mayaro virus (*14*), forms its own complex, rather than clustering within the Semliki Forest virus complex (*6*).

Identification of MIDV and SINV as possible neurologic pathogens in horses in South Africa prompted

Author affiliation: University of Pretoria, Pretoria, South Africa (J. Steyn, I. Fourie, J. Steyl, J. Williams, V. Stivaktas, E. Botha, S. van Niekerk, M. Venter); Mpumalanga Veterinary Services, Middelburg, South Africa (B. Reininghaus)

DOI: https://doi.org/10.3201/eid2606.191179

the investigation of undiagnosed neurologic and febrile disease or sudden unexplained death in wildlife, nonequine domestic animals, and birds. The purpose of our study was to investigate the host range and association of alphaviruses from Africa with neurologic disease and death, as well as to increase knowledge on pathogenesis and the zoonotic potential of these 2 viruses.

Materials and Methods

Clinical Infections

This study forms part of an ongoing passive surveillance study to detect zoonotic arboviruses in South Africa. A total of 608 EDTA-treated blood or postmortem specimens from animal species other than horses that had neurologic disease, acute febrile illness of unknown origin, or sudden unexpected death during February 2010–September 2018 in South Africa were submitted to the Centre for Viral Zoonoses, Department of Medical Virology, University of Pretoria (Pretoria, South Africa). Clinical cases were submitted by wildlife veterinarians and pathologists who identified cases that fit the case definition of febrile or neurologic signs or sudden unexpected deaths of unknown origin. EDTA-treated blood or serum samples were submitted when animals were alive, whereas tissues were submitted if the animal died. Preferred tissue type was brain matter or spinal cord and visceral organs, including lungs, spleen, and liver samples. The study was approved under Section 20 (no. 12/11/1/1) by the Department of Forestry and Fisheries and by the Animal Ethics Committee (no. V057–15 and H12/16).

We performed full necropsy examination at the Section of Pathology, Department of Paraclinical Sciences, Faculty of Veterinary Science, University of Pretoria, for animals that had clinically progressive quadriparesis, apparently normal mentation, and positive results for MIDV or SINV by reverse transcription PCR. We collected a wide range of organs and tissues from all wildlife cases and preserved the samples in 10% neutral buffered formalin for histologic examination. We microscopically examined routinely prepared, hematoxylin and eosin–stained (*18*) histologic sections by using a standard light microscope.

RNA Extraction and PCR

We extracted all specimens under Biosafety Level 3 (BSL-3) conditions in the Department of Forestry and Fisheries compliant BSL-3 laboratory at the Centre for Viral Zoonoses, University of Pretoria. We extracted virus RNA from blood or body fluids by using a Viral Mini Kit (QIAGEN, https://www.qiagen.com) according to the manufacturer's instructions and virus RNA from tissue samples by using the RNeasy Kit (QIAGEN). We analyzed all clinical specimens by using genus-specific nested real-time PCRs (*11*). We designed specific MIDV (forward ^{6285}5′-GCAGCCTTTTGTCCGTCYAA-23^{6305} and reverse ^{6633}5′-GGCTTCAAGTCRTAGGTTT-3′^{6614}) and SINV (forward ^{6285}5′-GCAACCTTYTGCCCCGCYAA-′3^{6305} and reverse ^{6633}5′-GGGACCAAATTATRCGTCT-32^{6613}) nested primers to increase the RNA-dependent RNA polymerase gene region from 198 bp to 348 bp for phylogenetic analysis by using the same conditions as in the alphavirus PCR (*11*). We designed primers on the basis of MIDV strain SAE_25/11 (GenBank accession no. KF680222) and SINV strain SA_AR86 (accession no. U38305). For differential diagnosis, we also screened all specimens for flaviviruses (*19*), equine encephalosis virus (*20*), and Shuni virus (*21*).

Sanger Sequencing and Phylogenetic Analysis

Arbovirus PCR-positive results were confirmed by sequencing at Inqaba Biotec (https://www.inqababiotec.co.za). We analyzed sequence data by using CLC Main Workbench 8 (QIAGEN) and MEGA 6.06 software (https://www.megasoftware.net). We performed multiple sequence alignments by using MAFFT version 7 software (http://mafft.cbrc.jp) with default parameters and used them to assemble sequences. We conducted maximum-likelihood analysis by using RaxML (*22*) and invoking the auto-MRE bootstopping function by applying a generalized time-reversible model with gamma distribution of rates across sites. We calculated bootstrap support values by using the autoMRE bootstopping criterion in RaxML. We conducted P-distance analysis in MEGA 6.06 and determined average within mean group distance between MIDV and SINV strains. We submitted sequences >200 bp to GenBank.

Virus Isolation

We subjected all PCR-positive samples to virus isolation on African green monkey kidney cells (Vero) and baby hamster kidney cells (BHK-21 clone 3). We maintained cells in Earle minimum essential medium (EMEM) containing L-glutamine (Lonza, https://www.lonza.com), MycoZap CL-Plus (Lonza), 10% fetal calf serum (FCS) (Lonza) for Vero or 20% FCS for BHK-21 clone 3 cells in an Intercool Incubator (Lasec, https://www.lasec.com) at 37°C and an atmosphere of 5.0% CO_2.

We performed isolations by using EMEM containing 10% fetal calf serum and Mycozap CL-Plus for

Vero cells and 20% fetal calf serum and Mycozap CL-Plus for BHK-21 clone 3 cells and incubated at 37°C in an atmosphere of 5% CO_2. We inoculated blood or serum samples (200 μL) from animals directly onto phosphate-buffered saline (PBS)–washed cells, incubated for 1 h, and washed once with PBS, then added 2% EMEM. We cut tissue specimens into pieces (≈5 mg) and homogenized with sterile glass beads (Merck, https://www.merck.com) at 100 × *g* for 6 min by using a TissueLyzer (QIAGEN). We then centrifuged homogenates at 1,000 × *g* for 10 min to collect debris. We used 200 μL of supernatant to infect PBS-washed cells, incubated them for 1 h, and then added 2% EMEM. We passaged cultures 3–4 times at 7-day intervals, observing monolayers daily for cytopathic effect. Between passages, we froze cultures at –80°C, thawed 3 times, and clarified by centrifuging at 1,000 × *g* for 5 min.

Data Analysis

We performed data and statistical analyses by using Epi Info version 7.2.0.1 (https://www.cdc.gov/epiinfo/index.html) and a Fisher exact test with 95% CIs and odds ratios (ORs) to calculate the association between clinical signs and infection. We excluded animals that were found dead (n = 76) or were aborted (n = 23) or stillborn (n = 13) from OR analysis.

Results

During the 9-year study period, we tested 608 animals that had unsolved neurologic, febrile, and respiratory signs or sudden unexpected death. We detected MIDV in 23 (3.8%, 95% CI 2.4%–5.5%) animals and SINV in 9 (1.5%, 95% CI 0.5%–2.4%) (Table 1). We detected MIDV in wildlife (16/361; 4.4%, 95% CI 2.3%–6.6%), domestic animals (5/196; 2.6%, 95% CI 0.3%–4.8%), and wild birds (2/51; 3.9%, 95% CI 0%–9.3%) and SINV in wildlife (7/608; 1.1%, 95% CI 0.5%–3.4%) and domestic animals (2/196; 1%, 95% CI 0%–2.4%) (Table 1). We did not detect SINV in clinical samples from birds.

The 608 animals tested were from 99 animal species, of which 14 species were positive for MIDV or SINV (Table l). We detected MIDV in white rhinoceros (9.2%, 95% CI 2.2%–16.3%), buffalo (3.7%, 95% CI 0%–8.7%), domestic bovids (5.4%, 95% CI 0.8%–10.0%), warthogs (7.7%, 95% CI 0%–18.0%), lions (22.2%, 95% CI 0%–49.4%), birds (lemon dove and blue crane; 3.9%, 95% CI 0%–9.2%), sable antelopes (3.8%, 95% CI 0%–8.9%), waterbucks (33.3%, 95% CI 0%–86.7%),

Table 1. Samples from wildlife, nonequine domestic animals, and birds tested for alphavirus by using nested real-time PCRs specific for MIDV and SINV, South Africa*

Animal	No. tested	No. positive (%, 95% CI)	
		MIDV	SINV
Buffalo (*Syncerus caffra*)	54	2 (3.7, 0.0–8.7)	1 (1.9, 0.0–5.4)
Avian†	51	2 (3.9, 0.0–9.2)	0
Sable antelope (*Hippotragus niger*)	53	2 (3.8, 0.0–8.9)	2 (3.8, 0.0–8.9)
Warthog (*Phaecocherus africanus*)	26	2 (7.7, 0.0–18.0)	0
White rhinoceros (*Ceratotherium simum*)	65	6 (9.2, 2.2–16.3)	1 (1.5, 0.0–4.5)
Lion (*Panthera leo*)	9	2 (22.2, 0.0–49.4)	0
Waterbuck (*Kobus ellipsiprymnus*)	3	1 (33.3, 0.0–86.7)	0
Genet (*Genetta genetta*)	2	1 (50.0, 0.0–119.3)	1 (50.0, 0.0–119.3)
Giraffe (*Giraffa camelopardalis*)	6	0	1 (16.7, 0.0–46.5)
Blesbuck (*Damaliscus pygargus phillipsi*)	4	0	1 (25.0, 0.0–67.4)
Crocodile (*Crocodylus niloticus*)	12	0	0
Springbok (*Antidorcas marsupialis*)	4	0	0
Roan antelope (*Hippotragus equinus*)	3	0	0
Other antelope‡	82	0	0
Elephant (*Loxodonta africana*)	6	0	0
Equine (zebra/donkeys)§	10	0	0
Carnivores¶	17	0	0
Alpaca	8	0	0
Domestic bovid	93	5 (5.4, 0.8–10.0)	0
Domestic sheep	45	0	1 (2.2, 0.0–6.5)
Domestic and other porcine	5	0	1 (20.0, 0.0–46.5)
Camel	8	0	0
Goat	1	0	0
Wildlife	361	16 (4.4, 2.3–6.6)	7 (1.9, 0.5–3.4)
Domestic	196	5 (2.6, 0.3–4.8)	2 (1.0, 0.0–2.4)
Avian	51	2 (3.9, 0.0–9.2)	0
Total	608	23 (3.8, 2.4–5.5)	9 (1.5, 0.5–2.4)

*MIDV, Middelburg virus; SINV, Sindbis virus.
†Avian MIDV-positive: laughing dove (*Spilopelia senegalensis*) and blue crane (*Grus paradisea*).
‡Kudu, wildebeest, impala.
§Zebra and donkeys.
¶Jackal, hyena, wild dog, civet.

and genets (50%, 95% CI 0%–119.3%) (Table 1). SINV was detected in buffalo (1.9%, 95% CI 0%–5.4%), sable antelopes (3.8%, 95% CI 0%–8.9%), rhinoceroses (1.5%, 95% CI 0%–4.5%), giraffes (16.7%, 95% CI 0%–46.5), European wild boar (16.7%, 95% CI 0%–46.5%), sheep (2.2%, 95% CI 0%–6.5%), blesbucks (25%, 95% CI 0%–67.4%), and genets (50%, 95% CI 0%–119.3%) (Table 1). One co-infection with MIDV and SINV was reported in a genet (Table 1). Two white rhinoceroses had co-infections (MVA07/10 with MIDV and Shuni virus, MVA11/10 with MIDV and equine encephalosis virus). Two animals, a domestic bovid (ZRU176/14/2) and a buffalo (ZRU160/18), had co-infections with MIDV and West Nile virus.

All SINV-positive animals and 20 (87%) of 23 MIDV PCR-positive animals had virus detected in postmortem specimens (Table 2). MIDV was detected primarily in the central nervous system (CNS; 14/23, 60.9%), followed by visceral organs (10/23, 43.5%), blood (5/23, 21.7%), and respiratory organs (2/23, 8.7%). SINV was detected primarily in the CNS (5/9, 55.6%), visceral organs (3/9, 33.3%), respiratory organs (2/9, 22.2%) and cerebrospinal fluid (1/9, 11.1%). All clinically sick animals infected with MIDV (22/22) (p = 0.06) and SINV (6/6) (p = 1) had neurologic manifestations as a primary diagnostic sign (Table 2). Tongue paralysis (OR 32.5, 95% CI 2.9–368.3) was associated with SINV-positive animals (p<0.05) (Table 2). Three animals were found dead and subsequently found to be positive for MIDV (waterbuck) and SINV (buffalo and blesbuck), and an aborted Merino sheep fetus was positive for SINV (Table 2).

Most MIDV infections were reported during 2010 (5/62, 8.1%) and 2015 (5/60, 8.3%), followed by 2017 (4/90, 4.4%), 2014 (3/69, 4.3%), 2018 (3/75, 4.0%), 2012 (1/30, 3.3%), and 2011 (2/80, 2.5%). No MIDV infections were detected during 2016 (Figure 1). SINV infections were highest in 2018 (4/75, 5.3%), followed

Table 2. Clinical signs associated with MIDV and SINV infections in wildlife, nonequine domestic animals, and birds, South Africa*

Virus, sign, and outcome	No. (%) positive, n = 22	No (%) negative, n = 474	Odds ratio (95% CI)	p value
MIDV				
Sign				
Fever	4 (18.2)	42 (8.9)	2.3 (0.7–7.1)	0.1
Neurologic signs	22 (100.0)	404 (85.2)	ND	0.06
Ataxia	4 (18.2)	100 (21.1)	0.8 (0.2–2.5)	1.0
Paralysis	4 (18.2)	60 (12.7)	1.5 (0.5–4.7)	0.7
Quadriparesis	6 (27.3)	114 (24.1)	1.8 (0.5–3.1)	0.8
Tongue paralysis	0	4 (0.8)	ND	1.0
Recumbency	4 (18.2)	101 (21.3)	0.8 (0.3–2.5)	1.0
Dyspnea	0	81 (17.1)	ND	1.0
Hemorrhage	0	11 (2.3)	ND	1.0
Congenital deformities	0	7 (1.5)	ND	1.0
Blindness	0	11 (2.3)	ND	1.0
Icterus	0	2 (0.4)	ND	1.0
Seizure	0	29 (6.1)	ND	1.0
Outcome	n = 23	n = 585		
Sudden unexpected death	1 (4.4)	75 (12.8)	0.3 (0.0–2.3)	0.3
Abortion	0	23 (4.1)	ND	1.0
Stillbirth	0	13 (2.7)	ND	1.0
Fatal	20 (87.0)	501 (85.6)	1.1 (0.3–3.9)	1.0
SINV	n = 6	n = 490		
Sign				
Fever	1 (16.7)	45 (9.2)	2.0 (0.2–17.3)	0.5
Neurologic signs	6 (100.0)	420 (85.7)	ND	1.0
Ataxia	2 (33.3)	102 (20.8)	1.9 (0.3–10.5)	0.6
Paralysis	1 (16.7)	63 (12.9)	1.4 (0.2–11.8)	0.7
Quadriparesis	0	120 (24.5)	ND	1.0
Tongue paralysis	1 (16.7)	3 (0.6)	32.5 (2.9–368.3)	<0.05
Recumbency	2 (33.3)	103 (21.0)	1.9 (0.3–10.4)	0.6
Dyspnea	1 (16.7)	80 (16.3)	1.0 (0.1–89)	1.0
Hemorrhage	0	11 (2.2)	ND	1.0
Congenital deformities	0	7 (1.4)	ND	1.0
Blindness	0	11 (2.4)	ND	1.0
Icterus	0	2 (0.4)	ND	1.0
Seizure	0	29 (5.9)	ND	1.0
Outcome	n = 9	n = 599		
Sudden unexpected death	2 (22.2)	74 (12.7)	0.5 (0.1–2.4)	0.3
Abortion	1 (11.1)	22 (3.8)	3.3 (0.4–27.4)	0.3
Stillbirth	0	13 (2.7)	ND	0.8
Fatal	9 (100.0)	512 (85.5)	ND	1.0

*ND, not determined; MIDV, Middelburg virus; SINV, Sindbis virus.

by 2014 (2/69, 2.9%), 2013 (1/50, 2%), and 2010 and 2015 (each 1/67, 1.5%). No SINV infections were reported during 2011, 2012, 2016, and 2017 (Figure 1). MIDV positivity was highest in April (5/55, 9.1%), followed by November (3/38, 7.9%) (Figure 1). No positive animals were reported during February, October, or December. SINV positivity was highest in September (3/65, 4.6%), followed by February (2/48, 4.2%) (Figure 1). Samples were received from all 9 provinces, although positive samples were detected in only 6 provinces (Figure 2).

No specific macroscopic lesions could be demonstrated at necropsy for cases submitted to the Section of Pathology, Faculty of Veterinary Science, University of Pretoria. Similar to other parenchymal tissues examined, no distinct cytologic nor architectural abnormalities could be demonstrated in the CNS of examined cases. Some of these animals died after a short period (<3 days) of recumbency. In these cases, secondary factors, such as dehydration and unrelenting high levels of stress, were suspected to contribute to death. In some instances, animals with severe cases were euthanized for humane reasons or as part of disease management for elective necropsy to determine the cause of outbreaks of neurologic signs in wildlife.

Phylogenetic analysis of the partial nonstructural protein 4 (nsP4) gene region (348 bp) confirmed all virus-positives cases as being infected with MIDV or SINV (Figure 3). Maximum-likelihood analysis resulted in a topology lacking strong support in deeper nodes for several alphavirus groups. However, we obtained bootstrapping values of 95 for MIDV clades and 93 for SINV clades (Figure 3). The MIDV complex had 2 separate clades within the group, and viruses detected in lions (Carnivora) were sister clades to viruses detected in rhinoceroses, warthogs, buffalo, sable antelopes, domestic bovids, and blue cranes, which clustered together (bootstrap value = 70) (Figure 3) and had a between-group mean distance of 96%. The SINV clade (Western equine encephalitis virus complex) also formed a separate cluster with the positive samples primarily from the 2018 group that was separate from positive samples reported in 2010, 2013, and 2014 (bootstrap value = 66) (Figure 3) and had a between group mean distance of 93.7%. Within-group mean nucleotide distances were 98.4% for MIDV and 95.4% for SINV.

Discussion

We identified a total of 32 alphavirus infections in wildlife, nonequine domestic animals, and 2 birds that had neurologic or febrile signs or unexplained death over a period of 9 years (2010–2018) as MIDV (n = 23) or SINV (n = 9). Detection of these viruses in the CNS indicates that they are able to cross the blood–brain barrier and suggests that they might cause pathologic changes, neurologic disease, and death in infected animals. Detection of viral RNA in respiratory organs and visceral organs suggest spread of these viruses throughout the body. The success rate of virus isolation from neural tissue is low because death is often the end stage of disease concurrent with a low virus titer, which can often only be detected by nested PCR. Virus isolation can also be related to the quality of clinical specimens received from wildlife and domestic animals, which were often found dead in remote areas and took some time to reach the laboratory, as compared with equine cases, which are often detected earlier by owners during the stage of clinical disease and therefore are sampled earlier.

All cases were accompanied by a case investigation form with clinical and epidemiologic data recorded by the submitting veterinarian. All animals that had clinical information available had neurologic signs suggesting infection with MIDV and SINV as likely etiologies of neurologic disease (p = 0.06) despite the small sample size of alphavirus-positive

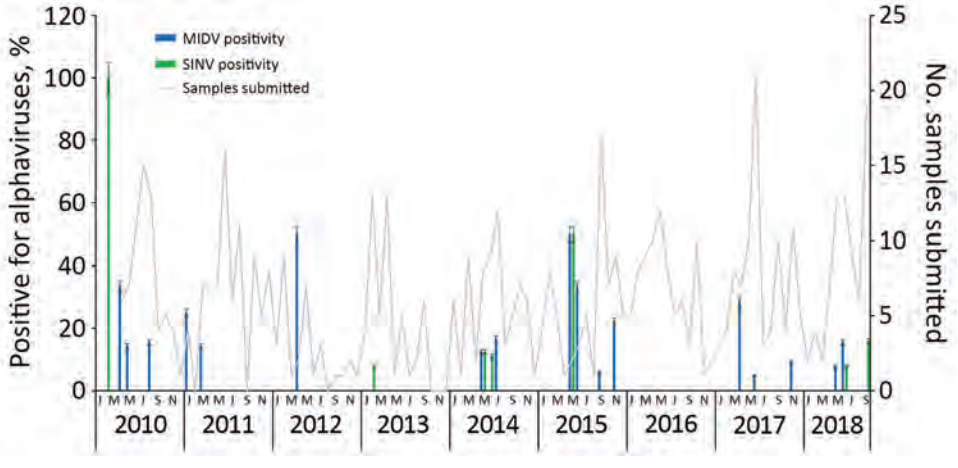

Figure 1. Seasonal detection of 32 alphavirus-positive infections of wildlife, nonequine domestic animals and birds, South Africa, February 2010–September 2018. Error bars indicate 95% CIs. MIDV, Middelburg virus; SINV, Sindbis virus.

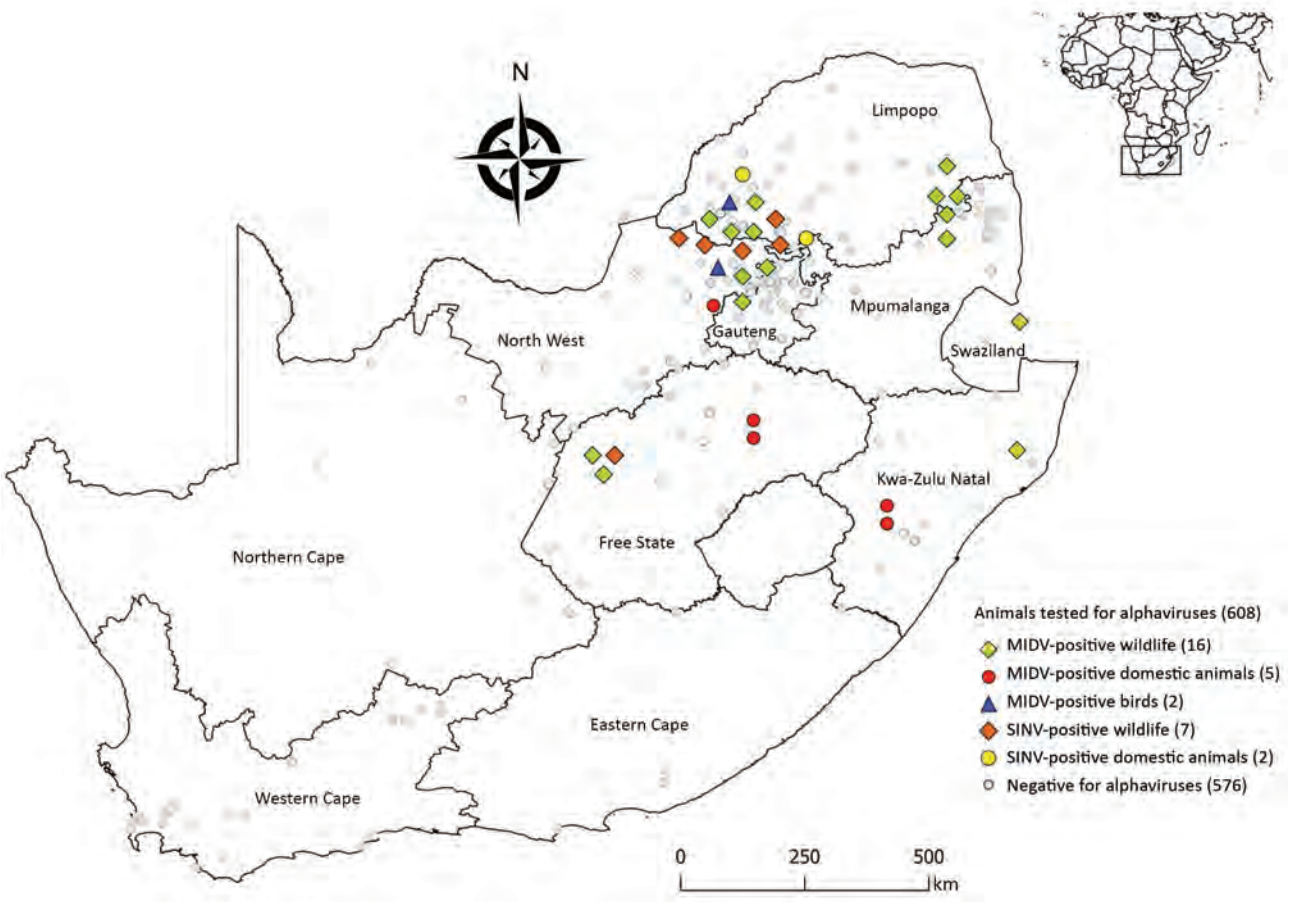

Figure 2. Locations of MIDV and SINV PCR-positive and –negative samples from wildlife, nonequid domestic animals, and avian species, South Africa, 2010–2018. Inset shows location of South Africa in Africa. Values in parentheses are number of animals. MIDV, Middelburg virus; SINV, Sindbis virus.

cases compared with alphavirus-negative cases. None of the other signs could clearly be associated with these viruses because of the small sample size of virus-positive animals. This finding suggests that these Old World alphaviruses might have similar characteristics to their New World relatives in some species (*11*,*23*). SINV was strongly associated with tongue paralysis, as observed in the giraffe (ZRU54_13). Although the overall positivity rate was low for samples tested during this study, specific species were positive more frequently for alphaviruses. These species include white rhinoceros, buffalo, and sable antelope, all of which had ≥1 infections for MIDV and SINV.

MIDV was reported more frequently in white rhinoceroses and domestic bovids. SINV was not detected in domestic bovids but was detected in sheep and domestic porcines. In a few instances, samples from an animal were submitted from a cluster of animal deaths and apparent outbreak scenarios. A MIDV-positive white rhinoceros (MVA004/10) was given a diagnosis after 9 rhinoceroses from the same population had similar clinical signs. All animals were subjected to postmortem investigation over a 2-year duration at the Faculty of Veterinary Science, University of Pretoria. CNS tissues from an adult white rhinoceros (MVA007/10) from Broederstroom, North West Province, showed positive results for MIDV and equine encephalosis virus. A rhinoceros calf that was kept in the same boma (livestock enclosure) had similar signs and had died 5 days earlier. A warthog (MVA51/10) was part of a disease outbreak involving ≈50 similar cases in contact animals of the same species in Marekele National Park, Limpopo Province. All warthogs of the specific sounder (group) showed signs of ataxia that lasted 3–7 days, after which some recovered and some died. A captive-bred African buffalo calf from Bloemfontein, Free State Province, also died after paralysis developed, and an uncountable number of animals in the herd were positive for MIDV. These 3 cases of disease can be regarded as disease outbreaks affecting multiple contact animals from the same epizootic unit.

Phylogenetic analyses based on the partial nsP4 gene support the monophyletic grouping of SINV with the New World viruses in the Western equine encephalitis virus complex (*24*,*25*). The analysis also supports the grouping of MIDV strains into a genetic complex, with a 95% bootstrap support (*23*), with MIDV sequences obtained from 2 lions (ZRU209_15 and ZRU211_15), forming a sister

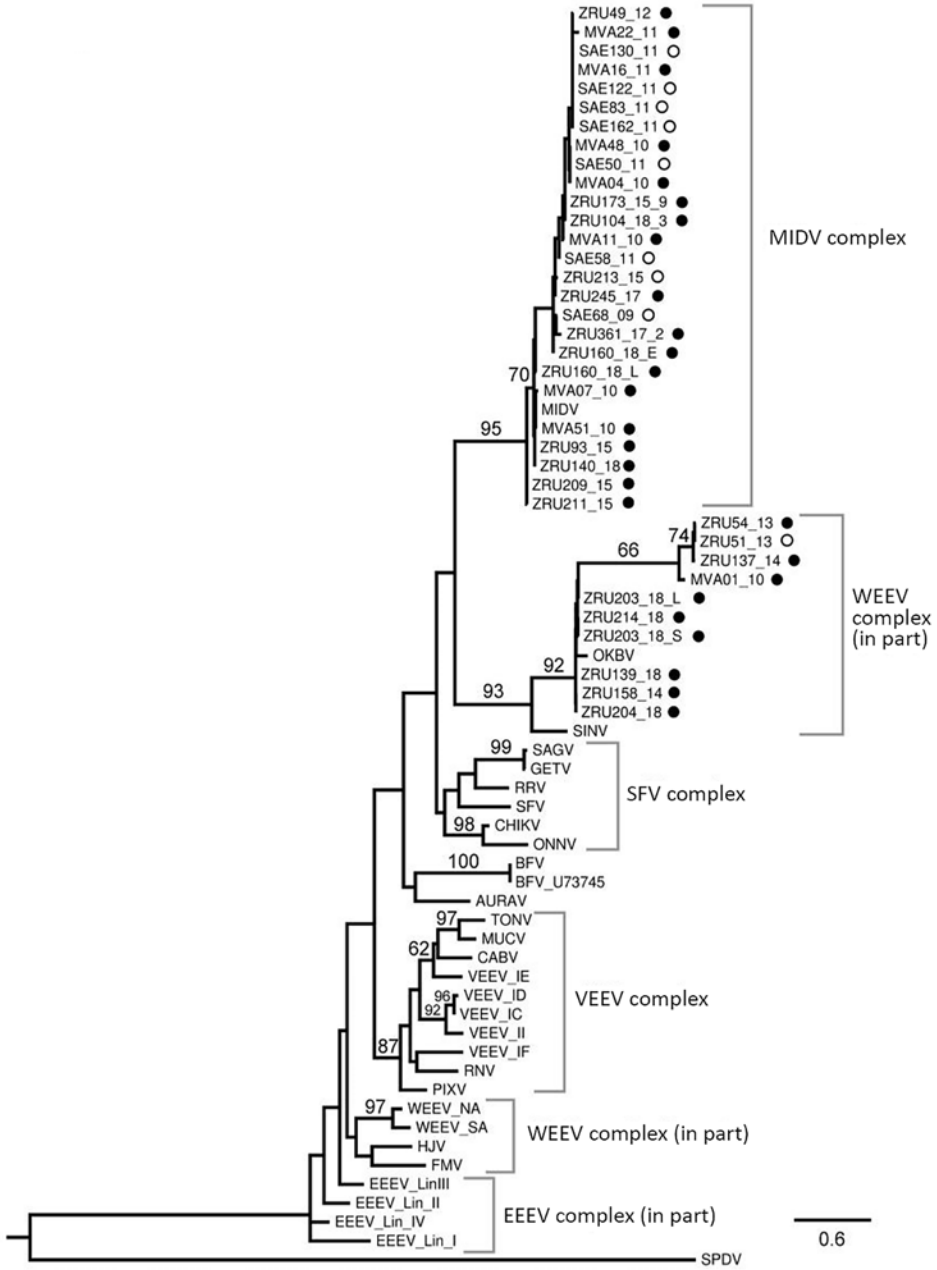

Figure 3. Phylogram of the RNA-dependent RNA polymerase gene (348-bp fragment) of alphaviruses rooted at the midpoint and created by using maximum-likelihood analysis (67 taxa, generalized time-reversible model with gamma distribution of rates across sites). Black circles indicate wildlife, domestic animals, and birds from South Africa, February 2010–September 2018, and open circles indicate previously reported virus-positive horses (*11*). Numbers on branches are bootstrap support values. Values are shown if they are >60. Sample identification and GenBank Accession numbers: MVA51/10, MK114099; ZRU139/18, MK114091; ZRU140/18, MK114087; ZRU158/14, MK114089; ZRU160/18, MK114092, ZRU203/18_Lung, MK114094; ZRU203/18_Spleen, MK114093; ZRU204/18, MK114095; ZRU209/15, MK114096; ZRU211/15, MK114097; ZRU214/18, MK114098; ZRU54/13, MK114090; ZRU93/15, MK114088. Reference strain, name, accession number, and origin are as described by Forrester et al. (*6*). Scale bar indicates nucleotide substitutions per site. EEEV, Eastern equine encephalitis virus; MIDV, Middelburg virus; SFV, Semliki Forest virus; SPDV, salmon pancreas disease virus; WEEV, Western equine encephalitis virus.

group to the other virus-positive animals. A mean nucleotide distance of 96% was observed between the 2 groups. The 2 MIDV-positive lions originated from Mpumalanga Province, and the rest of the MIDV-positive animals were from Gauteng, Limpopo, Free State, Northern Cape, Western Cape, and KwaZulu-Natal Provinces. This clade groups with MIDV strains previously identified in horses from these areas (*11*). These findings could indicate geographic clustering between strains.

Similar results were obtained for the SINV strains, although positive samples clustered according to year, with a between group mean nucleotide distance of 93.7%, possibly indicating changes in the strains circulating over time. Because birds are believed to be reservoir hosts for SINV, new strains might be introduced through migratory birds. P-distance analysis showed little or no nucleotide variation in the nsP4 gene region for MIDV and SINV strains respectively identified in this study, apart from the limited differences described above, indicating genetically similar strains. However, this gene segment is highly conserved, and sequence lengths were relatively short (198–348 bp). Attempts to amplify more gene regions, as well as virus isolation, were not successful.

The results of this study demonstrate that alphaviruses might be associated with neurologic disease in wildlife, nonequine domestic animals, and birds in South Africa. Wide geographic distribution of MIDV and SINV in Africa suggests that this distribution should be investigated in other regions. Humans living near wildlife and livestock, such as domestic bovids, sheep, and porcines, might have similar exposure to mosquito vectors and should therefore also be monitored for potential zoonotic infections. SINV has been shown to have birds as its reservoir host and is a well-known human pathogen in South Africa, although most described cases are nonneurologic and associated with febrile disease or arthralgia. Our study identified SINV in neural tissue of various wildlife and nonequine domestic species that had neurologic signs of infection. The geographic range, prevalence of infection in various species, species-specific differences, and seroprevalence need to be determined to define the epidemiology of these pathogens. Serologic evidence for MIDV in humans has been demonstrated in South Africa (*26*), although such evidence is less informative for SINV. This finding might be caused by host range preference and spread of the vectors associated with these viruses.

Reservoir hosts for MIDV are unknown. Our suggestion of a higher prevalence of MIDV relative to SINV warrants further investigation. Widespread distribution of MIDV suggest birds might play a role in the spread of this virus. However, a dove and blue crane were the only virus-positive birds identified, both submitted as postmortem specimens. Further investigation is needed regarding the potential of the identified species to function as reservoir and amplification hosts and potential for transmission of virus to vectors. Spillover of MIDV into humans through adaption to additional vectors should be monitored. Investigation of neurologic cases and deaths in wildlife and domestic animals suggested that most cases occur during January–July—from the second half of the summer months to late autumn or early winter in warmer parts of the country, where many wildlife reside—after which vector numbers usually decrease because of colder winter temperatures.

Future studies into the epidemiology of SINV and especially MIDV would greatly benefit from analysis of increased sample sizes or whole-genome sequencing, combined with serologic analyses of affected species, especially in outbreak investigations. Syndromic surveillance for febrile and neurologic disease in sensitive species might act as an early warning system for outbreaks of emerging and reemerging arboviruses and predict outbreaks in humans (*27*,*28*).

A limitation of our study is that all other possible infectious and noninfectious etiologies could not be excluded by comprehensive investigations for all cases, suggesting that the causative link with clinical signs still has to be regarded with caution. Also, serum samples from PCR-positive animals were not available because most animals were tested postmortem, which limited validation by serologic assays for this study. However, use of serum samples should be a focus of future investigations.

Most emerging zoonotic diseases are believed to be caused by pathogens that originate from wildlife (*29*). Wildlife might either assume the role of reservoir or amplification host with or without clinical disease or be dead end or incidental hosts that might have severe disease (*30*,*31*). To our knowledge, MIDV and SINV neurologic infections have not been reported in wildlife and nonequine domestic animals. Our study demonstrated a wide host range for these viruses, and detection of these viruses directly in the neurologic tissue in several cases suggests crossing of the blood–brain barrier and MIDV and SINV as the probable cause of neurologic signs. This finding highlights the need for surveillance of alphaviruses to prevent spillover events and outbreaks in humans.

Acknowledgments

We thank all veterinarians and veterinary pathologists across South Africa for submitting samples and Louwtjie Snyman for assisting with phylogenetic analyses. This study was cleared by section 20 (12/11/1/1) approval through the Department of Agriculture Forestry and Fisheries, by the animal ethics committee (V057-15) (J.S.) and (H12/16) (M.V.) of the University of Pretoria and the PhD research committee. Buffalo samples were transported under a Red Cross permit (LDK2016/9/1) to the BSL3 laboratory.

The study was supported by the US Centers for Disease Control and Prevention Global Disease Detection grant for zoonotic arboviruses (grant no. 1U19GH000571-01-GDD), Non-Research CoAg and National Health Service Laboratory project 23, and University of Pretoria Zoonotic Arbo and Respiratory virus program income-generated funds. J.S. received doctoral scholarships from the National Research Foundation (grant no. 95175), the Meat Industry Trust (grant no. IT8114/98), and the Poliomyelitis Research Foundation (grant no. 15/112), as well as a partial studentship from the US-CDC Cooperative Agreement (no. 5 NU2GGH001874-02-00) with the University of Pretoria.

About the Author

Dr. Steyn is a virologist at the Centre for Viral Zoonoses, University of Pretoria, Pretoria, South Africa. Her primary research interest is investigating arboviruses with zoonotic potential at human/animal interface areas.

References

1. Aguilar PV, Estrada-Franco JG, Navarro-Lopez R, Ferro C, Haddow AD, Weaver SC. Endemic Venezuelan equine encephalitis in the Americas: hidden under the dengue umbrella. Future Virol. 2011;6:721–40. https://doi.org/10.2217/fvl.11.50
2. Lambert AJ, Martin DA, Lanciotti RS. Detection of North American eastern and western equine encephalitis viruses by nucleic acid amplification assays. J Clin Microbiol. 2003;41:379–85. https://doi.org/10.1128/JCM.41.1.379-385.2003
3. Zacks MA, Paessler S. Encephalitic alphaviruses. Vet Microbiol. 2010;140:281–6. https://doi.org/10.1016/j.vetmic.2009.08.023
4. Powers AM, Brault AC, Tesh RB, Weaver SC. Re-emergence of chikungunya and O'nyong-nyong viruses: evidence for distinct geographical lineages and distant evolutionary relationships. J Gen Virol. 2000;81:471–9. https://doi.org/10.1099/0022-1317-81-2-471
5. Wahid B, Ali A, Rafique S, Idrees M. Global expansion of chikungunya virus: mapping the 64-year history. Int J Infect Dis. 2017;58:69–76. https://doi.org/10.1016/j.ijid.2017.03.006
6. Forrester NL, Palacios G, Tesh RB, Savji N, Guzman H, Sherman M, et al. Genome-scale phylogeny of the alphavirus genus suggests a marine origin. J Virol. 2012;86:2729–38. https://doi.org/10.1128/JVI.05591-11
7. Laine M, Luukkainen R, Toivanen A. Sindbis viruses and other alphaviruses as cause of human arthritic disease. J Intern Med. 2004;256:457–71. https://doi.org/10.1111/j.1365-2796.2004.01413.x
8. McIntosh B, Jupp P, Dos Santos I, Meenehan G. Epidemics of West Nile and Sindbis viruses in South Africa and *Culex* (*Culex*) *univittatus*. South African Journal of Science. 1976;72:295–300.
9. Lwande OW, Obanda V, Bucht G, Mosomtai G, Otieno V, Ahlm C, et al. Global emergence of Alphaviruses that cause arthritis in humans. Infect Ecol Epidemiol. 2015;5:29853. https://doi.org/10.3402/iee.v5.29853
10. Burt FJ, Goedhals D, Mathengtheng L. Arboviruses in southern Africa: are we missing something? Future Virol. 2014;9:993–1008. https://doi.org/10.2217/fvl.14.87
11. van Niekerk S, Human S, Williams J, van Wilpe E, Pretorius M, Swanepoel R, et al. Sindbis and Middelburg old world alphaviruses associated with neurologic disease in horses, South Africa. Emerg Infect Dis. 2015;21:2225–9. https://doi.org/10.3201/eid2112.150132
12. Kokernot RH, Smithburn KC, Weinbren MP. Neutralizing antibodies to arthropod-borne viruses in human beings and animals in the Union of South Africa. J Immunol. 1956;77:313–23.
13. Kokernot RH, De Meillon B, Paterson HE, Heymann CS, Smithburn KC. Middelburg virus; a hitherto unknown agent isolated from *Aedes* mosquitoes during an epizootic in sheep in the eastern Cape Province. S Afr J Med Sci. 1957;22:145–53.
14. Attoui H, Sailleau C, Mohd Jaafar F, Belhouchet M, Biagini P, Cantaloube JF, et al. Complete nucleotide sequence of Middelburg virus, isolated from the spleen of a horse with severe clinical disease in Zimbabwe. J Gen Virol. 2007;88:3078–88. https://doi.org/10.1099/vir.0.83076-0
15. Smithburn KC, Kokernot RH, Heymann CS, Weinbren MP, Zentkowsky D. Neutralizing antibodies for certain viruses in the sera of human beings residing in northern Natal. S Afr Med J. 1959;33:555–61.
16. Kokernot RH, Smithburn KC, Kluge E. Neutralizing antibodies against arthropod-borne viruses in the sera of domestic quadrupeds ranging in Tongland, Union of South Africa. Ann Trop Med Parasitol. 1961;55:73–85. https://doi.org/10.1080/00034983.1961.11686021
17. Hubálek Z, Rudolf I, Nowotny N. Arboviruses pathogenic for domestic and wild animals. Adv Virus Res. 2014;89:201–75. https://doi.org/10.1016/B978-0-12-800172-1.00005-7
18. Bancroft JD, Gamble M, editors. 2002. Theory and practice of histological techniques. Edinburgh: Churchill Livingstone; 2002.
19. Zaayman D, Human S, Venter M. A highly sensitive method for the detection and genotyping of West Nile virus by real-time PCR. J Virol Methods. 2009;157:155–60. https://doi.org/10.1016/j.jviromet.2008.12.014
20. van Niekerk M, Freeman M, Paweska JT, Howell PG, Guthrie AJ, Potgieter AC, et al. Variation in the NS3 gene and protein in South African isolates of bluetongue and equine encephalosis viruses. J Gen Virol. 2003;84:581–90. https://doi.org/10.1099/vir.0.18749-0
21. Van Eeden C, Zaayman D, Venter M. A sensitive nested real-time RT-PCR for the detection of Shuni virus. J Virol Methods. 2014;195:100–5. https://doi.org/10.1016/j.jviromet.2013.10.008
22. Stamatakis A. RAxML version 8: a tool for phylogenetic analysis and post-analysis of large phylogenies. Bioinformatics. 2014;30:1312–3. https://doi.org/10.1093/bioinformatics/btu033
23. Forrester NL, Palacios G, Tesh RB, Savji N, Guzman H, Sherman M, et al. Genome-scale phylogeny of the alphavirus

genus suggests a marine origin. J Virol. 2012;86:2729–38. https://doi.org/10.1128/JVI.05591-11
24. Powers AM, Brault AC, Shirako Y, Strauss EG, Kang W, Strauss JH, et al. Evolutionary relationships and systematics of the alphaviruses. J Virol. 2001;75:10118–31. https://doi.org/10.1128/JVI.75.21.10118-10131.2001
25. Weaver SC, Kang W, Shirako Y, Rumenapf T, Strauss EG, Strauss JH. Recombinational history and molecular evolution of western equine encephalomyelitis complex alphaviruses. J Virol. 1997;71:613–23. https://doi.org/10.1128/JVI.71.1.613-623.1997
26. McIntosh B. The epidemiology of arthropod-borne viruses in southern Africa. Pretoria (South Africa): University of Pretoria; 1980.
27. Adams AP, Aronson JF, Tardif SD, Patterson JL, Brasky KM, Geiger R, et al. Common marmosets (*Callithrix jacchus*) as a nonhuman primate model to assess the virulence of eastern equine encephalitis virus strains. J Virol. 2008;82:9035–42. https://doi.org/10.1128/JVI.00674-08
28. de Novaes Oliveira R, Iamamoto K, Silva ML, Achkar SM, Castilho JG, Ono ED, et al. Eastern equine encephalitis cases among horses in Brazil between 2005 and 2009. Arch Virol. 2014;159:2615–20. https://doi.org/10.1007/s00705-014-2121-4
29. Bengis RG, Leighton FA, Fischer JR, Artois M, Mörner T, Tate CM. The role of wildlife in emerging and re-emerging zoonoses. Rev Sci Tech. 2004;23:497–511.
30. Lederberg J, Shope RE, Oaks SC Jr. Emerging infections: microbial threats to health in the United States. Washington: National Academies Press; 1992.
31. Morse SS. Factors and determinants of disease emergence. Rev Sci Tech. 2004;23:443–51. https://doi.org/10.20506/rst.23.2.1494

Address for correspondence: Marietjie Venter, Faculty of Health Sciences, Department of Medical Virology, University of Pretoria, PO Box 2034, Pretoria 0001, South Africa; email: marietjie.venter@up.ac.za

Effectiveness and Tolerability of Oral Amoxicillin in Pregnant Women with Active Syphilis, Japan, 2010–2018

Takeshi Nishijima, Kei Kawana, Ichio Fukasawa, Naoko Ishikawa, Melanie M. Taylor, Hiroshige Mikamo, Kiyoko Kato, Jo Kitawaki, Tomoyuki Fujii, Women's Health Care Committee, Japan Society of Obstetrics and Gynecology

We conducted a nationwide retrospective study in Japan to evaluate the effectiveness of oral amoxicillin or ampicillin as alternatives to injectable benzathine penicillin G for treating pregnant women with syphilis and preventing congenital syphilis (CS). We investigated 80 pregnant women with active syphilis treated with amoxicillin or ampicillin during 2010–2018. Overall, 21% (15/71) had pregnancies resulting in CS cases, and 3.8% (3/80) changed therapies because of side effects. Among 26 patients with early syphilis, no CS cases occurred, but among 45 with late syphilis, 15 (33%) CS cases occurred. Among 57 patients who started treatment ≥60 days before delivery, 8 (14%) had CS pregnancy outcomes. We found oral amoxicillin potentially ineffective for preventing CS cases among pregnant women with late syphilis but potentially effective in those with early syphilis. Prospective studies are needed to definitively evaluate the efficacy of amoxicillin for the treatment of pregnant women with syphilis to prevent CS.

Syphilis is a sexually transmitted infection that can be passed from mother to infant during pregnancy and childbirth. Mother-to-child transmission (MTCT) of syphilis results in congenital syphilis (CS), which can cause serious outcomes, including miscarriage, stillbirth, neonatal death, preterm birth, low birth weight, and various illnesses and congenital deformities. The World Health Organization (WHO) estimated 988,000 active syphilis cases and 611,000 CS cases in pregnant women worldwide in 2016 (*1*), and syphilis is the second most common infectious cause of stillbirth worldwide (*2*).

Injectable benzathine penicillin G (BPG) is the only regimen recommended in WHO and US Centers for Disease Control and Prevention (CDC) guidelines (*3*–*5*) for the treatment of syphilis in pregnant women to prevent CS. Sufficient evidence is not available to recommend an alternative regimen. In a systematic review on alternative treatments for pregnant women with syphilis, only 21 pregnant women treated with regimens other than BPG could be identified (*6*). Erythromycin and azithromycin do not cross the placental barrier and thus cannot treat infections in the fetus (*6*). Macrolide-resistant *T. pallidum* has been reported in many countries (*7*). Tetracycline and doxycycline are contraindicated in the second and third trimesters of pregnancy, and data are not sufficient to recommend ceftriaxone for treatment of maternal syphilis and prevention of CS (*4*,*8*). During 2014–2016, shortages or stockouts of BPG were reported by 39 of 95 surveyed countries and territories (*9*), and in several countries, including Japan, intramuscular BPG is not available (*10*). A reliable alternative treatment for syphilis in pregnant women to prevent CS is urgently needed.

Because sales of BPG stopped in Japan in 1986, oral penicillins, such as amoxicillin or ampicillin, have been primarily used to treat pregnant women with syphilis. These regimens are indicated in the obstetrics and gynecology care guidelines of Japan

Author affiliations: National Center for Global Health and Medicine, Tokyo, Japan (T. Nishijima); World Health Organization Regional Office of the Western Pacific, Manila, the Philippines (T. Nishijima, N. Ishikawa); Nihon University School of Medicine, Tokyo, Japan (K. Kawana); Dokkyo Medical University, Tochigi, Japan (I. Fukasawa); World Health Organization, Geneva, Switzerland (M.M. Taylor); Centers for Disease Control and Prevention, Atlanta, Georgia, USA (M.M. Taylor); Aichi Medical University, Aichi, Japan (H. Mikamo); Kyushu University Graduate School of Medical Sciences, Fukuoka, Japan (K. Kato); Graduate School of Medical Science, Kyoto Prefectural University of Medicine, Kyoto, Japan (J. Kitawaki); Graduate School of Medicine, The University of Tokyo, Tokyo, Japan (T. Fujii)

DOI: https://doi.org/10.3201/eid2606.191300

(*11*), which follows the regimens recommended by the Japanese Society for Sexually Transmitted Infections diagnosis and treatment guidelines (*12*). These guidelines recommend oral amoxicillin or ampicillin with dosing of 1,500 mg/day (i.e., 500 mg 3×/d) for 2–4 weeks for primary syphilis, 4–8 weeks for secondary syphilis, and 8–12 weeks for tertiary or later-stage syphilis in pregnant women. However, effectiveness of this regimen for pregnant women and prevention of CS has not been reported, except for 1 pregnant woman who was treated with a much higher dosage of amoxicillin (6 g/d) plus probenecid (1 g/d) for 14 days (*13*). In this retrospective study, we investigated the effectiveness and tolerability of oral amoxicillin and ampicillin in pregnant women to treat active syphilis and prevent MTCT of syphilis.

Methods

Study Setting and Population

We conducted this nationwide, multicenter retrospective study in Japan as a joint research project between the Japan Society of Obstetrics and Gynecology and the WHO (Appendix, https://wwwnc.cdc.gov/EID/article/26/6/19-1300-App1.pdf) (*14*). The study was approved by the human research ethics committees of Nihon University School of Medicine (Tokyo, Japan), Dokkyo Medical University (Tochigi, Japan), and the Japan Society of Obstetrics and Gynecology (Tokyo, Japan). We also submitted the study protocol to the WHO Ethics Review Committee. Because our research involved anonymized patient data and not new data collection or an additional intervention, the study was determined to be exempt from WHO Ethics Review Committee review. The requirement for informed consent was waived because this study included only data gained from routine clinical practice. We conducted this study according to the principles expressed in the Declaration of Helsinki.

We included pregnant women with syphilis, regardless of their symptoms, who were treated with oral amoxicillin or ampicillin during 2010–2018; we only included those with serum rapid plasma reagin (RPR) titers ≥8 and positive results from treponemal tests, such as the *T. pallidum* hemagglutination test (*10*,*15*). We excluded patients with tertiary syphilis or neurosyphilis diagnoses that were based on findings from cerebrospinal fluid (CSF) samples (*10*,*16*) or patient symptoms (including ocular or auditory syphilis) and those with suspected reinfections after initiation of syphilis treatment (defined as patients with ≥4-fold rise in RPR titer after 4-fold decrement with or without symptoms) (*10*,*15*,*17*).

In Japan, the automated latex turbidimetric immunoassay and the conventional manual RPR card test are both used to determine RPR titers (*18*,*19*). The automated RPR test highly correlates with the manual test for syphilis diagnoses (*18*,*19*); just like the manual card test, for the automated test, a 4-fold decrement in RPR titer is a good criterion for successful treatment of syphilis (*19*). Thus, we treated the titers from the automated RPR test the same as those from the manual RPR test.

Definitions

We defined CS following the reporting criteria set by the Japanese Ministry of Health, Labour, and Welfare (*20*). Diagnosis of CS in newborns required fulfillment of any 1 of the following criteria: serum RPR titer ≥4-fold that of the mother's (*4*); fluorescent treponemal antibody absorption (FTA-ABS) test result positive for serum IgM (*12*,*21*,*22*); lesion tissue or body fluid samples positive by PCR (*4*); lesion or fluid samples positive for *T. pallidum* on dark field microscopy (*4*); or physical examination findings consistent with CS, such as nonimmune hydrops, jaundice, hepatosplenomegaly, skin rash, pseudoparalysis, and rhinitis (*4*,*20*,*23*). We classified the mother's stage of syphilis into early syphilis (primary, secondary, or early latent syphilis) and late syphilis (late latent syphilis or latent syphilis of unknown duration). We defined early latent syphilis as asymptomatic syphilis that could be linked to reported syphilis symptoms, a sexual exposure, or conversion from a prior negative syphilis test ≤1 year after diagnosis. These criteria occurring >1 year after diagnosis constituted a late latent case and at an undefined time point after diagnosis as a latent case of unknown duration (*4*,*10*,*24*). We defined miscarriage as the loss of a fetus before week 20 of pregnancy and stillbirth as the loss during or after week 20.

Data Collection, Outcome Measures, and Statistical Analysis

We collected data from medical charts at each facility, using a case report form (Appendix). The primary outcome of this study was effectiveness of prevention of MTCT of syphilis. We defined MTCT as a CS case and defined CS cases as live newborns with CS diagnoses, miscarriages, or still births. If a live newborn was not given a CS diagnosis, we interpreted the treatment given as successful for preventing MTCT (*5*). We evaluated the secondary outcome serologic effectiveness of treatment in the mother (4-fold decrement of serum RPR titer) at each of the following time points: delivery (*25*), 6 months after therapy (*4*), and 12 months after

therapy (*4*). We analyzed the primary outcome among all study patients and among those who initiated treatment ≥60 days before delivery. We used this subgroup to evaluate drug effectiveness among patients who initiated treatment within an adequate interval (defined by WHO as ≥30 days before delivery) (*26*). We used 60 days for this evaluation because of the long treatment duration recommended for oral penicillins in Japan's guidelines (*12*). We compared the percentage of CS cases between those who had early syphilis and late syphilis, between those treated with amoxicillin and those treated with ampicillin, and between those who were and were not Japanese.

We compared characteristics between groups using the Student *t*-test for continuous variables and using either the χ^2 test or Fisher exact test for categorical variables. We defined statistical significance as a 2-sided p value <0.05. We developed a multivariate logistic regression model to determine the effect of factors on CS cases. We performed this analysis with SAS version 9.4 (https://www.sas.com) and all other statistical analyses with SPSS Statistics 23 (https://www.ibm.com).

Results

Of 88 hospitals invited into the study, 44 (50%) participated and provided 131 case report forms (Appendix Figure). We excluded 51 cases, resulting in 80 cases being included in our analysis.

Median patient age was 23 (interquartile range [IQR] 21–27) years; 75 (94%) patients were Japanese, and only 1 patient was HIV positive (Table 1). In total, 31 patients had early syphilis (5 primary, 19 secondary, 7 early latent) and 49 had late syphilis (4 latent, 45 latent with unknown duration). Median RPR titer at diagnosis was 51 (IQR 29–72), and 66 (83%) patients were treated with amoxicillin and 14 (17%) with ampicillin. The median duration of treatment for pregnant women was 60 (IQR 29–90) days, and the median duration of treatment before delivery was 56 (28–86) days. In total, 61 (76%) patients were treated with 1,500 mg/day dosing, and 3 were concurrently prescribed probenecid. Median gestational age of fetus at CS diagnosis was 13.8 (IQR 11.7–26.3) weeks and at treatment initiation 15.8 (13.0–27.1) weeks. In total, 57 (71%) patients received syphilis diagnoses when the fetus had the gestational age of <20 weeks. A comparison of pregnant women by syphilis stage revealed that women with late syphilis and early syphilis had similar characteristics but women with late syphilis had longer durations of treatment (Table 2).

Of the 80 cases, we excluded 9 (6 with unknown outcomes, 3 involving abortions induced at 15–17 weeks of pregnancy) from the outcome analysis. Of the remaining 71 cases, 15 (21%, 95% CI 13.2%–32%) were classified as CS (13 live newborns with CS diagnoses, 1 miscarriage, 1 stillbirth; Tables 2, 3; Appendix Table 1). Effectiveness of treatment for preventing CS cases was significantly better among patients with early syphilis than late syphilis; CS cases developed in 0% (0/26, 95% CI 0%–12.9%) of patients with early syphilis and 33% (15/45, 95% CI 21.4%–47.9%; p<0.001) of patients with late syphilis.

Among pregnant women with early syphilis, 26 (84%) received 1,500 mg/day of either amoxicillin or ampicillin, and the median duration of antimicrobial drug treatment was 30 (IQR 28–64) days (Table 2). Among those with late syphilis, 35 (71%) received 1,500 mg/day of either amoxicillin or ampicillin, and the median duration of antimicrobial drug treatment was 78 (IQR 51–104) days. CS cases developed in 19% (11/58, 95% CI 10.9%–30.9%) of those treated with amoxicillin and 31% (4/13, 95% CI 12.7%–57.6%; p = 0.19) of those treated with ampicillin (Table 3). CS cases were frequently found among non-Japanese pregnant women (60% [3/5], 95% CI 23.1%–88.2%).

In the subgroup of women initiating syphilis treatment ≥60 days before delivery, 14% (8/56 95% CI 7.4%–25.7%) had pregnancies resulting in CS cases (Table 3). In the subgroup initiating treatment <60 days before delivery, 43% (6/14, 95% CI 21.4%–67.4%) had pregnancies resulting in CS. The proportions of women with early and late syphilis were not different between these 2 treatment initiation subgroups (p = 0.57 by χ^2 test). Among those who initiated syphilis treatment ≥60 days before delivery, 11% (5/45, 95% CI 4.8%–23.5%) of those treated with amoxicillin and 27% (3/11, 95% CI 9.7%–56.6%; p = 0.11) of those treated with ampicillin had pregnancies resulting in CS cases.

Because no CS cases developed among pregnant women with early syphilis, we applied exact logistic regression (*27*) to estimate exact odds ratios (ORs) and 95% CIs associated with various factors. Analyses showed late syphilis was associated with CS cases (late vs. early syphilis, adjusted exact OR 13.5, 95% CI 2.56–∞; p = 0.0025) and that starting treatment ≥60 days before delivery had a protective effect (≥60 days vs. <60 days, adjusted exact OR 0.11, 95% CI 0–0.69; p = 0.023) (Appendix Table 2).

Discontinuation of antimicrobial drug treatment occurred because of adverse events in 3 (3.8%) of 80 pregnant women. All 3 started amoxicillin and switched to other antimicrobial drugs because of skin rash only, itching only, or dizziness only; 1 of 3 of these patients had a newborn with a CS diagnosis.

Table 1. Characteristics of pregnant women with active syphilis treated with amoxicillin or ampicillin, by CS birth outcome, Japan, 2010–2018*

Characteristic	All cases, n = 80	CS cases,† n = 15	Cases of live birth without CS, n = 56‡	p value§
Age, y	23 (21–27)	24 (22–26)	26 (22–29.5)	0.46
Japanese	75/80 (94)	12/15 (80)	54/56 (96)	0.06
HIV co-infection	1/78 (1)	0/15	1/56 (2)	1.00
Syphilis stage				
Early syphilis	31/80 (39)	0/15	26/56 (46)	
Primary	5/80 (6)	0/15	5/56 (9)	
Secondary	19/80 (24)	0/15	14/56 (25)	
Early latent	7/80 (9)	0/15	7/56 (13)	
Late syphilis	49/80 (61)	15/15 (100)	30/56 (54)	
Late latent	4/80 (5)	0/15	4/56 (7)	
Latent with unknown duration	45/80 (56)	15/15 (100)	26/56 (46)	
Diagnosis and treatment				
Rapid plasma reagin titer at diagnosis	51 (29–72)	58 (28–105)	51 (27.1–71.8)	0.59
Amoxicillin	66/80 (82.5)	11/15 (73)	47/56 (84)	0.45
Ampicillin	14/80 (17.5)	4/15 (27)	9/56 (16)	
Antimicrobial drug dosage, mg/d	1,500 (1,500–1,500)	1,500 (1,500–1,500)	1,500 (1,500–1,500)	0.88
Received 1,500 mg/d	61/80 (76)	13/15 (87)	39/56 (70)	0.20
Co-administered probenecid	3/75 (4)	1/15 (7)	2/56 (4)	0.51
Total duration of treatment, d¶	60 (29–90)	70 (37–101)	56 (28–90)	0.49
Duration of treatment at delivery, d¶	56 (28–86)	68 (4–100)	56 (28–84)	0.84
Gestational age at diagnosis, wk¶	13.8 (11.7–26.3)	18.1 (12.3–34)	13.2 (11.5–21.6)	0.082
Gestational age at treatment, wk¶	15.8 (13.0–27.1)	18.3 (13.6–34.3)	15.9 (13.4–25.4)	0.22
Gestational age at delivery, wk¶	39.1 (37.9–40.6)	38.6 (35.6–40.9)	39.1 (37.9–40.3)	0.38
Time from treatment to delivery, wk¶	21.9 (8.5–26.3)	15.7 (0.4–25.9)	23 (16.7–27.2)	0.026
Started treatment <60 d before delivery¶	14/69 (20)	6/14 (43)	8/56 (14)	0.027
Birth outcomes				
Birth weight, g¶	2,936 (2,580–3,156)	2,704 (1,797–3,085)	2,959 (2,641–3,180)	0.094
Low birth weight, <2,500 g	11/69 (16)	4/13 (31)	7/56 (13)	0.20
Very low birth weight, <1,500 g	3/69 (4)	3/13 (23)	0/56	0.005

*Values are no./total (%) or median (interquartile range). Pregnancy outcome was missing for 9 patients. CS, congenital syphilis.
†CS cases include newborns with CS diagnoses, miscarriages, and stillbirths.
‡One pregnant woman delivered twins. The twin delivery was acknowledged as 1 birth outcome, and the birth weight of the first child born was used for the table and analyses.
§Student *t*-test for continuous variables and either χ^2 test or Fisher exact test for categorical variables.
¶Denominators varied because of missing data. Anywhere from 1 to 11 cases might be missing.

All 15 women who had CS pregnancy outcomes had latent syphilis of unknown duration (Appendix Table 1). The 13 newborns with CS diagnoses had the following findings: FTA-ABS test results positive for serum IgM (n = 10), positive serum RPR titers (n = 5), CSF findings (n = 3), very low (<1,500 g; n = 2) or extremely low (<1,000 g; n = 1) birth weight, clinical signs compatible with CS (n = 2), and cardiac anomaly (n = 1). (Appendix Table 1).

A 4-fold decrement in serum RPR titer was achieved in 35 (49%) pregnant women by delivery, 41 (53%) at 6 months after treatment, and 46 (82%) at 1 year after treatment (Table 4). The percentage of CS cases was not significantly different between pregnant women with (16%, n = 5) and without (23%, n = 8) a 4-fold titer decline at delivery (p = 0.54). However, RPR titers declined ≥4-fold in 91% (21/23) of women with early syphilis (group with 0 CS cases) and 76% (25/33) of women with late syphilis (group with 15 CS cases) (Table 4). The percentage who achieved a 4-fold decrement was higher among those with early syphilis than among those with late syphilis for all 3 endpoints (by delivery, 58% early vs. 44% late; 6 months, 67% early vs. 45% late; 1 year, 91% early vs. 76% late). Among those who started treatment ≥60 days before delivery, 63% (35/56) had late syphilis, and 81% (35/43) achieved a 4-fold RPR titer decline by 1 year after treatment (Tables 3, 4).

Discussion

In this nationwide, multicenter retrospective study, we evaluated effectiveness and tolerability of oral amoxicillin or ampicillin for treatment of pregnant women with active syphilis and prevention of MTCT of syphilis. Overall, 21% (15/71) of pregnancies resulted in CS cases, which we defined to include CS diagnoses in live newborns, miscarriages, and stillbirths. Among pregnancies in women who initiated syphilis treatment ≥60 days before delivery, 14% (8/56) resulted in CS cases. However, no CS cases were observed among the subgroup with early syphilis (n = 26), suggesting that oral amoxicillin with 1,500-mg dosing (500 mg 3×/d) for 30 days could be an optional regimen for treatment of pregnant women with early syphilis when intramuscular BPG is not available. In this study, we found a

high percentage of CS cases (33%, 15/45) among those with late syphilis treated with oral amoxicillin or ampicillin, suggesting these regimens should not be used in this population. Late initiation of treatment was also associated with CS independent of syphilis stage. Although further studies evaluating drug adherence are warranted before any recommendation can be made, these findings are valuable for implicating some alternative treatments, considering reports of syphilis increases among heterosexual populations, reports of CS increases in various countries (including Japan and the United States), and national shortages of BPG (*28*,*29*).

Our study has 3 strengths. First, we evaluated effectiveness of oral amoxicillin or ampicillin for the treatment of pregnant women with active syphilis and prevention of MTCT. The finding that 1,500 mg of oral amoxicillin for 30 days might be effective in treating pregnant women with early syphilis and preventing CS is clinically useful because intramuscular BPG, the only recommended regimen for this population, is not always available because of shortages or stockouts (*3*,*9*). High-dose oral amoxicillin (3,000 mg/d) plus probenecid has been reported to effectively treat syphilis in nonpregnant patients with HIV infection with a serologic effectiveness of 97.5% for early syphilis and 90.8% for late syphilis (*10*). Further studies are warranted to determine efficacy, optimal dosing, duration, and the need for co-administration of probenecid with oral amoxicillin as an alternative regimen for both early and late syphilis in pregnant women.

Second, the well-established and strict inclusion criteria of having both serum RPR titers ≥8 and positive treponemal test results, regardless of symptoms, for active syphilis was a strength of this study (*10*,*15*,*19*). Application of these criteria enabled us to exclude those with low RPR titers who might have had previous antimicrobial drug treatment or those with serofast status, for whom further treatment is not required (*30*). This inclusion criterion was necessary to exclude persons who had past (not current) infections, considering that various antimicrobial drugs can treat syphilis (*30*,*31*) and that patients can receive effective treatment for syphilis without recognizing it.

Third, we evaluated not only MTCT of syphilis but also treatment effectiveness of oral amoxicillin or ampicillin in women using serology. Serologic effectiveness 1 year after treatment was 82% overall and 91% among early syphilis cases, suggesting greater effectiveness of this regimen for early syphilis. Furthermore, as was the case for the report by Rac et al. (*25*), we showed that the percentage of CS cases was not different between patients with and without a 4-fold titer decline at delivery.

The effectiveness of antimicrobial drugs for the prevention of MTCT of syphilis needs to be carefully considered because evidence is limited and diagnostic criteria for pregnant women with syphilis and CS vary across studies (*5*,*8*,*25*). We included time between treatment and delivery and syphilis staging in analyses

Table 2. Characteristics and birth outcomes of pregnant women with active syphilis treated with amoxicillin or ampicillin, by syphilis stage, Japan, 2010–2018*

Category	Early syphilis, n = 31	Late syphilis, n = 49	p value†
Age, y	26 (21–28)	25 (22–27)	0.63
Japanese	29/31 (94)	46/49 (94)	1.00
HIV co-infection	0/31	1/49 (2)	1.00
Diagnosis and treatment			
Rapid plasma reagin titer at diagnosis	44 (27–64)	58 (29–83)	0.64
Amoxicillin	28/31 (90)	38/49 (78)	0.23
Ampicillin	3/31 (10)	11/49 (22)	
Antimicrobial drug dosage, mg/d	1,500 (1,500–1,500)	1,500 (1,500–1,500)	0.56
Received 1,500 mg/d	26/31 (84)	35/49 (71)	0.22
Total duration of treatment, d‡	30 (28–64)	78 (51–104)	0.004
Duration of treatment at delivery, d‡	30 (26–56)	70 (29-98)	0.016
Gestational age at diagnosis, wk‡	15.1 (11.1–27.5)	13.3 (12–25.6)	0.70
Gestational age at treatment, wk‡	17.3 (13.3–28.7)	14.7 (13–26)	0.62
Gestational age at delivery, wk‡	39.4 (38.1–40.6)	38.9 (37.7–40.5)	0.10
Time from treatment to delivery, wk‡	15.7 (0.4–25.9)	23 (16.7–27.2)	0.73
Birth outcomes			
Live birth with congenital syphilis diagnosis	0/26	13/45 (29)	0.009
Stillbirth	0/26	1/45 (2)	
Miscarriage	0/26	1/45 (2)	
Birth weight, g‡	2,902 (2,652–3,184)	2,942 (2,555–3,155)	0.88
Low birth weight, <2,500 g‡	3/26 (12)	8/45 (18)	0.52
Very low birth weight, <1,500 g‡	0/26	3/45 (7)	0.29

*Values are no./total (%) or median (interquartile range).
†Used the Student *t*-test for continuous variables and either the χ^2 test or Fisher exact test for categorical variables.
‡Denominators varied because of missing data. Anywhere from 1 to 11 cases might be missing.

Table 3. Birth outcomes of pregnant women with active syphilis treated with oral amoxicillin or ampicillin, Japan, 2010–2018*

Category	Total no.	No. missing	No. live births without CS diagnosis	No. adverse outcomes			Adverse outcomes, % (95% CI)	p value†
				Live births with CS diagnosis	Miscarriages	Stillbirths		
All patients	80	9	56	13	1	1	21.1 (13.2–32)	
Early syphilis	31	5	26	0	0	0	0 (0–12.9)	<0.001
Late syphilis	49	4	30	13	1	1	33.3 (21.4–47.9)	
Amoxicillin	66	8	47	9	1	1	19.0 (10.9–30.9)	0.19
Ampicillin	14	1	9	4	0	0	30.8 (12.7–57.6)	
Japanese	75	9	54	10	1	1	18.2 (10.7–29.1)	0.033
Non-Japanese	5	0	2	3	0	0	60.0 (23.1–88.2)	
Patients starting syphilis treatment ≥60 days before delivery‡								
All	57	1	48	8	0	0	14.2 (7.4–25.7)	
Early syphilis	21	0	21	0	0	0	0 (0–15.5)	0.017
Late syphilis	36	1	27	8	0	0	22.9(12.1–39)	
Amoxicillin	46	1	40	5	0	0	11.1 (4.8–23.5)	0.11
Ampicillin	11	0	8	3	0	0	27.3 (9.7–56.6)	
Japanese	54	1	47	6	0	0	11.3 (5.3–22.6)	0.026
Non-Japanese	3	0	1	2	0	0	66.7 (20.8–93.9)	
Patients starting syphilis treatment <60 days before delivery								
All	14	0	8	5	0	1	42.9 (21.4–67.4)	
Early syphilis	5	0	5	0	0	0	0 (0–43.5)	0.028
Late syphilis	9	0	3	5	0	1	66.7 (35.4–87.9)	
Amoxicillin	13	0	8	4	0	1	38.5 (17.7–64.5)	0.43
Ampicillin	1	0	0	1	0	0	100 (20.7–100)	
Japanese	12	0	7	4	0	1	41.7 (19.3–68.1)	0.86
Non-Japanese	2	0	1	1	0	0	50.0 (9.5–90.6)	

*Nine cases (including 3 cases of induced abortion) were excluded from this analysis because data on birth outcomes were not available. One miscarriage case is missing in the subgroup analysis because the exact date of miscarriage was unknown, CS, congenital syphilis.
†Used either the χ^2 test or Fisher exact test to measure the association between cases of live birth without CS diagnosis and cases of live birth with CS diagnosis, miscarriage, and stillbirth.
‡Outcome data for 1 patient is missing. Outcome data (whether CS or not) was not known because this patient was referred to another hospital before delivery. Because the birth date of this patient's infant was reported and available, we could group this patient with the appropriate group, which was the group that started syphilis treatment ≥60 days before delivery.

because these parameters influence MTCT; transmission is more likely to occur during early syphilis stages and among women with late treatment (*30*,*32*). The CDC-recommended regimen of intramuscular BPG once for early syphilis and three times at 1-week intervals for late syphilis was reported to prevent 98.2% of CS cases (97.1% for early syphilis, 100% for late syphilis including latent syphilis of unknown duration) among a cohort of pregnant women with syphilis diagnosed during 1987–1989 (*5*). However, note that the authors of that investigation applied loose inclusion criteria (positive for treponemal antibody and positive by either the venereal disease research laboratory test or the RPR test); their diagnostic criteria for CS was strict (*5*). That group of authors subsequently reported that, among a cohort of pregnant women with syphilis treated during 1981–2011 by CDC guidelines, 18% of infants subsequently required treatment for CS (*25*). Only 1 case series has been published on the use of ceftriaxone to treat pregnant women with syphilis and to prevent CS (*8*). In that study, 2 courses of intramuscular ceftriaxone with 250-mg dosing for 7–10 days was evaluated in 11 pregnant women with early syphilis, and this treatment resulted in no CS diagnoses.

Our study demonstrates the need for comparative trials to evaluate the use of amoxicillin in the prevention of MTCT of syphilis before recommending this regimen as an alternative to BPG for pregnant women with syphilis. Considering our study results, healthcare authorities in Japan and other countries where intramuscular BPG is not recommended should consider making intramuscular BPG available. When intramuscular BPG is not available to treat pregnant women with syphilis, physicians need to make difficult decisions regarding alternative regimens, often following recommendations for neurosyphilis, such as intravenous aqueous crystalline penicillin G or intravenous or intramuscular ceftriaxone, treatments with limited clinical evidence available on efficacy.

We found that 17% of pregnant women were treated with oral ampicillin, even though oral amoxicillin is favored over oral ampicillin for most indications because of greater bioavailability (*31*,*33*). Oral ampicillin is also used to prevent group B *Streptococcus* at some facilities in Japan, despite guidelines recommending the injectable form of ampicillin for such indications (*11*,*34*). Our study results showed that the effectiveness of oral amoxicillin and ampicillin were not significantly different; however, our sample size was small.

Our study has several limitations. First, the retrospective nature of the study could have introduced

Table 4. Serologic outcomes of pregnant women with active syphilis treated with amoxicillin or ampicillin, Japan, 2010–2018, by delivery, 6 months after treatment, and 1 year after treatment*

Patient group	No./total (%) with ≥4-fold decrement in RPR titer		
	By delivery	6 months after treatment	1 year after treatment
All	35/71 (49)	41/77 (53)	46/56 (82)
Live birth without CS diagnosis	27/54 (50)	29/54 (54)	31/39 (80)
CS cases†	5/13 (39)	6/15 (40)	9/11 (82)
Early syphilis	15/26 (58)	20/30 (67)	21/23 (91)
Late syphilis	20/45 (44)	21/47 (45)	25/33 (76)
Amoxicillin	27/58 (47)	32/63 (51)	36/44 (82)
Ampicillin	8/13 (62)	9/14 (64)	10/12 (83)
Japanese	34/66 (52)	39/72 (54)	44/52 (85)
Non-Japanese	1/5 (20)	2/5 (40)	2/4 (50)
Started syphilis treatment ≥60 days before delivery	32/55 (58)	32/55 (58)	35/43 (81)
Started syphilis treatment <60 days before delivery	0	5/17 (29)	6/8 (75)

*CS, congenital syphilis; RPR, rapid plasma reagin.
†CS cases include newborns with CS diagnoses, miscarriages, and stillbirths.

some selection and information bias, and variables were missing for some mothers and infants. Second, data on adherence of patients to the prescribed regimens were not available, could not be evaluated, and could have affected our findings. Third, the definition of CS is not universal; diagnostic criteria can differ in national surveillance guidelines of other countries, limiting the comparativeness of our findings with other studies (*4*,*12*,*22*). In this study, we followed the reporting criteria set by the Japanese Ministry of Health, Labour, and Welfare, which includes the criterion of FTA-ABS test positivity for serum IgM in newborns (*12*,*20*). In contrast to IgG, IgM does not cross the placenta, making IgM in the serum of newborns a reliable marker with high specificity for CS diagnosis (*21*,*35*). However, a sufficiently sensitive and specific IgM assay is not commercially available (*4*). CDC guidelines do not include FTA-ABS test positivity for serum IgM in newborns as a criterion for CS diagnosis (*4*), whereas the Japan and the European Centre for Disease Prevention and Control guidelines do (*12*,*20*,*22*). In our study, misclassification of infants with CS could have been possible because evaluation (including laboratory testing) of newborns was not always rigorously performed. CS can cause long bone and CSF findings; these criteria are used in the United States for CS diagnosis (*4*). Because long bone radiographs are not included in the reporting criteria for CS in Japan, these procedures are infrequently performed, and results were not available for review in this analysis. Among 71 cases with available birth outcomes, 60 had serum RPR test results and only 6 had CSF results (3 with remarkable findings). Fourth, even though we classified latent syphilis of unknown duration as late syphilis, this category could have included early latent syphilis; clearly distinguishing between these 2 groups is difficult. Last, our results should be interpreted with caution because of the small sample size.

In conclusion, we evaluated the effectiveness and tolerability of oral amoxicillin and ampicillin for the treatment of pregnant women with active syphilis and prevention of MTCT of syphilis in Japan. Although we cannot recommend oral amoxicillin or ampicillin as alternative regimens for the treatment of pregnant women with syphilis, this analysis suggests that 1,500 mg/day of oral amoxicillin for 30 days could effectively treat early syphilis and prevent CS. Further studies, preferably controlled comparative trials, are needed to establish the efficacy of oral amoxicillin as an alternative regimen for the treatment of pregnant women with syphilis and the prevention of CS.

Acknowledgements

The authors thank the following gynecologists and obstetricians at 44 hospitals across Japan who kindly collected the data and fulfilled the case report forms for this study: Yukio Wakui, Yoshihiro Akimoto, Yusaku Kumagai, Yuki Shimoda, Yutaka Fujiki, Maiko Ichikawa, Takashi Watanabe, Hidenori Sasa, Tomoko Amagata, Hisayo Fujimura, Yoshinori Iitsuka, Hironobu Hyodo, Miki Goto, Hideyuki Oda, Noriko Sato, Yasuko Nagasaka, Masahiro Shiba, Hiroko Tsuchiya, Junko Mochizuki, Soichiro Obata, Toru Arase, Hiroki Waki, Yasuko Nemoto, Tomoaki Kano, Saki Inuzuka, Noriko Kato, Kazuhiro Higuchi, Yasuyuki Noguchi, Shima Takamura, Masako Sawada, Masahiro Ohashi, Kuniko Hanabusa, Ikuko Sawada, Kayoko Harada, Masako Tomimoto, Yoshinori Takeda, Taihei Tsunemi, Yoshimasa Onohara, Hiroko Kurioka, Mika Sugihara, Yuriko Omori, Masakatsu Sase, Masaki Goto, Naotoshi Honda, Shoichi Kawakami, Junya Miyoshi, and Tadakazu Uesato. The authors would also like to thank Makoto Ohnishi, Motoyuki Tsuboi, Yosuke Inaba, and Naoko Tomita for their invaluable support for this study.

This work was supported by the Ministry of Health, Labour, and Welfare of Japan.

About the Author

Dr. Nishijima is a clinician-researcher at the National Center for Global Health and Medicine, Tokyo, Japan. His research interests include clinical trials and observational studies on HIV and sexually transmitted infections.

References

1. Korenromp EL, Rowley J, Alonso M, Mello MB, Wijesooriya NS, Mahiané SG, et al. Global burden of maternal and congenital syphilis and associated adverse birth outcomes-estimates for 2016 and progress since 2012 [Erratum in: PLoS One. 2019;14:e0219613]. PLoS One. 2019;14:e0211720. http://dx.doi.org/10.1371/journal.pone.0211720
2. Lawn JE, Blencowe H, Waiswa P, Amouzou A, Mathers C, Hogan D, et al.; Lancet Ending Preventable Stillbirths Series study group; Lancet Stillbirth Epidemiology investigator group. Stillbirths: rates, risk factors, and acceleration towards 2030. Lancet. 2016;387:587–603. http://dx.doi.org/10.1016/S0140-6736(15)00837-5
3. World Health Organization. WHO guidelines for the treatment of *Treponema pallidum* (syphilis). 2016 [cited 2020 Jan 30]. http://apps.who.int/iris/bitstream/10665/249572/1/9789241549806-eng.pdf
4. Workowski KA, Bolan GA; Centers for Disease Control and Prevention. Sexually transmitted diseases treatment guidelines, 2015. MMWR Recomm Rep. 2015;64(RR-03):1–137.
5. Alexander JM, Sheffield JS, Sanchez PJ, Mayfield J, Wendel GD Jr. Efficacy of treatment for syphilis in pregnancy. Obstet Gynecol. 1999;93:5–8.
6. Roberts CP, Raich A, Stafylis C, Klausner JD. Alternative treatments for syphilis during pregnancy. Sex Transm Dis. 2019;46:637–40. http://dx.doi.org/10.1097/OLQ.0000000000001050
7. Molini BJ, Tantalo LC, Sahi SK, Rodriguez VI, Brandt SL, Fernandez MC, et al. Macrolide resistance in *Treponema pallidum* correlates with 23S rDNA mutations in recently isolated clinical strains. Sex Transm Dis. 2016;43:579–83. http://dx.doi.org/10.1097/OLQ.0000000000000486
8. Zhou P, Gu Z, Xu J, Wang X, Liao K. A study evaluating ceftriaxone as a treatment agent for primary and secondary syphilis in pregnancy. Sex Transm Dis. 2005;32:495–8. http://dx.doi.org/10.1097/01.olq.0000170443.70739.cd
9. Nurse-Findlay S, Taylor MM, Savage M, Mello MB, Saliyou S, Lavayen M, et al. Shortages of benzathine penicillin for prevention of mother-to-child transmission of syphilis: an evaluation from multi-country surveys and stakeholder interviews. PLoS Med. 2017;14:e1002473. http://dx.doi.org/10.1371/journal.pmed.1002473
10. Tanizaki R, Nishijima T, Aoki T, Teruya K, Kikuchi Y, Oka S, et al. High-dose oral amoxicillin plus probenecid is highly effective for syphilis in patients with HIV infection. Clin Infect Dis. 2015;61:177–83. http://dx.doi.org/10.1093/cid/civ270
11. Japan Society of Obstetrics and Gynecology; Japan Association of Obstetricians and Gynecologists. The Japanese obstetrics and gynecology care guidelines [in Japanese]. 2017 [cited 2020 Jan 30]. http://www.jsog.or.jp/activity/pdf/gl_fujinka_2017.pdf
12. Japanese Society for Sexually Transmitted Infections. The Japanese STI diagnosis and treatment guidelines [in Japanese]. 2016 [cited 2020 Jan 30]. http://jssti.umin.jp/pdf/guideline-2016_v2.pdf
13. Katanami Y, Hashimoto T, Takaya S, Yamamoto K, Kutsuna S, Takeshita N, et al. Amoxicillin and ceftriaxone as treatment alternatives to penicillin for maternal syphilis. Emerg Infect Dis. 2017;23:827–9. http://dx.doi.org/10.3201/eid2305.161936
14. Takamatsu K, Kitawaki J. Annual report of the Women's Health Care Committee, Japan Society of Obstetrics and Gynecology, 2017. J Obstet Gynaecol Res. 2018;44:13–26. http://dx.doi.org/10.1111/jog.13470
15. Kenyon C, Lynen L, Florence E, Caluwaerts S, Vandenbruaene M, Apers L, et al. Syphilis reinfections pose problems for syphilis diagnosis in Antwerp, Belgium—1992 to 2012. Euro Surveill. 2014;19:20958. http://dx.doi.org/10.2807/1560-7917.ES2014.19.45.20958
16. Marra CM, Maxwell CL, Smith SL, Lukehart SA, Rompalo AM, Eaton M, et al. Cerebrospinal fluid abnormalities in patients with syphilis: association with clinical and laboratory features. J Infect Dis. 2004;189:369–76. http://dx.doi.org/10.1086/381227
17. Zetola NM, Engelman J, Jensen TP, Klausner JD. Syphilis in the United States: an update for clinicians with an emphasis on HIV coinfection. Mayo Clin Proc. 2007;82:1091–102. http://dx.doi.org/10.4065/82.9.1091
18. Lee JH, Lim CS, Lee MG, Kim HS. Comparison of an automated rapid plasma reagin (RPR) test with the conventional RPR card test in syphilis testing. BMJ Open. 2014;4:e005664. http://dx.doi.org/10.1136/bmjopen-2014-005664
19. Tsuboi M, Nishijima T, Aoki T, Teruya K, Kikuchi Y, Gatanaga H, et al. Usefulness of automated latex turbidimetric rapid plasma reagin test for diagnosis and evaluation of treatment response in syphilis in comparison with manual card test: a prospective cohort study. J Clin Microbiol. 2018;56:e01003-18. http://dx.doi.org/10.1128/JCM.01003-18
20. Government of Japan. Case report form of congenital syphilis [in Japanese] [cited 2020 Jan 30]. https://www.mhlw.go.jp/bunya/kenkou/kekkaku-kansenshou11/pdf/01-05-11-3-b.pdf
21. Herremans T, Kortbeek L, Notermans DW. A review of diagnostic tests for congenital syphilis in newborns. Eur J Clin Microbiol Infect Dis. 2010;29:495–501. http://dx.doi.org/10.1007/s10096-010-0900-8
22. European Union. Decisions. Commission implementing decision (EU) 2018/945 of 22 June 2018 on the communicable diseases and related special health issues to be covered by epidemiological surveillance as well as relevant case definitions. Off J Eur Union. 2018;61:L170/44–5 [cited 2020 Jan 30] https://eur-lex.europa.eu/legal-content/EN/TXT/PDF/?uri=OJ:L:2018:170:FULL&from
23. Cheng JQ, Zhou H, Hong FC, Zhang D, Zhang YJ, Pan P, et al. Syphilis screening and intervention in 500,000 pregnant women in Shenzhen, the People's Republic of China. Sex Transm Infect. 2007;83:347–50. http://dx.doi.org/10.1136/sti.2006.023655
24. Janier M, Hegyi V, Dupin N, Unemo M, Tiplica GS, Potočnik M, et al. 2014 European guideline on the management of syphilis. J Eur Acad Dermatol Venereol. 2014;28:1581–93. http://dx.doi.org/10.1111/jdv.12734
25. Rac MW, Bryant SN, Cantey JB, McIntire DD, Wendel GD Jr, Sheffield JS. Maternal titers after adequate syphilotherapy during pregnancy. Clin Infect Dis. 2015;60:686–90. http://dx.doi.org/10.1093/cid/ciu920
26. World Health Organization. Global guidance on criteria and processes for validation: elimination of mother-to-child transmission of HIV and syphilis. 2nd edition. 2017 [cited 2020 Jan 30]. https://www.who.int/reproductivehealth/publications/emtct-hiv-syphilis

27. Mehta CR, Patel NR. Exact logistic regression: theory and examples. Stat Med. 1995;14:2143–60. http://dx.doi.org/10.1002/sim.4780141908
28. Takahashi T, Arima Y, Yamagishi T, Nishiki S, Kanai M, Ishikane M, et al. Rapid increase in reports of syphilis associated with men who have sex with women and women who have sex with men, Japan, 2012 to 2016. Sex Transm Dis. 2018;45:139–43. http://dx.doi.org/10.1097/OLQ.0000000000000768
29. Centers for Disease Control and Prevention, National Center for HIV/AIDS, Viral Hepatitis, STD, and TB Prevention. Sexually transmitted disease surveillance 2017. 2018 Sep [cited 2019 Jun 10]. https://www.cdc.gov/std/stats17/2017-STD-Surveillance-Report_CDC-clearance-9.10.18.pdf
30. Clement ME, Okeke NL, Hicks CB. Treatment of syphilis: a systematic review. JAMA. 2014;312:1905–17. http://dx.doi.org/10.1001/jama.2014.13259
31. Bennett J, Dolin R, Blaser MJ. Mandell, Douglas, and Bennett's principles and practice of infectious diseases. 8th edition. London: Churchill Livingstone Elsevier; 2014
32. Sheffield JS, Sánchez PJ, Morris G, Maberry M, Zeray F, McIntire DD, et al. Congenital syphilis after maternal treatment for syphilis during pregnancy. Am J Obstet Gynecol. 2002;186:569–73. http://dx.doi.org/10.1067/mob.2002.121541
33. Klein JO, Finland M. The new penicillins. N Engl J Med. 1963;269:1129–34. http://dx.doi.org/10.1056/NEJM196311212692107
34. AmericanCollege of Obstetricians and Gynecologists Committee on Obstetric Practice. Prevention of group B streptococcal early-onset disease in newborns: ACOG committee opinion summary, number 797 [Erratum in: Obstet Gynecol. 2020;135:978–9]. Obstet Gynecol. 2020;135:e51–72. http://dx.doi.org/10.1097/AOG.0000000000003668
35. Johnston NA. Neonatal congenital syphilis. Diagnosis by the absorbed fluorescent treponemal antibody (IgM) test. Br J Vener Dis. 1972;48:464–9.

Address for correspondence: Kei Kawana, Department of Obstetrics and Gynecology, Nihon University School of Medicine, 30-1 Ohyaguchi Kamicho, Itabashi, Tokyo 173-8610, Japan; email: kkawana-tky@umin.org

Endemic Chromoblastomycosis Caused Predominantly by *Fonsecaea nubica*, Madagascar[1]

Tahinamandranto Rasamoelina, Danièle Maubon, Malalaniaina Andrianarison, Irina Ranaivo, Fandresena Sendrasoa, Njary Rakotozandrindrainy, Fetra A. Rakotomalala, Sébastien Bailly, Benja Rakotonirina, Abel Andriantsimahavandy, Fahafahantsoa R. Rabenja, Mala Rakoto Andrianarivelo, Muriel Cornet, Lala S. Ramarozatovo

Chromoblastomycosis is an implantation fungal infection. Twenty years ago, Madagascar was recognized as the leading focus of this disease. We recruited patients in Madagascar who had chronic subcutaneous lesions suggestive of dermatomycosis during March 2013–June 2017. Chromoblastomycosis was diagnosed in 50 (33.8%) of 148 patients. The highest prevalence was in northeastern (1.47 cases/100,000 persons) and southern (0.8 cases/100,000 persons) Madagascar. Patients with chromoblastomycosis were older (47.9 years) than those without (37.5 years) (p = 0.0005). Chromoblastomycosis was 3 times more likely to consist of leg lesions (p = 0.003). Molecular analysis identified *Fonsecaea nubica* in 23 cases and *Cladophialophora carrionii* in 7 cases. Of 27 patients who underwent follow-up testing, none were completely cured. We highlight the persistence of a high level of chromoblastomycosis endemicity, which was even greater at some locations than 20 years ago. We used molecular tools to identify the *Fonsecaea* sp. strains isolated from patients as *F. nubica*.

Chromoblastomycosis is a chronic, implantation, fungal disease caused by melanized fungi from a variety of genera of the order Chaetothyriales. This disease is included in a group of melanized infections and easily identifiable by verrucous lesions that eventually lead to cauliflower-like eruptions on the skin. Infection is acquired traumatically by implantation of infected plant material from thorns or wood splinters or by soil contamination of an existing wound (*1*,*2*). The causative agents are mainly *Fonsecaea* spp., *Cladophialophora* spp., and *Rhinocladiella* spp. However, rare cases caused by other genera, such as *Phialophora* spp. or *Exophiala* spp., have been reported (*1*,*3*). As is the case for other implantation mycoses, chromoblastomycosis lesions are located mainly on the lower limbs, particularly on the dorsal face of the feet, ankles, and legs (*1*,*4*–*6*).

Infection is caused by a lack of protective clothing or shoes for persons working in rural areas in which spiny plants are common. Chromoblastomycosis is linked to poverty and is highly prevalent in low-income resource countries. It was the first fungal infection to be recognized as a neglected tropical disease (along with mycetoma, which is not exclusively of fungal origin) (*7*).

The clinical manifestation of chromoblastomycosis is polymorphous but is dominated by verrucous and tumoral lesions resembling cauliflower. No clinical particularity associated with the fungal species or genera has been described (*1*,*4*,*5*,*7*). Infection begins with development of muriform cells in the skin, provoking a granulomatous immune response. Muriform cells are specific to chromoblastomycosis and described as large brown, thick-walled, compartmented cells. They are also found in the infected plants assumed to be the source of human contamination.

Albeit belonging to the same order, the species found in these plants and the soil are different from the pathogenic ones (*4*,*5*,*7*,*8*). Infection involves ≥1 nodules that develop into verrucous, hyperkeratotic, or papillomatous lesions or plaques. The lesions progress slowly, over a period of 2–20 years and become highly

Author affiliations: Université d'Antananarivo, Antananarivo, Madagascar (T. Rasamoelina, N. Rakotozandrindrainy, F.A. Rakotomalala, B. Rakotonirina, A. Andriantsimahavandy, M. Rakoto Andrianarivelo); Université Grenoble Alpes, Grenoble, France (D. Maubon, S. Bailly, M. Cornet); Hôpital Universitaire Joseph Raseta Befelatanana, Antananarivo (M. Andrianarison, I. Ranaivo, F. Sendrasoa, F.R. Rabenja, L.S. Ramarozatovo); Centre Hospitalier Universitaire de Befelatanana, Antananarivo (L.S. Ramarozatovo)

DOI: https://doi.org/10.3201/eid2606.191498

[1]Preliminary results from this study were presented at the 20th International Society for Human and Animal Mycology Conference; June 29–July 5, 2018; Amsterdam, the Netherlands.

disabling because of development of elephantiasis-type edema or superinfections. Itching and scratching favor dissemination (*1*). The usual diagnosis relies on detection of the muriform cells in superficial samples, which is sufficient to confirm chromoblastomycosis. However, culture, yielding black fungi, is required to identify the causative agent at the species level by morphologic and molecular analyses (*1*,*5*).

Chromoblastomycosis predominates in tropical and subtropical regions, and most reported cases are from Latin America (Brazil, Mexico, and Venezuela), the Caribbean (Dominican Republic and Cuba), Africa, Asia (India, Japan, and southern China) and Australia (*1*). In Madagascar, studies conducted by Institut Pasteur during 1955–1994 provided an inventory of the number of cases of chromoblastomycosis and identified this country as the leading focus of chromoblastomycosis worldwide. The mean annual incidence was estimated to be ≈1 cases/200,000 persons during this period. The most commonly isolated agents were *Fonsecaea pedrosoi* in the humid tropical areas and *Cladophialophora carrionii* in the semiarid zones of the southern Madagascar (*9*–*11*).

Since 2013, we have established a cross-sectional study to document the current epidemiology of implantation mycoses in Madagascar, including chromoblastomycosis (*12*). Clinical diagnosis and fungal identification were confirmed by using molecular biology methods. We describe the current prevalence and clinical manifestation of chromoblastomycosis in Madagascar and patient outcomes. We also report the species-level identification, genetic relatedness, and antifungal susceptibility of clinical isolates.

Materials and Methods

Study Design and Patient Recruitment

We conducted a cross-sectional study as described (*12*). We recruited patients with clinically suspected chromoblastomycosis or another chronic dermatomycosis during March 2013–June 2017 at the Dermatology Department of the Joseph Raseta Befelatanana University Hospital in Antananarivo or during advanced consultation campaigns in districts (Figure 1, panel A). A clinical and demographic information form was completed for each participant. This study was approved by the Ethics Committee for Biomedical Research of the Ministry of Public Health of Madagascar (authorization no. 66-MSANP/CE).

Case Definition

We provide clinical, mycological, histological, severity and prognostic criteria used for classifying cases in this study (Table 1). Cases were identified after a monthly consultation between the clinicians of the Department of Dermatology-Rheumatology of Joseph Ravoahangy Befelatanana University Hospital Center in Antananarivo and the teams of mycologists from the Charles Mérieux Infectiology Center and Université Grenoble Alpes.

Clinical Samples

We obtained consent from patients and collected specimens consisting of biopsy material or flakes of skin. We then sent samples to the laboratory of the Charles Mérieux Infectiology Center of Antananarivo, where they were processed immediately or after 24–48 hours of storage at 2°C–8°C.

Mycological Analysis

Cultures

We performed direct microscopic examination of clinical specimens with and without Chlorazol Black staining to detect muriform cells, which are typical of chromoblastomycosis (*2*). We then used samples to inoculate Sabouraud medium supplemented with chloramphenicol, on which samples were incubated at 30°C for 2–3 weeks. For positive cultures, we morphologically identified fungal isolates, extracted DNA, and froze the culture at -80°C.

Molecular Analysis

We used the QIAamp DNA Blood Mini Kit (QIAGEN, https://www.qiagen.com) for DNA purification from clinical samples and fungal colonies. We performed PCR amplification in 2 steps. In the first step, we used 2 panfungal PCRs targeting internal transcribed spacer (ITS) regions with primers ITS1/ITS4 and D1D2 regions with primers NL-1/NL-4 and NL-3/NL-4 (*13*–*15*). In the second step, we used a *C. carrionii*–specific PCR, primers Ccar-F 5′-ATCGCTGCGAAGCGTCTCG-3′ and Ccar-R 5′-ACCGTCCAACACCAAGCACAGG-3′, and specific *Fonsecaea* sp. and PCR primers that have been described (*16*). We sequenced panfungal PCR products by LGC Genomics GmbH, https://www.nucleics.com) by using the same primers as for amplification.

We aligned the sequences obtained for panfungal PCR with reference sequences in the International Society of Human and Animal Mycology Barcoding Database (http://its.mycologylab.org) for the ITS region and the National Center for Biotechnology Information (NCBI; https://www.ncbi.nlm.nih.gov) database for the D1D2 and ITS regions (*17*). We constructed a phylogenetic tree by using MEGA7 software (https://www.

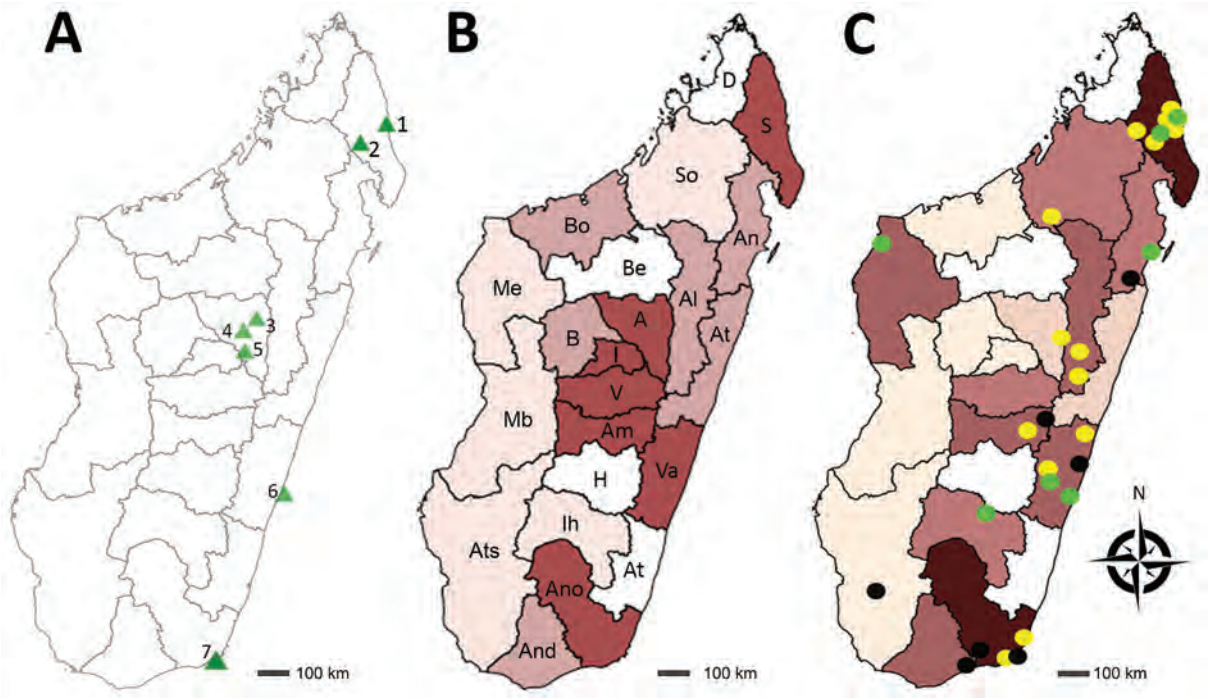

Figure 1. Recruitment of patients for study of chromoblastomycosis and prevalence by region, Madagascar, March 2013–June 2017. A) Recruitment sites (green triangles). Region of Sava: 1) Centre Hospitalier de Référence Régionale, Sambava District; 2) Centre Hospitalier de District and Hôpital Adventiste, Andapa District, Analamanga Region; 3) Centre de Santé de Base Alakamisy-Anjozorobe, Anjozorobe District; 4) Centre Hospitalier Universitaire Joseph Ravoahangy Befelatanana, Antananarivo District; 5) Centre de Santé de Base, Andramasina District, Vatovavy Fitovinany Region; 6) Fondation Médicale Ampasimanjeva, Manakara District; Anosy Region; 7) Centre Médical Tolagnaro, Centre Hospitalier de Référence Régionale Tolagnaro and Hôpital Luthérien Manambaro, Tolagnaro District. B) Geographic origin of patients recruited. Regions from north to south: D, Diana; S, Sava; I, Itasy; A, Analamanga; V, Vakinankaratra; B, Bongolava; So, Sofia; Bo, Boeny; Be, Betsiboka; Me, Melaky; Al, Alaotra-Mangoro; At, Atsinanana, An, Analanjirofo; Am, Amoron'I Mania; H, Haute Matsiatra; Va, Vatovavy-Fitovinany; Ato, Atsimo-Atsinanana; Ih, Ihorombe; Mb, Menabe; Ats, Atsimo Andrefana; And, Androy; Ano, Anôsy. No. patients recruited; dark purple, ≥6; medium purple, 3–5; light purple, <3; white, missing (none). C) Geographic distribution of chromoblastomycosis cases and causative fungal agents. Prevalence is no. cases/100,000 persons: dark purple, >0.5; medium purple, 0.1–0.5; light purple, <0.1; white, missing (none). Causative agent distribution: yellow dots, *Fonsecaea nubica*; black dots, *Cladophialophora carrionii*; green dots, *Fonsecaea* sp.

megasoftware.net) according to the protocol of Barry G. Hall (Bellingham Research Institute, Bellingham, WA, USA), based on the maximum-likelihood method.

Matrix-Assisted Laser Desorption/Ionization Time-of-Flight Mass Spectrometry Analysis

In-house main spectrum profiles (MSPs) were created on the Microflex Mass Spectrometer (Bruker Daltonics, https://www.bruker.com) according to the MALDI Biotyper MSP Creation version 1.1 protocol for reference strains of *C. carrionii*, *F. nubica*, *F. pedrosoi*, and *F. monophora* (1 of each) and 7 isolates formally identified by ITS DNA sequencing (Appendix Table, https://wwwnc.cdc.gov/EID/article/26/6/19-1498-App1.pdf). Isolates were cultured under 3 conditions: in Sabouraud–chloramphenicol agar for 4–7 days at 30°C, in liquid Sabouraud medium for 2–4 days at 25°C–30°C with shaking, and on solid peptone dextrose agar for 4–5 days at 30°C. We used an external validation of the new library performed with clinical isolates obtained during the study but not used to create the MSPs. We made a rapid identification by using a direct deposition method in accordance with MALDI Biotyper In Vitro Diagnostic Protocol Version 1.6 (Bruker Daltonics). We compared spectra obtained with Bruker Taxonomy (7,815 entries), Bruker Filamentous Fungi (364 MSP), NIH mold (365 profiles) (*18*), and MSP-chromoblastomycosis in-house databases and generated identification scores with the following quality criteria: score ≥2, species-level identification; score ≤1.7–<2, genus-level identification; score <1.7, no identification.

Susceptibility to Antifungal Drugs

The M38-A2 protocol of the Clinical and Laboratory Standard Institute for filamentous fungi was used on

Table 1. Classification criteria for cases of endemic chromoblastomycosis caused predominantly by *Fonsecaea nubica*, Madagascar*

Criteria	Description
Clinical	
Major	1) Nodular: moderately elevated, fairly soft, dull to pink violaceous growth; surface is smooth, verrucous, or scaly. 2) Verrucous: hyperkeratosis is the outstanding feature; warty dry lesions; frequently encountered along the border of the foot. 3) Tumorous: tumor-like masses, prominent, papillomatous, sometimes lobulated; cauliflower like; surface is partly or entirely covered with epidermal debris and crusts; more exuberant on lower extremities. 4) Cicatricial: nonelevated lesions that enlarge by peripheral extension with atrophic scarring, while healing takes place at the center; might expand centrifugally, usually with an annular, arciform, or serpiginous outline; tends to cover extensive areas of the body. 5) Plaque: least common type; slightly elevated with areas of infiltration of various sizes and shapes; red to violet color; a scaly surface, sometimes showing marked lines of cleavage; generally found on the higher portions of the limbs, shoulders, and buttocks. 6) Mixed form: association of the 5 basic types of lesions; usually observed in patients showing severe and advanced stages of the disease. 7) Clinical form on the face: erythematosquamous cup, central plate, atrophic, cicatricial, retractile, papular on the face, edema on the lips.
Minor	Pseudovacuolar and eczematous types in patients with a short time of evolution (<3 mo)
Mycological and histological	
Major	1) Muriform cells found by direct microscopic examination or histological analysis. 2) Molecular evidence of *Fonsecaea* spp., *Cladophialophora carrionii*, or *Rhinocladiella aquaspersa* by PCR with specific primers or internal transcribed spacer, BT2, or TF1 sequencing directly from clinical samples or a positive fungal culture of a melanized fungus morphologically reminiscent of *Fonsecaea* spp., *C. carrionii*, or *R. aquaspersa*. 3) Nonambiguous identification (score >2) of *Fonsecaea* spp., *C. carrionii*, or *R. aquaspersa* by MALDI-TOF MS with a validated main spectra profile.
Minor	Positive fungal culture of a melanized fungus morphologically reminiscent of *Fonsecaea* sp., *C. carrionii*, or *R. aquaspersa* from a clinical sample without molecular confirmation or ambiguous identification (score <2) of *Fonsecaea* spp., *C. carrionii*, or *R. aquaspersa* by MALDI-TOF MS with a home-made validated main spectra profile.
Classification	
Confirmed	≥1 of the major clinical criteria and ≥1 of the major mycological criteria or 1 minor clinical criterion and ≥1 of the major mycological criteria
Probable	≥1 of the major clinical criteria and 1 minor mycological or histological criterion and a complete or partial response to antifungal therapy
Possible	≥1 of the major clinical criteria without any (major or minor) mycological or histological criteria or ≥1 of the minor clinical criteria without any (major or minor) mycological or histological criteria and a complete or partial response to antifungal therapy
Severity	
Mild	Solitary plaque or nodule <5 cm in diameter
Moderate	Solitary or multiple lesions as nodular, verrucous, or plaque types existing alone or in combination, covering 1 or 2 adjacent cutaneous regions and measuring <15 cm in diameter
Severe	Any type of lesion alone or in combination covering extensive cutaneous regions whether adjacent or nonadjacent
Clinical response during antifungal therapy	
Major	Resolution of lesions with no relapse after 6 mo of follow-up. Reduction in the thickness/induration of lesions by 75% or reduction of the surface area affected by palpable lesions by 75%
Minor	Resolution of all cutaneous symptoms (i.e., pruritus) referable to the lesions and some objective improvement of lesions, less than a major response
Failure	Minor improvement or no change, worsening of lesions on therapy

*Adapted from Queiroz-Telles et al. (*1*). MALDI-TOF MS, matrix-assisted laser desorption/ionization time-of-flight mass spectrometry.

mycelial strains after subculture at 30°C to determine the MICs for antifungal agents (*19*). The following agents were tested at the concentrations indicated: posaconazole and isavuconazole, 0.016–8 μg/mL; amphotericin B and itraconazole, 0.006–32 μg/mL; and terbinafine, 0.008–4 μg/mL. MICs were determined after 120 h of culture at 30°C. We used a 100% inhibition endpoint for all drugs except for terbinafine, for which the endpoint was 80%.

Statistical Analysis

We compared chromoblastomycosis cases and other nonchromoblastomycosis cases by using χ^2 or Fisher exact tests for qualitative variables and Student *t*-tests for quantitative variables. Because this infection is chronic, we calculated prevalence by dividing the total number of cases at the end of the study period in June 2017 by the number of persons in the area concerned. We calculated the number of persons at the end of the period from the most recent figures available in 2013 from the official website of the National Institute of Statistics of Madagascar (*20*) and adjusted for the subsequent years with a growth rate of 2.7% per year (World Bank estimates of demographic growth in Madagascar). We analyzed data and generated maps by using Epi Info version 7.2.2.1(*21*) and R Studio version 1.0.153 (*22*).

Results

Demographic and Clinical Characteristics of Patients

During March 2013–June 2017, we included 148 patients with chronic cutaneous or subcutaneous lesions in the study. The mean (SD) age of the patients was 41 (18.8) years; 111 (75.0%) were males. The largest number of patients (n = 118, 79.7%) was enrolled at Joseph Raseta Befelatanana University Hospital, the permanent recruitment center (Figure 1, panel A). An analysis of the geographic origin of the patients showed that most (n = 90, 60.8%) patients came from the highlands, followed by the regions in the northeast (n = 23, 15.5%), east and southeast (n = 16, 10.8%), south and southwest (n = 13, 8.8%), and west (n = 6, 4.1%) (Figure 1, panel B). A comparison of the full years of recruitment (2014, 2015, and 2016) showed that the number of patients was higher in 2015 (n = 47, 31.8%) and 2016 (n = 36, 24.3%) than in 2014 (n = 28, 18.9%), but this difference was not significant (p = 0.47).

The largest proportion of the patients worked in agriculture (n = 76, 51.3%), followed by the service sector (n = 31, 21%), students (n = 20, 13.5%), craftsmen (n = 14, 9.5%), and the unemployed (n = 7, 4.7%). Lesions were located principally on the legs (62.8%) and arms (28.3%).

Patients with Chromoblastomycosis

At the first consultation, 58 of 148 patients had clinically suspected chromoblastomycosis. A diagnosis of chromoblastomycosis was made for 50 (33.8%) patients: confirmed for 41 (27.7%), probable for 3 (2.0%), and possible for 6 (4.0%). The frequency of chromoblastomycosis remained stable during 2013–2017 (21.4%–47.2%; p = 0.12 (Table 2) During 2014–2016, the mean (SD) number of annual chromoblastomycosis cases was 12 (5.5).

Patients who had chromoblastomycosis were significantly older (47.9 years) than those without chromoblastomycosis (37.5 years) (p = 0.0005). Analysis by age group showed that this trend was linked to a higher frequency of chromoblastomycosis in persons 33–48 years of age (44.0%) and 63–80 years of age (54.1%) (p = 0.001). The risk for having chromoblastomycosis was almost 5 times higher after the age of 33 years (odds ratio 5.44, 95% CI 2.04–17.10; p = 0.0001).

Male predominance was more marked in patients with chromoblastomycosis (92.0%) than in the other recruited patients (66.0%) (p = 0.001) (Table 2). Chromoblastomycosis patients were predominantly farmers and employees of the service sector (Table 2). The risk for chromoblastomycosis tended to be higher among farmers than among persons with other professions grouped together (OR 1.92, 95% CI 0.95–3.85; p = 0.09).

Location of lesions differed between chromoblastomycosis patients and other patients. Overall, 80.0% of patients with chromoblastomycosis had leg lesions, compared with 54.1% of patients without chromoblastomycosis (p = 0.005) (Table 2). A diagnosis of chromoblastomycosis was 3 times more likely than any other diagnoses for leg lesions (OR 3.36, 95% CI 1.45–8.4; p = 0.003).

Mixed and tumorous lesions were the most frequent forms in chromoblastomycosis cases (Table 2; Figure 2). Lesions were mostly severe (54%) and moderate (42%). All tumorous forms were severe. Chromoblastomycosis lesions had been present for >1–2 years in 90% of patients. The longest duration of lesion presence was 36 years. All but the verrucous forms were seen after 2 years of evolution (Table 2).

Prevalence and Geographic Distribution

We determined the geographic origin of patients with chromoblastomycosis, corresponding to the presumed origin of contamination. Most (84.0%) chromoblastomycosis patients originated from peripheral regions, such as the northern (40%), eastern and southeastern (22%), and southern and southwestern (20%) areas. We observed only 8 (16.0%) cases in the central highlands. In June 2017, the prevalence of chromoblastomycosis was highest (1.47 cases/100,000 persons) in the Sava region in northeastern Madagascar, followed by the Anosy region in south Madagascar (0.80 cases/100,000 persons) (Figure 1, panel C; Table 3).

Mycological Results

We collected 192 samples (151 biopsy specimens, 23 skin flake samples, and 18 pus samples) from 148 patients. For chromoblastomycosis patients, we analyzed 58 samples (47 biopsy specimens, 7 skin flake samples, and 4 pus samples). We compiled results of mycological investigations, including molecular analyses of samples from chromoblastomycosis patients (Appendix Table). Direct examination showed muriform cells in 33 (56.9%) samples, 145 (90.6%) biopsy specimens, and 13 (57.1%) skin flake samples (p = 0.11).

Culture

We obtained 172 cultures, including 41 from samples of 50 chromoblastomycosis patients. Overall, 26 (63.4%) cultures had macroscopic morphological features consistent with *Fonsecaea* sp. and *C. carrionii*,

and 2 (4.8%) cultures had microscopic morphological features consistent with *Fonsecaea* sp. and *C. carrionii*.

Molecular Analysis

The ITS panfungal PCR had lower sensitivity for clinical specimens than D1D2 PCR (21.6% vs. 91.9%; p<0.0001). The performances of the 2 panfungal PCR tests were relatively similar with cultures (75.0% vs. 92.5%; p = 0.07). Concerning the sensitivity of specific PCRs for clinical specimens, the PCR for *C. carrionii* was unable to confirm identification for any of the specimens, whereas the PCR for *Fonsecaea* spp. established a diagnosis in 16 (55.3%) of 30 cases caused by this genus (Appendix Table).

Comparison of the 31 reliable D1D2 sequences by using the NCBI database identified 20 isolates of *F. pedrosoi*, 4 of *F. monophora*, and 7 of *C. carrionii*. Comparison of the 28 reliable ITS sequences from the International Society of Human and Animal Mycology database confirmed 6 isolates of *C. carrionii* but identified 22 isolates of *F. nubica* as *Fonsecaea* spp. strains (Appendix Table). Identity ranged from 97.8% to 100.0% for *F. nubica* strains and from 99.5% to 99.8% for all *C. carrionii* isolates but 1 (which was 96.3%). Phylogenetic analysis confirmed that 22 *F. nubica* ITS sequences obtained from strains in Madagascar were grouped in the *F. nubica* clade (Figure 3). This clade also includes 2 sequences that correspond

Table 2. Characteristics of chromoblastomycosis cases in patients with chronic cutaneous and subcutaneous lesions, Madagascar, March 2013–June 2017*

Characteristic	Chromoblastomycosis				Other,‡ n = 98	p value
	Severe,† n = 27	Moderate,† n = 21	NA, n = 2	All, n = 50		
Period of recruitment						
2013, starting March 1	NS	NS	NS	6 (12.0)	10 (10.2)	0.12
2014	NS	NS	NS	6 (12.0)	22 (22.4)	NS
2015	NS	NS	NS	12 (24.0)	35 (35.7)	NS
2016	NS	NS	NS	17 (34.0)	19 (19.5)	NS
2017, through May 31	NS	NS	NS	9 (18.0)	12 (12.2)	NS
Mean age, y, (SD)	NS	NS	NS	47.9 (15.7)	37.5 (19.4)	0.0005
Age range, y						
3–17	NS	NS	NS	1 (2.0)	16 (16.3)	0.001
18–32	NS	NS	NS	5 (10.0)	26 (26.5)	NS
33–47	NS	NS	NS	21 (42.0)	26 (26.5)	NS
48–62	NS	NS	NS	10 (20.0)	19 (19.4)	NS
63–80	NS	NS	NS	13 (26.0)	11 (11.2)	NS
Sex						
M	NS	NS	NS	46 (92.0)	65 (66.3)	0.001
F	NS	NS	NS	4 (8.0)	33 (33.7)	NS
Occupation						NS
Farmer	17 (63.0)	12 (57.1)	2 (100.0)	31 (62.0)	45 (45.9)	0.006
Services sector	7 (25.9)	7 (33.3)	0	14 (28.0)	17 (17.4)	NS
Student	1 (3.7)	1 (4.8)	0	2 (4.0)	18 (18.4)	NS
Merchant-artisan	1 (3.7)	0	0	1 (2.0)	13 (13.3)	NS
Unemployed	1 (3.7)	1 (4.8)	0	2 (4.0)	5 (5.1)	NS
Anatomic location						
Lower limb	21 (77.8)	17 (81.0)	2 (100.0)	40 (80.0)	53 (54.1)	0.005
Upper limb	3 (11.1)	3 (14.3)	0	6 (12.0)	36 (37.7)	NS
Other§	3 (11.1)	1 (4.7)	0	4 (8.0)	9 (9.2)	NS
Duration of the lesion, y						
<1	2 (7.4)	1 (4.8)	0	3 (6.0)	56 (57.1)	<0.0001
1–2	1 (3.7)	1 (4.8)	0	2 (4.0)	14 (14.3)	NS
>2	24 (88.9)	19 (90.4)	2 (100.0)	45 (90.0)	28 (28.6)	NS
Clinical form						
Nodular	1 (3.7)	3 (14.3)	0	4 (8.0)	NS	NS
Verrucous	1(3.7)	4 (19.0)	0	5 (10.0)	NS	NS
Tumorous	5 (18.5)	0	0	5 (10.0)	NS	NS
Cicatricial	3 (11.1)	1 (4.8)	0	4 (8.0)	NS	NS
Plaque	3 (11.1)	7 (33.3)	0	10 (20.0)	NS	NS
Mixed	8 (29.6)	3 (14.3)	0	11 (22.0)	NS	NS
Mixed on the face	2 (7.4)	0	0	2 (4.0)	NS	NS
Modified by previous therapy	4 (14.8)	3 (14.3)	0	7 (14.0)	NS	NS
NA	0	0	2 (100.0)	2 (4.0)	NS	NS

*Values are no. (%) unless otherwise indicated. NA, not available; NS, not specified.
†For definitions, see Table 1.
‡Sporotrichosis (n = 63) (*12*); mycetoma (n = 4); carcinoma, eczema, and cutaneous tuberculosis (n = 2); carpitis, erysipela, fibrosarcoma, cutaneous lymphoma, porokeratosis of Mibelli, prurigo nodularis, pyoderma, and papillomavirus (n = 1); not specified (n = 17).
§Head and neck, thorax.

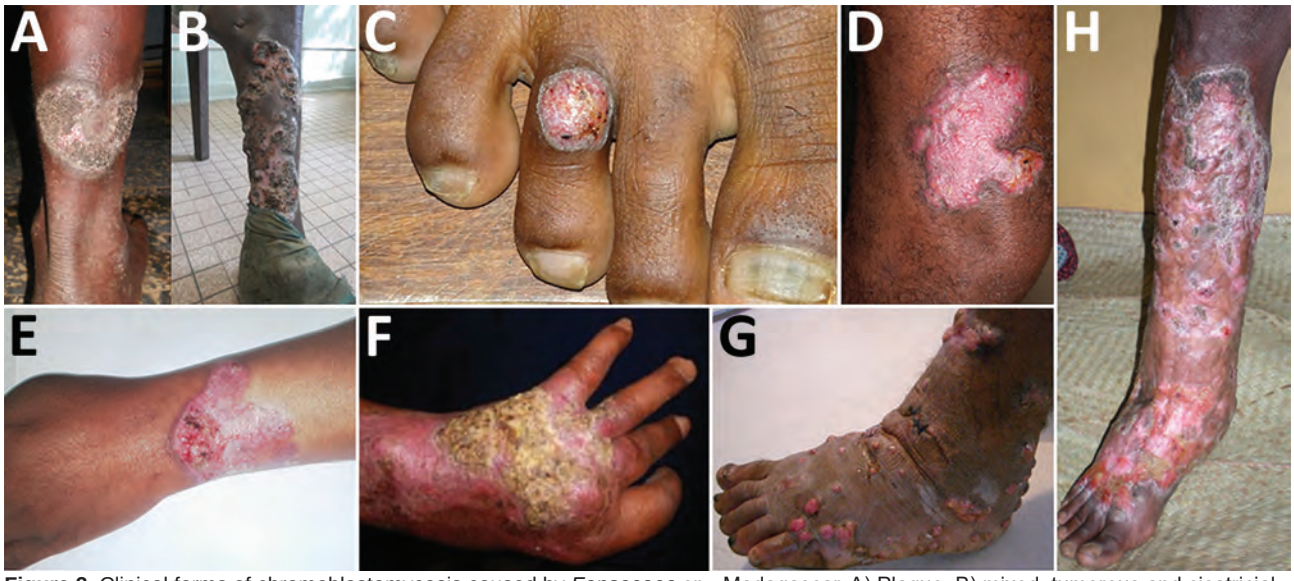

Figure 2. Clinical forms of chromoblastomycosis caused by *Fonsecaea* sp., Madagascar. A) Plaque; B) mixed: tumorous and cicatricial; C) nodular; D) raised plaque; E) plaque; F) cicatricial; G) tumorous caused by *Cladophialophora carrionii*; H) mixed: cicatricial and modified by previous therapy.

to *Fonsecaea* strains collected previously by Institut Pasteur in Madagascar and identified as *F. pedrosoi* (*23*). The *Fonsecaea* strains were isolated from patients who originated from the humid tropical zones of eastern Madagascar, whereas *C. carrionii* was restricted to the southern and eastern regions of this country (Figure 1, panel C).

Table 3. Prevalence of chromoblastomycosis, Madagascar, March 2013–June 2017

Region	No. persons*	No. cases	Prevalence
North and central north	3,629,908	20	0.55
Analanjirofo	1,151,536	2	0.17
Sava	1,091,102	16	1.47
Sofia	1,387,270	2	0.14
Highlands	7,850,950	8	0.10
Analamanga	3,725,377	3	0.08
Amoron'i Mania	795,434	3	0.38
Itasy and Bongolava	1,324,044	0	0
Vakinankaratra	2,006,095	2	0.10
West	1,870,459	1	0.05
Boeny and Menabe	1,548,299	0	0.00
Melaky	322,160	1	0.31
East and South East	4,131,928	11	0.27
Alaotra Mangoro	1,142,612	4	0.35
Atsinanana	1,413,572	1	0.07
Vatovavy Fitovinany	1,575744	6	0.38
South and South West	3,376,074	10	0.30
Androy	816,466	3	0.37
Anosy	747,352	6	0.80
Atsimo Andrefana	1,464,830	0	0
Ihorombe	347,427	1	0.29

*Determined at the end of the study period and calculated from the most recent figures available in 2013 and adjusted for subsequent years with a growth rate of 2.7%/year (World Bank estimates of demographic growth in Madagascar).
†No. cases/100,000 persons.

We used 11 reference strains or isolates identified by ITS sequencing for matrix-assisted laser desorption/ionization time-of-flight (MALDI-TOF) mass spectrometry analysis. We then validated the MSPs by identification of ITS sequenced isolates (Appendix Table). A comparison of the obtained spectra showed that the mean (SD) identification score was 2.01 (0.36) when compared with MSPs already present in reference databases. Statistical tests showed similar identification performance between the 3 culture conditions. In-house MSPs systematically outperformed the 2 sets of MSPs in the Bruker database and the set in the NIH database for *F. nubica* and *C. carrionii* identification, confirming their superiority for discrimination and identification at the species level. Our MSPs identified 1 additional isolate of *F. nubica*, which ITS sequencing failed to identify (MYC10081; Appendix Table).

Susceptibility of Strains to Antifungal Drugs and Patient Outcomes

A total of 15 *F. nubica* and 5 *C. carrionii* isolates were culturable after thawing for MIC determination. We determined MICs and their geometric means for the 5 antifungal drugs tested (Table 4). MICs were ≤1 μg/mL for itraconazole and ≤0.25 μg/mL for posaconazole and isavuconazole for all *F. nubica* and *C. carrionii* isolates. We observed low MICs (≤0.031 μg/mL) for terbinafine for all *F. nubica* and 4/5 *C. carrionii* isolates. Amphotericin B appeared to be less active than the other antifungal drugs.

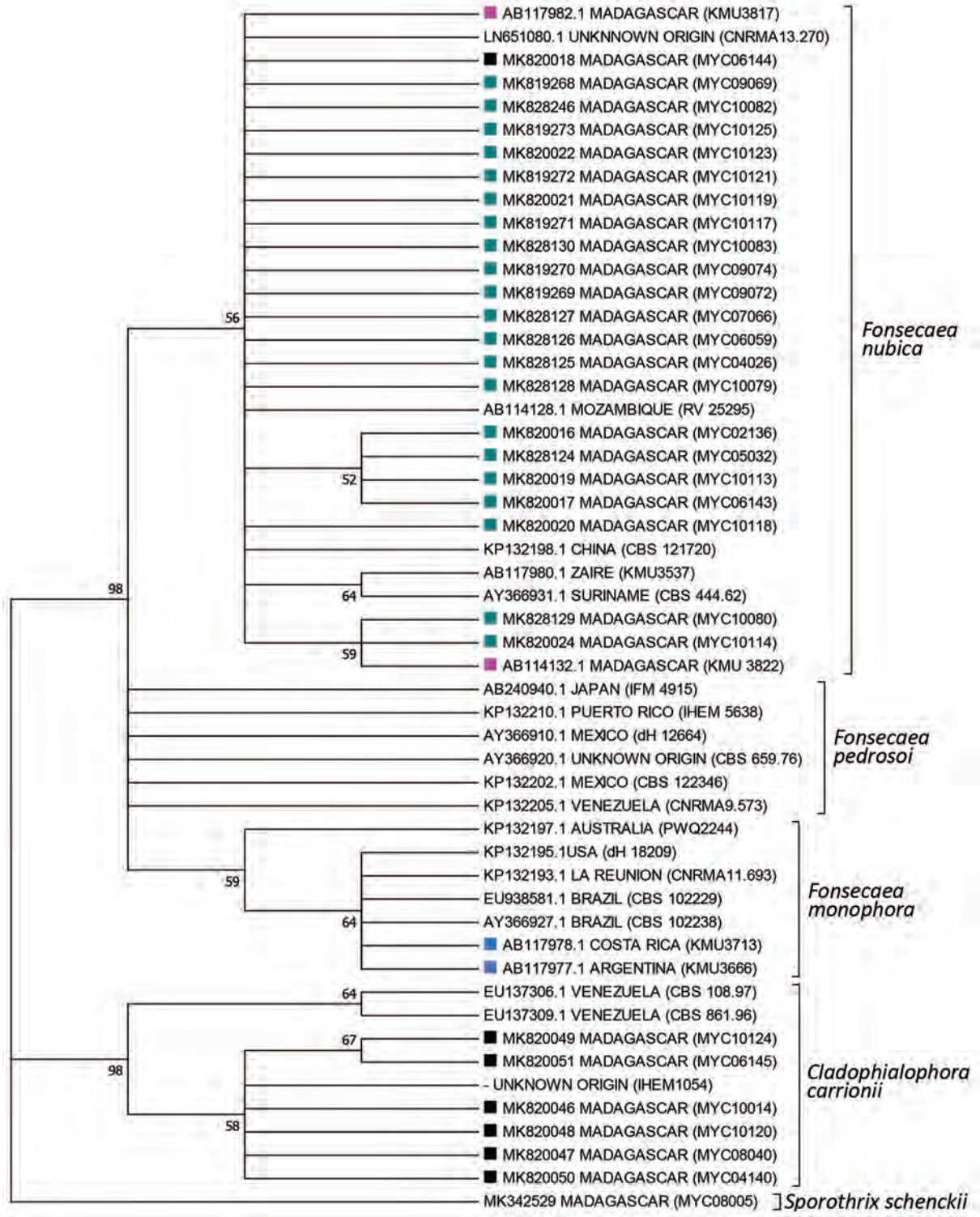

Figure 3. Phylogenetic tree of internal transcribed spacers sequences of fungal isolates from patients with chromoblastomycosis, Madagascar. Tree was constructed by using MEGA7.0 software (https://www.megasoftware.net) and applying the maximum-likelihood method based on the Kimura 2-parameter model (100 bootstrap replicates). Numbers along branches are bootstrap values. GenBank accession numbers are provided. Detailed information for strains is available (Appendix Table, https://wwwnc.cdc.gov/EID/article/26/6/19-1498-App1.pdf). *Sporpthrix schenckii* was used as the outgroup. Dark blue squares, *Fonsecaea nubica* sequences isolated in this study; black squares, *Cladophialophora carrionii* isolated in this study; pink squares, *F. nubica* previously identified as *F. pedrosoi*; light blue squares, *F. monophora* previously identified as *F. pedrosi.*

Table 4. Minimal inhibitory concentrations of 5 antifungal drugs for *Fonsecaea nubica*) and *Cladophialophora carrionii* (n = 5) strains, Madagascar*

Fungi, drug	MIC, μg/mL and no. isolates										Geometric mean, μg/mL (range)
	0.008	0.015	0.02	0.031	0.062	0.125	0.25	0.5	1.0	2.0	
F. nubica, n = 15											
ITZ	0	0	0	5	3	4	1	1	1	0	0.101 (0.031–1.0)
PSZ	0	11	0	2	2	0	0	0	0	0	0.021 (0.015–0.062)
ISZ	1	3	0	10	1	0	0	0	0	0	0.027 (0.008–0.006)
TRB	11	1	2	1	0	0	0	0	0	0	0.012 (0.008–0.003)
AMB	0	0	0	0	1	2	4	6	1	1	0.692 (0.062–4.0)
C. carrionii, n = 5											
ITZ	0	0	1	1	0	2	0	1	0	0	0.094 (0.031–1.0)
PSZ	0	0	2	2	0	0	1	0	0	0	0.071 (0.031–0.5)
ISZ	0	0	2	2	0	0	1	0	0	0	0.071 (0.031–0.5)
TRB	2	2	0	0	1	0	0	0	0	2	0.024 (0.008–0.125)
AMB	0	0	0	0	0	0	0	0	5	0	4.595 (2.0–8.0)

*AMB, amphotericin B; ISZ, isavuconazole; ITZ, itraconazole; PSZ, posaconazole; TRB, terbinafine.

A total of 27 (17 with severe cases and 10 with moderate cases) of the 50 chromoblastomycosis patients who were treated (itraconazole, 100 mg 2×/d) could have been followed-up. Patients were treated for 4–26 months independently of disease severity. A complete cure was never achieved, and a major response was seen in only 2 patients with severe forms. Other patients showed only a minor response.

Discussion

We conducted an epidemiologic study of chromoblastomycosis in Madagascar that went back to 1997, when the studies conducted by Institut Pasteur stopped. Our study confirmed the high endemicity and showed even higher burdens in some regions than described 20 years earlier. Although the climatic–geographic distribution of fungal pathogens was preserved for *Fonsecaea* spp. in the humid tropical climate of the east, north, and northwest regions and *C. carrionii* in the semiarid climate in the southern region, molecular identification led to a revision of *F. nubica* previously described as *F. pedrosoi* (*9*,*24*,*25*). On the basis of this study, we were able to develop and routinely implement molecular analyses in Madagascar, making positive species identification possible.

We report high regional prevalences of 1.47 cases/100,000 persons for the Sava region and 0.8 cases/100,000 persons for the Anosy region. These 2 regions were already perceived to be the major foci of the disease. These prevalences exceed the prevalence of 0.5 cases/100,000 persons estimated 20 years ago (*9*). Other regions, such as Amoron'i Mania, Melaky, or Vatovavy Fitovinany, had lower prevalences (0.31–0.38 cases/100,000 persons), similar to prevalences previously described (*9*). The frequency of chromoblastomycosis in some areas of western and southwestern Madagascar are unknown because these areas were not investigated by advanced consultation campaigns. More recently, Queiroz-Telles reported a prevalence of 0.26 cases/100,000 persons in Madagascar (*26*). Our results show at least a steady high level of endemicity, suggesting that this country could still be the leading focus of chromoblastomycosis worldwide (*9*). However, a comparison with data reported from other countries is challenging because these data are for mostly cumulative cases or series counts (*1*,*4*,*27*–*29*). Our study also confirms the low prevalence in the central highlands, where climatic conditions are different because of higher altitude (drier and cooler than for the northern and eastern coasts) (*9*).

Use of molecular methods, such ITS sequencing and MALDI-TOF mass spectrometry, enabled us to revise the identification of the *Fonsecaea* species endemic to Madagascar as *F. nubica* instead of *F. pedrosoi*. Phylogenetic analysis grouped all reliable *Fonsecaea* sequences obtained from the strains isolated in Madagascar and 2 sequences previously identified as *F. pedrosoi* (*23*) together into the Nubica clade. In addition, analysis of D1D2 sequences showed that the NCBI database was not reliable for identification of *F. nubica* at the species level.

The climato–geographic locations for case-patients infected with *F. nubica* corresponded to those described for *F. perdosoi* in the humid northern and eastern tropical coasts (*1*,*9*). Concerning the second causative pathogen (*C. carrionii*) found in Madagascar, we confirmed its location in the arid southern part of Madagascar. However, we detected 3/7 cases in patients who did not report any trip to the southern region and who originated from the humid zones (*1*,*9*). These results might suggest a larger distribution and lower restrictive climatic conditions for this species.

Patients with chromoblastomycosis were mostly men and farmers, and lesions were located mostly on lower limbs. Most patients were involved in raising crops, working with bare hands and feet, animal husbandry, rearing of livestock (e.g., pigs or

zebu cattle) near plantations, and woodcutting and charcoal-producing activities. In the Sava region, in which we found the highest prevalence, vanilla, coffee, sugar cane, and pineapple production are the main activities. In the dry southern area, the second focus of chromoblastomycosis, the flora are characterized by forests of thorny plants of the family *Didieraceae* and euphorbias. This region also contains sisal, which is used for manufacture of rope; eucalyptus, which is used for charcoal production; and cacti, which are used for construction materials (2). These rural activities provide many risks for injury by thorny plants or cutting leaves for persons working with bare hands and feet.

Clinical manifestations were mostly polymorphous, with an association of plaques and nodular and warty tumorous features, characterized by pink pimples with a typical cauliflower appearance. Nearly half of the patients were not available for follow-up examinations, mostly because of remoteness of their homes, lack of public transport in rural areas, and disabilities caused by their extensive lesions. We confirmed that chromoblastomycosis lesions are mostly refractory because only 7.0% of the patients showed major improvement. Nevertheless, observance of the treatment and monitoring of therapeutic drug use could not be assessed. Thus, we do not know if the lack of cure was caused by ineffectiveness of itraconazole or low observance of use or low absorption of this drug.

In conclusion, after 20 years without data, our study and update of the epidemiology of chromoblastomycosis in Madagascar confirms its high endemicity. This disease shows a high prevalence in the 2 main disease loci of 1.47 cases/100,00 persons in the northeast region and 0.8 cases/100,000 persons the southeast region of this country. Chromoblastomycosis has persisted in Madagascar, and its burden might be even greater than before, which fully supports the recognition by the World Health Organization that chromoblastomycosis is a neglected tropical disease. On the basis of this recent international effort, national control programs should be conducted to ensure prevention, improve management through the earlier detection of lesions, and facilitate access to treatment.

This study was supported by Fondation Mérieux (Lyon, France), Institut de Recherche pour le Développement, Société Française de Mycologie Médicale, and Campus France.

M.C. received research grants from Pfizer and travel grants from Basilea, Gilead, Merck Sharp & Dohme, and Pfizer. F.R.R., M.R.A., L.S.R., and M.C. designed the study; T.R., D.M., N.R., F.A.R., F.S., I.R., M.A., and B.R. collected data; T.R., D.M., S.B., A.A., F.R.R., M.R.A., L.S.R., and M.C. analyzed and interpreted data; and T.R., D.M., S.B., M.R.A., and M.C. wrote the manuscript. All authors reviewed and approved the manuscript.

About the Author

Dr. Rasamoelina is a research scientist at the Centre d'Infectiologie Charles Mérieux, Antananarivo, Madagascar. His research interests are the epidemiology and laboratory diagnosis of tropical infections.

References

1. Queiroz-Telles F, de Hoog S, Santos DW, Salgado CG, Vicente VA, Bonifaz A, et al. Chromoblastomycosis. Clin Microbiol Rev. 2017;30:233–76. https://doi.org/10.1128/CMR.00032-16
2. Rasamoelina T, Raharolahy O, Rakotozandrindrainy N, Ranaivo I, Andrianarison M, Rakotonirina B, et al. Chromoblastomycosis and sporotrichosis, two endemic but neglected fungal infections in Madagascar. J Mycol Med. 2017;27:312–24. https://doi.org/10.1016/j.mycmed.2017.08.003
3. Badali H, Bonifaz A, Barrón-Tapia T, Vázquez-González D, Estrada-Aguilar L, Oliveira NM, et al. *Rhinocladiella aquaspersa*, proven agent of verrucous skin infection and a novel type of chromoblastomycosis. Med Mycol. 2010;48:696–703. https://doi.org/10.3109/13693780903471073
4. Bonifaz A, Carrasco-Gerard E, Saúl A. Chromoblastomycosis: clinical and mycologic experience of 51 cases. Mycoses. 2001;44:1–7. https://doi.org/10.1046/j.1439-0507.2001.00613.x
5. Queiroz-Telles F, Esterre P, Perez-Blanco M, Vitale RG, Salgado CG, Bonifaz A. Chromoblastomycosis: an overview of clinical manifestations, diagnosis and treatment. Med Mycol. 2009;47:3–15. https://doi.org/ 10.1080/13693780802538001
6. Queiroz-Telles F, Nucci M, Colombo AL, Tobón A, Restrepo A. Mycoses of implantation in Latin America: an overview of epidemiology, clinical manifestations, diagnosis and treatment. Med Mycol. 2011;49:225–36. https://doi.org/10.3109/13693786.2010.539631
7. Queiroz-Telles F, Fahal AH, Falci DR, Caceres DH, Chiller T, Pasqualotto AC. Neglected endemic mycoses. Lancet Infect Dis. 2017;17:e367–77. https://doi.org/10.1016/S1473-3099(17)30306-7
8. Vicente VA, Najafzadeh MJ, Sun J, Gomes RR, Robl D, Marques SG, et al. Environmental siblings of black agents of human chromoblastomycosis. Fungal Divers. 2014;65:47–63. https://doi.org/10.1007/s13225-013-0246-5
9. Esterre P, Andriantsimahavandy A, Ramarcel ER, Pecarrere JL. Forty years of chromoblastomycosis in Madagascar: a review. Am J Trop Med Hyg. 1996;55:45–7. https://doi.org/10.4269/ajtmh.1996.55.45
10. Brygoo ER. Chromoblastomycosis in Madagascar [in French]. Sem Hop Paris. 1957;33:777–91.
11. Coulanges P, Locheron P. Chromoblastomycosis in Madagascar. Epidemiological data on the most important outbreak currently known in the world (counting 891 cases diagnosed from 1955 to 1987) [in French]. Arch Inst Pasteur Madagascar. 1981;48:69–95.

12. Rasamoelina T, Maubon D, Raharolahy O, Razanakoto H, Rakotozandrindrainy N, Rakotomalala FA, et al. Sporotrichosis in the highlands of Madagascar, 2013–2017. Emerg Infect Dis. 2019;25:1893–902. https://doi.org/10.3201/eid2510.190700
13. Irinyi L, Lackner M, de Hoog GS, Meyer W. DNA barcoding of fungi causing infections in humans and animals. Fungal Biol. 2016;120:125–36. https://doi.org/10.1016/j.funbio.2015.04.007
14. Kurtzman CP, Robnett CJ. Identification of clinically important ascomycetous yeasts based on nucleotide divergence in the 5′ end of the large-subunit (26S) ribosomal DNA gene. J Clin Microbiol. 1997;35:1216–23. https://doi.org/10.1128/JCM.35.5.1216-1223.1997
15. Abliz P, Fukushima K, Takizawa K, Nishimura K. Identification of pathogenic dematiaceous fungi and related taxa based on large subunit ribosomal DNA D1/D2 domain sequence analysis. FEMS Immunol Med Microbiol. 2004;40:41–9. https://doi.org/10.1016/S0928-8244(03)00275-X
16. Abliz P, Fukushima K, Takizawa K, Nieda N, Miyaji M, Nishimura K. Rapid identification of the genus *fonsecaea* by PCR with specific oligonucleotide primers. J Clin Microbiol. 2003;41:873–6. https://doi.org/10.1128/JCM.41.2.873-876.2003
17. Irinyi L, Serena C, Garcia-Hermoso D, Arabatzis M, Desnos-Ollivier M, Vu D, et al. International Society of Human and Animal Mycology (ISHAM)-ITS reference DNA barcoding database—the quality controlled standard tool for routine identification of human and animal pathogenic fungi. Med Mycol. 2015;53:313–37. https://doi.org/10.1093/mmy/myv008
18. Lau AF, Drake SK, Calhoun LB, Henderson CM, Zelazny AM. Development of a clinically comprehensive database and a simple procedure for identification of molds from solid media by matrix-assisted laser desorption ionization-time of flight mass spectrometry. J Clin Microbiol. 2013;51:828–34. https://doi.org/10.1128/JCM.02852-12
19. Clinical and Laboratory Standards Institute. Reference method for broth dilution antifungal susceptibility testing of filamentous fungi. Approved standard (document M38–A2). Wayne (PA): The Institute; 2008.
20. Madagascar in figures, population, and demography [in French] [cited 2020 Feb 7]. https://www.instat.mg
21. Centers for Disease Control and Prevention. Epi Info 7 [cited 2020 Feb 7]. https://www.cdc.gov/epiinfo/pdfs/UserGuide/EI7Full.pdf
22. Bivand R, Lewin-Koh N. Maptools: tools for reading and handling spatial objects. R package version 0.8–27 [cited 2020 Feb 7]. https://www.researchgate.net/publition/308748917_maptools_Tools_for_reading_and_handling_spatial_objects_R_package_version_08-27
23. Tanabe H, Kawasaki M, Mochizuki T, Ishizaki H. Species identification and strain typing of *Fonsecaea pedrosoi* using ribosomal RNA gene internal transcribed spacer regions. Nippon Ishinkin Gakkai Zasshi. 2004;45:105–12. https://doi.org/10.3314/jjmm.45.105
24. Esterre P, Andriantsimahavandy A, Raharisolo C. Natural history of chromoblastomycosis in Madagascar and the Indian Ocean [in French]. Bull Soc Pathol Exot. 1997;90:312–7.
25. Najafzadeh MJ, Sun J, Vicente V, Xi L, van den Ende AH, de Hoog GS. *Fonsecaea nubica* sp. nov, a new agent of human chromoblastomycosis revealed using molecular data. Med Mycol. 2010;48:800–6. https://doi.org/10.3109/13693780903503081
26. Queiroz-Telles F. Grades of severity and parameters for cure. Presented at: International Society for Human and Animal Mycology workshop on chromoblastomycosis; 2017 Dec 11; Havana, Cuba.
27. Xi L, Sun J, Lu C, Liu H, Xie Z, Fukushima K, et al. Molecular diversity of *Fonsecaea* (Chaetothyriales) causing chromoblastomycosis in southern China. Med Mycol. 2009;47:27–33. https://doi.org/10.1080/13693780802468209
28. Attapattu MC. Chromoblastomycosis: a clinical and mycological study of 71 cases from Sri Lanka. Mycopathologia. 1997;137:145–51. https://doi.org/10.1023/A:1006819530825
29. Agarwal R, Singh G, Ghosh A, Verma KK, Pandey M, Xess I. Chromoblastomycosis in India: review of 169 cases. PLoS Negl Trop Dis. 2017;11:e0005534. https://doi.org/10.1371/journal.pntd.0005534

Address for correspondence: Muriel Cornet, Laboratoire Innovations Translationnelles en Médecine et Complexité–Informatique et Mathématiques Appliquées de Grenoble, Équipe Thérapeutique Recombinante Expérimentale, Domaine de la Merci, 38706 La Tronche CEDEX, France; email: mcornet@chu-grenoble.fr

Emergence of New Non–Clonal Group 258 High-Risk Clones among *Klebsiella pneumoniae* Carbapenemase–Producing *K. pneumoniae* Isolates, France

Rémy A. Bonnin, Agnès B. Jousset, Adriana Chiarelli, Cécile Emeraud, Philippe Glaser, Thierry Naas, Laurent Dortet

The worldwide spread of *Klebsiella pneumoniae* carbapenemase–producing *Klebsiella pneumoniae* (KPC-*Kp*) isolates was reported to be caused by dissemination of 1 clonal complex (i.e., clonal group [CG] 258, which includes sequence types [STs] 258 and 512). We conducted whole-genome sequencing and epidemiologic analysis of all KPC-*Kp* isolates in France in 2018 and found that new successful high-risk clones of ST147, ST307, ST231, and ST383 are now the main drivers of bla_{KPC} genes. The bla_{KPC} genes were mostly carried by Tn*4401a* and Tn*4401d* structures and a new non–Tn*4401* element. Our epidemiologic investigations showed that the emergence of these non-CG258 KPC-*Kp* isolates in France was linked to dissemination of these clones from Portugal. Thus, KPC-*Kp* epidemiology has changed in Europe, at least in several non–KPC-endemic countries of western Europe, such as France and Portugal, where CG258 is not the most prevalent clone.

In *Klebsiella pneumoniae* bacteria, resistance to carbapenems results in 2 main mechanisms: the production of an extended spectrum β-lactamase or plasmid-borne cephalosporinase associated with a decrease in permeability of the outer membrane (especially through alteration of OmpK35 and OmpK36 porins), or the production of a carbapenemase (*1*,*2*). In France, these carbapenemases are Ambler's class A KPC enzymes; class B metallo-β-lactamases of NDM-, VIM- and, to a lesser extent, IMP-type; and Ambler's class D oxacillinases of OXA-48–like type (*3*,*4*).

K. pneumoniae carbapenemase (KPC) was first identified in United States in the early 2000s (*5*). Since then, this carbapenemase has spread and has become endemic in several countries, including the United States, Israel, Greece, China, and Italy. It has also been sporadically described in many countries of Europe (*1*). The worldwide spread of KPC has been linked to the dissemination of a main clone of *K. pneumoniae* (sequence type [ST] 258) and a single-locus variant (ST512) (*6*). In Asia (especially China), ST11, another single-locus variant of ST258, is mostly reported among bla_{KPC}-harboring *K. pneumoniae* isolates (*7*). In addition, a recently published study, conducted by the EUSCAPE working group in 2013 in Europe, revealed that the spread of carbapenemase-producing *K. pneumoniae* was driven by only a few clones (*8*). The most prevalent carbapenemase was KPC (45.5% [311/684 isolates]), and 72.7% (229/311) of KPC-producing *K. pneumoniae* (KPC-*Kp*) belong to the same clonal group (CG) 258, including ST258 and ST512. Whole-genome sequencing (WGS) analysis has suggested that ST258 and ST512 KPC-*Kp* spread out in Europe from 2 KPC-endemic countries: Greece (ST258) and Italy (ST512) (*6*,*9*–*11*). However, that study described the epidemiology of KPC in Europe in 2013, whereas the aim of our study was to describe the genomic characteristics of KPC isolates from a more recent period.

Author affiliations: Institut Pasteur–Assistance Publique/Hôpitaux de Paris–University Paris Sud, Paris, France (R.A. Bonnin, A.B. Jousset, A. Chiarelli, C. Emeraud, T. Naas, L. Dortet); Faculty of Medicine University Paris-Sud, University Paris–Saclay, Le Kremlin-Bicêtre, France (R.A. Bonnin, A.B. Jousset, C. Emeraud, T. Naas, L. Dortet); National Reference Center for Antibiotic Resistance: Carbapenemase Producing *Enterobacteriaceae*, Le Kremlin-Bicêtre, (R.A. Bonnin, A.B. Jousset, C. Emeraud, T. Naas, L. Dortet); Assistance Publique/Hôpitaux de Paris, Bicêtre Hospital, Le Kremlin-Bicêtre (A.B. Jousset, C. Emeraud, T. Naas, L. Dortet)

DOI: https://doi.org/10.3201/eid2606.191517

Analysis of the genetic context of bla_{KPC} has revealed that this gene is mostly localized into a class 2 transposon named Tn*4401* (*12*). Several variants of this Tn*4401* (Tn*4401a* through Tn*4401i*) have been reported with deletions upstream of bla_{KPC} within the promoter region (*13*,*14*). Consequently, expression of bla_{KPC} genes is complex and might involve different promoters, depending on the specific genetic environment and bacterial species. The 2 main promoters are named P1, which is in the vicinity of bla_{KPC}, and P2, a hybrid promoter located partly in the inverted repeat right of IS*Kpn7* (*15*). In rare cases, bla_{KPC} genes have been described in genetic structure not related to Tn*4401* and are named non–Tn*4401* elements (NTE) (*16*). However, in NTE, the expression of bla_{KPC} is mediated by other promoters. Our study aimed to deeply characterize the epidemiology of KPC-*Kp* circulating in France in 2018.

Material and Methods

Strains Collections and Culture Conditions

We included all KPC-*Kp* sent to France's National Reference Center for Antimicrobial Resistance during January 1–December 31, 2018. As previously described, we used isolates that were recovered from clinical and screening specimens and sent on a voluntary basis by any type of laboratory related to any health facility, such as private and public hospitals, nursing homes, and community laboratories (*3*,*4*). These laboratories were located throughout France, including overseas territories. KPC-*Kp* recovered by the National Reference Center for Antimicrobial Resistance represent ≈85%–90% of the KPC-*Kp* infection cases reported to the French Public Health Agency (R.A. Bonnin, L. Dortet, unpub. data). The collection used for WGS analysis represents a total of 63 nonduplicate isolates recovered from rectal screening (n = 45), urine (n = 12), blood cultures (n = 1), wound infections (n = 2), and respiratory samples (n = 2) and 1 isolate for which no recovery site information was available. Because the aim of the study was to evaluate the genetic diversity of KPC producers, we discarded from further analysis any duplicate isolates or isolates recovered from the same patient.

Antimicrobial Susceptibility Testing and Carbapenemase Detection

We performed antimicrobial susceptibility testing by using the disc diffusion method on Mueller-Hinton agar (Bio-Rad, https://www.bio-rad.com) and interpreted results according to European Committee on Antimicrobial Susceptibility Testing guidelines as updated in 2018 (http://www.eucast.org). We determined MICs for colistin by using broth microdilution (Sensititer Thermofisher, https://www.thermofisher.com). We performed carbapenemase detection by using Rapidec Carba NP (bioMérieux, https://www.biomerieux.com), followed by immunochromatographic detection of the carbapenemase enzyme using NG-Carba5 test (NG Biotech, https://ngbiotech.com).

WGS and Bioinformatic analysis

We sequenced all KPC-*Kp* isolates by using Illumina technology as previously described (*17*). We extracted total DNA from colonies by using the Ultraclean Microbial DNA Isolation Kit (MO BIO Laboratories, https://www.mobio.com) according to the manufacturer's instructions. We prepared the DNA library as previously described (*17*) and performed de novo assembly and read mappings by using CLC Genomics Workbench 12.0 (QIAGEN, https://www.qiagen.com). We identified the acquired antimicrobial resistance genes by using Resfinder 3.1 (https://cge.cbs.dtu.dk/services/ResFinder/) and the CARD database (https://card.mcmaster.ca). We annotated the genomes by using RAST (*18*). We performed phylogenic analysis by using CSIphylogeny 1.4 (https://cge.cbs.dtu.dk/services/CSIPhylogeny) and visualized the genomes by using FigTree 1.4.3 (http://tree.bio.ed.ac.uk/software/figtree). We performed sequences alignments by using ClustalW (https://www.genome.jp/tools-bin/clustalw). We analyzed single-nucleotide polymorphisms (SNPs) on the whole genome by using CSIphylogeny V1.4 with parameters as follows: select minimum depth at SNP position at 10×, minimum distance between SNPs at 10 bp, and minimum SNP quality score of 30.

We constructed the genetic contexts by using de novo assembly or by mapping with reference genomes from GenBank and verified by in-house PCR as previously described (*17*). We analyzed plasmid contents of clinical isolates by using PlasmidFinder 2.1 to search for the replicase gene and by conducting manual searches for genes showing homology with the replicase gene.

Results

Low Prevalence of KPC Producers among Carbapenem-Resistant *K. pneumoniae* in France

In 2018, a total of 3,931 carbapenem-resistant *Enterobacteriaceae* were collected, including 1,259 carbapenem-resistant *K. pneumoniae*, among which 1,010 were carbapenemase producers. OXA-48-like enzymes were the most prevalent carbapenemases (69.4%), followed by NDM (17.1%); 37 isolates (3.7%) had a

combination of both of these carbapenemases. KPC enzymes represent only 3.0% of all carbapenemases, corresponding to 6.8% (69 isolates, including 6 duplicated isolates) of all carbapenemase produced by *K. pneumoniae*. KPC also was produced by 13 non–*K. pneunomiae*, including 5 KPC-2 producers (2 *Escherichia coli*, 1 *Klebsiella oxytoca*, 1 *Enterobacter cloacae*, and 1 *Citrobacter koseri*) and 8 KPC-3 producers (5 *E. coli*, 1 *C. freundii*, 1 *E. cloacae*, and 1 *K. aerogenes*). Accordingly, *K. pneumoniae* is the most prevalent species (84.1%) among KPC producers.

Antimicrobial-Susceptibility of KPC-*Kp*

Susceptibility testing revealed that all KPC-*Kp* were resistant to all broad-spectrum cephalosporins (ceftazidime, cefotaxime, cefepime) and monobactam (Figure 1). All KPC-*Kp* were resistant to ertapenem. According to European Committee on Antimicrobial Susceptibility Testing breakpoints, 62.1% (41/66) KPC-*Kp* isolates remained susceptible to imipenem and 30.3% (20/66) to meropenem (Figure 1). Ceftazidime/avibactam (98.5% susceptibility) and colistin (92.2%) remained the most potent agents (Figure 1,

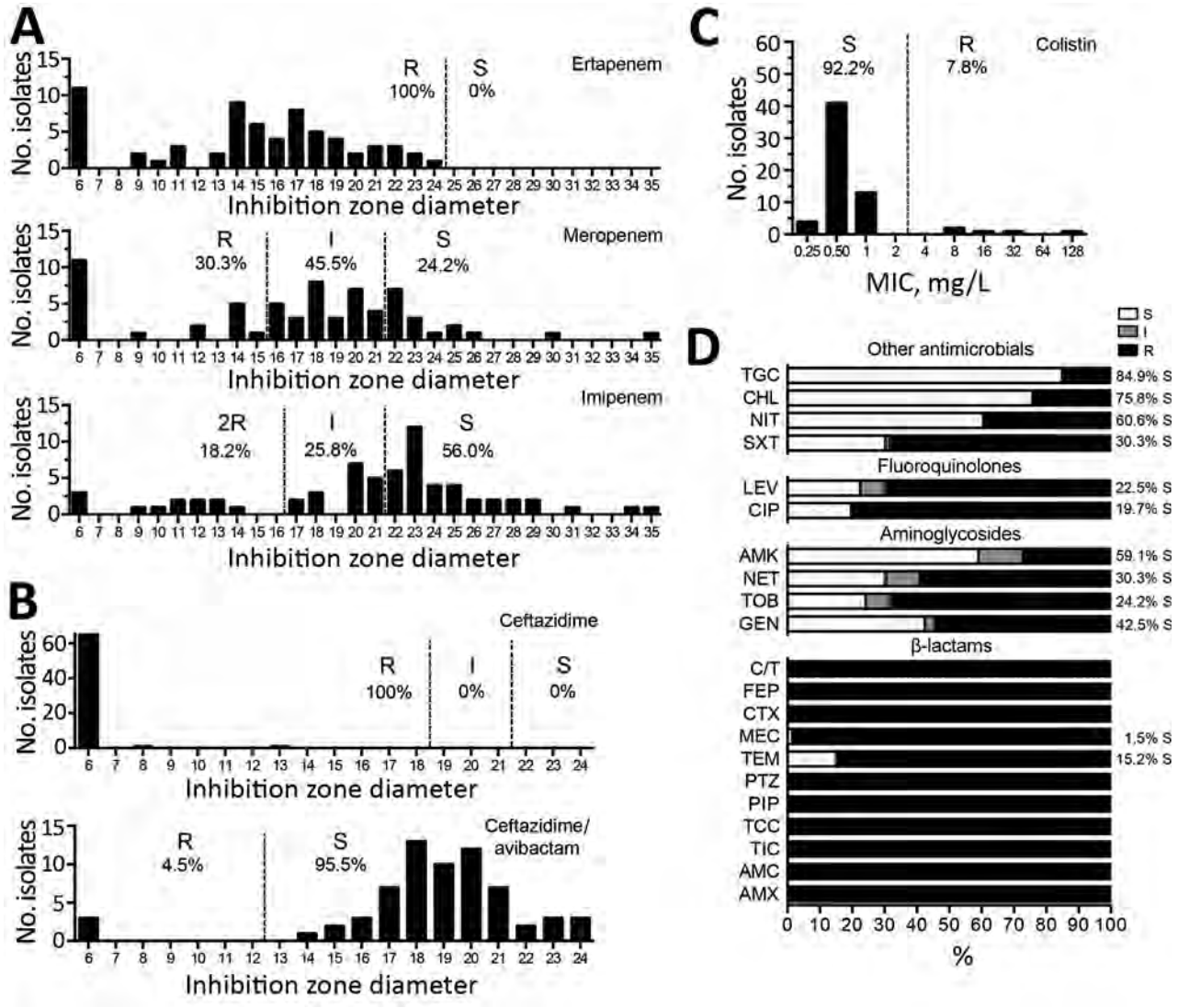

Figure 1. Susceptibility testing of *Klebsiella pneumoniae* carbapenemase–producing *K. pneumoniae* isolates, France, 2018. A) Antimicrobial susceptibility to carbapenems tested by using the disc diffusion method and interpreted according to European Committee on Antimicrobial Susceptibility Testing guidelines (http://www.eucast.org). B) Susceptibility to ceftazidime or ceftazidime/avibactam combination. C) MICs for colistin as determined by broth microdilution. D) Percentage of susceptibility to other antibiotic families. Where percentage of resistance is <100%, percentage of susceptible isolates is indicated. AMC, amoxicillin/clavulanate; AMK, amikacin; AMX, amoxicillin; CIP, ciprofloxacin; CHL, chloramphenicol; C/T, ceftolozane/tazobactam; CTX, cefotaxime; FEP, cefepime; GEN, gentamicin; I, intermediate; LEV, levofloxacin; MEC, mecillinam; NET, netilmicin; NIT, nitrofurane; PIP, piperacillin; PTZ, piperacillin/tazobactam; R, resistant; S, susceptible; TCC, ticarcillin/clavulanate; TEM, temocillin; TGC, tigecycline; TIC, ticarcillin.

panels B and C). However, we identified 1 isolate resistant to ceftazidime/avibactam but susceptible to carbapenems (Figure 1). This isolate produces a new variant of KPC, named KPC-39, that has been reported to possess increased ceftazidime catalytic activity but also to have concomitantly lost its carbapenemase activity (*19*). Among other antimicrobial families, 84.9% KPC-*Kp* isolates were susceptible to tigecycline, 30.3% to sulfamethoxazole/trimethoprim, and 19.7% to ciprofloxacin (Figure 1, panel D). Resistance to aminoglycosides varied from 40.9% for amikacin to 75.8% for tobramycin.

bla_{KPC} Variants and Associated Acquired Resistance Genes

We performed WGS on 63 nonduplicate KPC-*Kp* isolates and identified their resistomes by using Illumina technology. In this collection, 44 isolates possessed the bla_{KPC-3} gene (69.8%), and 18 (28.5%) possessed the bla_{KPC-2} gene. One isolate harbored a novel single-nucleotide variant of bla_{KPC-3}, bla_{KPC-39} (Figure 1, panel B). Two isolates produced 2 carbapenemases, including 1 isolate coharboring bla_{KPC-2} and bla_{VIM-1} and another 1 coharboring bla_{KPC-2} and bla_{NDM-4} (Figure 2). We identified additional antimicrobial-resistance determinants in all isolates (Appendix 1, https://wwwnc.cdc.gov/EID/article/26/6/19-1517-App1.xlsx). Approximately 46% of the KPC-*Kp* isolates carried an extended spectrum β-lactamase encoding gene, including 22 isolates harboring $bla_{CTX-M-15}$; 4 isolates coharboring $bla_{CTX-M-14}$ and $bla_{CTX-M-15}$; and 3 isolates with $bla_{CTX-M-14}$, $bla_{CTX-M-3}$, or $bla_{CTX-M-65}$. The other acquired β-lactam resistance determinants encoded for the narrow-spectrum β-lactamases OXA-9 and TEM-1. To decipher quinolone resistance, we analyzed the presence of plasmid-mediated resistance determinants and known mutations in gyrase and topoisomerases (*20*–*22*). Resistance to quinolones was mediated by either mutation in gyrase *gyrA* affecting the residues S83 (p.S83I, n = 42; p.S83F, n = 7; and p.S83Y, n = 2) or D87 (p.D87N, n = 7; p.D87G, n = 3; and p.D87A, n = 2) or *parC* affecting the residues p.S80 (p.S80I, n = 51) or the production of *Qnr* (Qnr66-like, QnrB6, or QnrS1). Aminoglycoside resistance was caused by the production of the 16S RNA methylase RmtB (n = 7) or an aminoglycoside-modifying enzyme (encoding by *aac(3')-IIa, aadA1, aadA2, aac(6')-Ib-cr, or strA/strB*). Colistin resistance (n = 5) resulted systematically in chromosome-encoded resistance with alteration of the *mgrB* gene. In these isolates, 2 possessed a nonsense substitution (p.Q30*), 1 missense involved in colistin resistance (p.C27W) (*23*), an IS*Kpn26*-like inserted (with direct repeats [DRs] of 4 bp: TTAA), and a missense mutation leading to the disappearance of the start codon. No isolate had plasmid-encoded resistance *mcr*-1.

Genetic Diversity of KPC-*Kp*

Phylogenetic analysis revealed that the 63 KPC-*Kp* belonged to 15 different clones (STs) circulating in France (Figure 2; Appendix 1). Although many studies have asserted that CG258 is responsible for the spread of bla_{KPC} (*6*,*8*–*11*), in our collection, only 8 isolates (12.7%) belonged to CG258 (4 each for ST258 and ST512). Furthermore, epidemiologic investigations revealed no link between these isolates (Figure 2). Because KPC is not widely disseminated in France, we did not expect to observe such clonal diversity. Indeed, the epidemiology of KPC in France is not comparable to what was reported in nearby countries in Europe where KPC is endemic, such as Greece and Italy, and where the spread of $bla_{KPC-2/-3}$ is clearly linked to CG258 (*24*,*25*). Among the 8 isolates we identified that belonged to CG258, 3 were recovered from patients with travel history in Greece (isolate 175C3 and isolate 177H5) and Italy (isolate 160C2). In France, the 3 most prevalent clones are ST307 (with 15 isolates), ST147 (12 isolates), and ST13 (7 isolates). By using the 21 SNP cutoff value proposed by David et al. to identity a single hospital outbreak caused by a ST258 and ST512 cluster (*8*), we identified that the ST307 clone was overrepresented because of an outbreak that included 11 isolates (Figure 2; Appendix 2, https://wwwnc.cdc.gov/EID/article/26/6/19-1517-App2.pdf). However, this ST307 also included 4 isolates that were not related to this outbreak, such as the 195I4 strain, which was isolated from a patient who traveled in Crete (Greece) and possesses an additional carbapenemase-encoding gene (bla_{NDM-4}). The second most prevalent clone, ST147, seemed to have disseminated upon distinct events (Appendix 2). Most of the ST147 isolates have been recovered from different areas with no epidemiologic link between the patients (Figure 2). A link with Portugal has been identified for most (9/11) patients infected or colonized with a KPC-3–producing *K. pneumoniae* of ST147 (Figure 2). The same link with Portugal was observed for 4 patients infected or colonized with a KPC-3–producing *K. pneumoniae* of ST231. Strains from ST383 represented a small outbreak for which cross contamination was evidenced (<20 SNPs between 4 isolates [Appendix 2]). One isolate (171J7) was distantly related to other clones and corresponded to *K. variicola*. KPC-2-producing *K. pneumoniae* isolates of ST11 were predominantly linked to patients who had a history of travel in Asia (China and Vietnam), where this ST is known to be the main vector of bla_{KPC} dissemination.

Diversity of Genetic Vehicle Involved in Spread of *bla*$_{KPC}$

Analysis of the close genetic context of *bla*$_{KPC}$ highlighted diversity in the genetic structures at the origin of the acquisition of the carbapenemase-encoding gene. The well-known Tn*4401a* (in 29 isolates) and Tn*4401d* (in 26 isolates) were the most prevalent structures identified (Figure 2 and 3; Appendix 1). The KPC-*Kp* of the 2 main clones ST307 and ST147, *bla*$_{KPC}$, is carried on Tn*4401a* in ST307 and Tn*4401d* in ST147. Two unrelated isolates (ST11–167I9 and the *K. variicola* 171J7 isolate) harbored *bla*$_{KPC}$ in the Tn*4401b* isoform. In the remaining 6 isolates (ST273–171J9, ST147–199D1, ST1788–189B3,

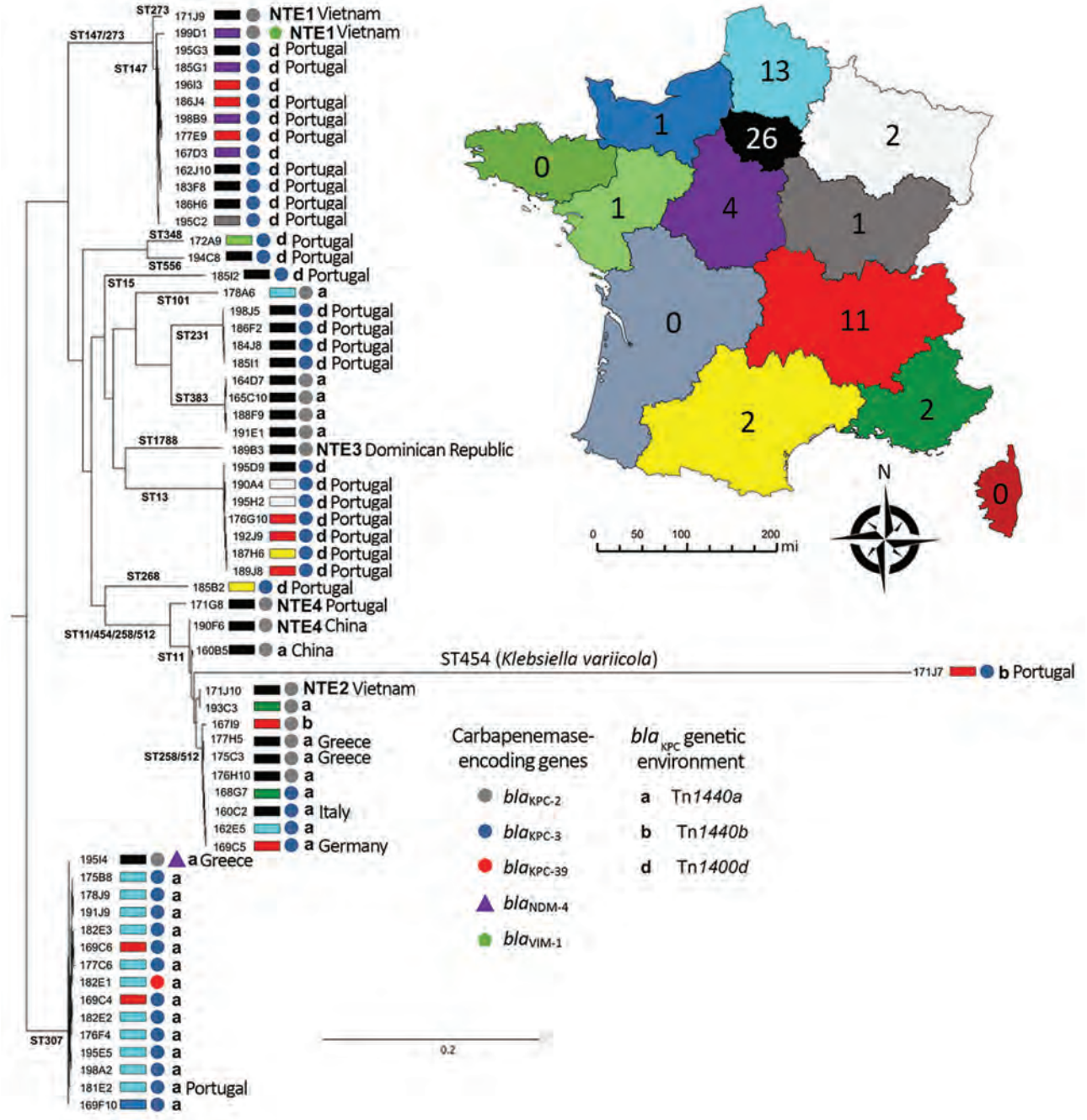

Figure 2. Phylogenetic analysis of *Klebsiella pneumoniae* carbapenemase–producing *K. pneumoniae* isolates, France, 2018. STs are indicated on the branches of the tree. Colored circles, triangles, or pentagons indicate carbapenemase type. Colored rectangles indicate region where isolates were recovered, as indicated on inset map; numbers on map indicate number of isolates. Genetic context indicated by isoform of Tn*4401* or NTE. Labels indicate links with foreign countries. Scale bar on tree indicates the number of single-nucleotide polymorpisms per position of common sequences. NTE, non-Tn*4401* element; ST, sequence type.

ST11–171G8, ST11–190F6, and ST11–171J10), bla_{KPC-2} is localized in an NTE element (Figures 2, 3). Although 3 isolates belonged to ST11, they displayed 200–800 SNPs of differences along their core genome, indicating that they were unrelated (Appendix 2). The links with 3 different countries (Portugal for ST11–171G8, China for ST11–190F6, and Vietnam for ST11–171J10) are consistent with this unrelatedness. Analysis of NTE elements revealed 4 different structures even if common features were observed (Figure 3). For instance, the presence of a fragment of IS*Kpn6* downstream of bla_{KPC} and a copy of IS*Kpn27* upstream were always present (Figure 3). DRs of TATAGG bracketing IS*Kpn27* indicated a transposition process that occurred inside the resolvase gene of Tn*3*. Immediately upstream of bla_{KPC-2} (74 bp), the presence of the inverted repeat right of Tn*3* is present in all NTE, indicating that all these structures were related. However, the NTE differed by the size of the deletions that are present between IS*Kpn27* and bla_{KPC-2} (from 280 bp in NTE-190F6 to 940 bp in NTE-199D1). We could observe a remnant of bla_{TEM-1} in longer structures, but it was not functional anymore. Analysis of the 4 NTE revealed that in NTE-199D1, several copies of IS*26* bracketed the whole structure, indicating that this IS might be involved in its acquisition by transposition or a recombination event. IS*26* has been recently demonstrated to be able to transpose and thus create a class I transposon by targeting another copy of IS*26* (*26*). NTE-171J10 is inserted in the *fip* gene of IncN-type plasmids with the presence of DRs surrounding the NTE-171J0 (Figure 3). The *fip* gene has already been demonstrated to be an integration hot spot in IncN-type plasmids (*27*,*28*). DRs as well as putative inverted repeats of Tn*3*-family transposon are present at the integration site (Figure 3). Moreover, the presence of the complete Tn*3* transposase gene indicated that NTE-171J10 might be functional. In NTE-189B3, a new class I transposon carrying a protein of unknown function has been identified. DRs bracketed IS*Apu1* and IS*Apu2*, indicating a transposition process mediated by these close insertion sequences (Figure 3).

Discussion

In France, KPC producers (84.1% of *K. pneumoniae*) represent only 6.8% of all carbapenemase producers,

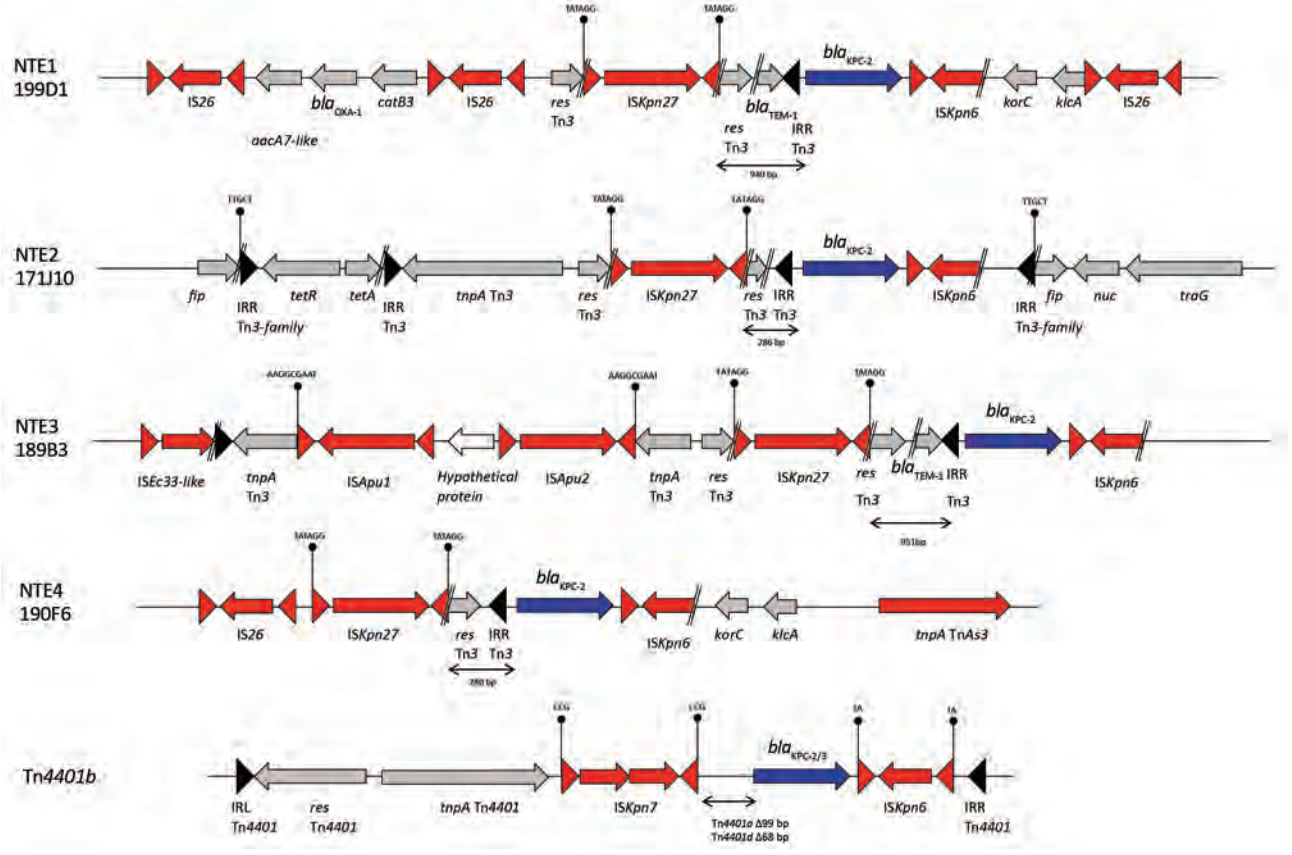

Figure 3. Analysis of genetic context of bla_{KPC} genes in *Klebsiella pneumoniae* carbapenemase–producing *K. pneumoniae* isolates, France, 2018. Different isoforms of NTE and Tn*4401* are represented. Inverted repeat sequences are indicated by triangles. Direct repeats are indicated by vertical lines. Genes are represented by arrows. NTE, non-Tn*4401* element.

far away from the global 72.7% found in Europe in 2013 (*8*). This relatively low prevalence of KPC producers in France compared with OXA-48–like and NDM producers has been reported since 2012 (*3*,*4*,*29*). We demonstrated unexpected clonal diversity among KPC-*Kp* isolated in France. A few overrepresented clones were identified (i.e., ST307, ST147, ST231, and ST13). However, ST307 was involved in a regional outbreak, whereas ST147 and ST13 were identified in different parts of France. Most of the patients colonized or infected with KPC-*Kp* had a clear link with Portugal, where these 4 STs were recently described to be the more prevalent (*30*,*31*). The KPC-2–producing *K. pneumoniae* isolates identified in France were predominantly recovered from patients with a history of travel in Greece (ST258) or Asia (ST11).

Regarding antimicrobial susceptibility of KPC-*Kp* in France, the relative high susceptibility to imipenem (30.3%) and meropenem to a lesser extent (18.2%) are in agreement with previous reports from Italy, where ST512 is highly prevalent (26.6% susceptibility to meropenem) (*32*). Conversely, data from the United States and Taiwan indicated that KPC-*Kp* are more resistant to carbapenems in those parts of the world, where ST258 is more prevalent (*33*,*34*).

Altogether, our results indicate that the KPC-*Kp* epidemiology has changed in Europe during the past 5 years. In 2018, ST258 and ST512 *K. pneumoniae* were no longer the main drivers of KPC resistance, at least in several non–KPC-endemic countries of western Europe, such as France and Portugal (*30*,*31*). KPC-*Kp* epidemiology also appears to have begun changing in some countries, such as Italy and Colombia, where CG-258 KPC-*Kp* was previously known to be endemic. This change is indicated by the reported emergence of ST307 and ST273 KPC-*Kp* in Sicilia (Italy) (*35*) and ST307 and ST14 KPC-*Kp* in Colombia (*36*). This change in the global epidemiology of KPC-*Kp* might have an effect on the identification of these carbapenemase producers with the molecular methods dedicated to the identification of GC258 *K. pneumoniae* (*37*,*38*).

In addition, our study highlights the dissemination of bla_{KPC} genes in high-risk clones of *K. pneumoniae* (ST307 and ST147), genetic features that might provide an advantage in adaptation to the hospital environment and the human host (*39*). These clones already convey several antimicrobial-resistance genes, including genes encoding other carbapenemases of NDM and OXA-48–like types (*40*,*41*). Accordingly, we might now fear the emergence of ST307 and ST147 high-risk clones of *K. pneumoniae* that can co-produce multiple carbapenemases. A recent study demonstrated the importance of ST307 in the dissemination of $bla_{OXA-181}$ in South Africa (*42*). In that study, >600 isolates belonging to ST307 were recovered and analyzed, and the results demonstrated the importance of this clone as a carrier of carbapenemase genes in all continents. Another study used Bayesian analysis to demonstrate that ST307 emerged in the mid-1990s (*43*). ST307 had been strongly associated with the diffusion of $bla_{CTX-M-15}$ (*43*) and now is associated with the dissemination of carbapenemase genes (*42*).

In conclusion, we found that the epidemiology of KPC-*Kp* has changed in Europe, in particular, with emergence of non–CG258 KPC-*Kp* isolates in France, linked to dissemination from Portugal. This change in epidemiology has to be considered by microbiologists because a few diagnostic assays specifically designed for the identification of ST-258 KPC-*Kp* isolates will not be able to detect non–CG258 KPC-*Kp* isolates.

This work was funded in part by the University Paris-Sud, France. L.D., T.N., and R.A.B. are members of the Laboratory of Excellence in Research on Medication and Innovative Therapeutics, which is supported by a grant from France's National Research Agency (grant no. ANR-10-LABX-33).

About the Author

Dr. Bonnin is an associate professor in Medical Microbiology at the University of Paris-Sud Medical School and a member of the Associated National Reference Center for Carbapenemase-Producing Enterobacteriaceae. His research focuses on bacterial genomes and transcriptomes with a special interest in mobile genetic elements and evolution.

References

1. Munoz-Price LS, Poirel L, Bonomo RA, Schwaber MJ, Daikos GL, Cormican M, et al. Clinical epidemiology of the global expansion of *Klebsiella pneumoniae* carbapenemases. Lancet Infect Dis. 2013;13:785–96. https://doi.org/10.1016/S1473-3099(13)70190-7
2. Tzouvelekis LS, Markogiannakis A, Psichogiou M, Tassios PT, Daikos GL. Carbapenemases in *Klebsiella pneumoniae* and other *Enterobacteriaceae*: an evolving crisis of global dimensions. Clin Microbiol Rev. 2012;25:682–707. https://doi.org/10.1128/CMR.05035-11
3. Dortet L, Cuzon G, Nordmann P. Dissemination of carbapenemase-producing *Enterobacteriaceae* in France, 2012. J Antimicrob Chemother. 2014;69:623–7. https://doi.org/10.1093/jac/dkt433
4. Dortet L, Cuzon G, Ponties V, Nordmann P. Trends in carbapenemase-producing *Enterobacteriaceae*, France, 2012 to 2014. Euro Surveill. 2017;22:22. https://doi.org/10.2807/1560-7917.ES.2017.22.6.30461
5. Nordmann P, Cuzon G, Naas T. The real threat of *Klebsiella pneumoniae* carbapenemase-producing bacteria. Lancet Infect Dis. 2009;9:228–36. https://doi.org/10.1016/S1473-3099(09)70054-4
6. Cuzon G, Naas T, Truong H, Villegas MV, Wisell KT, Carmeli Y, et al. Worldwide diversity of *Klebsiella pneumoniae*

that produce β-lactamase bla_{KPC-2} gene. Emerg Infect Dis. 2010;16:1349–56. https://doi.org/10.3201/eid1609.091389
7. Fu P, Tang Y, Li G, Yu L, Wang Y, Jiang X. Pandemic spread of bla $_{KPC-2}$ among *Klebsiella pneumoniae* ST11 in China is associated with horizontal transfer mediated by IncFII-like plasmids. Int J Antimicrob Agents. 2019;54:117–24. https://doi.org/10.1016/j.ijantimicag.2019.03.014
8. David S, Reuter S, Harris SR, Glasner C, Feltwell T, Argimon S, et al.; EuSCAPE Working Group; ESGEM Study Group. Epidemic of carbapenem-resistant *Klebsiella pneumoniae* in Europe is driven by nosocomial spread. Nat Microbiol. 2019;4:1919–29. https://doi.org/10.1038/s41564-019-0492-8
9. Chmelnitsky I, Shklyar M, Hermesh O, Navon-Venezia S, Edgar R, Carmeli Y. Unique genes identified in the epidemic extremely drug-resistant KPC-producing *Klebsiella pneumoniae* sequence type 258. J Antimicrob Chemother. 2013;68:74–83. https://doi.org/10.1093/jac/dks370
10. Fortini D, Villa L, Feudi C, Pires J, Bonura C, Mammina C, et al. Double copies of *bla*(KPC-3):Tn*4401a* on an IncX3 plasmid in *Klebsiella pneumoniae* successful clone ST512 from Italy. Antimicrob Agents Chemother. 2015;60:646–9. https://doi.org/10.1128/AAC.01886-15
11. Kitchel B, Rasheed JK, Patel JB, Srinivasan A, Navon-Venezia S, Carmeli Y, et al. Molecular epidemiology of KPC-producing *Klebsiella pneumoniae* isolates in the United States: clonal expansion of multilocus sequence type 258. Antimicrob Agents Chemother. 2009;53:3365–70. https://doi.org/10.1128/AAC.00126-09
12. Naas T, Cuzon G, Villegas MV, Lartigue MF, Quinn JP, Nordmann P. Genetic structures at the origin of acquisition of the β-lactamase bla_{KPC} gene. Antimicrob Agents Chemother. 2008;52:1257–63. https://doi.org/10.1128/AAC.01451-07
13. Araújo BF, Royer S, Campos PA, Ferreira ML, Gonçalves IR, Machado LG, et al. Insights into a novel Tn*4401* deletion (Tn*4401i*) in a multidrug-resistant *Klebsiella pneumoniae* clinical strain belonging to the high-risk clonal group 258 producing KPC-2. Int J Antimicrob Agents. 2018;52:525–7. https://doi.org/10.1016/j.ijantimicag.2018.08.011
14. Naas T, Cuzon G, Truong HV, Nordmann P. Role of IS*Kpn7* and deletions in bla_{KPC} gene expression. Antimicrob Agents Chemother. 2012;56:4753–9. https://doi.org/10.1128/AAC.00334-12
15. Girlich D, Bonnin RA, Jousset A, Naas T. Promoter characterization and expression of the bla_{KPC-2} gene in *Escherichia coli*, *Pseudomonas aeruginosa* and *Acinetobacter baumannii*. J Antimicrob Chemother. 2017;72:1597–601. https://doi.org/10.1093/jac/dkx044
16. Chen L, Mathema B, Chavda KD, DeLeo FR, Bonomo RA, Kreiswirth BN. Carbapenemase-producing *Klebsiella pneumoniae*: molecular and genetic decoding. Trends Microbiol. 2014;22:686–96. https://doi.org/10.1016/j.tim.2014.09.003
17. Girlich D, Bonnin RA, Bogaerts P, De Laveleye M, Huang DT, Dortet L, et al. Chromosomal amplification of the bla_{OXA-58} carbapenemase gene in a *Proteus mirabilis* clinical isolate. Antimicrob Agents Chemother. 2017;61:61.
18. Aziz RK, Bartels D, Best AA, DeJongh M, Disz T, Edwards RA, et al. The RAST Server: rapid annotations using subsystems technology. BMC Genomics. 2008;9:75. https://doi.org/10.1186/1471-2164-9-75
19. Jousset AB, Oueslati S, Creton E, Cotellon E, Sauvadet A, Emeraud C, et al. Resistance to ceftazidime-avibactam in a *Klebsiella pneumoniae* clinical isolate due to the production of KPC-39, a single amino-acid variant of KPC-3. Presented at: 29th European Congress of Clinical Microbiology and Infectious Diseases; Amsterdam, the Netherlands; 2019 April 13–16.
20. Ruiz J, Goñi P, Marco F, Gallardo F, Mirelis B, Jimenez De Anta T, et al. Increased resistance to quinolones in *Campylobacter jejuni*: a genetic analysis of *gyrA* gene mutations in quinolone-resistant clinical isolates. Microbiol Immunol. 1998;42:223–6. https://doi.org/10.1111/j.1348-0421.1998.tb02274.x
21. Vila J, Ruiz J, Goñi P, De Anta MT. Detection of mutations in *parC* in quinolone-resistant clinical isolates of *Escherichia coli*. Antimicrob Agents Chemother. 1996;40:491–3. https://doi.org/10.1128/AAC.40.2.491
22. Vila J, Ruiz J, Marco F, Barcelo A, Goñi P, Giralt E, et al. Association between double mutation in *gyrA* gene of ciprofloxacin-resistant clinical isolates of *Escherichia coli* and MICs. Antimicrob Agents Chemother. 1994;38:2477–9. https://doi.org/10.1128/AAC.38.10.2477
23. Poirel L, Jayol A, Nordmann P. Polymyxins: antibacterial activity, susceptibility testing, and resistance mechanisms encoded by plasmids or chromosomes. Clin Microbiol Rev. 2017;30:557–96. https://doi.org/10.1128/CMR.00064-16
24. Conte V, Monaco M, Giani T, D'Ancona F, Moro ML, Arena F, et al.; AR-ISS Study Group on Carbapenemase-Producing K. pneumoniae. Molecular epidemiology of KPC-producing *Klebsiella pneumoniae* from invasive infections in Italy: increasing diversity with predominance of the ST512 clade II sublineage. J Antimicrob Chemother. 2016;71:3386–91. https://doi.org/10.1093/jac/dkw337
25. Gartzonika K, Rossen JWA, Sakkas H, Rosema S, Priavali E, Friedrich AW, et al. Identification of a KPC-9-producing *Klebsiella pneumoniae* ST258 cluster among KPC-2-producing isolates of an ongoing outbreak in northwestern Greece: a retrospective study. Clin Microbiol Infect. 2018;24:558–60. https://doi.org/10.1016/j.cmi.2017.12.007
26. Harmer CJ, Hall RM. IS*26*-mediated formation of transposons carrying antibiotic resistance genes. MSphere. 2016;1:1. https://doi.org/10.1128/mSphere.00038-16
27. Gauthier L, Dortet L, Jousset AB, Mihaila L, Golse N, Naas T, et al. Molecular characterization of plasmid-encoded Tripoli MBL 1 (TMB-1) in *Enterobacteriaceae*. J Antimicrob Chemother. 2019;74:42–7.
28. Poirel L, Bonnin RA, Nordmann P. Analysis of the resistome of a multidrug-resistant NDM-1-producing *Escherichia coli* strain by high-throughput genome sequencing. Antimicrob Agents Chemother. 2011;55:4224–9. https://doi.org/10.1128/AAC.00165-11
29. Lee CR, Lee JH, Park KS, Kim YB, Jeong BC, Lee SH. Global dissemination of carbapenemase-producing *Klebsiella pneumoniae*: epidemiology, genetic context, treatment options, and detection methods. Front Microbiol. 2016;7:895. https://doi.org/10.3389/fmicb.2016.00895
30. Aires-de-Sousa M, Ortiz de la Rosa JM, Gonçalves ML, Pereira AL, Nordmann P, Poirel L. Epidemiology of carbapenemase-producing *Klebsiella pneumoniae* in a hospital, Portugal. Emerg Infect Dis. 2019;25:1632–8. https://doi.org/10.3201/eid2509.190656
31. Rodrigues C, Bavlovič J, Machado E, Amorim J, Peixe L, Novais Â. KPC-3-producing *Klebsiella pneumoniae* in Portugal linked to previously circulating non-CG258 lineages and uncommon genetic platforms (Tn*4401d*-IncFIA and Tn*4401d*-IncN). Front Microbiol. 2016;7:1000. https://doi.org/10.3389/fmicb.2016.01000
32. Cojutti P, Sartor A, Bassetti M, Scarparo C, Pea F. Is meropenem MIC increase against KPC-producing *Klebsiella pneumoniae* correlated with increased resistance rates against other antimicrobials with Gram-negative activity? J Glob Antimicrob Resist. 2018;14:238–41. https://doi.org/10.1016/j.jgar.2018.05.005

33. Chiu SK, Ma L, Chan MC, Lin YT, Fung CP, Wu TL, et al. Carbapenem nonsusceptible *Klebsiella pneumoniae* in Taiwan: dissemination and increasing resistance of carbapenemase producers during 2012–2015. Sci Rep. 2018;8:8468. https://doi.org/10.1038/s41598-018-26691-z
34. Kaiser RM, Castanheira M, Jones RN, Tenover F, Lynfield R. Trends in *Klebsiella pneumoniae* carbapenemase-positive *K. pneumoniae* in US hospitals: report from the 2007–2009 SENTRY Antimicrobial Surveillance Program. Diagn Microbiol Infect Dis. 2013;76:356–60. https://doi.org/10.1016/j.diagmicrobio.2013.03.032
35. Bonura C, Giuffrè M, Aleo A, Fasciana T, Di Bernardo F, Stampone T, et al.; MDR-GN Working Group. An update of the evolving epidemic of bla_{KPC} carrying *Klebsiella pneumoniae* in Sicily, Italy, 2014: emergence of multiple non-ST258 clones. PLoS One. 2015;10:e0132936. https://doi.org/10.1371/journal.pone.0132936
36. Ocampo AM, Chen L, Cienfuegos AV, Roncancio G, Chavda KD, Kreiswirth BN, et al. A two-year surveillance in five Colombian tertiary care hospitals reveals high frequency of non-CG258 clones of carbapenem-resistant *Klebsiella pneumoniae* with distinct clinical characteristics. Antimicrob Agents Chemother. 2015;60:332–42. https://doi.org/10.1128/AAC.01775-15
37. Chen L, Chavda KD, Mediavilla JR, Zhao Y, Fraimow HS, Jenkins SG, et al. Multiplex real-time PCR for detection of an epidemic KPC-producing *Klebsiella pneumoniae* ST258 clone. Antimicrob Agents Chemother. 2012;56:3444–7. https://doi.org/10.1128/AAC.00316-12
38. Yu F, Lv J, Niu S, Du H, Tang YW, Pitout JDD, et al. Multiplex PCR analysis for rapid detection of *Klebsiella pneumoniae* carbapenem-resistant (sequence type 258 [ST258] and ST11) and hypervirulent (ST23, ST65, ST86, and ST375) strains. J Clin Microbiol. 2018;56:56. https://doi.org/10.1128/JCM.00731-18
39. Villa L, Feudi C, Fortini D, Brisse S, Passet V, Bonura C, et al. Diversity, virulence, and antimicrobial resistance of the KPC-producing *Klebsiella pneumoniae* ST307 clone. Microb Genom. 2017;3:e000110. https://doi.org/10.1099/mgen.0.000110
40. Potel C, Ortega A, Martínez-Lamas L, Bautista V, Regueiro B, Oteo J. Interspecies transmission of the bla_{OXA-48} gene from a *Klebsiella pneumoniae* high-risk clone of sequence type 147 to different *Escherichia coli* clones in the gut microbiota. Antimicrob Agents Chemother. 2017;62:62. https://doi.org/10.1128/AAC.01699-17
41. Turton J, Davies F, Turton J, Perry C, Payne Z, Pike R. Hybrid resistance and virulence plasmids in "high-risk" clones of *Klebsiella pneumoniae*, including those carrying bla_{NDM-5}. Microorganisms. 2019;7:7. https://doi.org/10.3390/microorganisms7090326
42. Lowe M, Kock MM, Coetzee J, Hoosien E, Peirano G, Strydom K-A, et al. *Klebsiella pneumoniae* ST307 with $bla_{OXA-181}$, South Africa, 2014–2016. Emerg Infect Dis. 2019;25:739–47. https://doi.org/10.3201/eid2504.181482
43. Wyres KL, Hawkey J, Hetland MAK, Fostervold A, Wick RR, Judd LM, et al. Emergence and rapid global dissemination of CTX-M-15-associated *Klebsiella pneumoniae* strain ST307. J Antimicrob Chemother. 2019;74:577–81. https://doi.org/10.1093/jac/dky492

Address for correspondence: Laurent Dortet, Service de Bactériologie-Hygiène, Hôpital de Bicêtre, 78 rue du Général Leclerc, 94275 Le Kremlin-Bicêtre CEDEX, France; email: laurent.dortet@aphp.fr

Zoonotic Vectorborne Pathogens and Ectoparasites of Dogs and Cats in Eastern and Southeast Asia

Vito Colella, Viet L. Nguyen, Do Y. Tan, Na Lu, Fang Fang, Yin Zhijuan, Jiangwei Wang, Xin Liu, Xinghui Chen, Junyan Dong, Wisnu Nurcahyo, Upik K. Hadi, Virginia Venturina, Kenneth B.Y. Tong, Yi-Lun Tsai, Piyanan Taweethavonsawat, Saruda Tiwananthagorn, Thong Q. Le, Khanh L. Bui, Malaika Watanabe, Puteri A.M.A. Rani, Giada Annoscia, Frédéric Beugnet, Domenico Otranto, Lénaïg Halos

To provide data that can be used to inform treatment and prevention strategies for zoonotic pathogens in animal and human populations, we assessed the occurrence of zoonotic pathogens and their vectors on 2,381 client-owned dogs and cats living in metropolitan areas of 8 countries in eastern and Southeast Asia during 2017–2018. Overall exposure to ectoparasites was 42.4% in dogs and 31.3% in cats. Our data cover a wide geographic distribution of several pathogens, including *Leishmania infantum* and zoonotic species of filariae, and of animals infested with arthropods known to be vectors of zoonotic pathogens. Because dogs and cats share a common environment with humans, they are likely to be key reservoirs of pathogens that infect persons in the same environment. These results will help epidemiologists and policy makers provide tailored recommendations for future surveillance and prevention strategies.

Asia is the largest continent in the world, known for its thriving biocultural diversity. Today, countries in Asia are experiencing a rapid social, demographic, and economic transformation, thereby placing this region as an ever-growing economic powerhouse in the years to come. Sustained economic growth in Asia has resulted in increased demand for products and services and substantial urbanization (*1*). These factors have triggered a series of human-mediated environmental alterations, such as deforestation and encroachment of humans into natural ecosystems, that now link previously isolated ecologic niches and give pathogens new opportunities to thrive (*2*). During the past century, Asia has been in the limelight for emergence and pathogenicity of a large number of infectious diseases that have taken a substantial toll on the health of millions of persons (*1*). Striking examples include the emergence of severe acute respiratory syndrome, infections with the highly pathogenic avian influenza A(H5N1) virus, and coronavirus disease (COVID-19). Recently, human modification of natural habitats resulted in the emergence of a tick vector of Kyasanur Forest disease virus, a zoonotic vectorborne flavivirus that causes severe hemorrhagic fever with a fatality rate of 3%–10% (*3*).

Also implicated in the changing epidemiology of pathogens of public health concern in eastern and Southeast Asia are dogs and cats (*4*–*6*). In remote areas of eastern and Southeast Asia, three quarters of dogs are classified as stray or community dogs (*7*). Increases in living standards have led to a dramatic

Author affiliations: University of Melbourne, Melbourne, Victoria, Australia (V. Colella); University of Bari, Bari, Italy (V. Colella, V.L. Nguyen, G. Annoscia, D. Otranto); Boehringer Ingelheim Animal Health, Lyon, France (D.Y. Tan, Na Lu, F. Beugnet, L. Halos); Guangxi University, Nanning, China (F. Fang); KangBao Pet Hospital, Guilin, China (Y. Zhijuan); Sapphire Veterinary Hospital, Shanghai, China (J. Wang); Meilianzhonghe Veterinary Referral Center, Beijing, China (X. Liu); Chongyisheng Veterinary Hospital, Chengdu, China (X. Chen); Nanjing Police Dog Research Institute, Nanjing, China (J. Dong); Gadjah Mada University, Yogyakata, Indonesia (W. Nurcahyo); Bogor University Indonesia, Jakarta, Indonesia (U.K. Hadi); Central Luzon State University, Nueva Ecija, Philippines (V. Venturina); Animal & Avian Veterinary Clinic, Yishun, Singapore (K.B.Y. Tong); National Pingtung University of Science and Technology, Pingtung, Taiwan (Y.L. Tsai); Chulalongkorn University, Bangkok, Thailand (P. Taweethavonsawat); Chiang Mai University, Chiang Mai, Thailand (S. Tiwananthagorn); Nong Lam University, Ho Chi Minh City, Vietnam (T.Q. Le); Vietnam National University of Agriculture, Hanoi, Vietnam (K.L. Bui); University Putra Malaysia, Selangor, Malaysia (M. Watanabe, P.A.M.A. Rani)

DOI: https://doi.org/10.3201/eid2606.191832

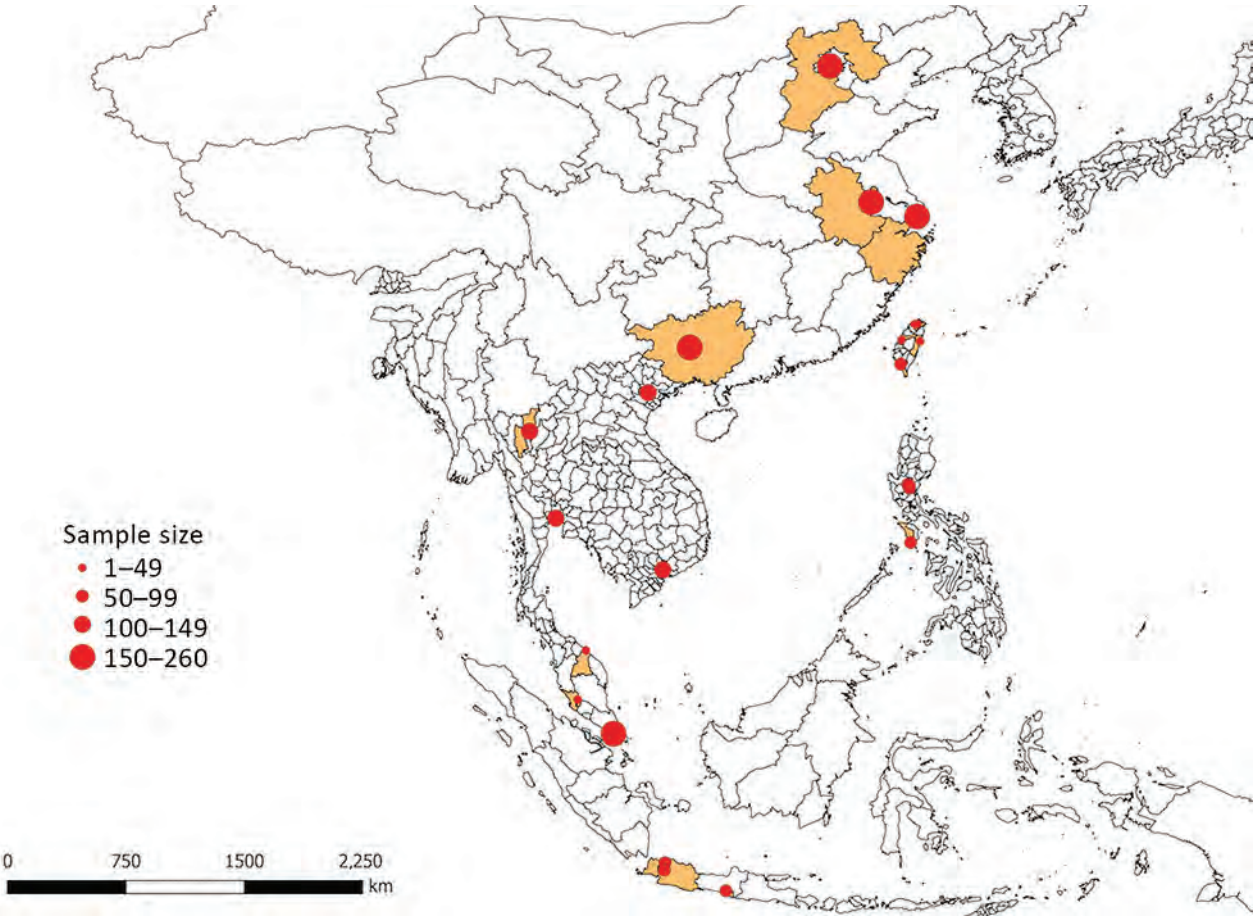

Figure 1. Geographic distribution and size of dog and cat samples in study of ectoparasites and vectorborne zoonotic pathogens of dogs and cats in Asia, 2017–2018. Highlighted areas represent the geographic regions from which samples were collected in China, Indonesia, Malaysia, the Philippines, Singapore, Taiwan, Thailand, and Vietnam.

surge in the number of pet dogs and cats living in metropolitan settings (*8*,*9*). In China, the population of pet dogs is estimated to grow by 5 million per year. Along with this increase in companion animal ownership, the risk of acquiring parasitic zoonoses from companion dogs and cats represents an ongoing, yet neglected, threat (*10*,*11*).

Implementation of effective measures to control zoonotic diseases must rely on the elucidation of pathogens and reservoir hosts in a given area. For most countries in Asia, limited knowledge about the agents parasitizing dogs and cats, including those transmissible to humans, hinders the establishment of proper strategies for treatment and prevention of zoonotic pathogens in animal and human populations. Although previous investigations have explored the occurrence of zoonotic diseases in animals living in remote areas (*4*–*7*), our year-long multicenter study explored the occurrence of vectorborne pathogens and ectoparasites in pet dogs and cats from metropolitan areas in eastern and Southeast Asia.

Methods

Our study involved academic institutions and private facilities of eastern Asia (China and Taiwan) and Southeast Asia (Indonesia, Malaysia, the Philippines, Singapore, Thailand, and Vietnam). To provide capacity building and compliance with the study procedures, trainings were performed at local institutions as needed. The protocol of this study was approved by the Ethics Committee of the Department of Veterinary Medicine, University of Bari (protocol no. 13/17). At partner institutions, animal owners read, approved, and signed an owner informed consent, which contained information about study procedures.

During 2017–2018, local investigators sampled 10 client-owned dogs and 10 client-owned cats each month for 12 months in each country, except China,

Table 1. Distribution of 1,229 dogs and 1,152 cats from select countries, by age group, husbandry, and sex, in study of ectoparasites and vectorborne zoonotic pathogens of dogs and cats, Asia, 2017–2018

Country (total no. animals; no. dogs, no. cats)	Age, y						Husbandry				Sex			
	≤1		>1 to ≤5		>5		Urban area		Rural area		M		F	
	Dogs	Cats	Dogs	Cats	Dogs	Cats	Dogs	Cats	Dogs	Cats	Dogs	Cats	Dogs	Cats
China (971; 481, 490)*	122	228	182		172	69	464	484	17	6	289	273	192	217
Indonesia (173; 95, 78)	30	22	50	46	15	10	68	63	27	15	51	39	44	39
Malaysia (91; 45, 46)	9	30	11	14	25	2	45	1	0	45	20	27	25	19
Philippines (235; 120, 115)	45	50	50	59	20	5	96	91	24	23	51	60	68	54
Singapore (245; 116, 129)	3	61	14	26	98	42	115	128	1	1	50	67	63	60
Taiwan (186; 132, 54)	10	26	45	20	77	8	81	35	51	19	62	28	69	26
Thailand (240; 120, 120)	15	35	49	66	54	19	89	101	31	19	69	49	51	71
Vietnam (240; 120, 120)	48	80	49	27	20	0	81	86	39	19	66	63	53	57
All (2,381; 1,229, 1,152)	282	532	450	451	481	155	1,039	989	190	147	658	606	565	543

*Beijing (240; 119, 121); Nanjing (240; 120, 120); Shanghai (240; 120, 120); Guangxi Province (251; 122, 129).

where 40 dogs and 40 cats each month were sampled. Inclusion criteria were a history of regular outdoor access and having not received recent antiparasitic treatments. Data on the animals' location, age, breed, and sex were recorded.

Veterinary Examination

Veterinarians performed a complete examination of the animals, reporting abnormalities in rectal temperature, overall physical condition, demeanor, nasal discharge, skin/haircoat, eyes, superficial lymph nodes, respiratory system (breathing), cardiovascular system (mucous membranes), and fecal consistency. The examinations included checking for the presence of ectoparasites (ticks, fleas, lice, and mites) by examining the whole-body surface for ≥5 minutes. The veterinarians inspected both eyes, including a thorough examination under the third eyelid to detect adult *Thelazia callipaeda* eyeworms. They also performed testing for lesions evocative of sarcoptic mange or demodicosis (deep skin scraping), cheyletiellosis (tape test), or otoacariosis (earwax examination).

Sampled parasites were stored in vials containing 70% ethanol and sent for morphologic and molecular identification at the University of Bari (Bari, Italy), where we examined adult and nymph ticks under a stereomicroscope. We clarified tick larvae, fleas, lice, and fur mites in 10% potassium hydroxide overnight, mounted in Hoyer's medium and observed under an optical microscope (*12*). We

Table 2. Frequency of tick, flea, and lice detection on 1,229 dogs and 1,152 cats, by country, in study of ectoparasites and vectorborne zoonotic pathogens of dogs and cats, Asia, 2017–2018

Country (no. dogs, no. cats)	Detection frequency, % (95% CI)					
	Ticks		Fleas		Lice	
	Dogs	Cats	Dogs	Cats	Dogs	Cats
China (481, 490)	6.0 (4.2–8.5)	0.2 (0.0–1.1)	3.1 (1.9–5.1)	4.5 (3.0–6.7)	0.6 (0.2–1.8)	0.8 (0.0–2.0)
Indonesia (95, 78)	42.1 (32.7–52.2)	10.3 (5.3–18.9)	16.8 (10.6–25.6)	53.9 (42.9–64.5)	6.3 (2.9–13.1)	33.3 (23.9–44.4)
Malaysia (45, 46)	4.4 (1.2–14.8)	0	4.4 (1.2–14.8)	89.1 (77.0–95.3)	0	8.7 (3.4–20.3)
Philippines (120, 115)	67.5 (58.7–75.2)	24.4 (17.4–32.9)	80.0 (72.0–86.2)	54.8 (45.7–63.6)	52.5 (43.6–61.2)	26.1 (18.9–34.8)
Singapore (116, 129)	8.6 (4.7–15.1)	1.6 (0.4–5.5)	0.9 (0.0–4.7)	3.9 (1.7–8.7)	0.9 (0.0–4.7)	3.9 (1.7–8.7)
Taiwan (132, 54)	12.9 (8.2–19.7)	5.6 (1.9–15.1)	9.1 (5.3–15.2)	20.4 (11.8–32.9)	0.8 (0.0–4.2)	1.9 (0.3–9.7)
Thailand (120, 120)	27.5 (20.3–36.1)	0	20.8 (14.5–28.9)	19.2 (13.1–27.1)	2.5 (0.8–7.1)	0
Vietnam (120, 120)	51.7 (42.8–60.4)	0.8 (0.1–4.6)	12.5 (7.7–19.6)	15.8 (10.4–23.4)	0.8 (0–4.6)	0
All (1,229, 1152)	22.3 (20.1–24.7)	3.7 (2.8–5.0)	14.8 (12.9–16.9)	19.6 (17.4–22.0)	6.4 (5.1–7.8)	6.1 (4.8–7.6)

Table 3. Frequency of mite detection on 1,229 dogs and 1,152 cats in study of ectoparasites and vectorborne zoonotic pathogens of dogs and cats, Asia, 2017–2018

Country (no. dogs, no. cats)	Detection frequency, % (95% CI)						
	Scabies mites		*Demodex* spp.		*Otodectes cynotis*		*Lynxacarus radovskyi*, cats
	Sarcoptes scabiei, dogs	*Notoedres cati*, cats	Dogs	Cats	Dogs	Cats	
China (481, 490)	0.6 (0.2–1.8)	0.2 (0–1.1)	0.6 (0.2–1.8)	0.2 (0–1.1)	1.3 (0.6–2.7)	5.1 (3.5–7.4)	0
Indonesia (95, 78)	3.2 (1.1–8.9)	34.6 (25.0–45.7)	1.1 (0.2–5.7)	0	0	12.8 (7.1–22.0)	5.1 (2.0–12.5)
Malaysia (45, 46)	0	0	0	0	0	17.4 (9.09–30.72)	4.4 (1.2–1.45)
Philippines (120, 115)	0	0.9 (0.1–4.7)	3.3 (1.3–8.3)	0.9 (0.1–4.7)	0	2.6 (0.9–7.4)	0
Singapore (116, 129)	2.7 (0.5–6.1)	0	4.3 (1.8–9.7)	0	0.9 (0.1–4.7)	19.4 (13.5–27.0)	34.9 (27.2–43.4)
Taiwan (132, 54)	0	0	0.2 (0.04–5.4)	0	2.3 (0.8–6.5)	7.4 (2.9–17.5)	0
Thailand (120, 120)	0	0	0	0	0	1.7 (0.0–5.8)	0
Vietnam (120, 120)	0.8 (0.1–4.6)	0	2.5 (0.8–7.1)	0	0.8 (0.1–4.6)	10 (5.8–16.7)	0
All (1,229, 1,152)	0.7 (0.4–1.4)	2.5 (1.7–3.4)	1.5 (0.9–2.3)	0.2 (0–0.6)	0.9 (0.5–1.6)	7.7 (6.3–9.4)	4.4 (3.4–5.6)

used morphologic keys to identify all ectoparasites to the species level (*13*–*20*). For mite identification, we minced crusty skin lesions by using disposable surgical blades, added drops of saline solution on a glass slide, observed the slides under an optical microscope, and identified the mites according to morphologic appearance (*18*,*21*). We mounted anterior and posterior extremities of adult *T. callipaeda* eyeworms in lactophenol and identified them (*22*).

Molecular Identification of Ectoparasites

To confirm morphologic identifications of ectoparasite species, we subjected a representative subpopulation (≈20%) of the ectoparasites to DNA extraction and amplification of target genes (Appendix Table, https://wwwnc.cdc.gov/EID/article/26/6/19-1832-App1.pdf). For ticks, fleas and lice, we isolated genomic DNA (gDNA) by using the DNeasy Blood and Tissue Kit (QIAGEN, https://www.qiagen.com) according to the manufacturer's instructions. We isolated gDNA from a small portion of the idiosoma of ticks (*23*) and from the anterior dorsal part of the abdomen of fleas (*24*). We selected individual lice and mites under an optical microscope and extracted gDNA by using a QIAamp DNA Micro Kit (QIAGEN).

Blood Collection and Processing

From each study animal, we collected ≈2 mL of blood in a tube with anticoagulant and processed it as follows. For dogs, we used an aliquot of the blood sample for the ELISA-based technology SNAP 4Dx Plus test (IDEXX Laboratories, Inc., https://www.idexx.com) to detect *Dirofilaria immitis* antigen and antibodies against *Anaplasma phagocytophilum*/*A. platys*, *Borrelia burgdorferi* sensu lato, and *Ehrlichia canis*/*E. ewingii* as described and the SNAP *Leishmania* test (IDEXX Laboratories, Inc.) to detect antibodies against *Leishmania infantum/L. donovani* as described. For cats, we used an aliquot of blood to detect antigens of feline leukemia virus (FeLV) and *D. immitis* and antibodies against feline immunodeficiency virus (FIV). We used the SNAP Combo FIV/FeLV and SNAP Heartworm RT Test (IDEXX Laboratories, Inc.). For dogs and cats, we blotted 2 spots of blood (125 µL each, total 250 µL/animal) onto Whatman FTA cards (Sigma-Aldrich Corp., https://www.sigmaaldrich.com), stored the cards overnight (≥6 h) at room temperature for blood to dry, and put them in a zip-locked plastic bag.

DNA Extraction, Amplification, Purification, and Sequencing

From each Whatman FTA card, we punched out 5 disks of 3.0-mm each (Uni-Core 150 punch; GE Healthcare, https://www.gelifesciences.com) and placed them in each well of a 96-well plate (QIAcube HT kit Plasticware; QIAGEN) and included a negative control (Whatman FTA card blotted with dog blood naive to the pathogens in this study) for each plate. Subsequently, we added a 200-µL solution (180 µL of buffer ATL and 20 µL of proteinase K) to each well and subjected samples to prelysate overnight incubation at 56°C in a 711 CT incubator (Asal s.r.l., http://www.asal.it). We extracted DNA by using a QIAcube HT and the QIAamp 96 DNA QIAcube HT

kit (QIAGEN) according to manufacturer instructions. We tested all gDNA isolated from dried blood samples by conventional PCR (cPCR) (Appendix Table). We detected *Leishmania* protozoa by quantitative PCR (qPCR) and further tested only samples scoring positive in duplicates by qPCR by cPCR on the internal transcribed spacer 2 region and kinetoplast DNA for species identification (Appendix Table).

For all PCRs, we included positive controls (DNA of pathogen-positive blood samples) and negative controls (DNA of pathogen-negative blood samples). We visualized PCR amplicons from nematodes and apicomplexan protozoa by capillary electrophoresis by using a QIAxcel DNA screening gel cartridge on a QIAxcel system (QIAGEN for each) and used a QX DNA Size Marker (QIAGEN) to size PCR products. We injected a QX Alignment Marker (QIAGEN), which consisted of 15-bp and 3,000-bp fragments, onto the cartridge with each sample. We then determined the PCR product sizes by using QIAxcel Screen Gel 1.4.0 software (QIAGEN). We subjected cPCR products from *Leishmania* spp. protozoa, *Thelazia* spp. eyeworms, ticks, fleas, lice, and mites to electrophoresis in a 2% agarose gel stained with Gel Red (VWR International PBI, https://it.vwr.com) and visualized them on a Kodak Gel Logic 100 gel documentation system (https://www.kodak.com).

We purified all cPCR amplicons obtained and sequenced them in both directions in an automated

Table 4. Frequency of tick detection on 1,229 dogs and 1,152 cats and molecular identification of ticks, in study of ectoparasites and vectorborne zoonotic pathogens of dogs and cats, Asia, 2017–2018

Ectoparasite	Location		Relative frequency of occurrence, % (95% CI)		GenBank accession nos.
	Dogs	Cats	Dogs	Cats	
Tick					
Rhipicephalus sanguineus	All countries	Philippines, Singapore, Indonesia, Taiwan, China	96.6 (93.6–98.2)	95 (83.5–98.6)	MN685287–321, MT320104–5
R. haemaphysaloides		Taiwan	0.8 (0.2–2.7)		MN653239–40
Haemaphysalis hystricis	Thailand		0.4 (0–2.1)		MN658833
H. wellingtoni	Thailand, Indonesia		0.8 (0.2–2.7)		MN658820–1
H. campanulata	China		0.4 (0–2.1)		MN658817
H. longicornis	China	China	0.8 (0.2–2.7)	2.5% (0.4–12.9)	MN658797–800
Ixodes sp.		Taiwan		2.5 (0.4–12.9)	MT035959
Fleas					
Ctenocephalides felis	All	All	65.1 (57.7–71.8)	98.7 (95.5–99.6)	MT027205–8, MT027227, MT027230
C. canis	Vietnam, Philippines, Indonesia, China	Philippines	15.7 (22.0–21.9)	0.6 (0.1–3.5)	Not applicable
C. orientis	Vietnam, Thailand, Philippines, Singapore, Indonesia, Taiwan		19.2 (14.0–25.7)		MT027193–99
Xenopsylla cheopis		Indonesia		0.6 (0.1–3.5)	MT027228
Lice					
Heterodoxus spiniger	Vietnam, Thailand, Philippines, Taiwan, China		72.8 (63.5–80.5)		MT027225
Trichodectes canis	Philippines, Singapore, Indonesia		25.2 (17.8–34.4)		MT027226
Felicola subrostratus	Indonesia	Philippines, Indonesia, China	1.9 (0.5–6.8)	1.8 (0.3–9.3)	Not applicable
Linognathus setosus		Malaysia			Not applicable
Mites					
Lynxacarus radovskyi		Singapore, Malaysia, Indonesia	Not applicable	Not applicable	MN639734, MN639736

Table 5. Serologic and molecular detection of vectorborne pathogens in dogs in study of ectoparasites and vectorborne zoonotic pathogens of dogs and cats, Asia, 2017–2018*

Country	Detection frequency, % (95% CI)				
	Ehrlichia canis, Ab	*Anaplasma platys*, Ab	*Dirofilaria immitis*, Ag, PCR, Ag + PCR	*Hepatozoon canis*, PCR	*Babesia gibsoni*, PCR
Overall	14.8 (12.9–16.9)	7.1 (5.8–8.7)	3.5 (2.6–4.6), 2.3 (1.58–3.3), 3.9 (3.0–5.1)	1.6 (1.1–2.5)	1.0 (0.6–1.7)
China	1.9 (1–3.5)	0.2 (–1.2)	0	0.8 (0.3–2.1)	2.3 (1.3–4.0)
Indonesia	36.2 (27.2–46.2)	11.7 (6.7–19.7)	0	0	0
Malaysia	11.1 (4.8–23.5)	11.1 (4.8–23.5)	6.7 (2.3–17.7), 6.7 (2.3–17.7), 6.7 (2.3–17.9)	2.2 (0.4–11.6)	0
Philippines	33.0 (25.0–42.2)	17 (11.1–25.0)	17.9 (11.9–26.0), 13.6 (8.27–21.5), 29.8 (21.9–39.2)	9.7 (5.4–17.0)	0
Singapore	5.3 (2.4–11.0)	2.6 (0.9–7.4)	2.6 (0.9–7.4)	0	0.9 (0.1–4.7)
Taiwan	1.5 (0.42–5.4)	3 (1.2–7.5)	8.3 (4.7–14.3), 4.8 (2.07–10.8), 13.2 (8.0–21.0)	0	0
Thailand	45 (36.4–53.9)	24.2 (17.4–32.5)	4.2 (1.8–9.5), 4.2 (1.8–9.4), 5.8 (2.8–11.5)	3.3 (1.3–8.3)	0
Vietnam	25.8 (18.8–34.3)	13.3 (8.4–20.6)	0, 0.8 (0.1–4.6), 0.8 (0.1–4.6)	0.8 (0.1–4.6)	0

**Leishmania* spp., *Borrelia* spp., and *Brugia* spp. not shown. Ab, antibodies; Ag, antigens; PCR samples positive by PCR-coupled Sanger sequencing.

sequencer ABI-PRISM 377 (ThermoFisher Scientific, https://www.thermofisher.com). We edited and aligned the sequences by using Geneious Prime software (https://www.geneious.com) and compared them with each other and with those available in the GenBank database by using BLAST (http://blast.ncbi.nlm.nih.gov/Blast.cgi).

Statistical Analyses

We calculated frequency values as the proportion of positive animals to the total number of examined animals and the relative frequency of occurrence of each species of parasite as the proportion of animals infested by a given parasite species/group within the total number of positive results within a given parasite species/group. We calculated 95% CIs by using the Wilson score interval.

We categorized animals into 3 age groups (≤1, >1 to ≤5, and >5 years). We used the χ^2 test to investigate associations between parasitic infection/exposure or infestation by ectoparasites and age group or clinical observations. We analyzed the Cohen κ coefficient and dependent and independent variables by using GraphPad Prism 8 (http://www.graphpad.com). We considered $p<0.01$ to indicate significance.

Results

Our study sample consisted of 2,381 animals (1,229 dogs and 1,152 cats). Samples were collected from animals living in 23 main cities (and neighboring localities) in 8 countries in Asia, specifically China (Beijing, Nanjing, Shanghai, and Guangxi Province), Taiwan (Taipei, Taoyuan, Changhua, Pingtung, and Hualien), Indonesia (Jakarta, Bogor, and Yogyakarta), Malaysia (Klang Valley region and Kota Bharu), the Philippines (Cabanatuan, San Jose, and Munoz), Singapore, Thailand (Bangkok and Chiang Mai), and Vietnam (Hanoi and Ho Chi Minh City) (Figure 1).

The dog population was composed of 565 (46.0%) females, 660 (53.7%) males, and 4 (0.3%) with unreported data; the cat population was composed of 543 (47.1%) females, 606 (52.6%) males, and 3 (0.3%) with unreported data. Ages of dogs ranged from 2 months to 20 years (mean 5.1 years, median 4.0 years), and ages of cats ranged from 2 months to 20 years (mean 2.7 years, median 2.0 years) (Table 1).

Overall, 42.4% (95% CI 39.7%–45.2%) of dogs and 31.3% (95% CI 28.4%–33.7%) of cats had ≥1 ectoparasite detected, exposure to vectorborne parasites, or both (Tables 2–6; Figures 2–6). In particular, 33.5% (95% CI 30.9%–36.2%) of dogs and 31.3% (95% CI 28.4%–34.0%) of cats were infested with ≥1 ectoparasite, and 22.8% (95% CI 20.5%–25.2%) of dogs and 0.5% (95% CI 0.2%–1.1%) of cats were detected with or exposed to ≥1 vectorborne parasite. *T. callipaeda* eyeworms were detected in 1.7% (95% CI 0.8%–3.3%) of dogs from China, specifically in 6.7% (95% CI 3.4–12.7) of dogs and 0.6% (95% CI 0.2%–1.8%) of cats from Beijing.

Table 6. Molecular identification and GenBank accession numbers of vectorborne parasites detected in study of ectoparasites and vectorborne zoonotic pathogens of dogs and cats, Asia, 2017–2018

Parasite species	GenBank accession nos.
Dirofilaria immitis filariae	MT027229
Brugia malayi filariae	MT027200–1
Brugia pahangi filariae	MT027202–4
Leishmania infantum protozoa	MN699319–20
Thelazia callipaeda nematodes	MT040339–44
Hepatozoon canis protozoa	MN689651–71
Babesia gibsoni protozoa	MN689634–48

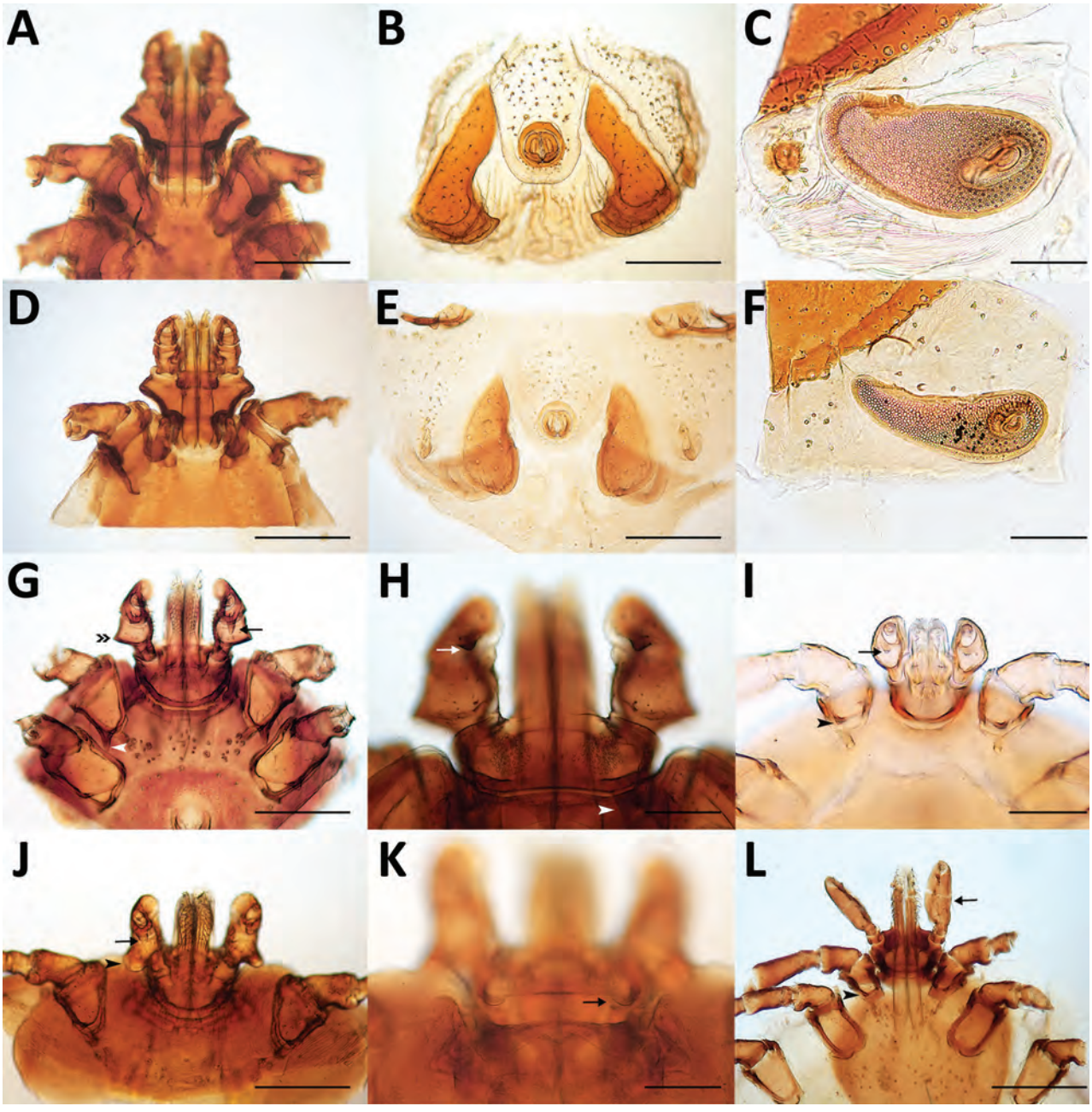

Figure 2. Morphologic characteristics of ticks collected from dogs and cats in study of ectoparasites and vectorborne zoonotic pathogens of dogs and cats in Asia, 2017–2018. A–C) Male *Rhipicephalus haemaphysaloides* tick with hexagonal basis capitulum (A); typical sickle-shape adanal plates (B); and spiracular plate with comma shape, broad throughout its length (C). D–F) Male *R. sanguineus* tick with hexagonal basis capitulum (D); subtriangular adanal plates (E); and comma-shaped spiracular plate, elongated throughout its length (F). G) Female *Haemaphysalis longicornis* tick with enlarged lateral palp article II (double arrowhead), ventral spur on palp article III (arrow), and internal spur on coxa I (white arrowhead), relatively long and pointed. H) *H. longicornis* tick palp article III with retrograde dorsal spur (arrow) and cornua one third the length of the basis capitulum (arrowhead). I) Larva of *Haemaphysalis wellingtoni* palp article II slightly broader than article III, internal spur on coxa I (arrowhead) and strong and sharp ventral spur on palpal article III (arrow). J–K) Female *Haemaphysalis campanulata* tick with well-defined ventral spur (arrow) on palp article III, palp article II strongly salient laterally, with flared and bell-shaped posterior margin (arrowhead) (J) and with short cornua (arrow) (K). L) *Ixodes* sp. female tick with long palp (arrow) and short spur on coxa I (arrowhead). Scale bars in panels A, B, D, E, G, J, and L indicate 500 μm; scale bars in panels C, F, H, and K indicate 200 μm; scale bar in panel I indicates 100 μm.

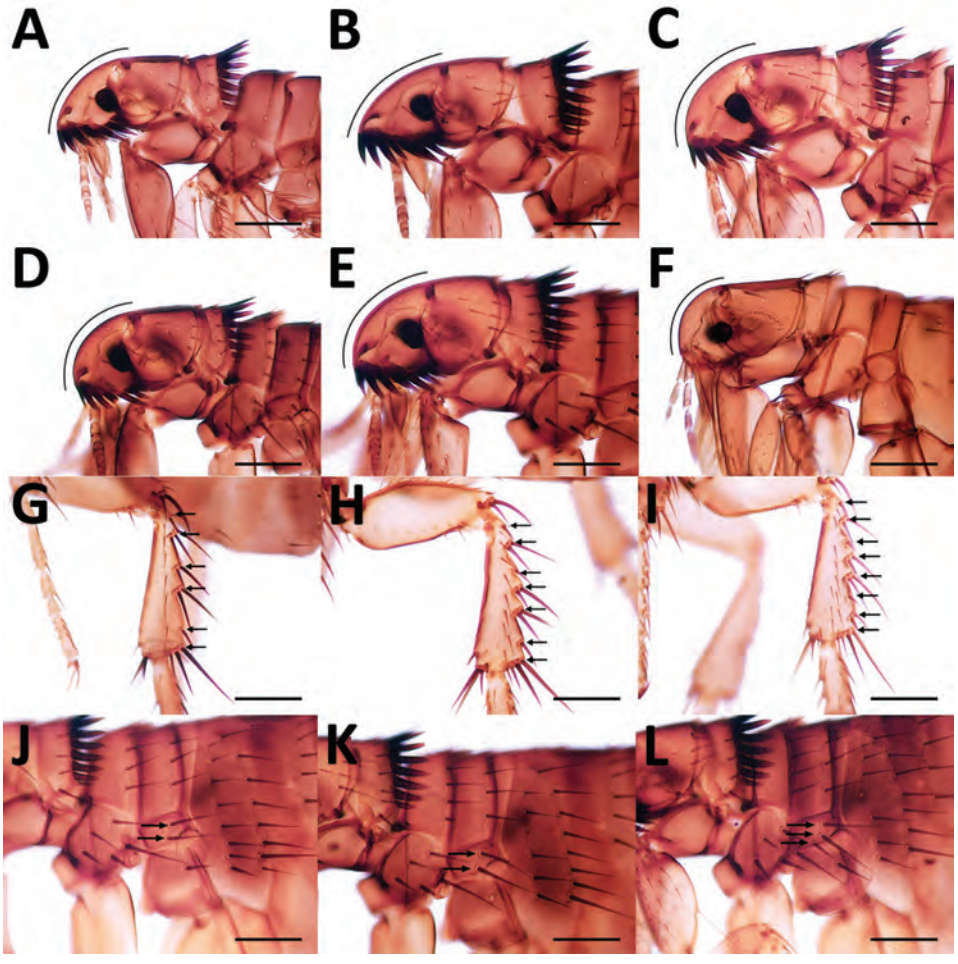

Figure 3. Morphologic characteristics of fleas collected from dogs and cats in study of ectoparasites and vectorborne zoonotic pathogens of dogs and cats in Asia, 2017–2018. A) *Ctenocephalides felis* male flea head; B) *C. felis* female flea head showing acute anterior margin; C) *C. canis* male flea; D) *Ctenocephalides orientis* male flea; E) *C. orientis* female flea; F) *Xenopsylla cheopis* male flea with strongly rounded anterior margin and absence of ctenidia; G) *C. felis* flea with 6 setae-bearing notches (arrows) on the dorsal margin of the hind tibia; H) *C. orientis* flea with 7 setae-bearing notches; I) *C. canis* flea with 8 setae-bearing notches; J) *C. felis* flea with 2 setae on the lateral metonotal area (arrows); K) *C. orientis* flea with 2 setae; L) *C. canis* fleas with 3 setae. Scale bars indicate 200 μm.

We detected co-infections with *Hepatozoon canis* and *D. immitis* heartworms in 4 dogs (2 each from Thailand and the Philippines). No tick infestations were found on dogs infected with *B. gibsoni*, but *Rhipicephalus sanguineus* ticks were detected on 50% of animals with *H. canis* infection. *H. canis* infection was correlated with infestation by *R. sanguineus* ticks (p = 0.0125).

A total of 4 dogs (0.3%, 95% CI 0.1%–0.8%) were positive for antibodies against *Leishmania infantum;* 2 of these dogs were from China (0.4%, 95% CI 0.1%–1.5%) and 1 each from Vietnam (0.8%, 95% CI 0.1%–4.6%) and the Philippines (0.9%, 95% CI 0.2%–5.0%). In addition, the 2 seropositive dogs from China were positive for *L. infantum* by qPCR and cPCR Sanger sequencing (Table 6).

A total of 2 dogs (0.2%, 95% CI 0–0.6) were positive for antibodies against *Borrelia burgdorferi* sensu lato. One was in the Philippines (0.9%, 95% CI 0.2%–4.9%), and 1 was in Indonesia (1.1%, 95% CI 0.2%–5.7%).

Overall, 5.2% (95% CI 4.1%–6.7%) of dogs were infected with filarial parasites according to antigen testing (3.5%, 95% CI 2.6%–4.6%), cPCR (2.7%, 95% CI 1.9%–3.7%), or both. cPCR-coupled sequencing identified *Brugia* spp. in 0.4% of dogs (95% CI 0.2%–0.9%) and in 15.2% (95% CI 6.6%–30.9%) of the samples positive for filariae by cPCR. Specifically, *B. pahangi* was found in dogs in Thailand (1.7%, 95% CI 0.5%–5.9%) and Malaysia (2.2%, 95% CI 0.4–11.6), and *B. malayi* was found in dogs in Vietnam (0.8%, 95% CI 0.1–4.6) and Thailand (0.8%, 95% CI 0.1%–4.6%). Using the kappa statistic, we found slight to fair agreement between antigen testing and cPCR (κ = 0.271, 95% CI 0.079–0.463) for the diagnosis of *D. immitis* in dogs. One cat (1.3%, 95% CI 0.2%–6.9%) from Indonesia was positive for *D. immitis* antigen.

H. canis infection was diagnosed for 1 cat from the Philippines (0.9%, 95% CI 0.2–5.1) and *B. gibsoni* for 3 cats in China (0.6%, 95% CI 0.2%–1.8%) and 1 cat in Singapore (0.8%, 95% CI 0.1–4.3). FIV antibodies were detected in 5.2% (95% CI 4.0%–6.6%) of cats and FeLV antigens in 2.9% (95% CI 2.1%–4.0%).

We compiled statistically significant associations for the detection of/exposure to ≥1 ectoparasite or

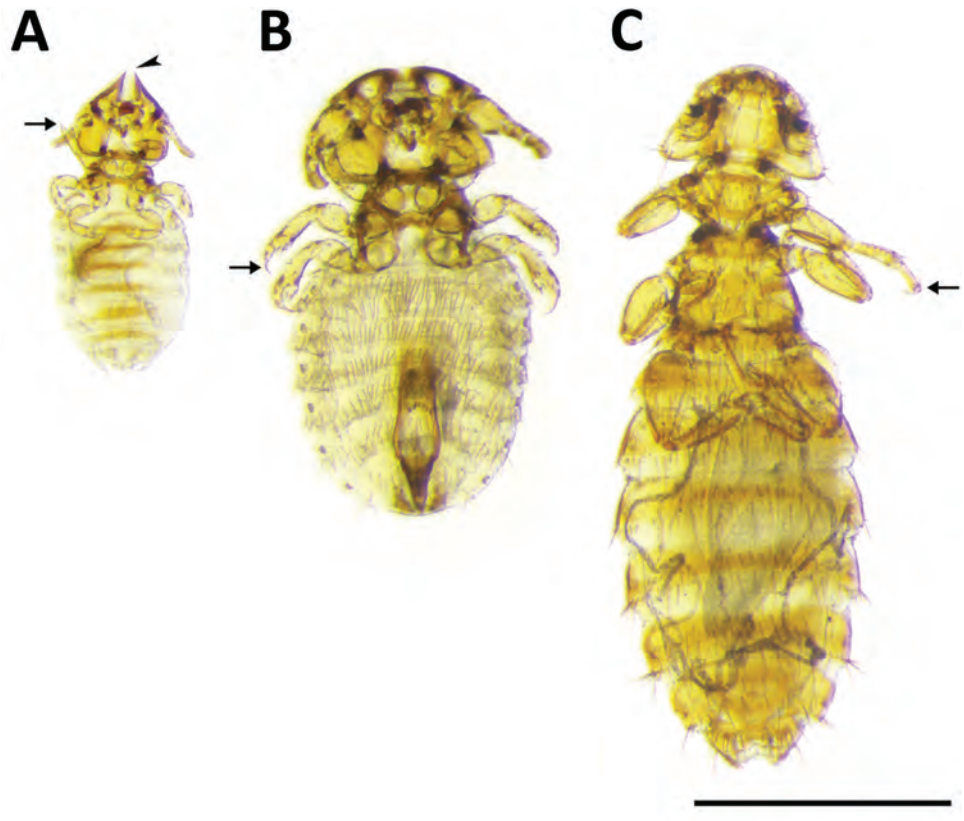

Figure 4. Chewing lice collected from dogs and cats in study of ectoparasites and vectorborne zoonotic pathogens of dogs and cats in Asia, 2017–2018. A) Female *Felicola subrostratus* louse with triangular head and pointed anteriorly. The median longitudinal groove (arrowhead) on the head fits around the shaft of the hair of the host. Thorax is short and legs are small, ending with a single claw (arrow). B) *Trichodectes canis* male louse with short thorax, flattened head with quadrangular shape, broader than long; each leg with only 1 claw on tarsus (arrow). C) *Heterodoxus spiniger* female louse with subtriangular head, rounded anteriorly. The thorax is considerably longer than wide. Each leg has 2 claws on the tarsus (arrow). Scale bar indicates 1 mm.

vectorborne pathogen, to ectoparasites or vectorborne parasites only, and to filarial parasites in dogs in different age classes (Appendix Figure 1). The finding of clinical signs (e.g., respiratory, lymph nodes, ocular, and skin abnormalities and increased body temperature) was statistically associated with the overall detection of/exposure to ≥1 parasite (Appendix Figure 2) and with ectoparasite infestation or detection of/exposure to vectorborne parasites in dogs (Appendix Figure 3). For cats, we found no association between age group and detection of parasites, whereas clinical signs (i.e., enlarged lymph nodes and skin abnormalities) were statistically associated with detection of ectoparasitic infestation (Appendix Figure 4). We found no statistical association between seropositivity for FIV antibodies and FeLV antigens and detection of ectoparasites, vectorborne pathogens, or both.

Discussion

The detection of zoonotic pathogens in client-owned dogs and cats living in metropolitan areas indicates that these animals serve as hosts for several parasitic agents in Asia. We provide data for an extended geographic distribution of zoonotic pathogens (e.g., *L. infantum* protozoa and zoonotic species of filariae) and of arthropods infesting animals (e.g., ticks of the *Haemaphysalis* and *Rhipicephalus* genera) where prior data unavailability made treatment and disease control strategies unachievable.

Nearly half of the dogs and one third of the cats in this study were infested with ≥1 ectoparasite or exposed to vectorborne pathogens; prevalence peaked in countries with a humid tropical climate (e.g., the Philippines, where 67% of dogs were infested with ticks, and Malaysia, where 89% of cats were infested with fleas). Such findings raise concern that vectorborne pathogens are responsible for several zoonotic diseases in Southeast Asia (*25*). The most prevalent tick on dogs and cats in this study was *R. sanguineus*. The taxonomic status of this tick group is a matter of debate with regard to *R. sanguineus* sensu lato including 2 lineages, so-called temperate and tropical (*26*–*28*). The tropical lineage of the *R. sanguineus* s.l. tick is prevalent in most countries in Asia and has been deemed accountable for the transmission of pathogens causing babesiosis, ehrlichiosis, and several rickettsial diseases in Asia (*25*,*29*,*30*). Despite the high proportion of tick-infested animals, the paucity of data on the ecology of *R. sanguineus* s.l. ticks in Asia makes their role as a vector difficult to ascertain.

Unexpectedly, we found tick species not classically associated with companion animals but with the potential to transmit zoonotic disease–causing pathogens in dogs. For example, *Haemaphysalis hystricis*

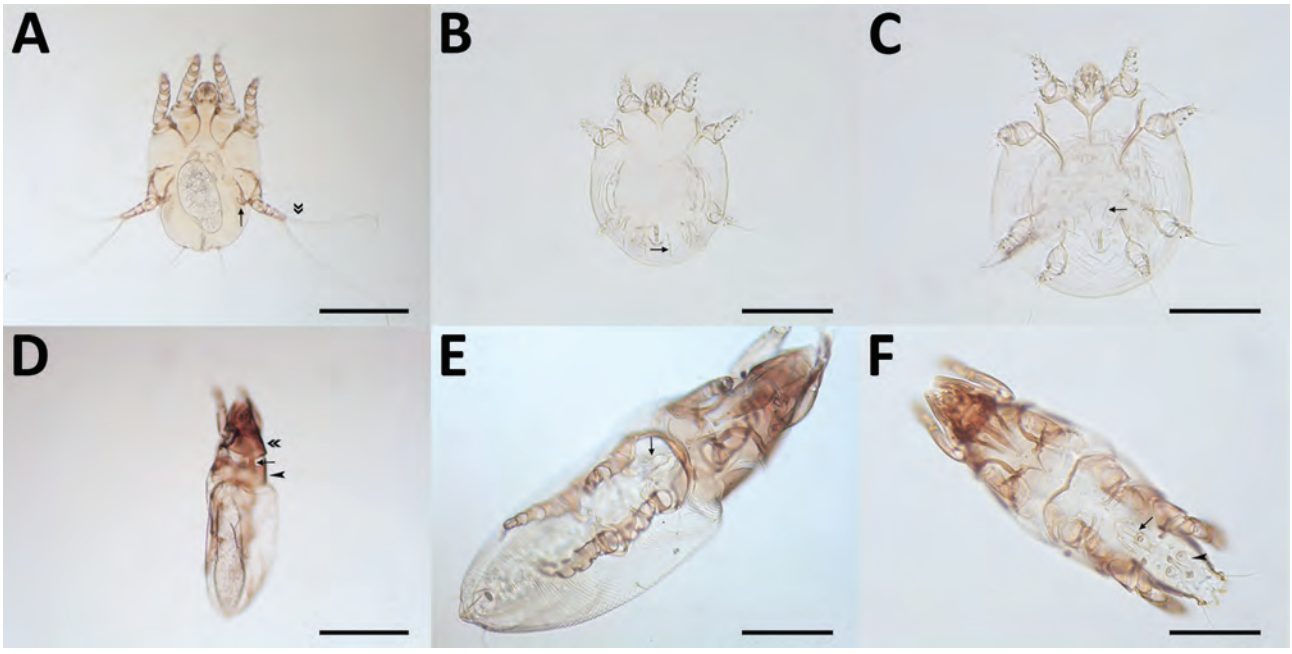

Figure 5. Mites collected from dogs and cats in study of ectoparasites and vectorborne zoonotic pathogens of dogs and cats in Asia, 2017–2018. A) *Otodectes cynotis* female mite with greatly reduced last pair of legs (arrow); the third pair of legs terminates in 2 long and whip-like setae (double arrowhead). B) *Sarcoptes scabiei* male mite with strong and spine-like dorsal setae (arrow). C) *Notoedres cati* mite with narrow and not spine-like setae. D) Female *Lynxacarus radovskyi* cat fur mite with cylindrical and heavily striated idiosoma, well-developed head plate (double arrowhead) with convex posterior margin; propodosomal plate (arrowhead) with posterior margin broadly rounded, connected mediodorsally to head plate by a narrow-sclerotized band (arrow). E) *L. radovskyi* female mite genital apparatus (arrow) positioned between coxae III in female. F) *L. radovskyi* male mite with genital apparatus (arrow) positioned between coxae IV (arrow) and circular genital discs (arrowhead). Scale bars in panels A and D indicate 200 μm; scale bars in panels B, C, E, and F indicate 100 μm.

ticks have been implicated as vectors of a novel *Borrelia* species closely related to the relapsing fever group (*31*), and *Haemaphysalis wellingtoni* ticks are vectors of Kyasanur Forest disease virus, which causes fatal epidemics among monkeys and leads to hospitalization of ≈500 persons/year in India (*3*). Moreover, dogs seropositive to *B. burgdorferi* s.l. in this study were from Indonesia and the Philippines. This finding is unexpected, considering that these bacteria have been detected outside the known distribution area of *Ixodes* tick species, the main vectors of *B. burgdorferi* s.l., and indicates a need for in-depth epidemiologic surveys of this group of pathogens in Southeast Asia.

These results update the list of pathogens and ectoparasites affecting companion animals in Asia, including ticks with multihost feeding behavior, which has the potential to extend the network of pathogen transmission further into urban areas. The same holds true for pet dogs, suggesting that these animals might have been overlooked as potential pathogen reservoirs in metropolitan settings in this geographic area.

Similarly, the *Ctenocephalides orientis* flea was identified in one fifth of flea-positive dogs. The host spectrum of this flea is wider, but apparently its geographic distribution is more limited than that of the well-known cat flea *Ctenocephalides felis*, and it is involved in the transmission of rickettsiae, including *Rickettsia* sp. genotype RF2125 and *Rickettsia* sp. TH2014 (*32*,*33*). The morphologic ambiguity of the *C. orientis* flea (probably misidentified as *Ctenocephalides canis* and previously reported as a subspecies of *C. felis*) has contributed to a substantial dearth of information on its global distribution and role as a vector. In contrast, the cosmopolitan *C. felis* flea has colonized different bioclimatic niches, mainly through human-mediated migration (*34*). As human and animal global transportation increase in Asia, constant vigilance regarding the introduction of *C. orientis* fleas outside their known range of distribution in developed and developing countries is essential, as supported by the recent report of detection of fleas of this species in Iran (*35*).

In Singapore, one of the countries with the highest human development index (*36*) and lowest proportion of animals affected by parasites, *Lynxacarus radovskyi*, a mite for which little is known regarding

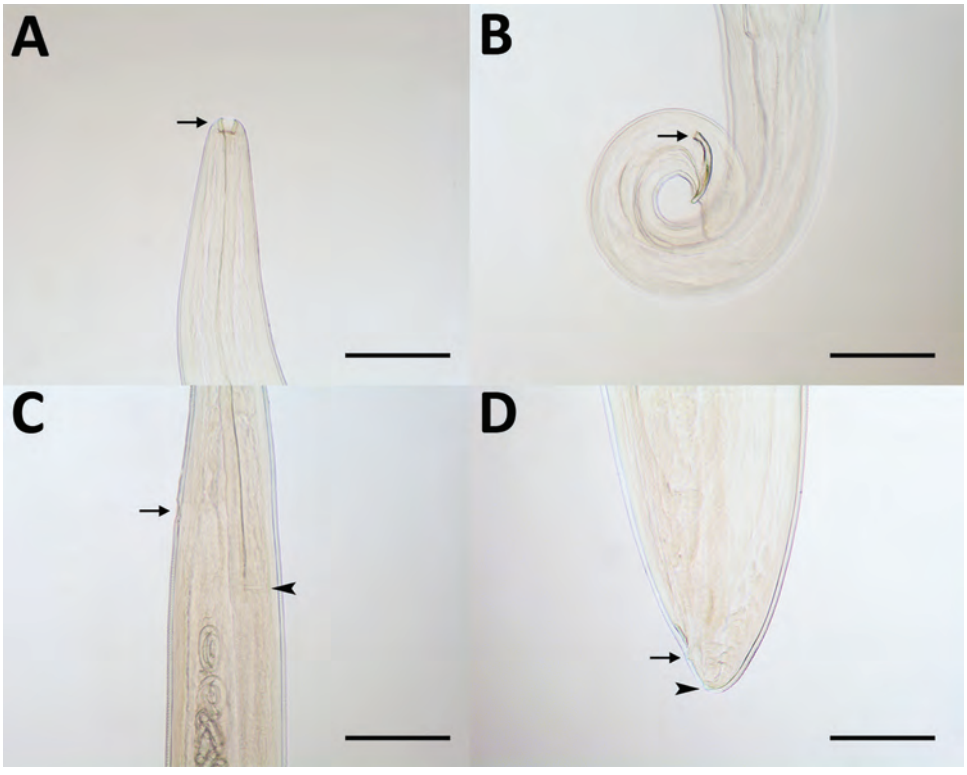

Figure 6. *Thelazia callipaeda* eyeworms collected from animals in China in study of ectoparasites and vectorborne zoonotic pathogens of dogs and cats in Asia, 2017–2018. A) *T. callipaeda* male eyeworm with buccal capsule (arrow); B) posterior end of male eyeworm with short and crescent-shaped spicule (arrow); C) anterior portion of *T. callipaeda* female eyeworm with vulva (arrow) located posterior to the esophagus-intestinal junction (arrowhead); and D) posterior end of female eyeworm showing anus (arrow) and phasmids (arrowhead). Scale bars indicate 200 μm.

its ecology, was detected on 35% of sampled cats. We have provided molecular data and updated morphologic information on this listophorid mite, which is an agent of papular dermatitis in humans (*37*). Furthermore, availability of appropriate diagnostics for this species or data on the efficacy of ectoparasiticides against it are limited.

Refined diagnostics are essential for assessing the distribution of filarial species in canine populations. For instance, the poor agreement (κ = 0.271) between cPCR and antigen-detection tests for *D. immitis* advocates for the use of integrated diagnostics to better appreciate the epidemiologic status of this species of filariae. Furthermore, the use of both tests revealed *B. pahangi* and *B. malayi* to also (in addition to *D. immitis*) affect companion animals in the regions investigated. These 3 species of filariae cause clinical manifestations in humans: lymphatic filariosis for *B. malayi* and *B. pahangi* (*38*,*39*) and pulmonary granulomas for *D. immitis* (*40*). In particular, lymphatic filariosis is among the most debilitating neglected tropical diseases; an estimated 70 million persons are infected, among which >50% live in Southeast Asia (*41*,*42*), and *D. immitis* infection of humans poses significant diagnostic challenges (*40*). Hence, for development and enactment of global elimination programs (*41*), surveillance of filarial species should be extended to animal populations in filariae-endemic countries (*42*).

Similarly, *Leishmania* spp. parasites currently cause ≈500,000 human infections/year in 62 countries (*43*), although their occurrence in eastern and Southeast Asia is poorly documented. We detected dogs positive for *L. infantum* by serology, qPCR, and sequencing in China and seropositive dogs in Thailand and Vietnam. In Thailand, the recent emergence of *L. martiniquensis* and *L. siamensis* caused immunocompetent and immunocompromised persons to seek medical assistance (*44*). A range of animals is involved in the zoonotic cycle of these 2 species (*44*,*45*), but dogs are the main reservoir for zoonotic leishmaniosis caused by *L. infantum* (*46*). The role of *Leishmania* spp. in human infections and as agents of disease in Southeast Asia requires urgent attention.

Further complicating knowledge of the transmission of zoonotic parasites in these regions of Asia are the large populations of free-roaming animals; the increased number of pet dogs and cats; and the complex social, economic, and ecologic changes currently occurring in Asia, (*1*,*2*,*4*,*25*,*47*,*48*). Integrated strategies that address all of these factors are therefore fundamental for the control of such parasitic agents. We investigated the presence of pathogens and ectoparasites in pet dogs and cats living in metropolitan areas in close proximity to humans. These animals share a common environment with humans, which makes them likely key reservoirs for pathogens with

the potential to infect persons living in such areas and settings.

The epidemiologic data presented in this study can be pivotal for building knowledge bases about the occurrence of zoonotic parasites infecting companion dogs and cats in eastern and Southeast Asia. This information could help epidemiologists and policy makers provide tailored recommendations in the blueprint of future surveillance and prevention strategies.

Acknowledgments

We are grateful to Isabelle Richtofen, Jianwei Zhang, Evonne Lim, Clair Cheng, Nadine Duperray, and Marielle Servonnet for their expertise and contributions to managing this logistically challenging study.

About the Author

Dr. Colella is a postdoctoral research fellow at the University of Melbourne, Australia. His main research is focused on the development of epidemiologic studies and strategies for interventions against zoonotic pathogens.

References

1. Coker RJ, Hunter BM, Rudge JW, Liverani M, Hanvoravongchai P. Emerging infectious diseases in southeast Asia: regional challenges to control. Lancet. 2011;377:599–609. https://doi.org/10.1016/S0140-6736(10)62004-1
2. Chongsuvivatwong V, Phua KH, Yap MT, Pocock NS, Hashim JH, Chhem R, et al. Health and health-care systems in southeast Asia: diversity and transitions. Lancet. 2011;377:429–37. https://doi.org/10.1016/S0140-6736(10)61507-3
3. Shah SZ, Jabbar B, Ahmed N, Rehman A, Nasir H, Nadeem S, et al. Epidemiology, pathogenesis, and control of a tick-borne disease—Kyasanur Forest disease: current status and future directions. Front Cell Infect Microbiol. 2018;8:149. https://doi.org/10.3389/fcimb.2018.00149
4. Conlan JV, Sripa B, Attwood S, Newton PN. A review of parasitic zoonoses in a changing Southeast Asia. Vet Parasitol. 2011;182:22–40. https://doi.org/10.1016/j.vetpar.2011.07.013
5. Chen J, Xu MJ, Zhou DH, Song HQ, Wang CR, Zhu XQ. Canine and feline parasitic zoonoses in China. Parasit Vectors. 2012;5:152. https://doi.org/10.1186/1756-3305-5-152
6. Inokuma H. Panorama of vector borne disease of pets in Asia & Japan. In: Beugnet F, editor. Guide to vector borne diseases of pets. Lyon (France): Merial; 2013. p. 94–107.
7. Traub RJ, Irwin P, Dantas-Torres F, Tort GP, Labarthe NV, Inpankaew T, et al. Toward the formation of a Companion Animal Parasite Council for the Tropics (CAPCT). Parasit Vectors. 2015;8:271. https://doi.org/10.1186/s13071-015-0884-4
8. Dong HP, Liu ZW, Chen H, Zhang LX. The situation and treatment of parasitic zoonoses of pets [in Chinese]. Hennan J Ani Sci. Vet Med. 2007;28:8–10.
9. Otranto D, Dantas-Torres F, Mihalca AD, Traub RJ, Lappin M, Baneth G. Zoonotic parasites of sheltered and stray dogs in the era of the global economic and political crisis. Trends Parasitol. 2017;33:813–25. https://doi.org/10.1016/j.pt.2017.05.013
10. Paul M, King L, Carlin EP. Zoonoses of people and their pets: a US perspective on significant pet-associated parasitic diseases. Trends Parasitol. 2010;26:153–4. https://doi.org/10.1016/j.pt.2010.01.008
11. Chomel BB, Sun B. Zoonoses in the bedroom. Emerg Infect Dis. 2011;17:167–72. https://doi.org/10.3201/eid1702.101070
12. Gibb TJ, Oseto CY. Arthropod collection and identification: field and laboratory techniques. 1st ed. Boston: Academic Press; 2006.
13. Tanskul P, Inlao I. Keys to the adult ticks of *Haemaphysalis* Koch, 1844, in Thailand with notes on changes in taxonomy (Acari: Ixodoidea: Ixodidae). J Med Entomol. 1989;26:573–601. https://doi.org/10.1093/jmedent/26.6.573
14. Hopkins GHE. Siphonaptera. In: Gressitt JL, editor. Insect of Micronesia. Hawaii (HI): Bishop Museum; 1961. p. 91–107.
15. Trapido H, Varma MGR, Rajagopalan PK, Singh KRP, Rebello MJ. A guide to the identification of all stages of the *Haemaphysalis* ticks of South India. Bull Entomol Res. 1964;55:249–70. https://doi.org/10.1017/S0007485300049439
16. Yamaguti N, Tipton VJ, Keegan HL, Toshioka S. Ticks of Japan, Korea, and the Ryukyu Islands. Brigham Young University Science Bulletin. Biological Series. 1971;15:Article 1.
17. Tenorio JM. A new species of *Lynxacarus* (Acarina: Astigmata: Listrophoridae) from *Felis catus* in the Hawaiian islands. J Med Entomol. 1974;11:599–604.
18. Kettle DS. Medical and Veterinary Entomology. 1st ed. Sydney (Australia): Croom Helm; 1984.
19. Lewis RE. Fleas (Siphonaptera). In: Lane RP, Crosskey RW, editors. Medical insects and arachnids. Dordrecht (Netherlands): Springer; 1993. p. 529–575.
20. Walker JB, Keirans JE, Horak IG. The genus *Rhipicephalus* (Acari, Ixodidae): a guide to the brown ticks of the world. Cambridge: Cambridge University Press; 2005.
21. Wall R, Shearer D. Veterinary Entomology. 1st ed. London: Chapman & Hall Press; 1997.
22. Otranto D, Lia RP, Traversa D, Giannetto S. *Thelazia callipaeda* (Spirurida, Thelaziidae) of carnivores and humans: morphological study by light and scanning electron microscopy. Parassitologia. 2003;45:125–33.
23. Oliver JH. Importance of systematics to public health: ticks, microbes, and disease. Ann Mo Bot Gard. 1996;83:37–46. https://doi.org/10.2307/2399966
24. Whiting MF, Whiting AS, Hastriter MW, Dittmar K. A molecular phylogeny of fleas (Insecta: Siphonaptera): origins and host associations. Cladistics. 2008;24:677–707. https://doi.org/10.1111/j.1096-0031.2008.00211.x
25. Irwin PJ, Jefferies R. Arthropod-transmitted diseases of companion animals in Southeast Asia. Trends Parasitol. 2004;20:27–34. https://doi.org/10.1016/j.pt.2003.11.004
26. Nava S, Mastropaolo M, Venzal JM, Mangold AJ, Guglielmone AA. Mitochondrial DNA analysis of *Rhipicephalus sanguineus* sensu lato (Acari: Ixodidae) in the Southern Cone of South America. Vet Parasitol. 2012;190:547–55. https://doi.org/10.1016/j.vetpar.2012.06.032
27. Dantas-Torres F, Latrofa MS, Annoscia G, Giannelli A, Parisi A, Otranto D. Morphological and genetic diversity of *Rhipicephalus sanguineus* sensu lato from the New and Old Worlds. Parasit Vectors. 2013;6:213. https://doi.org/10.1186/1756-3305-6-213
28. Nava S, Beati L, Venzal JM, Labruna MB, Szabó MPJ, Petney T, et al. *Rhipicephalus sanguineus* (Latreille, 1806): neotype designation, morphological re-description of all parasitic stages and molecular characterization. Ticks Tick

Borne Dis. 2018;9:1573–85. https://doi.org/10.1016/j.ttbdis.2018.08.001
29. Petney TN, Keirans JE. Ticks of the genera *Boophilus*, *Dermacentor*, *Nosomma* and *Rhipicephalus* (Acari: Ixodidae) in South-east Asia. Trop Biomed. 1996;13:73–84.
30. Inpankaew T, Hii SF, Chimnoi W, Traub RJ. Canine vector-borne pathogens in semi-domesticated dogs residing in northern Cambodia. Parasit Vectors. 2016;9:253. https://doi.org/10.1186/s13071-016-1552-z
31. Khoo JJ, Lim FS, Tan KK, Chen FS, Phoon WH, Khor CS, et al. Detection in Malaysia of a *Borrelia* sp. From *Haemaphysalis hystricis* (Ixodida: Ixodidae). J Med Entomol. 2017;54:1444–8. https://doi.org/10.1093/jme/tjx131
32. Hii SF, Lawrence AL, Cuttell L, Tynas R, Abd Rani PA, Šlapeta J, et al. Evidence for a specific host-endosymbiont relationship between '*Rickettsia* sp. genotype RF2125' and *Ctenocephalides felis orientis* infesting dogs in India. Parasit Vectors. 2015;8:169. https://doi.org/10.1186/s13071-015-0781-x
33. Kho KL, Tay ST. Identification of rickettsial infections (*Rickettsia* sp. TH2014) in *Ctenocephalides orientis* fleas (Siphonaptera: Pulicidae). J Med Entomol. 2019;56:526–32. https://doi.org/10.1093/jme/tjy169
34. Lawrence AL, Webb CE, Clark NJ, Halajian A, Mihalca AD, Miret J, et al. Out-of-Africa, human-mediated dispersal of the common cat flea, *Ctenocephalides felis*: the hitchhiker's guide to world domination. Int J Parasitol. 2019;49:321–36. https://doi.org/10.1016/j.ijpara.2019.01.001
35. Seyyed-Zadeh SJ, Bozorg-Omid F, Telmadarraiy Z, Terenius O, Chavshin AR. Evidence for the presence of *Ctenocephalides orientis* in livestock dwellings in northwest Iran. Med Vet Entomol. 2018;32:383–7. https://doi.org/10.1111/mve.12308
36. United Nations Development Programme. Human development indices and indicators: 2018 statistical update [cited 2019 Dec 28]. http://hdr.undp.org/en/content/human-development-indices-indicators-2018-statistical-update
37. Foley RH. Parasitic mites of dogs and cats. Compend Contin Educ Vet Med. 1991;13:783–800.
38. Tan LH, Fong MY, Mahmud R, Muslim A, Lau YL, Kamarulzaman A. Zoonotic *Brugia pahangi* filariasis in a suburbia of Kuala Lumpur City, Malaysia. Parasitol Int. 2011;60:111–3. https://doi.org/10.1016/j.parint.2010.09.010
39. Ramaiah KD, Ottesen EA. Progress and impact of 13 years of the Global Programme to Eliminate Lymphatic Filariasis on reducing the burden of filarial disease. PLoS Negl Trop Dis. 2014;8:e3319. https://doi.org/10.1371/journal.pntd.0003319
40. Centers for Disease Control and Prevention. Dirofilariasis FAQs [cited 2019 Dec 28]. https://www.cdc.gov/parasites/dirofilariasis/faqs.html
41. Specht S, Suma TK, Pedrique B, Hoerauf A. Elimination of lymphatic filariasis in South East Asia. BMJ. 2019;364:k5198. https://doi.org/10.1136/bmj.k5198
42. Mallawarachchi CH, Nilmini Chandrasena TGA, Premaratna R, Mallawarachchi SMNSM, de Silva NR. Human infection with sub-periodic *Brugia* spp. in Gampaha District, Sri Lanka: a threat to filariasis elimination status? Parasit Vectors. 2018;11:68. https://doi.org/10.1186/s13071-018-2649-3
43. Guerin PJ, Olliaro P, Sundar S, Boelaert M, Croft SL, Desjeux P, et al. Visceral leishmaniasis: current status of control, diagnosis, and treatment, and a proposed research and development agenda. Lancet Infect Dis. 2002;2:494–501. https://doi.org/10.1016/S1473-3099(02)00347-X
44. Leelayoova S, Siripattanapipong S, Manomat J, Piyaraj P, Tan-Ariya P, Bualert L, et al. Leishmaniasis in Thailand: a review of causative agents and situations. Am J Trop Med Hyg. 2017;96:534–42. https://doi.org/10.4269/ajtmh.16-0604
45. Chusri S, Thammapalo S, Chusri S, Thammapalo S, Silpapojakul K, Siriyasatien P. Animal reservoirs and potential vectors of *Leishmania siamensis* in southern Thailand. Southeast Asian J Trop Med Public Health. 2014;45:13–9.
46. Otranto D, Dantas-Torres F. The prevention of canine leishmaniasis and its impact on public health. Trends Parasitol. 2013;29:339–45. https://doi.org/10.1016/j.pt.2013.05.003
47. Huggins LG, Koehler AV, Ng-Nguyen D, Wilcox S, Schunack B, Inpankaew T, et al. A novel metabarcoding diagnostic tool to explore protozoan haemoparasite diversity in mammals: a proof-of-concept study using canines from the tropics. Sci Rep. 2019;9:12644. https://doi.org/10.1038/s41598-019-49118-9
48. Nguyen VL, Colella V, Iatta R, Bui KL, Dantas-Torres F, Otranto D. Ticks and associated pathogens from dogs in northern Vietnam. Parasitol Res. 2019;118:139–42. https://doi.org/10.1007/s00436-018-6138-6

Address for correspondence: Vito Colella, Faculty of Veterinary and Agricultural Sciences, The University of Melbourne, VIC 3010, Australia; email: vito.colella@unimelb.edu.au

Multihost Transmission of *Schistosoma mansoni* in Senegal, 2015–2018

Stefano Catalano,[1] Elsa Léger,[1] Cheikh B. Fall, Anna Borlase, Samba D. Diop, Duncan Berger, Bonnie L. Webster, Babacar Faye, Nicolas D. Diouf, David Rollinson, Mariama Sène, Khalilou Bâ, Joanne P. Webster

In West Africa, *Schistosoma* spp. are capable of infecting multiple definitive hosts, a lifecycle feature that may complicate schistosomiasis control. We characterized the evolutionary relationships among multiple *Schistosoma mansoni* isolates collected from snails (intermediate hosts), humans (definitive hosts), and rodents (definitive hosts) in Senegal. On a local scale, diagnosis of *S. mansoni* infection ranged 3.8%–44.8% in school-aged children, 1.7%–52.6% in *Mastomys huberti* mice, and 1.8%–7.1% in *Biomphalaria pfeifferi* snails. Our phylogenetic framework confirmed the presence of multiple *S. mansoni* lineages that could infect both humans and rodents; divergence times of these lineages varied (0.13–0.02 million years ago). We propose that extensive movement of persons across West Africa might have contributed to the establishment of these various multihost *S. mansoni* clades. High *S. mansoni* prevalence in rodents at transmission sites frequented by humans further highlights the implications that alternative hosts could have on future public health interventions.

The collective image of schistosomiasis in Africa remains that of a mainly human-driven disease; schistosomiasis inflicted a burden of >2.5 million disability-adjusted life-years in 2016 and required that ≈200 million persons be treated with preventive chemotherapy in 2017 (*1*). As pledged by the World Health Organization (*2*), the goal to eliminate schistosomiasis as a public health problem by 2030 can only be achieved through transdisciplinary programs that improve sanitation and hygiene and provide access to safe water sources, health education, and chemotherapeutic treatments for at-risk populations. Furthermore, answers on the host specificity of human schistosomes and the impact of multihost transmission on disease control strategies remain imperative (*3*). In Asia, vertebrate reservoirs for *Schistosoma japonicum* (largely ruminants, rodents, and other mammals) play a crucial role in perpetuating the transmission of this zoonotic parasite, even under strong multisectoral control pressures (*4*,*5*). Likewise, in the Caribbean and South America, where evidence supports the introduction of *Schistosoma mansoni* from West Africa via the transatlantic slave trade (*6*), rodent populations have become the main reservoirs of *S. mansoni*; transmission in this region can be maintained in absence of human activity (*7*,*8*).

The magnitude of *Schistosoma* zoonotic transmission, in which both domestic animals and wildlife are active participants, is yet to be determined in endemic countries across Africa. Sporadic investigations have attempted to answer whether schistosomes infecting humans are zoonotic and which, if any, other vertebrate species might be acting as definitive hosts (*9*–*11*). The emergence (or discovery) of hybridization events involving *S. mansoni*, *Schistosoma haematobium*, and other *Schistosoma* spp. in livestock and wildlife has raised the profile of these definitive hosts and the schistosomes they harbor (*12*,*13*). The interspecific interactions between *Schistosoma* spp. and the potential involvement of domestic and wild vertebrates in the transmission dynamics of these species might partially be a consequence of anthropogenic changes, loss

Author affiliations: Royal Veterinary College, University of London, Hatfield, UK (S. Catalano, E. Léger, A. Borlase, J.P. Webster); Université Cheikh Anta Diop, Dakar, Senegal (C.B. Fall, B. Faye); Big Data Institute, University of Oxford, Oxford, UK (A. Borlase); Université Alioune Diop de Bambey, Bambey, Senegal (S.D. Diop); Wellcome Sanger Institute, Hinxton, UK (D. Berger); Natural History Museum, London, UK (B.L. Webster, D. Rollinson); Université Gaston Berger, Saint-Louis, Senegal (N.D. Diouf, M. Sène); Institut de Recherche pour le Développement, Dakar (K. Bâ)

DOI: https://doi.org/10.3201/eid2606.200107

[1]These first authors contributed equally to this article.

of ecologic barriers, and movement of communities between endemic areas (*12*).

In 1986, the Diama Dam became operational and transformed the Senegal River Basin. The rice and sugarcane industries benefitted extensively from this change in land use, and the guaranteed freshwater supply favored the expansion of subsistence farming and livestock husbandry. In addition, communities attracted by employment opportunities migrated to the region, in particular to the town of Richard Toll and villages nearby the lake Lac de Guiers in northern Senegal (*14*,*15*). However, these anthropogenic changes in the area rapidly led to the first outbreaks of schistosomiasis in the early 1990s (*16*). As of April 2020, both intestinal schistosomiasis (caused by *S. mansoni*) and urogenital schistosomiasis (caused by *S. haematobium* and schistosome hybrids) remain endemic, with co-infections commonly observed across the Senegal River Basin (*17*). Records show a prevalence of 32%–40% for *S. mansoni* and 77%–81% for *S. haematobium* and schistosome hybrids in school-aged children and adults inhabiting towns surrounding Lac de Guiers and along the Senegal River (*18*,*19*). In this scenario, the role of animal hosts in the epidemiology of schistosomiasis is unclear. Wild rodents and humans seem to share the same *Schistosoma* species and hybrids at transmission foci (*20*,*21*). However, whether these schistosomes are truly multihost parasites or, in contrast, they have followed diverging evolutionary pathways indicative of definitive host specialization remains to be determined. Focusing on the regions of Richard Toll and Lac de Guiers, our objectives were to examine the evolutionary relationships and host use among *Schistosoma* isolates and the potential for rodent-to-human spillover.

Materials and Methods

Small Mammal Trapping

During October–December 2017, we captured small mammals at 21 sites that represented *Schistosoma* spp. transmission foci frequented by humans and their livestock because they are access points to fresh water (Appendix Figure 1, https://wwwnc.cdc.gov/EID/article/26/6/20-0107-App1.pdf). These study sites were situated within or adjacent to villages on the shores of Lac de Guiers and were considered independent from each other for trapping purposes; the shortest distance between adjacent sites was ≈500 m, greater than the maximum home range of endemic species (*22*). We baited locally made wire-mesh live traps (26 × 10 × 10 cm) with peanut butter and placed them in lines of 14–22 traps at intervals of 5 m adjacent to bodies of water in riparian habitats where reeds (*Phragmites* sp. and *Typha* sp.) were the dominant vegetation. We set traps each evening before dusk and inspected them the following morning after dawn for 2 consecutive nights per study site. We calculated the relative abundance of trapped species (no. animals captured/no. active traps) per night for each trap site (*23*).

We euthanized small trapped mammals with an intraperitoneal injection of sodium thiopental (300 mg/kg body weight) and confirmed their deaths by cervical dislocation and the absence of pedal reflex. We recorded each animal's species (based on morphologic identification), sex, age class, and anatomic measurements at postmortem examination (Appendix); dissected their thoracic and abdominal organs separately; and visually inspected these organs for helminths. We separated *Schistosoma* pairs, preserved them in separate vials containing 95% ethanol, and stored them at –20°C. We macerated dissected livers and large intestines of *Schistosoma*-positive hosts through 300 μm metal sieves using bottled spring water to hatch miracidia and then collected the free-swimming miracidia onto Whatman Indicating FTA Classic Cards (GE Healthcare Life Sciences, https://www.gelifesciences.com) for DNA storage and molecular analysis (*24*,*25*). We archived *Schistosoma* miracidia and adult worms in the Schistosomiasis Collection at the Natural History Museum (*26*).

Human and Snail Surveys

During October 2017–January 2018, as part of a large-scale program on the transmission dynamics of *Schistosoma* spp. across Senegal, we conducted a survey for parasites among randomly selected school-aged children (5–17 years of age, n = 290) and self-selected adults (18–78 years of age, n = 40) in the region of Richard Toll and Lac de Guiers. Each person provided 1 fecal sample; we diagnosed *Schistosoma* infections when eggs were observed in duplicate Kato-Katz thick smears (*27*). We processed each *Schistosoma*-positive fecal sample (30 g or the whole sample if <30 g) separately using the miracidial hatching technique (*25*) and pipetted the free-swimming miracidia onto Whatman Indicating FTA Classic Cards for DNA storage and molecular analysis (*24*). We archived *Schistosoma* miracidia in the Schistosomiasis Collection at the Natural History Museum (*26*).

During November 2015–April 2018, we sampled open freshwater sources within and nearby villages where we conducted surveys with human volunteers to identify snails acting as intermediate hosts of *Schistosoma* parasites. Throughout 5 surveys, we applied

standardized protocols in malacology, determined species of collected snails, and identified cercarial shedding to diagnose infections (*28*). We pipetted free-swimming *Schistosoma* cercariae, which we identified using a morphologic key (*29*), onto Whatman Indicating FTA Classic Cards for DNA storage and molecular analysis (*24*). We archived *Schistosoma* cercariae in the Schistosomiasis Collection at the Natural History Museum (*26*).

Molecular Analyses

We extracted DNA of individual adult schistosomes using the DNeasy Blood and Tissue Kit (QIAGEN, https://www.qiagen.com) following the manufacturer's instructions and extracted the DNA of miracidia and cercariae stored on Whatman Indicating FTA Classic Cards as previously described (*30*). We analyzed the following genomic regions because they are highly informative for phylogenetic identification and classification (*31*): the internal transcribed spacers (ITS) of the nuclear rDNA, the mitochondrial 12S rRNA gene, cytochrome *c* oxidase subunit 1 (*cox1*) and subunit 3 (*cox3*) genes of the mitochondrial DNA (mtDNA), and NADH dehydrogenase subunit 4 (*nad4*) and subunit 3 (*nad3*) genes of the mtDNA. We amplified these regions using 25-μL reactions containing 2.5 μL of 10× buffer, 200 μM of dNTPs, 0.5 μM of each primer, 0.2 units of KOD XL DNA Polymerase (EMD Millipore Corporation, https://www.emdmillipore.com), and 2 μL of DNA template (Appendix Tables 1 and 2). We purified and sequenced PCR products using Eurofins Genomics (https://www.eurofinsgenomics.com) and then edited and assembled contigs using CodonCode Aligner 8.0.1 (https://www.codoncode.com/index.htm). We aligned the noncoding ITS and 12S regions using MAFFT v7 (*32*) with automated selection of parameters and aligned the protein-coding mtDNA genes (i.e., *cox1*, *cox3*, *nad4*, and *nad3*) with respect to their amino acid translations using MACSE (*33*) as implemented in CodonCode Aligner 8.0.1. Molecular sequences from the *S. mansoni* samples are deposited in GenBank (accession nos. MN593375–434).

Phylogenetic Approach

We concatenated the 12S rRNA gene and the 4 protein-coding mtDNA genes of each *S. mansoni* specimen (i.e., adult worms and miracidia from rodents, miracidia from humans, and cercariae from snails), as well as those from *S. mansoni* specimens previously collected from Hubert's multimammate mice (*Mastomys huberti*) and Nile grass rats (*Arvicanthis niloticus*) in Senegal (*21*). In addition, we also obtained and concatenated the respective sequences from publicly available genomes of *S. mansoni* previously isolated from school-aged children in Uganda (*34*) and *Schistosoma rodhaini* from an undetermined intermediate host in Burundi (*6*). In brief, we downloaded an *S. mansoni* reference genome (GenBank accession no. SAMEA2272516) from WormBase ParaSite (*35*) and aligned the 5 specified mitochondrial genes with those of *S. mansoni* from Uganda and *S. rodhaini* from Burundi using BWA-MEM version 0.7.17 (Li H, unpub. data, https://arxiv.org/abs/1303.3997v2). For each sample, we used the Genome Analysis Toolkit (*36*) tools HaplotypeCaller version 3.6.0 to perform variant calling and FastaAlternateReferenceMaker version 3.6.1.0 to replace reference bases with single-nucleotide polymorphisms at variation sites.

We implemented maximum-likelihood analyses in RAxML version 8.2 (*37*) and Bayesian inference analyses in MrBayes 3.2.6 (*38*). Across 4 partitions (noncoding positions and protein-encoding first, second, and third codon positions), we selected the generalized time-reversible substitution model with rate heterogeneity for both maximum-likelihood and Bayesian inference. Bootstrap resampling was automatically arrested within the maximum-likelihood analysis. We performed Bayesian inference analysis using 2 independent Markov chain Monte Carlo runs including 4 chains and 10 million generations, sampling every 10,000 generations, and discarding the first 25% of trees as burn-in (Appendix).

We analyzed the temporal structure of the data by using Bayesian inference analysis and specifying independent Hasegawa-Kishino-Yano substitution models with rate heterogeneity across the 4 partitions, a coalescent constant population tree prior with default settings, and a strict clock model in BEAST 2.5.1 (*39*). We based divergence dating on previous estimates of mutation rates (8.1×10^{-9} substitutions/site/year) per generation time (0.2 years) that were determined by using whole-genome *S. mansoni* sequences (*6*). We inferred the resulting uniform clock rate prior of 4.05×10^{-8} substitutions/site/year. We computed 2 independent Markov chain Monte Carlo runs including 10 million generations, sampling every 1,000 generations, and discarding the first 10% of trees as burn-in. We inspected convergence and effective sample size values $\geq$200 using Tracer version 1.7.1 (https://beast.community/tracer) and generated the maximum clade credibility tree using TreeAnnotator version 2.5.1 (https://beast.community/treeannotator). We tested the association between phylogenetic clustering and geographic structure of *S. mansoni* isolates in BaTS (*40*) by implementing 1,000

null replicates, 5 discrete states, and an initial burn-in period of 10% (Appendix).

Ethical Considerations

We obtained informed written consent from all human participants or their legal guardians. All infected persons were treated with praziquantel 40 mg/kg either at school or at home. After explicit consent from local authorities and land owners, we targeted our small mammal trapping activities on animal populations classified as least concern by the International Union for the Conservation of Nature Red List. We recorded the trapping of nontarget animals (i.e., unidentified birds and anuran amphibians) and immediately released them at their point of capture. The examined animals were treated in accordance with published guidelines on animal welfare and the use of wildlife in research (*41*). All investigations were approved by the Comité National d'Ethique pour la Recherche en Santé of Senegal (reference no. SEN15/68), the Imperial College Research Ethics Committee of the United Kingdom (reference no. 03.36), and the Clinical Research Ethical Review Board of the Royal Veterinary College of the United Kingdom (reference nos. 2015-1327 and 2016-1505).

Results

A total of 1,618 traps were set over the course of 27 consecutive nights, and 195 *M. huberti* mice, 42 *A. niloticus* rats, and 14 *Crocidura* shrews were trapped and examined (Appendix Figure 2). We detected *Schistosoma* trematodes in 16 (8.2%) *M. huberti* mice (Appendix Table 3), specifically in the mesenteric vessels (in 81.2% of infected mice) and the portal system (in 68.7% of infected mice). On a local scale, 1.7%–52.6% of *M. huberti* mice were infected with *S. mansoni* (Table 1). In contrast, we did not observe *Schistosoma* infections in *A. niloticus* rats and *Crocidura* shews or at the dissection of the urogenital systems of any animals trapped during this study (Appendix Table 3). Miracidial hatching was successful for 8 of 16 infected *M. huberti* mice. No association was found between *Schistosoma* infection prevalence and *M. huberti* mice sex or age (Appendix). All adult schistosomes and miracidia from infected rodents were identified as *S. mansoni* on the basis of molecular analyses.

A total of 290 school-aged children were examined by duplicate Kato-Katz thick smears, and 37 (12.8%) had *S. mansoni* infections. We performed miracidial hatching on a randomly selected subset of *Schistosoma*–positive fecal samples and collected miracidia from samples from 4 infected persons. Molecular analysis confirmed the identification of *S. mansoni*. In contrast, none of the 40 adults examined by duplicate Kato-Katz thick smears had *S. mansoni* infections. On a local scale, 3.8%–44.8% of school-aged children were infected with *S. mansoni* (Table 1). A total of 407 *Biomphalaria pfeifferi* snails were observed for cercarial shedding and 9 (2.2%) had *S. mansoni* infections, which were identified by using molecular tools. On a local scale, 1.8%–7.1% of *B. pfeifferi* snails were infected with *S. mansoni* (Table 1).

The dataset including ITS, 12S rRNA, and the protein-coding mtDNA sequences (i.e., *cox1*, *cox3*, *nad4*, and *nad3*) of *S. mansoni* from school-aged children, rodents, and *B. pfeifferi* snails (Table 2) showed no intraspecific variability within the ITS alignment (914 bp), whereas variability was present within the 12S (760 bp, polymorphism ≤0.52%) and concatenated mtDNA (2,874 bp, polymorphism ≤0.77%) gene alignments. Intraspecific single-nucleotide

Table 1. *Schistosoma mansoni* infection rate and intensity by host and study site, Senegal, 2015–2018*

	Mastomys huberti mice		*Arvicanthis niloticus* rats		School-aged children		*Biomphalaria pfeifferi*, snails, no. infected/ total no. (%)
Study site	No. infected/ total no. (%)	Median (range) infection intensity	No. infected/ total no. (%)	Median (range) infection intensity	No. infected/ total no. (%)	Median (range) infection intensity	
Didjiery†	0/12	NA	0/69	NA	6/17 (35.3)	180 (12–408)	0/111
Ganket	2/4 (50.0)	18.5 (5–32)	0/4	NA	NA	NA	NA
Gueo	10/19 (52.6)	14 (2–64)	NA	NA	NA	NA	NA
Keur Momar Sarr	1/19 (5.3)	2	NA	NA	NA	NA	NA
Mbane†	0/60	NA	0/34	NA	1/26 (3.8)	264	1/55 (1.8)
Merina Guewel	1/12 (8.3)	2	NA	NA	6/16 (37.5)	42 (12–108)	NA
Nder†	1/60 (1.7)	2	0/11	NA	5/44 (11.4)	12 (12–24)	6/84 (7.1)
Ndombo	NA	NA	NA	NA	5/101 (5.0)	12 (12–24)	0/5
Richard Toll†	0/10	NA	1/73 (1.4)	4	13/29 (44.8)	180 (24–1,656)	0/4
Temeye†	8/43 (18.6)	4 (2–35)	0/4	NA	1/21 (8.3)	12	2/75 (2.7)
Thiago†	0/4	NA	NA	NA	NA	NA	0/2

*Only study sites where infected hosts were detected are included. Infection intensities were calculated by using eggs per gram of fecal samples for school-aged children and number of adult worms in rodents (*M. huberti* and *A. niloticus*). Infection intensity was not quantified for *B. pfeifferi* snails (intermediate host). NA, not applicable.
†For rodents, values include data previously reported (*21*).

Table 2. *Schistosoma* specimens from Senegal, Uganda, and Burundi, 2002–2018, included in phylogenetic analysis to determine if certain *S. mansoni* clades use multiple definitive hosts*

Source	Parasite	Stage†	No. isolates	Sampling locality	Isolation year	GenBank or ENA accession no.
Reference	*S. rodhaini*	Adult	1	Burundi	2002	SAMEA1979799
Definitive host						
Human	*S. mansoni*	Miracidium	4	Mayuge, Uganda	2014	SAMEA5366708, SAMEA5366733, SAMEA5366938, SAMEA5367037
	S. mansoni	Miracidium	1	Tororo, Uganda	2014	SAMEA5366700
	S. mansoni	Miracidium	1	Nder, Senegal	2017	MN593383–6
	S. mansoni	Miracidium	3	Temeye, Senegal	2017	MN593387–90
	S. mansoni	Miracidium	3	Didjiery, Senegal	2018	MN593375–82
Mastomys huberti mouse	*S. mansoni*	Adult	1	Nder, Senegal	2016	NA
	S. mansoni	Adult	10	Gueo, Senegal	2017	MN593427–34
	S. mansoni	Miracidium	1	Gueo, Senegal	2017	NA
	S. mansoni	Adult	2	Ganket, Senegal	2017	MN593419–22
	S. mansoni	Miracidium	2	Ganket, Senegal	2017	MN593411–4
	S. mansoni	Adult	2	Temeye, Senegal	2017	NA
	S. mansoni	Miracidium	4	Temeye, Senegal	2017	MN593415–8
	S. mansoni	Adult	2	Merina Guewel, Senegal	2017	MN593423–6
	S. mansoni	Miracidium	2	Merina Guewel, Senegal	2017	NA
Arvicanthis niloticus rat	*S. mansoni*	Adult	3	Richard Toll, Senegal	2016	MN593407–10
Intermediate host						
Biomphalaria pfeifferi snail	*S. mansoni*	Cercaria	1	Mbane, Senegal	2015	MN593391–4
	S. mansoni	Cercaria	4	Temeye, Senegal	2016	MN593395–402
	S. mansoni	Cercaria	2	Nder, Senegal	2016	MN593403–6

*ENA, European Nucleotide Archive; NA, not applicable.

polymorphisms within protein-coding mtDNA genes represented nonsynonymous amino acid substitutions in 4.4% (35/796) of codons, and saturation at model-corrected genetic distances was not detected (Appendix Figure 3). Maximum-likelihood and Bayesian inference analyses of the concatenated 12S and mtDNA gene sequences yielded consensus trees with congruent topologies, including different multihost *S. mansoni* lineages (Appendix Figure 4). The presence of multiple, well-supported *S. mansoni* clades within Senegal, 4 of which included samples collected from both humans and rodents, was confirmed by a phylogenetic analysis constructed by using a strict molecular clock (Figure, panel A; Appendix Figure 5). Different *S. mansoni* lineages prevalent in the Senegal River Basin diverged between 0.13 (95% highest posterior density interval [HPDI] 0.11–0.16) and 0.02 (95% HPDI 0.01–0.03) million years ago (MYA). Using uniform clock rate prior (4.05×10^{-8} substitutions/site/year), we determined that divergence between the sampled *S. mansoni* parasites from Uganda and Senegal occurred ≈0.19 (95% HPDI 0.15 0.23) MYA, whereas the speciation of *S. rodhaini* may have occurred ≈1.14 (95% HPDI 0.95 1.35) MYA. The association index, parsimony score, and monophyletic clade metrics of *S. mansoni* within Senegal were not significant in BaTS ($p>0.05$). These findings strongly support the null hypothesis of random phylogenetic trait associations and, therefore, that *S. mansoni* clades are not associated with the geographic structure on a local scale (Figure, panel B).

Discussion

In this study, we provide direct evidence of the zoonotic nature of *S. mansoni* in West Africa, revealing a potential ecologic cause for human reinfection after chemotherapeutic treatment. Our phylogenetic approach demonstrated that *S. mansoni* lineages responsible for intestinal schistosomiasis in humans also exploit rodent populations as reservoirs at transmission sites frequented by humans; prevalence could be as high as 52.6% in *M. huberti* mice at these sites. Therefore, we exclude the presence of an independent sylvatic life cycle and host specialization for *S. mansoni* in the Senegal River Basin. The phylogenetic similarity between parasite isolates collected from humans, rodents, and freshwater snails indicates that host use has not played a prominent role in the evolutionary pathway of *S. mansoni* in this region. Similar results were obtained during the analysis of specimens from different regions and hosts within the geographic distribution of *S. mansoni*, suggesting that murine isolates did not constitute monophyletic assemblages (*42*).

This lack of a geographic structure for *S. mansoni* on the local scale might be caused by disease foci of recent origin or the rapid dissemination of *S. mansoni* across the Senegal River Basin, which probably

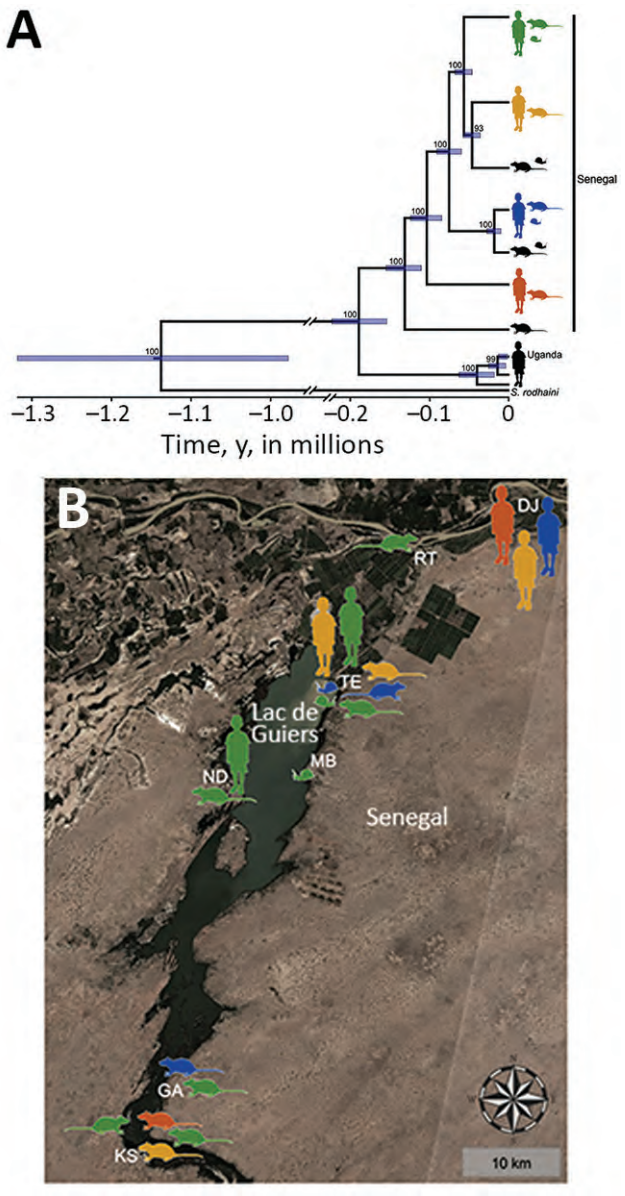

Figure. Phylogenetic analysis and geographic locations of *Schistosoma mansoni* lineages isolated from both humans and rodents (colored silhouettes) or from a single definitive host (black silhouettes), Senegal. Rodent silhouettes represent *Mastomys huberti* mice or *Arvicanthis niloticus* rats and snail silhouettes represent *Biomphalaria pfeifferi* snails (intermediate host). A) Bayesian tree made by using a strict molecular clock and the concatenated mitochondrial 12S rRNA and 4 protein-coding mitochondrial DNA gene sequences. *Schistosoma rodhaini* and *S. mansoni* samples from school-aged children in Uganda were included in the analysis. Posterior probabilities and 95% highest posterior density intervals (blue rectangles) are indicated for each node. Branches with nodal support ≤90% were collapsed. For complete tree, see Appendix Figure 5 (https://wwwnc.cdc.gov/EID/article/26/6/20-0107-App1.pdf). B) Geographic locations of multihost *S. mansoni* lineages, Richard Toll and Lac de Guiers regions. Satellite imagery from Sentinel Hub (Sinergise, https://www.sentinel-hub.com) was used as the base layer. DJ, Didjiery; GA, Ganket; KS, Keur Momar Sarr; MB, Mbane; ND, Nder; RT, Richard Toll; TE, Temeye.

occurred as a result of the land-use changes associated with the Diama Dam construction and transport infrastructure development (*14*–*16*). Furthermore, 3 decades of endemicity and the extensive movement of communities from within Senegal and other countries of West Africa could have substantially contributed to *S. mansoni* lineage diversification and gene flow in the Lac de Guiers region (*14*,*43*). The different *S. mansoni* clades detected herein might have diverged between 0.13 ± 0.03 MYA and 0.02 ± 0.01 MYA, firmly corroborating the hypothesis of their ramification from a common precursor during ancestral times. Multiple introduction events of various parasite populations could indicate that *M. huberti* mice and other rodent populations inhabiting periaquatic ecosystems act as competent alternative hosts for *S. mansoni* in many endemic areas across sub-Saharan Africa. The mainly nocturnal activity of *M. huberti* mice (vs. diurnal activity of *A. niloticus* rats) (*22*) may support the presence of different *S. mansoni* chronotypes characterized by differing circadian rhythms of cercarial emergence (*44*). Therefore, the risk for infection among local communities might not be limited to just the warmest hours of the day (diurnal transmission) but also extend to the early morning and late afternoon (crepuscular transmission). The high excretion rates of *S. mansoni* eggs by *M. huberti* mice during experimental infections (median intensity 720 eggs/g fecal sample) (*45*) and field observations (median intensity 262 eggs/g fecal sample) (*46*) are a warning about the potential contamination of freshwater bodies by parasitized rodents.

In our study, fully resolved spatial and temporal dynamics could not be determined. Future incorporation of *S. mansoni* sequences from multiple endemic regions across West Africa and Africa as a whole might help decipher the origin and radiation pattern of the various lineages observed in the Richard Toll and Lac de Guiers areas. Furthermore, the temporal estimates of *S. mansoni* evolution displayed herein should be interpreted with caution. The molecular clock calibration relied on previous estimates of the mutation rate and generation time calculated by using whole-genome *S. mansoni* data across its known geographic distribution (*6*). However, our reconstruction of the divergence between *S. rodhaini* and *S. mansoni* (1.14 ± 0.20 MYA) differs from previous dating (0.13 ± 0.02 MYA and 2.80 ± 0.19 MYA) (*6*,*42*). This conundrum highlights that further evidence is needed to characterize the evolutionary history within the genus *Schistosoma*. The application of a single calibration method in divergence dating remains subject to time-dependent bias

if not integrated by ancestral DNA, fossil records, or biogeographic events (*47*).

The zoonotic *S. japonicum* in Asia illustrates the pivotal role that animal reservoirs and multihost dynamics have as drivers of pathogen transmission and human reinfection, even after decades of multifaceted interventions (*4*,*5*). With the presence of multiple multihost *S. mansoni* lineages characterized by different divergence times circulating across the Senegal River Basin, our results support a similar scenario for *S. mansoni* in sub-Saharan Africa. Therefore, the parasite should be acknowledged as zoonotic, and public health campaigns must be planned considering the availability of alternative hosts (including wildlife, although *S. mansoni* prevalence in wildlife reservoirs can markedly vary) when transmission is maintained despite repeated interventions. The implementation of coprologic and DNA-based diagnostics within nonlethal sampling schemes can directly facilitate targeted surveillance where rodents might be contributing to the transmission of *S. mansoni*, other *Schistosoma* spp., and hybrids. However, the results of our study and previous surveys in endemic settings of Senegal (*21*) and Corsica, France (*48*), support the role of rodents as accidental (rather than maintenance) hosts of the *Schistosoma* hybrids responsible for urogenital schistosomiasis. Furthermore, although evidence suggests that rodents could be competent hosts of *Schistosoma bovis* (typically a schistosome of ruminants) across sub-Saharan Africa (*11*,*21*), we did not isolate any during this survey.

In conclusion, the multihost transmission dynamics of *S. mansoni* promote the recruitment of various definitive hosts spatially and temporally overlapping at transmission sites in the region of Lac de Guiers. In sub-Saharan Africa, the role of nonhuman vertebrates in the epidemiology of *Schistosoma* species and hybrids has yet to be fully determined, considering these could be spillover hosts incapable of maintaining transmission by themselves. However, our study supports that rodents have the potential to act as true reservoirs of *S. mansoni* and influence the evolution of this parasite (i.e., by providing opportunities for host switching and genetic exchange), which could thwart attempts to control or interrupt transmission of *S. mansoni* in human populations (*3*,*12*). Nevertheless, the presence of zoonotic pathogens in their animal reservoirs should not be considered synonymous with human disease risk, but rather a measure of underlying transmission potential, which is itself mediated by many additional intersecting ecologic and social drivers (*19*,*49*). The extent to which rodents contribute to the zoonotic transmission of *S. mansoni* and *Schistosoma* hybrids remains a question to be further developed by epidemiologic surveys, mathematical modelling, and genomics. As we move our efforts from disease control toward interruption of *S. mansoni* transmission and local elimination, the implication of alternative hosts in disease dynamics will be crucial and threaten to undermine future chemotherapeutic-focused interventions on local scales. Cross-disciplinary initiatives between the natural resource and public health sectors, including the long-term establishment of regional expertise, can be used to guide preventive measures not only for schistosomiasis but also for other rodentborne zoonoses across Africa and beyond.

Acknowledgments

We are extremely grateful for the contribution made by all the personnel who supported this study, in particular Alassane Ndiaye, Lucy Yasenev, Mapaté Gaye, and the Schistosomiasis Collection staff at the Natural History Museum (Aidan Emery, Fiona Allan, and Muriel Rabone). We thank Chiara Crestani and Kathryn Berger for their helpful advice during data analysis. Special thanks to Boubacar Bâ, Cheikh Thiam, and their families for enormously facilitating fieldwork and logistics. We are grateful to the communities involved in the study for their friendly participation and hospitality.

This work was funded by the Biotechnology and Biological Sciences Research Council, the Department for International Development, the Economic and Social Research Council, the Medical Research Council, the Natural Environment Research Council, and the Defense Science and Technology Laboratory under the Zoonoses and Emerging Livestock Systems program (BB/L018985/1 and BB/N503563/1).

About the Author

Dr. Catalano completed his doctoral studies in the Department of Pathobiology and Population Sciences, Royal Veterinary College, London, United Kingdom, during the publication of this research. His research interests focus on disease dynamics at the human–wildlife interface and biodiversity conservation initiatives.

References

1. World Health Organization. Schistosomiasis and soil-transmitted helminthiases: numbers of people treated in 2017. Wkly Epidemiol Rec. 2018;93:681–92. https://www.who.int/publications-detail/who-wer9350
2. World Health Organization. Ending the neglect to attain the sustainable development goals: a road map for neglected tropical diseases 2021–2030. 2020 Feb [cited 2020 Feb 24]. https://www.who.int/neglected_diseases/Ending-the-neglect-to-attain-the-SDGs--NTD-Roadmap.pdf?ua=1

3. Colley DG, Loker ES. New tools for old questions: how strictly human are "human schistosomes"—and does it matter? J Infect Dis. 2018;218:344–6. http://dx.doi.org/10.1093/infdis/jiy030
4. Rudge JW, Webster JP, Lu DB, Wang TP, Fang GR, Basáñez MG. Identifying host species driving transmission of schistosomiasis japonica, a multihost parasite system, in China. Proc Natl Acad Sci U S A. 2013;110:11457–62. http://dx.doi.org/10.1073/pnas.1221509110
5. Gordon CA, Kurscheid J, Williams GM, Clements ACA, Li Y, Zhou XN, et al. Asian schistosomiasis: current status and prospects for control leading to elimination. Trop Med Infect Dis. 2019;4:40. http://dx.doi.org/10.3390/tropicalmed4010040
6. Crellen T, Allan F, David S, Durrant C, Huckvale T, Holroyd N, et al. Whole genome resequencing of the human parasite *Schistosoma mansoni* reveals population history and effects of selection. Sci Rep. 2016;6:20954. http://dx.doi.org/10.1038/srep20954
7. Théron A, Sire C, Rognon A, Prugnolle F, Durand P. Molecular ecology of *Schistosoma mansoni* transmission inferred from the genetic composition of larval and adult infrapopulations within intermediate and definitive hosts. Parasitology. 2004;129:571–85. http://dx.doi.org/10.1017/S0031182004005943
8. Gentile R, Barreto MG, Gonçalves MM, Soares MS, D'Andrea PS. The role of wild rodents in the transmission of *Schistosoma mansoni* in Brazil. In: Rokni MB, editor. Schistosomiasis. London: IntechOpen Limited; 2012. p. 231–54. https://www.intechopen.com/books/schistosomiasis/the-role-of-wild-rodents-in-the-transmission-of-schistosoma-mansoni-in-brazil
9. Standley CJ, Dobson AP, Stothard JR. Out of animals and back again: schistosomiasis as a zoonosis in Africa. In: Rokni MB, editor. Schistosomiasis. London: IntechOpen Limited; 2012. p. 209–30. https://www.intechopen.com/books/schistosomiasis/out-of-animals-and-back-again-schistosomiasis-as-a-zoonosis-in-africa
10. Webster BL, Diaw OT, Seye MM, Webster JP, Rollinson D. Introgressive hybridization of *Schistosoma haematobium* group species in Senegal: species barrier break down between ruminant and human schistosomes. PLoS Negl Trop Dis. 2013;7:e2110. http://dx.doi.org/10.1371/journal.pntd.0002110
11. Hanelt B, Mwangi IN, Kinuthia JM, Maina GM, Agola LE, Mutuku MW, et al. Schistosomes of small mammals from the Lake Victoria Basin, Kenya: new species, familiar species, and implications for schistosomiasis control. Parasitology. 2010;137:1109–18. http://dx.doi.org/10.1017/S0031182010000041
12. Webster JP, Gower CM, Knowles SC, Molyneux DH, Fenton A. One Health–an ecological and evolutionary framework for tackling neglected zoonotic diseases. Evol Appl. 2016;9:313–33. http://dx.doi.org/10.1111/eva.12341
13. Léger E, Webster JP. Hybridizations within the genus *Schistosoma*: implications for evolution, epidemiology, and control. Parasitology. 2017;144:65–80. http://dx.doi.org/10.1017/S0031182016001190
14. Van den Broeck F, Maes GE, Larmuseau MH, Rollinson D, Sy I, Faye D, et al. Reconstructing colonization dynamics of the human parasite *Schistosoma mansoni* following anthropogenic environmental changes in northwest Senegal. PLoS Negl Trop Dis. 2015;9:e0003998. http://dx.doi.org/10.1371/journal.pntd.0003998
15. Jones I, Lund A, Riveau G, Jouanard N, Ndione RA, Sokolow SH, et al. Ecological control of schistosomiasis in Sub-Saharan Africa: restoration of predator-prey dynamics to reduce transmission. In: Roche B, Broutin H, Simard F, editors. Ecology and evolution of infectious disease: pathogen control and public health management in low-income countries. Oxford: Oxford University Press; 2018. p. 236–51.
16. Uhlir PF. Scientific data for decision making toward sustainable development: Senegal River Basin case study. Washington: The National Academies Press; 2002.
17. Knowles SCL, Webster BL, Garba A, Sacko M, Diaw OT, Fenwick A, et al. Epidemiological interactions between urogenital and intestinal human schistosomiasis in the context of praziquantel treatment across three West African countries. PLoS Negl Trop Dis. 2015;9:e0004019. http://dx.doi.org/10.1371/journal.pntd.0004019
18. Boon NAM, Van Den Broeck F, Faye D, Volckaert FAM, Mboup S, Polman K, et al. Barcoding hybrids: heterogeneous distribution of *Schistosoma haematobium* × *Schistosoma bovis* hybrids across the Senegal River Basin. Parasitology. 2018; 145:634–45. http://dx.doi.org/10.1017/S0031182018000525
19. Lund AJ, Sam MM, Sy AB, Sow OW, Ali S, Sokolow SH, et al. Unavoidable risks: local perspectives on water contact behavior and implications for schistosomiasis control in an agricultural region of northern Senegal. Am J Trop Med Hyg. 2019;101:837–47. http://dx.doi.org/10.4269/ajtmh.19-0099
20. Duplantier JM, Sène M. Rodents as reservoir hosts in the transmission of *Schistosoma mansoni* in Richard-Toll, Senegal, West Africa. J Helminthol. 2000;74:129–35. http://dx.doi.org/10.1017/S0022149X00000172
21. Catalano S, Sène M, Diouf ND, Fall CB, Borlase A, Léger E, et al. Rodents as natural hosts of zoonotic *Schistosoma* species and hybrids: an epidemiological and evolutionary perspective from West Africa. J Infect Dis. 2018;218:429–33. http://dx.doi.org/10.1093/infdis/jiy029
22. Granjon L, Duplantier JM. Les rongeurs de l'Afrique Sahélo-Soudanienne. Marseille (France): Muséum National d'Histoire Naturelle; 2009.
23. Whisson DA, Engeman RM, Collins K. Developing relative abundance techniques (RATs) for monitoring rodent populations. Wildl Res. 2005;32:239–44. http://dx.doi.org/10.1071/WR03128
24. Gower CM, Shrivastava J, Lamberton PHL, Rollinson D, Webster BL, Emery A, et al. Development and application of an ethically and epidemiologically advantageous assay for the multi-locus microsatellite analysis of *Schistosoma mansoni*. Parasitology. 2007;134:523–36. http://dx.doi.org/10.1017/S0031182006001685
25. Yu JM, de Vlas SJ, Jiang QW, Gryseels B. Comparison of the Kato-Katz technique, hatching test and indirect hemagglutination assay (IHA) for the diagnosis of *Schistosoma japonicum* infection in China. Parasitol Int. 2007;56:45–9. http://dx.doi.org/10.1016/j.parint.2006.11.002
26. Emery AM, Allan FE, Rabone ME, Rollinson D. Schistosomiasis collection at NHM (SCAN). Parasit Vectors. 2012;5:185. http://dx.doi.org/10.1186/1756-3305-5-185
27. Katz N, Chaves A, Pellegrino J. A simple device for quantitative stool thick-smear technique in *Schistosomiasis mansoni*. Rev Inst Med Trop Sao Paulo. 1972;14:397–400.
28. Allan F, Dunn AM, Emery AM, Stothard JR, Johnston DA, Kane RA, et al. Use of sentinel snails for the detection of *Schistosoma haematobium* transmission on Zanzibar and observations on transmission patterns. Acta Trop. 2013;128:234–40. http://dx.doi.org/10.1016/j.actatropica.2013.01.003
29. Frandsen F, Christensen NO. An introductory guide to the identification of cercariae from African freshwater snails

with special reference to cercariae of trematode species of medical and veterinary importance. Acta Trop. 1984; 41:181–202.
30. Webster BL, Rabone M, Pennance T, Emery AM, Allan F, Gouvras A, et al. Development of novel multiplex microsatellite polymerase chain reactions to enable high-throughput population genetic studies of *Schistosoma haematobium*. Parasit Vectors. 2015;8:432. http://dx.doi.org/10.1186/s13071-015-1044-6
31. Zarowiecki MZ, Huyse T, Littlewood DTJ. Making the most of mitochondrial genomes–markers for phylogeny, molecular ecology and barcodes in *Schistosoma* (Platyhelminthes: Digenea). Int J Parasitol. 2007;37:1401–18. http://dx.doi.org/10.1016/j.ijpara.2007.04.014
32. Katoh K, Rozewicki J, Yamada KD. MAFFT online service: multiple sequence alignment, interactive sequence choice and visualization. Brief Bioinform. 2019;20:1160–6. http://dx.doi.org/10.1093/bib/bbx108
33. Ranwez V, Harispe S, Delsuc F, Douzery EJ. MACSE: Multiple Alignment of Coding SEquences accounting for frameshifts and stop codons. PLoS One. 2011;6:e22594. http://dx.doi.org/10.1371/journal.pone.0022594
34. Crellen T, Walker M, Lamberton PHL, Kabatereine NB, Tukahebwa EM, Cotton JA, et al. Reduced efficacy of praziquantel against *Schistosoma mansoni* is associated with multiple rounds of mass drug administration. Clin Infect Dis. 2016;63:1151–9.
35. Protasio AV, Tsai IJ, Babbage A, Nichol S, Hunt M, Aslett MA, et al. A systematically improved high quality genome and transcriptome of the human blood fluke *Schistosoma mansoni*. PLoS Negl Trop Dis. 2012;6:e1455. http://dx.doi.org/10.1371/journal.pntd.0001455
36. McKenna A, Hanna M, Banks E, Sivachenko A, Cibulskis K, Kernytsky A, et al. The Genome Analysis Toolkit: a MapReduce framework for analyzing next-generation DNA sequencing data. Genome Res. 2010;20:1297–303. http://dx.doi.org/10.1101/gr.107524.110
37. Stamatakis A. RAxML version 8: a tool for phylogenetic analysis and post-analysis of large phylogenies. Bioinformatics. 2014;30:1312–3. http://dx.doi.org/10.1093/bioinformatics/btu033
38. Ronquist F, Teslenko M, van der Mark P, Ayres DL, Darling A, Höhna S, et al. MrBayes 3.2: efficient Bayesian phylogenetic inference and model choice across a large model space. Syst Biol. 2012;61:539–42. http://dx.doi.org/10.1093/sysbio/sys029
39. Bouckaert R, Vaughan TG, Barido-Sottani J, Duchêne S, Fourment M, Gavryushkina A, et al. BEAST 2.5: an advanced software platform for Bayesian evolutionary analysis. PLOS Comput Biol. 2019;15:e1006650. http://dx.doi.org/10.1371/journal.pcbi.1006650
40. Parker J, Rambaut A, Pybus OG. Correlating viral phenotypes with phylogeny: accounting for phylogenetic uncertainty. Infect Genet Evol. 2008;8:239–46. http://dx.doi.org/10.1016/j.meegid.2007.08.001
41. Sikes RS; Animal Care and Use Committee of the American Society of Mammalogists. 2016 guidelines of the American Society of Mammalogists for the use of wild mammals in research and education. J Mammal. 2016;97:663–88. http://dx.doi.org/10.1093/jmammal/gyw078
42. Morgan JA, Dejong RJ, Adeoye GO, Ansa ED, Barbosa CS, Brémond P, et al. Origin and diversification of the human parasite *Schistosoma mansoni*. Mol Ecol. 2005;14:3889–902. http://dx.doi.org/10.1111/j.1365-294X.2005.02709.x
43. Campbell G, Noble LR, Rollinson D, Southgate VR, Webster JP, Jones CS. Low genetic diversity in a snail intermediate host (*Biomphalaria pfeifferi* Krass, 1848) and schistosomiasis transmission in the Senegal River Basin. Mol Ecol. 2010;19:241–56. http://dx.doi.org/10.1111/j.1365-294X.2009.04463.x
44. Théron A. Chronobiology of trematode cercarial emergence: from data recovery to epidemiological, ecological and evolutionary implications. Adv Parasitol. 2015;88:123–64. http://dx.doi.org/10.1016/bs.apar.2015.02.003
45. Sène M, Duplantier JM, Marchand B, Hervé JP. Susceptibility of rodents to infection with *Schistosoma mansoni* in Richard-Toll (Senegal). Parasite. 1996;3:321–6. http://dx.doi.org/10.1051/parasite/1996034321
46. Catalano S, Symeou A, Marsh KJ, Borlase A, Léger E, Fall CB, et al. Mini-FLOTAC as an alternative, non-invasive diagnostic tool for *Schistosoma mansoni* and other trematode infections in wildlife reservoirs. Parasit Vectors. 2019;12:439. http://dx.doi.org/10.1186/s13071-019-3613-6
47. Hipsley CA, Müller J. Beyond fossil calibrations: realities of molecular clock practices in evolutionary biology. Front Genet. 2014;5:138. http://dx.doi.org/10.3389/fgene.2014.00138
48. Oleaga A, Rey O, Polack B, Grech-Angelini S, Quilichini Y, Pérez-Sánchez R, et al. Epidemiological surveillance of schistosomiasis outbreak in Corsica (France): are animal reservoir hosts implicated in local transmission? PLoS Negl Trop Dis. 2019;13:e0007543. http://dx.doi.org/10.1371/journal.pntd.0007543
49. Suzán G, García-Peña GE, Castro-Arellano I, Rico O, Rubio AV, Tolsá MJ, et al. Metacommunity and phylogenetic structure determine wildlife and zoonotic infectious disease patterns in time and space. Ecol Evol. 2015;5:865–73. http://dx.doi.org/10.1002/ece3.1404

Address for correspondence: Elsa Léger, Department of Pathobiology and Population Sciences, Royal Veterinary College, University of London, Hatfield AL9 7TA, UK; email: eleger@rvc.ac.uk

Statin Use and Influenza Vaccine Effectiveness in Persons ≥65 Years of Age, Taiwan

Lung-Wen Tsai,[1] Yung-Tai Chen,[1] Chia-Jen Shih, Shuo-Ming Ou, Pei-Wen Chao, Shih-Hsiu Lo

Medscape EDUCATION ACTIVITY

In support of improving patient care, this activity has been planned and implemented by Medscape, LLC and Emerging Infectious Diseases. Medscape, LLC is jointly accredited by the Accreditation Council for Continuing Medical Education (ACCME), the Accreditation Council for Pharmacy Education (ACPE), and the American Nurses Credentialing Center (ANCC), to provide continuing education for the healthcare team.

Medscape, LLC designates this Journal-based CME activity for a maximum of 1.00 ***AMA PRA Category 1 Credit(s)™***. Physicians should claim only the credit commensurate with the extent of their participation in the activity.

Successful completion of this CME activity, which includes participation in the evaluation component, enables the participant to earn up to 1.0 MOC points in the American Board of Internal Medicine's (ABIM) Maintenance of Certification (MOC) program. Participants will earn MOC points equivalent to the amount of CME credits claimed for the activity. It is the CME activity provider's responsibility to submit participant completion information to ACCME for the purpose of granting ABIM MOC credit.

All other clinicians completing this activity will be issued a certificate of participation. To participate in this journal CME activity: (1) review the learning objectives and author disclosures; (2) study the education content; (3) take the post-test with a 75% minimum passing score and complete the evaluation at http://www.medscape.org/journal/eid; and (4) view/print certificate. For CME questions, see page 1353.

Release date: May 15, 2020; Expiration date: May 15, 2021

Learning Objectives

Upon completion of this activity, participants will be able to:

- Evaluate the risks for poor outcomes in elderly patients (aged >65 years) who received influenza vaccinations with those in propensity score-matched elderly control individuals who did not receive influenza vaccinations, based on a large-scale, nationwide, Taiwanese population-based cohort study
- Compare vaccine effectiveness between elderly statin users and nonusers, based on a large-scale, nationwide, Taiwanese population-based cohort study
- Assess the clinical implications of comparative risks for poor outcomes in elderly patients who did or did not receive influenza vaccinations and those of comparative vaccine effectiveness between statin users and nonusers, based on a large-scale, nationwide, Taiwanese population-based cohort study

CME Editor

Amy J. Guinn, BA, MA, Copyeditor, Emerging Infectious Diseases. *Disclosure: Amy J. Guinn, BA, MA, has disclosed no relevant financial relationships.*

CME Author

Laurie Barclay, MD, freelance writer and reviewer, Medscape, LLC. *Disclosure: Laurie Barclay, MD, has disclosed no relevant financial relationships.*

Authors

Disclosures: ***Lung-Wen Tsai, PhD; Yung-Tai Chen, MD; Chia-Jen Shih, MD; Shuo-Ming Ou, MD; Pei-Wen Chao, MD;*** *and* ***Shih-Hsiu Lo, MD,*** *have disclosed no relevant financial relationships.*

Author affiliations: Taipei Medical University Hospital, Taipei, Taiwan (L.-W. Tsai, P.-W. Chao, S.-H. Lo); Taipei City Hospital, Taipei (Y.-T. Chen); University of Taipei, Taipei (Y.-T, Chen); National Yang-Ming University, Taipei (Y.-T. Chen, C.-J. Shih, S.-M. Ou); Taipei Veterans General Hospital, Taipei (S.-M. Ou)

DOI: https://doi.org/10.3201/eid2606.190646

[1]These authors contributed equally to this study.

Debates on whether statin use reduces the effectiveness of influenza vaccines against critical illness and death among persons ≥65 years of age continue. We conducted a study of 9,427,392 persons ≥65 years of age who did and did not receive influenza vaccinations during 12 consecutive influenza seasons, 2000–01 through 2011–12. Using data from Taiwan's National Health Insurance Research Database, we performed propensity score-matching to compare vaccinated persons with unvaccinated controls. After propensity score-matching, the vaccinated group had lower risks for in-hospital death from influenza and pneumonia and for hospitalization for pneumonia and influenza, circulatory conditions, and critical illnesses compared with the unvaccinated group. We stratified the 2 groups by statin use and analyzed data by interaction analysis and saw no statistically significant difference. We found that influenza vaccine effectively reduced risks for hospitalization and death in persons ≥65 years of age, regardless of statin use.

Epidemics of influenza occur nearly every winter and last through spring, causing an average of 226,054 influenza-related hospital admissions and 51,203 influenza-related deaths in the United States annually (*1*–*3*). Persons ≥65 years of age are at greater risk for serious complications of influenza and ≈90% of deaths due to influenza and pneumonia occur among this age group (*1*,*4*). Taiwan, like other high-income countries, recognizes the importance of influenza vaccination and strongly recommends annual vaccination to prevent complications of influenza and reduce hospitalization rates and death in older persons (*5*,*6*).

Persons ≥65 years of age also are at greater risk for coronary atherosclerosis and cardiovascular disease. Statin treatment in this population is crucial, but benefits and risks should guide its use (*7*,*8*). In addition to cholesterol-lowering effects that provide cardiovascular benefits, statins have been shown to suppress T-cell activation and exhibit antiinflammatory and immunomodulatory properties (*9*–*12*). Few studies have investigated the effect of statins on vaccine effectiveness, but concerns have been raised that statins might interfere with the immune response to influenza vaccines and seem to reduce their effectiveness (*13*,*14*). A study of 6,961 trial participants >65 years of age from Colombia, Panama, the Philippines, and the United States showed that hemagglutination-inhibiting geometric mean titers to influenza strains were much lower in chronic statin users compared with nonusers (*13*). Another large-scale retrospective cohort study based on a research database covering influenza seasons for 2002–2011 in the United States revealed reduced influenza vaccine effectiveness against respiratory illness in statin users (*14*). By contrast, data from another retrospective 5-year cohort study of 1,403,651 statin users matched to nonusers found that use of statins around the time of influenza vaccination does not dramatically affect the risk for influenza-related visits and influenza-related hospitalizations in older adults (*15*). Another large-scale nationwide population study evaluated whether statin therapy reduced vaccination effectiveness in terms of influenza-associated critical illness hospitalizations and death and suggested high-dose influenza vaccines or vaccines containing adjuvants to boost the immune response might be needed in older populations (*16*). However, previous studies did not match cases and controls for characteristics, underlying health conditions, or concomitant drug use and did not focus on the outcomes of influenza-related critical illness and death.

We designed a large-scale, nationwide, population-based cohort study to explore heterogeneity of influenza vaccine effectiveness between statin users and nonusers among persons ≥65 years of age in Taiwan. We assessed risks for hospitalization for pneumonia and influenza, circulatory conditions, or critical illness and for in-hospital death and in-hospital death from pneumonia in this age group. We compared the vaccinated group with propensity score-matched control subjects who did not receive influenza vaccinations.

Methods

Data Source

We used the data from Taiwan's National Health Insurance Research Database (NHIRD), which has been described in detail elsewhere (*17*–*19*). We extracted medical data for persons ≥65 years of age in Taiwan from an NHIRD dataset based on a regulation that prohibits use of the maximal amount of claims data and permits use of data from only one third of older beneficiaries for research purposes. Our dataset included information on all inpatient, emergency department, and outpatient visits; diagnosed illnesses and conditions; prescriptions; and procedures for one third of all persons ≥65 years of age in Taiwan. We used diagnostic and procedural codes from the International Classification of Diseases, 9th Revision, Clinical Modification (ICD-9-CM; https://www.cdc.gov/nchs/icd/icd9cm.htm) to ascertain details associated with inpatient and outpatient encounters. Because patient information in the NHIRD is secondary, deidentified, and encrypted, this study was exempted from a full ethics review by the institutional review

board of Taipei Medical University Hospital (IRB no. 105TMUH-SP-07).

Study Population

The study period encompassed 12 consecutive influenza seasons from 2000–01 through 2011–12 (*14*). The study sample was comprised of persons ≥65 years of age who resided in Taiwan during 2000–2012. Persons ≥65 years of age in Taiwan are encouraged to receive influenza vaccines, which are covered by insurance, between October 1 and December 31 each year. For our study, we defined the index date as the date of influenza vaccination for the vaccinated group. To avoid immortal time bias, for the unvaccinated group we randomly assigned index dates that corresponded to those in the vaccinated group. Because the same persons could be part of the unvaccinated group initially and later change to the vaccinated group during the influenza period each year, we did not include the unvaccinated period in our outcome analyses. In each year, we traced participants' NHIRD records from January 1 through September 30 or death.

Statin Exposure

For each year in the study period, we identified all drug prescriptions written for participants before the index date by using inpatient and ambulatory care order files. For statin users, we identified persons who had initial dispensing date of statin on or before the index date. We defined chronic statin users as those who received and filled a prescription for a statin medication for ≥30 days (*20*,*21*).

Outcomes

The outcomes of interest were in-hospital death and in-hospital death from pneumonia. Our analyses also included severe complications of influenza infections, including hospitalization for pneumonia, circulatory condition, and critical illness. We defined critical illness as hospitalization for acute respiratory failure (ICD-9-CM codes 518.5, 518.81, 518.82, or 96.7) or severe sepsis (ICD-9-CM codes 995.92 or 785.52) or organ dysfunction (*22*).

Statistical Analyses

We examined the differences of baseline characteristics between the vaccinated group and unvaccinated group by using standardized mean differences. For each participant, we calculated a propensity score for the likelihood of receiving influenza vaccination by using baseline covariates in a multivariate logistic regression model (Appendix Table 1, https://wwwnc.cdc.gov/EID/article/26/6/19-0646-App1.pdf). For each person in the vaccinated group, we identified 1 person in the unvaccinated group that was frequency-matched according to propensity score (*23*). We used Cox regression with adjusted imbalance covariates to calculate hazard ratios (HRs) for in-hospital death; in-hospital death from pneumonia; and hospitalization for pneumonia, circulatory conditions, and critical illness. We conducted a subgroup analyses and used a likelihood ratio test to explore heterogeneity of vaccine effectiveness between statin users and nonusers. We used SQL Server 2012 (Microsoft, https://www.microsoft.com) for data linkage, processing, and sampling. We performed all analyses by using 2-sided tests in Stata version 12.0 (StataCorp, https://www.stata.com) and considered $p<0.05$ statistically significant.

Results

Our study included 3,417,212 persons who received influenza vaccination and 6,010,180 who were not vaccinated during 12 consecutive influenza seasons. We matched demographic characteristics and baseline underlying conditions before and after propensity score matching (Table 1). Before propensity score matching, the vaccinated group was older (74.3 years of age) than the unvaccinated group (73.6 years of age) and had higher Charlson Comorbidity Index scores (7.7 ± 2.8) than the unvaccinated group (7.2 ± 2.8). The vaccinated group had higher rates of diabetes mellitus (40.3% vs. 33.3%) and coronary artery disease (48.9% vs. 38.9%) than the unvaccinated group. In addition, the vaccinated group had higher proportions of use of antiplatelet agents (16.4%) than the unvaccinated group (12.2%), and more used oral medications for diabetes (11.7%) than those in the unvaccinated group (9.2%). A total of 167,188 (4.9%) persons in the vaccinated group and 249,822 (4.2%) persons in the unvaccinated group were statin users.

Incidence rates of hospitalization for pneumonia and influenza increased over time. In 2000, the incidence rate was 26.71/1,000 person-years. By 2012, the incidence rate was 41.08/1,000 person-years (Table 2). During 2000–2012, hospitalization for pneumonia and influenza occurred on an average of 23,595 events per year (14,272–33,428 events/year).

Compared with the unvaccinated group, the vaccinated group had lower risks of in-hospital death (adjusted hazard ratio [aHR] 0.69, 95% CI 0.68–0.69), in-hospital death from pneumonia (aHR 0.72, 95% CI 0.70–0.73), hospitalization for pneumonia and influenza (aHR 0.84, 95% CI 0.84–0.85), hospitalization for circulatory conditions (aHR 0.90, 95% CI 0.90–0.90), and

hospitalization for critical illnesses (aHR 0.75, 95% CI 0.74–0.76) (Table 3). For subgroup analyses stratified by statin use, the effects of vaccination on in-hospital death ($P_{interaction}$ = 0.478), in-hospital death from pneumonia ($P_{interaction}$ = 0.493), hospitalization for pneumonia and influenza ($P_{interaction}$ = 0.138), hospitalization for circulatory condition ($P_{interaction}$ = 0.667), and hospitalization for critical illness ($P_{interaction}$ = 0.375) were consistent among statin users and nonusers. We also analyzed these data by using the Cox regression model, adjusted for propensity score only, and noted similar results (Appendix Table 2).

Table 1. Characteristics of persons ≥65 who received influenza vaccine versus those who did not receive influenza vaccine, Taiwan*

	Before propensity score-matching			Propensity score-matched		
Characteristics	Vaccinated	Unvaccinated	Standardized difference	Vaccinated	Unvaccinated	Standardized difference
No. patients	3,417,212	6,010,180		3,165,272	3,165,272	
Mean age, y (SD)	74.3 (6.4)	73.6 (6.8)	0.100	74.2 (6.4)	74.2 (6.9)	–0.002
Sex						
M	1,707,483 (50.0)	2,908,606 (48.4)	0.031	1,559,852 (49.3)	1,550,848 (49.0)	0.006
F	1,709,729 (50.0)	3,101,574 (51.6)		1,605,420 (50.7)	1,614,424 (51.0)	
Monthly income, $ Taiwan						
Dependent†	1,234,769 (36.1)	2,527,696 (42.1)	–0.122	1,190,930 (37.6)	1,197,102 (37.8)	–0.004
<19,100	794,513 (23.3)	1,365,600 (22.7)	0.013	728,908 (23.0)	721,281 (22.8)	0.006
19,100–41,999	1,367,022 (40.0)	2,054,058 (34.2)	0.121	1,224,632 (38.7)	1,226,438 (38.7)	–0.001
≥42,000	20,908 (0.6)	62,826 (1.0)	–0.048	20,802 (0.7)	20,451 (0.6)	0.001
Urbanization‡						
Level 1	988,136 (28.9)	1,833,258 (30.5)	–0.035	926,242 (29.3)	925,049 (29.2)	0.001
Level 2	2,194,465 (64.2)	3,793,218 (63.1)	0.023	2,025,556 (64.0)	2,025,109 (64.0)	0.000
Level 3	199,301 (5.8)	320,751 (5.3)	0.022	180,635 (5.7)	181,562 (5.7)	–0.001
Level 4	35,310 (1.0)	62,953 (1.0)	–0.001	32,839 (1.0)	33,552 (1.1)	–0.002
No. outpatient visits in the previous 12 mo						
0–10	504,028 (14.7)	1,831,616 (30.5)	–0.383	504,014 (15.9)	500,316 (15.8)	0.003
11–20	869,805 (25.5)	1,598,542 (26.6)	–0.026	851,438 (26.9)	854,335 (27.0)	–0.002
21–30	776,389 (22.7)	1,106,821 (18.4)	0.107	719,783 (22.7)	721,771 (22.8)	–0.001
31–40	522,170 (15.3)	651,142 (10.8)	0.132	462,035 (14.6)	462,408 (14.6)	0.000
>40	744,820 (21.8)	822,059 (13.7)	0.214	628,002 (19.8)	626,442 (19.8)	0.001
CCI score (SD)§	7.7 (2.8)	7.2 (2.8)	0.236	7.8 (2.8)	7.8 (2.9)	–0.006
Underlying conditions						
Cerebrovascular disease	1,151,954 (33.7)	1,703,465 (28.3)	0.116	1,047,165 (33.1)	1,052,107 (33.2)	–0.003
Diabetes	1,377,596 (40.3)	2,000,525 (33.3)	0.146	1,246,943 (39.4)	1,252,696 (39.6)	–0.004
Hypertension	2,568,836 (75.2)	3,931,874 (65.4)	0.215	2,344,103 (74.1)	2,351,157 (74.3)	–0.005
CAD	1,672,350 (48.9)	2,340,127 (38.9)	0.203	1,520,516 (48.0)	1,447,015 (45.7)	0.047
Myocardial infarction	158,688 (4.6)	228,094 (3.8)	0.042	143,777 (4.5)	144,573 (4.6)	–0.001
PVD	238,514 (7.0)	324,691 (5.4)	0.065	217,314 (6.9)	210,393 (6.6)	0.009
Heart failure	555,349 (16.3)	792,171 (13.2)	0.087	503,135 (15.9)	506,674 (16.0)	–0.003
Dyslipidemia	1,557,151 (45.6)	2,231,936 (37.1)	0.172	1,436,998 (45.4)	1,340,441 (42.3)	0.062
Chronic liver disease	1,067,001 (31.2)	1,460,809 (24.3)	0.155	950,911 (30.0)	951,575 (30.1)	0.000
CKD	664,324 (19.4)	917,408 (15.3)	0.110	596,302 (18.8)	597,911 (18.9)	–0.001
Peptic ulcer disease	1,904,442 (55.7)	2,764,223 (46.0)	0.196	1,720,590 (54.4)	1,723,618 (54.5)	–0.002
Dementia	249,766 (7.3)	370,758 (6.2)	0.045	228,856 (7.2)	231,226 (7.3)	–0.003
Valvular heart disease	424,657 (12.4)	596,580 (9.9)	0.079	383,055 (12.1)	384,592 (12.2)	–0.001
Drug abuse	48,591 (1.4)	74,326 (1.2)	0.016	45,499 (1.4)	45,816 (1.4)	–0.001
Atrial fibrillation	160,148 (4.7)	235,626 (3.9)	0.038	146,674 (4.6)	147,989 (4.7)	–0.002
Medications						
Antiplatelet agents	559,272 (16.4)	735,104 (12.2)	0.118	491,897 (15.5)	493,185 (15.6)	–0.001
Insulin	42,022 (1.2)	58,973 (1.0)	0.024	38,581 (1.2)	38,823 (1.2)	–0.001
Oral diabetic drugs	399,409 (11.7)	552,935 (9.2)	0.081	358,531 (11.3)	361,189 (11.4)	–0.003
Diuretics	301,500 (8.8)	420,868 (7.0)	0.067	270,816 (8.6)	272,637 (8.6)	–0.002
Calcium channel blockers	651,895 (19.1)	892,880 (14.9)	0.113	580,984 (18.4)	583,106 (18.4)	–0.002
Beta-blockers	413,542 (12.1)	583,937 (9.7)	0.077	371,599 (11.7)	372,374 (11.8)	–0.001
ACEI/ARB	508,701 (14.9)	719,943 (12.0)	0.085	459,520 (14.5)	461,934 (14.6)	–0.002
Statins	167,188 (4.9)	249,822 (4.2)	0.035	155,133 (4.9)	155,624 (4.9)	–0.001
Propensity score	0.42 (0.13)	0.33 (0.14)	0.662	0.406 (0.129)	0.406 (0.129)	0.000

*Values are no. (%) except as indicated. ACEI, angiotensin-converting enzyme inhibitor; ARB, angiotensin II receptor blocker; CAD, coronary artery disease; CCI, Charlson Comorbidity Index; CKD, chronic kidney disease; PVD, peripheral vascular disease.
†Dependent persons are those without an income.
‡Urbanization levels in Taiwan are divided into 4 strata according to the Taiwan National Health Research Institute publications. Level 1 designates the most urbanized areas, and level 4 designates the least urbanized areas.
§CCI score is used to determine overall systemic health. Increased CCI scores are indicative of stepwise increases in the cumulative mortality.

Table 2. Incidence of hospitalization for pneumonia and influenza in persons ≥65 years of age during 2000–2012, Taiwan

Year	No. events	Person-years	Incidence/1,000 person-years
2000	14,272	534,348	26.71
2001	17,342	596,594	29.07
2002	17,383	615,868	28.23
2003	19,298	610,215	31.62
2004	21,807	640,872	34.03
2005	19,909	662,198	30.07
2006	22,394	664,194	33.72
2007	24,148	699,617	34.52
2008	25,829	713,500	36.20
2009	28,226	730,645	38.63
2010	31,945	733,967	43.52
2011	33,428	746,025	44.81
2012	30,760	748,838	41.08

Discussion

In this nationwide population-based study in Taiwan, we investigated the effects of statin therapy on the risks for in-hospital death and severe complications of influenza infections in 9,427,392 persons ≥65 years of age during influenza seasons from 2000–01 through 2011–12. We found that vaccinated groups had lower risks than unvaccinated groups for in-hospital death; in-hospital death from pneumonia; and hospitalization for pneumonia and influenza, circulatory conditions, and critical illness. In the subgroup analysis stratified by statin use, the observed outcome differences across stain users and nonusers were consistent with chance.

Statins might exert antiinflammatory effects by inhibiting the major histocompatibility complex class II pathway of antigen presentation (*24*), preventing accumulation and recruitment of monocytes (*25*), reducing cytokine production by immune cells (*26*,*27*), and impairing the activation of T cells (*9*,*28*). Previous studies that directly address statin use and vaccine effectiveness have had conflicting results. A randomized clinical study of 150 healthy persons failed to find any difference in antibody responses to hepatitis A vaccine among those receiving atorvastatin and those receiving a placebo (*29*); that study was limited because only statin therapy initiated on the day of randomization, not prior chronic statin therapy, was considered. In contrast, another study of 105,874 vaccinated persons (39,342 statin users and 66,532 nonusers) and 141,714 unvaccinated persons (52,685 statin users and 89,029 nonusers) revealed reduced influenza vaccine effectiveness against acute respiratory illness among statin users compared with nonusers during influenza seasons (*14*). However, that study was limited by healthy-user bias (*30*,*31*) and did not match characteristics in controls.

Other large-scale studies have revealed suboptimal influenza vaccine effectiveness in persons ≥65 years of age because of age-related decline in the immune response, multiple underlying conditions, and concomitant medication use with possible secondary interactions (*32*,*33*). To address the potential negative effects of concomitant statin therapy on vaccine effectiveness, a prior post hoc analysis showed that influenza antibody titers were much lower in those receiving chronic statin therapy compared with those not receiving statin therapy (*13*). However, the association between antibody titers and adverse clinical outcomes was not characterized further, raising concern about the actual clinical implications. Another population-based retrospective cohort study of 1,403,651 Medicare beneficiaries ≥65 years of age in the United States matched statin users to nonusers and found that statin use does not dramatically affect the risk for influenza-related visits and influenza-related hospitalizations in this population (*15*). However, the study did not determine whether chronic statin use had any implication for major adverse cardiovascular events or death.

We found that, among persons ≥65 years of age, vaccinated statin users and nonusers had lower risks of in-hospital death and severe complications of influenza infections compared with unvaccinated groups. In further analyses, we found no statistically significant difference and interaction between statin use and hospitalization for pneumonia, influenza, or circulatory conditions. However, vaccine effectiveness against critical illness slightly increased in statin users compared with nonusers, suggesting that the context of benefits of statins for cardiovascular outcomes could play a role for critically ill patients (*34*).

The strengths of our study include the use of a large nationwide population-based dataset, encompassing data from 9,427,392 patients ≥65 years of age. Our study covered 12 influenza seasons, from 2000–01 through 2011–12, aiding comparison of the effects of statins on the risks for death and hospital admission for major pulmonary and circulatory events in older vaccinated and unvaccinated persons.

Our study has some limitations. First, relevant details enabling characterization of the geographic spread of influenza activity as sporadic, local, regional, or widespread, and information on influenza virus subtypes were not available in the NHIRD dataset. Therefore, we could not identify the effects of statin therapy on the spread of influenza. Second, we used data on persons registered in the national health insurance program, which included information on adverse clinical outcomes caused by local and widespread influenza, but we cannot rule out the possibility of diagnostic misclassification. Third, with a such large sample in our study, a statistical test would

Table 3. Comparison of statin users and nonusers ≥65 years of age for incidence and risk for hospitalization, pneumonia, circulatory conditions, critical illness, and death who are vaccinated and unvaccinated for influenza, Taiwan*

	Vaccinated			Unvaccinated (referent)			Hazard ratio (95% CI)†	
Characteristics	No.	Person-years	Incidence‡	No.	Person-years	Incidence‡	Crude	Adjusted
In-hospital death§	38,320	2,984,344	12.84	55,405	2,949,054	18.79	0.68 (0.67–0.69)	0.69 (0.68–0.69)
Statin user	1,478	147,164	10.04	22,097	146,668	14.30	0.70 (0.66–0.75)	0.71 (0.67–0.76)
Statin nonuser	36,842	2,837,180	12.99	53,308	2,802,386	19.02	0.68 (0.67–0.69)	0.68 | (0.68–0.69)
In-hospital death from pneumonia¶	15,057	2,984,931	5.04	20,699	2,950,157	7.02	0.72 (0.70–0.73)	0.72 (0.70–0.73)
Statin user	503	147,202	3.42	665	146,723	4.53	0.75 (0.67–0.85)	0.75 (0.67–0.85)
Statin nonuser	14,554	2,837,730	5.13	20,034	2,803,435	7.15	0.72 (0.70–0.73)	0.72 (0.70–0.73)
Hospitalization for pneumonia or influenza#	103,395	2,946,802	35.09	121,776	2,907,115	41.89	0.84 (0.83–0.84)	0.84 (0.84–0.85)
Statin user	3,967	145,687	27.23	4,810	144,805	33.22	0.82 (0.79–0.86)	0.82 (0.79–0.86)
Statin nonuser	99,428	2,801,115	35.50	116,966	2,762,309	42.34	0.84 (0.83–0.85)	0.84 (0.84–0.85)
Hospitalization for circulatory condition**	394,245	2,801,412	140.73	430,954	2,750,954	156.66	0.90 (0.90–0.90)	0.90 (0.90–0.90)
Statin user	25,141	134,914	186.35	27,991	132,843	210.71	0.89 (0.87–0.90)	0.90 (0.88–0.91)
Statin nonuser	369,104	2,666,498	138.42	402,963	2,618,111	153.91	0.90 (0.90–0.90)	0.90 (0.89–0.90)
Hospitalization for critical illness††	62,018	2,968,927	20.89	82,602	2,929,804	28.19	0.74 (0.73–0.75)	0.75 (0.74–0.76)
Statin user	2,614	146,432	17.85	3,574	145,677	24.53	0.73 (0.69–0.77)	0.74 (0.71–0.78)
Statin nonuser	59,404	2,822,496	21.05	79,028	2,784,127	28.39	0.74 (0.73–0.75)	0.75 (0.74–0.76)

*Values after propensity score-matching between persons who received and did not receive influenza vaccination.
†Calculated by Cox regression model with adjusted imbalance covariates listed in Table 1. In all cases, p<0.001.
‡Per 1,000 person-years.
§Interaction p = 0.478.
¶Interaction p = 0.493.
#Interaction p = 0.138.
**Interaction p = 0.667.
††Interaction p = 0.375.

easily demonstrate a significant difference. However, the risk difference in the vaccinated group compared with the unvaccinated group ranged from 10% to 31%, and the difference is not small. For subgroup analyses, the overall treatment effects also are consistent across subsets of patients. In addition, although we explored the interaction between statin use and the effectiveness of the influenza vaccine, whether other drugs exerting similar pleiotropic effects, such as aspirin and nonsteroidal antiinflammatory drugs, or other vaccines commonly used in this population, including pneumococcal and herpes vaccines, have similar interactions is unknown. Finally, our study included only persons ≥65 years of age, and our results cannot be extrapolated to younger persons who often elicit stronger immune responses after vaccination.

In conclusion, influenza vaccination was associated with lower risks of in-hospital death and hospitalization for pulmonary and circulatory adverse outcomes in persons ≥65 years of age in Taiwan. Of note, the rate of hospitalization for critical illness was slightly lower in statin users than that for nonusers. These findings indicate that influenza vaccination should continue to be encouraged in older populations because it reduces disease-specific hospitalization and death. In addition, statin use might enhance the protective effects of the vaccine against critical illness.

This study was based on data from the National Health Insurance Research Database provided by Bureau of National Health Insurance (BNHI) of the Department of Health and managed by the National Health Research Institute. The conclusions presented in this study are those of the authors and do not necessarily reflect the views of the BNHI, the Department of Health, or the National Health Research Institute.

This work was supported in part by the Novel Bioengineering and Technological Approaches to Solve Two Major Health Problems in Taiwan sponsored by the Taiwan Ministry of Science and Technology (MOST) Academic Excellence Program (MOST grant nos. 105-2633-B-009-003, 107-2314-B-075-052, and 108-2314-B-075-008); Wan Fang Hospital (grant nos. 105swf0 and, 106-swf-06); Taipei City Government (grant nos. 10701-62-054 and10801-62-051); Taipei Veterans General Hospital (grant nos. V105A-003, V106B-009, V107B-027, V108B-023, V109B-022, and V109D50-001-MY3-1); Taipei Veterans General Hospital-National Yang-Ming University Excellent Physician Scientists Cultivation Program (grant no. 104-V-B-044); Taipei Medical University Hospital (grant no. 105TMUH-SP-07).

About the Author

Dr. Tsai is a professor of infectious diseases at Tapai University. His research interests include epidemiology and public health.

References

1. Thompson WW, Shay DK, Weintraub E, Brammer L, Cox N, Anderson LJ, et al. Mortality associated with influenza and respiratory syncytial virus in the United States. JAMA. 2003;289:179–86. https://doi.org/10.1001/jama.289.2.179
2. Thompson WW, Shay DK, Weintraub E, Brammer L, Bridges CB, Cox NJ, et al. Influenza-associated hospitalizations in the United States. JAMA. 2004;292:1333–40. https://doi.org/10.1001/jama.292.11.1333
3. Chandrasekhar R, Sloan C, Mitchel E, Ndi D, Alden N, Thomas A, et al. Social determinants of influenza hospitalization in the United States. Influenza Other Respir Viruses. 2017;11:479–88. https://doi.org/10.1111/irv.12483
4. Sprenger MJ, Van Naelten MA, Mulder PG, Masurel N. Influenza mortality and excess deaths in the elderly, 1967–82. Epidemiol Infect. 1989;103:633–41. https://doi.org/10.1017/S0950268800031034
5. Nichol KL, Nordin JD, Nelson DB, Mullooly JP, Hak E. Effectiveness of influenza vaccine in the community-dwelling elderly. N Engl J Med. 2007;357:1373–81. https://doi.org/10.1056/NEJMoa070844
6. Wang CS, Wang ST, Lai CT, Lin LJ, Lee CT, Chou P. Reducing major cause-specific hospitalization rates and shortening hospital stays after influenza vaccination. Clin Infect Dis. 2004;39:1604–10. https://doi.org/10.1086/425323
7. Savarese G, Gotto AM Jr, Paolillo S, D'Amore C, Losco T, Musella F, et al. Benefits of statins in elderly subjects without established cardiovascular disease: a meta-analysis. J Am Coll Cardiol. 2013;62:2090–9. https://doi.org/10.1016/j.jacc.2013.07.069
8. Teng M, Lin L, Zhao YJ, Khoo AL, Davis BR, Yong QW, et al. Statins for primary prevention of cardiovascular disease in elderly patients: systematic review and meta-analysis. Drugs Aging. 2015;32:649–61. https://doi.org/10.1007/s40266-015-0290-9
9. Fehr T, Kahlert C, Fierz W, Joller-Jemelka HI, Riesen WF, Rickli H, et al. Statin-induced immunomodulatory effects on human T cells in vivo. Atherosclerosis. 2004;175:83–90. https://doi.org/10.1016/j.atherosclerosis.2004.02.016
10. Blanco-Colio LM, Tuñón J, Martín-Ventura JL, Egido J. Anti-inflammatory and immunomodulatory effects of statins. Kidney Int. 2003;63:12–23. https://doi.org/10.1046/j.1523-1755.2003.00744.x
11. Jain MK, Ridker PM. Anti-inflammatory effects of statins: clinical evidence and basic mechanisms. Nat Rev Drug Discov. 2005;4:977–87. https://doi.org/10.1038/nrd1901
12. Chow SC. Immunomodulation by statins: mechanisms and potential impact on autoimmune diseases. Arch Immunol Ther Exp (Warsz). 2009;57:243–51. https://doi.org/10.1007/s00005-009-0038-5
13. Black S, Nicolay U, Del Giudice G, Rappuoli R. Influence of statins on influenza vaccine response in elderly individuals. J Infect Dis. 2016;213:1224–8. https://doi.org/10.1093/infdis/jiv456
14. Omer SB, Phadke VK, Bednarczyk RA, Chamberlain AT, Brosseau JL, Orenstein WA. Impact of statins on influenza vaccine effectiveness against medically attended acute respiratory illness. J Infect Dis. 2016;213:1216–23. https://doi.org/10.1093/infdis/jiv457
15. Izurieta HS, Chillarige Y, Kelman JA, Forshee R, Qiang Y, Wernecke M, et al. Statin use and risks of influenza-related outcomes among older adults receiving standard-dose or high-dose influenza vaccines through Medicare during 2010–2015. Clin Infect Dis. 2018;67:378–87. https://doi.org/10.1093/cid/ciy100
16. Ortiz JR, Neuzil KM, Shay DK, Rue TC, Neradilek MB, Zhou H, et al. The burden of influenza-associated critical illness hospitalizations. Crit Care Med. 2014;42:2325–32. https://doi.org/10.1097/CCM.0000000000000545
17. Shih CJ, Ou SM, Chao PW, Kuo SC, Lee YJ, Yang CY, et al. Risks of death and stroke in patients undergoing hemodialysis with new-onset atrial fibrillation: a competing-risk analysis of a nationwide cohort. Circulation. 2016;133:265–72. https://doi.org/10.1161/CIRCULATIONAHA.115.018294
18. Ou SM, Shih CJ, Chao PW, Chu H, Kuo SC, Lee YJ, et al. Effects on clinical outcomes of adding dipeptidyl peptidase-4 inhibitors versus sulfonylureas to metformin therapy in patients with type 2 diabetes mellitus. Ann Intern Med. 2015;163:663–72. https://doi.org/10.7326/M15-0308
19. Shih CJ, Chu H, Chao PW, Lee YJ, Kuo SC, Li SY, et al. Long-term clinical outcome of major adverse cardiac events in survivors of infective endocarditis: a nationwide population-based study. Circulation. 2014;130:1684–91. https://doi.org/10.1161/CIRCULATIONAHA.114.012717
20. Lee CC, Lee MG, Hsu TC, Porta L, Chang SS, Yo CH, et al. A population-based cohort study on the drug-specific effect of statins on sepsis outcome. Chest. 2018;153:805–15. https://doi.org/10.1016/j.chest.2017.09.024
21. Chanin JM, Yang DC, Haider MA, Swaminathan RV, Kim LK, Charitakis K, et al. Impact of chronic statin therapy on postprocedural contrast-induced nephropathy in patients undergoing non-emergent percutaneous coronary intervention. J Invasive Cardiol. 2015;27:490–6.
22. Ortiz JR, Neuzil KM, Cooke CR, Neradilek MB, Goss CH, Shay DK. Influenza pneumonia surveillance among hospitalized adults may underestimate the burden of severe influenza disease. PLoS One. 2014;9:e113903. https://doi.org/10.1371/journal.pone.0113903
23. Stürmer T, Joshi M, Glynn RJ, Avorn J, Rothman KJ, Schneeweiss S. A review of the application of propensity score methods yielded increasing use, advantages in specific

settings, but not substantially different estimates compared with conventional multivariable methods. J Clin Epidemiol. 2006;59:437–47. https://doi.org/10.1016/j.jclinepi.2005.07.004
24. Ghittoni R, Napolitani G, Benati D, Ulivieri C, Patrussi L, Laghi Pasini F, et al. Simvastatin inhibits the MHC class II pathway of antigen presentation by impairing Ras superfamily GTPases. Eur J Immunol. 2006;36:2885–93. https://doi.org/10.1002/eji.200636567
25. Han KH, Ryu J, Hong KH, Ko J, Pak YK, Kim JB, et al. HMG-CoA reductase inhibition reduces monocyte CC chemokine receptor 2 expression and monocyte chemoattractant protein-1-mediated monocyte recruitment in vivo. Circulation. 2005;111:1439–47. https://doi.org/10.1161/01.CIR.0000158484.18024.1F
26. Azor MH, dos Santos JC, Futata EA, de Brito CA, Maruta CW, Rivitti EA, et al. Statin effects on regulatory and proinflammatory factors in chronic idiopathic urticaria. Clin Exp Immunol. 2011;166:291–8. https://doi.org/10.1111/j.1365-2249.2011.04473.x
27. Zhang J, Osawa S, Takayanagi Y, Ikuma M, Yamada T, Sugimoto M, et al. Statins directly suppress cytokine production in murine intraepithelial lymphocytes. Cytokine. 2013;61:540–5. https://doi.org/10.1016/j.cyto.2012.12.006
28. Ghittoni R, Patrussi L, Pirozzi K, Pellegrini M, Lazzerini PE, Capecchi PL, et al. Simvastatin inhibits T-cell activation by selectively impairing the function of Ras superfamily GTPases. FASEB J. 2005;19:605–7. https://doi.org/10.1096/fj.04-2702fje
29. Packard RR, Schlegel S, Senouf D, Burger F, Sigaud P, Perneger T, et al. Atorvastatin treatment and vaccination efficacy. J Clin Pharmacol. 2007;47:1022–7. https://doi.org/10.1177/0091270007302169
30. Brookhart MA, Patrick AR, Dormuth C, Avorn J, Shrank W, Cadarette SM, et al. Adherence to lipid-lowering therapy and the use of preventive health services: an investigation of the healthy user effect. Am J Epidemiol. 2007;166:348–54. https://doi.org/10.1093/aje/kwm070
31. Shrank WH, Patrick AR, Brookhart MA. Healthy user and related biases in observational studies of preventive interventions: a primer for physicians. J Gen Intern Med. 2011;26:546–50. https://doi.org/10.1007/s11606-010-1609-1
32. Goodwin K, Viboud C, Simonsen L. Antibody response to influenza vaccination in the elderly: a quantitative review. Vaccine. 2006;24:1159–69. https://doi.org/10.1016/j.vaccine.2005.08.105
33. Mannino S, Villa M, Apolone G, Weiss NS, Groth N, Aquino I, et al. Effectiveness of adjuvanted influenza vaccination in elderly subjects in northern Italy. Am J Epidemiol. 2012;176:527–33. https://doi.org/10.1093/aje/kws313
34. Westin GG, Armstrong EJ, Bang H, Yeo KK, Anderson D, Dawson DL, et al. Association between statin medications and mortality, major adverse cardiovascular event, and amputation-free survival in patients with critical limb ischemia. J Am Coll Cardiol. 2014;63:682–90. https://doi.org/10.1016/j.jacc.2013.09.073

Addresses for correspondence: Shih-Hsiu Lo, Department of Urology, Taipei Medical University Hospital, Taipei, Taiwan; email: 153031@h.tmu.edu.tw; Shuo-Ming Ou, Department of Nephrology, Taipei Veterans General Hospital, Taipei, 11217, Taiwan; email: okokyytt@gmail.com

Estimating Risk for Death from Coronavirus Disease, China, January–February 2020

Kenji Mizumoto, Gerardo Chowell

Since December 2019, when the first case of coronavirus disease (COVID-19) was identified in the city of Wuhan in the Hubei Province of China, the epidemic has generated tens of thousands of cases throughout China. As of February 28, 2020, the cumulative number of reported deaths in China was 2,858. We estimated the time-delay adjusted risk for death from COVID-19 in Wuhan, as well as for China excluding Wuhan, to assess the severity of the epidemic in the country. Our estimates of the risk for death in Wuhan reached values as high as 12% in the epicenter of the epidemic and ≈1% in other, more mildly affected areas. The elevated death risk estimates are probably associated with a breakdown of the healthcare system, indicating that enhanced public health interventions, including social distancing and movement restrictions, should be implemented to bring the COVID-19 epidemic under control.

Since the first case of coronavirus disease (COVID-19) was identified in December 2019 in the city of Wuhan in the Hubei Province of China, the novel virus (severe acute respiratory syndrome coronavirus 2 [SARS-CoV-2]) has continued to spread around the world, resulting in several thousand reported cases in multiple countries. In China, the cumulative number of reported deaths was 2,858 as of February 28, 2020, a figure that already dwarfed the number of persons that succumbed to severe acute respiratory syndrome during 2002–2003 (*1*).

In the context of an emerging infectious disease with pandemic potential, assessing its efficiency at spreading between humans is critical, as is determining the associated risk for death from the disease. In particular, the type and intensity of public health interventions are often set as a function of these epidemiologic metrics. In the absence of vaccines against SARS-CoV-2 or antiviral drugs for the treatment of COVID-19, the implementation of handwashing and other hygiene-related interventions, as well as nonpharmaceutical interventions such as social distancing and movement restrictions (all of which are the basic strategies available to mitigate disease spread in the population), also generate considerable pressure on the global economy (*2*).

As interventions are gradually implemented and calibrated during the course of an outbreak, early estimates of the case-fatality ratio (CFR) provide crucial information for policymakers to decide the intensity, timing, and duration of interventions. However, the assessment of epidemiologic characteristics, including the CFR, during the course of an outbreak tends to be affected by right censoring and ascertainment bias (*3*–*5*). The phenomenon of right censoring is caused by the gap in illness onset to death between the vulnerable population and the healthy population, resulting in underestimation, whereas ascertainment bias is attributable to the unreported bulk of infected persons who have mild symptoms or asymptomatic infections, potentially leading to overestimation. Assuming that ascertainment bias is consistent, we can adjust for right censoring by using established methods and available data (*6*,*7*). To assess the current severity of the epidemic in China, we derived estimates (and quantified uncertainty) of the time-delay adjusted CFR for COVID-19 for the city of Wuhan and for China excluding Wuhan, with quantified uncertainty.

Methods

Data Sources

We used 2 different types of epidemiologic data in our analysis. First, we extracted the daily series of confirmed cases and deaths in China from daily reports published by the respective governments of China, Hubei Province, and the city of Wuhan (*8*–*11*). Because >50% of the deaths are occurring in Hubei Province, and most of these have occurred in Wuhan, we categorized the

Author affiliations: Georgia State University, Atlanta, Georgia, USA (K. Mizumoto, G. Chowell); Kyoto University, Kyoto, Japan (K. Mizumoto)

DOI: https://doi.org/10.3201/eid2606.200233

data by geographic area: Wuhan City, Hubei Province excluding Wuhan, or China excluding Hubei Province. Diagnosis of COVID-19 relies solely on PCR testing because rapid diagnostic tests for this novel coronavirus are not widely available. Our analysis relies on epidemiologic data reported through February 11, 2020, because of the change in case definition that was announced by the government of China on February 12 (*12*).

We then obtained from several sources a total of 50 epidemiologic descriptions of patients who died from COVID-19 (*9*–*11*). After we checked for duplication and missing data, the sample size with data available was 39 patients for observed delays from illness onset to death and 33 for observed delays from hospitalization to death. We fitted a gamma distribution, an exponential distribution, and a lognormal distribution to these distributions and selected the best model based on the Akaike information criterion (AIC) (Appendix 1, https://wwwnc.cdc.gov/EID/article/26/6/20-0233-App1.pdf). The gamma distribution yielded the best fit for the distribution of delays from hospitalization to death (AIC 202.0), whereas the log-normal distribution gave the best fit for the distribution of delays from illness onset to death (AIC 263.3). On the basis of these 2 delay distributions, we incorporated the distribution of delays from hospitalization to death into the model.

Case-Fatality Ratio

We defined crude CFR as the number of cumulative deaths divided by the number of cumulative cases at a specific point in time. To estimate CFR in real time, we used the delay from hospitalization to death, h_s, which is assumed to be given by $h_s = H(s) - H(s\text{-}1)$ for $s>0$ where $H(s)$ is a cumulative density function of the delay from hospitalization to death and follows a gamma distribution with mean 10.1 days and SD 5.4 days, obtained from the available observed data. If $\pi_{a,ti}$ os the time-delay adjusted CFR on reported day ti in area a, the likelihood function of the estimate $\pi_{a\,ti}$ is

$$L(\pi_{a,t_i}; c_{a,t}) = \prod_{t_i}\left(\sum_{t=1}^{t_i} c_{a,t} \atop D_{a,t_i}\right)\left(\pi_{a,t_i}\frac{\sum_{t=2}^{t_i}\sum_{s=1}^{t-1} c_{a,t-s}h_s}{\sum_{t=1}^{t_i} c_{a,t}}\right)^{D_{a,t_i}} \left(1-\pi_{a,t_i}\frac{\sum_{t=2}^{t_i}\sum_{s=1}^{t-1} c_{a,t-s}h_s}{\sum_{t=1}^{t_i} c_{a.t}}\right)^{\sum_{t=1}^{ti} c_{a,t}-D_{a,t_i}}$$

where $c_{a,t}$ represents the number of new cases with reported day t in area a, and $D_{a,ti}$ is the cumulative number of deaths until reported day t_i in area a (*6*,*7*). Among the cumulative cases with reported day t in area a, $D_{a,ti}$ have died, and the remainder have survived the infection. The contribution of those who have died with biased death risk is shown in the middle parenthetical term, and the contribution of survivors is shown in the right parenthetical term. We assume that $D_{a,ti}$ is the result of the binomial sampling process with probability $\pi_{a,ti}$.

We estimated model parameters by using a Markov chain Monte Carlo method in a Bayesian framework. We estimated posterior distributions of the model parameters by sampling from the 3 Markov chains. For each chain, we drew 100,000 samples from the posterior distribution after a burn-in of 20,000 iterations. We evaluated convergence of Markov chain Monte Carlo chains by using the potential scale reduction statistic (*13*,*14*). Estimates and 95% credibility intervals (CrIs) for these estimates are based on the posterior probability distribution of each parameter and based on the samples drawn from the posterior distributions. All statistical analyses were conducted in R version 3.6.1 (R Foundation for Statistical Computing, https://www.r-project.org) using the rstan package.

Results

As of February 11, 2020, a total of 44,795 cases of COVID-19 had been reported in China, 1,117 of which had resulted in death (*9*–*11*; Appendix 2, https://wwwnc.cdc.gov/EID/article/26/6/20-0233-App2.xlsx). Of the 44,795 cases reported in China, 19,559 cases (43.7%) occurred in Wuhan, 13,894 cases (31.0%) occurred in Hubei Province excluding Wuhan, and 11,342 cases (25.3%) occurred in China excluding Hubei Province. Of the 1,117 deaths in China, 820 (73.4%) occurred in Wuhan, 248 (22.2%) occurred in Hubei Province excluding Wuhan, and 49 (4.4%) occurred in China excluding Hubei Province.

We charted the cumulative cases and deaths in Wuhan, Hubei Province excluding Wuhan, and China excluding Hubei Province (Figure 1). The curve of the cumulative number of deaths grows after that of the cumulative number of cases. Moreover, the increase in the number of deaths in Wuhan occurred more rapidly and the associated mortality rate was much higher than for the rest of China, whereas the cumulative case counts for the 3 areas in China are relatively similar.

We also charted the observed and model-based posterior estimates of crude CFR and the model-based posterior estimates of the time-delay adjusted CFR for Wuhan, Hubei Province excluding Wuhan, and China excluding Hubei Province (Figure 2). Our model-based crude CFR fitted the observed data well throughout the

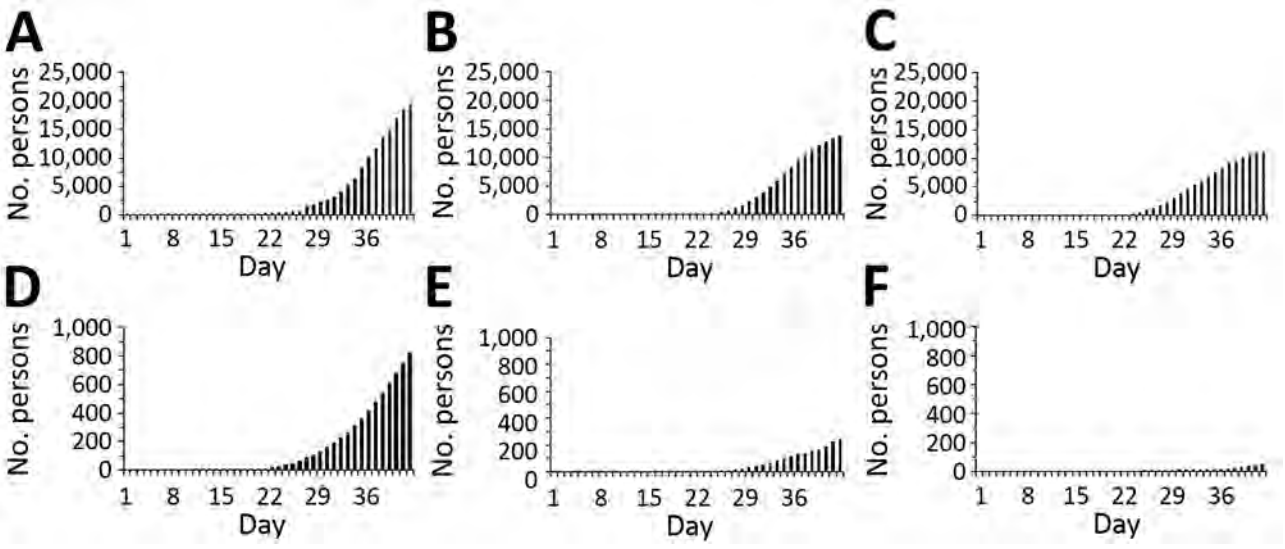

Figure 1. Temporal distribution of cases and deaths attributable to coronavirus disease in 3 areas in China, January 1–February 11, 2020. Cumulative cases in A) Wuhan, B) Hubei Province excluding Wuhan City, and C) China excluding Hubei Province, and cumulative deaths in D) Wuhan, E) Hubei Province excluding Wuhan, and F) China excluding Hubei Province. Day 1 corresponds to January 1, 2020. Because the dates of illness onset were not available, we used dates of reporting.

course of the epidemic except for the very early stage. During the course of the outbreak, our model-based posterior estimates of time-delay adjusted CFR have much higher values than the observed crude CFR, except for the early stage in Wuhan and the later stage in China excluding Hubei Province. Our estimates of the time-delay adjusted CFR appear to be decreasing almost consistently in Hubei Province excluding Wuhan and in China excluding Hubei Province, whereas in Wuhan, estimates were low at the early stage and then increased and peaked in the middle of the study period; the Wuhan estimates then followed a decreasing trend similar to the other 2 areas, reaching ≈12%.

As of February 11, estimates of the time-delay adjusted CFR were 12.2% (95% CrI 11.3%–13.1%) in Wuhan, 4.2% (95% CrI 3.7%–4.7%) in Hubei Province excluding Wuhan, and 0.9% (95% CrI 0.7%–1.1%) in China excluding Hubei Province. The observed crude CFR was 4.2% (95% CI 3.9%–4.5%) in Wuhan, 1.8% (95% CI 1.6%–2.0%) in Hubei Province excluding Wuhan, and 0.43% (95% CI 0.32%–0.57%) in China excluding Hubei Province (Table; Figure 3).

Discussion

We have derived estimates of the CFR for the ongoing COVID-19 epidemic in China. We have estimated time-delay adjusted CFR in 3 different geographic areas in China and found that the most severely affected areas were Wuhan as well as Hubei Province excluding Wuhan, whereas the rest of China (China excluding Hubei Province) experienced a less severe impact.

Our latest estimates (as of February 11, 2020) of the delay-adjusted CFR in Wuhan reach values as high as 12.2% (95% CrI 11.3%–13.1%), an estimate that is 3-fold higher than our estimate for Hubei Province excluding Wuhan and ≈14-fold higher than our estimate for China excluding Hubei Province. These findings suggest that the situation in Wuhan has been particularly dire compared with the other affected areas in China. We note that the upward trend of CFR during the early phase generally indicates increasing ascertainment bias.

An upward trend in the CFR should be interpreted with caution. Diagnosing cases of COVID-19 is difficult because the associated symptoms are not specific. Further, the fraction of asymptomatic patients with SAR-CoV-2 infection and COVID-19 patients who have mild symptoms is not minor; this fact complicates detection and diagnosis early after illness onset, leading to ascertainment bias (*15*,*16*). Indeed, out of a total of 566 residents of Japan who evacuated Wuhan by government-chartered plane during January 29–31, a total of 5 asymptomatic and 4 symptomatic COVID-19 patients were detected after undergoing detailed medical examinations (*17*). However, considering that this underestimation occurred during the course of outbreak and the number of deaths is reported fairly accurately, the upward trend indicates that the temporal disease burden exceeded the capacity of healthcare facilities and the surveillance system probably missed many cases during the early phase. In addition, hospital-based transmission has occurred, potentially affecting

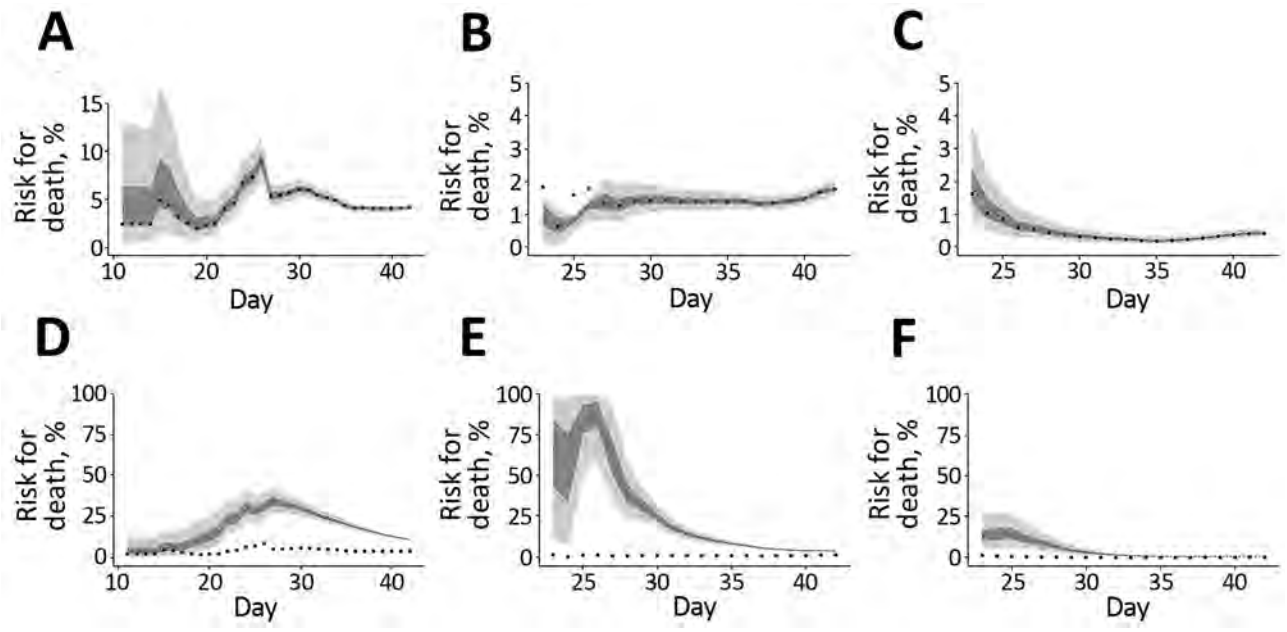

Figure 2. Temporal variation of risk for death associated with coronavirus disease in 3 areas in China, January 1–February 11, 2020. Observed and posterior estimates of A) crude case-fatality ratio in Wuhan, B) Hubei Province excluding Wuhan, and C) China excluding Hubei Province, and D) time-delay adjusted case-fatality ratio in Wuhan, E) Hubei Province excluding Wuhan, and F) China excluding Hubei Province. Day 1 corresponds to January 1, 2020. Black dots show crude case-fatality ratio, light gray area shows 95% credibility interval for posterior estimates, and dark gray area shows 50% credibility intervals for posterior estimates.

healthcare workers, inpatients, and visitors at healthcare facilities, which might explain an increasing trend and the elevated CFR estimates. Indeed, thousands of healthcare workers have succumbed to the disease in China (*18*), a pattern that resembles past nosocomial outbreaks of Middle East respiratory syndrome (MERS) and severe acute respiratory syndrome (*19*,*20*). During past MERS outbreaks, inpatients with underlying disease or elderly persons infected in the hospital setting have raised the CFR to values as high as 20% (*21*,*22*). A growing body of evidence indicates that COVID-19 transmission is facilitated in confined settings; for example, a large cluster (634 confirmed cases) of COVID-19 secondary infections occurred aboard a cruise ship in Japan, representing about one fifth of the persons aboard who were tested for the virus. This finding indicates the high transmissibility of COVID-19 in enclosed spaces (*23*,*24*).

A downward trend in CFR is suggestive of the extent of improvements in epidemiologic surveillance. In addition, this pattern indirectly indicates a substantial number of mild or asymptomatic cases in Wuhan and that the underlying transmission might prolong the end of the outbreak or further transmission to other areas unless effective social distancing measures are implemented until a vaccine becomes available. Furthermore, given that the delay-adjusted CFR and crude CFR estimates in Wuhan are ≈14-fold higher than our estimates for China excluding Hubei Province, a breakdown in healthcare delivery probably occurred, underscoring the critical need for urgent medical support in the epicenter of the epidemic.

We also found that the estimates of the delay-adjusted CFR for Hubei Province excluding Wuhan and for China excluding Hubei Province showed a declining trend as the epidemic progressed. A similar trend was previously reported for the 2015 MERS outbreak in South Korea, where a substantial fraction of the case-patients were elderly or had underlying conditions (*19*,*20*). The high proportion

Table. Summary results of time-delay adjusted CFR for COVID-19 in the 3 areas in China, January 1–February 11, 2020*

Area	Latest estimate, %	Median estimates during study period, %	Crude CFR (95% CI), %	No. deaths/ no. cases
Wuhan	12.2 (95% CrI 11.3–13.1)	4.1–34.8	4.2 (95% CI 3.9–4.5)	820/19,559
Hubei Province excluding Wuhan	4.2 (95% CrI 3.7–4.7)	4.2–88.3	1.8 (95% CI 1.6–2.0)	248/13,894
China excluding Hubei Province	0.9 (95% CrI 0.7–1.1)	0.8–14.8	0.35 (95% CI 0.32–0.57)	39/11,103

*CFR, case-fatality ratio; COVID-19, coronavirus disease; CrI, credibility interval.

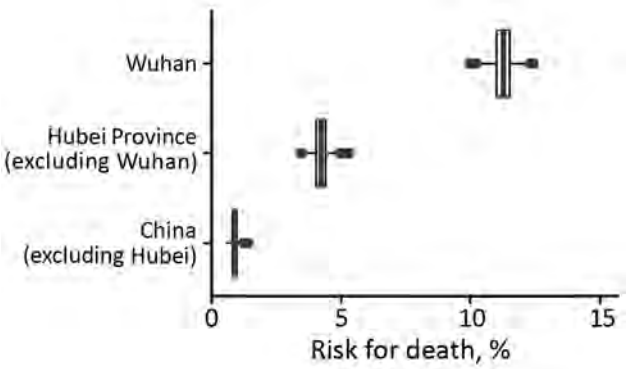

Figure 3. Latest estimates of time-delay adjusted risk for death from coronavirus disease in 3 areas in China, January 1–February 11, 2020.

of vulnerable case-patients at the early phase of the outbreak and the smaller number in the later stage could partly explain the observed decline. However, because the epidemic had yet to peak, this time-dependent decrease was probably caused by ascertainment bias. Moreover, the latest estimates of the delay-adjusted CFR and crude CFR in Hubei Province are ≈5-fold higher than our estimate for China excluding Hubei Province, where the healthcare system has not been overwhelmed. These findings also indicate the need to anticipate additional medical support to deliver medical care to the most vulnerable patients, including those with preexisting health conditions, who are at the highest risk for succumbing to the disease. For comparison, the crude CFR has been estimated at 0.9% in Beijing (*25*), 1.4% among 1,099 patients across China (*26*), and 4.3% in a meta-analysis among 50,466 hospitalized patients (*27*).

Our study has limitations. First, our CFR estimate is influenced by ascertainment bias, which might influence estimates upward. For those infectious diseases characterized by a large fraction of patients with mild illness or asymptomatic infections, the infection-fatality risk (e.g., the number of deaths divided by the total number of persons infected) is a more appropriate index of disease burden (*28*,*29*). Therefore, mass serologic surveillance and surveys to assess the presence or absence of symptoms is strongly recommended to disentangle the threat of emerging infectious diseases, including COVID-19. In addition, because our estimates of CFR are based on the number of confirmed cases reported before the February 12 change in the case definition, caution will be needed when comparing our estimates with other CFR estimates that include epidemiologic data from on or after February 12, which would be lower. Second, in our estimation we employed a distribution of delays from illness onset to death (n = 39 patients), which was obtained from secondary sources, but the available epidemiologic data does not include either the date of illness onset or the date of confirmation. For this reason, we used the time delay from hospitalization to death (n = 33 patients).

In conclusion, our estimates of the risk for death from COVID-19 in China as of February 11, 2020, were as high as 12% in the epicenter of the epidemic and as low as ≈1% in the less severely affected areas in China. Because the risk for death from COVID-19 is probably associated with a breakdown of the healthcare system in the absence of pharmaceutical interventions (i.e., vaccination and antiviral drugs), enhanced public health interventions (including social distancing measures, quarantine, enhanced infection control in healthcare settings, and movement restrictions), as well as enhanced hygienic measures in the general population and an increase in healthcare system capacity, should be implemented to rapidly contain the epidemic.

K.M. acknowledges support from the Japan Society for the Promotion of Science (KAKENHI grant no. 15K20936), the Program for Advancing Strategic International Networks to Accelerate the Circulation of Talented Researchers (grant no. G2801), and the Leading Initiative for Excellent Young Researchers from the Ministry of Education, Culture, Sport, Science, and Technology of Japan. G.C. acknowledges support from the National Science Foundation (grant no. 1414374) as part of the joint National Science Foundation–National Institutes of Health–US Department of Agriculture Ecology and Evolution of Infectious Diseases Program, and support from the United Kingdom Biotechnology and Biological Sciences Research Council (grant no. BB/M008894/1).

About the Authors

Dr. Mizumoto works as an assistant professor at the Graduate School of Advanced Integrated Studies in Human Survivability, Kyoto University, Japan. His research interests include mathematical and statistical epidemiology and modeling of infectious diseases.

Dr. Chowell is professor of Epidemiology and Biostatistics and chair of the Department of Population Health Sciences at the Georgia State University School of Public Health. He is also a senior research fellow at the Fogarty International Center of the National Institutes of Health. His research interests include mathematical modeling of infectious disease dynamics and control.

References

1. World Health Organization. Summary of probable SARS cases with onset of illness from 1 November 2002 to 31 July 2003 [cited 2020 Feb 7]. https://www.who.int/csr/sars/country/table2004_04_21
2. Chowell G, Fenimore PW, Castillo-Garsow MA, Castillo-Chavez C. SARS outbreaks in Ontario, Hong Kong and Singapore: the role of diagnosis and isolation as a control mechanism. J Theor Biol. 2003;224:1–8. https://doi.org/10.1016/S0022-5193(03)00228-5
3. Ghani AC, Donnelly CA, Cox DR, Griffin JT, Fraser C, Lam TH, et al. Methods for estimating the case fatality ratio for a novel, emerging infectious disease. Am J Epidemiol. 2005;162:479–86. https://doi.org/10.1093/aje/kwi230
4. Kucharski AJ, Edmunds WJ. Case fatality rate for Ebola virus disease in west Africa. Lancet. 2014;384:1260. https://doi.org/10.1016/S0140-6736(14)61706-2
5. Jewell NP, Lei X, Ghani AC, Donnelly CA, Leung GM, Ho LM, et al. Non-parametric estimation of the case fatality ratio with competing risks data: an application to Severe Acute Respiratory Syndrome (SARS). Stat Med. 2007;26:1982–98. https://doi.org/10.1002/sim.2691
6. Nishiura H, Klinkenberg D, Roberts M, Heesterbeek JA. Early epidemiological assessment of the virulence of emerging infectious diseases: a case study of an influenza pandemic. PLoS One. 2009;4:e6852. https://doi.org/10.1371/journal.pone.0006852
7. Tsuzuki S, Lee H, Miura F, Chan YH, Jung SM, Akhmetzhanov AR, et al. Dynamics of the pneumonic plague epidemic in Madagascar, August to October 2017. Euro Surveill. 2017;22:22. https://doi.org/10.2807/1560-7917.ES.2017.22.46.17-00710
8. Garske T, Legrand J, Donnelly CA, Ward H, Cauchemez S, Fraser C, et al. Assessing the severity of the novel influenza A/H1N1 pandemic. BMJ. 2009;339(jul14 3):b2840.
9. The State Council of the People's Republic of China. Update on new coronavirus pneumonia [in Chinese] [cited 2020 Feb 7]. http://www.nhc.gov.cn/yjb/pzhgli/new_list.shtml
10. Health Commission of Hubei Province. China. Pneumonia epidemic prevention and control of new coronavirus infection [in Chinese] [cited 2020 Feb 7]. http://wjw.hubei.gov.cn/fbjd/dtyw
11. Health Commission of Wuhan City. Hubei Province, China. Wuhan Municipal Commission of Health and Health on pneumonia of new coronavirus infection [in Chinese] [cited 2020 Feb 7]. http://wjw.hubei.gov.cn/fbjd/dtyw
12. The State Council of the People's Republic of China. Clinical guideline for COVID-19, version 5 [in Chinese]. 2020 [cited 2020 Feb 29]. http://www.gov.cn/zhengce/zhengceku/2020-02/05/5474791/files/de44557832ad-4be1929091dcbcfca891.pdf
13. Gamerman D, Lopes HF. Markov chain Monte Carlo: stochastic simulation for Bayesian inference. 2nd edition. London: Chapman and Hall/CRC Press; 2006.
14. Gelman A, Rubin DB. Inference from iterative simulation using multiple sequences. Stat Sci. 1992;7:457–72. https://doi.org/10.1214/ss/1177011136
15. Rothe C, Schunk M, Sothmann P, Bretzel G, Froeschl G, Wallrauch C, et al. Transmission of 2019-nCoV infection from an asymptomatic contact in Germany. N Engl J Med. 2020;382:970–1. https://doi.org/10.1056/NEJMc2001468
16. Kupferschmidt K. Study claiming new coronavirus can be transmitted by people without symptoms was flawed [cited 2020 Feb 4]. https://www.sciencemag.org/news/2020/02/paper-non-symptomatic-patient-transmitting-coronavirus-wrong
17. Ministory of Health, Labour and Welfare, Japan. List of press releases (new coronavirus) [in Japanese]. 2020 [cited 2020 Feb 28]. https://www.mhlw.go.jp/stf/seisakunitsuite/bunya/0000121431_00086.html
18. Gan N, Thomas N, Culver D. CNN. Over 1,700 frontline medics infected with coronavirus in China, presenting new crisis for the government. 2020 [cited 2020 Mar 2]. https://edition.cnn.com/2020/02/13/asia/coronavirus-health-care-workers-infected-intl-hnk/index.html
19. Chowell G, Abdirizak F, Lee S, Lee J, Jung E, Nishiura H, et al. Transmission characteristics of MERS and SARS in the healthcare setting: a comparative study. BMC Med. 2015;13:210. https://doi.org/10.1186/s12916-015-0450-0
20. Abdirizak F, Lewis R, Chowell G. Evaluating the potential impact of targeted vaccination strategies against severe acute respiratory syndrome coronavirus (SARS-CoV) and Middle East respiratory syndrome coronavirus (MERS-CoV) outbreaks in the healthcare setting. Theor Biol Med Model. 2019;16:16. https://doi.org/10.1186/s12976-019-0112-6
21. Mizumoto K, Endo A, Chowell G, Miyamatsu Y, Saitoh M, Nishiura H. Real-time characterization of risks of death associated with the Middle East respiratory syndrome (MERS) in the Republic of Korea, 2015. BMC Med. 2015;13:228. https://doi.org/10.1186/s12916-015-0468-3
22. Mizumoto K, Saitoh M, Chowell G, Miyamatsu Y, Nishiura H. Estimating the risk of Middle East respiratory syndrome (MERS) death during the course of the outbreak in the Republic of Korea, 2015. Int J Infect Dis. 2015;39:7–9. https://doi.org/10.1016/j.ijid.2015.08.005
23. Mizumoto K, Kagaya K, Zarebski A, Chowell G. Estimating the asymptomatic proportion of coronavirus disease 2019 (COVID-19) cases on board the Diamond Princess cruise ship, Yokohama, Japan, 2020. Euro Surveill. 2020;25:25. https://doi.org/10.2807/1560-7917.ES.2020.25.10.2000180
24. Mizumoto K, Chowell G. Transmission potential of the novel coronavirus (COVID-19) onboard the Diamond Princess Cruises ship, 2020. Infect Dis Model. 2020;5:264–70. https://doi.org/10.1016/j.idm.2020.02.003
25. Tian S, Hu N, Lou J, Chen K, Kang X, Xiang Z, et al. Characteristics of COVID-19 infection in Beijing. J Infect. 2020 Feb 27 [Epub ahead of print].
26. Guan WJ, Ni ZY, Hu Y, Liang WH, Ou CQ, He JX, et al. China Medical Treatment Expert Group for Covid-19. Clinical characteristics of coronavirus disease 2019 in China. N Engl J Med. 2020 Feb 28 [Epub ahead of print]. https://doi.org/10.1056/NEJMoa2002032
27. Sun P, Qie S, Liu Z, Ren J, Li K, Xi J. Clinical characteristics of 50466 hospitalized patients with 2019-nCoV infection. J Med Virol. 2020 Feb 28 [Epub ahead of print]. https://doi.org/10.1002/jmv.25735
28. Wong JY, Wu P, Nishiura H, Goldstein E, Lau EH, Yang L, et al. Infection fatality risk of the pandemic A(H1N1)2009 virus in Hong Kong. Am J Epidemiol. 2013;177:834–40. https://doi.org/10.1093/aje/kws314
29. Presanis AM, De Angelis D, Hagy A, Reed C, Riley S, Cooper BS, et al.; New York City Swine Flu Investigation Team. The severity of pandemic H1N1 influenza in the United States, from April to July 2009: a Bayesian analysis. PLoS Med. 2009;6:e1000207. https://doi.org/10.1371/journal.pmed.1000207

Address for correspondence: Kenji Mizumoto, Graduate School of Advanced Integrated Studies in Human Survivability, Kyoto University, 1 Yoshida-Nakaadachi-cho, Sakyo-ku, Kyoto 606-8306, Japan; email: mizumoto.kenji.5a@kyoto-u.ac.jp

Epidemiology of Coronavirus Disease in Gansu Province, China, 2020

Jingchun Fan, Xiaodong Liu, Weimin Pan, Mark W. Douglas, Shisan Bao

To determine the epidemiology of coronavirus disease (COVID-19) in a remote region of China, far from Wuhan, we analyzed the epidemiology of COVID-19 in Gansu Province. From January 23 through February 3, 2020, a total of 35 (64.8%) of 54 reported cases were imported from COVID-19–epidemic areas. Characteristics that differed significantly during the first and second waves of illness in Gansu Province were mean patient age, occupation, having visited epidemic areas, and mode of transportation. Time from infection to illness onset for family clusters was shorter in Gansu Province than in Wuhan, consistent with shortened durations from onset to first medical visit or hospitalization. Spatial distribution pattern analysis indicated hot spots and spatial outliers in Gansu Province. As a result of adequate interventions, transmission of the COVID-19 virus in Gansu Province is decreasing.

The outbreak of coronavirus disease (COVID-19) was first reported on December 31, 2019, in Wuhan, China (*1*). Within a few weeks, the virus had spread rapidly throughout China and within 1 month to several other countries, including Italy (*2*), the United States (*3*), and Germany (*4*). Difficulty controlling such aggressive spread resulted partly from the size of Wuhan, which has a full-time population of >9 million and a transient population of an additional 5.10 million, for a total population of ≈14 million (*5*,*6*). Wuhan is located in central China and has a wide range of transportation links, including airplanes, trains, interstate buses, and private transportation. In an attempt to reduce virus transmission, on January 23, 2020, authorities locked down Wuhan, but by that time, ≈5 million persons had already left (*7*). Reasons for leaving included returning to hometowns for the Chinese New Year (most persons) or leaving for holidays, but some left because of fear of COVID-19 (*7*). Consequently, COVID-19 has now been identified in every province or autonomous region in China, although the highest number of cases is still in Wuhan (*7*).

Gansu Province is located in northwestern China, and as of February 3, 2020, the number of COVID-19 cases identified has been small, most in persons coming from Wuhan. As of January 23, the date of the Wuhan lockdown, the Gansu Provincial Centre for Disease Control and Prevention (Lanzhou, China) had identified only 2 cases of COVID-19 in Lanzhou, the capital of Ganzu Province: 1 patient had traveled from Wuhan and another had been in contact with persons from Wuhan (*8*). Within 2 weeks, however, 54 cases of COVID-19 in Gansu Province were confirmed, indicating the seriousness of this outbreak and triggering the alarm for the Gansu Province government to make it mandatory that face masks be worn in public places from January 28 until further notice (*9*). From a public health point of view, the epidemiology of the COVID-19 event in Lanzhou (*10*), a relatively remote region of China, may provide critical information to help control the spread of this disease to other provinces and countries. We therefore explored the epidemiology of COVID-19 in Gansu Province, remote from the outbreak epicenter in Wuhan.

Materials and Methods

We split the 12-day study period in half. The early period began January 23, the date of the first

Author affiliations: School of Public Health, Gansu University of Chinese Medicine, Lanzhou, China (J. Fan); Institute of Immunization and Prevention Management, Shandong Center for Disease Control and Prevention, Jinan, China (X. Liu); Gansu Provincial Center for Disease Control and Prevention, Lanzhou (W. Pan); Centre for Infectious Diseases and Microbiology, Westmead Hospital, Sydney, New South Wales, Australia (M.W. Douglas); Storr Liver Centre and Marie Bashir Institute for Infectious Diseases and Biosecurity, University of Sydney, Sydney (M.W. Douglas); School of Medical Sciences and Bosch Institute, Charles Perkins Centre, University of Sydney, Sydney (S. Bao)

DOI: https://doi.org/10.3201/eid2606.200251

confirmed case of COVID-19 reported in Gansu Province, and continued through January 28, the date when the Gansu government decreed it mandatory to wear face masks in public places. The late period, the subsequent 6 days, extended from January 29 through February 3. To analyze the epidemiology of the COVID-19 outbreak in Gansu Province, we compared cases diagnosed during the early and late periods. Our aim was to compare groups to determine if the restriction order was effective for controlling transmission. The definition of primary versus secondary cases refers to whether persons traveled from Wuhan (primary) or never left Gansu Province (secondary). The aim of this distinction was to explore potential transmission.

The first wave of infection was seen in persons who arrived from Wuhan, whereas later infections resulted from virus transmission from the first group of persons. To compare the demographic and clinical characteristics of persons with primary and secondary infection, we collected data about transmission and family clusters, including the date of return from epidemic areas, first day of close contact, date of symptom onset, date of first medical visit and hospitalization, and relationships between patients with primary and secondary cases.

Setting

Gansu Province (32°31′N–42°57′N, 92°13′E–108°46′E) is located in northwestern China (Figure 1). Gansu is the seventh largest province in China, comprising 12 prefecture-level cities and 2 autonomous prefectures (86 counties and districts), with a total land area of 454,000 km2 and a population of 26,257,100 in 2019 (*11*). It is a long, handle-shaped province, and Lanzhou is located on the Yellow River. The complex landforms of Gansu Province include mountainous regions, plateaus, plains, river valleys, and desert. With a population of 3.8 million and 13,100 km2, the population density of Lanzhou is 287 persons/km2 (Figure 2), although Lanzhou is classified as a third-tier city in China (*10*).

Materials

COVID-19 diagnoses in Gansu Province from January 23 through February 3, 2020, were confirmed in the laboratory of Gansu Provincial Centre for Disease Control and Prevention (*12*). Suspected cases of COVID-19 infection were identified in hospitals and confirmed in the same laboratory by specific nucleic acids. We collected demographic data, including patient sex, age, occupation, place of residence, and exposure history, from the official website of the Gansu

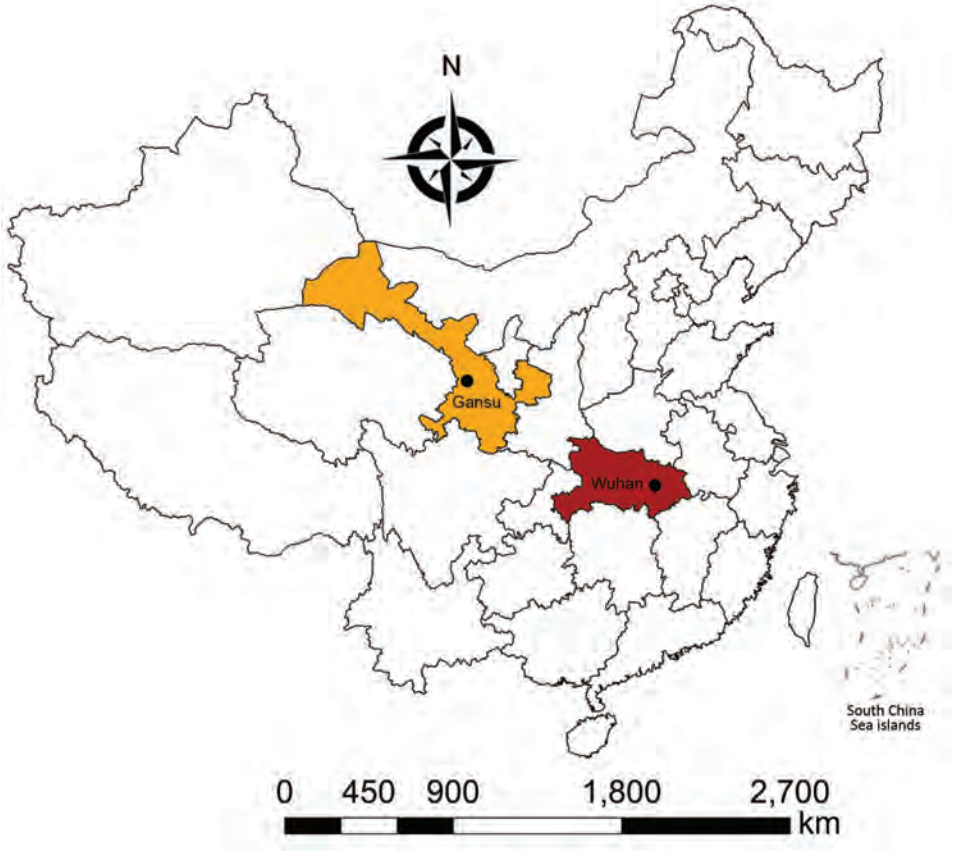

Figure 1. Location of Gansu Province and Wuhan, China. Circles indicate capital cities.

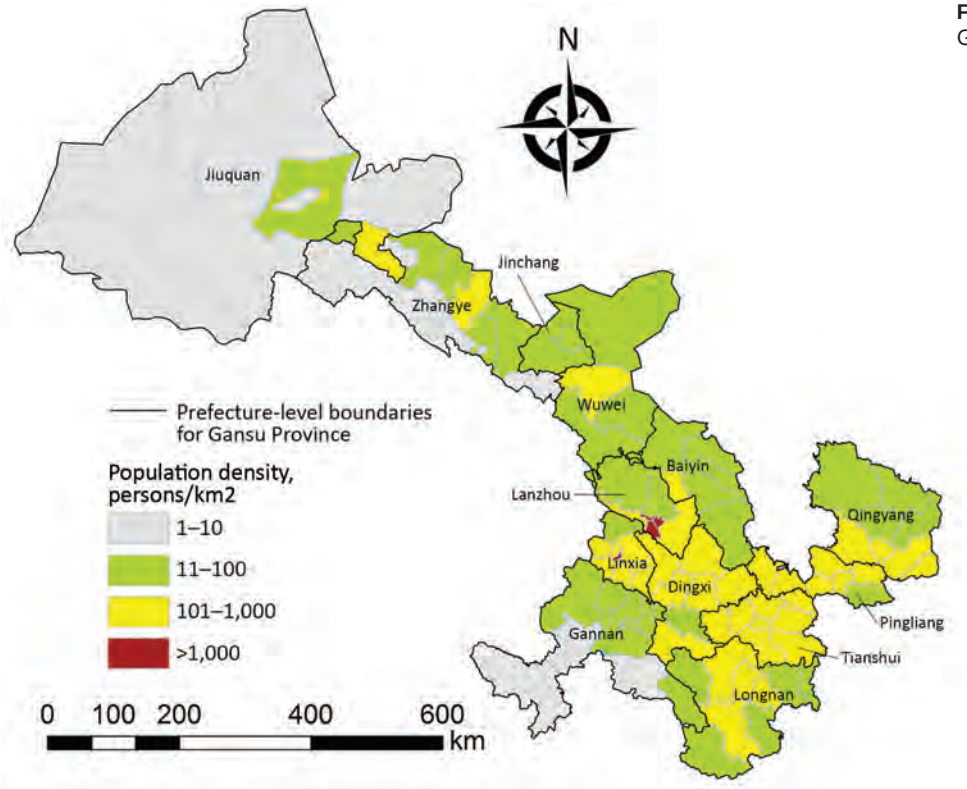

Figure 2. Population density of Gansu Province, China, in 2018.

Provincial Center for Disease Control and Prevention (http://gscdc.net).

Within each prefecture or prefecture-level city in Gansu Province are districts, counties or autonomous counties, and county-level cities. For this study, we classified all counties and county-level cities as counties for simplicity and for data analysis. To conduct a geographic information system (GIS)–based analysis on the spatial distribution of COVID-19 cases, we applied the county-level polygon map (county layers) at 1:250,000 scale from Data Sharing Infrastructure of Earth System Science (http://www.geodata.cn), on which we generated a county-level layer containing information regarding latitudes and longitudes of cases in county layers (central points) of each county.

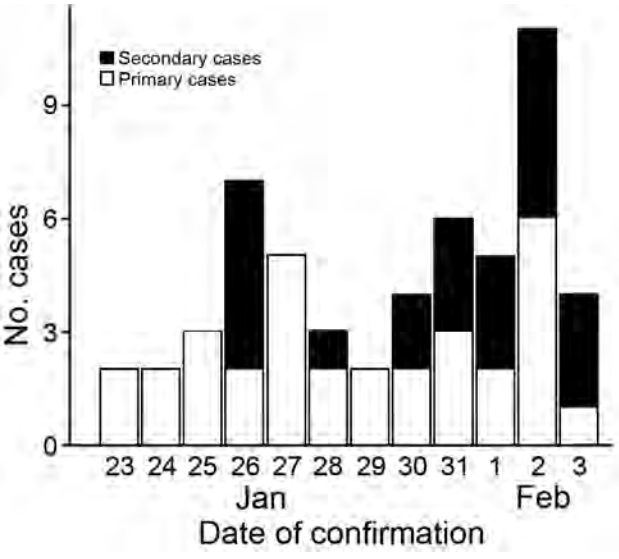

Figure 3. Time series of coronavirus disease case identification in Gansu Province, China, 2020.

Statistical Analyses

The 54 patients were assigned numbers from 1 to 54 according to time of diagnosis. The statistical descriptions included demographic characteristics, exposure history, whether the cases were primary or secondary, and potential spread of disease. Because the ages of case-patients were not normally distributed, we performed nonparametric Brown-Mood tests to compare medians between early and late cases. For expected cell sizes <5, we used the Fisher exact test to compare the frequency between or among groups; otherwise, we used the χ^2 test. We estimated days from illness onset to first medical visit and days from illness onset to hospitalization by fitting a Weibull distribution to the dates of illness onset, first medical visit, and hospital admission (*13*).

GIS Mapping and Spatial Analyses

We geocoded all COVID-19 cases and matched them to the county-level layers of polygon and point by

Table 1. Characteristics of patients with coronavirus disease, Gansu Province, China, 2020*

Characteristics	Jan 23–28, n = 24	Jan 29–Feb 3, n = 30	p value
Median age (range), y	34 (20–83)	48 (1.67–94)	0.014
Age group, no./total no. (%), y			0.821
<18	0/24	1/30 (3)	
18–64	22/24 (92)	25/30(83)	
≥65	2/24 (8)	4/30(13)	
Sex			0.854
M	11/24 (46)	13/30 (43)	
F	13/24 (54)	17/30 (57)	
Occupation			0.009
Cadres and professionals	3/24 (8)	8/30 (27)	
Laborers	7/24 (29)	3/30 (10)	
Farmers	3/24 (13)	0/30	
Business service providers	3/24 (13)	2/30 (7)	
Students	2/24 (8)	3/30 (10)	
Scatter children† and retires	4/24 (17)	16/30 (47)	
Healthcare workers	2/24 (8)	0/30	
Urban residence	14/24 (58)	20/30 (67)	0.529
Primary case	19/24 (79)	17/30 (56)	0.081
Exposure to epidemic area			0.043
Hubei Province	16/24 (66)	14/30 (47)	
Other area	3/24 (13)	2/30 (7)	
No exposure to Hubei/other area	5/24 (21)	14/30 (46)	
Main mode of transportation			0.193
Airplane	6/24 (25)	3/30 (10)	
Train	7/24 (29)	8/30 (27)	
Airplane and train	6/24 (25)	5/30 (17)	
Local, did not leave Gansu Province	5/24 (21)	14/30 (46)	
Frequency of transfer between transportation modes			0.024
≤3	7/24 (29)	11/30 (37)	
>3	12/24 (50)	5/30 (16)	
Local, did not leave Gansu Province	5/24 (21)	14/30 (47)	

*Data are no./total no. (%) unless otherwise indicated.
†Children who stayed at home, did not attend childcare facilities.

administrative codes by using ArcGIS 10.2.2 software (https://www.arcgis.com). To explore the spatial distribution pattern of COVID-19 cases on the county level during the study periods, we applied local indicators of spatial association (LISA [*14*]). Using LISA, we could identify the type and degree of spatial clustering, including significant hot spots (high-high), cold spots (low-low), and spatial outliers (high-low and low-high) between a given location and surrounding spatial units by calculating the local Moran's I (*14*,*15*). We used the Z statistic to determine the significance of clustering based on a significance level of 0.05. A significant positive Z indicates high-value regions surrounded by high-value regions (high-high) or low value regions surrounded by low-value regions (low-low). A significant negative Z indicates high-value regions surrounded by low-value regions (high-low) or low-value regions surrounded by high-value regions (low-high) (*16*).

Ethics Approval

Our study was approved by the institutional review board, Gansu University of Chinese Medicine. We collected data from the official website of Gansu Provincial Center for Disease Control and Prevention, which was considered exempt from approval.

Results

Patient Characteristics

Of the total 54 cases of COVID-19 in Gansu Province, 35 were imported primary and 19 were indigenous secondary cases. Serious/critical illness was experienced by 6 (17.1%) of the 35 patients with primary cases and by 3 (15.7%) of the 19 patients with secondary cases; the difference was not significant (p = 0.899). A total of 24 cases were reported during the early period and 30 during the late period (Figure 3). On January 26, the first secondary case of COVID-19 was identified in Longnan, a city located in southern of Gansu Province. The youngest patient was 1 year and 8 months of age; the oldest was 94 years of age. We used Cox proportional hazards regression to correct for covariates but found no significant differences between the early and late groups. No survival pattern could be calculated because, to date, no COVID-19–associated deaths in Gansu Province have been reported.

Table 2. Interval between primary and secondary cases in 6 family clusters of coronavirus disease, Gansu Province, China, 2020*

Family cluster patient no.	No. primary cases	No. secondary cases	Date of close contact	Date of symptom onset	Serial interval, d†
1	1	9	Jan 18	22 Jan	4
2	1	26	Jan 18	26 Jan	8
3	1	27	Jan 18	26 Jan	8
4	4	14	Jan 19	25 Jan	6
5	4	46	19 Jan	27 Jan	8
6	6	10	15 Jan	21 Jan	6
7	6	11	15 Jan	21 Jan	6
8	6	12	15 Jan	24 Jan	9
9	6	13	15 Jan	24 Jan	9
10	6	23	15 Jan	23 Jan	8
11	29	39	25 Jan	30 Jan	5
12	29	47	22 Jan	26 Jan	4
13	Family gathering‡	43	26 Jan	28 Jan	2
14	Interstate business‡	44	15 Jan	23 Jan	8
15	36	48	20 Jan	23 Jan	3
16	36	49	21 Jan	24 Jan	3
17	36	50	20 Jan	30 Jan	10
18	36	51	20 Jan	30 Jan	10
19	36	52	20 Jan	30 Jan	10

*Because incidence was derived from a family gathering, dates of close contact and symptom onset are similar.
†Days between close contact and symptom onset.
‡Local residents for whom primary cases could not be traced.

Comparing patients who sought care in the early and late periods, we found significant differences for age (median age 34 years for the early period vs. 48 years for the late period; p = 0.014) and for occupation (more laborers in the early period vs. more retired persons in the late period; p = 0.009) but not for patient sex or whether the patients lived in urban or rural areas (Table 1). In addition, more case-patients in the early period had visited epidemic areas (p = 0.043) and returned to their destination (p = 0.024) than had patients in the late period.

Key Time-to-Event Distributions of COVID-19

For the 54 cases of COVID-19 diagnosed in Gansu Province from January 23 through February 3, the days from illness onset to first medical visit ranged from 0 to 10 and the days from first medical visit to hospitalization ranged from 0 to 7. The days from infection to symptom onset for 19 case-patients in a family cluster, confirmed by epidemiologic survey, ranged from 2 to 10 days (mean 6.7 days); the 95th percentile of the distribution was 12.5 days (95% CI 9.2–18 days) (Table 2; Figure 4, panel A). Among the 24 COVID-19 cases confirmed in the early period, the estimated mean time from illness onset to first medical visit was 2.8 days (95% CI 1.7–3.8); that is, there was a trend toward longer delay for case-patients in the early period than the mean of 2.3 days (95% CI 1.3–3.2) for the 30 case-patients in the late period (Figure 4, panel B), but this difference did not reach statistical significance (p>0.05). The mean duration from first medical visit to hospital admission was 1.9 days (95% CI 1.2–2.6 days) among 24 case-patients with illness onset during the early period, shorter than among 30 case-patients with illness onset during the second period, among whom the mean duration from first medical visit to hospital admission was 3.3 days (95% CI 2.7–4.0 days) (Figure 4, panel C).

Spatial Distribution of COVID-19

The 54 COVID-19 cases reported in Gansu Province from January 23 through February 3 were distributed in 11 prefectures and 24 counties. The 2 cities with the most COVID-19 case-patients were Lanzhou (26 cases) and Tianshui (8 cases). The area with the most COVID-19 cases was Chengguan District, the political and economic center of Lanzhou (Figure 5, panel A). Patients with secondary cases seem to have been infected by persons with primary cases; we identified 6 family clusters: 3 in Lanzhou, 1 in Tianshui, 1 in Longnan, and 1 in Linxia. LISA analysis demonstrated hot spots (high-high) and outliers (high-low and low-high). The high-high cluster included 4 counties, accounting for 4.55% of all counties, mainly distributed in the eastern capital city of Lanzhou. High-low and low-high outliers were sporadically distributed in eastern-central Gansu Province (Figure 5, panel B).

Discussion

Our data suggest that most COVID-19 cases that occurred in the first 6 days (January 23–28, 2020) were imported from Wuhan (the coronavirus epicenter). Most secondary cases occurred in the second 6 days (January 29–February 3, 2020).

In Gansu Province, the patients identified in the early period were younger than those identified in the late period, but overall the 54 patients were younger (median age 38 years) than patients identified in the early stage of the outbreak in Wuhan (median age 59 years) (*13*). This finding is most likely because Wuhan is where the outbreak originated in China (*17*). Patients from the early period were younger and had mainly imported primary cases, possibly because most of them were labor workers in Wuhan who traveled back to Gansu Province; in contrast, a greater proportion of patients in the late period were senior retirees with secondary indigenous cases. The proportions of COVID-19 patients who had visited an epidemic area and the frequencies of transfer were 3 times greater during the early than the late period, suggesting that exposure risk would decrease from epidemic areas and public places as the epidemic spread. The current situation may result from the travel bans from Wuhan or other places as well as most persons' awareness and education about COVID-19 (*18*), but human transportation had spread the virus before Wuhan was locked down. (*19*).

In our study, distribution of illness by sex did not differ significantly between the early and late periods, but female patients predominated slightly. In contrast, Chen and colleagues reported more male than female patients in the Wuhan outbreak (*20*). One possible explanation is that in Wuhan, men dominate the labor market and probably had close contact with the seafood market in Wuhan (the source of the outbreak), resulting in more male patients in the Wuhan study. In contrast, the COVID-19 outbreak in Gansu was 2 weeks later, during the Chinese New Year festival, in which family members of both sexes participated. Thus, our data further support the need for broad infection control measures in surrounding areas, irrespective of age, sex, place of residence, or mode of transportation.

The first case of secondary infection was identified in a patient who had had close contact with the first case-patient with primary COVID-19 in Gansu Province, after a lag of 4 days. Subsequently, 6 family clusters were identified over 12 days. These data confirm direct human-to-human transmission of the COVID-19 virus, severe acute respiratory syndrome coronavirus 2 (SARS-CoV-2), through close contact (*21*). This finding supports the government restriction of persons gathering in large groups, to reduce or minimize virus transmission. The 95% percentile range for the incubation period found in our study is consistent with the findings for Wuhan, which almost completely overlap (*13*), suggesting that within this short time, SARS-CoV-2 has not mutated sufficiently to affect incubation time (*22*).

The proportion of persons who visited a medical center or hospital within 2 days from illness onset was 61% in Gansu Province, compared with 27%

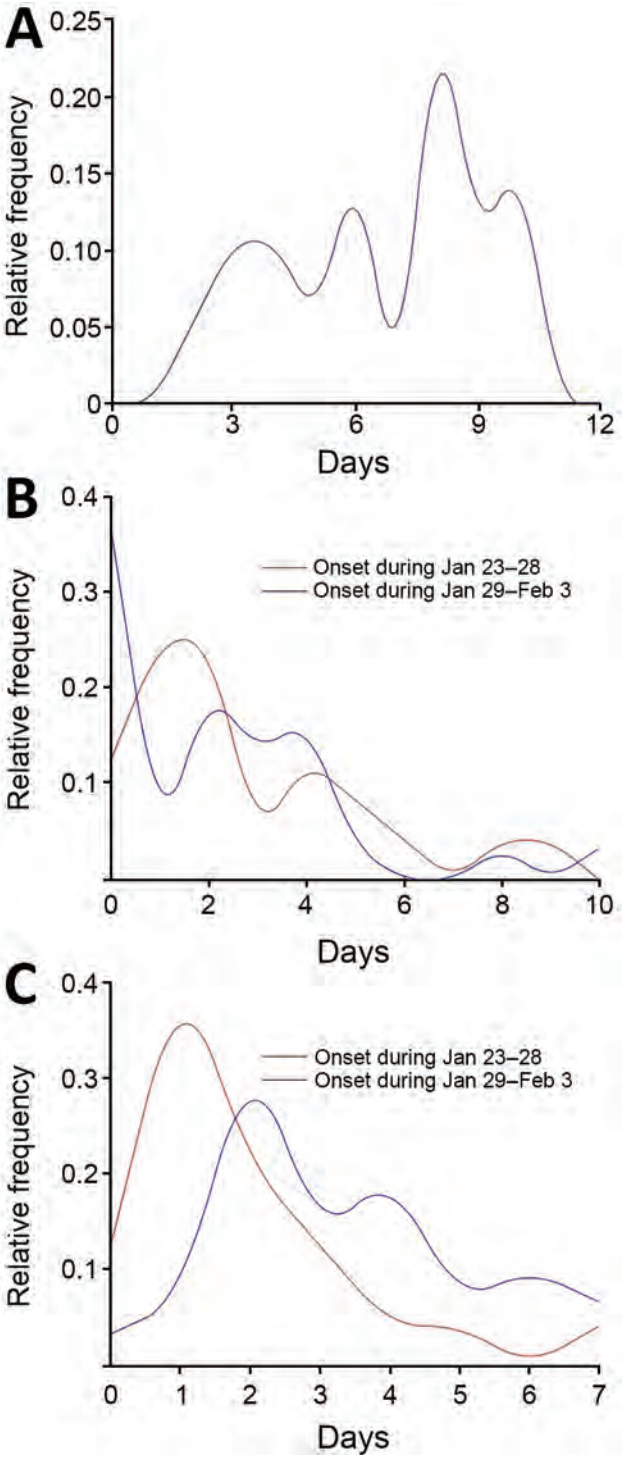

Figure 4. Key time-to-event distributions of coronavirus disease cases in Gansu Province, China, 2020. A) Incubation period (i.e., days from infection to illness onset). B) Days from illness to first medical visit. C) Days from illness to hospitalization.

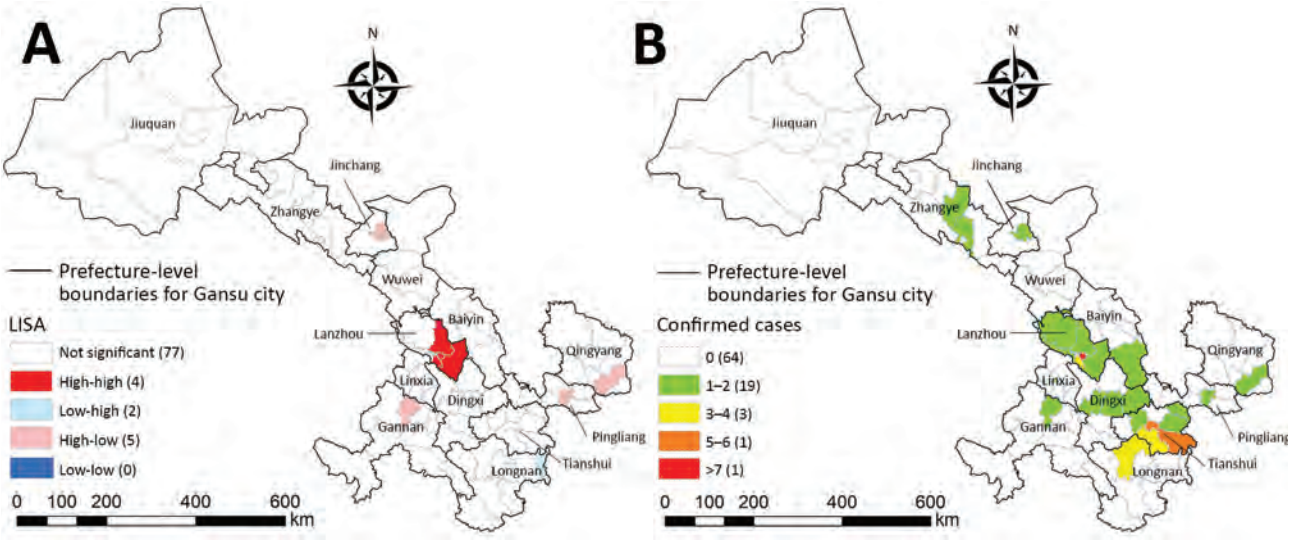

Figure 5. Distribution of reported coronavirus disease cases (A) and local indicators of spatial association cluster map (B) for Gansu Province, January 23–February 3, 2020. Numbers in parentheses indicate number of counties.

in Wuhan (*13*). In addition, 68% of patients in Gansu Province were hospitalized within 5 days after illness onset, whereas only 11% of patients in Wuhan were hospitalized in the early stages of the disease (*13*). These differences between Gansu Province and Wuhan may partially result from differences in numbers of staff and medical resources between Wuhan and Gansu Province, relative to the number of COVID-19 patients. Another potential factor is advanced warning about COVID-19 in Gansu Province via various channels. Although knowledge about COVID-19 was minimal at the beginning of the outbreak, the seriousness of COVID-19 was well broadcast throughout China, including Gansu Province, after the initial outbreak. Compared with the initial stage of the COVID-19 outbreak in Wuhan, the reduced incidence of COVID-19 in Gansu Province over this period may be associated with reinforcement of mandatory control and prevention interventions, patients voluntarily seeking medical assistance after being educated by the media, or possibly both.

Our study demonstrates a significant spatial heterogeneity of COVID-19 cases in Gansu Province over this 2-week period; cases were mostly concentrated in Lanzhou and surrounding areas. LISA analysis findings are in agreement with the spatial distribution of COVID-19 at the county levels of Gansu Province. This analysis confirms that the distribution of cases was not random: hot spots were mainly restricted to the Chengguan District of Lanzhou, the most densely populated and most developed area (*11*). This case aggregation is closely associated with the development characteristics of Gansu Province, which is at the high end of economic, medical, population, and cultural development. Consequently, Chengguan District was the most common pathway for most persons returning from Wuhan and other cities, who end up in or transit through Lanzhou. Land formations in Gansu Province limit travel, particularly in mountainous rural areas, which may have slowed down or restricted the spread of COVID-19 across Gansu Province. For example, cases have been reported in Wuwei, a city in a remote, mountainous, hard-to-reach area in Gansu Province. Our findings are supported by other studies, which demonstrate a close correlation with population and economy in other major cities of China where outbreaks of COVID-19 occurred within 1–2 weeks of the original outbreak in Wuhan (*23*–*25*).

Although case numbers are small, in Gansu Province the severity of COVID-19 illness did not differ between persons with primary and secondary cases, suggesting that the virus does not mutate to decrease virulence during ongoing transmission. This finding is consistent with recent reports from Italy and the United States, which suggest that mutations that reduce transmission do not spontaneously develop in SARS-CoV-2 (*2*,*3*). In Gansu Province, we observed fewer severe clinical cases of COVID-19, lower rates of patients in critical condition (13%), and no deaths, compared with Wuhan, where ≈30% patients were admitted to intensive care and 4% died (*26*). One possible explanation is insufficient medical staff and resources in Wuhan to deal with the large outbreak and only extremely serious

or critical patients being hospitalized, in contrast to Gansu Province, where relatively more medical staff and resources were available. Furthermore, a large proportion of the Wuhan population who left the city before the lockdown were migrant workers, commercial personnel, and college students; the population remaining in Wuhan after the lockdown therefore comprised mostly elderly persons with compromised immunity (*27*). The incubation period in Gansu Province was longer than that in Wuhan (3–6 days for Wuhan) (*28*,*29*). This finding may be the result of the government's intensive provision of information for the whole nation about controlling and preventing COVID-19.

A limitation of our study is the difficulty of calculating county-level incidence or estimating the risk factors affecting SARS-CoV-2 transmission in Gansu Province because of the relatively small number of cases and the short study period (i.e., 12 days), which may not reflect the entire epidemiology of the virus in Gansu Province and will only become clear over time. Whether the outbreak will be controlled soon, and if so when, will be answered in due course.

In conclusion, our study demonstrates the epidemiology of a relatively small-scale outbreak of COVID-19 outside of Wuhan. Our cohort included primary cases from Wuhan and subsequent secondary cases, including several family clusters. Such information should be useful for other regions and countries to help combat the spread of this lethal disease (*30*) by informing the development of more effective local infection control policies and recommendations.

This study was funded by Talent Introduction Program of Gansu University of Chinese Medicine (no. 2016YJRC-01 to J.F.) and Shanghai Jiao Tong University grants 2019, The University of Sydney (to S.B.).

About the Author

Dr. Fan is a principal investigator at the School of Public Health, Gansu University of Chinese Medicine. Her research interests focus on population epidemiology and statistics, including the effects of environmental factors on population health.

References

1. World Health Organization. Novel coronavirus—China [cited 2020 Jan 12]. https://www.who.int/csr/don/12-january-2020-novel-coronavirus-china
2. Giovanetti M, Benvenuto D, Angeletti S, Ciccozzi M. The first two cases of 2019-nCoV in Italy: where they come from? J Med Virol. 2020 Feb 5 [Epub ahead of print]. https://doi.org/ 10.1002/jmv.25699
3. Centers for Disease Control and Prevention. Coronavirus disease 2019 (COVID-19) in the U.S. [cited 2020 Feb 21]. https://www.cdc.gov/coronavirus/2019-ncov/cases-in-us.html
4. Rothe C, Schunk M, Sothmann P, Bretzel G, Froeschl G, Wallrauch C, et al. Transmission of 2019-nCoV infection from an asymptomatic contact in Germany. N Engl J Med. 2020;382:970–1. https://doi.org/10.1056/NEJMc2001468
5. Hubei Provincial Bureau of Statistics. Hubei statistical yearbook—2018. Wuhan (China): Hubei Provincial Bureau of Statistics; 2019.
6. Lu H, Stratton CW, Tang YW. Outbreak of pneumonia of unknown etiology in Wuhan, China: the mystery and the miracle. J Med Virol. 2020;92:401–2. https://doi.org/10.1002/jmv.25678
7. Ma J; WND News Services. 5 million left Wuhan before lockdown, 1,000 new coronavirus cases expected in city [cited 2020 Jan 26]. https://ph.news.yahoo.com/5-million-residents-left-wuhan-142328311.html
8. Health Commission of Gansu Province. Two cases of novel coronavirus 2019 (2019-nCoV) have been confirmed in Gansu Province [in Chinese] [cited 2020 Jan 23]. http://wsjk.gansu.gov.cn/single/10910/82997.html
9. www.Chinanews.com|Gansu. Face masks are made mandatory in Wuhan [in Chinese] [cited 2020 Jan 27]. http://www.gs.chinanews.com.cn/news/2020/01-27/326475.shtml
10. The State Council, The People's Republic of China. China to apply new city classification standards [cited 2014 Nov 20]. http://english.www.gov.cn/policies/latest_releases/2014/11/25/content_281475015213546.htm
11. Gansu Provincial Bureau of Statistics. Gansu statistical yearbook—2018. Lanzhou (China): Gansu Provincial Bureau of Statistics; 2019.
12. Gansu Provincial Center of Disease Control and Prevention. Gansu Provincial Center of Disease Control and Prevention outbreak bulletin [in Chinese] [cited 2020 Feb 4]. http://www.gscdc.net/index.php?s=news&c=category&id=60
13. Li Q, Guan X, Wu P, Wang X, Zhou L, Tong Y, et al. Early transmission dynamics in Wuhan, China, of novel coronavirus-infected pneumonia. N Engl J Med. 2020 Jan 29 [epub ahead of print]. https://doi.org/10.1056/NEJMoa2001316
14. Anselin L. Local indicators of spatial association—LISA. Geogr Anal. 1995;27:93–115. https://doi.org/10.1111/j.1538-4632.1995.tb00338.x
15. Wang LY, Zhang WY, Ding F, Hu WB, Soares Magalhaes RJ, Sun HL, et al. Spatiotemporal patterns of Japanese encephalitis in China, 2002–2010. PLoS Negl Trop Dis. 2013;7:e2285. PubMed https://doi.org/10.1371/journal.pntd.0002285
16. Anselin L. Local indicators of spatial association—LISA (Geospatial analysis, 6th edition, 2020 update) [cited 2019 Jul 23]. http://www.spatialanalysisonline.com/HTML/index.html?local_indicators_of_spatial_as.htm
17. Bassetti M, Vena A, Giacobbe DR. The novel Chinese coronavirus (2019-nCoV) infections: challenges for fighting the storm. Eur J Clin Invest. 2020;50:e13209. https://doi.org/10.1111/eci.13209
18. Department of Dissemination Science, Chinese Medical Association. Diagnosis and prevention of 2019-nCov infection pneumonia in children [in Chinese] [cited 2020 Jan 29]. https://en.cma.org.cn/art/2020/1/29/art_1822_32177.html
19. Du Z, Wang L, Cauchemez S, Xu X, Wang X, Cowling BJ, et al. Risk for transportation of coronavirus disease from Wuhan to other cities in China. Emerg Infect Dis. 2020; Feb 13; 26 [Epub ahead of print]. https://doi.org/10.3201/eid2605.200146

20. Chen N, Zhou M, Dong X, Qu J, Gong F, Han Y, et al. Epidemiological and clinical characteristics of 99 cases of 2019 novel coronavirus pneumonia in Wuhan, China: a descriptive study. Lancet. 2020 Jan 30 [Epub ahead of print]. https://doi.org/10.1016/S0140–6736(20)30211–7.
21. Chan JF, Yuan S, Kok KH, To KK, Chu H, Yang J, et al. A familial cluster of pneumonia associated with the 2019 novel coronavirus indicating person-to-person transmission: a study of a family cluster. Lancet. 2020 Jan 24 [Epub ahead of print]. https://doi.org/10.1016/S0140–6736(20)30154–9.
22. Zhou P, Yang XL, Wang XG, Hu B, Zhang L, Zhang W, et al. A pneumonia outbreak associated with a new coronavirus of probable bat origin. Nature. 2020 Feb 3 [Epub ahead of print]. https://doi.org/10.1038/s41586-020-2012-7
23. Wu JT, Leung K, Leung GM. Nowcasting and forecasting the potential domestic and international spread of the 2019-nCoV outbreak originating in Wuhan, China: a modelling study. Lancet. 2020;395:689–97. https://doi.org/10.1016/S0140-6736(20)30260-9
24. Li RQ, Richmond P, Roehner BM. Effect of population density on epidemics. Physica A. 2018;510:713–24. https://doi.org/10.1016/j.physa.2018.07.025
25. Hakeem MA. Effect of population density on the level of development [cited 2017 Nov 1]. https://mpra.ub.uni-muenchen.de/82301
26. Wilson ME, Chen LH. Travelers give wings to novel coronavirus (2019-nCoV). J Travel Med. 2020 Feb 3 [Epub ahead of print]. https://doi.org/10.1093/jtm/taaa015
27. Horton R. Offline: 2019-nCoV outbreak-early lessons. Lancet. 2020;395:322. https://doi.org/10.1016/S0140-6736(20)30212-9
28. Sovran B, Hugenholtz F, Elderman M, Van Beek AA, Graversen K, Huijskes M, et al. Age-associated impairment of the mucus barrier function is associated with profound changes in microbiota and immunity. Sci Rep. 2019;9:1437. https://doi.org/10.1038/s41598-018-35228-3
29. Huang C, Wang Y, Li X, Ren L, Zhao J, Hu Y, et al. Clinical features of patients infected with 2019 novel coronavirus in Wuhan, China. Lancet. 2020;395:497–506.
30. The Lancet. Emerging understandings of 2019-nCoV. Lancet. 2020;395:311. https://doi.org/10.1016/S0140-6736(20)30186-0

Address for correspondence: Shisan Bao, Discipline of Pathology, School of Medical Sciences and Bosch Institute, Charles Perkins Centre, The University of Sydney, Sydney, NSW 2006, Australia; email: bob.bao@sydney.edu.au

Severe Acute Respiratory Syndrome Coronavirus 2 from Patient with Coronavirus Disease, United States

Jennifer Harcourt,[1] Azaibi Tamin,[1] Xiaoyan Lu, Shifaq Kamili, Senthil K. Sakthivel, Janna Murray, Krista Queen, Ying Tao, Clinton R. Paden, Jing Zhang, Yan Li, Anna Uehara, Haibin Wang, Cynthia Goldsmith, Hannah A. Bullock, Lijuan Wang, Brett Whitaker, Brian Lynch, Rashi Gautam, Craig Schindewolf, Kumari G. Lokugamage, Dionna Scharton, Jessica A. Plante, Divya Mirchandani, Steven G. Widen, Krishna Narayanan, Shinji Makino, Thomas G. Ksiazek, Kenneth S. Plante, Scott C. Weaver, Stephen Lindstrom, Suxiang Tong, Vineet D. Menachery,[2] Natalie J. Thornburg[2]

The etiologic agent of an outbreak of pneumonia in Wuhan, China, was identified as severe acute respiratory syndrome coronavirus 2 in January 2020. A patient in the United States was given a diagnosis of infection with this virus by the state of Washington and the US Centers for Disease Control and Prevention on January 20, 2020. We isolated virus from nasopharyngeal and oropharyngeal specimens from this patient and characterized the viral sequence, replication properties, and cell culture tropism. We found that the virus replicates to high titer in Vero-CCL81 cells and Vero E6 cells in the absence of trypsin. We also deposited the virus into 2 virus repositories, making it broadly available to the public health and research communities. We hope that open access to this reagent will expedite development of medical countermeasures.

Author affiliations: Centers for Disease Control and Prevention, Atlanta, Georgia, USA (J. Harcourt, A. Tamin, X. Lu, K. Queen, Y. Tao, C.R. Paden, Y. Li, C. Goldsmith, B. Whitaker, R. Gautam, S. Lindstrom, S. Tong, N.J. Thornburg); Eagle Medical Services, Atlanta (S. Kamili, S.K. Sakthivel, J. Murray, B. Lynch); IHRC, Atlanta (J. Zhang, H. Wang); Oak Ridge Institute for Science and Education, Oak Ridge, Tennessee, USA (A. Uehara); Synergy America, Inc., Atlanta (H.A. Bullock, L. Wang); University of Texas Medical Branch, Galveston, Texas, USA (C. Schindewolf, K.G. Lokugamage, D. Mirchandani, S. Widen, K. Narayanan, S. Makino, T.G. Ksiazek, S.C. Weaver, V.D. Menachery); World Reference Center for Emerging Viruses and Arboviruses, Galveston (D. Scharton, J.A. Plante, T.G. Ksiazek, K.S. Plante, S.C. Weaver, V.D. Menachery)

DOI: https://doi.org/10.3201/eid2606.200516

A novel coronavirus, severe acute respiratory syndrome coronavirus 2 (SARS-CoV-2), has been identified as the source of a pneumonia outbreak in Wuhan, China, in late 2019 (*1*,*2*). The virus was found to be a member of the β coronavirus family, in the same species as SARS-CoV and SARS-related bat CoVs (*3*,*4*). Patterns of spread indicate that SARS-CoV-2 can be transmitted person-to-person, and may be more transmissible than SARS-CoV (*5*–*7*). The spike protein of coronaviruses mediates virus binding and cell entry. Initial characterization of SARS-CoV-2 spike indicates that it binds the same receptor as SARS-CoV angiotensin-converting enzyme, which is expressed in both upper and lower human respiratory tracts (*8*).

The unprecedented rapidity of spread of this outbreak represents a critical need for reference reagents. The public health community requires viral lysates to serve as diagnostic references, and the research community needs virus isolates to test antiviral compounds, develop new vaccines, and perform basic research. In this article, we describe isolation of SARS-CoV-2 from a patient who had coronavirus disease (COVID-19) in the United States and described its genomic sequence and replication characteristics. We have made the virus isolate available to the public health community by depositing it into 2 virus reagent repositories.

[1]These authors contributed equally to this article.

[2]These senior authors contributed equally to this article.

Methods

Specimen Collection

Virus isolation from patient samples was deemed not to be human subjects research by the National Center for Immunizations and Respiratory Diseases, Centers for Disease Control and Prevention (CDC) (research determination no. 0900f3eb81ab4b6e). Clinical specimens from a case-patient who had acquired COVID-19 during travel to China and who was identified in Washington, USA, were collected as described (*1*). Nasopharyngeal (NP) and oropharyngeal (OP) swab specimens were collected on day 3 postsymptom onset, placed in 2–3 mL of viral transport medium, used for molecular diagnosis, and frozen. Confirmed PCR-positive specimens were aliquoted and refrozen until virus isolation was initiated.

Cell Culture, Limiting Dilution, and Virus Isolation

We used Vero CCL-81 cells for isolation and initial passage. We cultured Vero E6, Vero CCL-81, HUH 7.0, 293T, A549, and EFKB3 cells in Dulbecco minimal essential medium (DMEM) supplemented with heat-inactivated fetal bovine serum (5% or 10%) and antibiotics/antimycotics (GIBCO, https://www.thermofisher.com). We used both NP and OP swab specimens for virus isolation. For isolation, limiting dilution, and passage 1 of the virus, we pipetted 50 μL of serum-free DMEM into columns 2–12 of a 96-well tissue culture plate, then pipetted 100 μL of clinical specimens into column 1 and serially diluted 2-fold across the plate. We then trypsinized and resuspended Vero cells in DMEM containing 10% fetal bovine serum, 2× penicillin/streptomycin, 2× antibiotics/antimycotics, and 2× amphotericin B at a concentration of 2.5×10^5 cells/mL. We added 100 μL of cell suspension directly to the clinical specimen dilutions and mixed gently by pipetting. We then grew the inoculated cultures in a humidified 37°C incubator in an atmosphere of 5% CO_2 and observed for cytopathic effects (CPEs) daily. We used standard plaque assays for SARS-CoV-2, which were based on SARS-CoV and Middle East respiratory syndrome coronavirus (MERS-CoV) protocols (*9*,*10*).

When CPEs were observed, we scraped cell monolayers with the back of a pipette tip. We used 50 μL of viral lysate for total nucleic acid extraction for confirmatory testing and sequencing. We also used 50 μL of virus lysate to inoculate a well of a 90% confluent 24-well plate.

Inclusivity/Exclusivity Testing

From the wells in which CPEs were observed, we performed confirmatory testing by using real-time reverse transcription PCR (CDC) and full-genome sequencing (*1*). The CDC molecular diagnostic assay targets 3 portions of the nucleocapsid gene, and results for all 3 portions must be positive for a sample to be considered positive (https://www.cdc.gov/coronavirus/2019-ncov/lab/rt-pcr-detection-instructions.html and https://www.cdc.gov/coronavirus/2019-ncov/lab/rt-pcr-panel-primer-probes.html). To confirm that no other respiratory viruses were present, we performed Fast Track Respiratory Pathogens 33 Testing (FTD Diagnostics, http://www.fast-trackdiagnostics.com).

Whole-Genome Sequencing

We designed 37 pairs of nested PCRs spanning the genome on the basis of the coronavirus reference sequence (GenBank accession no. NC045512). We extracted nucleic acid from isolates and amplified by using the 37 individual nested PCRs. We used positive PCR amplicons individually for subsequent Sanger sequencing and also pooled them for library preparation by using a ligation sequencing kit (Oxford Nanopore Technologies, https://nanoporetech.com), subsequently for Oxford Nanopore MinION sequencing. We generated consensus nanopore sequences by using Minimap version 2.17 (https://github.com) and Samtools version 1.9 (http://www.htslib.org). We generated consensus sequences by Sanger sequencing from both directions by using Sequencher version 5.4.6 (https://www.genecodes.com), and further confirmed them by using consensus sequences generated from nanopore sequencing.

To sequence passage 4 stock, we prepared libraries for sequencing by using the Next Ultra II RNA Prep Kit (New England Biolabs, https://www.neb.com) according to the manufacturer's protocol. In brief, we fragmented ≈70–100 ng of RNA for 15 min, followed by cDNA synthesis, end repair, and adaptor ligation. After 6 rounds of PCR, we analyzed libraries by using an Agilent Bioanalyzer (https://www.agilent.com) and quantified them by using a quantitative PCR. We pooled samples and sequenced samples by using a paired-end 75-base protocol on an Illumina (Illumina, Inc., https://www.illumina.com) MiniSeq instrument and using the High-Output Kit and then processed reads by using Trimmomatic version 0.36 (*11*) to remove low-quality base calls and any adaptor sequences. We used the de novo assembly program ABySS (*12*) to assemble the reads into contigs by using several different sets of reads and kmer values ranging from 20 to 40. We compared contigs >400 bases against the National Center for Biotechnology Information (Bethesda, MD, USA) nucleotide collection using BLAST

(https://blast.ncbi.nlm.nih.gov). A nearly full-length viral contig obtained in each sample had 100% identity to the 2019-nCoV/USA-WA1/2020 strain (GenBank accession no. MN985325.1). All the remaining contigs mapped to either host cell rRNA or mitochondria. We mapped the trimmed reads to the reference sequence by using BWA version 0.7.17 (*13*) and visualized these reads by using the Integrated Genomics Viewer (*14*) to confirm the identity with the USA-WA1/2020 strain.

Electron Microscopy

We scraped infected Vero cells from the flask, pelleted by low-speed centrifugation, rinsed with 0.1 mol/L phosphate buffer, pelleted again, and fixed for 2 h in 2.5% buffered glutaraldehyde. We then postfixed specimens with 1% osmium tetroxide, en bloc stained with 4% uranyl acetate, dehydrated, and embedded in epoxy resin. We cut ultrathin sections, stained them with 4% uranyl acetate and lead citrate, and examined them by using a Thermo Fisher/FEI Tecnai Spirit electron microscope (https://www.fei.com).

Protein Analysis and Western Blotting

We harvested cell lysates by using Laemmli sodium dodecyl sulfate–polyacrylamide gel electrophoresis sample buffer (Bio-Rad, https://www.bio-rad.com) containing 2% SDS and 5% β-mercaptoethanol. We removed the cell lysates from a Biosafety Level 3 Laboratory, boiled them, and loaded them onto a polyacrylamide gel. We subjected the lysates to sodium dodecyl sulfate–polyacrylamide gel electrophoresis, followed by transfer to a polyvinylidene difluoride polyvinylidene fluoride membrane. We then blocked the membrane in 5% nonfat dry milk dissolved in Tris-buffered saline containing 0.1% Tween-20 (TBS-T) for 1 h, followed by a short wash with TBS-T. We incubated the membrane overnight with primary antibody, either rabbit polyclonal serum against the SARS-CoV spike protein (#40150-T52; Sino Biological, https://www.sinobiological.com), β-actin antibody (#4970; Cell Signaling Technology, https://www.cellsignal.com), or a custom rabbit polyclonal serum against SARS-CoV nucleocapsid. We then washed the membrane with 3 times with TBS-T and applied horseradish peroxidase-conjugated secondary antibody for 1 h. Subsequently, we washed the membrane 3 times with TBS-T, incubated with Clarity Western ECL Substrate (#1705060S; Bio-Rad), and imaged with a multipurpose imaging system.

Generation of SARS-CoV Nucleocapsid Antibodies

We used the plasmid pBM302 (*15*) to express SARS-CoV nucleocapsid protein, with a C-terminal His6 tag, to high levels within the inclusion bodies of *Escherichia coli* and the recombinant protein was purified from the inclusion bodies by using nickel-affinity column chromatography under denaturing conditions. We used stepwise dialysis against Tris/phosphate buffer to refold the recombinant SARS-CoV nucleocapsid protein with decreasing concentrations of urea to renature the protein. We then immunized rabbits with the renatured, full-length, SARS-CoV nucleocapsid protein to generate an affinity-purified rabbit anti–SARS-CoV nucleocapsid protein polyclonal antibody.

Results

A patient was identified with confirmed COVID-19 in Washington State on January 22, 2020. CPE was not observed in mock infected cells (Figure 1, panel A). Cycle threshold (C_t) values were 18–20 for NP specimens and 21–22 for OP specimens (*1*). The positive clinical specimens were aliquoted and refrozen inoculated into cell culture on January 22, 2020. We observed CPE 2 days postinoculation and harvested viral lysate on day 3 postinoculation (Figure 1, panels B, C). We used 50 μL of passage 1 viral lysates for nucleic acid extraction to confirm the presence of SARS-CoV-2 by using the CDC molecular diagnostic assay (*1*). The C_t values of 3 nucleic acid extractions were 16.0–17.1 for nucleocapsid portion 1, 15.9–17.1 for nucleocapsid portion 2, and 16.2–17.3 for nucleocapsid portion 3, which confirmed isolation of SARS-CoV-2 (C_t <40 is considered a positive result). We also tested extracts for 33 additional different respiratory pathogens by using the Fast Track 33 Assay. No other pathogens were detected. Identity was additionally supported by thin-section electron microscopy (Figure 1, panel D). We observed a morphology and morphogenesis characteristic of coronaviruses.

We used isolates from the first passage of an OP and an NP specimen for whole-genome sequencing. The genomes from the NP specimen (GenBank accession MT020880) and OP specimen (GenBank accession no. MT020881) showed 100% identity with each other. The isolates also showed 100% identity with the corresponding clinical specimen (GenBank accession no. MN985325).

After the second passage, we did not culture OP and NP specimens separately. We passaged virus isolate 2 more times in Vero CCL-81 cells and titrated by determining the 50% tissue culture infectious dose ($TCID_{50}$). Titers were 8.65×10^6 $TCID_{50}$/mL for the third passage and 7.65×10^6 $TCID_{50}$/mL for the fourth passage.

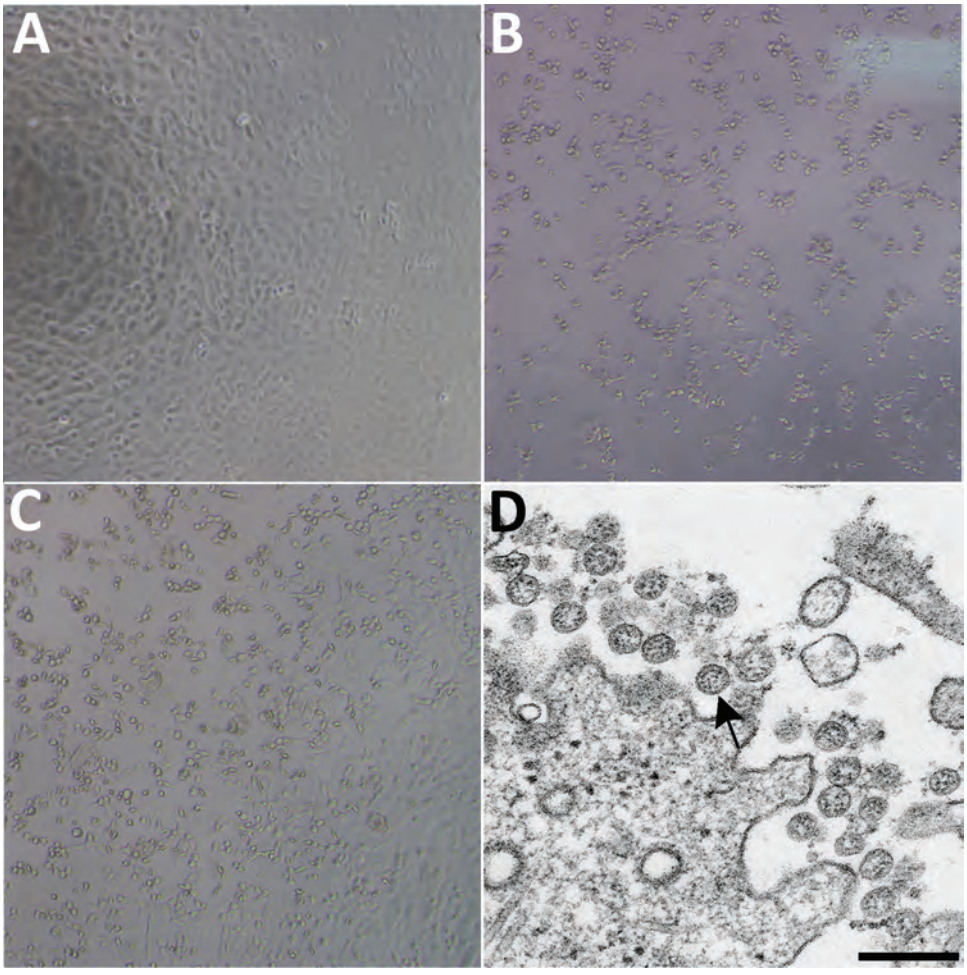

Figure 1. Cytopathic effect caused by severe acute respiratory syndrome coronavirus 2 from patient with coronavirus disease, United States, 2020. A–C) Phase-contrast microscopy of Vero cell monolayers at 3 days postinoculation: A) Mock, B) nasopharyngeal specimen, C) oropharyngeal specimen. Original magnifications ×10). D) Electron microscopy of virus isolate showing extracellular spherical particles with cross-sections through the nucleocapsids (black dots). Arrow indicates a coronavirus virion budding from a cell. Scale bar indicates 200 nm.

We passaged this virus in the absence of trypsin. The spike protein sequence of SARS-CoV-2 has an RRAR insertion at the S1-S2 interface that might be cleaved by furin (*16*). Highly pathogenic avian influenza viruses have highly basic furin cleavage sites at the hemagglutinin protein HA1-HA2 interface that permit intracellular maturation of virions and more efficient viral replication (*17*). The RRAR insertion in SARS-CoV-2 might serve a similar function.

We subsequently generated a fourth passage stock of SARS-CoV-2 on VeroE6 cells, another fetal rhesus monkey kidney cell line. We sequenced viral RNA from SARS-CoV-2 passage 4 stock and confirmed it to have no nucleotide mutations compared with the original reference sequence (GenBank accession no. MN985325). SARS-CoV has been found to grow well on VeroE6 cells and MERS-CoV on Vero CCL81 cells (*18,19*). To establish a plaque assay and determine the preferred Vero cell type for quantification, we titered our passage 4 stock on VeroE6 and VeroCCL81 cells. After infection with a dilution series, SARS-CoV-2 replicated in both Vero cell types; however, the viral titers were slightly higher in VeroE6 cells than in Vero CCL81 cells (Figure 2, panel A). In addition, plaques were more distinct and visible on Vero E6 cells (Figure 2, panel B). As early as 2 days postinoculation, VeroE6 cells produced distinct plaques visible by staining with neutral red. In contrast, Vero CCL81 cells produced less clear plaques and was most easily quantitated by staining with neutral red 3 days postinoculation. On the individual plaque monolayers, SARS-CoV-2 infection of Vero E6 cells produced CPE with areas of cell clearance (Figure 2, panel C). In contrast, Vero CCL81 cells had areas of dead cells that had fused to form plaques, but the cells did not clear. Together, these results suggest that VeroE6 cells might be the best choice for amplification and quantification, but both Vero cell types support amplification and replication of SARS-CoV-2.

Because research has been initiated to study and respond to SARS-CoV-2, information about cell lines and types susceptible to infection is needed. Therefore, we examined the capacity of SARS-CoV-2 to infect and replicate in several common primate and human cell lines, including human adenocarcinoma

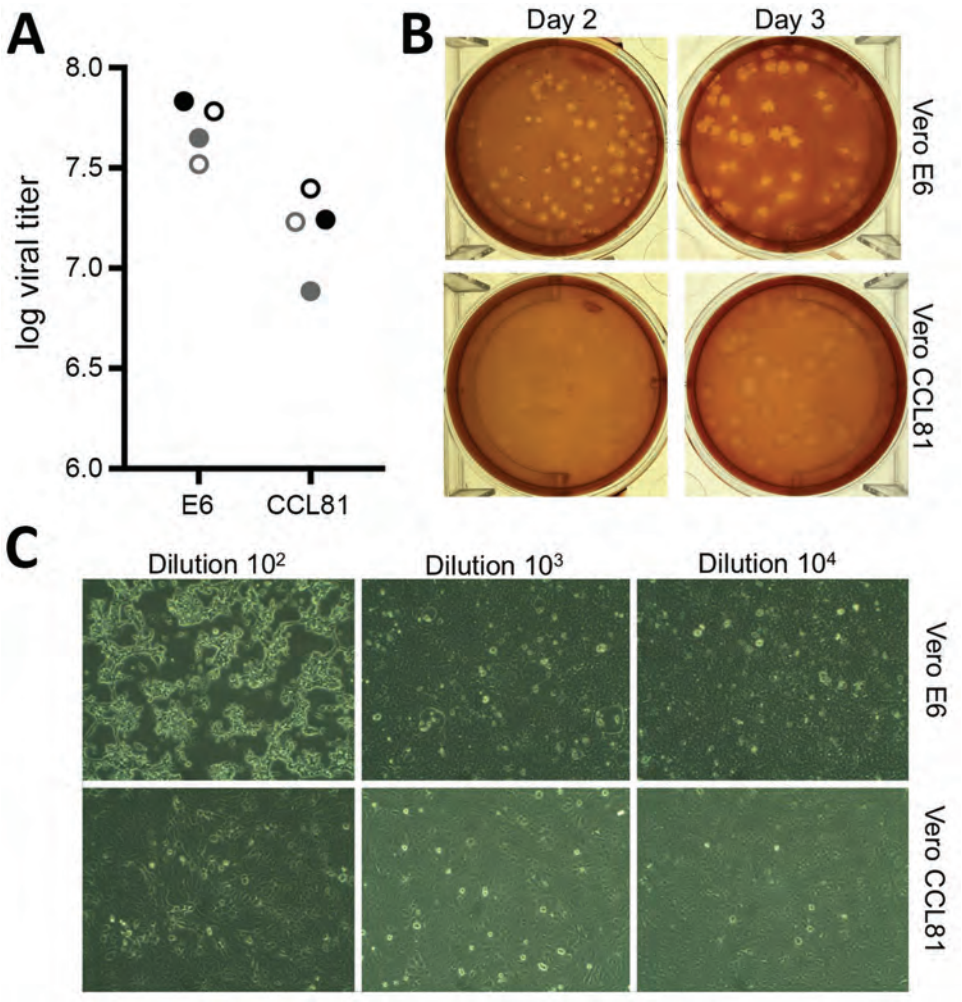

Figure 2. Viral propagation and quantitation of severe acute respiratory syndrome coronavirus 2 from patient with coronavirus disease, United States, 2020. A) Two virus passage 4 stocks (black and gray circles) were quantified by using plaque assay at day 2 (solid circles) and day 3 (open circles) postinfection of Vero E6 and Vero CCL81 cells. B) Plaque morphology for virus on Vero E6 and Vero CCL81 at day 2 and day 3 postinoculation. C) Cell monolayers 2 days postinfection of Vero E6 (top) and Vero CCL81 (bottom) at 3 dilutions. Original magnifications ×40.

cells (A549), human liver cells (HUH7.0), and human embryonic kidney cells (HEK-293T), in addition to Vero E6 and Vero CCL81 cells. We also examined an available big brown bat kidney cell line (EFK3B) for SARS-CoV-2 replication capacity. Each cell line was inoculated at high multiplicity of infection and examined 24 h postinfection (Figure 3, panel A). No CPE was observed in any of the cell lines except in Vero cells, which grew to >10^7 PFU at 24 h postinfection. In contrast, HUH7.0 and 293T cells showed only modest viral replication, and A549 cells were incompatible with SARS-CoV-2 infection. These results are consistent with previous susceptibility findings for SARS-CoV and suggest other common culture systems, including MDCK, HeLa, HEP-2, MRC-5 cells, and embryonated eggs, are unlikely to support SARS-CoV-2 replication (*20*–*22*). In addition, SARS-CoV-2 did not replicate in bat EFK3B cells, which are susceptible to MERS-CoV. Together, the results indicate that SARS-CoV-2 maintains a similar profile to SARS-CoV in terms of susceptible cell lines.

Having established robust infection with SARS-CoV-2 in several cell types, we next evaluated the cross-reactivity of SARS-CoV antibodies against the SARS-CoV-2. Cell lysates from infected cell lines were probed for protein analysis; we found that polyclonal serum against the SARS-CoV spike protein and nucleocapsid proteins recognize SARS-CoV-2 (Figure 3, panels B, C). The nucleocapsid protein, which is highly conserved across the group 2B family, retains >90% amino acid identity between SARS-CoV and SARS-CoV-2. Consistent with the replication results (Figure 3, panel A), SARS-CoV-2 showed robust nucleocapsid protein in both Vero cell types, less protein in HUH7.0 and 293T cells, and minimal protein in A549 and EFK3B cells (Figure 3, panel B). The SARS-CoV spike protein antibody also recognized SARS-CoV-2 spike protein, indicating cross-reactivity (Figure 3, panel C). Consistent with SARS CoV, several cleaved and uncleaved forms of the SARS-CoV-2 spike protein were observed. The cleavage pattern of the SARS spike positive control from Calu3 cells, a respiratory

cell line, varies slightly and could indicate differences between proteolytic cleavage of the spike proteins between the 2 viruses because of a predicted insertion of a furin cleavage site in SARS-CoV-2 (*16*). However, differences in cell type and conditions complicate this interpretation and indicate the need for further study in equivalent systems. Overall, the protein expression data from SARS-CoV nucleocapsid and spike protein antibodies recapitulate replication findings and indicate that SARS-CoV reagents can be used to characterize SARS-CoV-2 infection.

Finally, we evaluated the replication kinetics of SARS-CoV-2 in a multistep growth curve. In brief, we infected Vero CCL-81 and HUH7.0 cells with SARS-CoV-2 at a low multiplicity of infection (0.1) and evaluated viral replication every 6 h for 72 h postinoculation, with separate harvests in the cell-associated and supernatant compartments (Figure 4). Similar to SARS-CoV, SARS-CoV-2 replicated rapidly in Vero cells after an initial eclipse phase, achieving 10^5 $TCID_{50}$/mL by 24 h postinfection and peaking at >10^6 $TCID_{50}$/mL. We observed similar titers in cell-associated and supernatant compartments, which indicated efficient egress. Despite peak viral titers by 48 h postinoculation, major CPE was not observed until 60 h postinoculation and peaked at 72 h postinoculation, indicating that infected monolayers should be harvested before peak CPE is observed. Replication in HUH7.0 cells also increased quickly after an initial eclipse phase but plateaued by 24 h postinoculation in the intracellular compartment at 2 × 10^3 $TCID_{50}$/mL and decreased after 66 h postinoculation. Virus was not detected in the supernatant of infected HUH7 cells until 36 h postinoculation and exhibited lower titers at all timepoints (Figure 4). Major CPE was never observed in HUH7.0 cells. These results are consistent with previous reports for SARS-CoV and MERS-CoV, which suggested similar replication dynamics between the zoonotic CoV strains (*23*,*24*).

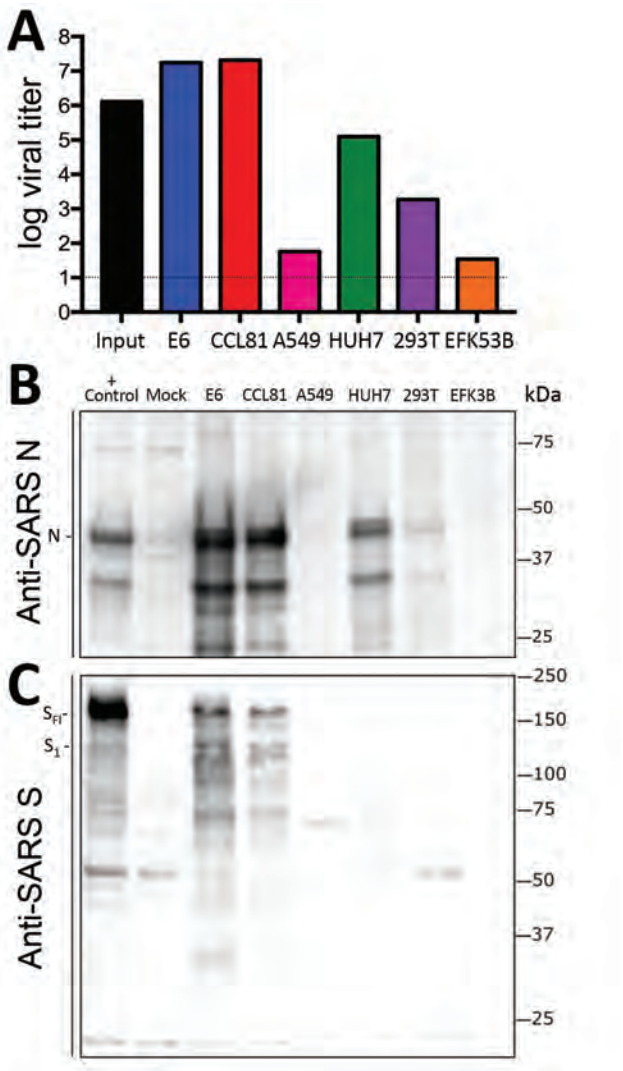

Figure 3. Cell lines from patient with coronavirus disease, United States, 2020, susceptible to SARS coronavirus 2 (SARS-CoV-2). Cell lines were infected with a high multiplicity of infection (>5), washed after adsorption, and subsequently harvested 24 h postinfection for viral titer and protein lysates. A) Viral titer for SARS-CoV-2 quantitated by plaque assay on Vero E6 cells 2 days postinoculation. Infected cell protein lysates were probed by using Western blotting with B) rabbit polyclonal anti-SARS N antibody or C) anti–SARS-CoV S protein antibody. Full-length spike protein (S_{FL}) and spike protein S1 (S_1) are indicated. N, nucleocapsid; S, spike protein; SARS, severe acute respiratory syndrome.

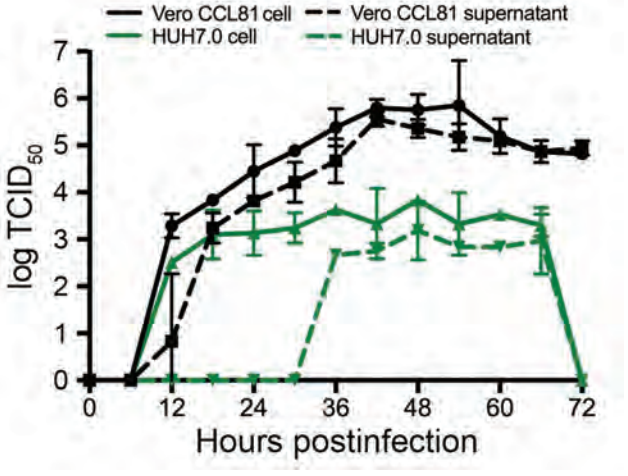

Figure 4. Multistep growth curve for severe acute respiratory syndrome coronavirus 2 from patient with coronavirus disease, United States, 2020. Vero CCL81 (black) and HUH7.0 cells (green) were infected at a multiplicity of infection of 0.1, and cells (solid line) and supernatants (dashed line) were harvested and assayed for viral replication by using $TCID_{50}$. Circles, Vero CCL81 cells; squares, Vero CCL81 supernatants; triangles, HUH7.0 cells; inverted triangles, HUH7.0 supernatants. Error bars indicate SEM. $TCID_{50}$, 50% tissue culture infectious dose.

Discussion

We have deposited information on the SARS-CoV-2 USA-WA1/2020 viral strain described here into the Biodefense and Emerging Infections Research Resources Repository (https://www.beiresources.org) reagent resources (American Type Culture Collection, https://www.atcc.org) and the World Reference Center for Emerging Viruses and Arboviruses, University of Texas Medical Branch (https://www.utmb.edu/wrceva), to serve as the SARS-CoV-2 reference strain for the United States. The SARS-CoV-2 fourth passage virus has been sequenced and maintains a nucleotide sequence identical to that of the original clinical strain from the United States. These deposits make this virus strain available to the domestic and international public health, academic, and pharmaceutical sectors for basic research, diagnostic development, antiviral testing, and vaccine development. We hope broad access will expedite countermeasure development and testing and enable a better understanding of the transmissibility and pathogenesis of this novel emerging virus.

Acknowledgments

We thank Mavanur R. Suresh for providing plasmid pBM302, which expresses the SARS-CoV nucleocapsid protein.

The reagent described is available through the Biodefense and Emerging Infections Research Resources Repository, National Institutes of Allergy and Infectious Diseases, National Institutes of Health: SARS-related coronavirus 2, isolate USA-WA1/2020, NR-52281.

This study was supported by grants from the National Institute on Aging and the National Institutes of Allergy and Infectious Diseases of the National Institutes of Health (U19AI100625 and R00AG049092 to V.D.M., R24AI120942 to S.C.W., and AI99107 and AI114657 to S.M.); a STARs Award provided by the University of Texas System to V.D.M.; the Institute for Human Infections and Immunity at the University of Texas Medical Branch (S.M.); and trainee funding provided by the McLaughlin Fellowship Fund at the University of Texas Medical Branch.

About the Author

Dr. Harcourt is a microbiologist in the National Center for Immunization and Respiratory Diseases, Centers for Disease Control and Prevention, Atlanta, GA. Her research interests are emerging coronavirus replication and antibody responses.

References

1. Holshue ML, DeBolt C, Lindquist S, Lofy KH, Wiesman J, Bruce H, et al.; Washington State 2019-nCoV Case Investigation Team. First case of 2019 novel coronavirus in the United States. N Engl J Med. 2020;382:929–36. https://doi.org/10.1056/NEJMoa2001191
2. Zhu N, Zhang D, Wang W, Li X, Yang B, Song J, et al.; China Novel Coronavirus Investigating and Research Team. A novel coronavirus from patients with pneumonia in China, 2019. N Engl J Med. 2020;382:727–33. https://doi.org/10.1056/NEJMoa2001017
3. Lu R, Zhao X, Li J, Niu P, Yang B, Wu H, et al. Genomic characterisation and epidemiology of 2019 novel coronavirus: implications for virus origins and receptor binding. Lancet. 2020;395:565–74. https://doi.org/10.1016/S0140-6736(20)30251-8
4. Chan JF, Kok KH, Zhu Z, Chu H, To KK, Yuan S, et al. Genomic characterization of the 2019 novel human-pathogenic coronavirus isolated from a patient with atypical pneumonia after visiting Wuhan. Emerg Microbes Infect. 2020;9:221–36. https://doi.org/10.1080/22221751.2020.1719902
5. Li Q, Guan X, Wu P, Wang X, Zhou L, Tong Y, et al. Early transmission dynamics in Wuhan, China, of novel coronavirus-infected pneumonia. N Engl J Med. 2020 Jan 29 [Epub ahead of print]. https://doi.org/10.1056/NEJMoa2001316
6. Chen N, Zhou M, Dong X, Qu J, Gong F, Han Y, et al. Epidemiological and clinical characteristics of 99 cases of 2019 novel coronavirus pneumonia in Wuhan, China: a descriptive study. Lancet. 2020;395:507–13. https://doi.org/10.1016/S0140-6736(20)30211-7
7. Chan JF, Yuan S, Kok KH, To KK, Chu H, Yang J, et al. A familial cluster of pneumonia associated with the 2019 novel coronavirus indicating person-to-person transmission: a study of a family cluster. Lancet. 2020;395:514–23. https://doi.org/10.1016/S0140-6736(20)30154-9
8. Wan Y, Shang J, Graham R, Baric RS, Li F. Receptor recognition by novel coronavirus from Wuhan: an analysis based on decade-long structural studies of SARS. J Virol. 2020 Jan 29 [Epub ahead of print]. https://doi.org/10.1128/JVI.00127-20
9. Sims AC, Tilton SC, Menachery VD, Gralinski LE, Schäfer A, Matzke MM, et al. Release of severe acute respiratory syndrome coronavirus nuclear import block enhances host transcription in human lung cells. J Virol. 2013;87:3885–902. https://doi.org/10.1128/JVI.02520-12
10. Josset L, Menachery VD, Gralinski LE, Agnihothram S, Sova P, Carter VS, et al. Cell host response to infection with novel human coronavirus EMC predicts potential antivirals and important differences with SARS coronavirus. MBio. 2013;4:e00165–13. https://doi.org/10.1128/mBio.00165-13
11. Bolger AM, Lohse M, Usadel B. Trimmomatic: a flexible trimmer for Illumina sequence data. Bioinformatics. 2014;30:2114–20. https://doi.org/10.1093/bioinformatics/btu170
12. Simpson JT, Wong K, Jackman SD, Schein JE, Jones SJ, Birol I. ABySS: a parallel assembler for short read sequence data. Genome Res. 2009;19:1117–23. https://doi.org/10.1101/gr.089532.108
13. Li H, Durbin R. Fast and accurate short read alignment with Burrows-Wheeler transform. Bioinformatics. 2009;25:1754–60. https://doi.org/10.1093/bioinformatics/btp324
14. Robinson JT, Thorvaldsdóttir H, Winckler W, Guttman M, Lander ES, Getz G, et al. Integrative genomics viewer. Nat Biotechnol. 2011;29:24–6. https://doi.org/10.1038/nbt.1754

15. Das D, Suresh MR. Copious production of SARS-CoV nucleocapsid protein employing codon optimized synthetic gene. J Virol Methods. 2006;137:343–6. https://doi.org/10.1016/j.jviromet.2006.06.029
16. Coutard B, Valle C, de Lamballerie X, Canard B, Seidah NG, Decroly E. The spike glycoprotein of the new coronavirus 2019-nCoV contains a furin-like cleavage site absent in CoV of the same clade. Antiviral Res. 2020;176:104742. https://doi.org/10.1016/j.antiviral.2020.104742
17. Stieneke-Gröber A, Vey M, Angliker H, Shaw E, Thomas G, Roberts C, et al. Influenza virus hemagglutinin with multibasic cleavage site is activated by furin, a subtilisin-like endoprotease. EMBO J. 1992;11:2407–14. https://doi.org/10.1002/j.1460-2075.1992.tb05305.x
18. Li W, Moore MJ, Vasilieva N, Sui J, Wong SK, Berne MA, et al. Angiotensin-converting enzyme 2 is a functional receptor for the SARS coronavirus. Nature. 2003;426:450–4. https://doi.org/10.1038/nature02145
19. Chan JF, Chan KH, Choi GK, To KK, Tse H, Cai JP, et al. Differential cell line susceptibility to the emerging novel human betacoronavirus 2c EMC/2012: implications for disease pathogenesis and clinical manifestation. J Infect Dis. 2013;207:1743–52. https://doi.org/10.1093/infdis/jit123
20. Gillim-Ross L, Taylor J, Scholl DR, Ridenour J, Masters PS, Wentworth DE. Discovery of novel human and animal cells infected by the severe acute respiratory syndrome coronavirus by replication-specific multiplex reverse transcription-PCR. J Clin Microbiol. 2004;42:3196–206. https://doi.org/10.1128/JCM.42.7.3196-3206.2004
21. Kaye M, Druce J, Tran T, Kostecki R, Chibo D, Morris J, et al. SARS-associated coronavirus replication in cell lines. Emerg Infect Dis. 2006;12:128–33. https://doi.org/10.3201/eid1201.050496
22. Swayne DE, Suarez DL, Spackman E, Tumpey TM, Beck JR, Erdman D, et al. Domestic poultry and SARS coronavirus, southern China. Emerg Infect Dis. 2004;10:914–6. https://doi.org/10.3201/eid1005.030827
23. Scobey T, Yount BL, Sims AC, Donaldson EF, Agnihothram SS, Menachery VD, et al. Reverse genetics with a full-length infectious cDNA of the Middle East respiratory syndrome coronavirus. Proc Natl Acad Sci U S A. 2013;110:16157–62. https://doi.org/10.1073/pnas.1311542110
24. Yount B, Curtis KM, Fritz EA, Hensley LE, Jahrling PB, Prentice E, et al. Reverse genetics with a full-length infectious cDNA of severe acute respiratory syndrome coronavirus. Proc Natl Acad Sci U S A. 2003;100:12995–3000. https://doi.org/10.1073/pnas.1735582100

Address for correspondence: Natalie J. Thornburg, Center for Disease Control and Prevention, 1600 Clifton Rd NE, Mailstop H18-6, Atlanta GA 30329-4027, USA; email: nax3@cdc.gov

Syphilis in Maria Salviati (1499–1543), Wife of Giovanni de' Medici of the Black Bands

Antonio Fornaciari, Raffaele Gaeta, Simona Minozzi, Valentina Giuffra

Researchers from the Division of Paleopathology of Pisa University (Pisa, Italy) exhumed the well-preserved skeleton of Maria Salviati (1499–1543), wife of Giovanni de' Medici, named "Giovanni of the Black Bands," in Florence in 2012. Many lytic lesions had affected the skull of Maria on the frontal bone and on the parietal bones. These lesions are pathognomonic for syphilis. An ancient diagnosis of syphilis for Maria Salviati does not emerge from the historical sources, although the symptoms manifested in her last years of life are compatible with a colorectal localization, including severe hemorrhages, caused by syphilitic infection. The case of Maria Salviati can be compared with those of other famous Italian noblewomen of the Renaissance, such as Isabella of Aragon (1470–1524) and Maria of Aragon (1503–1568). Paleopathology made it possible to directly observe a "secret illness" to which noblewomen were susceptible as a result of the sexual conduct of their husbands.

Syphilis today is a reemerging infectious disease that affects not only the developing countries but also the Western world. In recent years, a new increase has occurred in the incidence of sexually transmitted diseases, among which syphilis is one of the most common (*1*). Especially in the United States, the rates of primary and secondary syphilis have increased since 2000–2001. A total of 27,814 syphilis cases were reported in 2016 (*2*). During 2015–2016, the US syphilis rate increased by 17.6%, reaching 8.7 cases/100,000 population, the highest rate reported since 1993 (*2*). Europe experienced a similar trend; in 2016, a total of 29,365 confirmed syphilis cases were reported in 28 countries, a rate of 6.1 cases/100,000 population. The highest rates (cases/100,000 population) in Europe were observed in the United Kingdom (9.9), Malta (9.2), Iceland (9.0), and Germany (8.7) (*3*).

Author affiliation: University of Pisa, Pisa, Italy

DOI: https://doi.org/10.3201/eid2606.180786

Venereal syphilis is a treponematosis caused by the bacterium *Treponema pallidum* subsp. *pallidum*, the most widespread disease among the 4 treponematoses. Pinta (*T. carateum* infection) is spread only in tropical areas of the Americas, yaws (*T. pallidum* subsp. *pertenue* infection) in humid tropical and subtropical regions, and bejel (*T. pallidum* subsp. *endemicum* infection) in arid-temperate and subtropical rural areas. All these diseases involve the human bone, with the exception of pinta. Three clinical stages are typical of venereal syphilis: the primary stage is a painless lesion (chancre) on the genitals, which heals in 2–6 weeks; some months later, the secondary stage is characterized by a widespread skin rash; and several years later, the tertiary stage involves different organs, including the skeleton (*4*).

Venereal syphilis first emerged in Europe at the end of the 15th century, as a result of the sexual and social behavior of the time (*5*). Soon after the disease's arrival, its sexually transmitted nature was recognized, becoming a mark of immoral behavior (*6*); however, the social implication of syphilis was not the same for men and women, especially in the aristocracy (*7*). In fact, the sexual conduct of the noblemen and the possible infectious diseases that followed were not subject to moral censorship; instead, there was severe moral judgement for venereal diseases in noblewomen (*7*–*9*). Some paleopathological cases have indicated the impact of syphilis on the aristocratic classes of the Renaissance (*10*–*12*). Paleopathology offers a source for increasing the diagnosis of infection in the past and for understanding the social and cultural impact of infectious diseases in previous populations. The models obtained can be compared with what happens today with emerging and reemerging diseases and can serve to refine the systems of prevention and fight against future infection outbreaks (*13*). The study of the skeletal remains of Maria Salviati (1499–1543), wife of Giovanni de'

Figure 1. Portrait of Maria Salviati and Giulia de' Medici depicted by Pontormo (Jacopo Carucci) in 1537 c. Oil on panel. 34.65 × 28.07 in. (88 × 71.3 × 1 cm). (The Walters Art Museum, Baltimore.)

Medici, which revealed lesions typical of third-stage syphilis, has enabled us to understand the dynamics of the infection in one of the most famous families of the Renaissance and to examine the perception of the illness in 16th century Europe.

Syphilis in the 16th Century

After the 1494 invasion of Italy by the troops of Charles VIII, King of France (1470–1498), venereal syphilis had a pandemic spread in Italy and in Europe (*9*). The origin of the disease remains one of the greatest issues in the history of medicine and is still discussed by scholars. One theory suggests the disease originated in the Americas and was introduced by Columbus' crew returning to Europe from the New World in 1493. According to a second theory, syphilis previously existed in the Old World but went unrecognized until the late 15th century, when there was increased prevalence and virulence of the disease (*14*). In the past few years, further paleopathologic evidence has indicated the presence of the disease in Europe before 1492 (*15*,*16*). However, the transmission at the end of the 15th century is undeniable and can be explained in the light of the wider sociocultural context of the period (*17*,*18*).

From the late 15th to mid-16th centuries, Italy was a great field of war and an ideal social environment for the spread of the disease. In the Renaissance, before the advent of the Catholic Counter-Reformation, Italy experienced an increase in the volume of trade exchanges, new contacts between populations, migration from other countries, and, above all, a time of greater sexual liberty (*5*,*19*). The activity of prostitution among the troops and the civilians in the towns, as well as the opportunities for extramarital sex created by the permanence of armies, generated a perfect basis for the spread of syphilis (*7*,*9*). Because of its sexual connotation, the disease embodied the concept of divine ill-punishment, which, as an archetype, pervaded the popular religious sensibility of European populations of the early modern age (*20*). The early pandemic and violent phase of syphilis, before the classical chronicization to three stages, had an impressive impact on European society (*5*,*21*).

The first physician observing syphilis was Alessandro Benedetti, field doctor of the Italian confederate army fighting against the French during the battle of Fornovo in 1495 (*22*). Girolamo Fracastoro (1548) successfully coined the name of the disease in his famous

Figure 2. Portrait of an Elderly Lady (Maria Salviati) depicted by Agnolo Bronzino in 1542–1543 c. Oil on panel. 50 × 39.4 in. (127 × 100 cm). (San Francisco, The Fine Arts Museum of San Francisco, Gift of Mr. Samuel H. Kress, 53670. Image courtesy the Fine Arts Museums of San Francisco).

poem "Syphilis sive morbus gallicus [Syphilis or the French disease]" (*23*). Contemporary physicians described the manifestation of the disease, consisting in the appearance of an ulceration on the penis, followed by pustules and sores all over the face and body with joint pain and pruritus. The doctors quickly acknowledged that the infection had been transmitted through sexual intercourse (*17*). After the most aggressive first phase of the "new" disease, syphilis quickly changed from an acute and debilitating disease into a less severe chronic infection, probably because the selection of the less virulent strains represented an evolutionary advantage for the pathogen (*21*).

Syphilis was rife in all social classes and affected many members of the aristocracy. Many noblemen undertook military careers as captains of mercenary troops, which typically involved extramarital affairs, not only with regular lovers but also, and frequently, with prostitutes (*24*). Famous are the cases of Cesare Borgia (1476–1507), son of Pope Alexander VI, who had to wear a leather mask covering half of his face, which had been disfigured by syphilis in his later years (*25*), and of Francesco II Gonzaga (1466–1519), Marquis of Mantua, who had a form of tertiary syphilis (*23*). Evidence that the disease was widespread in the 16th century aristocratic classes is also demonstrated by paleopathology. The cases of Maria of Aragon, Marquise of Vasto (1503–1568) (*10*), Vespasiano Gonzaga, Duke of Sabbioneta (1531–1591) (*11*), and Cardinal Giulio Della Rovere (1533–1578) (*12*) are some of the most famous Renaissance figures for whom syphilis was diagnosed.

Brief Biography and Nosography of Maria Salviati

Maria Salviati, daughter of Lucrezia de' Medici and Jacopo Salviati and granddaughter of Lorenzo the Magnificent, was born in Florence in 1499. Her marriage to Giovanni de' Medici (1498–1526) took place in 1516. Giovanni died of gangrene and septicemia (*26*) on November 30, 1526, complications resulting from an injury and amputation of his right leg after the Battle of Governolo, near Mantua, leaving his wife a widow at the age of 27. Maria never remarried. Cosimo, the son of Maria and Giovanni, was called to govern Florence after the death of Duke Alessandro de' Medici (1537), giving rise to the Grand Ducal Medici branch, which ruled Tuscany until 1737.

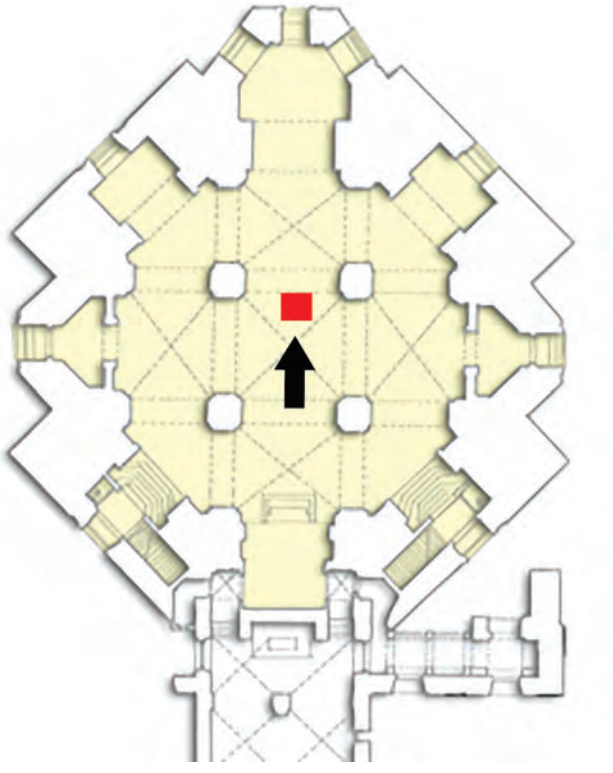

Figure 3. Plan of the crypt of the Medici Chapel with the position of the tomb of Maria Salviati. (Archive of the Division of Paleopathology. University of Pisa.)

Archival research by Gaetano Pieraccini was able to reveal important information about Maria Salviati, with particular regard to the last years of her life (*24*). Until 1540, she enjoyed good health, except for a brief episode of fever of unknown origin recorded

Figure 4. The skeletal remains of Maria Salviati at exhumation in 2012. (Archive of the Division of Paleopathology. University of Pisa.)

in 1517. In the last 3 years of her life, from May 1541 to her death on December 29, 1543, many symptoms of severe illness were described in letters sent by Andrea Pasquali, the court physician, to Duke Cosimo, including abundant recurring proctorrhagias (bleeding from the rectum from ½ to 3 libras of blood [i.e., 180 g to ≈1 L]), rectal and perianal ulcers, headaches, and abdominal colic. The letters also report "chronic weakness…, shortness of breath, frequent lipothymic episodes, severe syncopes, cold extremities, vomit and agitation…" and note "the pulse was deeply reduced, the frequency increased" (*24*). The symptoms were certainly the expression of a severe anemia caused by chronic leakages of blood.

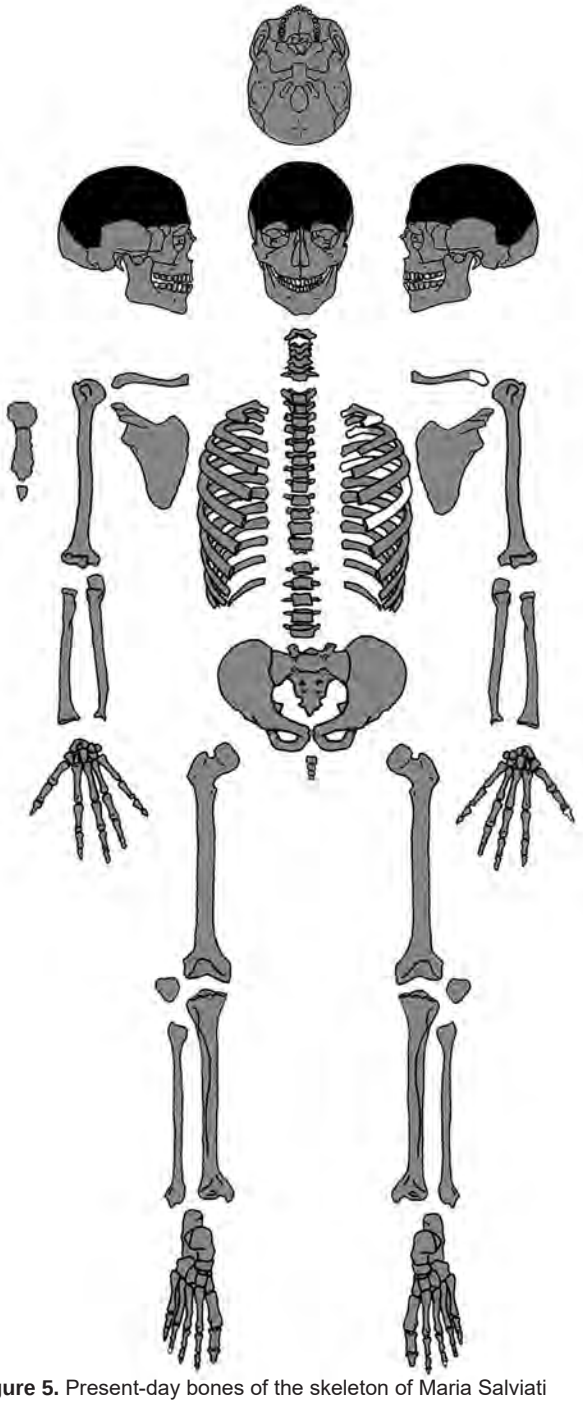

Figure 5. Present-day bones of the skeleton of Maria Salviati (gray). Distribution of lesions (black). (Archive of the Division of Paleopathology. University of Pisa.)

The portraits of Maria Salviati clearly show the significant changes that occurred in her aspect, marking the progress in terms both of age and of illness. A portrait by Jacopo Pontormo (Figure 1), painted in 1537 and preserved at the Uffizi Museum, shows Maria as a beautiful lady, still young; but only 6 years later, in a portrait by Bronzino (Figure 2), she appears as a very old woman. Rather than to the artistic choices of the painter, this transformation seems to be strongly related to the accelerating physical decay of Maria, which was probably connected to the illness in the last years of her life.

Historical, Archeological, and Taphonomic Background

Almost all the bodies of the Medici, and also that of Maria Salviati, were embalmed before burial (*24*), but it was not until the mid-19th century that they were given a definitive grave location. Until the 19th century, the bodies of the Medici of the Grand Duchy dynasty were preserved in wooden coffins inside the 2 sacristies of the Basilica of San Lorenzo in Florence. During 1857–58, the Gran Duke of Tuscany Leopold II of Lorrain arranged the bodies of the Medici in the crypt of the Medici Chapel to give a proper and dignified burial place to the founders of the Grand Duchy of Tuscany (*27*). The body of Maria Salviati, identified in 1857 thanks to the presence of a copper epigraph on the coffin (*28*), was deposed, together with that of her husband Giovanni "of the Black Bands," in a tomb at the center of the crypt floor (Figure 3). We have a description of this event given by Luigi Passerini-Rilli, director of the State Archive of Florence and responsible for the recognition of the bodies of the Grand Dukes (*28*): "The body, although reduced to almost a skeleton in the face, was however very well preserved in the other parts.... The head lay on two bricks.... The clothing that covered it resembled that of a nun, i.e. a black cloth, but eaten by the moths: the leftovers of the wimple were still discernible, though the veil that at first covered the head, was worn...."

In 1946, Gaetano Pieraccini and the anthropologist Giuseppe Genna conducted an exhumation (*29*); they heavily manipulated the skeletal remains of Maria with the removal of residual soft tissues before reburial in a small zinc coffin (*27*). On this occasion, they made a plaster cast of the skull, which is now in the Museum

Figure 6. The skull of Maria Salviati in frontal view. Cavitations on the frontal bone are apparent. (Archive of the Division of Paleopathology. University of Pisa.)

of Anthropology of Florence. In November 2012 the last exhumation took place, under the management of the Division of Paleopathology of the University of Pisa, during some architectural checks of the stability of the floor of the Chapel. The paleopathologists found that the remains of Maria were in excellent state of preservation, unconnected in a small zinc coffin bearing an epigraph with her name (Figure 4).

Anthropologic and Paleopathologic Study

We examined the nearly complete skeleton of Maria Salviati macroscopically (Figure 5) and performed radiographic and computed tomography (CT) scans. We compared the skull bone recovered during exhumation with the skull cast, and they showed the same lesions. The anthropologic study of the skeleton revealed a female individual (*30*), 40–45 years of age (*31*–*34*), with a stature of 1.56 m (*34*). Maria had severe periodontal disease, as evidenced by the resorption of alveolar edges and an abscess at the buccal portion of the third right maxillary molar. Nonpenetrating caries affected 10 teeth, of which 4 were mandibular and 6 maxillary. The poor dental health of Maria is consistent with that of the other members of the Medici family (*35*). We detected many lytic lesions on the skull. Two circular ectocranial depressions are visible on the frontal bone, on the glabella and above the left supraorbital ridge. They are irregularly elliptical in shape, measuring ≈1 × 0.7 cm and 0.5 × 0.4 cm, respectively, with a central destructive focus and a reactive compact bone formation on the margins (Figure 6). These frontal bone lesions are consistent with 2 destructive osteolytic inflammatory processes, in advanced reparative phase, as clearly revealed by CT examination (Figures 7, 8). Furthermore, the cranial vault on the parietal bones shows several osteolytic lesions in the form of circumvallate depressed areas with fine scar lines radiating inside the shallow depressions (Figures 9, 10). CT examination confirms the lytic and reparative nature of the lesions, which are morphologically similar to internodular stellate depressions. We observed no other lesions in the postcranial bones macroscopically, by radiograph, or by CT scan. The presence of strong bone reaction excludes metastatic osteolytic carcinoma, multiple myeloma, tuberculosis, and fungal bone infections (*36*,*37*). The presence of superficial circumvallated cavitations with radial scars is pathognomonic of cranial syphilis (caries sicca) (*38*).

Discussion

The combination of crater-like lesions, such as circumvallate cavitations on the frontal bone (phase 4

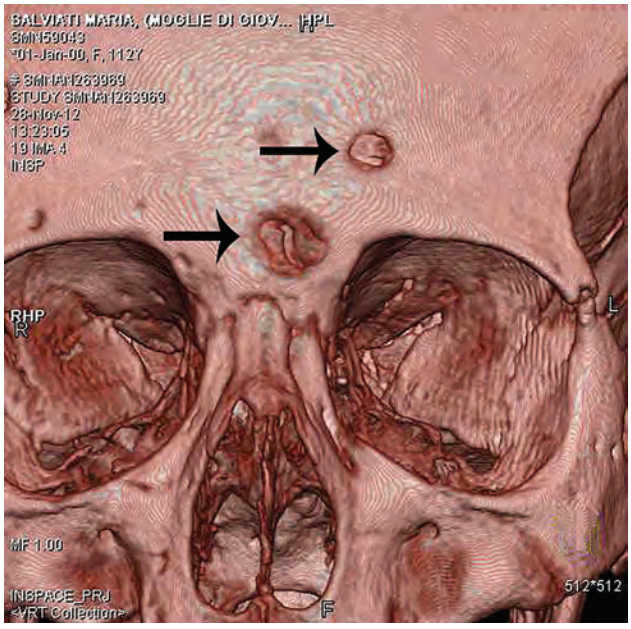

Figure 7. Volume rendering of the skull of Maria Salviati. Two destructive osteolytic inflammatory processes, in advanced reparative phase (circumvallate cavitations), are apparent. (Archive of the Division of Paleopathology. University of Pisa.)

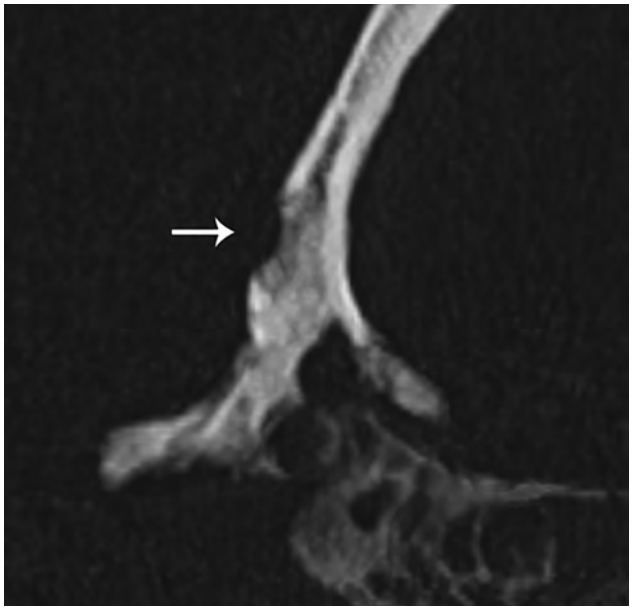

Figure 8. Computed tomography scan of frontal bone with an osteolytic lesion with sclerotic walls (circumvallate cavitations). (Archive of the Division of Paleopathology. University of Pisa.)

in the Caries Sicca sequence depicted in Hackett [*38*]), and circumvallate cavitations with radial scars on the parietal bones (phase 5 in the Caries Sicca sequence [*38*]) is pathognomonic for tertiary syphilis. Pathography attests that Maria had abundant recurring proctorrhagias. This symptom strongly suggests tertiary syphilis with cranial and possible colorectal localization. Apart from proctorrhagias, the other symptoms, such as frequent fever and headache, abdominal colic, rectal and perianal ulcers, reported by the written sources are very compatible with tertiary syphilis (*4*,*39*,*40*) but were not attributed to syphilis by the physicians of that time nor by the nosographic scholars in recent times (*24*). Nevertheless, rectal syphilis is a rare disease that usually shows proctitis with perianal ulcers but lacks pathognomonic clinical symptoms, making diagnosis difficult. In clinical medicine, anal syphilis could be easily misdiagnosed as cancer or advanced stage hemorrhoids, upholding the reputation of syphilis as the "great mimicker" (*41*).

One hypothesis is that the contemporary physicians might have correctly diagnosed and recognized Maria Salviati's disease but concealed the sexual component of the infection. Another hypothesis is that Maria Salviati, who never allowed the physicians to inspect her genitals (*24*), might have hidden the symptoms of her disease out of modesty. A further explanation, based on political reasons, is that the mother of Duke Cosimo I could not appear to be affected by venereal syphilis, to avoid corrupting the image of the Medici family that Cosimo was laboriously trying to promote among the royal rank. The fact that in her last years of life Maria was always portrayed with a veil might indicate her intention to hide the luetic skin lesions.

Syphilis is likely to have been more widespread among the noblewomen of the Renaissance than is attested by the written sources. Paleopathology has in some cases revealed some hidden illnesses of the Italian noblewomen, as in the case of Isabella of Aragon, Duchess of Milan (1470–1524), and Maria of Aragon (1503–1568), Marquise of Vasto and wife of the governor of Milan Alfonso of Avalos (1502–1546). Isabella was probably affected by syphilis, despite the absence of bone lesions on her skeletal remains. The syphilitic infection was diagnosed indirectly, on the basis of the paleopathologic analyses performed on her teeth (*42*). On the buccal surfaces of the teeth, Isabella showed a strong abrasion caused by pumice powder and toothpicks of cuttlebone that she used to remove the blackish patina produced by her mercurial therapy. In fact, energy-dispersive spectroscopic analysis of the dark material detected a massive presence of mercury, largely employed in the treatment of syphilis since the early 16th century in the form of salves, fumigations, and ointments (*43*,*44*). The care given to Isabella of Aragon

Figure 9. Parietal bones of Maria Salviati, showing several radial scars typical of tertiary syphilis. (Archive of the Division of Paleopathology. University of Pisa.)

clearly demonstrates her willingness to erase the evident traces of chronic mercury intoxication caused by the antisyphilitic therapy. However, no references to syphilis are reported in the written documents about the life of Isabella. In the artificial mummy of Maria of Aragon, the histologic, immunohistochemical, and ultrastructural study of a cutaneous ulcer of the left arm led to the direct identification of *Treponema pallidum* and the diagnosis of tertiary venereal syphilis (*10*). The biographic sources report that Maria of Aragon periodically spent time at the Agnano Baths, near Naples (*45*), probably to treat a skin disease with the sulfuric waters. However, in the written sources, there is no mention of any possible syphilitic infection affecting the noblewoman, who was famous at that time for her beauty and cultural refinement.

It is difficult to speculate on how Maria Salviati contracted the disease, but she is likely to have been infected by her husband Giovanni before his death in 1526, and more probably after the birth of her son Cosimo (June 12, 1519); indeed, the historical sources do not reveal any details about a possible infection of the child, nor do the skeletal remains of the first Grand Duke of Tuscany show any signs of congenital syphilis (*46*). The lifestyle of Giovanni "of the Black Bands" (Figure 11) was characterized by intense sexual extramarital affairs, as witnessed by many documents of the time preserved in the archives of Florence (*24*). On October 20, 1521, Giovanni wrote to his treasurer and lieutenant Francesco Albizi to dispose of war supplies during the military campaign against the French army in Northern Italy: "send me that Greek whore I left in Viterbo" (*47*). On September 22, 1522, during some military actions in the Marche region on behalf of the Pope, Giovanni wrote again to Francesco Albizi, ordering him to kidnap "Lucrezia, courtesan of Rome" and to bring her to him by force (*48*). A considerable series of names of prostitutes frequented by Giovanni are cited in his correspondence: Flora from Padua, Nicolosa "the painted Jewess," Camilla Orsini, Giulia, Angelica "the Venetian," Lorenzina "the Greek slave," Baccia from Rome, Lucrezia nicknamed "Matrema non vole [Mom does not want]," and Paolina (*49*,*50*). The skeleton of Giovanni de' Medici does not reveal any lesion of syphilis (*26*), probably because he died at the age of 28 years, before the development of the tertiary stage of the disease.

Extramarital affairs were common among aristocrats (*7*); therefore, syphilis could be considered a disease characterizing the pathocenosis of high social classes. Noblewomen were at risk for contracting sexually transmitted diseases caused by the lifestyle of their husbands, who led an unregulated sexual life

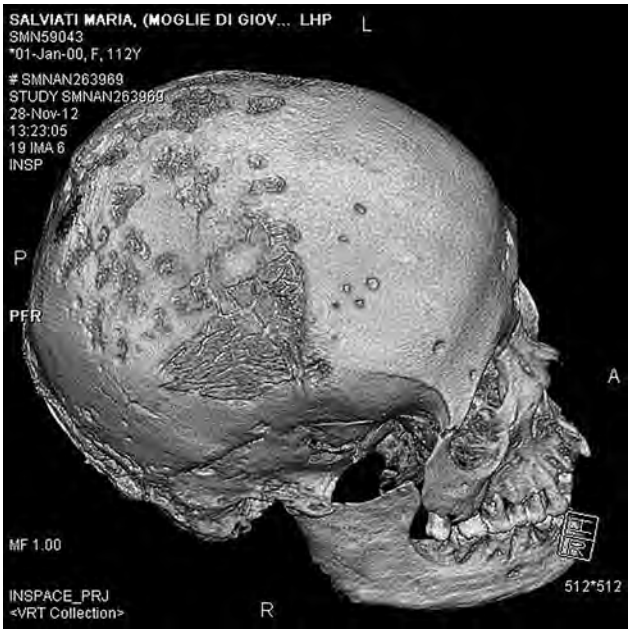

Figure 10. Volume rendering of the skull of Maria Salviati, showing contemporary presence of lytic (superficial cavitations) and reparative lesions (radial scars).(Archive of the Division of Paleopathology. University of Pisa.)

characterized by occasional relationships with prostitutes. It was already a well-known fact at the time that syphilis was transmitted sexually (*5*); therefore, some preventive practices were undertaken by the noblewomen, wives, or lovers of the men affected by the disease. Just like Isabella d'Este, wife of Francesco II Gonzaga, Marquise of Mantua, these women sometimes refused to have sexual intercourse with their partners (*7*). Although the disease had no consequences on the reputation of the men, whose sexual conduct was not subject to moral censorship, the situation was different for the women, who tried to hide their sexually transmitted infections (*6*).

Conclusions

A diagnosis of syphilis for Maria Salviati does not emerge from the historical sources, although the symptoms that manifested in the last years of her life are compatible with a colorectal localization and severe hemorrhages caused by syphilitic infection. In her final years, Maria had a very withdrawn life, possibly to conceal the signs of the illness and certainly for the social complications caused by her recurrent anal hemorrhages (*24*). However, we have no reports that she was marginalized from the ducal court; instead, she was held in high regard as the mother of the reigning duke. In the famous portrait painted by Bronzino during 1542–1543 (Figure 2),

she appears veiled and in widow's clothes, as if to hide the signs of illness.

The paleopathologic study of Maria Salviati reveals osteolytic and reparative lesions on the skull, which are pathognomonic for syphilis. The diagnosis of syphilis for Maria Salviati enables us to directly observe the gender-based consequences of a pathology to which the Renaissance noblewomen were subjected as a consequence of the sexual conduct of their husbands. The real nature of the disease might have been kept secret at the time for reasons of political opportunity and privacy. A disease that was not a reason of particular shame for sovereigns, princes, and gentlemen, that did not affect their political role and leadership, and was therefore unnecessary to hide, was instead jealously concealed by noblewomen as a "secret illness" that often did not seep outside the private apartments and perhaps did not even reach the attention of the court physicians. This attitude reveals a disparity of perception and of mentality, symptomatic of gender discrimination that was well implanted in the heart of Renaissance society (*6*,*20*)

Figure 11. Portrait of Giovanni de' Medici of the Black Bands, depicted by Francesco de' Rossi circa 1546–1548. Oil on panel. 25.6 × 18.1 in. (65 × 46 cm). (Florence, Istituti Museali della Soprintendenza Speciale per il Polo Museale Fiorentino, Palazzo

Acknowledgments

We are grateful to Gino Fornaciari for his revision of the text, to Laura Cignoni for the linguistic revision of the manuscript, and the anonymous consultants for their helpful suggestions. We also thank Roberto Carpi for providing CT data.

The Fondazione Arpa and the Associazione Ortopedica Italiana supported this research. .

About the Author

Dr. Fornaciari is a postdoctoral fellow in History of Medicine and Paleopathology at the Division of Paleopathology, University of Pisa. His primary research interests are paleopathology, archaeology, and the history of medicine of the medieval and postmedieval age.

References

1. Peeling RW, Mabey D, Kamb ML, Chen XS, Radolf JD, Benzaken AS. Syphilis. Nat Rev Dis Primers. 2017;3:17073. https://doi.org/10.1038/nrdp.2017.73
2. Centers for Disease Control and Prevention. Sexually transmitted disease surveillance, 2016. Atlanta: US Department of Health and Human Services; September 2017.
3. European Centre for Disease Prevention and Control. Syphilis. Annual epidemiological report for 2016. Stockholm: The Centre; 2018.
4. Lukehart SA. Syphilis. In: Fauci AS, Braunwald E, Kasper DL, Hauser SL, Longo DL, Jameson JL, et al., editors. Harrison's principles of internal medicine. 17th edition. New York: McGraw-Hill; 2008. p. 1038–46.
5. Tognotti E. The rise and fall of syphilis in Renaissance Europe. J Med Humanit. 2009;30:99–113. https://doi.org/10.1007/s10912-009-9079-3
6. Schleiner W. Moral attitudes toward syphilis and its prevention in the Renaissance. Bull Hist Med. 1994;68:389–410.
7. Tognotti E. Prevention strategies and changes in sexual mores in response to the outbreak of syphilis in Europe in the early modern age. J Anc Dis Prev Rem. 2014;2:113. https://doi.org/10.4172/2329-8731.1000113
8. Boehrer BT. Early modern syphilis. J Hist Sex. 1990;1: 197–214.
9. Foa A. The new and the old: the spread of syphilis (1494–1530). In: Muir E, Ruggiero G, editors. Sex and gender in historical perspective. Baltimore: Johns Hopkins University Press; 1990. p. 26–45.
10. Fornaciari G, Castagna M, Tognetti A, Tornaboni D, Bruno J. Syphilis in a Renaissance Italian mummy. Lancet. 1989;2:614. https://doi.org/10.1016/S0140-6736(89)90729-0
11. Mallegni F, Bedini E, Fornaciari G. The study of human remains in Vespasiano Gonzaga's tomb 400 years later [in Italian]. Sabbioneta (Italy): Edizioni A Passo d'Uomo; 1991. p. 55–110.
12. Fornaciari G, Vitiello A. The tombs of Della Rovere. In: Vastano A, editor. Enigmas and new discoveries: the monastery of Santa Chiara in Urbino [in Italian]. Urbino (Italy): Arti Grafiche Editoriali; 2012. p. 143–66.
13. Grmek M. Diseases at the beginning of the Western civilization [in French]. Paris: Payot; 1983.
14. Harper KN, Zuckerman MK, Harper ML, Kingston JD, Armelagos GJ. The origin and antiquity of syphilis

revisited: an appraisal of Old World pre-Columbian evidence for treponemal infection. Am J Phys Anthropol. 2011;146(Suppl 53):99–133. https://doi.org/10.1002/ajpa.21613
15. Walker D, Powers N, Connell B, Redfern R. Evidence of skeletal treponematosis from the medieval burial ground of St. Mary Spital, London, and implications for the origins of the disease in Europe. Am J Phys Anthropol. 2015;156:90–101. https://doi.org/10.1002/ajpa.22630
16. Roberts CA, Millard AR, Nowell GM, Gröcke DR, Macpherson CG, Pearson DG, et al. Isotopic tracing of the impact of mobility on infectious disease: The origin of people with treponematosis buried in hull, England, in the late medieval period. Am J Phys Anthropol. 2013;150:273–85. https://doi.org/10.1002/ajpa.22203
17. Arrizabalaga J, Henderson J, French R, French RK. The great pox: the French disease in Renaissance Europe. New Haven (CT): Yale University Press; 1997.
18. Meyer C, Jung C, Kohl T, Poenicke A, Poppe A, Alt KW. Syphilis 2001—a palaeopathological reappraisal. Homo. 2002;53:39–58. https://doi.org/10.1078/0018-442X-00037
19. Oriel JD. The scars of Venus. A history of venereology. London: Springer Verlag; 1984.
20. Siena K, editor. Sins of the flesh: responding to sexual disease in early modern Europe. Toronto: Centre for Reformation and Renaissance Studies; 2005.
21. Knell RJ. Syphilis in renaissance Europe: rapid evolution of an introduced sexually transmitted disease? Proc Biol Sci. 2004;271(Suppl 4):S174–6.
22. Benedetti A. Diary of the Caroline War. Schullian DM, editor. New York: Renaissance Society of America; 1967.
23. Tognotti E. The other face of Venus. Syphilis from the early modern age to the advent of AIDS (15th–20th century) [in Italian]. Milan: Franco Angeli, 2006.
24. Pieraccini G. The Medici of Cafaggiolo [in Italian]. Vol. 2. Florence (Italy): Nardini Editore, 1986.
25. Bradford S. Ceasare Borgia: his life and times. London: Futura Publications; 1981.
26. Fornaciari G, Bartolozzi P, Bartolozzi C, Rossi B, Menchi I, Piccioli A. A great enigma of the Italian Renaissance: paleopathological study on the death of Giovanni dalle Bande Nere (1498–1526) and historical relevance of a leg amputation. BMC Musculoskelet Disord. 2014;15:301. https://doi.org/10.1186/1471-2474-15-301
27. Lippi D. Unmourned graves. Curiosity and scientific research in history of the Medici exhumations [in Italian]. Florence (Italy): Firenze University Press; 2006.
28. Sommi Picenardi G. Exhumation and recognition of the ashes of the Medici Princes in the year 1857. Minutes and notes [in Italian]. Arch Stor Ital. 1888;165:333–60.
29. Genna G. Anthropological research on the Medici family [in Italian]. Atti Accademia Nazionale dei Lincei, Classe di Scienze Fisiche. Matematiche e Naturali. 1948;15:589–93.
30. Buikstra J, Ubelaker D. Standards for data collection from human skeletal remains. Fayetteville (AR): Arkansas Archaeological Survey Research Series No. 44; 1994.
31. Lovejoy CO. Dental wear in the Libben population: its functional pattern and role in the determination of adult skeletal age at death. Am J Phys Anthropol. 1985;68:47–56. https://doi.org/10.1002/ajpa.1330680105
32. Brooks ST, Suchey JM. Skeletal age determination based on the os pubis: a comparison of the Acsadi–Nemeskeri and Suchey–Brooks methods. Hum Evol. 1990;5:227–38. https://doi.org/10.1007/BF02437238
33. Loth SR, Iscan MY. Morphological assessment of age in the adult: the thoracic region. In: Iscan MY, editor. Age markers in the human skeleton. Springfield (IL): Charles C. Thomas Publisher; 1989. p. 105–35.
34. Trotter M, Gleser GC. Corrigenda to "Estimation of stature from long limb bones of American Whites and Negroes" Am. J. Phys. Anthrop. (1952). Am J Phys Anthropol. 1977;47:355–6. https://doi.org/10.1002/ajpa.1330470216
35. Colagrande S, Villari N, Pierleoni F, Weber D, Fornaciari G, Lippi D. Teeth of the Renaissance: a paleopathological and historic-medical study of the jaws of the Medici Family. Journal of Forensic Radiology and Imaging. 2013;1:193–200. https://doi.org/10.1016/j.jofri.2013.07.004
36. Waldron T. Paleopathology. Cambridge: Cambridge University Press; 2012.
37. Roberts CA, Buikstra JE. Bacterial Infections. In: Buikstra JE, editor. Ortner's identification of pathological conditions in human skeletal remains. New York: Academic Press 2019; p. 321–439.
38. Hackett C. Diagnostic criteria of syphilis, yaws and treponarid (treponematoses) and of some other diseases in dry bones (for use in osteo-archaeology). Berlin: Springer-Verlag; 1976.
39. Scolari EG, Giannotti B. Syphilis and other venereal diseases [in Italian]. Turin (Italy): UTET; 1972.
40. Serigado J, Lewis E, Kim G. Rectal bleeding caused by a syphilitic inflammatory mass. BMJ Case Rep. 2019;12:e226595. https://doi.org/10.1136/bcr-2018-226595
41. Arnold CA, Roth R, Arsenescu R, Harzman A, Lam-Himlin DM, Limketkai BN, et al. Sexually transmitted infectious colitis vs inflammatory bowel disease: distinguishing features from a case-controlled study. Am J Clin Pathol. 2015;144:771–81. https://doi.org/10.1309/AJCPOID4JIJ6PISC
42. D'Errico F, Villa G, Fornaciari G. Dental esthetics of an Italian Renaissance noblewoman, Isabella d'Aragona. A case of chronic mercury intoxication. Ossa. 1988;13:207–28.
43. O'Shea JG. 'Two minutes with venus, two years with mercury'—mercury as an antisyphilitic chemotherapeutic agent. J R Soc Med. 1990;83:392–5. https://doi.org/10.1177/014107689008300619
44. Tilles G, Wallach D. History of the treatment of syphilis with mercury: five centuries of uncertainty and toxicity [in French]. Rev Hist Pharm (Paris). 1996;44(suppl):347–51. https://doi.org/10.3406/pharm.1996.6244
45. Fiorentino F. Studies and portraits of the Renaissance [in Italian]. Bari (Italy): Giuseppe Laterza & Figli; 1911.
46. Fornaciari G, Vitiello A, Giusiani S, Giuffra V, Fornaciari A, Villari N. The Medici Project. First anthropological results of the exploration of the Medici Tombs in Florence. Med Secoli. 2007;19:521–44.
47. Gauthiez P. New documents about Giovanni de' Medici named delle Bande Nere [in Italian]. Arch Stor Ital. 1902;227:333–60.
48. Milanesi C. Unpublished letters and testament of G. de 'M. called delle Bande Nere with others by Maria and Jacopo Salviati of princes, cardinals, captains, family members and soldiers gathered by cav. Filippo Moisè [in Italian]. Arch Stor Ital. 1859;9:3–29.
49. Orlando F, Baccini G. Courtesans of the XVI century. Letters–Curiosity–News–Anecdotes [in Italian]. Florence (Italy): Il "Giornale di Erudizione" Editore; 1892.
50. De Gubernatis A. Love letters of women to Giovanni dalle B. N. [in Italian]. Rivista D'Italia. 1902;8.

Address for correspondence: Antonio Fornaciari, Department of Translational Research and New Technologies in Medicine and Surgery, University of Pisa, Via Roma 57, 56126 Pisa, Italy; email: antonio.fornaciari@med.unipi.it

Yaws Disease Caused by *Treponema pallidum* subspecies *pertenue* in Wild Chimpanzee, Guinea, 2019

Benjamin Mubemba,[1] Emeline Chanove,[1] Kerstin Mätz-Rensing, Jan F. Gogarten, Ariane Düx, Kevin Merkel, Caroline Röthemeier, Andreas Sachse, Helene Rase, Tatyana Humle, Guillaume Banville, Marine Tchoubar, Sébastien Calvignac-Spencer, Christelle Colin, Fabian H. Leendertz

Yaws-like lesions are widely reported in wild African great apes, yet the causative agent has not been confirmed in affected animals. We describe yaws-like lesions in a wild chimpanzee in Guinea for which we demonstrate infection with *Treponema pallidum* subsp. *pertenue*. Assessing the conservation implications of this pathogen requires further research.

Several monkey species in sub-Saharan Africa are infected with *Treponema pallidum* subspecies *pertenue* (TPE) and typically manifest yaws-like lesions on the face and distal extremities or syphilis-like lesions in the anogenital region (*1*). Reports of nonhuman primates (NHPs) infected with TPE came from West Africa in the 1960s. These studies were based on seroprevalence studies finding that yellow baboons (*Papio cynocephalus cynocephalus*) had a 60% seroprevalence rate for treponemal-specific antibodies (*2*,*3*). Whole-genome sequencing of the isolate collected from these baboons later revealed similarities with TPE causing yaws in humans (*3*,*4*). In the late 1980s in Gombe National Park in Tanzania, olive baboons (*Papio anubis*) with genital ulcerations were found to have yaws-like infections of the skin (*5*). Later genetic and serologic studies confirmed infections with *T. pallidum* in olive baboons at many sites in Tanzania (*6*,*7*).

Both genital and orofacial lesions attributable to TPE infection have been documented in several NHP species across sub-Saharan Africa (African green monkeys [*Chlorocebus sabaeus*] in Bijilo Forest Park, The Gambia, and Niokola-Koba National Park, Senegal; sooty mangabeys [*Cercocebus atys atys*] in Taï National Park, Côte d'Ivoire) (*1*; B. Mubemba et al., unpub. data, https://doi.org/10.1101/848382). Two studies observed that TPE infections remain geographically widespread in Tanzania and affect olive baboons, yellow baboons, vervet monkeys (*Chlorocebus pygerythrus*), and blue monkeys (*Cercopithecus mitis*), as well as grivet monkeys (*Chlorocebus aethiops*) from Ethiopia (*8*,*9*).

Symptoms and skeletal deformation have also been observed in great apes, specifically gorillas (*Gorilla gorilla*) in the Republic of Congo, Gabon, and Cameroon (*10*), as well as in chimpanzees (*Pan troglodytes*) in Cameroon, Uganda, and Côte d'Ivoire, and are suggestive of TPE infections (*10*; F.H. Leendertz, pers. comm., 2019 Nov 1), but matching diagnostics are currently unavailable. The only diagnostic evidence is based on TPE DNA from 2 chimpanzee (*P. troglodytes verus*) bones (*11*) and gorilla feces (*9*) of unknown individual great apes, so no link between diagnostics and clinical signs can be made. We present matching clinical and molecular evidence of TPE infection in a wild great ape.

The Study

We found a cachectic wild adult female chimpanzee (*Pan troglodytes verus*) with severe yaws-like lesions on the mouth and lips in a mining concession in Sangaredi area, Guinea (Figure 1, panel A). The chimpanzee

Author affiliations: Copperbelt University, Kitwe, Zambia (B. Mubemba); Robert Koch Institute, Berlin, Germany (B. Mubemba, J.F. Gogarten, A. Düx, K. Merkel, C. Röthemeier, A. Sachse, S. Calvignac-Spencer, F.H. Leendertz); University of Agricultural Sciences and Veterinary Medicine, Cluj-Napoca, Romania (E. Chanove); Chimpanzee Conservation Center, Somoria, Faranah, Republic of Guinea (E. Chanove, H. Rase, G. Banville, M. Tchoubar, C. Colin); Leibniz Institute for Primate Research, Göttingen, Germany (K. Mätz-Rensing); University of Kent, Canterbury, UK (T. Humle)

DOI: https://doi.org/10.3201/eid2606.191713

[1]These authors contributed equally to this article.

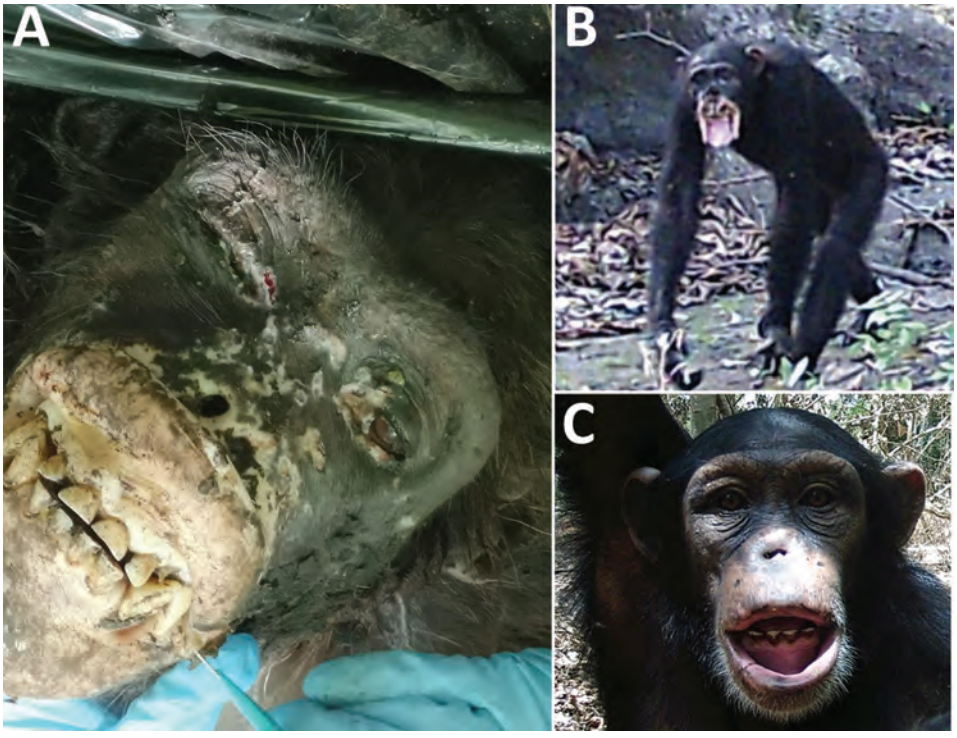

Figure 1. Yaws-like lesions in wild chimpanzees, Guinea. A) Yaws-like lesions observed during a necropsy of an adult female chimpanzee found in the Sangaredi area, Guinea. B, C) Camera trap images showing yaws-like lesions on adult (B) and juvenile (C) chimpanzees in Haut Niger National Park, Guinea.

was in visible agony and had to be euthanized; we performed a necropsy on the body. Gross pathology of the skin revealed a marked depigmentation on hypertrophied edematous lips; crusts and ulcers were present on the head, and much of the nose was missing. The eyes were shrunken and purulent and surrounded by crusts, and the corneas were opaque. We preserved samples of lesioned skin in 10% formalin and RNAlater (Thermo Fisher, https://www.thermofisher.com).

We analyzed formalin-fixed skin samples with both histological and immunohistochemical methods, as previously described (*6*). Histopathological features of the skin biopsies were compatible with treponemal infection (Figure 2, panel A). Skin lesions were characterized by irregular epidermal proliferation of different extents. The epidermis developed hyperkeratosis and hypertrophy of the epidermal rete pegs, which branched and projected deeply into the corium. Admixed areas with severe superficial erosions or deep ulcerations were visible. A moderate to severe mixed cell infiltration composed of lymphocytes and histiocytes was present in the underlying dermal layer. The cellular reaction was most pronounced around the dermal blood vessels and hair follicles, resulting in superficial and deep perivascular dermatitis. The epidermal surface was covered with a dried serosanguineous discharge. Immunohistochemical analyses failed to visualize treponemes, which is a frequent problem resulting from low numbers of bacteria at lesion sites (*6*).

We extracted DNA from 2 facial lesion biopsies stored in RNAlater and performed molecular investigations (Appendix, https://wwwnc.cdc.gov/EID/article/26/6/19-1713-App1.pdf). High-throughput sequencing analysis resulted in a 24-fold average coverage of the TPE genome; 98.6% of the genome was covered by ≥1 read and 97.6% by ≥3 reads. Bayesian Markov chain Monte Carlo analysis of a genomic alignment comprising this reconstructed TPE genome, all other available TPE and *Treponema pallidum* subsp. *endemicum* (TEN, bejel) genomes, and a selection of *Treponema pallidum* subsp. *pallidum* (TPA, syphilis) genomes available in Genbank (Appendix Table) revealed that the chimpanzee-derived genome clustered within the well-supported TPE clade, indicating that TPE is responsible for the clinical picture observed in this particular wild chimpanzee (Figure 2, panel B). More precisely, this new chimpanzee-derived genome belongs to a clade consisting of TPE strains isolated from NHPs in far western Africa in Gambia, Guinea Bissau, Senegal, and Guinea, in agreement with recent observations that genomic diversity of TPE strains infecting NHPs appears to be geographically structured (*9*; B. Mubemba et al., unpub. data, https://doi.org/10.1101/848382). Yaws is principally a skin disease, and it seems likely that the poor condition of this animal was caused by another

unknown but likely traumatic cause, perhaps coupled with associated secondary infections, although our field necropsy was not able to identify an alternative cause of her cachectic condition.

To determine whether TPE might affect other chimpanzees in Guinea, we examined videos collected by camera traps set near the Chimpanzee Conservation Center in Haut Niger National Park. During 2018–2019, in 10 different camera trap locations, we observed 12 chimpanzees (1 juvenile, 3 subadults, and 8 adults) with severe lesions. The lesions observed in these images closely resembled those of the wild female from

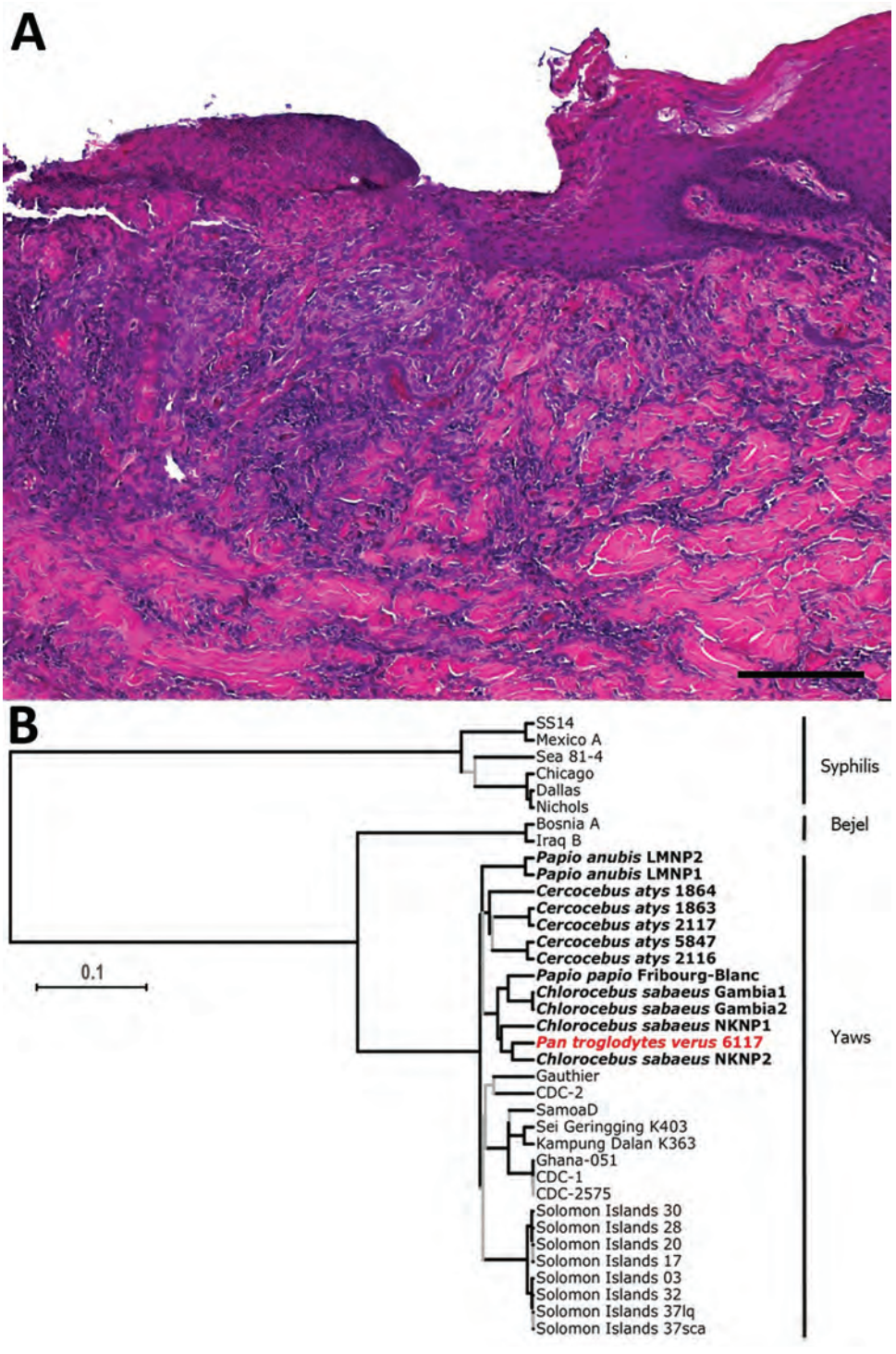

Figure 2. Histopathologic analysis of yaws-like lesions in a wild chimpanzee, Guinea, and phylogenetic placement of the *Treponema pallidum* subspecies *pertenue* strain. A) Histopathologic evidence suggestive of a treponemal infection. Shown here is superficial ulcerative pyogranulomatous dermatitis including formation of a mixed inflammatory cell infiltration, predominantly neutrophil granulocytes. Deeper dermal layers show the formation of a perivascular lymphocytic inflammatory cell infiltrate, focal folliculitis, and perifolliculitis. Skin areas adjacent to ulcerated parts show irregular epidermal hyperplasia, consistent with treponemal infections. The ulcerated areas were covered by a serocellular crust. Scale bar indicates 200 μm. B) Maximum clade credibility tree of *T. pallidum* strain genomes. Red indicates the chimpanzee genome generated in this study. All simian-infecting strains are shown in bold with labels showing the species of nonhuman primate, and the diseases caused by each type of bacteria are shown at right. Branches supported by posterior probabilities <0.95 in the Bayesian Markov chain Monte Carlo tree are indicated in gray. Scale bar indicates nucleotide substitutions per variable site.

the Sangaredi region described in this article, including shrunken eyes, deformation of the face, absence of the nose, and hypertrophied and depigmented lips (in 1 case, the lips were completely missing; Figure 1, panels B, C). Molecular investigations of the pathogen(s) causing these infections is clearly warranted, perhaps through noninvasive screening of TPE in feces, bones, or primate-associated flies (*9*,*12*).

Conclusions

This study links yaws-like pathology to the actual detection of TPE in a wild chimpanzee, providing evidence that at least part of the suggestive lesions often observed in wild great apes are caused by this pathogen. These data join a growing body of evidence demonstrating that many NHP species across sub-Saharan Africa are infected with TPE (*1*,*9*). This finding could potentially be problematic for the ongoing campaign to eradicate TPE globally by 2030 (*13*), although, clearly, data from TPE-infected humans in this region are needed to determine whether zoonotic transmission of this pathogen occurs. Given the severity of lesions, it is evident that individual animal fitness is affected. The impact of this disease on NHP populations is unknown but could be assessed through long-term monitoring.

Acknowledgments

For their collaboration and help, we thank the Office Guinéen des Parcs et Resérves and Haut Niger National Park Authorities. We are also grateful to the Convention on International Trade in Endangered Species, Germany and CITES, Guinea for facilitating the import of samples from Guinea to Germany.

The Tusk Trust funded the camera trap project and the German Research Foundation Great Ape Health project no. LE1813/14-1 funded the laboratory investigations. B.M. was supported through the Robert Koch Institute's PhD program, Berlin, Germany.

About the Author

Dr. Mubemba is a PhD student with the Epidemiology of Highly Pathogenic Organisms research group at the Robert Koch Institute, Berlin, Germany. Dr. Chanove is the veterinarian in charge at the Chimpanzee Conservation Center, Somoria, Faranah, Republic of Guinea. Both Dr. Mubemba and Dr. Chanove are veterinarians interested in infectious diseases of wildlife with a focus on wild nonhuman primates.

References

1. Knauf S, Gogarten JF, Schuenemann VJ, Nys HM De, Düx A, Strouhal M, et al. Nonhuman primates across sub-Saharan Africa are infected with the yaws bacterium *Treponema pallidum* subsp. *pertenue*. Emerg Microbes Infect. 2018;7:1–4. https://doi.org/10.1038/s41426-018-0156-4
2. Fribourg-Blanc A, Mollaret HH, Niel G. Serologic and microscopic confirmation of treponemosis in Guinea baboons [in French]. Bull Soc Pathol Exot Filiales. 1966;59:54–9.
3. Fribourg-Blanc A, Mollaret HH. Natural treponematosis of the African primate. Primates Med. 1969;3:113–21.
4. Zobaníková M, Strouhal M, Mikalová L, Cejková D, Ambrožová L, Pospíšilová P, et al. Whole genome sequence of the *Treponema* Fribourg-Blanc: unspecified simian isolate is highly similar to the yaws subspecies. PLoS Negl Trop Dis. 2013;7:e2172. https://doi.org/10.1371/journal.pntd.0002172
5. Wallis J, Lee DR. Primate conservation: the prevention of disease transmission. Int J Primatol. 1999;20:803–26. https://doi.org/10.1023/A:1020879700286
6. Knauf S, Batamuzi EK, Mlengeya T, Kilewo M, Lejora IAV, Nordhoff M, et al. *Treponema* infection associated with genital ulceration in wild baboons. Vet Pathol. 2012;49:292–303. https://doi.org/10.1177/0300985811402839
7. Harper KN, Fyumagwa RD, Hoare R, Wambura PN, Coppenhaver DH, Sapolsky RM, et al. *Treponema pallidum* infection in the wild baboons of East Africa: distribution and genetic characterization of the strains responsible. PLoS One. 2012;7:e50882. https://doi.org/10.1371/journal.pone.0050882
8. Chuma IS, Batamuzi EK, Collins DA, Fyumagwa RD, Hallmaier-Wacker LK, Kazwala RR, et al. Widespread *Treponema pallidum* infection in nonhuman primates, Tanzania. Emerg Infect Dis. 2018;24:1002–9. https://doi.org/10.3201/eid2406.180037
9. Chuma IS, Roos C, Atickem A, Bohm T, Anthony Collins D, Grillová L, et al. Strain diversity of *Treponema pallidum* subsp. *pertenue* suggests rare interspecies transmission in African nonhuman primates. Sci Rep. 2019;9:14243. https://doi.org/10.1038/s41598-019-50779-9
10. Knauf S, Liu H, Harper KN. Treponemal infection in non human primates as possible reservoir for human yaws. Emerg Infect Dis. 2012;19:2058–60. https://doi.org/10.3201/eid1912.130863
11. Gogarten JF, Düx A, Schuenemann VJ, Nowak K, Boesch C, Wittig RM, et al. Tools for opening new chapters in the book of *Treponema pallidum* evolutionary history. Clin Microbiol Infect. 2016;22:916–21. https://doi.org/10.1016/j.cmi.2016.07.027
12. Gogarten JF, Düx A, Mubemba B, Pléh K, Hoffmann C, Mielke A, et al. Tropical rainforest flies carrying pathogens form stable associations with social nonhuman primates. Mol Ecol. 2019;28:4242–58. https://doi.org/10.1111/mec.15145
13. Dyson L, Mooring EQ, Holmes A, Tildesley MJ, Marks M. Insights from quantitative and mathematical modelling on the proposed 2030 goals for Yaws. Gates Open Res. 2019;3:1576. https://doi.org/10.12688/gatesopenres.13078.1

Address for correspondence: Fabian H. Leendertz, Robert Koch Institute, Epidemiology of Highly Pathogenic Microorganisms, Seestr. 10, Berlin 13353, Germany; email: LeendertzF@rki.de

Fatal Encephalitis Caused by Cristoli Virus, an Emerging Orthobunyavirus, France

Christophe Rodriguez, Guillaume Gricourt,[1] Melissa Ndebi,[1] Vanessa Demontant, Lila Poiteau, Sonia Burrel, David Boutolleau, Paul-Louis Woerther, Vincent Calvez, Sebastian Stroer, Jean-Michel Pawlotsky

We report the discovery of a new orthobunyavirus, Cristoli virus, by means of shotgun metagenomics. The virus was identified in an immunodepressed patient with fatal encephalitis. Full-length genome sequencing revealed high-level expression of a virulence factor, possibly explaining the severity of the infection. The patient's recent history suggests circulation in France.

The *Orthobunyavirus* genus of the *Peribunyaviridae* family contains numerous viruses, usually transmitted by mosquitoes (*1*). New members are regularly discovered through mosquito screening campaigns, but most of them are not pathogenic (*2*–*4*). Global warming implies changes in the distribution of their vectors, possibly exposing humans to the onset of new diseases.

Broad-spectrum diagnostic tests, such as metagenomics methods, are useful to discover new viruses, especially in patients with encephalitis of unknown etiology (*2*,*5*). We have developed an original method based on shotgun metagenomics (MetaMIC) for the diagnosis of bacterial, viral, fungal, and parasitic infections from any human fluid or tissue (*6*). We used it to discover a previously unknown member of the *Orthobunyavirus* genus of the *Peribunyaviridae* family, Cristoli virus, in a patient with fatal encephalitis. The study was approved by the Créteil Institutional Review Board (Créteil, France).

The Study

A 58-year-old woman living in the Paris, France, area was hospitalized in September 2018 for isolated fever resistant to amoxicillin/clavulanic acid. She had a history of complete remission of non-Hodgkin lymphoma, decompensated cirrhosis related to autoimmune hepatitis treated with sirolimus, possibly congenital hypogammaglobulinemia associated with B-lymphopenia, and episodes of lower respiratory tract and digestive infections in the years preceding her admission. She last traveled to Italy and on a Mediterranean cruise in summer 2017. Although her fever declined on ofloxacin, she was admitted again in October 2018 for deterioration of her general health, anorexia, and psychomotor retardation. Her neurologic symptoms worsened during the following 6 months. Multiple electroencephalograms showed nonspecific slowing of background activity. Magnetic resonance imaging revealed limbic and cerebellar abnormalities compatible with inflammatory or infectious encephalitis (Figure). Results of testing for multiple cerebrospinal fluid samples showed only an increase in α interferon; no microbial agent was identified. A cerebral biopsy was performed in March 2019 for shotgun metagenomics testing. The patient's condition continued to deteriorate, and she died in the intensive care unit on March 27, 2019.

We ground the cerebral biopsy material in a sterile isotonic solution. We performed preextraction using bead beating combined with chemical cell disruption, then a combined DNA/RNA extraction using QIAsymphony (QIAGEN, https://www.qiagen.com). We tested a negative environmental control (isotonic sterile solution) in parallel. We prepared DNA libraries with Nextera XT DNA, and RNA libraries with RNA Human RiboZero TruSeq Stranded Total RNA Library Prep Kit (Illumina, https://www.illumina.com). We pair-end sequenced libraries, 2 × 150 bp, with High Output Kit version 2 on a NextSeq500 device (Illumina). We analyzed the sequences with MetaMIC software (*6*).

Author affiliations: Henri Mondor Hospital, Assistance Publique des Hôpitaux de Paris at University of Paris-Est, Créteil, France (C. Rodriguez, G. Gricourt, M. Ndebi, V. Demontant, L. Poiteau, P.-L. Woerther, J.-M. Pawlotsky); Pitié-Salpêtrière Hospital, Assistance Publique des Hôpitaux de Paris at Sorbonne-Université, Paris, France (S. Burrel, D. Boutolleau, V. Calvez, S. Stroer)

DOI: https://doi.org/10.3201/eid2606.191431

[1]These authors contributed equally to this article.

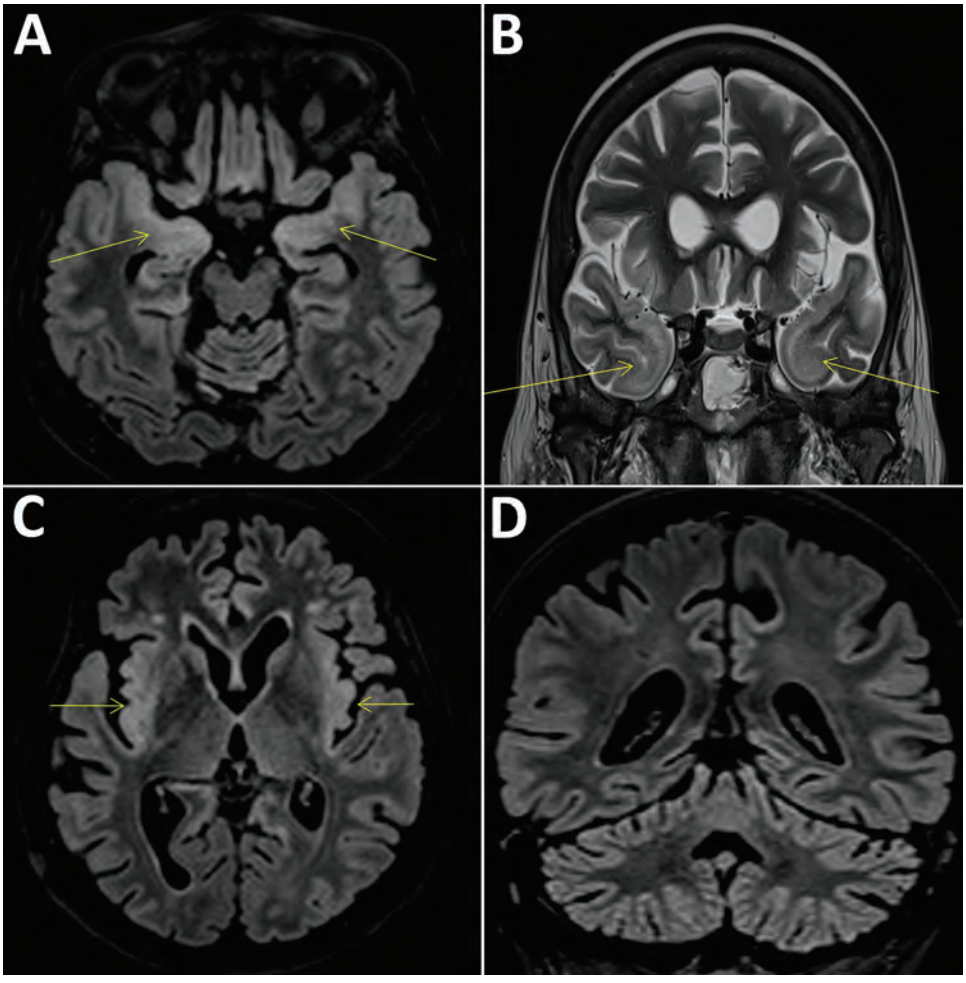

Figure. Cerebral magnetic resonance imaging scans compatible with the diagnosis of encephalitis in a 58-year-old woman, France. Fluid-attenuated inversion recovery (FLAIR) and T2 hypersignals in limbic system structures, including both amygdalae (A, arrows), temporal poles (B, arrows), and insular cortex (C), associated with FLAIR hyperintensities of the cerebellar cortex (D).

Identification of nonhuman sequences uses different databases, including cleaned National Center for Biotechnology Information nucleotide and nonredundant databases (GenBank release 229, December 2018) that contain all known microorganisms. For new species, we conducted verification using an algorithm combining de novo assembly with Meta-SPAdes version 3.12.0 (http://cab.spbu.ru/software/meta-spades) and contig alignment with the ViPR database (https://www.viprbrc.org). After manual curation of full-length viral sequences, we performed alignment and phylogenetic analyses with the closest known viral species using Muscle version 3.8.31 (http://www.drive5.com/muscle) and IQ-Tree version 1.3.11.1 (http://www.iqtree.org). We used the general time reversible plus gamma 4 plus invariate sites model of nucleotide substitution and 10,000 full maximum-likelihood bootstrap replicates.

Shotgun metagenomics revealed the presence of sequences from a new member of the *Orthobunyavirus* genus of the *Peribunyaviridae* family; the sequences were not present in the negative environmental control. This new virus was named Cristoli virus after the city of Créteil where it was described. We reconstructed the full-length sequence of the viral genome de novo in silico. The large (L), medium (M), and small (S) segments were individualized and could be aligned with similar sequences from known orthobunyaviruses (*1*) (Appendix 1 Figure 1, panels A, B, https://wwwnc.cdc.gov/EID/article/26/6/19-1431-App1.pdf). Cristoli virus segregated within serogroup Turlock; the closest related virus was Umbre virus. These viruses cluster on a different branch from all other known orthobunyaviruses with a 100% bootstrap (Appendix 1 Figure 1, panel C). Cristoli virus differed from Umbre virus by 11.4% of L, 12.3% of M, and 7.0% of S segments (differences with other orthobunyaviruses) (Appendix 2, https://wwwnc.cdc.gov/EID/article/26/6/19-1431-App2.xlsx).

We identified a 6,783-bp open reading frame (ORF), coding for a protein of 2,261 aa in the L segment, which, by analogy with other orthobunyaviruses, corresponded to the RNA-dependent RNA polymerase (Appendix 1 Figure 1). The conserved

Table. Amino acid differences coded by open reading frames in Cristoli virus compared with Umbre virus*

Open reading frame			
Large	Medium	Small	Nonstructural
A16T, M135I, H138Y, Q231L, S249A, R252K, E252D, P318H, V382I, N384T, E408D, V425I, K433R, A452T, R477K, G488E, V566I, V568I, N630S, I792V, V904I, E931S, T939A, R942K, T943S, I966V, V1080I, R1206K, I1444V, G1481D, K1566R, K1662R, D1665H, N1669D, G1987S, AQ2058V, D2074E, N2085D, K2130R, T2168I, T2232S, L2255F, T2258I, G2270E	M2V, V3I, S10L, A12V, L14F, S16N, R32K, D99N, V203I, I332V, A338I, C340Y, V358I, I376V, V382I, K390R, N393S, G427E, R451K, M452L, A458V, I465L, D468N, A473T, A474T, V484I, D504N, K511R, V514E, V515I, S521G, M546V, S578N, T594I, T627A, M692V, N701D, S724L, T746V, P758del, R759del, T760P, K761R, I762V, R772K, S773L, I790V, G791D, V827I, D837E, V839I, S847N, N853D, I860V, S888K, A889T, A904M, V921I, T923M, A967S, V989A, V994I, N996S, I1002M, I1008V, V1020M, T1031A, N1168D, F1206Y, T1254A, T1322M, S1323T, T1378I, T1406A, R1419K, T1443A, A1444T, N1446S	F12Y A53P T87A S115N	H3R L52P R56K

*Differences are indicated using the formula X#Y, where X indicates the presence of an amino acid in Umbre virus, Y a different amino acid in Cristoli virus, and # the position of the difference. A, alanine; C, cysteine; D, aspartic acid; E, glutamic acid; F, phenylalanine; G, glycine; H, histidine; I, isoleucine; K, lysine; L, leucine; M, methionine; N, asparagine; P, proline; Q, glutamine; R, arginine; S, serine; T, threonine; V, vazline; Y, tyrosine.

H….PD….DxK orthobunyavirus catalytic domain (*7*) was present between positions 37 and 101, identical to that of Umbre virus. Umbre and Cristoli viruses differed by 44 aa in the RNA polymerase (Table).

In segment M, we identified a 4,336-bp ORF coding for a protein of 1,445 aa, corresponding to a polyprotein processed into the 2 envelope glycoproteins n and c (Gn and Gc) and nonstructural protein m (NSm) in orthobunyaviruses (Appendix 1 Figure 1). Cristoli and Umbre viruses differed by 78 aa in the M segment, including 2 deletions (P758del and R759del) (Table). R759del corresponds to a trypsin cleavage site used for bunyavirus characterization (*8*). The conserved RxxR cleavage motif at the C-terminus of the Gn domain was conserved in Cristoli virus at positions 298–301. All conserved cysteine positions (*9*) were also conserved.

We identified 2 overlapping ORFs in the S segment, one corresponding to the nucleocapsid (N) protein (714 bp, 238 aa), the other to nonstructural protein s (NSs, 240 bp, 80 aa). We found few differences with Umbre virus for these proteins (Table).

The amounts of viral RNAs we semiquantified by shotgun metagenomics were 5.4 log viral genomes/mg of biopsy for segment L, log viral genomes/mg of biopsy 5.0 for segment M, and 6.2 log viral genomes/mg of biopsy for segment S. For confirmation, we designed specific reverse transcription PCRs for Cristoli virus segments L, M, and S. Brain extracts were positive for all three, with amplicon sequences identical to those in the full-length genome (Appendix 1 Figure 2). We deposited the annotated genome sequence into Genbank (accession nos. MN488996 [S segment], MN488997 [M segment], and MN488998 [L segment]).

Conclusions

The etiologic diagnosis of encephalitis is difficult because >25% of cases remain of unknown cause (*5*). Diagnostic methods without prior knowledge of the microorganisms sought, such as metagenomics, detect infectious agents when other techniques have failed (*10*). We used an original shotgun metagenomics approach and in-house software MetaMIC to discover a new virus belonging to the *Orthobunyavirus* genus of the *Peribunyaviridae* family in an immunodepressed patient with slowly progressive fatal encephalitis. Cristoli virus is close to Umbre virus, a member of the Turlock serogroup not previously associated with human disease. Because the patient had not traveled during the year preceding the onset of her symptoms, our findings suggest that Cristoli virus is endemic to France. Like other members of its family, it could have been transmitted through a mosquito bite. Changes in the distribution of mosquito species related to climate change may make such transmissions more frequent in the future. In this context, the metagenomics method we developed is particularly useful to detect unusual or emerging infectious agents in patients with unassigned infectious syndromes.

Full-length sequence analysis of Cristoli virus revealed a classical *Peribunyaviridae* genome organization with conserved motifs. The genome segment coding for the NSs protein was found in an amount 10 times higher than that of the other segments. Because NSs has been described as a virulence factor (*11*,*12*), its high-level expression in a context of immune depression could explain the unusual severity of the disease. If efficacious antiviral treatments become available (*13*), a rapid etiologic diagnosis of orthobunyavirus infections will become necessary. The shotgun metagenomics method we developed fulfills the criteria for such routine diagnosis.

The authors declare that the planning, conduct, and reporting of the case was in line with the Declaration of Helsinki and French laws for biomedical research. It only

involved the use of archived, residual samples that were sent for routine diagnosis and sequence characterization with nonopposition for leftover sample to be used in other assays.

C.R., G.G., V.D. and J.-M.P. are co-inventors of a patent protecting the shotgun metagenomics method and MetaMIC software.

Author contributions: C.R and J.-M.P conceived the study. C.R., G.G., M.N. and V.D. performed sequence analyses, developed the algorithms, and ran computational analyses. S.D., S.S, S.B., D.B., and V.C. provided and interpreted the clinical, radiologic, and virologic data. L.P. developed the confirmation RT-PCR methods. C.R., P.-L.W., and J.-M.P. analyzed the findings and wrote the manuscript. All authors discussed the results and contributed to the final manuscript.

About the Author

Dr. Rodriguez is an assistant professor in the Department of Microbiology at Henri Mondor Hospital, University of Paris-Est-Créteil, Créteil, France, and the head of the institution's genomics platform. He has implemented a clinical metagenomics technique in diagnostic routine and is working on the exploration of complex infectious diseases using this tool.

References

1. Elliott RM. Orthobunyaviruses: recent genetic and structural insights. Nat Rev Microbiol. 2014;12:673–85. https://doi.org/10.1038/nrmicro33322.
2. Li D. A highly pathogenic new bunyavirus emerged in China. Emerg Microbes Infect. 2013;2:e1. https://doi.org/10.1038/emi.2013.13.
3. Huang YS, Higgs S, Vanlandingham DL. Emergence and re-emergence of mosquito-borne arboviruses. Curr Opin Virol. 2019;34:104–9. https://doi.org/10.1016/j.coviro.2019.01.0014.
4. Huang B, Allcock R, Warrilow D. Newly characterized arboviruses of northern Australia. Virol Rep. 2016;6:11–7. https://doi.org/10.1016/j.virep.2016.01.0015.
5. Granerod J, Ambrose HE, Davies NW, Clewley JP, Walsh AL, Morgan D, et al.; UK Health Protection Agency (HPA) Aetiology of Encephalitis Study Group. Causes of encephalitis and differences in their clinical presentations in England: a multicentre, population-based prospective study. Lancet Infect Dis. 2010;10:835–44. https://doi.org/10.1016/S1473-3099(10)70222-X6.
6. Rodriguez CJ, Hua C, Woerther PL, Bosc R, Desroches M, Sitterlé E, et al. Pathogen identification by shotgun metagenomics of patients with necrotizing soft-tissue infections. Br J Dermatol. 2019. https://doi.org/10.1111/bjd.186117.
7. Reguera J, Weber F, Cusack S. *Bunyaviridae* RNA polymerases (L-protein) have an N-terminal, influenza-like endonuclease domain, essential for viral cap-dependent transcription. PLoS Pathog. 2010;6:e1001101. https://doi.org/10.1371/journal.ppat.10011018.
8. Fazakerley JK, Gonzalez-Scarano F, Strickler J, Dietzschold B, Karush F, Nathanson N. Organization of the middle RNA segment of snowshoe hare Bunyavirus. Virology. 1988;167:422–32. https://doi.org/10.1016/S0042-6822(88)90104-39.
9. Briese T, Rambaut A, Lipkin WI. Analysis of the medium (M) segment sequence of Guaroa virus and its comparison to other orthobunyaviruses. J Gen Virol. 2004;85:3071–7. https://doi.org/10.1099/vir.0.80122-010.
10. Wilson MR, Sample HA, Zorn KC, Arevalo S, Yu G, Neuhaus J, et al. Clinical metagenomic sequencing for diagnosis of meningitis and encephalitis. N Engl J Med. 2019;380:2327–40. https://doi.org/10.1056/NEJMoa180339611.
11. Bridgen A, Weber F, Fazakerley JK, Elliott RM. Bunyamwera bunyavirus nonstructural protein NSs is a nonessential gene product that contributes to viral pathogenesis. Proc Natl Acad Sci U S A. 2001;98:664–9. https://doi.org/10.1073/pnas.98.2.66412.
12. Weber F, Bridgen A, Fazakerley JK, Streitenfeld H, Kessler N, Randall RE, et al. Bunyamwera bunyavirus nonstructural protein NSs counteracts the induction of alpha/beta interferon. J Virol. 2002;76:7949–55. https://doi.org/10.1128/JVI.76.16.7949-7955.200213.
13. Ter Horst S, Conceição-Neto N, Neyts J, Rocha-Pereira J. Structural and functional similarities in bunyaviruses: perspectives for pan-bunya antivirals. Rev Med Virol. 2019;29:e2039. https://doi.org/10.1002/rmv.2039

Address for correspondence: Christophe Rodriguez, Department of Microbiology, Hôpital Henri Mondor, 51 avenue du Maréchal de Lattre de Tassigny, 94010 Créteil CEDEX, France; email: christophe.rodriguez@aphp.fr

Increased Community-Associated *Clostridioides difficile* Infections in Quebec, Canada, 2008–2015[1]

Veronica Zanichelli, Christophe Garenc, Jasmin Villeneuve, Danielle Moisan, Charles Frenette, Vivian Loo, Yves Longtin; Québec *C.difficile* Infection Surveillance Program (SPIN-CD)

The annual incidence rate of community-associated *Clostridioides difficile* infections in Quebec, Canada, has increased by 33.3%, from 0.51 (2008) to 0.68 (2015) cases/100,000 population, while incidence of healthcare-associated cases remained relatively stable. Possible causes include increased disease severity, increased antimicrobial drug use, emergence of virulent strains, and heightened physician awareness.

Clostridioides difficile infections (CDIs) are commonly acquired in healthcare settings (*1*). In 2003, an outbreak of CDI in the province of Quebec, Canada (population, 8.2 million), required implementation of mitigation strategies and prompted introduction of a surveillance program (*2*,*3*). Afterward, incidence of healthcare-associated CDIs (HA-CDIs) in the province decreased from 13.7 cases/10,000 patient-days in 2004–2005 to 6.9/10,000 patient-days in 2014–2015. Although CDIs afflict mainly hospitalized patients, recent studies report increased incidence of community-associated CDIs (CA-CDIs) (*4*–*6*). Whereas most of the focus in North America has been on HA-CDI, we describe and compare long-term trends in incidence rates for HA-CDI and CA-CDI in Quebec.

The Study

To evaluate HA-CDI and CA-CDI trends in Quebec, we performed a quasi-experimental study. We used prospectively collected data from the Quebec Health Ministry *C. difficile* Infection Surveillance Program (SPIN-CD), a mandatory surveillance program introduced in 2004 (*7*). As of 2018, all 90 acute-care hospitals with ≥1,000 admissions annually participate in SPIN-CD. These hospitals, which represent 97% of all admissions in the province, use a centralized web portal to report HA-CDI incidence density, computed as the aggregate number of cases divided by the aggregate number of patient-days per 4-week period. CA-CDI incidence rates are expressed as the number of CA-CDIs/100,000 population as reported by the Quebec Institute of Statistics (*8*).

CDI is defined as diarrhea (≥3 unformed stools in <24 hours with symptoms lasting ≥24 hours) with no other etiology and either a positive toxigenic *C. difficile* test result or evidence of pseudomembranes during histopathologic or colonoscopic examination (*9*). A case is considered to be HA-CDI if symptoms appear ≥72 hours after admission or ≤4 weeks after discharge. A CA-CDI case is defined as illness in a hospitalized patient for whom symptoms developed within 72 hours of admission and who had not been hospitalized or received ambulatory care in the previous 4 weeks. Nonhospitalized CA-CDI case-patients and recurrences (i.e., new CDI episodes within 8 weeks of a previous episode) are not reportable to SPIN-CD. Definitions did not change during the study period. The type of laboratory assay used to detect *C. difficile* was at the discretion of each center (*10*).

To focus the analysis on the postepidemic period (April 2008–March 2015), we excluded data from the epidemic period (August 2004–March 2008). We used Poisson regression models on time series

Author affiliations: Sir Mortimer B. Davis Jewish General Hospital, Montreal, Quebec, Canada (V. Zanichelli, Y. Longtin); Centre de Recherche du CHU de Quebec, Quebec City (C. Garenc); Institut National de Santé Publique du Québec, Quebec City, Quebec, Canada (C. Garenc, J. Villeneuve); CSSS Rivière-du-Loup, Rivière-du-Loup, Québec, Canada (D. Moisan); McGill University Health Centre, Montreal (C. Frenette, V. Loo, Y. Longtin)

DOI: https://doi.org/10.3201/eid2606.190233

[1]Preliminary results from this study were presented at the IDweek 2018 conference; 2018 Oct 3–7; San Francisco, California, USA (abstract no. 477).

Table 1. Annual incidence rate of community-associated and healthcare-associated *Clostridioides difficile* infections in the province of Quebec, Canada, 2008–2015

	Community-associated cases				Healthcare- associated cases		
Years	No. cases	Mean annual population	Rate/100,000 population	% Total cases	No. cases	No. patient-days	Rate/10,000 patient-days
2008–2009	510	7,764,759	0.51	13.6	3,244	4,915,666	6.60
2009–2010	568	7,846,295	0.56	15.1	3,206	4,855,739	6.60
2010–2011	619	7,930,943	0.60	14.9	3,544	4,898,891	7.23
2011–2012	605	8,009,614	0.58	14.1	3,697	4,927,050	7.50
2012–2013	697	8,084,741	0.66	15.9	3,695	4,941,796	7.48
2013–2014	753	8,150,131	0.71	17.2	3,615	4,880,472	7.41
2014–2015	729	8,209,599	0.68	17.8	3,372	4,843,433	6.96

data, including trend and periodic seasonal terms to calculate incidence rate ratios (IRRs) with 95% CIs and to assess trends in CA-CDIs and HA-CDIs. We also used interrupted time series analysis with segmented regression because of a change in the level and trend in HA-CDI incidence rate from 2011 on (*11*). We compared the change in trends in HA-CDI and CA-CDI incidence by using Z-tests of the difference of the natural logarithm of incidence rates. We used SAS software version 9.3 (https://www.sas.com) for analyses and considered $p<0.05$ to be significant.

During the study period, a total of 28,854 cases of HA-CDI (84.5%) and CA-CDI (15.5%) were reported. The annual number of CA-CDI cases and the proportion of CDI cases that were reported as CA-CDI increased gradually from 510 (13.6% of HA-CDI) to 729 (17.8% of CA-CDI) cases (Table 1). Furthermore, the CA-CDI incidence rate increased ≈6.5% annually and overall significantly by 33.3%, from 0.51 to 0.68 cases/100,000 population (IRR per 4-week period 1.005, 95% CI 1.004–1.006; $p<0.0001$) (Figure 1). By contrast, the incidence of HA-CDI did not change significantly (IRR per 4-week period 1.000, 95% CI 0.999–1.000; $p = 0.23$). Accordingly, incidence rate trends for CA-CDI differed significantly from trends for HA-CDI (IRR 1.005, 95% CI 1.004–1.006; $p<0.0001$).

An inflection point in HA-CDI incidence in April 2011 was demonstrated by a significant decreasing change in trend (IRR 0.996, 95% CI 0.994–0.998; $p = 0.001$). By contrast, no concomitant change occurred in the trend of CA-CDI at the inflection point (Figure 2, Table 2).

Conclusions

Although the incidence of HA-CDI has been decreasing in Canada since 2009 (*12*), our study suggests possible emergence of CA-CDI in the province of Quebec because the number, incidence, and proportion of reported cases have been steadily increasing since 2008. This increased incidence contrasts markedly with the overall decreasing trend of HA-CDI incidence after April 2011.

Emergence of CA-CDI has been reported in other countries (*4–6*,*13*). A 2008–2013 study in Finland reported an increase in probable CA-CDI cases at an annual rate of 4.3% compared with a concomitant decrease in HA-CDI cases at an annual rate of 8.1% (*4*). In the United Kingdom, an analysis of hospital administrative data detected an increase in the proportion of CDI cases that were community acquired, from 7% in 1998 to 13% in 2010, while the overall incidence of CDI cases fell to less than half of peak rate (*13*). The US Veterans

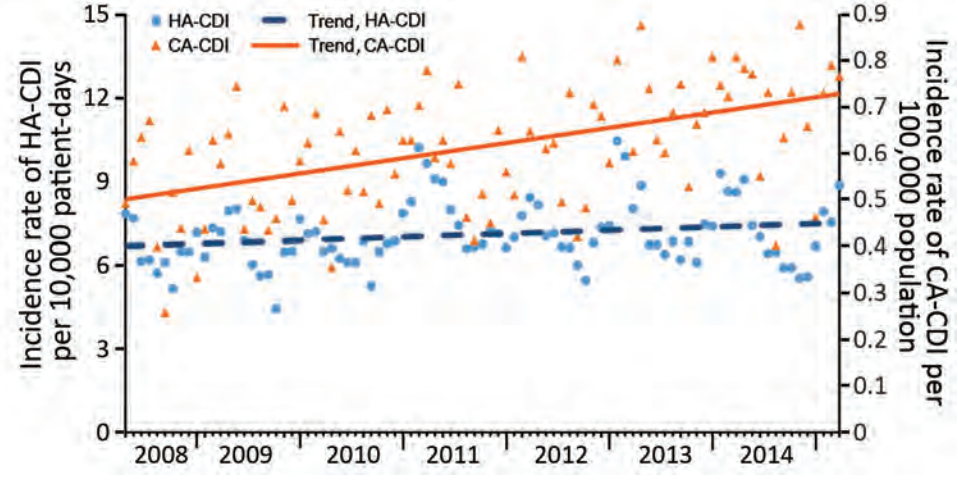

Figure 1. Incidence density of HA-CDIs and CA-CDIs per 4-week period, according to standardized surveillance definitions, Quebec, Canada, April 2008–March 2015. CDI, *Clostridioides difficile* infection; CA-CDI, community-associated CDI; HA-CDI, healthcare-associated CDI.

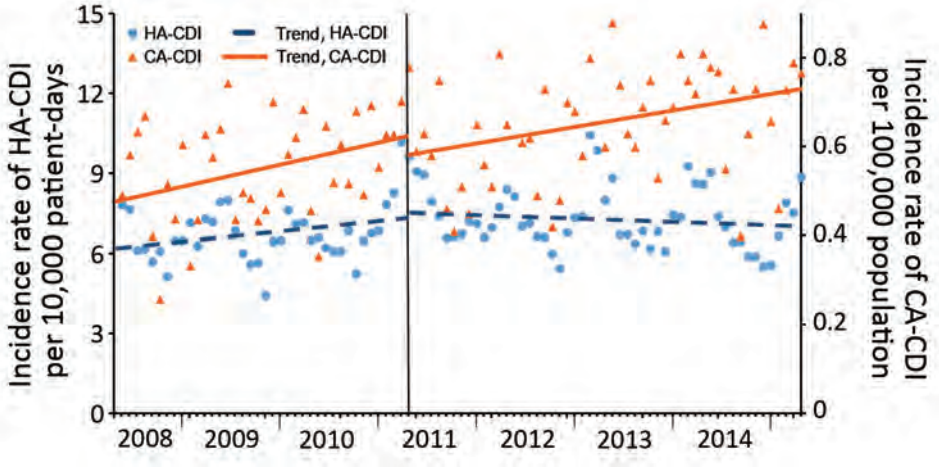

Figure 2. Trends in incidence of HA-CDIs and CA-CDIs analyzed by using linear segmented regression (inflection point of HA-CDI in April 2011) per 4-week period, according to standardized surveillance definitions, Quebec, Canada, April 2008–March 2015. CDI, *Clostridioides difficile* infection; CA-CDI, community-associated CDI; HA-CDI, healthcare-associated CDI.

Healthcare Administration reported similar findings of an increased proportion of CDI cases that were community-associated (from 8.3% in 2003 to 26.7% in 2014) (*5*). Electronic patient records analysis in Hong Kong identified a 3-fold increase in the incidence of CA-CDI cases, from 0.86/100,000 population in 2006 to 2.96/100,000 population in 2014 (*6*). These reports suggest that CA-CDI may be increasing worldwide; however, because the studies relied on retrospective extraction of data that were not specifically collected for CDI surveillance, they may be susceptible to misclassification and reporting biases (*14*).

The factors underlying this apparent increase in CA-CDI incidence are unclear. However, we hypothesize that this rise may result from any combination of the following: increased disease severity, leading to a greater proportion of case-patients being hospitalized; increased use of antimicrobial drugs or proton-pump inhibitors in the community; emergence of community-specific novel virulent *C. difficile* strains; and heightened awareness by physicians to consider the diagnosis of CDI.

Our study has many strengths. We used prospectively collected data from a well-established surveillance program enrolling virtually all persons admitted to acute-care hospitals in the province, thereby limiting selection bias, and we used standardized case definitions to avoid misclassification issues. However, our study also has several limitations. Only persons hospitalized with CA-CDI were reported to the surveillance program; therefore, milder cases were not captured. Thus, the actual incidence of CA-CDI may be underestimated. Because no clinical data regarding patients in whom CDI develops were collected, we cannot characterize patients or investigate potential changes in the affected population. We could not investigate the effect of diagnostic assay modifications on the observed change in trend because this information was not collected. Nucleic acid amplification tests are more sensitive than enzyme immunoassays for detecting toxigenic *C. difficile*; thus, increased use of these tests could lead to increased CA-CDI incidence rates. However, use of a more sensitive assay would be expected to affect CA-CDI and HA-CDI incidence similarly, whereas these trends are clearly divergent.

In conclusion, CA-CDI incidence in the province of Quebec increased significantly during 2008–2015 despite an overall decrease in HA-CDI incidence. This divergence in trends suggests a need to devote more attention to CA-CDI.

Table 2. Segmented regression of HA-CDI and CA-CDI in the province of Quebec, Canada, 2008–2015*

	2008–2009 to 2010–2011		2011–2012 to 2014–2015			
Rate	Overall trend before the breakpoint, IRR (95% CI)	p value	Immediate change after the breakpoint, IRR (95% CI)	p value	Change in trend after the breakpoint, IRR (95% CI)	p value
HA-CDI rate/10,000 patient-days	1.003 (1.001–1.005)	0.001	0.998 (0.945–1.053)	0.93	0.996 (0.994–0.998)	0.001
CA-CDI rate/100,000 population	1.007 (1.003–1.012)	0.002	0.95 (0.841–1.074)	0.41	0.997 (0.992–1.002)	0.30
Group difference	1.002 (0.997–1.007)	0.35	0.971 (0.851–1.107)	0.66	1.002 (0.996–1.008)	0.53

*Breakpoints were identified in April 2011. CA, community-acquired; HA, hospital-acquired; CDI, *Clostridioides difficile* infection; IRR, incidence rate ratio (calculated per 4-week period).

Acknowledgement

We thank the hospitals that participated in the prospective surveillance program.

Funding was provided by the Institut National de Santé Publique du Québec.

About the Author

Dr. Zanichelli is an infectious disease physician working as a research assistant at the Lady Davis Institute for Medical Research in Montreal, Canada. Her current research focuses on CDIs and antibiotic stewardship in the inpatient setting.

References

1. Levy AR, Szabo SM, Lozano-Ortega G, Lloyd-Smith E, Leung V, Lawrence R, et al. Incidence and costs of *Clostridium difficile* infections in Canada. Open Forum Infect Dis. 2015;2:ofv076. https://doi.org/10.1093/ofid/ofv076
2. Loo VG, Poirier L, Miller MA, Oughton M, Libman MD, Michaud S, et al. A predominantly clonal multi-institutional outbreak of *Clostridium difficile*-associated diarrhea with high morbidity and mortality. N Engl J Med. 2005;353:2442–9. https://doi.org/10.1056/NEJMoa051639
3. Institut National de Santé Publique du Québec (INSPQ). Surveillance provinciale des diarrhées à *Clostridium difficile* (DACD)–typage des souches de *C. difficile* causant la DACD au Québec, 2005–2015 [cited 2018 Nov 26]. https://www.inspq.qc.ca/publications/2444
4. Kotila SM, Mentula S, Ollgren J, Virolainen-Julkunen A, Lyytikäinen O. Community- and healthcare-associated *Clostridium difficile* infections, Finland, 2008–2013. Emerg Infect Dis. 2016;22:1747–53. https://doi.org/10.3201/eid2210.151492
5. Reveles KR, Pugh MJV, Lawson KA, Mortensen EM, Koeller JM, Argamany JR, et al. Shift to community-onset *Clostridium difficile* infection in the national Veterans Health Administration, 2003-2014. Am J Infect Control. 2018; 46:431–5. https://doi.org/10.1016/j.ajic.2017.09.020
6. Ho J, Dai RZW, Kwong TNY, Wang X, Zhang L, Ip M, et al. Disease burden of *Clostridium difficile* infections in adults, Hong Kong, China, 2006–2014. Emerg Infect Dis. 2017;23:1671–9. https://doi.org/10.3201/eid2310.170797
7. Institut National de Santé Publique du Québec (INSPQ). Surveillance des diarrhées à *Clostridium difficile* (DACD) [cited 2018 Nov 18]. https://www.inspq.qc.ca/infections-nosocomiales/spin/dacd
8. Institut de la Statistique du Québec. Le bilan démographique du Québec, édition 2017 [cited 2018 Nov 26]. http://www.stat.gouv.qc.ca/statistiques/population-demographie/bilan2017.pdf
9. Institut National de Santé Ppublique du Québec (INSPQ). Surveillance provinciale des diarrhées à *Clostridium difficile* au Québec protocole [cited 2018 Nov 19]. https://www.inspq.qc.ca/sites/default/files/documents/infectionsnosocomiales/protocole_dacd_2018.pdf
10. Bogaty C, Lévesque S, Garenc C, Frenette C, Bolduc D, Galarneau LA, et al.; Quebec Clostridium difficile Infection Surveillance Program (QCISP). Trends in the use of laboratory tests for the diagnosis of *Clostridium difficile* infection and association with incidence rates in Quebec, Canada, 2010-2014. Am J Infect Control. 2017;45:964–8. https://doi.org/10.1016/j.ajic.2017.04.002
11. Wagner AK, Soumerai SB, Zhang F, Ross-Degnan D. Segmented regression analysis of interrupted time series studies in medication use research. J Clin Pharm Ther. 2002;27:299–309. https://doi.org/10.1046/j.1365-2710.2002.00430.x
12. Katz KC, Golding GR, Choi KB, Pelude L, Amaratunga KR, Taljaard M, et al.; Canadian Nosocomial Infection Surveillance Program. The evolving epidemiology of *Clostridium difficile* infection in Canadian hospitals during a postepidemic period (2009–2015). CMAJ. 2018;190:E758–65. https://doi.org/10.1503/cmaj.180013
13. Jen MH, Saxena S, Bottle A, Pollok R, Holmes A, Aylin P. Assessment of administrative data for evaluating the shifting acquisition of *Clostridium difficile* infection in England. J Hosp Infect. 2012;80:229–37. https://doi.org/10.1016/j.jhin.2012.01.001
14. Albert K, Ross B, Calfee DP, Simon MS. Overreporting healthcare-associated *C. difficile*: a comparison of NHSN LabID with clinical surveillance definitions in the era of molecular testing. Am J Infect Control. 2018;46:998–1002. https://doi.org/10.1016/j.ajic.2018.03.001

Address for correspondence: Yves Longtin, Rm E-0057, Infection Prevention and Control Unit, Jewish General Hospital SMBD, 3755 Côte-Sainte-Catherine Rd, Montreal, QB H3T 1E2, Canada; email: yves.longtin@mcgill.ca

Melioidosis in a Resident of Texas with No Recent Travel History, United States

Caitlin M. Cossaboom, Atanaska Marinova-Petkova, Jonathan Strysko, Gretchen Rodriguez, Trevor Maness, Jaime Ocampo, Jay E. Gee, Mindy G. Elrod, Christopher A. Gulvik, Lindy Liu, William A. Bower, Alex R. Hoffmaster, David D. Blaney, Johanna S. Salzer, Jonathan S. Yoder, Mia C. Mattioli, Thomas J. Sidwa, Lillian Ringsdorf, Gale Morrow, Elvia Ledezma, Amanda Kieffer

To our knowledge, environmental isolation of *Burkholderia pseudomallei*, the causative agent of melioidosis, from the continental United States has not been reported. We report a case of melioidosis in a Texas resident. Genomic analysis indicated that the isolate groups with *B. pseudomallei* isolates from patients in the same region, suggesting possible endemicity to this region.

Burkholderia pseudomallei, which causes melioidosis, is a gram-negative saprophytic bacterium endemic to tropical and subtropical environments worldwide; to our knowledge, isolation from the continental United States has not been reported (*1*–*3*). The most overrepresented risk factor for melioidosis is diabetes mellitus (*3*,*4*). *B. pseudomallei* is resistant to many antimicrobial drugs (*3*). Laboratory exposures might occur without appropriate biosafety precautions (*2*,*5*).

Surveillance is challenging because melioidosis is not nationally notifiable; however, *B. pseudomallei* is a Tier 1 overlap Select Agent (*6*), and the Centers for Disease Control and Prevention (CDC) receives voluntary reports (*2*,*7*). We report a case of melioidosis in a Texas resident who had no recent travel history.

Author affiliations: Centers for Disease Control and Prevention, Atlanta, Georgia, USA (C.M. Cossaboom, A. Marinova-Petkova, J. Strysko, J.E. Gee, M.G. Elrod, C.A. Gulvik, L. Liu, W.A. Bower, A.R. Hoffmaster, D.D. Blaney, J.S. Salzer, J.S. Yoder, M.C.Mattioli); Texas Department of State Health Services, San Antonio, Texas, USA (G. Rodriguez, T. Maness, J. Ocampo, L. Ringsdorf, G. Morrow, E. Ledezma, A. Kieffer); Texas Department of State Health Services, Austin, Texas, USA (T.J. Sidwa)

DOI: https://doi.org/10.3201/eid2606.190975

The Study

On November 17, 2018, a 63-year-old man from Atascosa County, Texas, came to hospital A with fever, chest pain, and dyspnea of 3 days' duration. At admission, he reported congenital unilateral renal agenesis. Renal function measures were unremarkable. Increased hemoglobin A1c level and hyperglycemia (glucose >200 mg/dL) suggested undiagnosed type 2 diabetes.

Computed tomography of chest and abdomen with intravenous contrast showed left lower lobe pneumonia with a small left pleural effusion. Empiric antimicrobial drug therapy with intravenous azithromycin and ceftriaxone was initiated. Blood culture yielded presumptive *B. pseudomallei*, which was sent for confirmation to the laboratory response network (LRN) site in Houston, Texas.

On November 20, a localized, violaceous, cutaneous lesion developed on the central anterior chest wall of the patient and progressed to become purulent and ulcerated (Figure 1). The next day, he experienced respiratory failure, was emergently intubated, and was transferred to hospital B.

Hospital B was not aware of the presumptive diagnosis and performed a blood and chest wound culture. Both cultures showed gram-negative rods; blood analysis showed acute kidney injury. On November 25, *B. pseudomallei* susceptible to trimethoprim/sulfamethoxazole and ceftazidime (Table) was identified, and treatment was switched to ceftazidime by using dosing for continuous renal replacement therapy (*4*).

On November 26, the patient was extubated and began hemodialysis (3 ×/wk). He was discharged on December 9 and received 3 months of daily trimethoprim/sulfamethoxazole (*4*). Subsequent follow-up showed clinically recovery and resolution of z renal insufficiency.

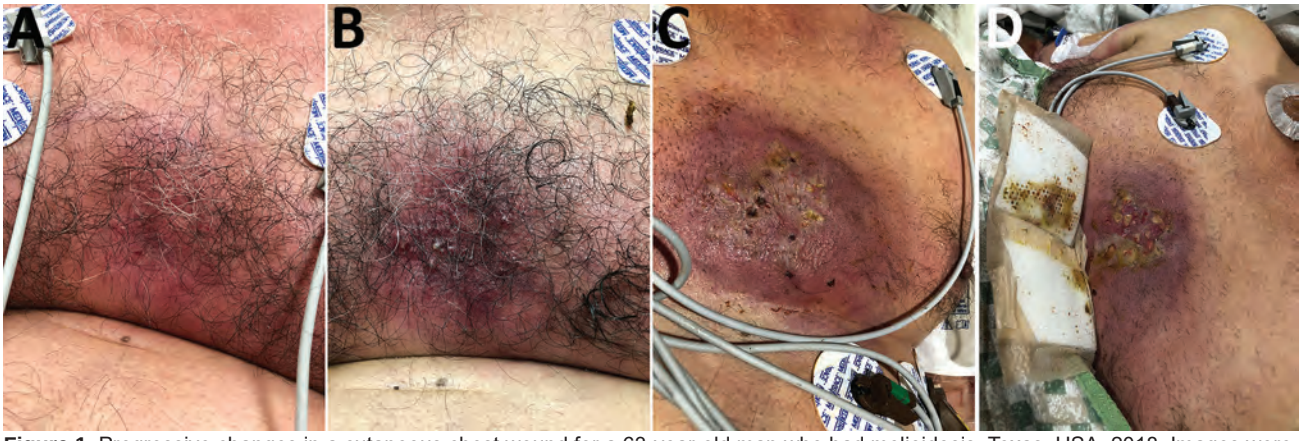

Figure 1. Progressive changes in a cutaneous chest wound for a 63-year-old man who had melioidosis, Texas, USA, 2018. Images were obtained on A) day 3, B) day 4, C) day 9, and D) day 10 after his initial visit to hospital A on November 17, 2018.

Because the isolate had an unremarkable resistance profile and *B. pseudomallei* was not specifically listed on the Texas Notifiable Conditions List, the automated system at hospital B did not generate an alert indicating it required LRN confirmation, and the isolate was not promptly reported to Texas Department of State Health Services (DSHS). On November 27, Houston LRN reported to DSHS Region 8 (San Antonio, TX, USA) confirmation of the isolate from hospital A as *B. pseudomallei*. The Houston LRN and hospital A destroyed the remaining isolates because of regulations surrounding handling of select agents.

DSHS and CDC collaboratively investigated the source of the patient's exposure to *B. pseudomallei* and performed risk assessments to identify potential laboratory exposures at both hospitals.

The patient's only reported travel outside Texas was a visit to Monterrey, Mexico, 30 years before illness onset. Before becoming ill, he resided on a small rural ranch without running water from a municipal source or private well. He purchased water for nondrinking use from a local chlorinated municipal water utility. He used a 500-gallon uncovered tank to store the water and then pumped the water into a 1,600-gallon storage tank. He cleaned the tank 1–2 times/month by climbing inside to scrub the walls. The last cleaning was 2 days before illness onset.

Table. Drug susceptibility profile for *Burkholderia pseudomallei* isolate from culture of chest wound from a 63-year-old man, Texas, USA*

Drug	MIC, μg/mL	Result
Amikacin	>32	R
Ampicillin	>16	R
Ampicillin/sulbactam	>16/8	R
Aztreonam	>16	R
Cefazolin	>16	R
Cefepime	>16	R
Cefotaxime	32	R
Cefoxitin	>16	R
Ceftazidime	8	S
Ceftriaxone	>32	R
Cefuroxime	>16	R
Ciprofloxacin	>2	R
Gentamicin	>8	R
Ertapenem	>1	R
Meropenem	≤1	S
Piperacillin/tazobactam	≤16	S
Tobramycin	>8	R
Trimethoprim/sulfamethoxazole	≤2/38	S

*R, resistant; S, susceptible.

During environmental sampling in December 2018, we collected 56 specimens from the patient's home and property. We concentrated large-volume (30–190 L) water samples on site and processed as described (*8*). We collected soil samples (50 mL) at a depth of 30 cm (*9*) from 8 sites in moist soil. Other environmental samples included surface swabs (10 × 10 inch) of the inside of both water storage tanks and swabs of indoor and outdoor plumbing fixtures. We processed specimens by using international guidelines (*9*) and tested for presence of *B. pseudomallei* by using culture and real-time quantitative PCR (*10*). All specimens were negative for *B. pseudomallei*.

We identified 7 laboratory personnel at hospitals A and B who had low-risk exposures to the *B. pseudomallei* isolates (*5*). Recommendations included temperature monitoring twice a day for 21 days and collecting serum samples at 1, 2, 4 and 6 weeks postexposure (*5*). We performed serologic testing by using an indirect hemagglutination assay (*11*). All samples were negative for *B. pseudomallei* antibodies (cutoff value 1:40).

Hospital B submitted the patient's blood culture isolate (TX2018b) for whole-genome sequencing (National Center for Biotechnology BioProject no. PRJNA545616). Multilocus sequence typing identified the isolate as sequence type 297 (*12*). The 8 other sequence type 297 isolates are all associated with North

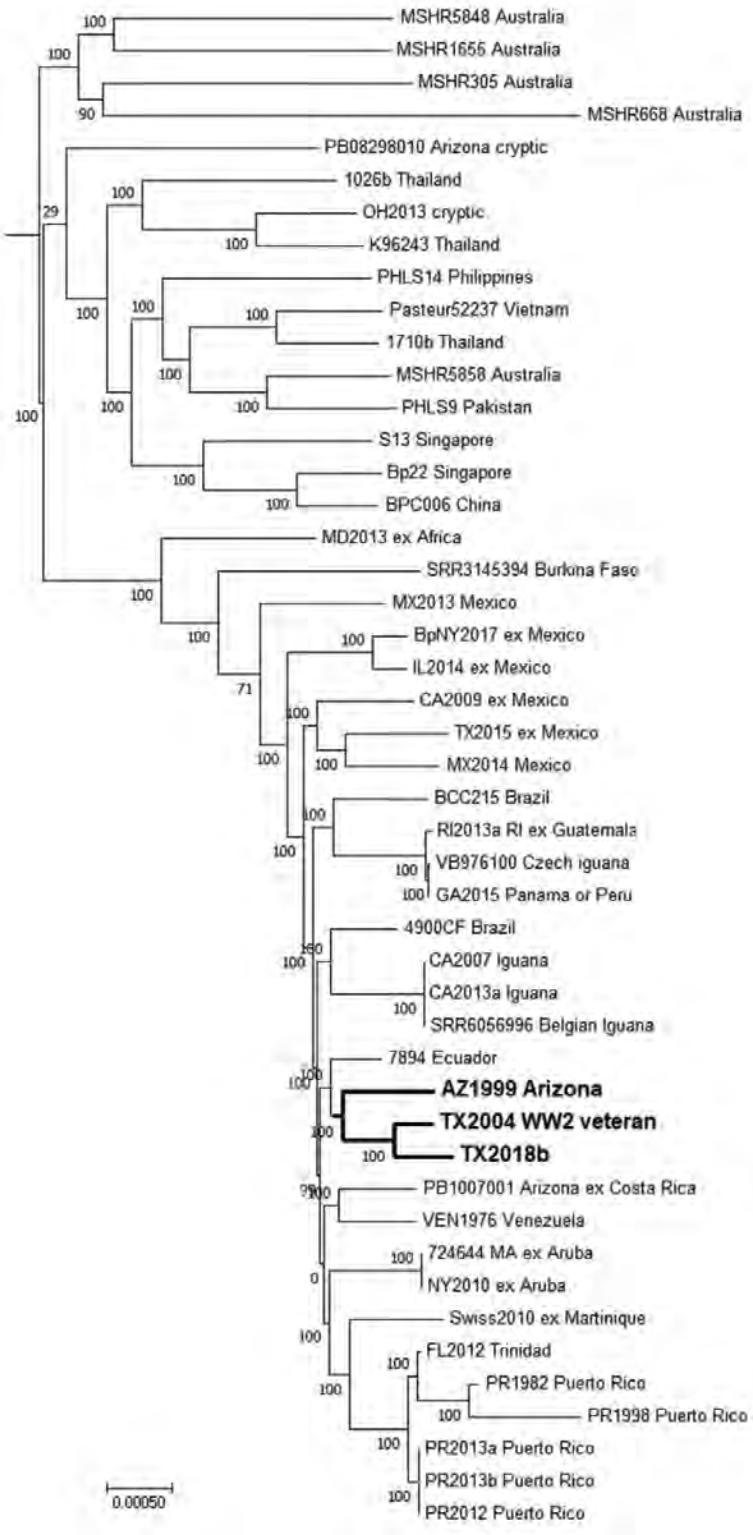

Figure 2. Dendrogram for characterization of *Burkholderia pseudomallei* isolate TX2018b from a 63-year-old man in Texas, USA, by comparison with reference genomes. Maximum-parsimony phylogenetic analysis based on core single-nucleotide polymorphisms (SNP) by using Parsnp, a component of the Harvest 1.3 software (https://github.com/marbl/harvest). Bold indicates clusters of genomes associated with the southwestern United States; the 2004 patient resided in the same county as the patient described in this article. Numbers at each node are bootstrap percentages. Scale bar indicates nucleotide substitutions per SNP.

America (*1*). A higher resolution single-nucleotide polymorphism comparison of the draft genome assembly with other public assemblies containing geographic data also indicated that the isolate is associated with others from North America. TX2018b grouped closest to TX2004 and to a lesser extent to AZ1999 (BioProject no. PRJNA545640) (Figure 2).

TX2004 was isolated in 2004 from a patient residing in the same Texas county as our patient (*13*). It was originally hypothesized that the 2004 patient was infected 62 years before disease onset, while serving during World War II in Southeast Asia (*13*). However, TX2004 is not related to strains from Southeast Asia but to strains from the Americas (*1*). Other regional travel by the 2004 patient was not reported. AZ1999 was isolated from a patient treated in 1999 in Arizona who had recently emigrated from El Salvador. Where exposure occurred for that patient is unknown, but that isolate groups closer to TX2004 and TX2018b than to other examples associated with Central America (Figure 2).

Conclusions

The source of this patient's infection remains unknown. However, genomic analysis showed that the patient isolate groups with existing isolates collected from other patients in the southwestern United States. Isolates TX2004 and TX2018b were collected ≈15 years apart from patients living in the same Texas county at time of illness onset and group together, a finding that suggests *B. pseudomallei* might be present in the environment in this area. Furthermore, these 2 isolates might represent a new clade endemic to the continental United States. Further investigation is warranted because this region is predicted to have suitable habitats for *B. pseudomallei* (*14*).

These findings call into question possible reactivation of melioidosis decades after travel to melioidosis-endemic regions. Instead of a 62-year incubation period, the patient infected with TX2004 might have had an unknown local environmental exposure that preceded symptom onset. A 1991 case report of an 18-year latency for a Vietnam War veteran indicated that this patient was also living in the southwestern United States (New Mexico) at time of symptom onset and had not traveled outside the continental United States since 1971 (*15*). On the other hand, although geographic and genotypic links between the 2 Texas cases suggest a local source, *B. pseudomallei* exposure for the patient infected with TX2018b could have occurred 30 years earlier, while visiting Mexico, and the patient infected with TX2004 might have had unreported regional travel before illness onset. Only when *B. pseudomallei* is isolated from the environment can it be definitively stated that *B. pseudomallei* is endemic to the continental United States.

B. pseudomallei infection should be included in a differential diagnosis for a patient with compatible disease, even without reported travel history. Increased awareness among healthcare workers and diagnostic laboratory personnel for melioidosis as a disease potentially endemic to the southwestern United States is critical to improve case outcomes and prevent laboratory exposures.

In addition, melioidosis is caused by a Tier 1 overlap Select Agent, but reporting of cases to CDC is voluntary (*2*,*7*). Making melioidosis nationally notifiable could improve surveillance and recognition and clarify distribution and potential sources of *B. pseudomallei* infection in the United States.

Acknowledgments

We thank the patient and his family for providing photographs of the patient's progressing cutaneous chest wound and the Arizona Department of Health and Maricopa County Department of Health for providing background information on strain AZ1999.

About the Author

Dr. Cossaboom is a veterinary epidemiologist in the Division of High-Consequence Pathogens and Pathology, National Center for Emerging and Zoonotic Infectious Diseases, Centers for Disease Control and Prevention, Atlanta, GA. Her primary research interests include epidemiology of and outbreak response for zoonotic diseases of public health importance.

References

1. Gee JE, Gulvik CA, Elrod MG, Batra D, Rowe LA, Sheth M, et al. Phylogeography of *Burkholderia pseudomallei* isolates, Western Hemisphere. Emerg Infect Dis. 2017;23:1133–8. https://doi.org/10.3201/eid2307.161978
2. Benoit TJ, Blaney DD, Doker TJ, Gee JE, Elrod MG, Rolim DB, et al. A Review of melioidosis cases in the Americas. Am J Trop Med Hyg. 2015;93:1134–9. https://doi.org/10.4269/ajtmh.15-0405
3. Wiersinga WJ, Virk HS, Torres AG, Currie BJ, Peacock SJ, Dance DA, et al. Melioidosis. Nat Rev Dis Primers. 2018;4:17107. https://doi.org/10.1038/nrdp.2017.107
4. Currie BJ. Melioidosis: evolving concepts in epidemiology, pathogenesis, and treatment. Semin Respir Crit Care Med. 2015;36:111–25. https://doi.org/10.1055/s-0034-1398389
5. Peacock SJ, Schweizer HP, Dance DA, Smith TL, Gee JE, Wuthiekanun V, et al. Management of accidental laboratory exposure to *Burkholderia pseudomallei* and *B. mallei*. Emerg Infect Dis. 2008;14:e2. https://doi.org/10.3201/eid1407.071501
6. Federal Select Agent Program, 2017 [cited 2019 Apr 21]. http://www.selectagents.gov

7. Adams DA, Thomas KR, Jajosky RA, Foster L, Baroi G, Sharp P, et al.; Nationally Notifiable Infectious Conditions Group. Summary of notifiable infectious diseases and conditions—United States, 2015. MMWR Morb Mortal Wkly Rep. 2017;64:1–143. https://doi.org/10.15585/mmwr.mm6453a1
8. Mull B, Hill VR. Recovery of diverse microbes in high turbidity surface water samples using dead-end ultrafiltration. J Microbiol Methods. 2012;91:429–33. https://doi.org/10.1016/j.mimet.2012.10.001
9. Limmathurotsakul D, Dance DA, Wuthiekanun V, Kaestli M, Mayo M, Warner J, et al. Systematic review and consensus guidelines for environmental sampling of *Burkholderia pseudomallei*. PLoS Negl Trop Dis.2013;7:e2105. https://doi.org/10.1371/journal.pntd.0002105
10. Novak RT, Glass MB, Gee JE, Gal D, Mayo MJ, Currie BJ, et al. Development and evaluation of a real-time PCR assay targeting the type III secretion system of *Burkholderia pseudomallei*. J Clin Microbiol. 2006;44:85–90. https://doi.org/10.1128/JCM.44.1.85-90.2006
11. Alexander AD, Huxsoll DL, Warner AR Jr, Shepler V, Dorsey A. Serological diagnosis of human melioidosis with indirect hemagglutination and complement fixation tests. Appl Microbiol. 1970;20:825–33. https://doi.org/10.1128/AEM.20.5.825-833.1970
12. Godoy D, Randle G, Simpson AJ, Aanensen DM, Pitt TL, Kinoshita R, et al. Multilocus sequence typing and evolutionary relationships among the causative agents of melioidosis and glanders, *Burkholderia pseudomallei* and *Burkholderia mallei*. J Clin Microbiol. 2003;41:2068–79. https://doi.org/10.1128/JCM.41.5.2068-2079.2003
13. Ngauy V, Lemeshev Y, Sadkowski L, Crawford G. Cutaneous melioidosis in a man who was taken as a prisoner of war by the Japanese during World War II. J Clin Microbiol. 2005;43:970–2. https://doi.org/10.1128/JCM.43.2.970-972.2005
14. Limmathurotsakul D, Golding N, Dance DA, Messina JP, Pigott DM, Moyes CL, et al. Predicted global distribution of *Burkholderia pseudomallei* and burden of melioidosis. Nat Microbiol. 2016;1:15008. https://doi.org/10.1038/nmicrobiol.2015.8
15. Koponen MA, Zlock D, Palmer DL, Merlin TL. Melioidosis. Forgotten, but not gone! Arch Intern Med. 1991;151:605–8. https://doi.org/10.1001/archinte.1991.00400030135027

Address for correspondence: Caitlin M. Cossaboom, Centers for Disease Control and Prevention, 1600 Clifton Rd NE, Mailstop H24-12; Atlanta, GA 30329-4027, USA; email: nrm9@cdc.gov

No Adaptation of the Prion Strain in a Heterozygous Case of Variant Creutzfeldt-Jakob Disease

Aileen Boyle, Chris Plinston, Fraser Laing, Graeme Mackenzie, Robert G. Will, Jean C. Manson, Abigail B. Diack

We investigated a clinical case of variant Creutzfeldt-Jakob Disease in a person heterozygous for methionine/valine at codon 129 of the prion protein gene and identified the same strain properties in variant Creutzfeldt-Jakob disease in methionine homozygous persons and in bovine spongiform encephalopathy. These results indicate no adaptation of the agent in a different genetic background.

In 2016, a definite case of clinical variant Creutzfeldt-Jakob disease (vCJD) in a person heterozygous for methionine/valine (MV) at codon 129 of the prion protein gene (*PRNP* 129MV) was reported in the United Kingdom (*1*). Given the relatively atypical clinical features in this case, we considered it important to ascertain the strain of prion agent to determine whether there had been strain adaption or whether the patient's genetic background may have influenced the disease phenotype. We conducted a study to determine whether we could isolate the same prion strain from this case of vCJD in a 129MV individual as was identified in previous 129 methionine homozygous (129MM) genotype vCJD cases, consistent with the hypothesis of a causal link to bovine spongiform encephalopathy (BSE).

The clinical features for this patient were consistent with a diagnosis of either vCJD or sporadic Creutzfeldt-Jakob disease (sCJD). Results from magnetic resonance imaging (MRI) of the patient's brain were suggestive of sCJD on diffusion-weighted imaging (DWI) sequences, although the single coronal fluid-attenuated inversion recovery (FLAIR) sequence in this case was not diagnostic because of movement artifact. Results of cerebrospinal fluid (CSF) real-time quaking-induced conversion assay analysis and the direct detection assay for vCJD infection in the blood were negative. However, at autopsy, neuropathological examination revealed florid plaques, and biochemical analysis of prion protein (PrP) from the brain confirmed a type 2B profile, both characteristic of vCJD (*1*). Abnormal PrP was also detected in peripheral tissues. Recent studies in which researchers used protein misfolding cyclic amplification in CSF were positive in this case of vCJD, but not in sCJD cases, including those with a heterozygous genotype (*2*).

The Study

We injected 18 RIII mice with 10% wt/vol frozen central nervous system tissue, 0.02 mL intracerebrally and 0.1 mL intraperitoneally, from a 129MV patient with a clinical case of vCJD (*1*). The vCJD tissue samples were provided by the NHS National Prion Clinic, University College London (UCL) Hospitals (London, UK), and MRC Prion Unit at UCL and sourced through the MRC Edinburgh Brain Bank (Edinburgh, Scotland, UK). The Brain Bank has full ethics approval and consent for the use of tissue in research (East of Scotland Research Ethics Service, Ref 16/ES/0084) and works within the framework of the Human Tissue (Scotland) Act 2006. We conducted inoculation, clinical scoring, and neuropathological and biochemical analysis of the mice as previously described (*3*–*5*). Animal studies were conducted according to the regulations of the UK Home Office Animals (Scientific Procedures) Act 1986.

The isolate from the brain of the 129MV patient transmitted successfully; clinical and neuropathological signs associated with prion disease appeared in the mice. We compared the mean incubation period, neuropathological signs, and biochemical analysis with archived records of UK 129MM vCJD central nervous system transmissions and UK BSE transmissions. Methods used for inoculation, clinical scoring, and neuropathological and biochemical analysis of the mice were described in previous publications (*3*–*5*).

Author affiliations: The Roslin Institute, Easter Bush, Scotland, UK (A. Boyle, C. Plinston, F. Laing, A.B. Diack); Western General Hospital, Edinburgh, Scotland, UK (G. Mackenzie); University of Edinburgh, Edinburgh (R.G. Will, J.C. Manson)

DOI: https://doi.org/10.3201/eid2606.191116

Clinical signs with individual incubation periods ranging from 300 to 392 days postinfection (dpi) were apparent in the mice. The major clinical signs were a loss of body weight and body condition with eye winking and gait abnormalities. Toward the end of the clinical phase, a wet genital area could also be observed. Pathologically confirmed disease developed in 14 of 16 mice (mean incubation period ± SEM 341 ± 6 dpi). This finding is within the range of previous transmission studies for UK vCJD in this mouse line (mean incubation 306–387 dpi) and similar to those for BSE (mean incubation 316–335 dpi).

We also generated a transmissible spongiform encephalopathy (TSE) vacuolation profile from clinically affected RIII mice and compared it with profiles from UK vCJD and BSE transmissions (Figure 1). We observed a mild-to-moderate gray matter vacuolation in the medulla, hypothalamus, and septum and moderate vacuolation in the cochlear nucleus and dorsal raphe (Figure 1; Figure 2, panels A, B).

We conducted an immunohistochemical analysis, which showed abnormal PrP deposition throughout the brain of both a granular and punctate nature (Figure 2, panels C–K). There was heavy staining in the brainstem, particularly the superior vestibular and cochlear nuclei, and lower midbrain, where the substantia nigra was often targeted. Most of the thalamic nuclei exhibited staining, but staining was more intense in the habenular, hypothalamus, and the CA2 region of the hippocampus (Figure 2, panels F–K). Punctate staining was also apparent in the mid-layer of the cortex throughout the brain. This pattern of staining was very similar to that observed in a vCJD and BSE transmission in the United Kingdom, with additional observations of granular deposition in the cerebellar cortex and small plaques occurring in the corpus callosum in 2 of the samples.

Biochemical analysis of the MV isolate confirmed the presence of protease-resistant PrP (PrP^{res}). We identified a similar type 2B–like pattern and glycosylation profile in the RIII mice. This profile is characterized by a predominance of the diglycosylated form of PrP^{res} at ≈30 kDa, a monoglycosylated form at ≈27kDa, and an unglycosylated band at ≈19kDa (Appendix Figure, https://wwwnc.cdc.gov/EID/article/26/6/19-1116-App1.pdf). The biochemical profile appears identical between the RIII-MV, RIII-MM, and RIII-BSE isolates tested, although the RIII-BSE isolate appeared to have less PrP^{res}.

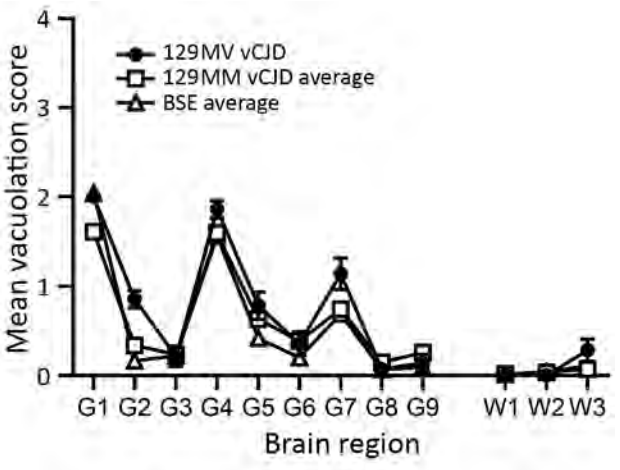

Figure 1. Vacuolation profiles of a clinical case of vCJD in a prion protein gene codon 129MV individual, pooled data from UK 129MM cases (n = 7) and pooled data from UK bovine spongiform encephalopathy cases (n = 8) show similarities in vacuolar pathology intensity and distribution in wild-type mouse brains. Data show mean ± SEM of clinical and pathological positive mice (n≥6 per group). G1–G9, gray matter scoring regions: G1, medulla; G2, cerebellum; G3, superior colliculus; G4, hypothalamus; G5, thalamus; G6, hippocampus; G7, septum; G8, retrosplenial and adjacent motor cortex; G9, cingulate and adjacent motor cortex. W1–W3, white matter scoring regions: W1, cerebellar white matter; W2, mesencephalic tegmentum; W3, cerebral peduncle. MM, methionine homozygous; MV, methionine/valine; vCJD, variant Creutzfeldt-Jakob disease.

Conclusions

This transmission study in RIII mice provides evidence that the prion strain isolated from this confirmed case of vCJD in a 129MV person is the same as that identified in typical 129MM vCJD and BSE cases. Further characterization in a range of mouse models is ongoing. However, transmission to RIII mice in previous studies has led to definitive identification of several strains, vCJD and BSE in particular (*6*,*7*).

PRNP codon 129 genotype has been shown to be a major factor influencing disease characteristics of Creutzfeldt-Jakob disease (*8*), but it has not been established if the same is true of vCJD, because previous vCJD infections in 129MV persons exposed to contaminated blood products have been asymptomatic (*9*,*10*). Earlier studies using gene-targeted mice inoculated with vCJD predicted that codon 129 genotype would determine disease susceptibility and incubation periods (*11*), whereas other transgenic mouse studies demonstrated that BSE could transmit with a different phenotype in mice expressing 129MV than that observed in mice expressing 129MM (*12*).

The clinical diagnosis in the MV case we report was uncertain while the patient was alive, and it was only at autopsy that neuropathology and biochemistry confirmed vCJD. The neurologic features alone

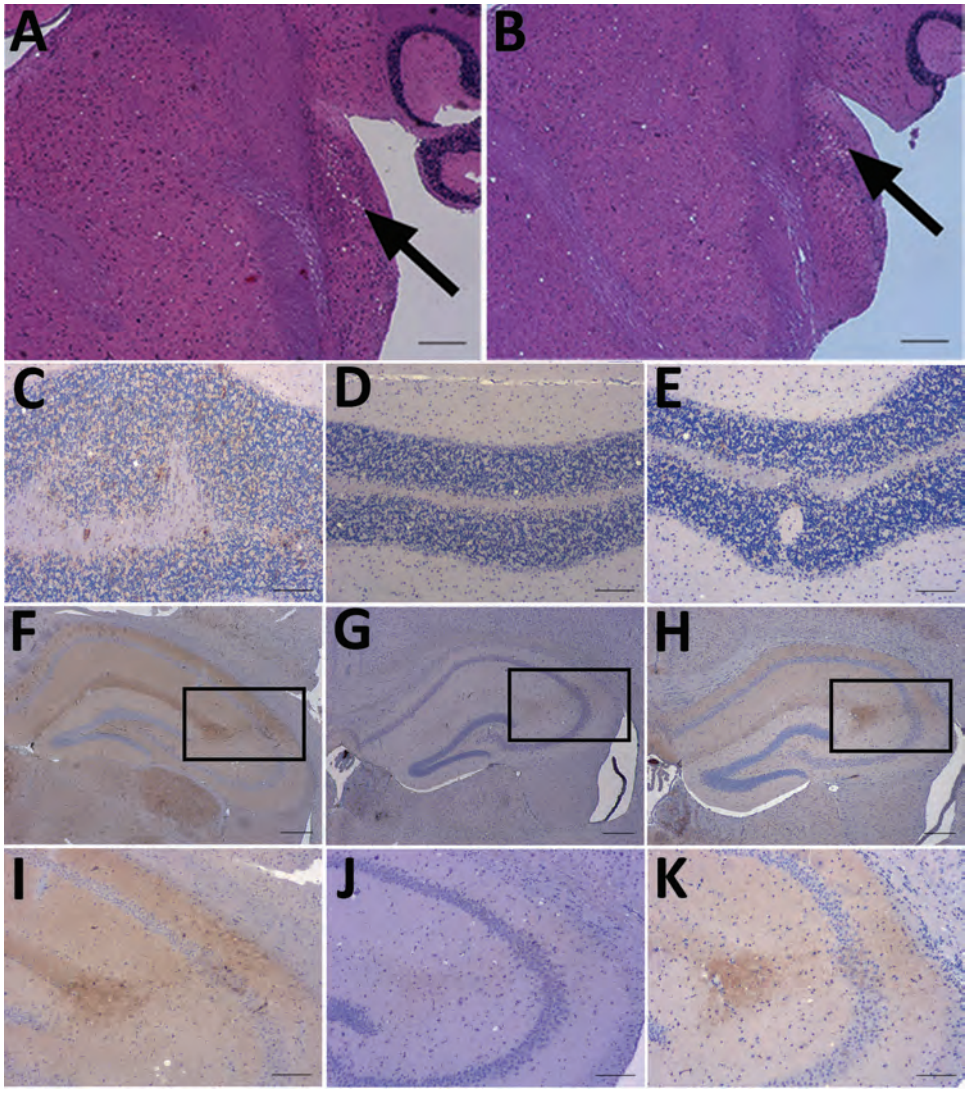

Figure 2. Neuropathology of RIII mice inoculated with material from a clinical case of vCJD in a prion protein gene codon 129MV individual, a typical 129MM case of vCJD, and BSE. A, B) Haemotoxylin and Eosin staining of transmissible spongiform encephalopathy vacuolation in the cochlear nucleus of mice inoculated with material from a clinical 129MV case (arrows). C–E) Abnormal PrP deposition in the cerebellum of mice inoculated with C) clinical 129MV case, D) typical 129MM case, and E) BSE. F–H) Abnormal PrP deposition in the hippocampus of mice inoculated with samples of F) clinical 129MV case, G) typical 129MM case, and H) BSE. I–K) Abnormal PrP deposition in the CA2 region of the hippocampus; I) inset from panel F; J) inset from panel G; K) inset from panel H. Monoclonal antibody: 6H4. Scale bars: A–B, F–H: 200 μm. C–E, I–K: 100 μm. BSE, bovine spongiform encephalopathy; MM, methionine homozygous; MV, methionine/valine; PrP, prion protein; vCJD, variant Creutzfeldt-Jakob disease.

cannot be used to discriminate between sCJD and vCJD, and the MRI findings on DWI imaging favored a diagnosis of sCJD. However, the high sensitivity and specificity of MRI for vCJD were determined by analyzing FLAIR images primarily (*13*) and recent review suggests that DWI imaging may be less specific than FLAIR imaging in vCJD. It is possible that the phenotype of vCJD in this case may have been altered by the heterozygous *PRNP* background and investigations including CSF protein misfolding cyclic amplification (*2*), tonsil biopsy, and perhaps FLAIR MRI may contribute to accurate diagnosis of future heterozygous cases.

The identification of vCJD in a 129MV person may indicate the start of a second wave of vCJD in association with the 129MV genotype which is present in around 45% of the UK population (*14*), although no further cases have been reported since 2016. This case highlights the need to continue surveillance to identify new cases of vCJD and the need for autopsy and strain typing in persons with prion diseases. Changes in clinical disease phenotype could mask the true diagnosis and may be indicative of potential changes in prion disease strains and infectious properties. Strain identification and assessing the infectious properties of prion diseases are essential components in the management of these diseases and have important implications for public health and in determining the prevalence of BSE-related prion disease in humans.

Acknowledgments

We thank the staff of the Biological Research Facility, Roslin Institute, and of Easter Bush Pathology, R(D)SVS, University of Edinburgh, for technical support. We thank David Summers (University of Edinburgh) for input and discussion on MRI imaging of vCJD.

The vCJD tissue samples were acquired through the Edinburgh Brain Bank, which is supported by the Medical Research Council (MR/L016400/1).

This report presents independent research commissioned and funded by the Department of Health and Social Care, Policy Research Programme (Strain typing of vCJD, 007/0195). The views expressed in this publication are those of the author(s) and not necessarily those of the Department of Health and Social Care. The Diack laboratory is also supported by BBSRC Project BBS/E/D/20002173.

About the Author

Ms. Boyle is a research scientist at The Roslin Institute, University of Edinburgh. Her research interests focus on the strain characterization of human and animal prion diseases using in vivo models.

References

1. Mok T, Jaunmuktane Z, Joiner S, Campbell T, Morgan C, Wakerley B, et al. Variant Creutzfeldt-Jakob disease in a patient with heterozygosity at PRNP codon 129. N Engl J Med. 2017;376:292–4. https://doi.org/10.1056/NEJMc1610003
2. Bougard D, Bélondrade M, Mayran C, Bruyère-Ostells L, Lehmann S, Fournier-Wirth C, et al. Diagnosis of methionine/valine variant Creutzfeldt-Jakob disease by protein misfolding cyclic amplification. Emerg Infect Dis. 2018;24:1364–6. https://doi.org/10.3201/eid2407.172105
3. Wiseman FK, Cancellotti E, Piccardo P, Iremonger K, Boyle A, Brown D, et al. The glycosylation status of PrPC is a key factor in determining transmissible spongiform encephalopathy transmission between species. J Virol. 2015;89:4738–47. https://doi.org/10.1128/JVI.02296-14
4. Dickinson AG, Meikle VMH, Fraser H. Identification of a gene which controls the incubation period of some strains of scrapie agent in mice. J Comp Pathol. 1968;78:293–9. https://doi.org/10.1016/0021-9975(68)90005-4
5. Fraser H, Dickinson AG. The sequential development of the brain lesions of scrapie in three strains of mice. J Comp Pathol. 1968;78:301–11. https://doi.org/10.1016/0021-9975(68)90006-6
6. Bruce ME, Will RG, Ironside JW, McConnell I, Drummond D, Suttie A, et al. Transmissions to mice indicate that 'new variant' CJD is caused by the BSE agent. Nature. 1997;389:498–501. https://doi.org/10.1038/39057
7. Bruce ME. TSE strain variation: an investigation into prion disease diversity Br Med Bull. 2003;66:99–108. https://doi.org/ 10.1093/bmb/66.1.99
8. Parchi P, Strammiello R, Notari S, Giese A, Langeveld JP, Ladogana A, et al. Incidence and spectrum of sporadic Creutzfeldt-Jakob disease variants with mixed phenotype and co-occurrence of PrP^{Sc} types: an updated classification. Acta Neuropathol. 2009;118:659–71. https://doi.org/10.1007/s00401-009-0585-1
9. Peden A, McCardle L, Head MW, Love S, Ward HJ, Cousens SN, et al. Variant CJD infection in the spleen of a neurologically asymptomatic UK adult patient with haemophilia. Haemophilia. 2010;16:296–304. https://doi.org/10.1111/j.1365-2516.2009.02181.x
10. Peden AH, Head MW, Ritchie DL, Bell JE, Ironside JW. Preclinical vCJD after blood transfusion in a PRNP codon 129 heterozygous patient. Lancet. 2004;364:527–9. https://doi.org/10.1016/S0140-6736(04)16811-6
11. Bishop MT, Hart P, Aitchison L, Baybutt HN, Plinston C, Thomson V, et al. Predicting susceptibility and incubation time of human-to-human transmission of vCJD. Lancet Neurol. 2006;5:393–8. https://doi.org/10.1016/S1474-4422(06)70413-6
12. Asante EA, Linehan JM, Gowland I, Joiner S, Fox K, Cooper S, et al. Dissociation of pathological and molecular phenotype of variant Creutzfeldt-Jakob disease in transgenic human prion protein 129 heterozygous mice. Proc Natl Acad Sci U S A. 2006;103:10759–64. https://doi.org/10.1073/pnas.0604292103
13. Collie DA, Summers DM, Sellar RJ, Ironside JW, Cooper S, Zeidler M, et al. Diagnosing variant Creutzfeldt-Jakob disease with the pulvinar sign: MR imaging findings in 86 neuropathologically confirmed cases. AJNR Am J Neuroradiol. 2003;24:1560–9.
14. Bishop MT, Pennington C, Heath CA, Will RG, Knight RS. PRNP variation in UK sporadic and variant Creutzfeldt Jakob disease highlights genetic risk factors and a novel non-synonymous polymorphism. BMC Med Genet. 2009;10:146. https://doi.org/10.1186/1471-2350-10-146

Address for correspondence: Abigail B. Diack, The Roslin Institute, Easter Bush, Scotland, UK email: abigail.diack@roslin.ed.ac.uk

Prevalence of *Escherichia albertii* in Raccoons (*Procyon lotor*), Japan

Atsushi Hinenoya, Keigo Nagano, Sharda P. Awasthi, Noritoshi Hatanaka, Shinji Yamasaki

Natural reservoirs of *Escherichia albertii* remain unclear. In this study, we detected *E. albertii* by PCR in 248 (57.7%) of 430 raccoons from Osaka, Japan, and isolated 143 *E. albertii* strains from the 62 PCR-positive samples. These data indicate that raccoons could be a natural reservoir of *E. albertii* in Japan.

Escherichia albertii is a gram-negative facultative anaerobic bacterium and an emerging human enteropathogen. This bacterium belongs to the group of attaching and effacing pathogens, which can form pedestal-structured lesions on intestinal epithelium by using an *eae*-encoded adhesin called intimin and a type 3 secretion system. *E. albertii* commonly carries cytolethal distending toxin genes; in addition, certain strains carry Shiga toxin 2 (*stx2a*, *stx2f*) genes (*1*), suggesting that *E. albertii* has a potential to cause severe diseases such as hemorrhagic colitis and hemolytic uremic syndrome in humans, similar to Shiga toxin–producing *E. coli*. An increase in human outbreaks and sporadic cases of *E. albertii* have been reported recently from several countries, including Japan (*1*–*3*). However, the reservoir and transmission routes of *E. albertii* to humans have not yet been identified. We surveyed wild raccoons (*Procyon lotor*) captured in Osaka, Japan, for the presence of *E. albertii* to determine if raccoons could be a reservoir of *E. albertii* in Japan.

The Study

We collected 430 rectal swabs from wild raccoons in Osaka during 2016–2017 (Appendix, https://wwwnc.cdc.gov/EID/article/26/6/19-1436-App1.pdf). To determine the presence of *E. albertii*, we first subjected fecal specimens to an *E. albertii*–specific *cdt* (*Eacdt*) gene-based PCR assay (*4*) after enrichment in tryptic soy broth. Of these 430 specimens, 248 (57.7%) yielded a 449-bp PCR amplicon specific for *E. albertii* (Table 1). By using XRM-MacConkey agar developed for the isolation of *E. albertii* (Appendix), we isolated and selected 143 *E. albertii* isolates from the 62 PCR-positive specimens (1–8 isolates/sample) with species identity confirmed by 2 different *E. albertii*–specific PCRs using primers targeting *Eacdt* (*4*), and *yejH* and *yejK* (*5*).

To determine the phylogenetic relationships among the isolates, we performed pulsed-field gel electrophoresis (PFGE) using *Xba*I-digested genomic DNA. The 143 isolates showed 59 pulsotypes (Figure), indicating that *E. albertii* isolates from raccoons were genetically diverse. We obtained 2–7 *E. albertii* isolates, which were determined to be clonal by PFGE, from 26 of 29 raccoons. The isolates from each of 3 raccoons (R305, R318, R419) showed 2–3 different DNA fingerprints with >3 bands different from each other, indicating that multiclonal *E. albertii* strains coexisted in the intestine of each of these 3 raccoons (Figure). In addition, we frequently observed that the isolates from different raccoons displayed exactly the same PFGE pattern (e.g., R7, R8, and R335; Figure), although the raccoons were usually captured in different locations in Osaka.

To evaluate the human pathogenic potential of *E. albertii* isolated from raccoons, we selected 1 isolate from each pulsotype (n = 59) and tested for the presence of virulence determinants in clinical *E. albertii* isolates (Appendix). We detected the *eae* gene in 59 strains (100%), *Eccdt*-I in 5 strains (8.5%), and *stx2f* genes in 2 strains (3.4%). By sequencing the entire *eae* gene in 59 strains (Appendix), we determined the intimin subtypes to be ρ (n = 8), ι2 (n = 5), ο (n = 4), ς (n = 4), γ5 (n = 2), ξ (n = 2), α8 (n = 1), β3 (n = 1), and unknown (n = 32) (Appendix Table 3). Among the 32 unknown subtypes, 16 were grouped into the 5 subtypes (N1–N5) that were recently identified in clinical *E. albertii* strains from Japan (*6*). Two subtypes were homologous to those identified in clinical *E. albertii* strains 1251–6/89, 2 were homologous to strain 4281–7/89 (*7*), and 3 were homologous to those identified in strain 2013C-4143 (GenBank accession no. CP030787). We also identified 2 novel subtypes (UT1 and UT2;

Author affiliation: Osaka Prefecture University, Osaka, Japan

DOI: https://doi.org/10.3201/eid2606.191436

Table 1. Prevalence of *Escherichia albertii* in Japanese wild raccoon fecal specimens and number of isolates

Sampling year and month	No. specimens	No. (%) PCR positive	No. specimens from which *E. albertii* was isolated	No. *E. albertii* isolates
2016				
Jun	57	25 (43.9)	7	17
Jul	55	34 (61.8)	4	8
Aug	22	14 (63.6)	0	0
Sep	7	2 (28.6)	0	0
Oct	8	3 (37.5)	0	0
Dec	14	7 (50.0)	0	0
2017				
Feb	3	2 (66.7)	0	0
Mar	16	3 (18.8)	0	0
Jul	88	56 (63.6)	14	21
Aug	104	63 (60.6)	21	56
Sep	56	39 (69.6)	16	41
Total	430	248 (57.7)	62	143

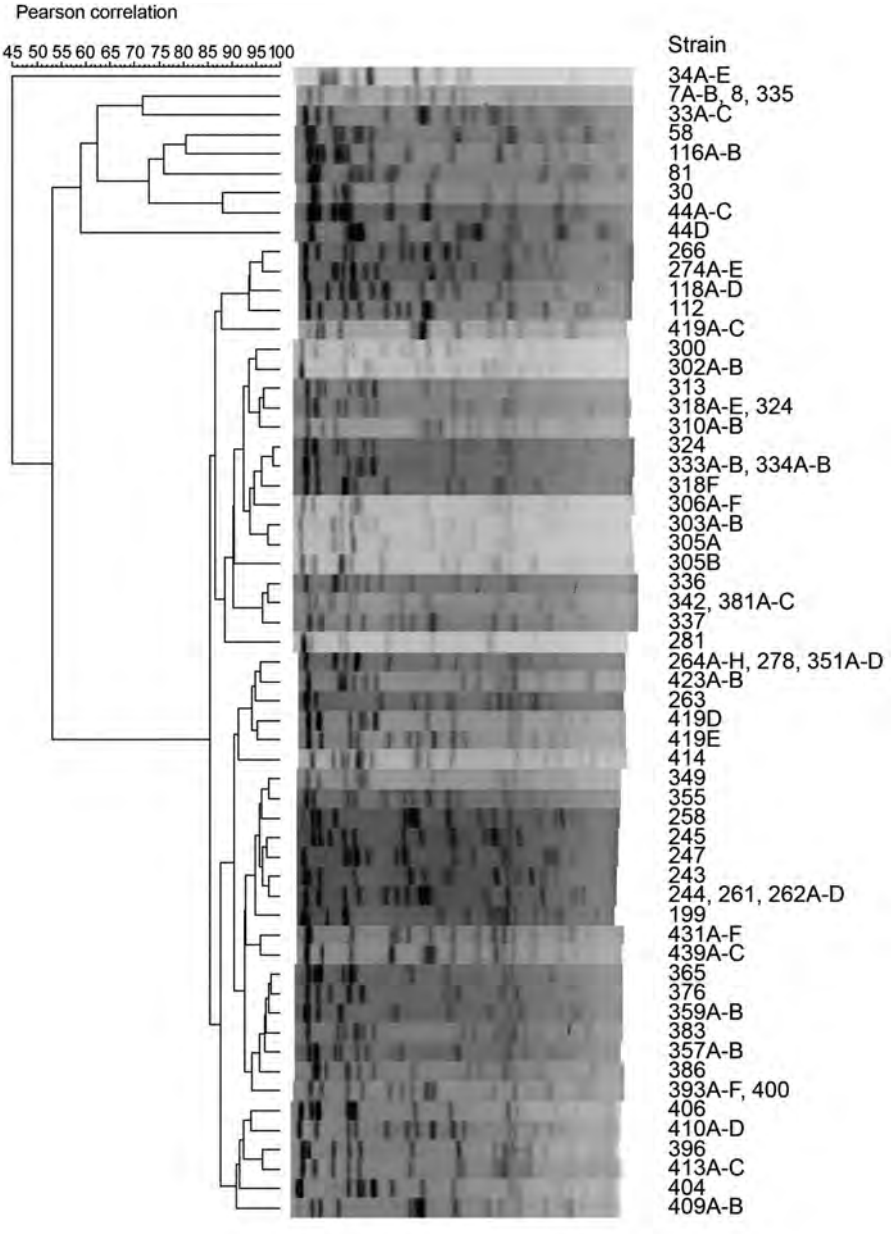

Figure. Phylogenetic analysis of raccoon *Escherichia albertii* strains by pulsed-field gel electrophoresis (PFGE). *Xba*I-digested genomic DNA of 143 raccoon *E. albertii* strains isolated in this study were analyzed by PFGE. The dendrogram was constructed based on DNA fingerprints obtained (Appendix, https://wwwnc.cdc.gov/EID/article/26/6/19-1436-App1.pdf). The number in each strain name represents a specific raccoon identification number.

Appendix Table 3) in the remaining 9 strains; each showed <95% nt and aa identities with any known subtypes. We identified complete *stx2f* genes in the *stx2f* gene-positive strains RAC-199 and RAC-247. The culture supernatants caused Vero cell deaths, which were neutralized by anti-Stx2fA serum, indicating that both strains produced biologically active Stx2f. The toxin activity was enhanced in the presence of mitomycin C, indicating that the *stx2f* genes could be located on inducible prophage genomes (Table 2). The fold change of Stx2f production by mitomycin C in the strains RAC-199 and RAC-247 were comparable to that of Stx2 production in human clinical strains *E. albertii* AKT5 and EHEC O157:H7 Sakai. These data suggest that the *E. albertii* strains isolated from raccoons have a potential to cause serious human diseases.

Conclusions

E. albertii is known to be an emerging zoonotic pathogen and has been isolated from various animals, such as pigs, cats, and birds (*6*,*8*,*9*). Although much effort has been devoted to identify the natural reservoir, *E. albertii* was not detected in vertebrate animals such as fish (n = 138), amphibians (n = 106), reptiles (n = 447), and mammals (n = 1,063) (*3*) but was found in 1.4% (9/634) of birds in Australia and 0.9% (9/1,204) of birds in Korea. Thus, the natural reservoir of *E. albertii* is still unclear; this information would be essential to determine transmission dynamics and prevent *E. albertii* infections. Given that patients in clinical outbreaks in Japan might be infected thorough waters (spring and well waters) or vegetables, but not meats (*3*), the natural reservoir of *E. albertii* might not be major food animals (e.g., cattle and chickens, the reservoirs for Shiga toxin–producing *E. coli* and *Campylobacter jejuni*, respectively). Another possibility is wild animals, which may contaminate environmental water and vegetables. Among the wild animals, the raccoon is a synanthropic animal with the ability to reside in a wide range of habitats, including agricultural, forested, and urban areas. Raccoons are omnivorous and forage within vegetable fields. They also prefer riparian environments. Furthermore, raccoons are known to carry various pathogenic microorganisms (*10*–*12*). Thus, they can contaminate vegetables and waters with pathogens, possibly including *E. albertii*, leading to human infections. Therefore, we performed a survey targeting raccoons and found that *E. albertii* was highly prevalent (248/430; 57.7%) in wild raccoons in Japan, indicating that carriage of *E. albertii* by raccoons is not incidental. The *E. albertii* strains isolated from raccoons also possessed virulence determinants (*eae*, *Eacdt, Eccdt-I*, or *stx2f*) present in human clinical strains. Almost all the intimin subtypes of the raccoon strains were those identified in human clinical *E. albertii* strains. Two strains produced functional Stx2f, which may have a potential to cause severe diseases in humans. Taken together, these data suggested that raccoons constitute a major reservoir of *E. albertii* and could be a source of human infection in Japan.

Raccoons originated from North America and were introduced as pets or game animals into other countries, including Japan and countries in Europe. Some of these have escaped and settled in the wild. The number of raccoons has increased because of their adaptability to various environments, omnivorous feeding habits, high reproductive potential, and lack of predators in the environment (*13*).

In addition to Japan, *E. albertii* has been clinically isolated in other countries where raccoons reside (*9*,*14*,*15*). Interactions between raccoons and other animals, such as wild mice and wild boars, can also be possible. Therefore, further epidemiologic studies to survey raccoons and other wild animals in Osaka, other areas of Japan, and other countries are highly warranted to evaluate the significance of raccoons as a natural reservoir of *E. albertii*.

Table 2. Stx2 production by *stx2f* gene-positive *Escherichia albertii* raccoon strains.

Species	Strains	Toxin gene	Mitomycin C	Toxin titer*	Neutralization†
E. albertii	RAC199	*stx2f*	Negative	4	Yes
			Positive	512	Yes
	RAC247	*stx2f*	Negative	32	Yes
			Positive	1,024	Yes
	AKT5	*stx2f*	Negative	512	Yes
			Positive	32,768	Yes
E. coli	Sakai	*stx1*, *stx2a*	Negative	256	Not done
			Positive	16,384	Not done
	C600	None	Negative	<1	Not done
			Positive	<1	Not done

*Reciprocal of highest dilution that resulted in death in >50% of cells is shown as toxin titer.
†Neutralization of cytotoxic effect by anti-Stx2f rabbit serum. Filtrated culture supernatants in LB-broth with and without mitomycin C were used as toxin samples.

Acknowledgments

We thank the Osaka Livestock Hygiene Service Center for providing raccoon fecal samples.

This work was supported in part by Japan Society for the Promotion of Science KAKENHI (grant no. 17H04651) and AMED (grant no. JP16jk021007).

About the Author

Dr. Hinenoya is an associate professor at the Graduate School of Life and Environmental Sciences, Osaka Prefecture University, Osaka, Japan. His research interests include molecular epidemiology and pathogenicity of pathogenic bacteria, especially zoonotic pathogens.

References

1. Bhatt S, Egan M, Critelli B, Kouse A, Kalman D, Upreti C. The evasive enemy: insights into the virulence and epidemiology of the emerging attaching and effacing pathogen *Escherichia albertii*. Infect Immun. 2018;87 :e00254-18. https://doi.org/10.1128/IAI.00254-18
2. National Institute of Infectious Diseases and Tuberculosis and Infectious Diseases Control Division, Ministry of Health, Labour and Welfare. Food poisoning due to *Escherichia albertii*, May 2017—Utsunomiya city in Japan [in Japanese]. Infect Agents Surveillance Rep. 2017;38:175–6.
3. Ooka T. Emerging enteropathogen, *Escherichia albertii* [in Japanese]. Jpn J Food Microbiol. 2017;34:151–7. https://doi.org/10.5803/jsfm.34.151
4. Hinenoya A, Ichimura H, Yasuda N, Harada S, Suzuki M, Iijima Y, et al. Development of a specific cytolethal distending toxin (*cdt*) gene (*Eacdt*)–based PCR assay for the detection of *Escherichia albertii*. Diagn Microbiol Infect Dis. 2019;95:119–24. https://doi.org/10.1016/j.diagmicrobio.2019.04.018
5. Ooka T, Ogura Y, Katsura K, Seto K, Kobayashi H, Kawano K, et al. Defining the genome features of *Escherichia albertii*, an emerging enteropathogen closely related to *Escherichia coli*. Genome Biol Evol. 2015;7:3170–9.
6. Ooka T, Seto K, Kawano K, Kobayashi H, Etoh Y, Ichihara S, et al. Clinical significance of *Escherichia albertii*. Emerg Infect Dis. 2012;18:488–92. https://doi.org/10.3201/eid1803.111401
7. Lima MP, Yamamoto D, Santos ACM, Ooka T, Hernandes RT, Vieira MAM, et al. Phenotypic characterization and virulence-related properties of *Escherichia albertii* strains isolated from children with diarrhea in Brazil. Pathog Dis. 2019;77:ftz014. https://doi.org/10.1093/femspd/ftz014
8. Hinenoya A, Shima K, Asakura M, Nishimura K, Tsukamoto T, Ooka T, et al. Molecular characterization of cytolethal distending toxin gene-positive *Escherichia coli* from healthy cattle and swine in Nara, Japan. BMC Microbiol. 2014;14:97. https://doi.org/10.1186/1471-2180-14-97
9. Oaks JL, Besser TE, Walk ST, Gordon DM, Beckmen KB, Burek KA, et al. *Escherichia albertii* in wild and domestic birds. Emerg Infect Dis. 2010;16:638–46. https://doi.org/10.3201/eid1604.090695
10. Hagiwara K, Matoba Y, Asakawa M. Borna disease virus in raccoons (*Procyon lotor*) in Japan. J Vet Med Sci. 2009;71:1009–15. https://doi.org/10.1292/jvms.71.1009
11. Hattori K, Donomoto T, Manchanayake T, Shibahara T, Sasai K, Matsubayashi M. First surveillance and molecular identification of the *Cryptosporidium skunk* genotype and *Cryptosporidium parvum* in wild raccoons (*Procyon lotor*) in Osaka, Japan. Parasitol Res. 2018;117:3669–74. https://doi.org/10.1007/s00436-018-6089-y
12. Lee K, Iwata T, Nakadai A, Kato T, Hayama S, Taniguchi T, et al. Prevalence of *Salmonella, Yersinia* and *Campylobacter* spp. in feral raccoons (*Procyon lotor*) and masked palm civets (*Paguma larvata*) in Japan. Zoonoses Public Health. 2011;58:424–31. https://doi.org/10.1111/j.1863-2378.2010.01384.x
13. Beltrán-Beck B, García FJ, Gortázar C. Raccoons in Europe: disease hazards due to the establishment of an invasive species. Eur J Wildl Res. 2012;58:5–15. https://doi.org/10.1007/s10344-011-0600-4
14. Brandal LT, Tunsjø HS, Ranheim TE, Løbersli I, Lange H, Wester AL. Shiga toxin 2a in *Escherichia albertii*. J Clin Microbiol. 2015;53:1454–5. https://doi.org/10.1128/JCM.03378-14
15. Lindsey RL, Rowe LA, Batra D, Smith P, Strockbine NA. PacBiol genome sequences of eight *Escherichia albertii* strains isolated from humans in the United States. Microbiol Resour Announc. 2019;8:e01663-18. https://doi.org/10.1128/MRA.01663-18

Address for correspondence: Shinji Yamasaki, Graduate School of Life and Environmental Sciences, Osaka Prefecture University, 1-58, Rinku ourai-kita, Izumisano, Osaka 598-8531, Japan; email: shinji@vet.osakafu-u.ac.jp

Cannabis Use and Fungal Infections in a Commercially Insured Population, United States, 2016

Kaitlin Benedict, George R. Thompson III, Brendan R. Jackson

Case reports have identified invasive fungal diseases in persons who use cannabis, and fungal contamination of cannabis has been described. In a large health insurance claims database, persons who used cannabis were 3.5 (95% CI 2.6–4.8) times more likely than persons who did not use cannabis to have a fungal infection in 2016.

Cannabis can contain fungal pathogens that cause serious and often fatal infections in persons with immunocompromising conditions, such as cancer, transplant, or infection with HIV (*1*). In these patients, some reasons for using cannabis include pain and nausea relief and appetite stimulation. The frequency of fungal infections associated with cannabis is unknown but is a growing concern as more states legalize its medicinal and recreational use. We used health insurance claims data from 2016 to evaluate the prevalence of fungal infection diagnosis codes among persons who use cannabis and persons who do not use cannabis and to compare demographic and clinical features between these 2 groups.

The Study

The 2016 IBM MarketScan Research Databases (https://www.ibm.com/products/marketscan-research-databases) include claims from outpatient visits and prescriptions and hospitalizations for >27 million employees, dependents, and retirees throughout the United States. MarketScan represents one of the largest collections of such data in the country and captures patient interactions across the full spectrum of healthcare. We used Treatment Pathways, a web-based platform (https://www.ibm.com/us-en/marketplace/marketscan-treatment-pathways), which enable users to query data for persons whose health insurance plans or employers contribute prescription drug data to MarketScan. Because data are fully deidentified, this analysis was not subject to review by the Centers for Disease Control and Prevention institutional review board.

We studied persons with continuous insurance enrollment in 2016, excluding those with diagnosis codes from the International Classification of Diseases, 10th Revision, Clinical Modification (ICD-10-CM), for presumed ocular histoplasmosis syndrome (H32 plus B39.4 or B39.9) assigned at an eye care provider (*2*). We identified patients with ICD-10-CM codes for mold infections (aspergillosis [B44], mucormycosis [B46]) and certain other fungal infections (blastomycosis [B40], coccidioidomycosis [B38], cryptococcosis [B45], histoplasmosis [B39]) among persons who used cannabis (F12.1, F12.2, F12.9) and persons who did not use cannabis. We further explored differences between ICD-10-CM codes for cannabis abuse or dependence (F12.1 and F12.2) and unspecified cannabis use (i.e., without mention of abuse or dependence) (F12.9). We defined immunocompromised status as HIV (B20, O9872, O9873), solid organ or hematopoietic stem cell transplant (Z94, T86), malignant neoplasms (C00–C80 excluding C44), and hematologic malignancies (C81–C96) and also identified tobacco use (Z27.0 or F17.2). We analyzed categorical variables by using χ^2 tests and logistic regression.

Forty (0.08%) of 53,217 persons who used cannabis and 6,294 (0.03%) of 21,559,558 persons who did not use cannabis had a fungal infection (odds ratio [OR] 2.6, 95% CI 1.9–3.5). After adjusting for age and immunocompromised status, the adjusted OR (aOR) was 3.5 (95% CI 2.6–4.8). Specifically, persons who use cannabis were more likely than persons who did not use cannabis to have mold infections (0.03% vs. 0.01%; OR 3.4, 95% CI 2.1–5.3, aOR 4.6, 95% CI 2.9–7.4) and other fungal infections (0.04% vs. 0.02%; OR 2.2, 95% CI 1.4–3.3, aOR 2.9, 95% CI 1.9–4.5).

Author affiliations: Centers for Disease Control and Prevention, Atlanta, Georgia, USA (K. Benedict, B.R. Jackson); University of California Davis Medical Center, Davis, California, USA (G.R. Thompson III)

DOI: https://doi.org/10.3201/eid2607.191570

Among patients with fungal infections, persons who used cannabis were significantly younger than persons who did not use cannabis (median age 41.5 years vs. 56.0 years; p<0.001), more likely to be immunocompromised (43% vs. 21%; p<0.001), more likely to be hospitalized on the fungal infection diagnosis date (40% vs. 13%; p<0.001), and more likely to have tobacco use codes (40% vs. 9%; p<0.001) (Table). Sixty percent (n = 24) of persons who used cannabis and had fungal infections had cannabis abuse or dependence codes, compared with 79% of persons who used cannabis and did not have fungal infections, and 48% (n = 19) of persons who used cannabis and had fungal infections had unspecified cannabis use codes, compared with 29% of persons who used cannabis and did not have fungal infections. Persons who used cannabis and had fungal infections and unspecified cannabis use codes were older (median age 52 years vs. 28 years) and more frequently immunocompromised (63% vs. 25%) than persons who used cannabis and had dependence codes.

Conclusions

In this large commercially insured population in the United States, cannabis use was associated with a higher prevalence of certain fungal infections. Although these infections were uncommon, they can result in substantial illness and even death, particularly in immunocompromised persons.

Several hypotheses could explain our findings. First, on the basis of immunocompromised status and hospitalizations, persons who used cannabis appeared to be sicker than persons who did not use cannabis and were therefore presumably at higher risk for fungal infections in general. Some persons who used cannabis might be using medical cannabis to help manage their underlying conditions. In this analysis, it was not possible to determine the source of infection, although contaminated cannabis has been previously implicated in aspergillosis, mucormycosis, and cryptococcal meningitis (*3*–*5*). We are not aware of any reports of blastomycosis, histoplasmosis, or coccidioidomycosis acquired from contaminated cannabis. However, a small risk likely exists; 1 histoplasmosis outbreak occurred in a cannabis field (*6*), and fomites, such as hay and vegetables, are involved in rare coccidioidomycosis cases (*7*). Another possible explanation is that smoking-induced structural and immunological lung damage confers increased susceptibility to infection (*8*), although the lung effects of cannabis might differ from those of tobacco (*9*). Confounding by tobacco smoking might be another explanation because tobacco use is typically more common among persons who use cannabis (*10*). Tobacco can also be contaminated with fungi, possibly to a lesser extent than cannabis (*11*).

Our results could also reflect medical coding artifacts. In general, cannabis use is likely greatly underrepresented by ICD codes (*12*), supported by the

Table. Characteristics of patients with fungal infections, by cannabis use status, United States, 2016*

Characteristic	Persons who use cannabis, n = 40	Persons who do not use cannabis, n = 6,294	p value
Median age, y (range)	41.5 (7–70)	56 (0–99)	<0.001
0–17	1 (3)	341 (5)	
18–34	16 (40)	659 (10)	
35–44	4 (10)	745 (12)	
45–54	5 (13)	1,226 (19)	
55–64	13 (33)	1,816 (29)	
≥65	1 (3)	1,507 (24)	
Sex			
M	25 (63)	3,078 (49)	0.086
F	15 (37)	3,216 (51)	
US Census Region†			0.964
Northeast	5 (13)	689 (11)	
Midwest	10 (25)	1,581 (25)	
South	12 (30)	2,099 (33)	
West	13 (33)	1,915 (30)	
Immunocompromised	17 (43)	1,303 (21)	<0.001
Inpatient on fungal infection diagnosis date	16 (40)	820 (13)	<0.001
Type of fungal infection			
Aspergillosis	17 (43)	2,091 (33)	
Blastomycosis	1 (3)	218 (3)	
Coccidioidomycosis	10 (25)	1,661 (26)	
Cryptococcosis	4 (10)	338 (5)	
Histoplasmosis	7 (18)	1,945 (31)	
Mucormycosis	1 (3)	82 (1)	
Tobacco use	16 (40)	558 (9)	<0.001

*Values are no. (%) unless otherwise indicated.
†Of primary beneficiary's residence.

finding that <0.3% of our study population had cannabis use codes, whereas ≈9% of the US population reported using cannabis in the past month (*13*). Although ICD-10-CM codes cannot distinguish between medical and recreational cannabis use, the higher frequency of immunocompromising conditions and older age among persons who use cannabis and persons who used cannabis and had unspecified cannabis use codes suggests medical cannabis use among some of these patients. We were also unable to differentiate smoking cannabis from other modes of use (e.g., ingestion), which is relevant because smoking might lead to greater fungal exposure through inhalation. Injection drug use, which also might be more common among persons who use cannabis, is an emerging risk factor for some fungal infections, such as invasive candidiasis, although this mode of acquisition seems less likely for the fungal infections described here, which are typically acquired through inhalation. Another limitation is that we did not evaluate immunocompromised status associated with medications such as corticosteroids and tumor necrosis factor inhibitors.

The similar geographic distribution of fungal infections between persons who use cannabis and persons who did not use cannabis is notable because state laws vary substantially regarding medical and recreational use. There is more legalization overall in the western and northeastern United States.

Despite the limitations inherent in administrative data and our inability to infer causality between cannabis use and fungal infections, our study adds to emerging evidence about this association. This finding is consistent with a recommendation that solid organ transplant recipients avoid smoking cannabis (*14*). Patients with other immunocompromising conditions should be also aware of the possible link between cannabis smoking and fungal infections and might also consider avoiding this exposure. Physicians should remain aware of the possible link between fungal infections and cannabis use.

About the Author

Ms. Benedict is an epidemiologist in the Mycotic Diseases Branch, Division of Foodborne, Waterborne, and Environmental Diseases, National Center for Emerging and Zoonotic Infectious Diseases, Centers for Disease Control and Prevention, Atlanta, GA. Her research interests include the epidemiology and prevention of fungal infections.

References

1. McHardy I, Romanelli A, Harris LJ, Opp G, Gaudino R, Torres A, et al. Infectious risks associated with medicinal cannabis: potential implications for immunocompromised patients? J Infect. 2018;76:500–1. https://doi.org/10.1016/j.jinf.2018.01.010
2. Benedict K, Beer KD, Jackson BR. Histoplasmosis-related healthcare use, diagnosis, and treatment in a commercially insured population, United States. Clin Infect Dis. 2019;Apr 30:pii:ciz324. https://doi.org/10.1093/cid/ciz324
3. Remington TL, Fuller J, Chiu I. Chronic necrotizing pulmonary aspergillosis in a patient with diabetes and marijuana use. CMAJ. 2015;187:1305–8. https://doi.org/10.1503/cmaj.141412
4. Stone T, Henkle J, Prakash V. Pulmonary mucormycosis associated with medical marijuana use. Respir Med Case Rep. 2019;26:176–9. https://doi.org/10.1016/j.rmcr.2019.01.008
5. Shapiro BB, Hedrick R, Vanle BC, Becker CA, Nguyen C, Underhill DM, et al. Cryptococcal meningitis in a daily cannabis smoker without evidence of immunodeficiency. BMJ Case Rep. 2018;2018:bcr-2017–221435. https://doi.org/10.1136/bcr-2017-221435
6. Ramírez J. Acute pulmonary histoplasmosis: newly recognized hazard of marijuana plant hunters. Am J Med. 1990;88:60N–2N.
7. Albert BL, Sellers TF Jr. Coccidioidomycosis from fomites. Report of a case and review of the literature. Arch Intern Med. 1963;112:253–61. https://doi.org/10.1001/archinte.1963.03860020151021
8. Bagaitkar J, Demuth DR, Scott DA. Tobacco use increases susceptibility to bacterial infection. Tob Induc Dis. 2008;4:12. https://doi.org/10.1186/1617-9625-4-12
9. Ribeiro LI, Ind PW. Effect of cannabis smoking on lung function and respiratory symptoms: a structured literature review. NPJ Prim Care Respir Med. 2016;26:16071. https://doi.org/10.1038/npjpcrm.2016.71
10. Agrawal A, Budney AJ, Lynskey MT. The co-occurring use and misuse of cannabis and tobacco: a review. Addiction. 2012;107:1221–33. https://doi.org/10.1111/j.1360-0443.2012.03837.x
11. Verweij PE, Kerremans JJ, Voss A, Meis JF. Fungal contamination of tobacco and marijuana. JAMA. 2000;284:2875. https://doi.org/10.1001/jama.284.22.2869
12. Vin-Raviv N, Akinyemiju T, Meng Q, Sakhuja S, Hayward R. Marijuana use and inpatient outcomes among hospitalized patients: analysis of the nationwide inpatient sample database. Cancer Med. 2017;6:320–9. https://doi.org/10.1002/cam4.968
13 Substance Abuse and Mental Health Services Administration. Key substance use and mental health indicators in the United States: Results from the 2016 National Survey on Drug Use and Health. HHS Publication No. SMA 17–5044, NSDUH Series H-52. Rockville (MD): Center for Behavioral Health Statistics and Quality, Substance Abuse and Mental Health Services Administration; 2017 [cited 2020 Feb 25]. https://www.samhsa.gov/data/sites/default/files/NSDUH-FFR1-2016/NSDUH-FFR1-2016.htm
14. Avery RK, Michaels MG; AST Infectious Diseases Community of Practice. Strategies for safe living following solid organ transplantation—guidelines from the American Society of Transplantation Infectious Diseases Community of Practice. Clin Transplant. 2019;33:e13519. https://doi.org/10.1111/ctr.13519

Address for correspondence: Kaitlin Benedict, Centers for Disease Control and Prevention, 1600 Clifton Rd NE, Mailstop H24-9, Atlanta, GA 30329-4027, USA; email: jsy8@cdc.gov

Leishmania infantum in Tigers and Sand Flies from a Leishmaniasis-Endemic Area, Southern Italy

Roberta Iatta, Andrea Zatelli, Pietro Laricchiuta, Matteo Legrottaglie, David Modry, Filipe Dantas-Torres, Domenico Otranto

We detected *Leishmania infantum* infection in 45% of tigers and 5.3% of sand flies tested at a zoo in southern Italy in 2019. These infections in tigers and the abundance of *Phlebotomus perniciosus* sand flies represent a potential risk to other animals and humans living in or visiting the zoo.

Visceral leishmaniasis, caused by infection with *Leishmania infantum* protozoa, is listed among the most neglected tropical diseases, affecting thousands of persons, most of whom are among the world's most vulnerable populations (*1*). The disease is associated with the presence of phlebotomine sand fly vectors; domestic dogs typically act as reservoirs. Among felids, domestic cats have recently gained prominence as putative reservoirs of *L. infantum* (*2*), whereas cases of infection in other felids have been reported occasionally (*3*–*5*).

In February 2019, a tiger (index case), born and raised in a zoologic park in southern Italy, had a nonhealing laceration that tested positive for *L. infantum* DNA on a skin punch biopsy. Because tigers are considered an endangered species, the presence of an active *L. infantum* transmission focus in a facility visited by thousands of visitors each year deserves attention. Therefore, we conducted an epidemiologic study to investigate the prevalence of *L. infantum* infection in the local tiger and sand fly populations, along with the sand flies' host blood-feeding preferences.

Author affiliations: University of Bari, Bari, Italy (R. Iatta, A. Zatelli, F. Dantas-Torres, D. Modry, D. Otranto); Zoo Safari di Fasano, Brindisi, Italy (P. Laricchiuta, M. Legrottaglie); University of Veterinary and Pharmaceutical Sciences, Brno, Czech Republic (D. Modry); Czech Academy of Sciences, Ceske Budejovice, Czech Republic (D. Modry); Masaryk University, Brno (D. Modry); Fundação Oswaldo Cruz (Fiocruz), Recife, Brazil (F. Dantas-Torres); Bu-Ali Sina University, Hamedan, Iran (D. Otranto).

DOI: https://doi.org/10.3201/eid2606.191668

The Study

During March–June 2019, we tested 20 tigers born at the zoologic park (Safari Park, Apulia region, Brindisi Province, southern Italy) and living in an open enclosure for *L. infantum* infection. We smeared lymph node aspirates on slides for the cytologic examination; we also cultured and processed these specimens, along with whole blood, skin punch biopsy, and conjunctival, nasal and oral swab specimens, for the detection of *L. infantum* DNA by quantitative PCR (qPCR) (*6*). We tested for feline leukemia virus (FeLV) and feline immunodeficiency virus (FIV) by using proviral DNA from blood, as described previously (*7*). We detected *L. infantum* antibodies by using an immunofluorescence antibody test (IFAT), as described previously in a study in cats (*2*). During May–November 2019, we collected sand flies in the tigers' enclosure biweekly by using sticky traps and light traps and identified each specimen by using morphologic keys. We performed conventional PCR for blood-meal identification in sand flies by using primers cyto 1 (5′-CCATCAAACATCTCAGCATGAAA-3′) and T2893R (5′-GTTGGCGGGGATGTAGTTATC-3′), which target the mitochondrial cytochrome b. The protocol of this study was approved by the ethics committee of the Department of Veterinary Medicine at the University of Bari (Bari, Italy).

Tigers enrolled in the study ranged in age from 6 months to 11 years and weighed 70–220 kg (Table 1); all were apparently healthy or had unrelated conditions, except for 1 (index case), which had a large nonhealing laceration extending from the left loin region to the left thoracic region (Figure). Overall, 9 (45%) of the 20 tigers tested positive for *L. infantum* by IFAT, 5 (25%) tested positive by qPCR, and 5 (25%) tested positive by both methods (Table 1). The tigers were positive by qPCR on lymph node aspirates and skin punch biopsy. None of the conjunctival swab specimens tested positive. We did not detect *L. infantum*

Table 1. Serologic and molecular results for *Leishmania infantum* in 20 tigers, southern Italy*

Month of sample collection	Case no.	Age, y/sex	Weight, kg	IFAT/Ab titer	qPCR results					
					PB	LN	CS	NS	OS	SPB
March	1	7/F	150	1:160	–	+	–	–	–	+
April	2	6/M	160	1:80	–	NT	–	–	–	–
April	3	7/M	220	1:80	–	–	–	–	–	–
April	4	8/M	210	1:80	–	NT	–	+	+	–
April	5	7/M	220	–	–	–	–	–	–	–
April	6	9/F	150	–	–	–	–	–	–	–
May	7	2/F	135	1:640	–	+	–	+	–	+
May	8	2/M	180	–	–	NT	–	–	–	–
May	9	2/F	150	1:40	+	+	–	–	–	+
May	10	2/M	170	1:40	+	+	–	–	+	+
May	11	8/F	190	1:40	–	–	–	–	–	–
May	12	6/M	220	–	–	–	–	–	–	–
May	13	7/F	160	–	–	–	–	–	–	–
May	14	11/F	120	–	–	–	–	–	–	–
June	15	1/M	130	–	–	–	–	–	–	–
June	16	1/F	110	–	–	–	–	–	–	–
June	17	7/F	150	1:80	–	–	–	–	–	–
June	18	0.5/F	70	–	–	–	–	–	–	–
June	19	0.5/F	70	–	–	–	–	–	–	–
June	20	0.5/F	70	–	–	–	–	–	–	–

*Ab, antibody; CS, conjunctival swab; IFAT, immunofluorescence antibody test; LN, lymph node; NS, nasal swab; NT, not tested; OS, oral swab; PB, peripheral blood; qPCR, quantitative PCR; SPB, skin punch biopsy; –, negative; +, positive.

cytology or culture of lymph node aspirates in any of the tigers. All tigers were negative for FeLV and FIV.

During May–November 2019, we collected a total of 580 sand flies. The most abundant species was *Phlebotomus perniciosus* (n = 491), followed by *Sergentomyia minuta* (n = 69) and *P. neglectus* (n = 20). Of the 190 females collected, 151 (26%) were *P. perniciosus*, 4 (<1%) were *P. neglectus*, and 35 (6%) were *S. minuta*. Specimens for 8 (5.3%) *P. perniciosus* sand flies and 1 (2.9%) *S. minuta* sand fly tested positive for *L. infantum* DNA. Of the 190 females examined, 63 (33.1%) *P. perniciosus*, 3 (1.6%) *P. neglectus*, and 2 (1.1.%) *S. minuta* sand flies tested positive for tiger DNA (Table 2); we detected no other mammalian DNA (e.g., from cats, dogs, rats, or humans) in blood-fed or -unfed specimens.

Figure. Large nonhealing laceration, attributable to *Leishmania infantum* infection, extending from the left loin region to the left thoracic region of a tiger, southern Italy.

Consensus sequences of the vertebrate host mitochondrial cytochrome b from all female sand flies (positive specimens) displayed 100% identity to the nucleotide sequences of *Panthera tigris* available in the GenBank database (accession nos. MH124112 and KC879295).

Conclusions

The high prevalence (45%) of *L. infantum* infection recorded indicates that tigers living in the zoologic park are highly exposed to sand flies and thus have a high risk for acquiring the parasite. The finding of engorged sand flies that fed on tigers and were also positive for *L. infantum* suggest that tigers could be an alternative host of this parasite; however, the possibility that *L. infantum*–positive sand flies had acquired the infection from another host, before feeding on tigers, cannot be ruled out.

Although *Leishmania* spp. infection has been scantly described in wild felids (*3*–*5*), the diagnosis of this parasitic infection should also be considered while screening these animals for pathogens potentially impairing their health and welfare. No information is available on the immune response against *L. infantum* infection in tigers, and serologic tests have not been validated for this host, but one could reasonably suspect that their antibody production would follow a pattern similar to that occurring in cats. Nonetheless, the absence of *L. infantum* DNA in tigers that were positive for *L. infantum* antibodies (4/9 tigers [44.4%]) could be expected, given that this lack of correlation between molecular and serologic positivity has also been observed in cats (*2*), indicating that the diagnosis of the infection in these animals might

Table 2. Number of phlebotomine sand fly species by sex, positivity for *Leishmania infantum* by quantitative PCR, and blood meal on tigers, southern Italy*

Sand fly species	Sex		Total	No. (%) positive for *L. infantum*	Blood meal source	
	F	M			No. positive	No. positive/engorged
Phlebotomus perniciosus	151	340	491	8/151 (5.3)	63/151	48/63
Sergentomyia minuta	35	34	69	1/35 (2.9)	2/35	–
Phlebotomus neglectus	4	16	20	–	3/4	–
Total	190	390	580	–	68/190	48/63

*–, no result.

be a difficult task, as it is in cats. The detection of *L. infantum* DNA in the lymph node aspirate and skin biopsy suggests that these tissues are more suitable than blood for the diagnosis of this infection, as previously reported in dogs and cats (*8*,*9*). Otherwise, the conjunctival swab seems to be not as good a sample for this purpose in tigers. Unlike some studies with cats (*2*), no correlation between *L. infantum* infection and FIV, FELV, or both FIV and FELV infection has been observed in the tigers in our study.

The predominance of *P. perniciosus* sand flies, along with their positivity for *L. infantum* DNA already recorded in southern Italy (*10*,*11*), is somewhat expected, given that this sand fly species is recognized as the main vector for *L. infantum* in different foci of visceral leishmaniasis in Italy (*12*). The high proportion of *L. infantum*–infected sand flies suggests that the risk for parasite transmission in this environment should be considered. Furthermore, the detection of *L. infantum* DNA in *S. minuta* sand flies has already been reported in southern Italy (4.2%) and Portugal (4%) (*11*,*13*). In addition, although consideration of the role played by *S. minuta* (the proven vector of *L. tarentolae*) in the circulation of *Leishmania* spp. of zoonotic concern has been raised (*11*,*14*), further studies are necessary to fully assess its vector role.

P. perniciosus sand flies frequently feed on tigers, because dogs are not allowed to roam in the zoo, the role of tigers as local reservoir hosts needs to be ascertained. Because *P. perniciosus* sand flies feed on a wide range of domestic and wild animals, and because *L. infantum* might infect the sand flies after taking a blood meal from infected felids (*15*), the role of tigers in the transmission cycle of *L. infantum* is probable.

In summary, *L. infantum* infection should be included in the differential diagnosis of infectious diseases in tigers in areas where visceral leishmaniasis is endemic. The role of tigers as sentinels for *L. infantum*, the occurrence of *P. perniciosus* sand flies infected by the protozoan, and its abundance in the study area might represent an eminent risk for animals and humans living in or visiting the zoo. Therefore, prevention measures are needed for providing protection against *L. infantum* infection in these animals and for controlling sand flies.

About the Author

Dr. Iatta is an associate professor at the Department of Veterinary Medicine, University of Bari "Aldo Moro" in Italy. Her research interests include the diagnosis, epidemiology, and prevention of parasitic infectious diseases.

References

1. World Health Organization. Leishmaniasis 2018 [cited 2018 Dec 22]. https://www.who.int/leishmaniasis
2. Iatta R, Furlanello T, Colella V, Tarallo VD, Latrofa MS, Brianti E, et al. A nationwide survey of *Leishmania infantum* infection in cats and associated risk factors in Italy. PLoS Negl Trop Dis. 2019;13:e0007594. https://doi.org/10.1371/journal.pntd.0007594
3. de Oliveira AR, de Carvalho TF, Arenales A, Tinoco HP, Coelho CM, Costa MELT, et al. Mandibular squamous cell carcinoma in a captive Siberian tiger (*Panthera tigris altaica*). Braz J Vet Pathol. 2018;11:97–101. https://doi.org/10.24070/bjvp.1983-0246.v11i3p97-101
4. Libert C, Ravel C, Pratlong F, Lami P, Dereure J, Keck N. *Leishmania infantum* infection in two captive barbary lions (*Panthera leo leo*). J Zoo Wildl Med. 2012;43:685–8. https://doi.org/10.1638/2012-0056.1
5. Dahroug MA, Almeida AB, Sousa VR, Dutra V, Turbino NC, Nakazato L, et al. *Leishmania* (*Leishmania*) *chagasi* in captive wild felids in Brazil. Trans R Soc Trop Med Hyg. 2010;104:73–4. https://doi.org/10.1016/j.trstmh.2009.08.003
6. Francino O, Altet L, Sánchez-Robert E, Rodriguez A, Solano-Gallego L, Alberola J, et al. Advantages of real-time PCR assay for diagnosis and monitoring of canine leishmaniosis. Vet Parasitol. 2006;137:214–21. https://doi.org/10.1016/j.vetpar.2006.01.011
7. Stiles J, Bienzle D, Render JA, Buyukmihci NC, Johnson EC. Use of nested polymerase chain reaction (PCR) for detection of retroviruses from formalin-fixed, paraffin-embedded uveal melanomas in cats. Vet Ophthalmol. 1999;2:113–6. https://doi.org/10.1046/j.1463-5224.1999.00066.x
8. Pennisi MG, Lupo T, Malara D, Masucci M, Migliazzo ALG. Serological and molecular prevalence of *Leishmania infantum* infection in cats from southern Italy. J Feline Med Surg. 2012;14:656–7.
9. Otranto D, Paradies P, de Caprariis D, Stanneck D, Testini G, Grimm F, et al. Toward diagnosing *Leishmania infantum* infection in asymptomatic dogs in an area where leishmaniasis is endemic. Clin Vaccine Immunol. 2009;16:337–43. https://doi.org/10.1128/CVI.00268-08
10. Tarallo VD, Dantas-Torres F, Lia RP, Otranto D. Phlebotomine sand fly population dynamics in a leishmaniasis endemic peri-urban area in southern Italy. Acta Trop. 2010;116:227–34. https://doi.org/10.1016/j.actatropica.2010.08.013
11. Latrofa MS, Iatta R, Dantas-Torres F, Annoscia G, Gabrielli S, Pombi M, et al. Detection of *Leishmania infantum*

DNA in phlebotomine sand flies from an area where canine leishmaniosis is endemic in southern Italy. Vet Parasitol. 2018;253:39–42. https://doi.org/10.1016/j.vetpar.2018.02.006
12. Maroli M, Feliciangeli MD, Bichaud L, Charrel RN, Gradoni L. Phlebotomine sandflies and the spreading of leishmaniases and other diseases of public health concern. Med Vet Entomol. 2013;27:123–47. https://doi.org/10.1111/j.1365-2915.2012.01034.x
13. Pereira S, Pita-Pereira D, Araujo-Pereira T, Britto C, Costa-Rego T, Ferrolho J, et al. First molecular detection of *Leishmania infantum* in *Sergentomyia minuta* (Diptera, Psychodidae) in Alentejo, southern Portugal. Acta Trop. 2017;174:45–8. https://doi.org/10.1016/j.actatropica.2017.06.020
14. Maia C, Depaquit J. Can *Sergentomyia* (Diptera, Psychodidae) play a role in the transmission of mammal-infecting *Leishmania?* Parasite. 2016;23:55. https://doi.org/10.1051/parasite/2016062
15. Maroli M, Pennisi MG, Di Muccio T, Khoury C, Gradoni L, Gramiccia M. Infection of sandflies by a cat naturally infected with *Leishmania infantum.* Vet Parasitol. 2007;145:357–60. https://doi.org/10.1016/j.vetpar.2006.11.009

Address for correspondence: Domenico Otranto, Department of Veterinary Medicine, University of Bari, Strada Provinciale per Casamassima km 3, 70010, Valenzano (BA) 70010, Italy; email: domenico.otranto@uniba.it

Origin of 3 Rabid Terrestrial Animals in Raccoon Rabies Virus–Free Zone, Long Island, New York, USA, 2016–2017

Scott Brunt, Heather Solomon, Hilaire Leavitt, Erica Lasek-Nesselquist, Pascal LaPierre, Matt Shudt, Laura Bigler, Navjot Singh, April D. Davis

During 2016–2017, three rabid terrestrial animals were discovered in the raccoon rabies virus–free zone of Long Island, New York, USA. Whole-genome sequencing and phylogenetic analyses revealed the likely origins of the viruses, enabling the rabies outbreak response (often costly and time-consuming) to be done less expensively and more efficiently.

Rabies has been endemic to the eastern United States in raccoons (*Procyon lotor*) since 1960 and endemic to New York, USA, since the 1990s (*1*). The spread of rabies virus from raccoons in the mid-Atlantic states to species in New York has been reconstructed with spatiogenetic and phylogenic analyses (*2*). Despite this spread, a few locations in the region, including Suffolk and Nassau Counties on Long Island, New York, have been considered to be rabies free since 2011 (*3*). Maintaining these areas as low risk for rabies substantially decreases the likelihood of human and animal exposure to rabies virus and dramatically reduces the expenses paid for postexposure rabies virus treatments and rabies control (*4*).

To identify any breaches in the elimination zone, Nassau and Suffolk County health departments, veterinarians, and wildlife control officers routinely submit animals with clinical signs compatible with rabies for rabies virus testing to the New York State Department of Health Rabies Laboratory (Slingerlands, New York, USA). Before 2016, rabies had not been reported in Suffolk County since 2009 or in Nassau County since 2007 (Figure 1) (*5*). During 2016–2017, rabies reappeared in Nassau and Suffolk Counties in 3 terrestrial animals: a raccoon (*Procyon lotor*), a river otter (*Lontra canadensis*), and a domestic cat (*Felis catus*). Here, we describe our efforts to identify the origins of these rabid animals and our contingency plans to eliminate further cases and restore the rabies virus–free zone status.

Author affiliations: New York State Department of Health, Albany, New York, USA (S. Brunt, H. Solomon, E. Lasek-Nesselquist, P. LaPierre, M. Shudt, N. Singh, A.D. Davis); Connecticut Department of Health, Rocky Hill, Connecticut, USA (H. Leavitt); Cornell University, Ithaca, New York, USA (L. Bigler)

DOI: https://doi.org/10.3201/eid2606.191700

The Study

In March 2016, a rabid raccoon with neurologic signs was trapped in Hicksville in Nassau County. Real-time reverse transcription PCR (*6*) and Sanger sequencing demonstrated that the animal was infected with a raccoon rabies virus variant. A phylogenetic analysis of the full nucleoprotein and partial glycoprotein gene sequences did not provide us the resolution required for us to confidently identify where the virus had originated. At the time of this original analysis, whole-genome sequencing (WGS) was not available in our laboratory. We initiated enhanced rabies surveillance for ≈12 months in Babylon and Huntington of Nassau County to determine if rabies virus was circulating locally by increasing the number of wild animals submitted for testing via trapping, roadkill collection, and animal control activities, but no animals were positive for rabies.

In December 2016, an employee of the New York State Department of Environmental Conservation (Albany, New York, USA) found a river otter on Sound Beach on the North Shore of Suffolk County; the otter was submitted to the Rabies Laboratory of the New York State Department of Health in February 2017. After the otter was determined to be rabies virus positive, our goal was to ascertain by WGS and sequence analysis where the otter was exposed,

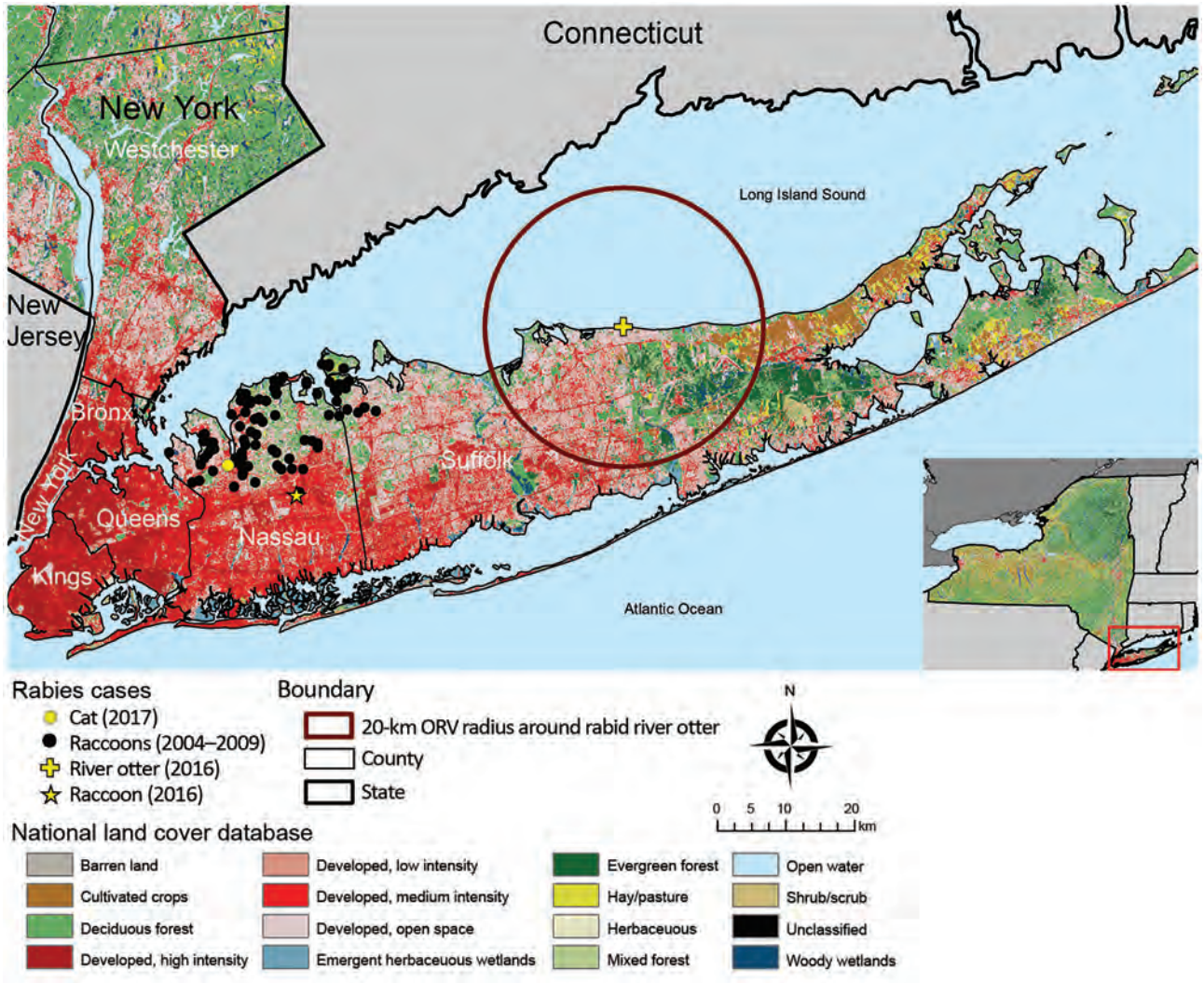

Figure 1. Locations of rabid raccoon, river otter, and cat in raccoon rabies virus–free zone, Nassau and Suffolk Counties, Long Island, New York, USA, 2016–2017. Locations of rabid raccoons found in these counties before they became raccoon rabies virus free are also indicated. The 20-km radius originally proposed for the distribution of ORV if rabies virus had become reestablished in raccoon rabies virus–free zone is indicated. Inset indicates location of Long Island in New York. ORV, oral rabies vaccine.

which would help us determine which supplementary contingency actions were required.

In November 2017, a cat with neurologic signs that bit a veterinary staff member in Nassau County was submitted for testing. After determining this cat was positive for rabies virus, we included this case in the study.

When the raccoon was originally discovered on Long Island, we had contacted multiple state and federal agencies to discuss contingency plans for containing a possible rabies outbreak. We agreed to limit the contingency actions at that juncture to 12 months' enhanced surveillance, public health alerts to educate citizens, and reminders about free rabies virus vaccine clinics for domestic animals. Only in the event that other rabid animals were discovered during this time would wildlife trap, vaccinate, and release programs be implemented and oral rabies virus vaccine baits be distributed (*4*,*5*,*7*). These vaccination programs can be expensive, so they are used conservatively as last resort efforts. The cost of the raccoon rabies virus elimination program that occurred on Long Island during 2006–2010 was ≈$2.6 million (*4*).

The contingency plan to respond to the rabid river otter was initially to deploy oral rabies vaccine around a 20-km radius of Sound Beach Long Island, covering nearly all of central Suffolk County (Figure 1). Costs would have exceeded $200,000 as 120,000 baits would need to have been spread by foot, vehicle, and aircraft over a 636.6-km^2 area during spring 2017.

Because Wadsworth Center Sequencing Core (Slingerlands, New York, USA) charged ≈$250/sample for WGS, we were able to save time and money by sampling animals and ruling out some areas as having local transmission and deescalating the initial plan. Applying WGS to priority samples has previously

Table. Information on rabies viruses used for phylogenetic analysis of viruses isolated from rabid animals found in raccoon rabies virus–free zone, Nassau and Suffolk Counties, Long Island, New York, USA, 2016–2017*

Laboratory ID no.	Collection date	Species	Location	Clade	GenBank accession no.
731-18	2018 Feb 5	Raccoon	Denville, NJ, USA	1	MN418142
2006-18	2018 Apr 23	Raccoon	Lincoln Park, NJ, USA	1	MN418156
2834-17	2017 Jun 16	Red Fox	New City, NY, USA	1	MN418149
KY026420	2004 Jun 21	Raccoon	Genoa, NY, USA	1	†
7686-17	2017 Oct 6	Skunk	Troy, NY, USA	1	MN418168
9049-17	2017 Dec 16	Raccoon	Hudson, NY, USA	1	MN418162
259-17	2017 Jan 23	Raccoon	Clinton, NY, USA	1	MN418178
8952-08	2008 Nov 26	Raccoon	Lloyd Harbor, NY, USA	1	MN418143
135-09	2009 Jan 8	Raccoon	Huntington, NY, USA	1	MN418164
7346-17	2017 Sep 21	Raccoon	Bronx, NY, USA	1	MN418174
7314-17	2017 Sep 20	Raccoon	Bronx, NY, USA	1	MN418157
7869-17	2017 Aug 18	Raccoon	Tarrytown, NY, USA	1	MN418153
4980-17	2017 Aug 8	Gray Fox	Mahopac, NY, USA	1	MN418183
8210-17	**2017 Nov 4**	**Cat**	**Sea Cliff, NY, USA**	**1**	**MN418154**
2677-18	2018 May 26	Raccoon	Midland Park, NJ, USA	1	MN418169
854-18	2018 Feb 16	Raccoon	Upper Saddle River, NJ, USA	1	MN418171
871-17	2017 Mar 3	Raccoon	New Paltz, NY, USA	1	MN418145
3617-17	2016 Jul 12	Raccoon	Cornwallville, NY, USA	1	MN418152
8423-17	2017 Nov 11	Skunk	Accord, NY, USA	1	MN418172
2847-17	2017 Jun 6	Gray Fox	Monticello, NY, USA	1	MN418158
849-17	2017 Mar 19	Raccoon	Slate Hill, NY, USA	1	MN418167
KY026481	2008 Sep 18	Raccoon	Charlotte, VT, USA	1 subclade 1	†
KY026478	2006 Nov 16	Raccoon	Stowe, VT, USA	1 subclade 1	†
8775-17	2017 Dec 3	Raccoon	Westerlo, NY, USA	1 subclade 1	MN418144
5318-17	2017 Aug 11	Raccoon	Cobleskill, NY, USA	1 subclade 1	MN418147
KY026483	2011 Oct 23	Skunk	Walden, VT, USA	1 subclade 1	†
KY026482	2008 Sep 28	Raccoon	Stowe, VT, USA	1 subclade 1	†
760-18	2017 Aug 29	Raccoon	Brownsville, VT, USA	1 subclade 1	MN418146
763-18	2017 Jun 20	Gray Fox	Arlington, VT, USA	1 subclade 1	MN418177
752-18	2017 Apr 21	Raccoon	Vergennes, VT, USA	1 subclade 1	MN418175
751-18	2017 Mar 3	Red Fox	Bristol, VT, USA	1 subclade 1	MN418165
KY026479	2006 Dec 5	Skunk	Bethel, VT, USA	1 subclade 1	†
KY026480	2007 Dec 10	Raccoon	Braintree, VT, USA	1 subclade 1	†
CT608844	2016 Jul 6	Raccoon	Ridgefield, CT, USA	1 subclade 2	MN418151
CT641269	2016 Nov 15	Raccoon	Ridgefield, CT, USA	1 subclade 2	MN418163
738-16	**2016 Mar 3**	**Raccoon**	**Hicksville, NY, USA**	**1 subclade 2**	**MN418159**
CT682858	2017 May 1	Raccoon	Weston, CT, USA	1 subclade 2	MN418160
CT627067	2016 Feb 1	Raccoon	Fairfield, CT, USA	1 subclade 2	MN418182
CT607469	2016 Jun 30	Raccoon	Bridgeport, CT, USA	1 subclade 2	MN418155
CT648095	2016 Dec 14	Raccoon	Weston, CT, USA	1 subclade 2	MN418181
441-17	**2016 Dec 14**	**Otter**	**Sound Beach, NY, USA**	**1 subclade 2**	**MN418161**
466-17	2017 Feb 15	Raccoon	Greene, NY, USA	2	MN418176
KY026416	1995 Dec 22	Raccoon	Hounsfield, NY, USA	2	†
KY026426	2000 Jan 12	Raccoon	Wolfe Island, Ontario, Canada	2	†
KY026424	1999 Dec 10	Raccoon	Wolfe Island, Ontario, Canada	2	†
KY026427	2000 Jan 13	Raccoon	Wolfe Island, Ontario, Canada	2	†
KY026422	1999 Jul 14	Raccoon	Prescott, Ontario, Canada	2	†
KY026423	1999 Sep 17	Raccoon	Oxford Station, Ontario, Canada	2	†
KY026450	2001 Apr 18	Raccoon	Leeds, Ontario, Canada	2	†
KY026417	1998 Nov 9	Raccoon	Canton, NY, USA	2	†
37-18	2018 Jan 3	Raccoon	Plymouth, MA, USA	3	MN418173
CT633269	2017 Oct 1	Skunk	Groton, CT, USA	3	MN418148
7844-17	2017 Oct 12	Cat	Providence, RI, USA	3	MN418170
761-18	2017 Aug 19	Raccoon	Woodstock, VT, USA	3	MN418179
186-18	2017 Dec 6	Skunk	Cutler, ME, USA	3	MN418180
8994-17	2017 Dec 15	Raccoon	Washington, ME, USA	3	MN418184
KY026414	2013 May 21	Raccoon	Waldo, ME, USA	3	†
CT661885	2016 Feb 1	Raccoon	New London, CT, USA	3	MN418150

*Bold indicates rabies virus isolates that were found in the rabies virus–free zone. ID, identification.
†Previously deposited in GenBank (*8*).

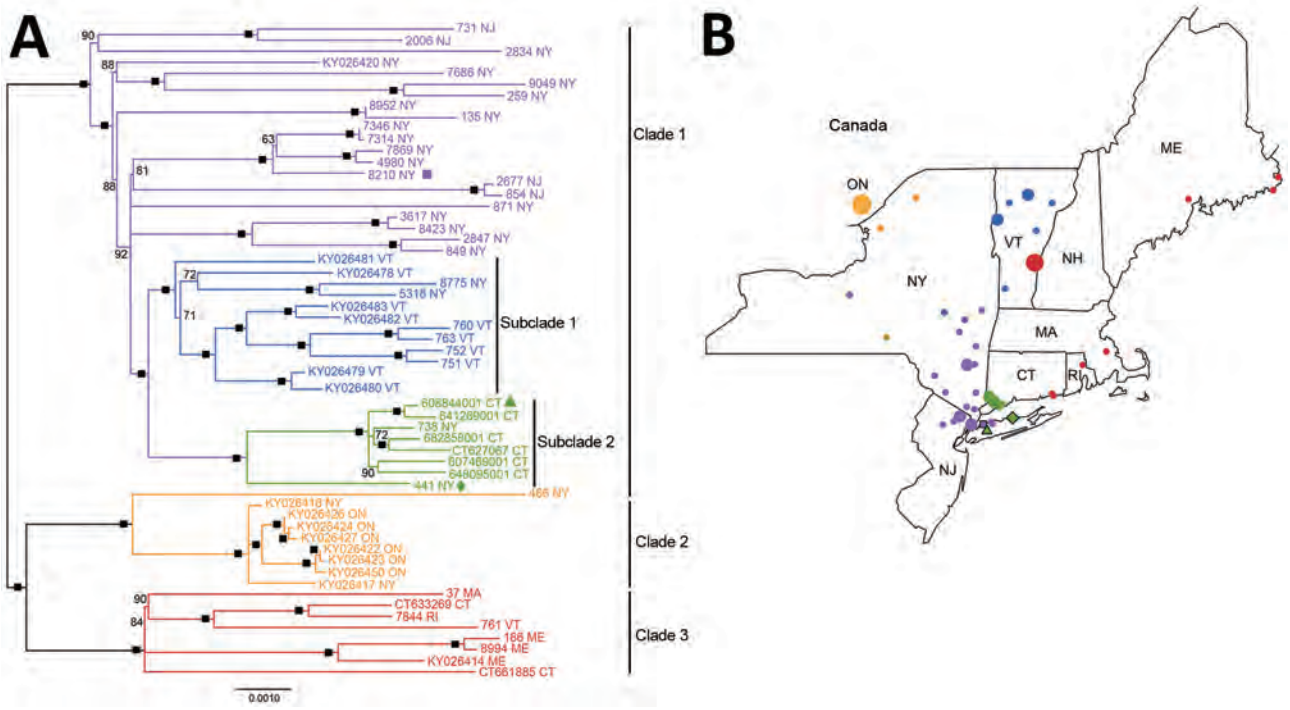

Figure 2. Maximum-likelihood whole-genome phylogeny and geographic location of rabies virus variants, northeastern United States and Canada, 2016–2017, including the rabid raccoon (green triangle), river otter (green diamond), and cat (purple square) found in raccoon rabies virus–free zones, Nassau and Suffolk Counties, Long Island, New York, USA . A) Midpoint-rooted, maximum-likelihood sequence analysis depicts the relationships among variants collected from New York, New Jersey, Massachusetts, Connecticut, Rhode Island, Vermont, and Maine, USA, and Ontario, Canada. Black boxes indicate nodes with ≥95% bootstrap support. Bootstrap support ≤50% is not shown. Scale bar indicates nucleotide substitutions per site. B) Location (by county) of virus isolation. Colors represent the major clades or subclades depicted in tree, and the size of symbols is proportional to the number of rabies samples isolated in that county. ON, Ontario.

been shown to be a viable strategy for public health laboratories to use in epidemiologic applications (*8*).

Using phylogenetic analysis (Table; Figure 2), we found that the raccoon in Hicksville was infected with a rabies virus variant consistent with those found in southwestern Connecticut. Considering the absence of local rabid wildlife with a similar rabies virus variant, we hypothesized that this raccoon was either accidentally or purposefully translocated into Long Island by human activity. Such translocation events were previously demonstrated with the linkage of an outbreak in Canada to a clade of raccoon rabies virus from upstate and central New York (*9*) and the spread of raccoon rabies virus up the East Coast of the United States (*2*,*8*). Furthermore, although the range of the average raccoon is highly dependent on many factors, raccoon ranges have been established to rarely exceed 4 km (2.5 miles) (*10*,*11*), well short of the 56-km (35-mile) distance from the Connecticut panhandle to Hicksville, New York.

Our phylogenetic analysis could not be used to conclusively determine where the rabies virus variant found in the river otter circulates, although the clade from Connecticut demonstrated the highest sequence similarity. Otters are found on the South Shores of Connecticut, Massachusetts, and Rhode Island and the North Shore of Long Island (*12*). They can swim >32 km (20 miles) a day and occupy territories of considerable size (*13*). When found, the otter was extremely decomposed to the extent of being borderline untestable. We deduced that the otter was likely from coastal or even inland Connecticut on the basis of phylogenetic data, tissue quality, and species behavior and habitat, but we do not know for certain. Additional sampling from Connecticut could potentially result in the virus from the otter being nested definitively within clade 1 subclade 2.

The rabid otter and raccoon most likely represent 2 separate incursion events, evidenced by the phylogenetic analysis. Because enhanced surveillance did not lead to the discovery of additional rabid animals during January 2017–December 2019 in the entirety of Suffolk and Nassau Counties, we can confidently stipulate that these were isolated events. Although we cannot state with conviction that no other animals

became infected, these incursions appear to be short lived and self-limiting.

The rabid cat from November 2017 was briefly considered a continuation of this tentative Long Island rabies outbreak, but after several conversations with public health authorities and the pet owner, this cat was determined to have been unvaccinated and adopted ≈80 km (50 miles) away in Westchester County. Phylogenetic analysis confirmed the virus variant was consistent with those found in downstate New York (clade 1). Although international pet adoption often garners headlines, domestic animal adoption (*14*) and incidental rabies translocation remains a constant threat that can jeopardize the results of multimillion-dollar rabies elimination programs.

Conclusions

Using WGS of an assortment of viruses, we revealed the likely origins of 3 raccoon rabies virus variants from 3 animals that had unexpectedly broken into a rabies-free zone. Through intensified enhanced rabies surveillance and WGS, an expensive contingency plan to distribute baits on Long Island ultimately became unnecessary and was not implemented. This study demonstrates the utility of WGS and phylogenetics as part of a multifaceted rabies investigation with tangible real-world consequences.

Acknowledgments

We are grateful to Susan Nadin-Davis and Christine Fehlner-Gardiner for their invaluable discussions on WGS. Thank you to the Connecticut, Vermont, and New York City Public Health Laboratories for sharing their samples with us. We are also grateful to Wadsworth Center Sequencing core for their assistance and advice.

About the Author

Mr. Brunt is a research scientist working at the Rabies Laboratory of the New York State Department of Health in Slingerlands, New York, USA. His research interests include molecular diagnostics, whole-genome sequencing, and bioinformatics.

References

1. Recuenco S, Eidson M, Cherry B, Kulldorff M, Johnson G. Factors associated with endemic raccoon (*Procyon lotor*) rabies in terrestrial mammals in New York State, USA. Prev Vet Med. 2008;86:30–42. http://dx.doi.org/10.1016/j.prevetmed.2008.03.001
2. Biek R, Henderson JC, Waller LA, Rupprecht CE, Real LA. A high-resolution genetic signature of demographic and spatial expansion in epizootic rabies virus. Proc Natl Acad Sci U S A. 2007;104:7993–8. http://dx.doi.org/10.1073/pnas.0700741104
3. Ma X, Monroe BP, Cleaton JM, Orciari LA, Li Y, Kirby JD, et al. Rabies surveillance in the United States during 2017. J Am Vet Med Assoc. 2018;253:1555–68. http://dx.doi.org/10.2460/javma.253.12.1555
4. Elser JL, Bigler LL, Anderson AM, Maki JL, Lein DH, Shwiff SA. The economics of a successful raccoon rabies elimination program on Long Island, New York. PLoS Negl Trop Dis. 2016;10:e0005062. http://dx.doi.org/10.1371/journal.pntd.0005062
5. Bigler L, Ochwat J, Scarpitta S, Matthews B, Rudd R, Lein D. Oral rabies vaccination strategies toward raccoon rabies elimination in suburban Nassau and Suffolk Counties (Long Island, New York, USA). J Wildl Dis. 2019 In press.
6. Szanto AG, Nadin-Davis SA, Rosatte RC, White BN. Re-assessment of direct fluorescent antibody negative brain tissues with a real-time PCR assay to detect the presence of raccoon rabies virus RNA. J Virol Methods. 2011;174:110–6. http://dx.doi.org/10.1016/j.jviromet.2011.04.009
7. Slavinski S, Humberg L, Lowney M, Simon R, Calvanese N, Bregman B, et al. Trap-vaccinate-release program to control raccoon rabies, New York, USA. Emerg Infect Dis. 2012;18:1170–2. http://dx.doi.org/10.3201/eid1807.111485
8. Nadin-Davis SA, Colville A, Trewby H, Biek R, Real L. Application of high-throughput sequencing to whole rabies viral genome characterisation and its use for phylogenetic re-evaluation of a raccoon strain incursion into the province of Ontario. Virus Res. 2017;232:123–33. http://dx.doi.org/10.1016/j.virusres.2017.02.007
9. Van Paassen K. Southeastern N.Y. likely the source of Ontario racoon rabies. 2016 Jun 17 [cited 2019 Jan 14]. https://www.theglobeandmail.com/news/national/southeastern-ny-likely-the-source-of-ontario-raccoon-rabies-outbreak/article30503340
10. Jenkins SR, Perry BD, Winkler WG. Ecology and epidemiology of raccoon rabies. Rev Infect Dis. 1988;10 (Suppl 4):S620–5. http://dx.doi.org/10.1093/clinids/10.Supplement_4.S620
11. Rosatte R, Sobey K, Donovan D, Bruce L, Allan M, Silver A, et al. Behavior, movements, and demographics of rabid raccoons in Ontario, Canada: management implications. J Wildl Dis. 2006;42:589–605. http://dx.doi.org/10.7589/0090-3558-42.3.589
12. Lariviere S, Walton LR. *Lontra canadensis*. Mamm Species. 1998;587:1–8. https://doi.org/10.2307/3504417
13. New York State Department of Environmental Conservation. River otter [cited 2019 Jan 19]. https://www.dec.ny.gov/animals/9355.html
14. Singh AJ, Chipman RB, de Fijter S, Gary R, Haskell MG, Kirby J, et al. Translocation of a stray cat infected with rabies from North Carolina to a terrestrial rabies-free county in Ohio, 2017. MMWR Morb Mortal Wkly Rep. 2018;67:1174–7. http://dx.doi.org/10.15585/mmwr.mm6742a2

Address for correspondence: Scott Brunt, New York State Department of Health, 5668 State Farm Rd, Slingerlands, NY 12159, USA; email: scott.brunt@health.ny.gov

Community Transmission of Severe Acute Respiratory Syndrome Coronavirus 2, Shenzhen, China, 2020

Jiaye Liu,[1] Xuejiao Liao,[1] Shen Qian, Jing Yuan, Fuxiang Wang, Yingxia Liu, Zhaoqin Wang, Fu-Sheng Wang, Lei Liu, Zheng Zhang

Since early January 2020, after the outbreak of coronavirus infection in Wuhan, China, ≈365 confirmed cases have been reported in Shenzhen, China. The mode of community and intrafamily transmission is threatening residents in Shenzhen. Strategies to strengthen prevention and interruption of these transmissions should be urgently addressed.

In December 2019, an outbreak of a novel coronavirus infection (COVID-19), occurred in Wuhan, China (*1*). Although China launched an emergency response early in the outbreak, the infection rapidly spread to metropolitan areas in China and around the world. The growing number of cases suggests that the epidemic has continued to spread. Several research articles have reported the epidemiologic characteristics of the outbreak in Wuhan and Hubei Province (*1*–*4*); however, to our knowledge, an analysis of the epidemic in metropolis areas around Wuhan has not yet been reported. To predict the epidemic trend and guide control measures, especially in similar metropolitan areas, outbreak investigations are needed.

Shenzhen, a modern and international metropolitan city, is located in southern China (Appendix Figure 1, https://wwwnc.cdc.gov/EID/article/26/6/20-0239-App1.pdf) and has a population of 13 million persons, among which >1 million are from Hubei Province and >70,000 from Wuhan. After the first cluster of COVID-19 cases was confirmed in Shenzhen in early January 2020 (W.J. Guan et al., unpub. data, https://doi.org/10.1101/2020.02.06.20020974), other cases spread within the city, involving all districts. To summarize the epidemiologic characteristics and provide updated information to aid in the development of control measures, we analyzed data for the first 365 laboratory-confirmed cases of COVID-19 in Shenzhen.

The Cases

In early January 2020, a total of 24 days after the index COVID-19 case occurred in Wuhan, a familial cluster of COVID-19 case-patients who had traveled to Wuhan from December 29, 2019, through January 4, 2020, was identified in Shenzhen (*5*). Subsequently, more cases in the city were reported. Analysis of spatiotemporal dynamics indicated that the infection spread more broadly throughout the city (Figure; Appendix Figure 2). Since January 17, infections increased substantially, peaking January 22–30. The decline since January 30 is probably the result of underascertainment of cases with recent onset and delayed identification or reporting (Figure).

Evaluation of the potential risk for local transmission will help determine whether patients with newly reported cases had definite exposure, defined by either having had definite contact with confirmed case-patients or having traveled to Wuhan or other cities in Hubei, or both, over the past 14 days. Overall, most (91%) cases that we report had definite exposure. On January 14, the first infected case-patient without definite exposure was reported in Shenzhen. Since January 20, growing numbers of cases without definite exposure were observed. Compared with the proportion before January 24, the proportion of case-patients without definite exposure was much higher from

Author affiliations: Shenzhen Third People's Hospital, Shenzhen, China (J. Liu, X. Liao, S. Qian, J. Yuan, F. Wang, Y. Liu, Z. Wang, L. Liu, Z. Zhang); Southern University of Science and Technology, Shenzhen (Y. Liu, L. Liu, Z. Zhang); The Fifth Medical Center of PLA General Hospital, Beijing, China (F.-S. Wang)

DOI: https://doi.org/10.3201/eid2606.200239

[1]These authors contributed equally to this article.

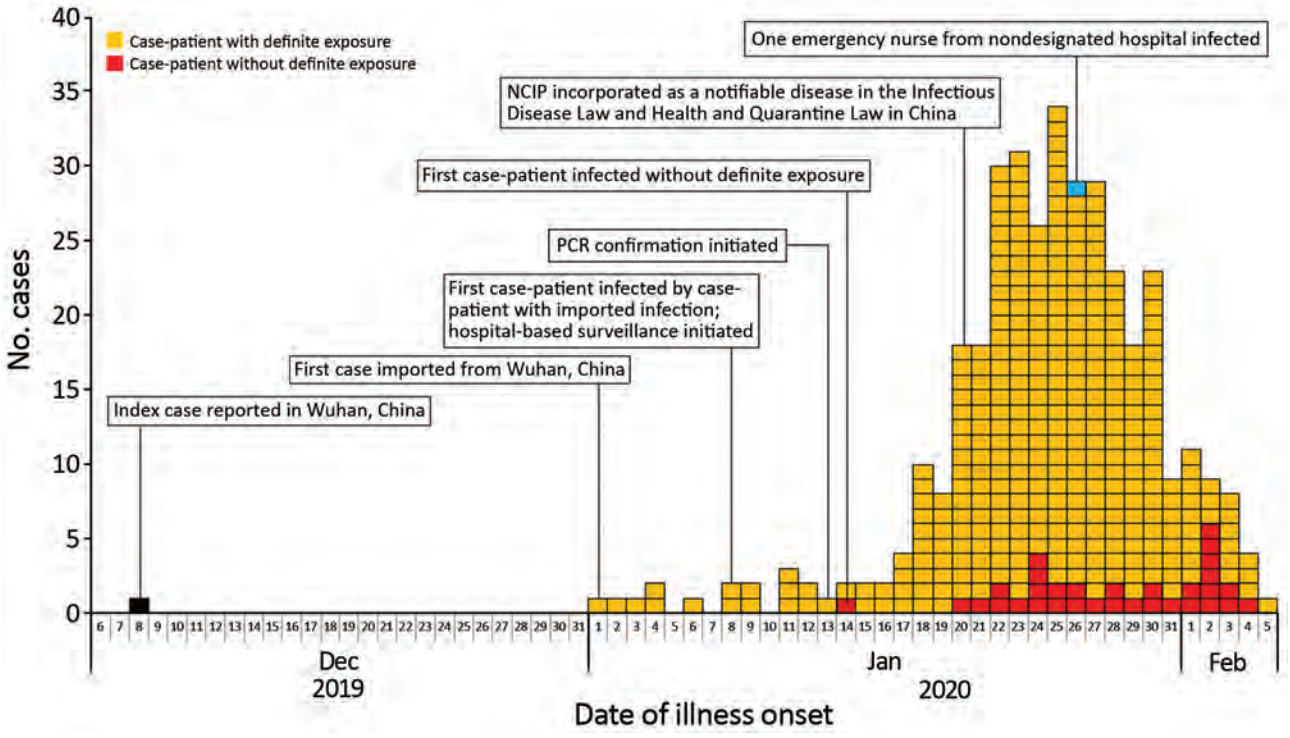

Figure. Onset of illness timeline for the first 365 confirmed COVID-19 case-patients in Shenzhen, China. The decline in incidence after January 30, 2020, probably resulted from delays in diagnosis and laboratory confirmation. All cases in this curve were confirmed. Hospital-based surveillance began January 8, 2020, for patients with suspected cases, defined by having a history of travel to Wuhan within the past 14 days, fever, and radiographic evidence of viral pneumonitis. PCR confirmation began January 13, 2020, and subsequently expanded the criteria for patients with suspected cases, defined by having typical clinical manifestations of COVID-19 and excluding infection caused by type A and B influenza and respiratory syncytial virus, regardless of travel history. NCIP, novel coronavirus–infected pneumonia (now called COVID-19).

January 25 through February 5 (11% vs. 6%; p<0.001) and increased to 36% (12/33) on both January 31 and February 5. These data suggest an increasing risk for community transmission (Table 1; Figure).

We analyzed the clinical and epidemiologic characteristics of 365 persons with laboratory-confirmed cases in Shenzhen. The median case-patient age was 46 (range 1–86) years; 182 (50%) case-patients were male. To investigate the shift of the epidemic, we compared characteristics of case-patients during 2 periods: before January 24 (the Chinese Spring Festival) and after January 25 (until February 5). Because of delays between

Table 1. Characteristics of patients with severe acute respiratory syndrome coronavirus 2 infection in Shenzhen, China, as of February 5, 2020

Characteristic	Before Jan 24, n = 166	Jan 25–Feb 5, n = 199	p value
Median age (range), y	52 (1–81)	40 (1–86)	<0.001
Age group, no. (%)			<0.001
<15	4 (2)	26 (13)	
15–34	30 (18)	44 (22)	
35–54	60 (36)	70 (35)	
≥55	72 (43)	59 (30)	
Patient sex, no. (%)			0.428
M	79 (48)	103 (52)	
F	87 (52)	96 (48)	
Exposure history, no. (%)			<0.001
Contact with confirmed case-patients	71 (43)	109 (55)	
Wuhan	78 (47)	42 (21)	
Cities other than Wuhan in Hubei Province	7 (4)	26 (13)	
No definite exposure	10 (6)	22 (11)	
First visited designated hospital, no. (%)	22 (13)	29 (15)	0.717
Days between illness onset and visiting hospital, median (range)	3 (0–15)	1 (0–9)	<0.001

Table 2. Estimated incubation periods for severe acute respiratory syndrome coronavirus 2, stratified by exposure classification, Shenzhen, China, as of February 5, 2020

Exposure	No. patients	Mean, d	Median, d	Interquartile range, d	Range, d
Contact with confirmed symptomatic case-patient	33	6.1	5	3–8	1–16
Traveled to Wuhan and stayed ≤1 day	25	6.0	5	3–8	1–15
Total	58	6.0	5	3–8	1–16

infection to illness onset or illness onset to confirmation, the following comparisons between the 2 periods might be biased because of misclassification.

We found a sharply increasing proportion of infected children (from 2% before January 24 to 13% for January 25–February 5; p<0.001), implying that increased exposure for children and intrafamily transmission might contribute substantially to the epidemic. Although substantially higher after January 25, 2020, the proportion of infected children in our study before January 24, 2020, was similar to the proportions reported by Li et al (*1*) (0/425, based on cases as of January 22, 2020) and Guan et al. (W.J. Guan et al., unpub. data, https://doi.org/10.1101/2020.02.06.20020974) (9/1,099 as of January 29, 2020). The possible reasons for the discrepancy after January 25 might be the low proportion of children exposed early in the outbreak; early detection for children who had had close contact with persons with diagnosed or suspected cases after strict control measures were conducted comprehensively; and difficult identification of the relatively milder clinical signs and symptoms in young patients than in infected adults (*6*), especially in the setting of limited resources in the early phase of the outbreak in Wuhan.

We explored the incubation periods for 58 case-patients with definite exposure and detailed investigation information. The estimated mean incubation periods were 6.1 (range 1–16) days among 33 case-patients who had had close contact with symptomatic confirmed case-patients and 6.0 (range 1–15) days among 25 case-patients who had traveled to Wuhan and stayed ≤1 day over the previous 3 weeks (Table 2; Appendix Table 1). Estimated incubation periods were consistent with those previously reported (*1*). We analyzed the characteristics of 74 clusters involving 183 cases (2–6 cases/cluster). Among 12 clusters of single intracluster transmission cases, 15 case-patients were infected within 5.5 days of the mean interval between illness onset of the infector and illness onset of the infectee. Among 56 clusters of single co-exposure cases, the mean interval of symptom onset between the primary and second case-patient within a cluster was 3.1 days, and the mean interval of symptom onset between the primary and last case-patient within a cluster was 3.6 days (Appendix Table 2).

With continuous implementation of strict control measures, we observed a shortened span (median days declining from 3 to 1; p<0.001) between illness onset and hospital visits for case-patients (Table 1). This finding may result from strict infection control management (e.g., early screening for suspected cases, monitoring for close-contact persons, and improved health consciousness of the general population).

To control the infection, confirmed case-patients should be separated and managed centrally; thus, the government has designated special hospitals to admit patients with suspected or confirmed cases. Nevertheless, as of February 5, to our knowledge, 1 case of a healthcare worker having been infected has been reported; an emergency nurse from a nondesignated hospital became ill on January 26, 2020, a total of 8 days after having been in close contact with a confirmed case-patient in the outpatient setting. We found that only 13%–15% of patients with confirmed cases went to the designated hospital first during the epidemic period. This finding means that a substantial number of case-patients visited ≥1 nondesignated hospital before they were admitted to the designated hospital, which increases the risk for nosocomial infection.

Conclusions

Essential for the control of this extremely contagious disease are close monitoring and timely reporting of the epidemic to the public as well as evaluation of the current control strategy. On the basis of this epidemiologic analysis, we found that COVID-19 has become endemic to Shenzhen, China. We suspect that community transmission and intrafamily transmission have potentially become the new transmission modes in the city. Also, nosocomial infection and transmission might pose a potential risk for COVID-19 control.

To control this outbreak in Shenzhen, maintaining basic and essential strategies is crucial. Early screening, diagnosis, isolation, and treatment are necessary to prevent further spread (*7*). Throughout the city, management of persons in close contact with persons with diagnosed and suspected cases, restriction of public activity, and use of personal protection measures should be continued. Strengthening effective and efficient measures, including but not limited to personal protection within families and communities with a high risk for exposure, will prevent and interrupt community and intrafamily transmission. To prevent nosocomial infection and transmission, a

designated hospital should be the first choice for persons who had close contact with confirmed case-patients or who themselves have clinical signs indicative of COVID-19.

Acknowledgment

We acknowledge the work and contribution of all health providers from Shenzhen Third People's Hospital and Shenzhen Center for Disease Control and Prevention in the detection, treatment, and control of the outbreak. We also acknowledge Zhiqiang Yao for his review of the manuscript.

About the Author

Dr. J. Liu is a clinical epidemiologist at The Institute of Hepatology, Shenzhen Third People's Hospital, Shenzhen, China. His research interests include the epidemiology, molecular characterization, and clinical outcomes of HIV/hepatitis B virus infection, and the control of emerging infectious diseases.

References

1. Li Q, Guan X, Wu P, Wang X, Zhou L, Tong Y, et al. Early transmission dynamics in Wuhan, China, of novel coronavirus–infected pneumonia. NEJM. 2020 Jan 31 [cited 2020 Feb 7]. https://www.nejm.org/doi/full/10.1056/NEJMoa2001316
2. Huang C, Wang Y, Li X, Ren L, Zhao J, Hu Y, et al. Clinical features of patients infected with 2019 novel coronavirus in Wuhan, China. Lancet. 2020;395:497–506 [cited 2020 Feb 7]. https://doi.org/10.1016/S0140-6736(20)30183-5
3. Chen N, Zhou M, Dong X, Qu J, Gong F, Han Y, et al. Epidemiological and clinical characteristics of 99 cases of 2019 novel coronavirus pneumonia in Wuhan, China: a descriptive study. Lancet. 2020;395:507–13 [cited 2020 Feb 7]. https://doi.org/10.1016/S0140-6736(20)30211-7
4. Wang DW, Hu B, Hu C, Zhu F, Liu X, Zhang J, et al. Clinical characteristics of 138 hospitalized patients with 2019 novel coronavirus–infected pneumonia in Wuhan, China. JAMA. 2020 Feb 7 [cited 2020 Feb 16]. https://doi.org/10.1001/jama.2020.1585
5. Chan JF, Yuan S, Kok KH, To KK, Chu H, Yang J, et al. A familial cluster of pneumonia associated with the 2019 novel coronavirus indicating person-to-person transmission: a study of a family cluster. Lancet. 2020;395:514–23 [cited 2020 Feb 7]. https://doi.org/10.1016/S0140-6736(20)30154-9
6. Chen ZM, Fu JF, Shu Q, Chen YH, Hua CZ, Li FB, et al. Diagnosis and treatment recommendations for pediatric respiratory infection caused by the 2019 novel coronavirus. World J Pediatr. 2020 Feb 5 [cited 2020 Feb 7]. https://doi.org/10.1007/s12519-020-00345-5
7. Wang FS, Zhang C. What to do next to control the 2019-nCoV epidemic? Lancet. 2020;395:391–3 [cited 2020 Feb 7]. https://doi.org/10.1016/S0140-6736(20)30300-7

Address for correspondence: Zheng Zhang or Lei Liu, Shenzhen Third People's Hospital, Bulan Rd No. 29, Longgang District, Shenzhen, Guangdong 518112, China; email: zhangzheng1975@aliyun.com or liulei3322@aliyun.com

Co-infection with SARS-CoV-2 and Influenza A Virus in Patient with Pneumonia, China

Xiaojing Wu, Ying Cai, Xu Huang, Xin Yu, Li Zhao, Fan Wang, Quanguo Li, Sichao Gu, Teng Xu, Yongjun Li, Binghuai Lu, Qingyuan Zhan

Author affiliations: China-Japan Friendship Hospital, Beijing, China (X. Wu, Y. Cai, X. Huang, X. Yu, L. Zhao, S. Gu, B. Lu, Q. Zhan); The Sixth Medical Center of PLA General Hospital, Beijing (F. Wang); Weifang No. 2 People's Hospital, Weifang, China (Q. Li); Vision Medicals Co., Ltd., Guangzhou, China (T. Zu, Y. Li)

DOI: https://doi.org/10.3201/eid2606.200299

We report co-infection with severe acute respiratory syndrome coronavirus 2 (SARS-CoV-2) and influenza A virus in a patient with pneumonia in China. The case highlights possible co-detection of known respiratory viruses. We noted low sensitivity of upper respiratory specimens for SARS-CoV-2, which could further complicate recognition of the full extent of disease.

In December 2019, a series of cases of pneumonia of unknown cause was reported in Wuhan, Hubei Province, China. On January 7, 2020, the causative pathogen was identified as a virus subsequently named severe acute respiratory syndrome coronavirus 2 (SARS-CoV-2) (*1*–*3*). We report a case of co-infection with SARS-CoV-2 and influenza A virus in China.

A 69-year-old man was seen in the clinic of China-Japan Friendship Hospital on January 23, 2020, for fever and dry cough. The patient visited Wuhan from December 18, 2019–January 22, 2020, and began having symptoms January 23. He reported no underlying medical conditions. Routine blood tests revealed a leukocyte count of 5.70 × 10^9 cells/L (reference range 3.5–9.5 × 10^9 cells/L) and lymphocyte count of 2.18 × 10^9 cells/L (reference range 1.1–3.2 × 10^9 cells/L). Chest computed tomography revealed a mass, ground-glass consolidation in the right inferior lobe of the lungs (Figure, panel A). Because of the patient's travel history, he was isolated for suspected coronavirus disease (COVID-19).

We obtained a nasopharyngeal swab specimen and conducted real-time reverse transcription-PCR (rRT-PCR) for SARS-CoV-2 by using reagents provided by Shanghai BioGerm Medical Technology Co., Ltd. (http://www.bio-germ.com), and Da An Gene Co., Ltd. (Sun Yat-Sen University, http://en.daangene.com), on a LightCycler 480 (Roche, https://lifescience.roche.com). However, both tests returned negative results 8 hours later. We obtained another nasopharyngeal swab specimen for detection of SARS-CoV-2 and for differentiation of influenza A and B and respiratory syncytial viruses by using Xpert Flu/RSV Xpress assay (Cepheid, https://www.cepheid.com). The sample was negative for SARS-CoV-2 but positive for influenza A. The patient was discharged with oral oseltamivir and instructed to stay home for isolation.

On January 30, the patient returned to the hospital reporting persistent fever and aggravated dyspnea. Routine blood tests showed a leukocyte count of 8.23 × 10^9 cells/L and lymphocyte count of 0.77 × 10^9 cells/L. A chest radiograph showed diffuse exudative shadows in bilateral lungs, indicating acute respiratory distress syndrome (Figure, panel B). Physical examination revealed respiratory rate of 30 breaths/min and oxygen saturation of 83% on ambient air. We administered oxygen and screened another nasopharyngeal swab specimen, which was negative for SARS-CoV-2. Considering his clinical features, we performed a fourth test for SARS-CoV-2 by using a sputum sample, which also was negative. The patient's dyspnea and

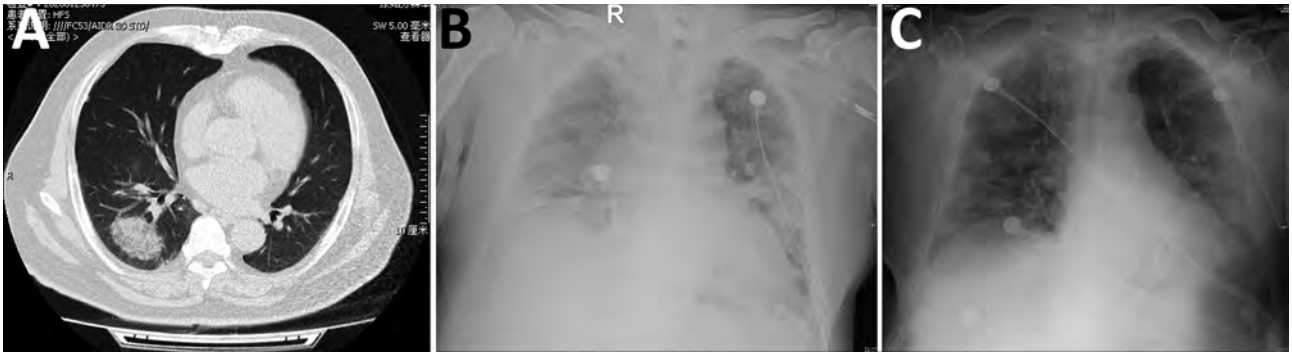

Figure. Radiographs of patient co-infected with severe acute respiratory syndrome coronavirus 2 and influenza A virus, China, 2020. A) Chest computed tomography demonstrating a mass, ground-glass consolidation in the right inferior lobe. B) Chest radiograph showing bilateral diffuse exudative shadows, indicating acute respiratory distress syndrome. C) Chest radiograph showing improved lung fields after 4 days in the intensive care unit.

respiratory distress increased, and his oxygenation index was <200. We admitted the patient to the single negative-pressure ward of the medical intensive care unit for severe influenza A pneumonia and administered endotracheal intubation because of severe hypoxemia.

Four days later, the patient's oxygenation and chest radiographs improved (Figure, panel C). We performed a bronchoscopy and obtained bronchoalveolar lavage fluid (BALF) for metagenomic next-generation sequencing (mNGS) to identify potential pathogens. On February 5, mNGS reported 3,460 sequences that showed 99.8% identity and covered 98.69% of the SARS-CoV-2 genome NC_045512.2|SARS-CoV-2|Wuhan-Hu-1 (GenBank accession no. NC_045512.2). We then performed rRT-PCR by using newly collected sputum and stored BALF, which also tested positive. Cycle threshold values were 34 for sputum and 30 for BALF. However, a fourth nasopharyngeal swab collected concurrently with the second sputum sample remained negative. The next day, the patient was transferred to a designated hospital for further critical care.

This case highlights 2 challenges in the diagnosis of COVID-19. First, the sensitivity of tests to detect SARS-CoV-2 from upper respiratory specimens might be insufficient. Repeated rRT-PCR testing of nasopharyngeal swabs was negative for SARS-CoV-2 before the patient was admitted to the intensive care unit. To date, diagnosis of COVID-19 is made mainly on the basis of nucleic acid detection from nasopharyngeal swabs. For suspected cases, 2 negative findings from nasopharyngeal swabs performed ≥24 hours apart would exclude a COVID-19 diagnosis (*4*). In this case, without the clinicians' persistence because of the patient's travel history, a COVID-19 diagnosis might never have been established. SARS-CoV-2 finally was identified by using mNGS and rRT-PCR of a BALF sample. Therefore, suitable sputum or BALF specimens are necessary to maximize detection in cases of high clinical suspicion; mNGS also might be a helpful tool for identifying SARS-CoV-2 (*1*,*5*).

Second, differentiating other causes of respiratory illness from COVID-19 is difficult, especially during influenza season, because common clinical manifestations of COVID-19, including fever, cough, and dyspnea, mimic those of influenza (*6*–*8*). In patients with COVID-19, blood tests typically show leucopenia and lymphopenia and most chest computed tomography scans show ground-glass opacity and consolidation with bilateral lung involvement (*7*–*9*). Unfortunately, influenza A and other respiratory viruses share these characteristics (*10*). Co-detection of SARS-CoV-2 and influenza A virus in this case demonstrates that additional challenges to detection remain, especially when patients test negative for SARS-CoV-2 but positive for another virus.

In summary, our case suggests that COVID-19 might be underdiagnosed because of false-negative tests for upper respiratory specimens or co-infection with other respiratory viruses. Broader viral testing might be needed when an apparent etiology is identified, particularly if it would affect clinical management decisions.

This study was supported by the National Key Research and Development Program of China (grant no. 2016YFC1304300 to Q.Z. and grant nos. 2018YFC1200100 and 2018YFC1200102 to B.L.), National Natural Science Foundation of China (grant no. 81870072 to Q.Z.), and Chinese Academy of Medical Sciences Innovation Fund for Medical Sciences (grant no. 2018-I2M-1-003 to Q.Z.).

About the author

Dr. Wu is a pulmonary and critical care physician specializing in respiratory infection at China-Japan Friendship Hospital, Beijing, China. Her research interests include severe lower respiratory infection and new respiratory infectious diseases.

References

1. Zhu N, Zhang D, Wang W, Li X, Yang B, Song J, et al.; China Novel Coronavirus Investigating and Research Team. A Novel coronavirus from patients with pneumonia in China, 2019. N Engl J Med. 2020;382:727–33. https://doi.org/10.1056/NEJMoa2001017
2. World Health Organization. Novel coronavirus–China. Disease outbreak news: update 12 January [cited 2020 Feb 12]. https://www.who.int/csr/don/12-january-2020-novel-coronavirus-china/en
3. Tan WZX, Zhao X, Ma X, Wang W, Niu P, Xu W, et al. A novel coronavirus genome identified in a cluster of pneumonia cases—Wuhan, China 2019–2020. China CDC Weekly 2020;2:61–62.
4. National Health Commission of People's Republic of China. Diagnosis and treatment for the novel coronavirus pneumonia (trial version 5) [cited 2020 Feb 8]. http://www.nhc.gov.cn/xcs/zhengcwj/202002/3b09b894ac9b4204a79db5b8912d4440/files/7260301a393845fc87fcf6dd52965ecb.pdf
5. World Health Organization. Pneumonia of unknown cause—China. Disease outbreak news: 5 January 2020 [cited 2020 Feb 12]. https://www.who.int/csr/don/05-january-2020-pneumonia-of-unkown-cause-china
6. Chen N, Zhou M, Dong X, Qu J, Gong F, Han Y, et al. Epidemiological and clinical characteristics of 99 cases of 2019 novel coronavirus pneumonia in Wuhan, China: a descriptive study. Lancet. 2020;395:507–13. https://doi.org/10.1016/S0140-6736(20)30211-7
7. Huang C, Wang Y, Li X, Ren L, Zhao J, Hu Y, et al. Clinical features of patients infected with 2019 novel coronavirus in

Wuhan, China. Lancet. 2020;395:497–506. https://doi.org/10.1016/S0140-6736(20)30183-5
8. Wang D, Hu B, Hu C, Zhu F, Liu X, Zhang J, et al. Clinical characteristics of 138 hospitalized patients with 2019 novel coronavirus-infected pneumonia in Wuhan, China. JAMA. 2020 Feb 7 [Epub ahead of print]. https://doi.org/10.1001/jama.2020.1585
9. Chan JF, Yuan S, Kok KH, To KK, Chu H, Yang J, et al. A familial cluster of pneumonia associated with the 2019 novel coronavirus indicating person-to-person transmission: a study of a family cluster. Lancet. 2020;395:514–23. https://doi.org/10.1016/S0140-6736(20)30154-9
10. Sullivan SJ, Jacobson RM, Dowdle WR, Poland GA. 2009 H1N1 influenza. Mayo Clin Proc. 2010;85:64–76. https://doi.org/10.4065/mcp.2009.0588

Address for correspondence: Binghuai Lu and Qingyuan Zhan, No. 2, East Yinghua Rd, Chaoyang District, Beijing 1000293, China; email: zs25041@126.com or zhanqycjfh@163.com

Incursions of *Candida auris* into Australia, 2018

Courtney R. Lane, Torsten Seemann, Leon J. Worth, Marion Easton, William Pitchers, Jenny Wong, Donna Cameron, Francesca Azzato, Richard Bartolo, Cristina Mateevici, Caroline Marshall, Monica A. Slavin, Benjamin P. Howden, Deborah A. Williamson

Author affiliations: The University of Melbourne at the Peter Doherty Institute for Infection and Immunity, Melbourne, Victoria, Australia (C.R. Lane, T. Seemann, W. Pitchers, D. Cameron, B.P. Howden, D.A. Williamson); VICNISS Coordinating Centre at the Peter Doherty Institute for Infection and Immunity, Melbourne (L.J. Worth); University of Melbourne, Parkville, Victoria, Australia (L.J. Worth, C. Marshall, M.A. Slavin); Peter MacCallum Cancer Centre, Melbourne (L.J. Worth, M.A. Slavin); Victorian Department of Health and Human Services, Melbourne (M. Easton, D. Cameron); Dorevitch Pathology—Western Health, Footscray, Victoria (J. Wong); Royal Melbourne Hospital at the Peter Doherty Institute for Infection and Immunity, Melbourne (F. Azzato, C. Marshall, M.A. Slavin); Western Health, Footscray (R. Bartolo, C. Mateevici); Royal Melbourne Hospital, Parkville (C. Marshall, D.A. Williamson); Austin Health, Heidelberg, Victoria, Australia (B.P. Howden)

DOI: https://doi.org/10.3201/eid2606.190936

Candida auris is an emerging global healthcare-associated pathogen. During July–December 2018, four patients with *C. auris* were identified in Victoria, Australia, all with previous overseas hospitalization. Phylogenetic analysis revealed putative transmission between 2 patients and suspected overseas acquisition in the others. Vigilant screening of at-risk patients is required.

The fungal pathogen *Candida auris* is an emerging global health threat associated with a range of invasive infections, most commonly candidemia; it is often resistant to multiple antifungal drugs (*1*). First identified in Japan in 2009, *C. auris* has been reported across all 6 populated continents with outbreaks in healthcare settings, particularly intensive care and high-dependence units (*1*,*2*). Four genetic lineages of *C. auris* with phylogeographic variation have been identified (*3*).

Before July 2018, only 1 case of *C. auris* had been reported in Australia, none in the state of Victoria (population 6.5 million) (*4*); no centralized surveillance or mandatory reporting has been implemented on a state or national level, and local screening policies are limited. However, Victoria has experienced large interfacility and intrafacility healthcare-associated outbreaks of other multidrug-resistant organisms (*5*) and has increasingly implemented genomics in both the investigation of outbreaks and routine surveillance (C.R. Lane et al., unpub. data, https://papers.ssrn.com/sol3/papers.cfm?abstract_id=3498431).

In July 2018, *C. auris* was cultured from a patient hospitalized in a Victoria healthcare facility. In response, the Victoria Department of Health and Human Services (DHHS) convened an incident management team and issued a Chief Health Officer alert to all health services and laboratories recommending admission screening for patients with recent overseas hospitalization. Also recommended was consideration of *C. auris* in patients with cultured non–*C. albicans* species and risk factors for fungal infection, including diabetes mellitus and recent antimicrobial drug use. The alert specified that all *C. auris* and nonspeciated non–*C. albicans* isolates from high-risk patients be referred to Victorian Public Health laboratories for speciation and characterization and reported to the DHHS (*6*). We report on the use of genomics to investigate putative transmission of *C. auris* in Victoria during July 1–December 31, 2018.

Isolates of *C. auris* were referred to the Victorian Infectious Diseases Reference Laboratory, where they underwent species identification and antimicrobial susceptibility testing. All isolates were then referred to the Microbiological Diagnostic Unit Public Health Laboratory for DNA extraction, whole-genome sequencing, and bioinformatic analysis.

During July–December 2018, we identified *C. auris* in 4 patients. Three patients (patients 1, 2, and 4 chronologically) were identified through clinically indicated samples, whereas patient 3 was screened on transfer from an overseas healthcare facility. Patients 1 and 2 were admitted to the same hospital at specimen collection, and patients 3 and 4 were admitted to different facilities. All patients reported previous overseas hospitalization (Figure).

We obtained 7 *C. auris* isolates from these 4 patients and performed core genome phylogenetic analysis on all isolates (Appendix, https://wwwnc.cdc.gov/EID/article/26/6/19-0936-App1.pdf). We downloaded publicly available *C. auris* sequences and included those meeting quality control metrics (Appendix Table 1). Phylogenetic analysis revealed all 7 isolates fell within the previously described South Asian clade (Figure, panel A).

We identified putative transmission during a concurrent hospital stay between patients 1 and 2 (Figure, panel B); transmission was epidemiologically validated and reported elsewhere (*7*). Because both patients reported overseas hospitalization, it is unclear which constituted the index case. Isolates from patients 3 and 4 were not closely related to each other, or any other included isolates, consistent with independent overseas acquisition.

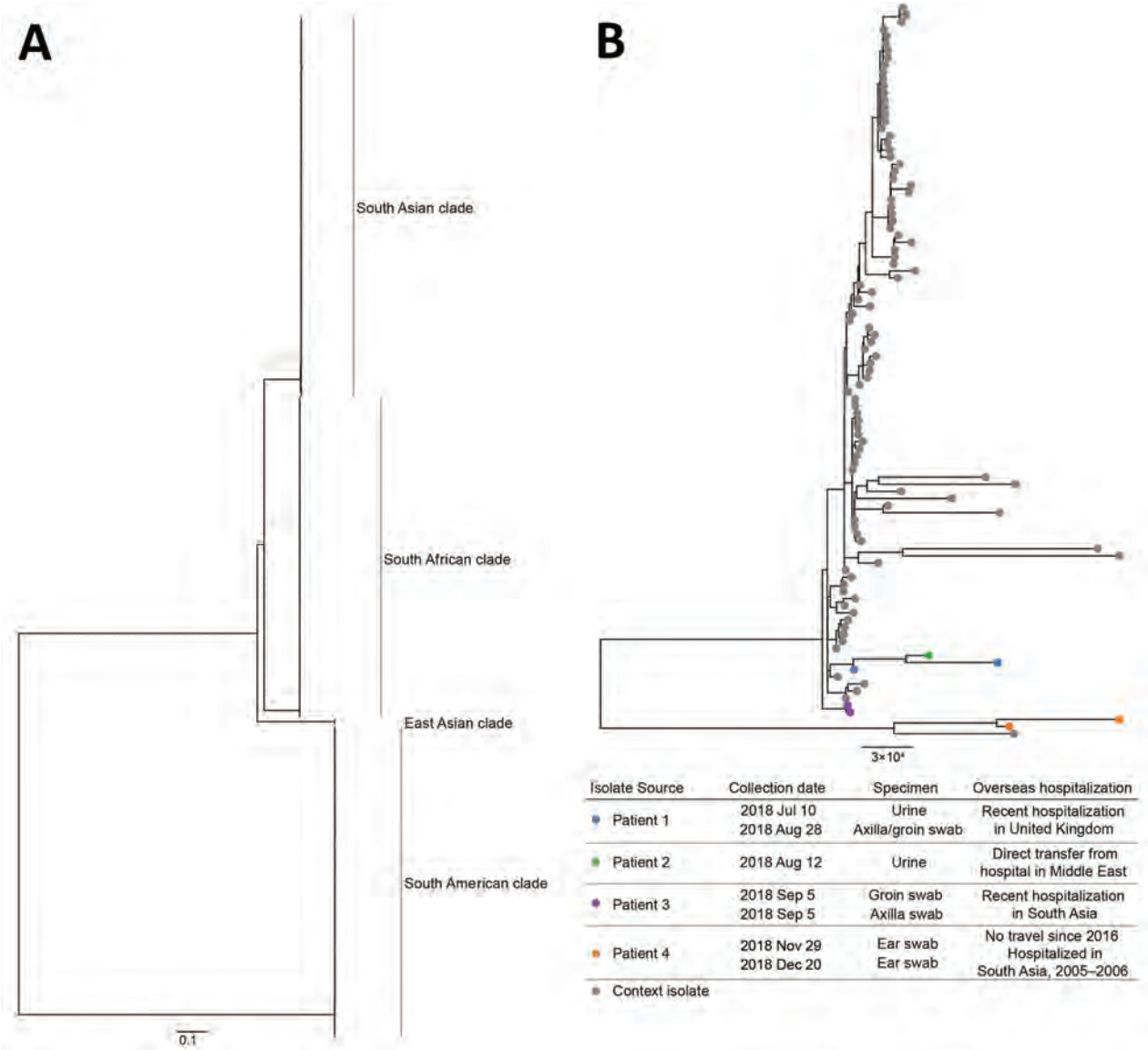

Figure. Maximum-likelihood phylogenetic trees of *Candida auris* isolates from Victoria, Australia, in the context of international publicly available genomes. A) Complete tree; B) South Asian clade. Isolates from 4 patients in Victoria are indicated by colored dots on the inset tree; isolate details and patient travel history are provided in the key. Scale bars indicate substitutions per site.

We reported results of phylogenetic analyses prospectively and concurrently to the incident management team and affected facilities. Because all patients reported overseas hospitalization, the combined analysis of genomic and epidemiologic data enabled assessment of alternative hypotheses, identifying putative local transmission between patients 1 and 2 and excluding patients 3 and 4 from the outbreak. These results justified targeted infection control measures.

In late 2015, Victoria introduced combined phylogenetic and epidemiologic surveillance for carbapenemase-producing *Enterobacterales*, a similar low-prevalence multiresistant organism (*8*). Using a search-and-destroy approach, this method enabled early identification of local transmission and complemented standard laboratory, screening, and outbreak control measures across the state. Leveraging from this work, a similar system was introduced for the control of *C. auris* in September 2019, with statewide mandatory notification of *C. auris* introduced in December 2019 (*9*,*10*). These measures address limitations in the current study, such as the inability to identify patients with *C. auris* because of noncompliance with screening recommendations, nonreporting, or decreased sensitivity of laboratory methods for the detection of *C. auris*.

A representative sample of international isolates enables inference of local transmission through local cluster identification and can indicate the source of local strains. The emergence of *C. auris* highlights the need for greater surveillance of nonbacterial multiresistant organisms and international data sharing. Sequences from our study were submitted to GenBank.

Our findings demonstrate the importance of proactive screening programs and of strict isolation and containment actions. Despite Australia's geographic isolation, vigilance is necessary to ensure that patients hospitalized overseas are identified and screened for the presence of multiresistant organisms such as *C. auris* upon hospital admission.

About the Author

Ms. Lane is an epidemiologist and PhD candidate at the University of Melbourne. Her primary research interest is the use of genomics in the surveillance of antimicrobial resistance and pathogens of public health concern.

References

1. Rhodes J, Abdolrasouli A, Farrer RA, Cuomo CA, Aanensen DM, Armstrong-James D, et al. Genomic epidemiology of the UK outbreak of the emerging human fungal pathogen *Candida auris*. Emerg Microbes Infect. 2018;7:43. https://doi.org/10.1038/s41426-018-0045-x
2. Centers for Disease Control and Prevention. Tracking *Candida auris* January 22, 2019: case count updated as of December 31, 2018 [cited 2019 Mar 6]. https://www.cdc.gov/fungal/candida-auris/tracking-c-auris.html
3. Lockhart SR, Etienne KA, Vallabhaneni S, Farooqi J, Chowdhary A, Govender NP, et al. Simultaneous emergence of multidrug-resistant *Candida auris* on 3 continents confirmed by whole-genome sequencing and epidemiological analyses. Clin Infect Dis. 2017;64:134–40. https://doi.org/10.1093/cid/ciw691
4. Australian Bureau of Statistics. Quarterly population estimates (ERP), by state/territory, sex and age [cited 2019 Mar 6]. http://stat.data.abs.gov.au/Index.aspx?DataSetCode=ERP_QUARTERLY
5. Kwong JC, Lane CR, Romanes F, Gonçalves da Silva A, Easton M, Cronin K, et al. Translating genomics into practice for real-time surveillance and response to carbapenemase-producing *Enterobacteriaceae*: evidence from a complex multi-institutional KPC outbreak. PeerJ. 2018;6:e4210. https://doi.org/10.7717/peerj.4210
6. Victorian Department of Health and Human Services. *Candida auris* case detected in Victoria [cited 2019 Mar 6]. https://www2.health.vic.gov.au/about/news-and-events/healthalerts/candida-auris-case-detected-in-victoria
7. Worth LJ, Harrison SJ, Dickinson M, van Diemen A, Breen J, Harper SE, et al. *Candida auris* in an Australian healthcare facility: importance of screening high-risk patients. Med J Aust. In press 2020.
8. Victorian Department of Health and Human Services. Victorian guideline on carbapenemase-producing *Enterobacteriaceae* for health services—version 2.1. Melbourne: Victorian Government; 2018 [cited 2020 Mar 23]. https://www2.health.vic.gov.au/Api/downloadmedia/%7BF1FDFD1D-C4D7-4131-A2FF-9EB24B5293E4%7D
9. Victorian Department of Health and Human Services. Victorian guideline on *Candida auris* for health services. Melbourne: Victorian Government; 2019 [cited 2020 Mar 23]. https://www2.health.vic.gov.au/Api/downloadmedia/%7BE72DE677-88A3-4AF4-8557-C20DEA78638F%7D
10. Parliament of Victoria. Public Health and Wellbeing Regulations 2019(Vic)(Austrl.). Parliament of Victoria; 2019 [cited 2020 Mar 23]. http://classic.austlii.edu.au/au/legis/vic/num_reg/phawr2019n135o2019412

Address for correspondence: Courtney R. Lane or Deborah Williamson, Microbiological Diagnostic Unit Public Health Laboratory, Doherty Institute for Infection & Immunity, 792 Elizabeth St, Melbourne, VIC 3000, Australia; email: courtney.lane@unimelb.edu.au or deborah.williamson@unimelb.edu.au

Donor-Derived Transmission of *Cryptococcus gattii* sensu lato in Kidney Transplant Recipients

Daniel W.C.L. Santos, Ferry Hagen, Jacques F. Meis, Marina P. Cristelli, Laila A. Viana, Fabiola D.C. Bernardi, Hélio Tedesco-Silva, José O. Medina-Pestana, Arnaldo L. Colombo

Author affiliations: Hospital do Rim, São Paulo, Brazil (D. W.C.L. Santos, M.P. Cristelli, L.A. Viana, H. Tedesco-Silva, J.O. Medina-Pestana); Escola Paulista de Medicina, Universidade Federal de São Paulo, São Paulo (D.W.C.L. Santos, A.L. Colombo); Canisius Wilhelmina Hospital, Nijmegen, the Netherlands (F. Hagen, J.F. Meis); Westerdijk Fungal Biodiversity Institute, Utrecht, The Netherlands (F. Hagen).Centre of Expertise in Mycology Radboudumc/CWZ, Nijmegen, the Netherlands (J.F. Meis); Faculdade de Ciências Médicas da Santa Casa de São Paulo, São Paulo (F.D.C. Bernardi)

DOI: https://doi.org/10.3201/eid2606.191765

We describe cases of donor-derived transmission of *Cryptococcus deuterogattii* in 2 kidney transplant recipients in Brazil and published information on other cases. Prompt reduction of immunosuppression and initiation of antifungal therapy was required to successfully control the fungal infections and preserve engraftment.

After antiretroviral therapy for HIV patients was introduced, solid organ transplant recipients became one of the major risk groups for developing cryptococcosis, possibly transmitted from donors (*1*,*2*). We describe 2 cases of donor-derived transmission of *Cryptococcus deuterogattii* in Brazil. The donor in both of these cases was a 43-year-old man with an antemortem history of an unspecified brain tumor who had been declared brain dead after respiratory arrest.

Case-patient 1 was a 51-year-old man who received a kidney from the donor. Physicians initiated induction therapy with antithymocyte globulin and maintenance therapy with tacrolimus, prednisone, and azathioprine. On day 7 after the procedure, doctors performed a kidney biopsy after the patient experienced delayed graft function. Histopathology of the graft showed organisms consistent with *Cryptococcus* yeast cells, suggesting fungal pyelonephritis. The patient had no respiratory or neurologic complaints. Results from his laboratory tests showed 7,000 leukocytes/mm^3, 201,000 platelets/μL, serum creatinine 13.29 mg/dL, and serum urea 132 mg/dL. Brain and thorax radiographs revealed no abnormalities. Results of a lumbar puncture showed an opening pressure of 18 cm H_2O, 2 leukocytes/mm^3, protein 63 mg/dL, and glucose 77 mg/dL; a *Cryptococcus* antigen latex (CrAg-latex) agglutination test result was positive (titer 1:8). Blood and urine cultures indicated *Cryptococcus* species, and the serum CrAg-latex agglutination test result was positive (titer 1:1,024).

After the diagnosis of cryptococcosis in the first patient, a 59-year-old woman (case-patient 2) who had received a kidney from the same donor was contacted for evaluation. Physicians had initiated induction therapy with antithymocyte globulin and maintenance therapy with tacrolimus, prednisone, and mycophenolic acid. She was discharged on day 8 after the procedure and was asymptomatic when recalled on day 10. Clinicians performed blood and urine cultures, radiographs of the chest and the brain, and a lumbar puncture. The radiograph revealed no abnormalities. Results of lumbar puncture showed opening pressure of 15 cm H_2O, 3 leukocytes/mm^3, protein 35 mg/dL, and glucose 174 mg/dL. Results of India ink and CrAg-latex agglutination tests were positive (titer: 1:64). Blood cultures and a urine sample indicated *Cryptococcus* species. No fungal growth was detected in a cerebrospinal fluid sample. The serum CrAg-latex agglutination was positive (titer 1:1,024).

A revised histology of the brain biopsy of the donor showed yeasts of *Cryptococcus* species that had not been detected previously. Results of a CrAg-latex agglutination test performed on a stored serum sample from the donor was positive (titer: 1:1,024). To rule out infection by *Cryptococcus* species in the organ recipients prior to the transplantations, CrAg-latex agglutination tests were performed on stored pretransplant serum samples from both recipients; results for both were negative.

Both patients were treated with amphotericin B lipid complex (5 mg/kg 1×/d for 21 d) in combination with 5-fluorocytosine (25 mg/kg 4×/d for 14 d); dosages of immunosuppressive drugs were lowered. Therapy was switched to intravenous fluconazole (400 mg/d) after results of blood and urine cultures became negative. After clinical and microbiological remission of the infection, dosage was adjusted on the basis of renal function to 300 mg/d of oral fluconazole and was maintained for 2 years. Three years after stopping all antifungal therapy, no relapse of cryptococcosis was documented.

All 6 isolates from the recipients were characterized at a reference laboratory at Universidade Federal de São Paulo (São Paulo, Brazil) and sent to Canisius-Wilhelmina Hospital (Nijmegen, The Netherlands). We performed AFLP (amplified fragment length polymorphism) fingerprinting and multilocus sequencing typing, which showed that all isolates were *C. deuterogattii* genotype AFLP6/VGII. The revision of slides from formalin-fixed paraffin-embedded tissue blocks from donor brain biopsies showed *Cryptococcus* yeasts. We performed fungal DNA extraction and amplified parts of *CAP59*, *GPD1*, *IGS1*, *LAC1*, *PLB1*, *SOD1*, and *URA5* loci (2). Phylogenetic analysis showed genetic similarity between the *C. deuterogattii* isolates from the kidney recipients and those from the donor's brain (Figure).

We searched the literature for other cases of fungal infections from solid organ donors in transplant

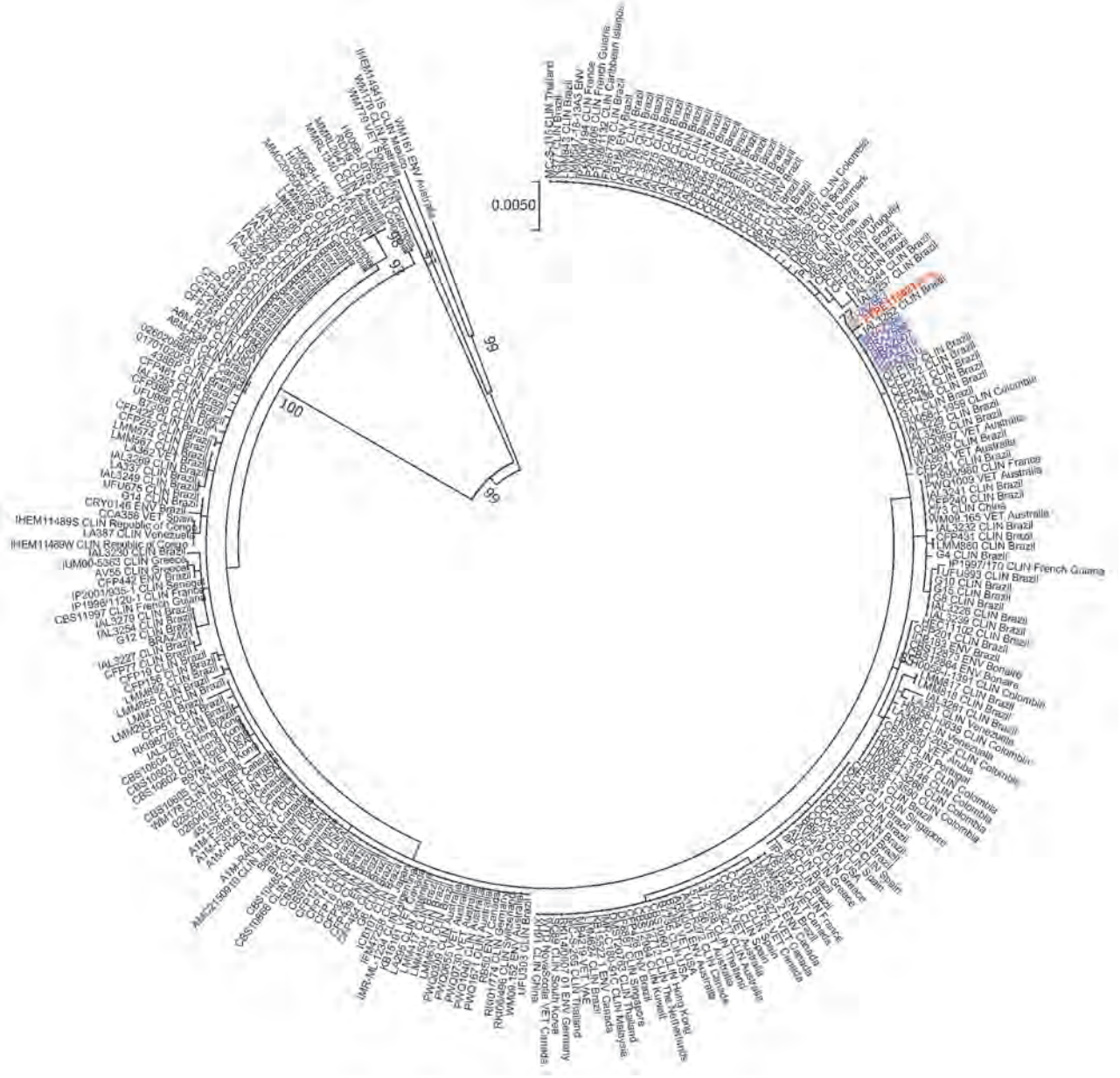

Figure. Phylogenetic maximum-likelihood analysis of 6 *Cryptococcus deuterogattii* isolates from 2 kidney transplant recipients in Brazil (blue), the organ donor (red), and cases from the literature (Appendix, https://wwwnc.cdc.gov/EID/article/26/6/19-1765-App1.pdf), along with reference isolates. Isolates from the 2 transplant recipients came from blood and urine; the genetic material from the donor came from a formalin-fixed paraffin-embedded brain tissue block. The GenBank accession numbers are KU642696-KU642701 (*CAP59*), KU642741-KU642746 (*GPD1*), KU642786-KU642791 (IGS1), KU642831-KU642836 (*LAC1*), KU642876-KU642881 (*PLB1*), KU642967-KU642972 (*SOD1*) and KU642921-KU642926 (*URA5*). Tree represents 1,000x bootstraps. Scale bar represents substitutions per site.

recipients and found 12 additional cases of presumed or confirmed donor-derived cryptococcosis (Appendix, https://wwwnc.cdc.gov/EID/article/26/6/19-1765-App1.pdf). Molecular identification was provided in only 6 out of 14 graft recipients (*3*–*10*). On the basis of the 2 cases we describe and data from the literature review, we suggest the following procedures for effective clinical management: performing blood and urine cultures, radiograph of the lungs and brain, and lumbar puncture to rule out dissemination; reducing immunosuppression to control infection; promptly initiating induction combination therapy with an amphotericin B lipid complex and 5-fluorocytosine; preserving the infected engraftment, if possible, in the absence of large fungal masses and abscesses; and extending the length of antifungal therapy when fungal elements persist in tissues.

In conclusion, we found that *C. deuterogattii* may be transmitted by infected allografts, representing a medical concern in countries to which *C. gattii* species complex is endemic. Cryptococcosis incidence might be reduced by excluding organ donor candidates with a history of neurologic disease without a clear definition of its etiology. Ensuring that clinicians are trained to recognize and treat this fungal infection would likely further reduce transmission from donors.

Acknowledgment

We are grateful to the team of infectious diseases and nephrologists responsible for the medical assistance to solid organ transplant recipients at the Hospital do Rim (UNIFESP).

There is no funding source for the research in question. There is no organization with a financial interest in the subject matter. The authors report no conflicts of interest for this research and are responsible for the content and writing of this paper. All the authors reviewed, approved, and contributed to the final version of the manuscript.

About the Author

Dr. Santos is a PhD student at the Federal University of São Paulo (UNIFESP), an infectious diseases specialist at the Kidney Hospital, São Paulo, and a clinical researcher at the Special Mycology Laboratory, Division of Infectious Diseases, Escola Paulista de Medicina, UNIFESP. His main research is on melanized fungal infections (phaeohyphomycosis and chromoblastomycosis) and infections in solid organ transplant patients.

References

1. Baddley JW, Forrest GN, AST Infectious Diseases Community of Practice. Cryptococcosis in solid organ transplantation—guidelines from the American Society of Transplantation Infectious Diseases Community of Practice. Clin Transplant. 2019;33:e13543. https://doi.org/10.1111/ctr.13543
2. Hagen F, Khayhan K, Theelen B, Kolecka A, Polacheck I, Sionov E, et al. Recognition of seven species in the *Cryptococcus gattii*/*Cryptococcus neoformans* species complex. Fungal Genet Biol. 2015;78:16–48. https://doi.org/10.1016/j.fgb.2015.02.009
3. Ooi BS, Chen BT, Lim CH, Khoo OT, Chan DT. Survival of a patient transplanted with a kidney infected with *Cryptococcus neoformans*. Transplantation. 1971;11:428–9. https://doi.org/10.1097/00007890-197104000-00018
4. Beyt BE Jr, Waltman SR. Cryptococcal endophthalmitis after corneal transplantation. N Engl J Med. 1978;298:825–6. https://doi.org/10.1056/NEJM197804132981506
5. Kanj SS, Welty-Wolf K, Madden J, Tapson V, Baz MA, Davis RD, et al. Fungal infections in lung and heart-lung transplant recipients: report of 9 cases and review of the literature. Medicine (Baltimore). 1996;75:142–56. https://doi.org/10.1097/00005792-199605000-00004
6. de Castro LE, Sarraf OA, Lally JM, Sandoval HP, Solomon KD, Vroman DT. *Cryptococcus albidus* keratitis after corneal transplantation. Cornea. 2005;24:882–3. https://doi.org/10.1097/01.ico.0000157404.34774.1a
7. Baddley JW, Schain DC, Gupte AA, Lodhi SA, Kayler LK, Frade JP, et al. Transmission of *Cryptococcus neoformans* by organ transplantation. Clin Infect Dis. 2011;52:e94–8. https://doi.org/10.1093/cid/ciq216
8. MacEwen CR, Ryan A, Winearls CG. Donor transmission of *Cryptococcus neoformans* presenting late after renal transplantation. Clin Kidney J. 2013;6:224–7. https://doi.org/10.1093/ckj/sft006
9. Chang CM, Tsai CC, Tseng CE, Tseng CW, Tseng KC, Lin CW, et al. Donor-derived *Cryptococcus* infection in liver transplant: case report and literature review. Exp Clin Transplant. 2014;12:74–7. https://doi.org/10.6002/ect.2012.0288
10. Camargo JF, Simkins J, Schain DC, Gonzalez AA, Alcaide ML, Anjan S, et al. A cluster of donor-derived *Cryptococcus neoformans* infection affecting lung, liver, and kidney transplant recipients: case report and review of literature. Transpl Infect Dis. 2018;20:e12836. https://doi.org/10.1111/tid.12836

Address for correspondence: Arnaldo L. Colombo, Laboratório Especial de Micologia, Disciplina de Infectologia, Universidade Federal de São Paulo, São Paulo-SP. Rua Botucatu, 740. CEP 04023-062, São Paulo, Brazil; e-mail: arnaldolcolombo@gmail.com

Sabiá Virus–Like Mammarenavirus in Patient with Fatal Hemorrhagic Fever, Brazil, 2020

Fernanda de Mello Malta,[1] Deyvid Amgarten,[1] Ana Catharina de Seixas Santos Nastri, Yeh-Li Ho, Luciana Vilas Boas Casadio, Marcela Basqueira, Gloria Selegatto, Murilo Castro Cervato, Amaro Nunes Duarte-Neto, Hermes Ryoiti Higashino, Felipe Arthur Faustino Medeiros, José Luiz Pinto Lima Gendler, Anna S. Levin, João Renato Rebello Pinho

Author affiliations: Hospital Israelita Albert Einstein, São Paulo, Brazil (F.M. Malta, D. Amgarten, M. Basqueira, M.C. Cervato, J.R.R. Pinho); Universidade de São Paulo, São Paulo (D. Amgarten, A.C. de Seixas Santos Nastri, Y.-L. Ho, L.V.R. Casadio, G. Selegatto, A.N. Duarte-Neto, H.R. Higashino, F.A.F. Medeiros, J.L.P.L. Gendler, A.S. Levin, J.R.R. Pinho)

DOI: https://doi.org/10.3201/eid2606.200099

New World arenaviruses can cause chronic infection in rodents and hemorrhagic fever in humans. We identified a Sabiá virus–like mammarenavirus in a patient with fatal hemorrhagic fever from São Paulo, Brazil. The virus was detected through virome enrichment and metagenomic next-generation sequencing technology.

Viral infections have become an important public health issue in South America during the past 2 decades. Outbreaks of arboviral disease, such as dengue, chikungunya, Zika, and yellow fever, have increased concern about improving surveillance and diagnosis of viral infections in anticipation of the next threat (*1*–*4*). South American arenaviruses belong to the New World serogroups, cause chronic infection in rodents, and have been associated with neurologic symptoms and hemorrhagic fever in humans (*5*).

We report a fatal case of a new Sabiá virus (SABV)–like mammarenavirus infection in São Paulo, Brazil, in a previously healthy 52-year-old man. On December 30, 2019, he sought care at a basic health facility for odynophagia, epigastric pain radiating to the chest, nausea, vertigo, xerostomy, and myalgia. During the next few days, his signs and symptoms worsened to intense myalgia, fever, drowsiness, and hypotension, so he was referred to the Hospital das Clinicas, Faculdade de Medicina da Universidade de São Paulo (São Paulo, Brazil), on January 6, 2020. At admission, he had bilateral conjunctivitis, diffuse skin rash, cervical lymphadenopathy, and altered mental status.

Blood samples were sent to the Laboratorio de Tecnicas Especiais (LATE), Hospital Israelita Albert Einstein (São Paulo, Brazil). Results of serologic and molecular tests were negative for yellow fever, dengue, Zika, and chikungunya viruses; viral hepatitis; enteroviruses; and herpesviruses. Further testing was performed with a newly implemented routine test for RNA viruses, a virome enrichment technique, and metagenomic next-generation sequencing (NGS) technology. In brief, total RNA was extracted from plasma, and human rRNA was depleted. Reverse transcription of RNA was performed with a 2-step cDNA random synthesis, followed by PCR amplification, adapted from Greninger et al. (*6*). We then generated DNA libraries using Illumina Nextera XT (Illumina, https://www.illumina.com) and sequenced them using Illumina NextSeq 550. We used the data generated as input for an in-house bioinformatics pipeline, performed as follows: raw data quality control, human decontamination, first round of pathogen identification, reads assembly, second round of identification with contigs, and finding confirmation through mapping and calculating quality metrics.

The patient's condition deteriorated, and he died on January 11. Main autopsy findings were cerebral edema, hepatomegaly with steatotic aspect, and pulmonary hemorrhage. Microscopy showed panlobular hepatitis, with steatotic and apoptotic hepatocytes, hyperplasic Kupffer cells, and mild inflammatory reaction in the liver. Ischemic coagulative necrosis around central vein was also noted. Other findings included bronchopneumonia, acute tubular necrosis, and hemophagocytosis in the bone marrow. Detailed histologic studies are under way.

The report of the virome test from the patient's plasma sample identified the presence of a mammarenavirus, SP2019-01. Further bioinformatics analysis enabled recovery of 2 complete fragments of the viral genome corresponding to the small (S [3,308 bp]) and large (L [7,056 bp]) segments of an arenavirus; NGS average coverage was 117× for the S and 1,146× for the L segment. The S segment had 87% identity and the L segment had 89% identity in a full nucleotide alignment with SABV strain SPH114202 (Figure, panel A). We submitted sequences to GenBank (accession nos. MN956773 [L segment] and MN956774 [S segment]). A maximum-likelihood tree of the species within the Arenaviridae family shows strain SP2019-01 as a SABV-like mammarenavirus based on the alignment

[1]These authors contributed equally to this article.

of arenavirus complete nucleotide sequences of the L segment (Figure, panel B).

SABV is a New World arenavirus that was previously isolated in São Paulo in 1994 in a patient with fatal hemorrhagic fever (*7*). Four additional New World arenavirus are known to be associated with human disease in South America: Junin, Machupo, Guanarito, and Chapare (*8*). Chapare virus is closely related to SABV and has been recently implicated in an outbreak of 5 cases (3 fatal) of hemorrhagic fever in Bolivia (*8*,*9*).

Little is known about the natural history of SABV infection. The wild reservoir species for this virus is still unknown but is probably a rodent (*10*). Three additional SABV cases in humans have been

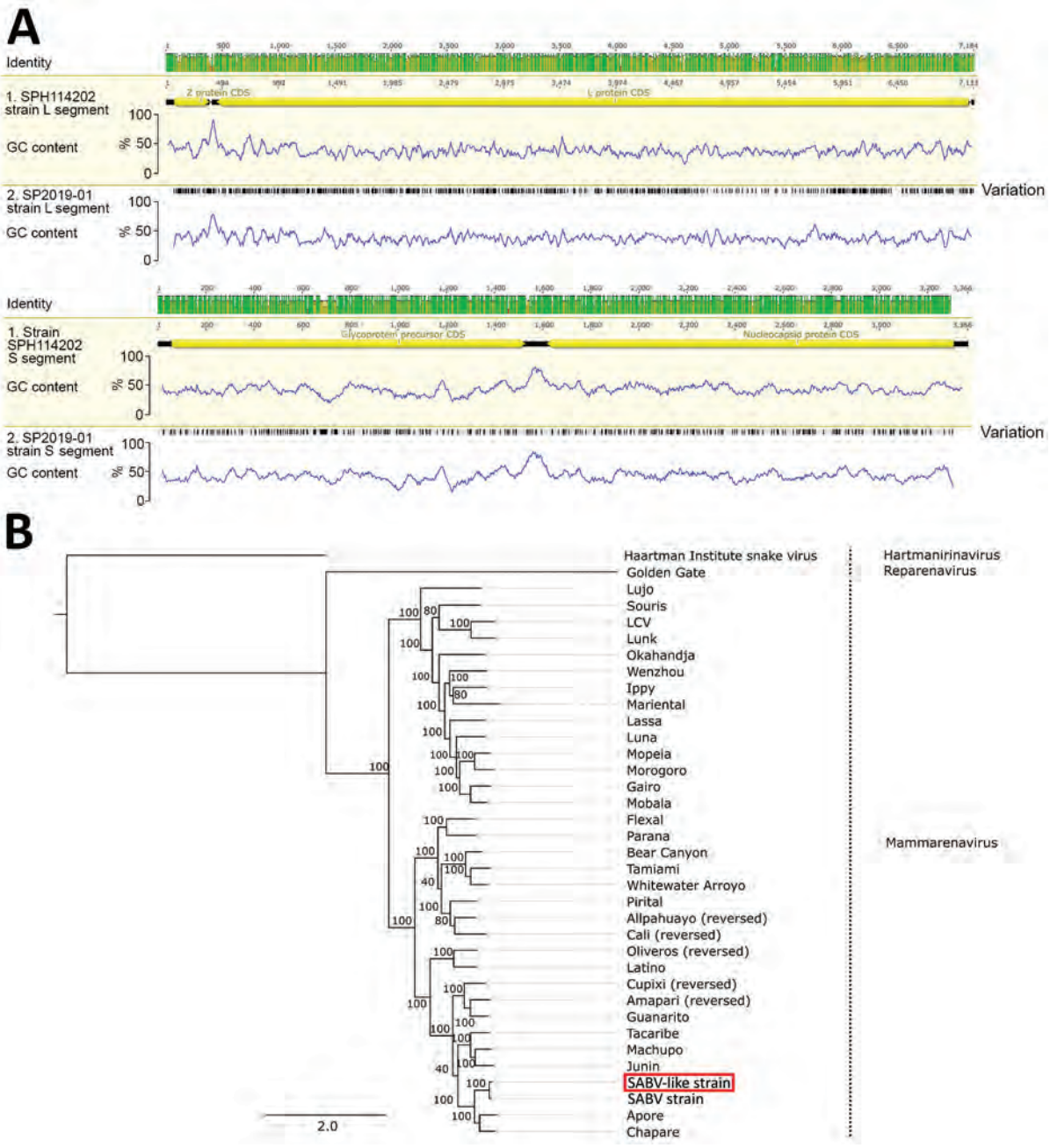

Figure. Genomic and phylogenetic analysis of SABV-like mammarenavirus (SP2019-01) from a patient with fatal hemorrhagic fever, Brazil, 2020. A) Genome plots comparing strain SP2019-01 with SABV strain SPH114202, showing identity throughout the genome and variant sites (black lines). B) Maximum-likelihood tree of SP2019-01 (red box) based on the alignment of arenavirus sequences. Tree was rooted in the Haartman Institute virus isolate sequence, and bootstrap values are shown next to the branches. CDS, coding sequence; GC, content of guanosine and cytosine; L, large; S, small; SABV, Sabiá virus. Scale bar indicates nucleotide substitutions per site.

reported since 1994 including 2 in laboratory workers handling SABV samples, raising concern about the potential for aerosol transmission (*10*).

After the virome test report from this investigation was issued, the laboratory team took all measures to remove biological samples from laboratory routine testing and store them at -80°C. Persons who had any contact with the patient were informed and monitored and did not develop symptoms. Brazil health and surveillance authorities, as well as the US Centers for Disease Control and Prevention, were also informed. Our finding of an SABV-like arenavirus strain causing a fatal human infection in a region with a recent outbreak of yellow fever show the potential role of virome enrichment technique and metagenomic NGS for the etiologic diagnosis and identification of new pathogens in patients with hemorrhagic fever.

Acknowledgments

We thank HCFMUSP Infectious Diseases Department healthcare workers for their dedication to assisting patients, Venancio Alves for continuous support, and Cristóvão Luis Pitangueira Mangueira and Rubia Anita Ferraz Santana and the technical staff of Laboratorio de Tecnicas Especiais, Hospital Israelita Albert Einstein, for scientific and technical support.

About the Author

Dr. Malta is a senior laboratory analyst at the Laboratorio de Tecnicas Especiais, Hospital Israelita Albert Einstein, São Paulo. Her primary research interests include molecular characterization of virus genome (hepatitis C virus, hepatitis B virus, and yellow fever virus) DNA sequencing techniques.

References

1. Morens DM, Fauci AS. Emerging infectious diseases: threats to human health and global stability. PLoS Pathog. 2013;9:e1003467. http://dx.doi.org/10.1371/journal.ppat.1003467
2. Grubaugh ND, Ladner JT, Lemey P, Pybus OG, Rambaut A, Holmes EC, et al. Tracking virus outbreaks in the twenty-first century. Nat Microbiol. 2019;4:10–9. http://dx.doi.org/10.1038/s41564-018-0296-2
3. Deng X, Achari A, Federman S, Yu G, Somasekar S, Bártolo I, et al. Metagenomic sequencing with spiked primer enrichment for viral diagnostics and genomic surveillance. Nat Microbiol. 2020;5:443–54. [Erratum in: Nat Microbiol. 2020;5:525.] PubMed http://dx.doi.org/10.1038/s41564-019-0637-9
4. Chong HY, Leow CY, Abdul Majeed AB, Leow CH. Flavivirus infection—a review of immunopathogenesis, immunological response, and immunodiagnosis. Virus Res. 2019;274:197770. http://dx.doi.org/10.1016/j.virusres.2019.197770
5. Brisse ME, Ly H. Hemorrhagic fever-causing arenaviruses: Lethal pathogens and potent immune suppressors. Front Immunol. 2019;10:372. http://dx.doi.org/10.3389/fimmu.2019.00372
6. Greninger AL, Naccache SN, Federman S, Yu G, Mbala P, Bres V, et al. Rapid metagenomic identification of viral pathogens in clinical samples by real-time nanopore sequencing analysis. Genome Med. 2015;7:99. http://dx.doi.org/10.1186/s13073-015-0220-9
7. Lisieux T, Coimbra M, Nassar ES, Burattini MN, de Souza LT, Ferreira I, et al. New arenavirus isolated in Brazil. Lancet. 1994;343:391–2. http://dx.doi.org/10.1016/S0140-6736(94)91226-2
8. Delgado S, Erickson BR, Agudo R, Blair PJ, Vallejo E, Albariño CG, et al. Chapare virus, a newly discovered arenavirus isolated from a fatal hemorrhagic fever case in Bolivia. PLoS Pathog. 2008;4:e1000047. http://dx.doi.org/10.1371/journal.ppat.1000047
9. Escalera-Antezana JP, Rodriguez-Villena OJ, Arancibia-Alba AW, Alvarado-Arnez LE, Bonilla-Aldana DK, Rodríguez-Morales AJ. Clinical features of fatal cases of Chapare virus hemorrhagic fever originating from rural La Paz, Bolivia, 2019: A cluster analysis. Travel Med Infect Dis. 2020 Feb 17 [Epub ahead of print]. http://dx.doi.org/10.1016/j.tmaid.2020.101589
10. Ellwanger JH, Chies JAB. Keeping track of hidden dangers—the short history of the Sabiá virus. Rev Soc Bras Med Trop. 2017;50:3–8. http://dx.doi.org/10.1590/0037-8682-0330-2016

Address for correspondence: João Renato Rebello Pinho, Hospital das Clinicas da Faculdade de Medicina da Universidade de São Paulo, Divisão de Laboratório Central, Biologia Molecular, Avenida Dr. Eneas de Carvalho Aguiar, 155, 2nd Fl, São Paulo, SP, Brazil; email: jrrpinho@usp.br

Lack of Vertical Transmission of Severe Acute Respiratory Syndrome Coronavirus 2, China

Yang Li,[1] Ruihong Zhao,[1] Shufa Zheng,[1] Xu Chen, Jinxi Wang, Xiaoli Sheng, Jianying Zhou, Hongliu Cai, Qiang Fang, Fei Yu, Jian Fan, Kaijin Xu, Yu Chen, Jifang Sheng

DOI: https://doi.org/10.3201/eid2606.200287

Author affiliations: The First Affiliated Hospital, College of Medicine, Zhejiang University, Hangzhou, China

A woman with coronavirus disease in her 35th week of pregnancy delivered an infant by cesarean section in a negative-pressure operating room. The infant was negative for severe acute respiratory coronavirus 2. This case suggests that mother-to-child transmission is unlikely for this virus.

The recent outbreak of severe acute respiratory syndrome coronavirus 2 (SARS-CoV-2), which causes coronavirus disease (COVID-19), is a public health emergency that has drawn international concern (*1*). Like SARS-CoV and Middle East respiratory syndrome coronavirus, SARS-CoV-2 is a member of the coronavirus family for which no evidence of mother-to-fetus transmission has been found (*2*–*4*). We report a pregnant woman with confirmed SARS-CoV-2 infection who underwent cesarean section delivery of a SARS-CoV-2–negative infant in Zhejiang Province, China.

On February 6, 2020, a 30-year-old pregnant woman at 35 weeks' gestation sought treatment at a college hospital because of a 2-day history of dry cough without fever, chills, or shortness of breath. The previous day, she had been confirmed positive for SARS-CoV-2 infection at her local hospital on the basis of a sputum sample.

We analyzed her epidemiologic history by asking questions to determine the timeline of her virus infection. Beginning on January 12, her mother-in-law and father-in-law, who lived in Hubei Province, visited her house for 18 days. After the pregnant woman's hospital admission, the asymptomatic parents-in-law were suspected of having SARS-CoV-2 infection and therefore quarantined in a hospital. However, they tested negative for SARS-CoV-2 twice, even though radiographs of the lungs of both persons suggested lesions. The pregnant woman's husband, who denied any contact with others except his wife and his parents, experienced fever on February 1. His condition worsened, and he went to the hospital, where he tested positive for SARS-CoV-2.

On day 1 of her hospitalization, the pregnant woman had dry cough and a temperature of 37.2°C. Chest auscultation was slightly thicker in the right lung but not the left lung. Chest radiography showed scattered multiple patchy infiltrates in both lungs. Laboratory findings were slightly abnormal (Appendix Table 1, https://wwwnc.cdc.gov/EID/article/26/6/20-0287-App1.pdf). We considered this an ordinary case on the basis of mild symptoms and radiologic imaging. She received antiviral treatment (oral lopinavir 200 mg and ritonavir 50 mg, each 2×/d), as well as methylprednisolone (40 mg 1×/d) to relieve inflammation effusion (Figure). Her cough resolved on day 2 of hospitalization.

On February 8 (day 3 of hospitalization), SARS-CoV-2 RNA remained in the woman's sputum, and the fetal heart rate monitor showed 110 beats/min. Consultation with an obstetrician resulted in a recommendation for emergency cesarean section. The woman underwent a lower uterus cesarean section in a negative-pressure operating room. All persons in the room wore protective suits. Cefoperazone sodium/sulbactam sodium (intravenous drip, 2 g/ 8 h) was infused to prevent infection at the surgical site, and the methylprednisolone dose was doubled. She delivered a normal baby boy without complications. An oropharyngeal swab specimen, obtained immediately after he was taken from the uterus, indicated he was negative for SARS-CoV-2, and he was sent to the negative-pressure ward. During the next 2 days, the infant's oropharyngeal swab, blood, feces, and urine samples remained negative for SARS-CoV-2 throughout testing at 7 different times.

On the delivery day, although the woman's sputum was positive, serum, urine, feces, amniotic fluid, umbilical cord blood and placenta, and breast milk samples were negative. On days 4 and 5 of hospitalization, the woman's sputum tests were negative for SARS-CoV-2, and she remained afebrile. Her respiratory specimens were positive for SARS-CoV-2 after 4 days of serial testing (Appendix Table 2). No SARS-CoV-2 RNA was detected in fecal, urine, and blood samples. The woman was discharged from the hospital on February 19, and her infant was discharged on February 24.

[1]These authors contributed equally to this article.

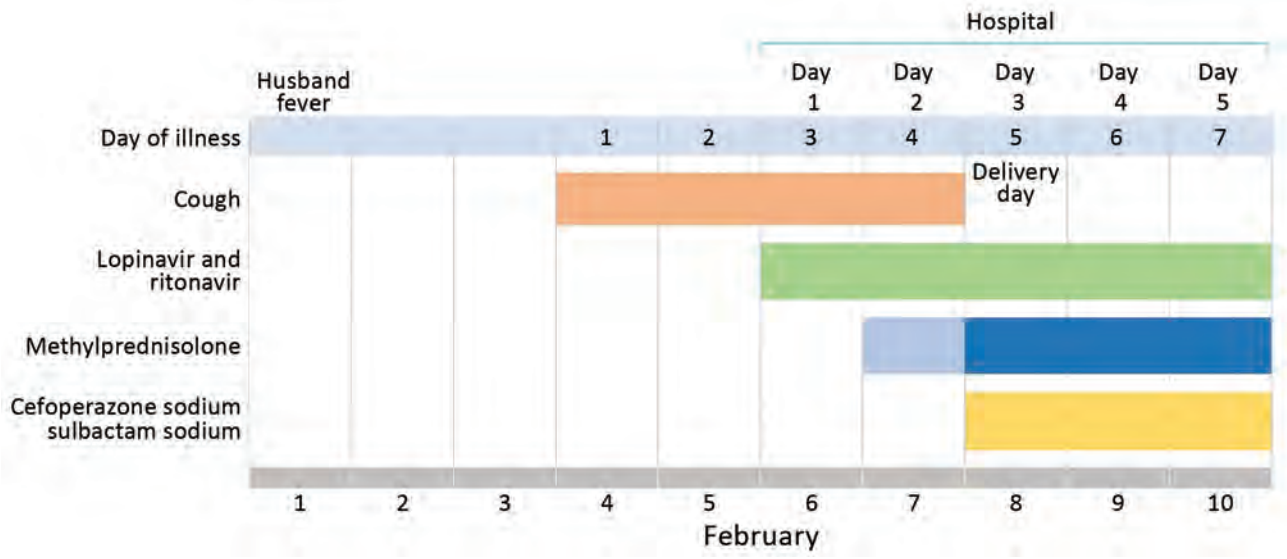

Figure. Course of illness and treatment for a 30-year-old pregnant woman infected with severe acute respiratory syndrome coronavirus 2, China.

In a descriptive study of SARS-CoV-2 infection, 7 of 9 pregnant women delivered their infants through caesarean section and 2 delivered through vaginal delivery; 10 SARS-CoV-2–negative infants were born (*5*). During caesarean section delivery, N95 mask, goggles, medical protective suit; gentle procedures to avoid droplets from the surgical site; and strict aseptic operation are required. Protective measures are crucial, and the surgery should be performed in a negative-pressure operating room. The virus is now known to interact with human respiratory epithelial cells through its spike protein (*6*). Therefore, it is mainly transmitted through droplets and aerosols.

In conclusion, we report a pregnant woman with SARS-CoV-2 infection who delivered a healthy infant, suggesting that mother-to-child transmission is unlikely for this virus. We believe that effective implementation of protection measures during delivery, including a negative-pressure delivery room, may help prevent the infant from acquiring SARS-CoV-2 infection. Because our conclusions are limited by our sample size of 1, we cannot definitively state whether cesarean section is better than vaginal delivery for preventing transmission from a pregnant mother with SARS-CoV-2 infection.

Acknowledgments

We thank all the medical staff members involved in treating this woman and her baby.

About the Author

Dr. Li is a deputy chief physician in the Department of Obstetrics, The First Affiliated Hospital, College of Medicine, Zhejiang University, Hangzhou, China. Her primary research interests include critical illness in obstetrics, prenatal diagnosis, and fetal medicine.

References

1. Zhu N, Zhang D, Wang W, Li X, Yang B, Song J, et al.; China Novel Coronavirus Investigating and Research Team. A novel coronavirus from patients with pneumonia in China, 2019. N Engl J Med. 2020;382:727–33. https://doi.org/10.1056/NEJMoa2001017
2. Ng PC, Leung CW, Chiu WK, Wong SF, Hon EKL. SARS in newborns and children. Biol Neonate. 2004;85:293–8. https://doi.org/10.1159/000078174
3. Stockman LJ, Lowther SA, Coy K, Saw J, Parashar UD. SARS during pregnancy, United States. Emerg Infect Dis. 2004;10:1689–90. https://doi.org/10.3201/eid1009.040244
4. Alserehi H, Wali G, Alshukairi A, Alraddadi B. Impact of Middle East respiratory syndrome coronavirus (MERS-CoV) on pregnancy and perinatal outcome. BMC Infect Dis. 2016;16:105. https://dx.org/10.1186/s12879-016-1437-y
5. Zhu H, Wang L, Fang C, Peng S, Zhang L, Chang G, et al. Clinical analysis of 10 neonates born to mothers with 2019-nCoV pneumonia. Transl Pediatr. 2020;9:51–60. https://doi.org/10.21037/tp.2020.02.06
6. Xu X, Chen P, Wang J, Feng J, Zhou H, Li X, et al. Evolution of the novel coronavirus from the ongoing Wuhan outbreak and modeling of its spike protein for risk of human transmission. Sci China Life Sci. 2020;63:457–60. http://dx.doi.org/10.1007/s11427-020-1637-5

Address for correspondence: Yu Chen or Jifang Sheng, Department of Clinical Laboratory, The First Affiliated Hospital, College of Medicine, Zhejiang University, 79 Qingchun Rd, Hangzhou 310003, China; email: chenyuzy@zju.edu.cn or jifang_sheng@zju.edu.cn

Detection of Novel Coronavirus by RT-PCR in Stool Specimen from Asymptomatic Child, China

An Tang,[1] Zhen-dong Tong,[1] Hong-ling Wang,[1] Ya-xin Dai,[1] Ke-feng Li, Jie-nan Liu, Wen-jie Wu, Chen Yuan, Meng-lu Yu, Peng Li, Jian-bo Yan

Author affiliation: Zhoushan Center for Disease Control and Prevention, Zhoushan, China

DOI: https://doi.org/10.3201/eid2606.200301

We report an asymptomatic child who was positive for a coronavirus by reverse transcription PCR in a stool specimen 17 days after the last virus exposure. The child was virus positive in stool specimens for at least an additional 9 days. Respiratory tract specimens were negative by reverse transcription PCR.

An outbreak of coronavirus disease (COVID-19) began in Wuhan, China, during December 2019 and has rapidly spread throughout China and to many countries (*1*,*2*). Common symptoms include fever, dry cough, and myalgia (*3*). Ten laboratory-confirmed cases and several asymptomatic cases of COVID-19 have been identified in Zhoushan, China, since January 19, 2020. We report the epidemiologic and diagnostic features for 1 case in an asymptomatic child.

On January 30, 2020, we identified a 10-year-old boy who had no fever or cough but had close contact with 2 confirmed case-patients with laboratory-confirmed COVID-19 (Figure). The boy was a primary school student who lived with his parents in an apartment of a college. The complex had several confirmed COVID-19 case-patients during January 19–31.

Interviews of the boy and his parents confirmed his multiple exposures to the previously confirmed case-patients. On January 9 and 15, he participated in 2 parties with his parents and their colleagues. Two persons at these parties were positive for severe acute respiratory syndrome coronavirus 2 (SARS-CoV-2) by reverse transcription PCR (RT-PCR) on January 20 and 22. During January 12–15, the boy played football at a football club with a teammate who had a virus-positive RT-PCR result on January 22. The parents of the boy were asymptomatic and their stool, nasopharyngeal, and sputum specimens collected on February 1 and 14 were negative for SARS-CoV-2.

We collected nasopharyngeal swab and sputum samples from the boy 15 days after the last close contact and tested these specimens for SARS-CoV-2 by using RT-PCRs targeting the open reading frame lab (ORF1ab) and nucleoprotein gene regions (*4*). We obtained equivocal results: cycle threshold (C_t) values were negative for ORFlab and 37.5 for the nucleoprotein gene. However, on February 1 (17 days after his last contact), a stool specimen was positive for SARS-CoV-2 by RT-PCR. (ORF1ab C_t 32.6; nucleoprotein gene C_t 33.7). He was then hospitalized in isolation and for monitoring.

Since January 22, The area of residence for the boy had been isolated, and community physicians monitored quarantined residents twice a day for signs and symptoms including fever, cough, and myalgia. During January 9–31, the boy had no signs or symptoms.

In the hospital, a routine blood test performed on February 2 showed cell counts within reference ranges, and a computed tomography scan on February 5 showed no abnormalities. After additional stool specimens collected on February 2 (ORF1ab C_t 25.6; nucleoprotein gene C_t 25.8) and February 4 (ORF1ab C_t 25.6; nucleoprotein gene C_t 28.3) were positive, the patient received abidol hydrochloride (100 mg 3×/d), interferon α-2b spray (2.5 million U 2×/d) and traditional Chinese medical therapy on February 5. Stool specimens collected on February 7 (ORF1ab C_t 26.3; nucleoprotein gene C_t 27.6), February 8 (ORF1ab C_t 31.4; nucleoprotein gene C_t 30.6), and February 9 (ORF1ab C_t 27.0; nucleoprotein gene C_t 27.0) were positive, but stool specimens collected on February 12 and 14 were negative.

Early symptoms in most COVID-19 patients include fever, myalgia, cough, and sore throat (*5*), which are common in other acute respiratory virus infections (*6*). Most cases appear to be mild, and most hospitalized patients have pneumonia with ground glass opacities on chest radiographs. Few children with SARS-CoV-2 infections have been reported, and most of them had mild clinical symptoms (*7*).

The boy we report had close contact with confirmed COVID-19 case-patients on several occasions before he showed an equivocal RT-PCR result for respiratory specimens and subsequently positive results for stool specimens. Despite these positive test results, he had no detectable fever or other clinical symptoms consistent with COVID-19 for ≥30 days from his last documented exposure. Although positive RT-PCR results do not necessarily indicate presence of infectious virus, our findings reinforce the need for RT-PCR testing of asymptomatic persons with exposure to COVID-19 patients.

[1]These authors contributed equally to this article.

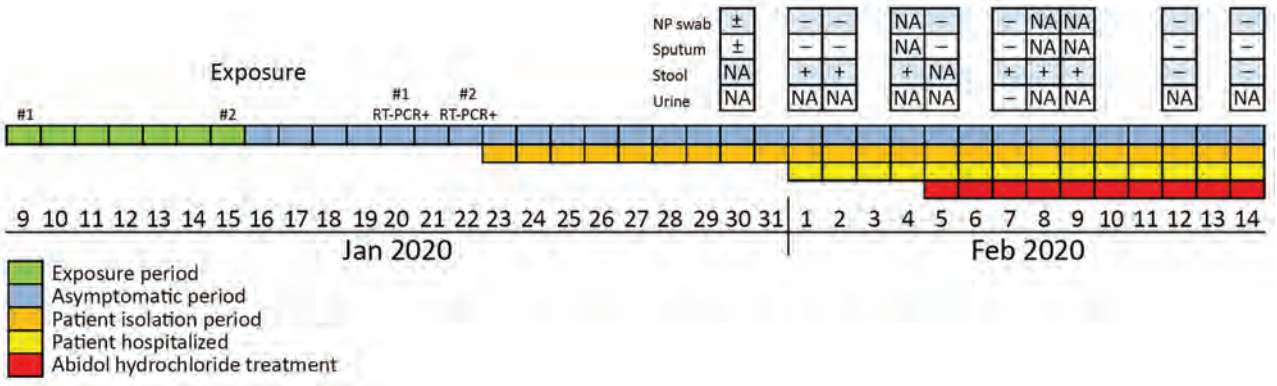

Figure. Timeline for detection of novel coronavirus by RT-PCR in stool specimen from asymptomatic child, China, January 9–February 14, 2020. NA, not available; NP, nasopharyngeal; RT-PCR, reverse transcription PCR; +, positive for novel coronavirus RNA by RT-PCR; ±, equivocal for novel coronavirus RNA by RT-PCR; –, negative for novel coronavirus RNA by RT-PCR.

Asymptomatic infections complicate efforts to curtail SARS-CoV-2 transmission and implement effective control procedures.

SARS-CoV-2 is believed to be transmitted through large respiratory droplets (*8*) and close contact (*9*). Indirect transmission by contaminated fomites might also play a role. During the SARS pandemic of 2002–2003, positive RT-PCR results for stool specimens from SARS patients suggested that stools or sewage might be virus sources (*10*). Our finding of multiple positive stool specimens in this case similarly raises the concern that stool from COVID-19 patients might serve as another vehicle for virus transmission. Moreover, detection of virus by RT-PCR in stool specimens when respiratory tract specimens are negative suggests that stool might be considered, in addition to respiratory tract specimens, for routine diagnostic screening.

Our study had several limitations. The delay in RT-PCR testing after the first recognition of virus exposure prevented a more accurate estimation of the incubation time from exposure to RT-PCR positivity. The failure to test other specimens, such as blood and urine, prevented determination of the full spectrum of virus shedding for the case-patient. Although we urge caution in making policy decisions on the basis of 1 case, expanded testing of various clinical specimens from symptomatic and asymptomatic case-patient contacts at multiple time points would be warranted to help confirm our findings.

Acknowledgment

We thank all members of the Zhoushan Center for Disease Control and Prevention for their involvement during the response to the outbreak.

This study was supported by the Zhoushan Science And Technology Project (grant nos. 2020C31004, 2020C31005, and 2020C31006); the Zhejiang Scientific and Technological Major Project under the 2020 Emergency (grant no. 2020C03124); the Zhejiang University special scientific research fund for COVID-19 prevention and control; and the Zhejiang Natural Project on Emergency Research about Community Prevention, Control, Early Warning, and Prediction of the novel coronavirus outbreak (grant no. LEZ20H260001)

About the Author

Dr. Tang is a public health research scientist at the Zhoushan Center for Disease Control and Prevention, Zhoushan, China. His research interests are epidemiology and control of infectious diseases.

References

1. Xiang YT, Yang Y, Li W, Zhang L, Zhang Q, Cheung T, et al. Timely mental health care for the 2019 novel coronavirus outbreak is urgently needed. Lancet Psychiatry. 2020;7:228–9 [Epub ahead of print]. https://doi.org/10.1016/S2215-0366(20)30046-8
2. Holshue ML, DeBolt C, Lindquist S, Lofy KH, Wiesman J, Bruce H, et al.; Washington State 2019-nCoV Case Investigation Team. First case of 2019 novel coronavirus in the United States. N Engl J Med. 2020;382:929–36. https://doi.org/10.1056/NEJMoa2001191
3. Wang D, Hu B, Hu C, Zhu F, Liu X, Zhang J, et al. Clinical characteristics of 138 hospitalized patients with 2019 novel coronavirus-infected pneumonia in Wuhan, China. JAMA. 2020 Feb 7 [Epub ahead of print]. https://doi.org/10.1001/jama.2020.1585
4. Zhu N, Zhang D, Wang W, Li X, Yang B, Song J, et al.; China Novel Coronavirus Investigating and Research Team. A novel coronavirus from patients with pneumonia in China, 2019. N Engl J Med. 2020;382:727–33. https://doi.org/10.1056/NEJMoa2001017
5. Chen N, Zhou M, Dong X, Qu J, Gong F, Han Y, et al. Epidemiological and clinical characteristics of 99 cases of

2019 novel coronavirus pneumonia in Wuhan, China: a descriptive study. Lancet. 2020;395:507–13. https://doi.org/10.1016/S0140-6736(20)30211-7
6. Kim JY, Choe PG, Oh Y, Oh KJ, Kim J, Park SJ, et al. The first case of 2019 novel coronavirus pneumonia imported into Korea from Wuhan, China: implication for infection prevention and control measures. J Korean Med Sci. 2020;35:e61. https://doi.org/10.3346/jkms.2020.35.e61
7. Del Rio C, Malani PN. Novel coronavirus-important information for clinicians. JAMA. 2020 Feb 5 [Epub ahead of print]. https://doi.org/10.1001/jama.2020.1490
8. Kampf G, Todt D, Pfaender S, Steinmann E. Persistence of coronaviruses on inanimate surfaces and their inactivation with biocidal agents. J Hosp Infect. 2020;104:246–51. https://doi.org/10.1016/j.jhin.2020.01.022
9. To KK, Tsang OT, Chik-Yan Yip C, Chan KH, Wu TC, Chan JMC, et al. Consistent detection of 2019 novel coronavirus in saliva. Clin Infect Dis. 2020 Feb 12 [Epub ahead of print] https://doi.org/10.1093/cid/ciaa149
10. Wang XW, Li JS, Guo TK, Zhen B, Kong QX, Yi B, et al. Concentration and detection of SARS coronavirus in sewage from Xiao Tang Shan Hospital and the 309th Hospital. J Virol Methods. 2005;128:156–61. https://doi.org/10.1016/j.jviromet.2005.03.022

Address for correspondence: Ya-xin Dai or Jian-bo Yan, Zhoushan Center for Disease Control and Prevention, No. 568 Wengshan Rd, Zhejiang, Zhoushan 316021, China: email: daiyaxin.712@163.com or yanjianbo02@163.com

Case-Fatality Risk Estimates for COVID-19 Calculated by Using a Lag Time for Fatality

Nick Wilson, Amanda Kvalsvig, Lucy Telfar Barnard, Michael G. Baker

Author affiliations: University of Otago Department of Public Health, Wellington, New Zealand

DOI: https://doi.org/10.3201/eid2606.200320

We estimated the case-fatality risk for coronavirus disease cases in China (3.5%); China, excluding Hubei Province (0.8%); 82 countries, territories, and areas (4.2%); and on a cruise ship (0.6%). Lower estimates might be closest to the true value, but a broad range of 0.25%–3.0% probably should be considered.

The coronavirus disease (COVID-19) is spreading globally; as of March 5, 2020, cases were reported in China and 85 other countries, territories, and areas (*1*). Disease severity is a particularly crucial parameter for understanding this new disease (*2*), but accurately estimating the case-fatality risk is difficult because milder cases are not being diagnosed and death is delayed.

We used data from the World Health Organization (WHO) (*1*) to calculate crude estimates of the case-fatality risk on March 5, 2020, for 4 populations: China; China, excluding Hubei Province; a group of 82 countries, territories, and areas; and passengers and crew of a cruise ship (Table 1). However, given the critical need to consider time lags to death when calculating case-fatality risk (*3*), we used time lags from a recent study from China (*4*). Yang et al. (*4*) reported that the median time from symptom onset to radiological confirmation of pneumonia was 5 days (interquartile range [IQR] 3–7 days); from symptom onset to intensive care unit (ICU) admission was 11 days (IQR 7–14 days); and from ICU admission to death was 7 days (IQR 3–11 days). Therefore, a median of 13 days passed from pneumonia confirmation to death ([11–5] + 7 = 13).

For our calculation, we assumed that the day of radiological confirmation of pneumonia approximately equated to the reporting date for laboratory-confirmed cases of COVID-19 to WHO. We obtained cumulative COVID-19 case counts reported by WHO on February 21 (*5*), which was 13 days before March 5, the date we used for calculating the crude case-fatality risk. Our approach is broadly comparable to a study that used earlier data to estimate the median time delay of 13 days from illness onset to death (*6*).

By using the number of cumulative cases on February 21 as the denominator for the adjusted case-fatality risk (aCFR), we assumed that half of the additional cumulative reported deaths on March 5 could be matched with cases reported on February 21. We acknowledge our approach is fairly simplistic and that it can be superseded when higher quality cohort-based analyses become available.

The case-fatality risks, when adjusted for a 13-day lag time from reporting to death, were 3.5% in China; 0.8% in China, excluding Hubei Province; 4.2% in the group of 82 countries, territories, and areas; and 0.6% for the cruise ship (Table). Our result for China, excluding Hubei Province, is similar to a previous estimate of 0.9% (95% CI 0.6%–1.3%) by using a time-delay adjusted case-fatality risk for the same area (K. Mizumoto and G. Chowell, unpub. data; https://www.medrxiv.org/content/10.1101/2020.02.19.20025163v1).

Table. Crude and adjusted estimates of case-fatality risk for COVID-19 in 4 populations*

Location	Cumulative deaths†	Cumulative confirmed cases†	Crude CFR, %	Adjusted deaths‡	Adjusted cumulative confirmed cases‡	Adjusted CFR, % (95% CI)§
China¶	3,015	80,565	3.74	2,627	75,569	3.48 (3.35–3.61)
China, excluding Hubei Province#	113	13,099	0.86	104	12,907	0.81 (0.67–0.98)
82 countries, territories, and areas**	27	2,285	1.18	15	354	4.24 (2.58–6.87)
Cruise ship	6	706	0.85	4	634	0.63 (0.25–1.61)

*CFR, case-fatality risk; COVID-19, coronavirus disease.
†Calculated by using data on laboratory-confirmed COVID-19 cases reported by the World Health Organization on March 5, 2020 (*1*).
‡Calculated by using cumulative confirmed cases as of February 21, 2020.
§Calculated using OpenEpi v3 (http://www.openepi.com) by using the Score (Wilson) method.
¶Includes Hong Kong, Macau, and Taiwan.
#We excluded Hubei Province because COVID-19 appears to have originated in this province and cases might have been missed because of shortages of appropriate diagnostic tests or health system overload.
**Includes 82 countries, territories, and areas outside of China and reporting cases on March 5, 2020; excludes areas with >500 cases (i.e., Italy, Iran, and South Korea) because of the possibility of uncontrolled spread and missed diagnoses in these localities.

Of our results, the least generalizable might be the result for China, which could be elevated because of undiagnosed mild cases, initial shortages of test kits, and elevated risk for death due to initial high demands on the healthcare system in Wuhan. The aCFR for the group of 82 countries, territories, and areas also might be affected by missed mild cases if some of the areas had undetected transmission. In terms of undiagnosed mild cases, the aCFR for the cruise ship population likely is the most accurate even though the 95% CI is broad. In addition, the aCFR for the cruise ship had a higher denominator due to inclusion of asymptomatic test-positive cases. Among 3,711 crew and passengers, 255 asymptomatic cases were identified (*7*); some of these persons subsequently might have developed symptoms. Thus, the aCFR for the cruise ship partially could reflect an infection-fatality risk. Also of note, 2,165 persons on the cruise ship were ≥60 years of age (*7*), and data from China indicates a much higher case-fatality risk among this age group (*8*); thus, a higher case-fatality risk might be expected in the cruise ship population than in other communities sampled. Considering these issues of generalizability, the aCFR of 0.8% for China, excluding Hubei Province, might be most accurate.

Nevertheless, given the residual uncertainties, health sector decision-makers and disease modelers probably should consider a broad range of 0.25%–3.0% for COVID-19 case-fatality risk estimates. The higher values could be more appropriate in resource poor settings where the quality of hospital and intensive care might be constrained. Higher values might also be appropriate in high-income countries with limited surge capacity in hospital services because elevated case-fatality risks could be seen at the peak of local epidemics. Because COVID-19 is expected to further spread globally, ongoing work using country-specific cohorts will be needed to more robustly clarify the case-fatality risk of this new disease.

This report was done as part of work for the New Zealand Ministry of Health (contract and funding support pending at the time of submission).

About the Author

Dr. Wilson is a professor of public health at the University of Otago, New Zealand. He has a long-standing research interest in historical and contemporary pandemics.

References

1. World Health Organization. Coronavirus disease 2019 (COVID-19) situation report—45, 5 Mar 2020 [cited 2020 Mar 6]. https://www.who.int/docs/default-source/coronaviruse/situation-reports/20200305-sitrep-45-covid-19.pdf
2. Cowling BJ, Leung GM. Epidemiological research priorities for public health control of the ongoing global novel coronavirus (2019-nCoV) outbreak. Euro Surveill. 2020 Feb 25 [Epub ahead of print]. https://doi.org/10.2807/1560-7917.ES.2020.25.6.2000110
3. Donnelly CA, Ghani AC, Leung GM, Hedley AJ, Fraser C, Riley S, et al. Epidemiological determinants of spread of causal agent of severe acute respiratory syndrome in Hong Kong. Lancet. 2003;361:1761–6. https://doi.org/10.1016/S0140-6736(03)13410-1
4. Yang X, Yu Y, Xu J, Shu H, Xia J, Liu H, et al. Clinical course and outcomes of critically ill patients with SARS-CoV-2 pneumonia in Wuhan, China: a single-centered, retrospective, observational study. Lancet Respir Med. 2020 Feb 24 [Epub ahead of print]. https://doi.org/10.1016/S2213-2600(20)30079-5
5. World Health Organization. Coronavirus disease 2019 (COVID-19) situation report—32, 21 Feb 2020 [cited 2020 Mar 6]. https://www.who.int/docs/default-source/coronaviruse/situation-reports/20200221-sitrep-32-covid-19.pdf
6. Linton NM, Kobayashi T, Yang Y, Hayashi K, Akhmetzhanov AR, Jung SM, et al. Incubation period and other epidemiological characteristics of 2019 novel coronavirus infections with right truncation: a statistical analysis of publicly available case data. J Clin Med. 2020;9:538. https://doi.org/10.3390/jcm9020538
7. National Institute of Infectious Diseases, Japan. Field briefing: Diamond Princess COVID-19 cases, 19 February 2020 [cited 2020 Feb 29]. https://www.niid.go.jp/niid/en/2019-ncov-e/9407-covid-dp-fe-01.html
8. The Novel Coronavirus Pneumonia Emergency Response Epidemiology Team. The epidemiological characteristics

of an outbreak of 2019 novel coronavirus diseases (COVID-19)—China, 2020. China CDC Weekly 2020 [cited 2020 Feb 29]. http://weekly.chinacdc.cn/en/article/id/e53946e2-c6c4-41e9-9a9b-fea8db1a8f51

Address for correspondence: Nick Wilson, Department of Public Health, University of Otago Wellington, Mein St, Newtown, Wellington 6005, New Zealand; email: nick.wilson@otago.ac.nz

Serial Interval of COVID-19 among Publicly Reported Confirmed Cases

Zhanwei Du,[1] Xiaoke Xu,[1] Ye Wu,[1] Lin Wang, Benjamin J. Cowling, Lauren Ancel Meyers

Author affiliations: University of Texas at Austin, Austin, Texas, USA (Z. Du, L.A. Meyers); Dalian Minzu University, Dalian, China (X. Xu); Beijing Normal University Computational Communication Research Center, Zhuhai, China (Y. Wu); Beijing Normal University School of Journalism and Communication, Beijing, China (Y. Wu); Institut Pasteur, Paris, France (L. Wang); University of Hong Kong, Hong Kong, China (B.J. Cowling); Santa Fe Institute, Santa Fe, New Mexico, USA (L.A. Meyers)

We estimate the distribution of serial intervals for 468 confirmed cases of coronavirus disease reported in China as of February 8, 2020. The mean interval was 3.96 days (95% CI 3.53–4.39 days), SD 4.75 days (95% CI 4.46–5.07 days); 12.6% of case reports indicated presymptomatic transmission.

DOI: https://doi.org/10.3201/eid2606.200357

Key aspects of the transmission dynamics of coronavirus disease (COVID-19) remain unclear (*1*). The serial interval of COVID-19 is defined as the time duration between a primary case-patient (infector) having symptom onset and a secondary case-patient (infectee) having symptom onset (*2*). The distribution of COVID-19 serial intervals is a critical input for determining the basic reproduction number (R_0) and the extent of interventions required to control an epidemic (*3*).

To obtain reliable estimates of the serial interval, we obtained data on 468 COVID-19 transmission events reported in mainland China outside of Hubei Province during January 21–February 8, 2020. Each report consists of a probable date of symptom onset for both the infector and infectee, as well as the probable locations of infection for both case-patients. The data include only confirmed cases compiled from online reports from 18 provincial centers for disease control and prevention (https://github.com/MeyersLabUTexas/COVID-19).

Fifty-nine of the 468 reports indicate that the infectee had symptoms earlier than the infector. Thus, presymptomatic transmission might be occurring. Given these negative-valued serial intervals, COVID-19 serial intervals seem to resemble a normal distribution more than the commonly assumed gamma or Weibull distributions (*4*,*5*), which are limited to positive values (Appendix, https://wwwnc.cdc.gov/EID/article/26/7/20-0357-App1.pdf). We estimate a mean serial interval for COVID-19 of 3.96 (95% CI 3.53–4.39) days, with an SD of 4.75 (95% CI 4.46–5.07) days (Figure), which is considerably lower than reported mean serial intervals of 8.4 days for severe acute respiratory syndrome (*5*) to 14.6 days (*6*) for Middle East respiratory syndrome. The mean serial interval is slightly but not significantly longer when the index case is imported (4.06 [95% CI 3.55–4.57] days) versus locally infected (3.66 [95% CI 2.84–4.47] days), but slightly shorter when the secondary transmission occurs within the household (4.03 [95% CI 3.12–4.94] days) versus outside the household (4.56 [95% CI 3.85–5.27] days). Combining these findings with published estimates for the early exponential growth rate COVID-19 in Wuhan (*7*), we estimate an R_0 of 1.32 (95% CI 1.16–1.48) (*5*), which is lower than published estimates that assume a mean serial interval exceeding 7 days (*7*,*8*).

These estimates reflect reported symptom onset dates for 752 case-patients from 93 cities in China, who range in age from 1 to 90 years (mean 45.2 years, SD 17.21 years). Recent analyses of putative COVID-19 infector–infectee pairs from several countries have indicated average serial intervals of 4.0 days (95% CI 3.1–4.9 days; n = 28; unpub. data, H. Nishiura et al., unpub. data, https://doi.org/10.1101/2020.02.03.20019497), 4.4 days (95% CI 2.9–6.7 days, n = 21; S. Zhao et al., unpub. data, https://doi.org/10.1101/2020.02.21.20026559], and 7.5 days (95% CI 5.3–19, n = 6; *8*). Whereas none of these studies report negative serial intervals in which the infectee had symptoms before the infector, 12.6% of the serial intervals in our sample were negative.

[1]These first authors contributed equally to this article.

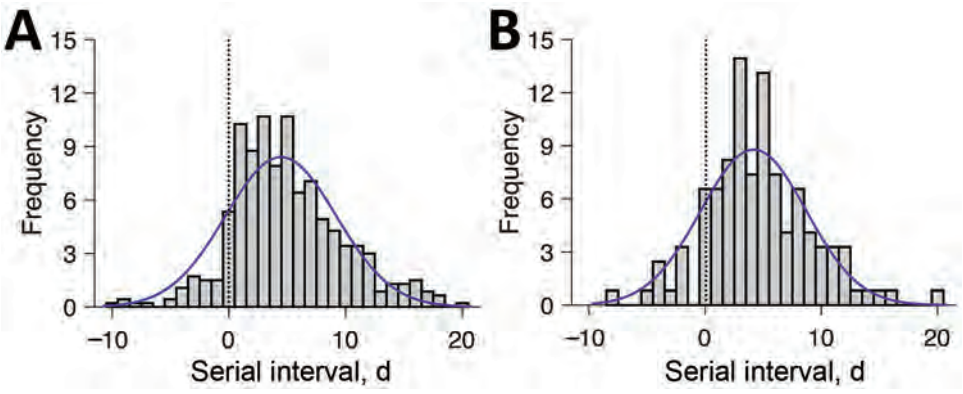

Figure. Estimated serial interval distribution for coronavirus disease (COVID-19) based on 468 reported transmission events, China, January 21–February 8, 2020. A) All infection events (N = 468) reported across 93 cities of mainland China as of February 8, 2020; B) the subset infection events (n = 122) in which both the infector and infectee were infected in the reporting city (i.e., the index patient's case was not an importation from another city). Gray bars indicate the number of infection events with specified serial interval, and blue lines indicate fitted normal distributions. Negative serial intervals (left of the vertical dotted lines) suggest the possibility of COVID-19 transmission from asymptomatic or mildly symptomatic case-patients.

We note 4 potential sources of bias. First, the data are restricted to online reports of confirmed cases and therefore might be biased toward more severe cases in areas with a high-functioning healthcare and public health infrastructure. The rapid isolation of such case-patients might have prevented longer serial intervals, potentially shifting our estimate downward compared with serial intervals that might be observed in an uncontrolled epidemic. Second, the distribution of serial intervals varies throughout an epidemic; the time between successive cases contracts around the epidemic peak (*9*). A susceptible person is likely to become infected more quickly if they are surrounded by 2 infected persons instead of 1. Because our estimates are based primarily on transmission events reported during the early stages of outbreaks, we do not explicitly account for such compression and interpret the estimates as basic serial intervals at the outset of an epidemic. However, if some of the reported infections occurred amid growing clusters of cases, then our estimates might reflect effective (compressed) serial intervals that would be expected during a period of epidemic growth. Third, the identity of each infector and the timing of symptom onset were presumably based on individual recollection of past events. If recall accuracy is impeded by time or trauma, case-patients might be more likely to attribute infection to recent encounters (short serial intervals) over past encounters (longer serial intervals). In contrast, the reported serial intervals might be biased upward by travel-related delays in transmission from primary case-patients that were infected in Wuhan or another city before returning home. If their infectious period started during travel, then we might be unlikely to observe early transmission events with shorter serial intervals. The mean serial interval is slightly higher for the 218 of 301 unique infectors reported to have imported cases.

Given the heterogeneity in type and reliability of these sources, we caution that our findings should be interpreted as working hypotheses regarding the infectiousness of COVID-19, requiring further validation. The potential implications for COVID-19 control are mixed. Although our lower estimates for R_0 suggest easier containment, the large number of reported asymptomatic transmission events is concerning.

We acknowledge the financial support from the US National Institutes of Health (grant no. U01 GM087719) and the National Natural Science Foundation of China (grant no. 61773091).

About the Author

Dr. Du is a postdoctoral researcher in the Department of Integrative Biology at the University of Texas at Austin. He develops mathematical models to elucidate the transmission dynamics, surveillance, and control of infectious diseases.

References

1. Cowling BJ, Leung GM. Epidemiological research priorities for public health control of the ongoing global novel coronavirus (2019-nCoV) outbreak. Euro Surveill. 2020;25. https://doi.org/10.2807/1560-7917.ES.2020.25.6.2000110
2. Svensson A. A note on generation times in epidemic models. Math Biosci. 2007;208:300–11. https://doi.org/10.1016/j.mbs.2006.10.010
3. Wallinga J, Lipsitch M. How generation intervals shape the relationship between growth rates and reproductive numbers. Proc Biol Sci. 2007;274:599–604. https://doi.org/10.1098/rspb.2006.3754
4. Kuk AYC, Ma S. The estimation of SARS incubation distribution from serial interval data using a convolution likelihood. Stat Med. 2005;24:2525–37. https://doi.org/10.1002/sim.2123
5. Lipsitch M, Cohen T, Cooper B, Robins JM, Ma S, James L, et al. Transmission dynamics and control of severe acute

respiratory syndrome. Science. 2003;300:1966–70. https://doi.org/10.1126/science.1086616
6. Park SH, Kim Y-S, Jung Y, Choi SY, Cho N-H, Jeong HW, et al. Outbreaks of Middle East respiratory syndrome in two hospitals initiated by a single patient in Daejeon, South Korea. Infect Chemother. 2016;48:99–107. https://doi.org/10.3947/ic.2016.48.2.99
7. Li Q, Guan X, Wu P, Wang X, Zhou L, Tong Y, et al. Early transmission dynamics in Wuhan, China, of novel coronavirus-infected pneumonia. N Engl J Med. 2020 Jan 29 [Epub ahead of print]. https://doi.org/10.1056/NEJMoa2001316
8. Wu JT, Leung K, Leung GM. Nowcasting and forecasting the potential domestic and international spread of the 2019-nCoV outbreak originating in Wuhan, China: a modelling study. Lancet. 2020;395:689–97. https://doi.org/10.1016/S0140-6736(20)30260-9
9. Kenah E, Lipsitch M, Robins JM. Generation interval contraction and epidemic data analysis. Math Biosci. 2008;213:71–9. https://doi.org/10.1016/j.mbs.2008.02.007

Address for correspondence: Lauren Ancel Meyers, J.T. Patterson Labs Bldg, University of Texas at Austin, 2415 Speedway, Austin, TX 78712, USA; email: laurenmeyers@austin.utexas.edu

Indirect Virus Transmission in Cluster of COVID-19 Cases, Wenzhou, China, 2020

Jing Cai,[1] Wenjie Sun,[1] Jianping Huang,[1] Michelle Gamber, Jing Wu, Guiqing He

Author affiliations: Wenzhou Sixth People's Hospital, Wenzhou Central Hospital Medical Group, Wenzhou, China (J. Cai, J. Huang, G. He); The Second Affiliated Hospital of Fujian Traditional Chinese Medical University, Fuzhou, China (W. Sun); Robert Stempel College of Public Health and Social Work, Florida International University, Miami, Florida, USA (W. Sun); Shenandoah University, Winchester, Virginia, USA (M. Gamber); Huashan Hospital, Fudan University, Shanghai, China (J. Wu)

DOI: https://doi.org/10.3201/eid2606.200412

To determine possible modes of virus transmission, we investigated a cluster of coronavirus disease cases associated with a shopping mall in Wenzhou, China. Data indicated that indirect transmission of the causative virus occurred, perhaps resulting from virus contamination of common objects, virus aerosolization in a confined space, or spread from asymptomatic infected persons.

[1]These authors contributed equally to this article.

Severe acute respiratory syndrome coronavirus 2 (SARS-CoV-2), the causative agent of coronavirus disease (COVID-19), is presumed to spread primarily via respiratory droplets and close contact. However, these transmission modes do not explain all cases. To determine how the virus may have spread among a cluster of COVID-19 cases associated with a shopping mall in Wenzhou (a city with 8 million residents), China, we monitored and traced close contacts and hypothesized possible transmission modes. We analyzed clinical and laboratory data for cases by using real-time reverse transcription PCR (*1*). The study was approved with written consent from the Ethics Committee of Wenzhou Central Hospital and written informed consent from all case-patients.

On January 20, 2020, a 23-year-old man (patient E) sought care at a hospital after 11 days of fever and headache. On January 21, COVID-19 was confirmed for patient E and his co-worker, patient G. The Wenzhou Center for Disease Control and Prevention traced and tested their contacts, and by January 28, COVID-19 was confirmed for 7 persons (patients A–G) from the same office (on floor 7).

Patient A, a 30-year-old woman, the only case-patient who indicated that she had been in Wuhan, China, returned from Wuhan on December 18, 2019. On January 15–16, 2020, she had a fever, but symptoms resolved without treatment. Despite symptom resolution, on January 30 she was confirmed to have SARS-CoV-2 infection. If patient A is the index patient, infected in Wuhan, her incubation period would have been 28 days, which would be extremely long, according to updated information (W.J. Guan et al., unpub. data, https://www.medrxiv.org/content/10.1101/2020.02.06.20020974v1). Asymptomatic carrier transmission has been reported for SARS-CoV-2 (*2*); hence, patient A could have been screened as a close contact during her incubation period and then hospitalized on the basis of a positive test (PCR) result only. However, her clinical symptoms did not appear until after hospitalization. Because persons with asymptomatic COVID-19 can spread the virus, patient A also could have been an asymptomatic carrier with a persistent infection (*3*).

On January 22, the mall was shut down. During January 19–February 9, COVID-19 was diagnosed for 7 mall staff from floors B1–3 and for 10 mall customers. Close contacts associated with the mall were traced, and COVID-19 was confirmed for 11 persons. Sixteen patients had had direct contact with other patients or had gone shopping in the mall. The average incubation period was 7.3 (range 1–17) days.

The mall has 8 floors above ground and several basement levels; floors B1 to 6 are commercial

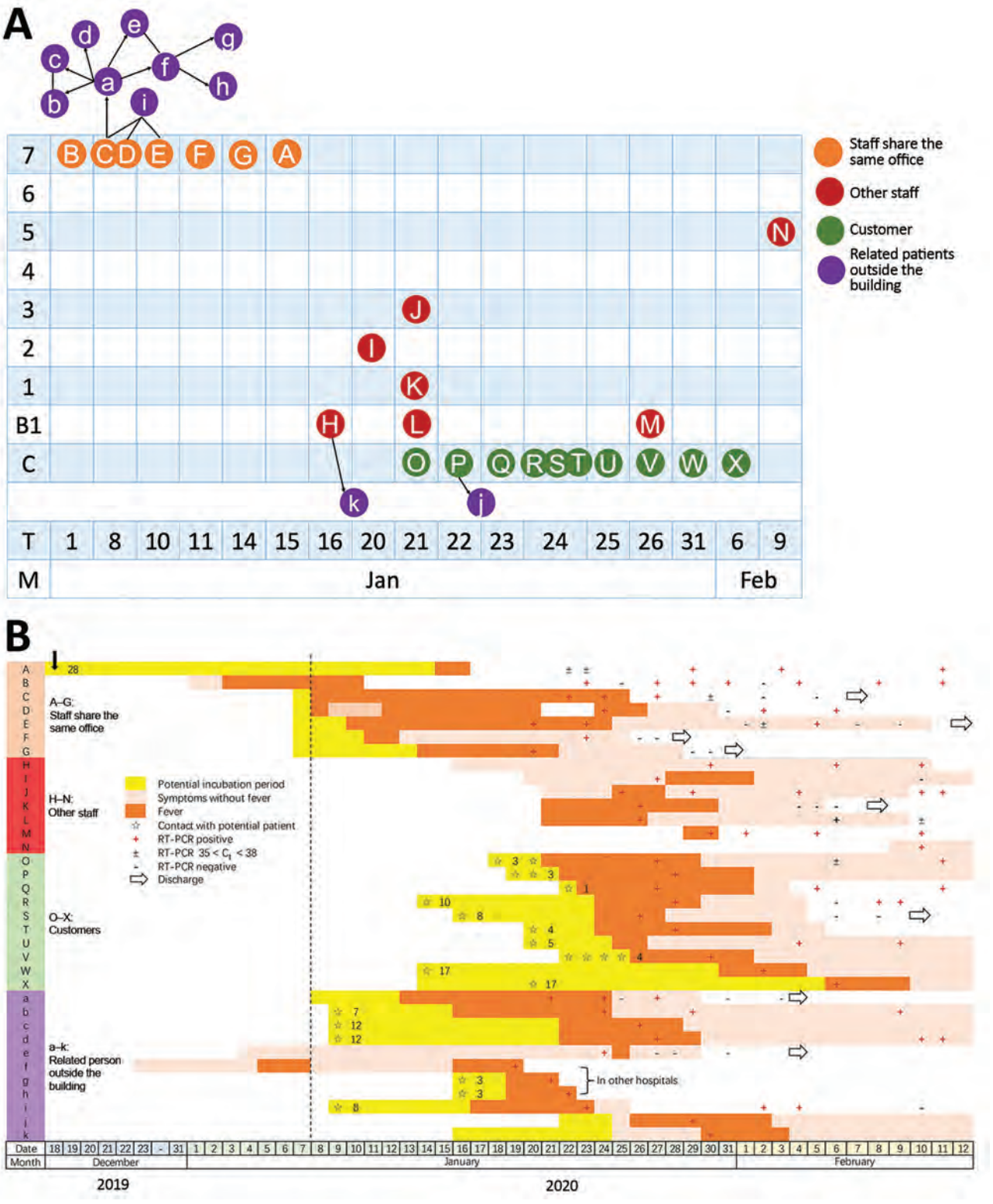

Figure. Cluster of COVID-19 cases associated with a shopping mall in Wenzhou, China. A) Distribution of COVID-19 case-patients by mall floor, time, and internal relationship. B) Dates of symptom onset, confirmed test results, and hospitalization information. Numbers within yellow bars indicate length of incubation period. Black vertical arrow indicates date when patient A returned from Wuhan, China. B1–7, mall floors; C, customer; COVID-19 coronavirus disease; C_t, cycle threshold; T, date of symptom onset; M, month; RT-PCR, reverse transcription PCR.

shopping space, and floor 7 contains shopping and office space. We created an illustration showing the floors where the eventual COVID-19 case-patients worked or shopped, along with dates of symptom onset, potential incubation periods, symptom durations, confirmed times of positive diagnosis, and times of discharge (Figure 1, panel A).

Except for those who had been on floor 7, all other case-patients denied direct close contact with other case-patients. The possibility of customers being infected from other sources cannot be excluded. However, most customers reported early symptom onset in a concentrated time frame (Figure 1, panel B). We found no convincing evidence of definitive transmission pathways in this building. Patients A–G (Figure 1, panel A) worked in the same room on floor 7. Other case-patients who had been on other floors denied any direct contact with confirmed patients from floor 7, but they shared common building facilities (e.g., restrooms, elevators). Also, staff from floor 7 visited shops on other floors daily.

Until now, no evidence has shown that SARS-CoV-2 can survive outside the body for long. However, Middle East respiratory syndrome coronavirus demonstrates high robustness and a strong capability to survive outside the body and can remain infectious for up to 60 minutes after aerosolization (*4*). Hence, the rapid spread of SARS-CoV-2 in our study could have resulted from spread via fomites (e.g., elevator buttons or restroom taps) or virus aerosolization in a confined public space (e.g., restrooms or elevators). All case-patients other than those on floor 7 were female, including a restroom cleaner, so common restroom use could have been the infection source. For case-patients who were customers in the shopping mall but did not report using the restroom, the source of infection could have been the elevators. The Guangzhou Center for Disease Control and Prevention detected the nucleic acid of SARS-CoV-2 on a doorknob at a patient's house (*5*), but Wenzhou Center for Disease Control and Prevention test results for an environmental sample from the surface of a mall elevator wall and button were negative.

We cannot exclude the possibility of unknown infected persons (e.g., asymptomatic carriers) spreading the virus. However, according to screening protocols implemented by the Wenzhou Center for Disease Control and Prevention, we traced all close contacts and included all patients with positive PCR results, including the asymptomatic carrier (patient A), in this study. Our findings appear to indicate that low intensity transmission occurred without prolonged close contact in this mall; that is, the virus spread by indirect transmission.

The work was supported by Major Project of Wenzhou Municipal Science and Technology Bureau (ZY202004).

About the Author

Dr. Cai is deputy chief physician and deputy director of the comprehensive internal medicine department. Her major research interest focuses on infectious diseases and gastrointestinal diseases.

References

1. National Microbiology Data Center. Novel Coronavirus National Science and Technology Resource Service System [cited 2020 Jan 30]. http://nmdc.cn/nCoV
2. Bai Y, Yao L, Wei T, Tian F, Jin DY, Chen L, et al. Presumed asymptomatic carrier transmission of COVID-19. JAMA. 2020 Feb 21 [Epub ahead of print]. https://doi.org/10.1001/jama.2020.2565
3. Rothe C, Schunk M, Sothmann P, Bretzel G, Froeschl G, Wallrauch C, et al. Transmission of 2019-nCoV Infection from an asymptomatic contact in Germany. N Engl J Med. 2020;382:970–1. https://doi.org/10.1056/NEJMc2001468
4. Pyankov OV, Bodnev SA, Pyankova OG, Agranovski IE. Survival of aerosolized coronavirus in the ambient air. Journal of Aerosol Science. 2018;115:158–63.
5. Meiping G. Coronavirus detected on doorknob in S. China's Guangzhou. 2020 [cited 2020 Feb 3]. https://news.cgtn.com/news/2020-02-03/Coronavirus-detected-on-doorknob-in-S-China-s-Guangzhou-NMua1LcOWY/index.html

Address for correspondence: Guiqing He, Department of Infectious Diseases, Infectious Diseases Laboratory, Wenzhou Sixth People's Hospital, Wenzhou Central Hospital Medical Group, Wenzhou, 325000 China; email: hegq123@126.com; Jing Wu, Department of Infectious Diseases, #5-504, Huashan Hospital, Fudan Universit, 12 Wulumuqizhong Rd, Jing'an District Shanghai 200040, China; email: jingee@fudan.edu.cn

COVID-19 in 2 Persons with Mild Upper Respiratory Symptoms on a Cruise Ship, Japan

Takeshi Arashiro, Keiichi Furukawa, Akira Nakamura

Author affiliation: Asahi General Hospital, Chiba, Japan

DOI: https://doi.org/10.3201/eid2606.200452

We describe 2 cases of coronavirus disease in patients with mild upper respiratory symptoms. Both patients worked on a cruise ship quarantined off the coast of Japan. One patient had persistent, low-grade upper respiratory tract symptoms without fever. The other patient had rapid symptom cessation but persistent viral RNA detection.

Since December 2019, an outbreak of coronavirus disease (COVID-19) caused by severe acute respiratory syndrome coronavirus 2 (SARS-CoV-2) has been spreading globally (*1*). On January 25, 2020, a passenger disembarked a cruise ship in Hong Kong and on February 1 tested positive for SARS-CoV-2 (*2*). The ship docked in Yokohama, Japan, on February 3 for quarantine and isolation. On February 7, passengers and crew were provided thermometers and asked to check their temperature several times daily. Crew members were instructed to continue duties, report fever or respiratory symptoms, and follow quarantine instructions.

By February 28, a total of 705 COVID-19 cases were confirmed among 4,061 passengers and crew tested; 392 cases were asymptomatic, 36 persons were admitted to intensive care units, and 6 patients died (*2*). All case-patients from the ship were transferred to designated medical institutions in Japan (*3*).

Preliminary reports describe COVID-19 manifesting as pneumonia (*4*–*6*), but most cases are milder and could have more transmission potential because patients might not seek medical attention (*7*). Because of the lower threshold for testing persons on board, the cruise ship created an opportunity to observe mild COVID-19 cases and monitor patient symptoms. We describe 2 COVID-19 cases in persons with mild upper respiratory symptoms. The patients provided written, informed consent to share their clinical details.

Case 1 occurred in a 35-year-old woman from South Asia who worked as a restaurant server on the ship. On day 1 of her illness, February 7, she experienced throat dryness and a slight cough (Figure, panel A). She and her roommate shared a bathroom with 2 others who had similar symptoms earlier. Case-patient 1 reported her symptoms but continued to work because she was afebrile. On day 3, she had throat soreness, stayed in her room, and was tested for SARS-CoV-2 by reverse transcription PCR (RT-PCR). On days 4–5, her symptoms diminished. On day 6, she was told she tested positive and was transferred to Asahi General Hospital (Chiba, Japan). At admission, she had a slight sore throat and cough. Her temperature was 36.5°C; blood pressure, 113/85 mm Hg; pulse, 92 bpm; respiration, 16 breaths/min; and oxygen saturation, 95% on ambient air. She had no underlying medical conditions and was taking no routine medication. On examination, her throat was bright red without exudates, lung auscultation was clear, and chest radiographs and blood tests were not clinically significant (Appendix Figure 1, panel A, Table 1, http://wwwnc.cdc.gov/EID/article/26/6/20-0452-App1.pdf). We did not suspect pneumonia and did not perform computed tomography. On day 8, she reported slight rhinorrhea. On day 9, RT-PCR again was positive for SARS-CoV-2. Her symptoms continued to diminish, and by day 10 she had discontinued all medications. RT-PCR results were positive on days 13 and 15, negative on day 19, positive again on day 20, and negative again on days 22 and 23, meeting the criteria for discharge, 2 consecutive negative assays. She never had fever, shortness of breath, or sputum, and daily lung auscultation was clear, suggesting absence of pneumonia.

Case 2 occurred in a 27-year-old man from South Asia who worked as a kitchen cleaner on the ship. On day 1 of his illness, February 8, he had a fever (38.6°C), sore throat, and cough. His roommate had similar symptoms that started 2 days before. Case-patient 2 reported his symptoms but continued to work. On day 2, he was tested for SARS-CoV-2 but continued to work. On day 3, his fever persisted, so he stayed in his room. By day 4, his symptoms resolved. On day 5, he was told he tested positive for SARS-CoV-2 and was transferred to Asahi General Hospital. At admission, he had no respiratory or other symptoms. He had no underlying medical conditions and was taking no routine medication. His temperature was 36.0°C; blood pressure, 132/85 mm Hg; pulse, 87 bpm; respirations, 16 breaths/min; and oxygen saturation, 95% on ambient air. On examination, his throat was bright red without exudates (Appendix Figure 2), lung auscultation was clear, and chest radiographs and blood tests were not clinically significant

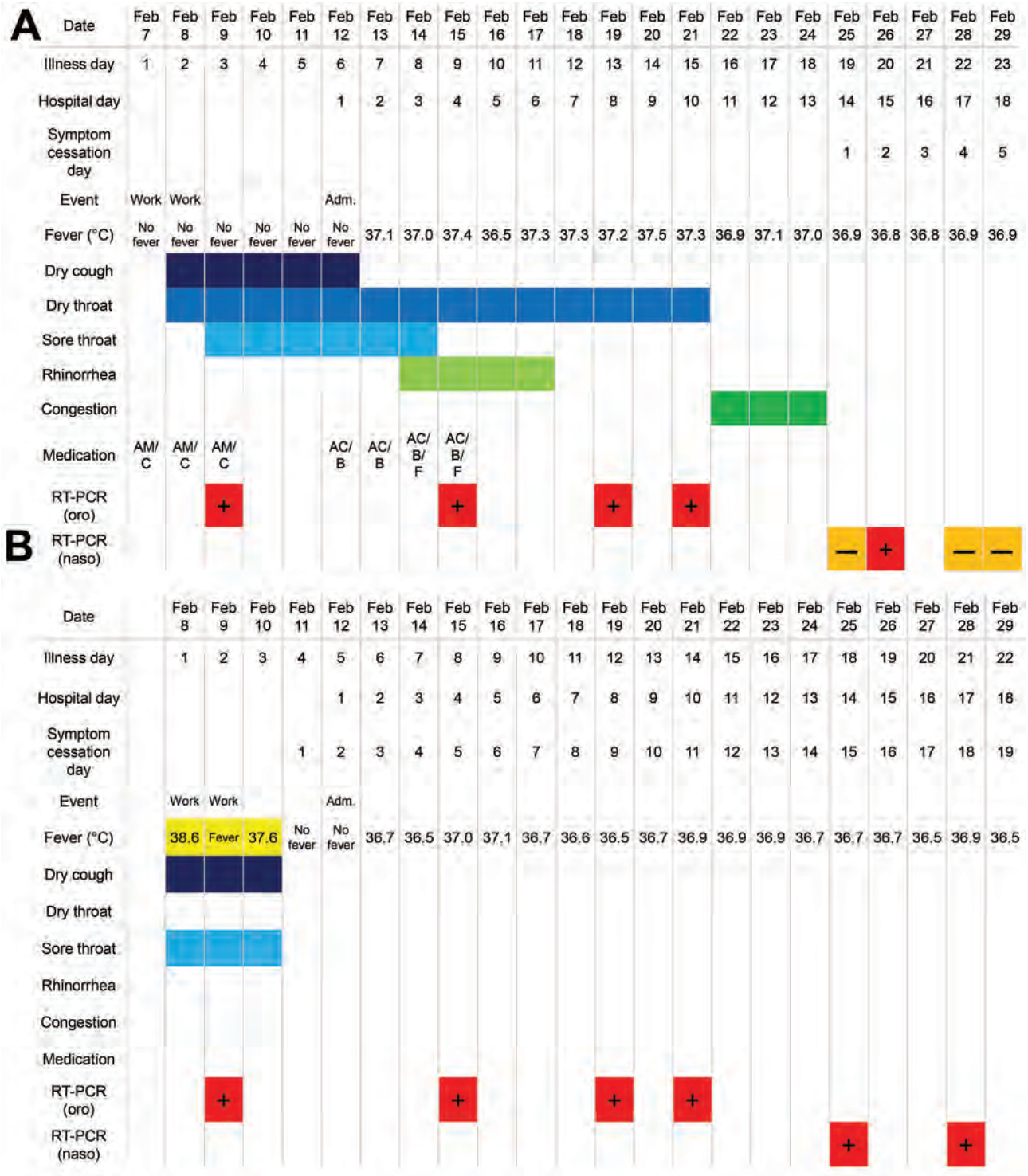

Figure. Clinical courses of 2 case-patients with coronavirus disease (COVID-19) admitted from a cruise ship docked in Japan, 2020. A) Case-patient 1, a 25-year-old woman who worked on the ship as a restaurant server. B) Case-patient 2, a 27-year-old man who worked on the ship as a kitchen cleaner. Acetaminophen was administered on an as-needed basis >2×/day after taking body temperature, so measured body temperature is not affected. Nasopharyngeal swabs were used after February 21, 2020, because a study by Zou et al. (*10*) suggested higher sensitivity of nasopharyngeal swab specimens over oropharyngeal swab specimens. AC, acetaminophen; Adm., admission; AM, amoxicillin; B, bakumondoto, a multiherb kampo medicine for dry cough; C, codeine-containing cough syrup; F, fexofenadine; naso, nasopharyngeal swab; oro, oropharyngeal swab; RT-PCR, reverse transcription PCR.

(Appendix Figure 1, panel B, Table 2). He remained asymptomatic, but on day 8, RT-PCR results were positive; results remained positive on days 12, 14, 18, and 21. His throat redness did not improve, but he did not report throat soreness or discomfort. He never experienced shortness of breath or sputum, and daily lung auscultations were clear.

We describe 2 mild cases of COVID-19 without discernable pneumonia, which could represent the clinical course in young, healthy persons. Worldwide, cases are appearing without apparent epidemiologic links (*8*). As the virus spreads, more mild COVID-19 cases are likely, and clinicians should be aware of clinical manifestations in the absence of severe symptoms. Case-patient 2's symptoms rapidly decreased, but detectable viral RNA persisted for >2 weeks. As of February 27, patients in Japan must have 2 consecutive negative RT-PCR results before they can be discharged (*9*). Viral RNA detection does not necessarily indicate infectivity, so we urgently need guidance for detection and management of mild COVID-19 to prepare for a possible pandemic and avoid overwhelming healthcare systems.

Acknowledgments

We thank the staff of the Kaiso Public Health Center and Chiba Prefectural Public Health Institute for public health support and testing, Ashley Stucky for thoughtful review of the manuscript, and Yuzo Arima and Takahiro Asami for intellectual discussion. We also thank the quarantine officers, cruise ship company, and healthcare personnel involved in the COVID-19 outbreak globally for their selfless dedication.

Addendum

As of April 6, a total of 712 coronavirus disease cases had been confirmed among 3,711 passengers and crew of the cruise ship (19.2%) (https://www.mhlw.go.jp/stf/houdou/houdou_list_202004.html). At the time of testing, 410 (57.6%) were asymptomatic; of those, 79 (11.1%) had symptoms develop within the 14-day self-monitoring period, leaving 331 persons who tested positive and remained asymptomatic after the self-monitoring period (46.5% of all cases). Forty (5.6%) patients were admitted to intensive care units (ICUs); 12 patients died (1.7%), including 1 person reported by the government of Australia to have died after transferring home. Of the cases we reported, case-patient 2 remained asymptomatic; RT-PCR results were negative on day 24, positive again on day 25, and negative again on days 27 and 28, meeting the criteria for discharge. His throat redness had improved by discharge. By March 27, both patients had been sent back to their home country by air and instructed to self-isolate at home for an additional 14 days.

About the Author

Dr. Arashiro is a junior resident at Asahi General Hospital in Chiba, Japan, and a collaborating researcher with the Infectious Diseases Surveillance Center in the National Institute of Infectious Diseases, Tokyo, Japan. His research interests include infectious disease epidemiology and global health.

References

1. World Health Organization. Coronavirus disease (COVID-19) outbreak, 2020 [cited 2020 Feb 26]. https://www.who.int/emergencies/diseases/novel-coronavirus-2019
2. Ministry of Health, Labour and Welfare, Japan. Regarding COVID-19 cases on a cruise ship, 2020 Feb 26 [in Japanese] [cited 2020 Feb 26]. https://www.mhlw.go.jp/stf/houdou/houdou_list_202002.html
3. Ministry of Health, Labour and Welfare, Japan. Cabinet order to designate novel coronavirus infection 2019 as designated infectious disease, 2020 Jan 28 [in Japanese] [cited 2020 Feb 26]. https://www.mhlw.go.jp/content/10900000/000589747.pdf
4. Huang C, Wang Y, Li X, Ren L, Zhao J, Hu Y, et al. Clinical features of patients infected with 2019 novel coronavirus in Wuhan, China. Lancet. 2020;395:497–506. https://doi.org/10.1016/S0140-6736(20)30183-5
5. Chen N, Zhou M, Dong X, Qu J, Gong F, Han Y, et al. Epidemiological and clinical characteristics of 99 cases of 2019 novel coronavirus pneumonia in Wuhan, China: a descriptive study. Lancet. 2020;395:507–13. https://doi.org/10.1016/S0140-6736(20)30211-7
6. Chang D, Lin M, Wei L, Xie L, Zhu G, Dela Cruz CS, et al. Epidemiologic and clinical characteristics of novel coronavirus infections involving 13 patients outside Wuhan, China. JAMA. 2020 Feb 7 [Epub ahead of print]. https://doi.org/10.1001/jama.2020.1623
7. Munster VJ, Koopmans M, van Doremalen N, van Riel D, de Wit E. A novel coronavirus emerging in China—key questions for impact assessment. N Engl J Med. 2020;382:692–4. https://doi.org/10.1056/NEJMp2000929
8. World Health Organization. Emergency ministerial meeting on COVID-19 organized by the African Union and the Africa Centres for Disease Control and Prevention, 2020 Feb 22 [cited 2020 Feb 26]. https://www.who.int/dg/speeches/detail/emergency-ministerial-meeting-on-covid-19-organized-by-the-african-union-and-the-africa-centres-for-disease-control-and-prevention
9. Ministry of Health, Labour and Welfare, Japan. Discharge criteria for COVID-19 patients, 2020 Feb 18 [in Japanese] [cited 2020 Feb 26]. https://www.mhlw.go.jp/content/10900000/000597947.pdf
10. Zou L, Ruan F, Huang M, Liang L, Huang H, Hong Z, et al. SARS-CoV-2 viral load in upper respiratory specimens of infected patients. N Engl J Med. 2020 Feb 19 [Epub ahead of print]. https://doi.org/10.1056/NEJMc2001737

Address for correspondence: Takeshi Arashiro, Asahi General Hospital, I 1326, Asahi City, Chiba 289-2511, Japan; email: arash003@umn.edu

The Pandemic Century: One Hundred Years of Panic, Hysteria and Hubris

Mark Honigsbaum; W.W. Norton, New York City, 2019; ISBN-10: 1787381218; ISBN-13: 978-1787381216; Pages: 450; Price: Hardcover $29.95; Audiobook narrated by John Lee; 13 h 40 min; HighBridge, a division of Recorded Books; $23.70–$33.09

Long before microbes were discovered, a sudden occurrence of disease in a society would trigger fear, accompanied by rational and irrational responses. A mysterious, highly contagious disease that spread across the Mediterranean and killed a quarter of the population of Athens is the first recorded pandemic (*1*).

The Pandemic Century: One Hundred Years of Panic, Hysteria and Hubris by Mark Honigsbaum, a medical historian at the City University of London (UK), focuses on large-scale outbreaks since 1900. The author uses 9 examples to shine a light on epidemiological blind spots to avoid in future investigations. For example, he suggests that the initial lackluster response to the 1918 influenza pandemic can be attributed in part to false confidence in Richard Pfeiffer's 1892 discovery of *Bacillus influenzae*, now known as *Haemophilus influenzae.* We later learned that *H. influenzae* occasionally is found in persons with influenza but was not the cause of the pandemic.

Through colorful and engaging narrative, Honigsbaum probes the social context of early 20th Century America that led investigators to attribute differences in pneumonia rates among African Americans to racial factors compared with white soldiers at Camp Funston, Kansas, thought to be an early site of the 1918 influenza pandemic. He details how public hysteria, fear, and conspiracy theories hindered public health responses in other outbreaks, such as in the 1976 Legionnaires' disease outbreak in Philadelphia, Pennsylvania. He includes laboratory and epidemiological investigations that led to identification of *Legionella pneumophila* in 1977 (Figure). The film, Influenza 1918, which aired on the Public Broadcasting Service, also profiles the pandemic (*2*).

The book at times offers a gloomy assessment of how, in today's era of international travel, ecological disturbances and human behaviors have tipped the scales in favor of pathogens. It also highlights lapses that occurred during outbreak investigations, such as how mishandled laboratory samples delayed recognition of severe acute respiratory syndrome (SARS) in 2002 and how cross-border travel and the lack of appreciation for local cultural practices by investigators facilitated spread of Ebola virus in West Africa during 2014–2016.

The text concludes with a description of global efforts to anticipate pandemics, such as Resolve, a public health initiative supported by philanthropic institutions including the Bill and Melinda Gates Foundation. Honigsbaum notes uncertainties and gaps here too, such as Madagascar's ineligibility to receive support to respond to a massive *Yersinia pestis* outbreak from a World Bank fund. The fund was established after the Ebola outbreak in West Africa and only can be used for diseases caused by viruses that have certain characteristics and threaten to spread internationally (*3*).

This book appealed to me because it condenses events spanning a century into readable segments told by an author known for in depth historical accounts. *The Pandemic Century* could appeal to diverse categories of readers, including epidemiologists, public health workers, students, and anyone interested in understanding why, despite impressive gains in global public health preparedness and advances in disease prevention and control, pandemics continue to surprise and terrify us.

Nkuchia M. M'ikanatha

Author affiliation: Pennsylvania Department of Health, Harrisburg, Pennsylvania, USA

DOI: https://doi.org/10.3201/eid2606.191739

References

1. Littman RJ. The plague of Athens: epidemiology and paleopathology. Mt Sinai J Med. 2009;76:456–67. https://doi.org/10.1002/msj.20137
2. Influenza 1918. American Experience. Public Broadcasting Service. 2010 Jan 18 [cited 2020 Apr 14]. https://www.pbs.org/video/american-experience-influenza-1918
3. The World Bank. World Bank launches first-ever pandemic bonds to support $500 million pandemic emergency financing facility [cited 2019 Nov 30]. https://www.worldbank.org/en/news/press-release/2017/06/28/world-bank-launches-first-ever-pandemic-bonds-to-support-500-million-pandemic-emergency-financing-facility

Address for correspondence: Nkuchia M. M'ikanatha, Pennsylvania Department of Health, Division of Infectious Disease Epidemiology, Health and Welfare Building, 7th and Forster St, Room 933, Harrisburg, PA 17120, USA; email: nmikanatha@pa.gov

Notice to Readers

Readers may learn more about this month's cover image, ***Portrait of Maria Salviati and Giulia de' Medici***, by reading the historical review article Syphilis in Maria Salviati (1499–1543), Wife of Giovanni de' Medici of the Black Bands, which appears in this issue (https://wwwnc.cdc.gov/eid/article/26/6/18-0786_article). This image is also included as Figure 1 in that article (page 1274).

Jacopo Carucci Pontormo (1494–1557). ***Portrait of Maria Salviati and Giulia de' Medici*** **(c. 1537).** Oil on panel, 34.65 in × 28.07 in/88 cm × 71.3 cm. Digital image courtesy of The Walters Art Museum, Baltimore, Maryland, USA.

EMERGING INFECTIOUS DISEASES®

Upcoming issue

- Case Manifestations and Public Health Response for Outbreak of Meningococcal W Disease, Central Australia
- Macrolide-Resistant *Mycoplasma pneumoniae* Infections in Pediatric Community-Acquired Pneumonia
- Transmission of Chikungunya Virus in an Urban Slum, Brazil
- Public Health Role of Academic Medical Center in Community Outbreak of Hepatitis A, San Diego County, California, USA, 2016–2018
- Identifying Locations with Possible Undetected Imported Severe Acute Respiratory Syndrome Coronavirus 2 Cases by Using Importation Predictions
- Atypical Manifestations of Cat-Scratch Disease, United States, 2005–2014
- Severe Acute Respiratory Syndrome Coronavirus 2–Specific Antibody Responses in Coronavirus Disease Patients
- Bat and Lyssavirus Exposure among Humans in Region that Celebrates a Bat Festival, Nigeria, 2010 and 2013
- High Contagiousness and Rapid Spread of Severe Acute Respiratory Syndrome Coronavirus 2
- Efficient Surveillance of *Plasmodium knowlesi* Genetic Subpopulations, Malaysian Borneo, 2000–2018
- Countrywide Outbreak of Invasive Listeriosis Associated with Blood Sausage Consumption, Germany, 2018–2019
- Rickettsioses as Major Etiologies of Unrecognized Acute Febrile Illness, Sabah, East Malaysia
- Meningococcal W 135 Disease Vaccination Intent, the Netherlands, 2018–2019
- Coccidioidomycosis Among Hispanic Farm Workers, California, USA, 2018
- Policy Decisions and Use of Information Technology to Fight Coronavirus Disease, Taiwan
- Early Introduction of Severe Acute Respiratory Syndrome Coronavirus 2 into Europe
- Shuni Virus in Wildlife and Nonequine Domestic Animals, South Africa
- Approach to Cataract in an Ebola Virus Disease Survivor with Prior Ocular Viral Persistence
- Transmission of Legionnaires' Disease through Toilet Flushing
- Clinical Characteristics of Patients Hospitalized with Coronavirus Disease, Thailand
- Clinical Management of Argentine Hemorrhagic Fever using Ribavirin and Favipiravir, Belgium, 2020
- Sub-Saharan Africa and Eurasia Ancestry of Reassortant Highly Pathogenic Avian Influenza A(H5N8) Virus, Europe, December 2019
- Inactivation of Severe Acute Respiratory Syndrome Coronavirus 2 by WHO-Recommended Hand Rub Formulations and Alcohols
- Aerosol and Surface Distribution of Severe Acute Respiratory Syndrome Coronavirus 2 in Hospital Wards, Wuhan, China, 2020
- Severe Acute Respiratory Syndrome Coronavirus 2 Infection among Returnees to Japan from Wuhan, China, 2020
- Carbapenem Resistance Conferred by OXA-48 in K2-ST86 Hypervirulent *Klebsiella pneumoniae*, France
- Possible Bat Origin of Severe Acute Respiratory Syndrome Coronavirus 2
- Serologic Evidence of Severe Fever with Thrombocytopenia Syndrome Virus and Related Viruses in Pakistan
- Surveillance and Testing for Middle East Respiratory Syndrome Coronavirus, Saudi Arabia, March 2016–March 2019

Complete list of articles in the July issue at http://www.cdc.gov/eid/upcoming.htm

Earning CME Credit

To obtain credit, you should first read the journal article. After reading the article, you should be able to answer the following, related, multiple-choice questions. To complete the questions (with a minimum 75% passing score) and earn continuing medical education (CME) credit, please go to http://www.medscape.org/journal/eid. Credit cannot be obtained for tests completed on paper, although you may use the worksheet below to keep a record of your answers.

You must be a registered user on http://www.medscape.org. If you are not registered on http://www.medscape.org, please click on the "Register" link on the right hand side of the website.

Only one answer is correct for each question. Once you successfully answer all post-test questions, you will be able to view and/or print your certificate. For questions regarding this activity, contact the accredited provider, CME@medscape.net. For technical assistance, contact CME@medscape.net. American Medical Association's Physician's Recognition Award (AMA PRA) credits are accepted in the US as evidence of participation in CME activities. For further information on this award, please go to https://www.ama-assn.org. The AMA has determined that physicians not licensed in the US who participate in this CME activity are eligible for AMA PRA Category 1 Credits™. Through agreements that the AMA has made with agencies in some countries, AMA PRA credit may be acceptable as evidence of participation in CME activities. If you are not licensed in the US, please complete the questions online, print the AMA PRA CME credit certificate, and present it to your national medical association for review.

Article Title

Manifestations of Toxic Shock Syndrome in Children, Columbus, Ohio, USA, 2010–2017

CME Questions

1. Your patient is a 2-year-old boy who appears to have some findings consistent with toxic shock syndrome (TSS), but who has no rash. On the basis of a retrospective chart review from a large tertiary care center by Cook and colleagues, which one of the following statements about clinical characteristics of pediatric TSS is correct?

A. Three quarters of patients with STSS had a characteristic rash
B. One quarter of patients had clinical and laboratory findings that are not part of TSS criteria
C. Pulmonary infiltrates were present in 73% of patients with TSS at diagnosis and admission, but only 12% of patients had primary admission and discharge diagnosis of pneumonia
D. In patients with nonstreptococcal TSS (NSTSS), thrombocytopenia was the only coagulation abnormality identified

2. According to the retrospective chart review by Cook and colleagues, which one of the following statements about diagnostic decisions regarding pediatric TSS in a large tertiary care center and their implications for published criteria is correct?

A. The findings support existing CDC criteria for TSS diagnosis and management.
B. Clinicians often rely incorrectly on typical presentations of TSS (eg, fever, hypotension, and rash) before they make the diagnosis of TSS
C. The findings support separate diagnostic criteria for STSS and NSTSS
D. The findings support use of diagnostic criteria regarding creatine phosphokinase (CPK) and renal and hepatic involvement

3. On the basis of the retrospective chart review from a large tertiary care center by Cook and colleagues, which one of the following statements about treatment and management of pediatric TSS is correct?

A. Many patients had a prolonged preadmission course that could delay their treatment start time
B. Treatment with clindamycin and intravenous immunoglobulin (IVIg) led to significantly better outcomes than treatment with IVIg alone
C. Presence or absence of rash did not affect timing of recommended treatment initiation in patients with STSS
D. Patients with NSTSS received clindamycin and IVIg sooner than those with STSS and stayed ~57% fewer inpatient days

Earning CME Credit

To obtain credit, you should first read the journal article. After reading the article, you should be able to answer the following, related, multiple-choice questions. To complete the questions (with a minimum 75% passing score) and earn continuing medical education (CME) credit, please go to http://www.medscape.org/journal/eid. Credit cannot be obtained for tests completed on paper, although you may use the worksheet below to keep a record of your answers.

You must be a registered user on http://www.medscape.org. If you are not registered on http://www.medscape.org, please click on the "Register" link on the right hand side of the website.

Only one answer is correct for each question. Once you successfully answer all post-test questions, you will be able to view and/or print your certificate. For questions regarding this activity, contact the accredited provider, CME@medscape.net. For technical assistance, contact CME@medscape.net. American Medical Association's Physician's Recognition Award (AMA PRA) credits are accepted in the US as evidence of participation in CME activities. For further information on this award, please go to https://www.ama-assn.org. The AMA has determined that physicians not licensed in the US who participate in this CME activity are eligible for AMA PRA Category 1 Credits™. Through agreements that the AMA has made with agencies in some countries, AMA PRA credit may be acceptable as evidence of participation in CME activities. If you are not licensed in the US, please complete the questions online, print the AMA PRA CME credit certificate, and present it to your national medical association for review.

Article Title

Statin Use and Influenza Vaccine Effectiveness in Persons >65 Years of Age, Taiwan

CME Questions

1. You are advising a large geriatric practice regarding the likelihood of efficacy of influenza vaccine in patients receiving statins. On the basis of the large-scale, nationwide, Taiwanese population-based cohort study by Tsai and colleagues, which one of the following statements about the risks for poor outcomes in elderly patients (aged >65 years) who received influenza vaccinations compared with those in propensity score-matched elderly control individuals who did not receive influenza vaccinations is correct?

A. The vaccinated group had lower risks for in-hospital death from pneumonia (28% lower risk; adjusted hazard ratio [aHR], 0.72) and hospitalization for pneumonia and influenza (16% lower risk; aHR, 0.84)
B. The vaccinated group did not have significantly lower risks for in-hospital death or hospitalization for critical illnesses than the unvaccinated group
C. Hospitalization for circulatory conditions did not differ between groups
D. Before propensity score matching, the groups did not differ in comorbidities or concomitant drug use

2. According to the large-scale, nationwide, Taiwanese population-based cohort study by Tsai and colleagues, which one of the following statements about comparative vaccine effectiveness between elderly statin users and nonusers is correct?

A. Statin use has been proven to eliminate influenza vaccine effectiveness against critical illness and mortality among vaccinated elderly patients
B. When stratified by statin use and analyzed by interaction analysis, there was no significant difference in outcomes between statin users and nonusers
C. Using a Cox regression model adjusted for propensity score only showed that statin users had worse outcomes than nonusers
D. The rate of hospitalization for critical illness was significantly higher in statin users than in nonusers

3. On the basis of the large-scale, nationwide, Taiwanese population-based cohort study by Tsai and colleagues, which one of the following statements about clinical implications of comparative risks for poor outcomes in elderly patients who did or did not receive influenza vaccinations, and of comparative vaccine effectiveness between statin users and nonusers, is correct?

A. The findings suggest that elderly patients using statins should not receive influenza vaccination
B. Statins appear to increase cytokine production by immune cells
C. The study proves that in middle-aged adults, statin use will not affect influenza vaccine effectiveness
D. Statins may inhibit the major histocompatibility complex class II pathway of antigen presentation

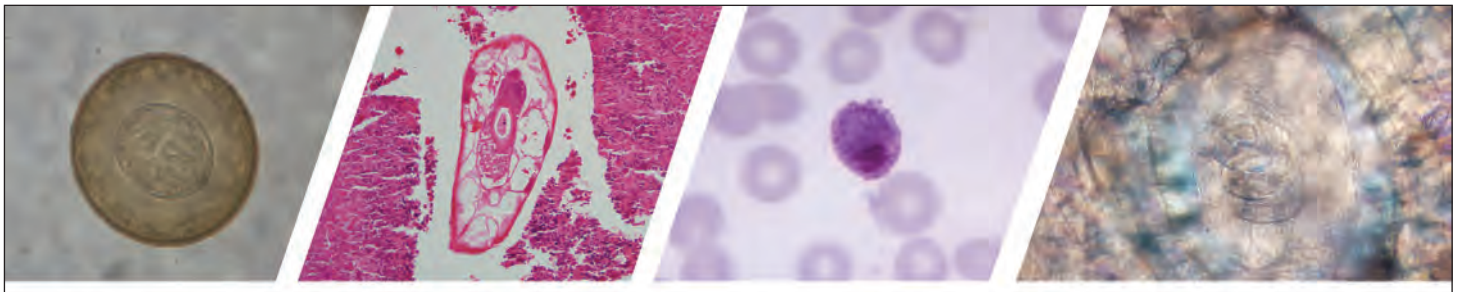

DPDx

Diagnostic Assistance and Training in Laboratory Identification of Parasites

A free service of CDC available to laboratorians, pathologists, and other health professionals in the United States and abroad

- Diagnosis from photographs of worms, histological sections, fecal, blood, and other specimen types
- Expert diagnostic review
- Formal diagnostic laboratory report
- Submission of samples via secure file share

Visit the DPDx website for information on laboratory diagnosis, geographic distribution, clinical features, parasite life cycles, and training via Monthly Case Studies of parasitic diseases.

www.cdc.gov/dpdx
dpdx@cdc.gov

U.S. Department of Health and Human Services
Centers for Disease Control and Prevention

CS272346-DE